AJNR

AMERICAN JOURNAL OF NEURORADIOLOGY

MAY 2014
VOLUME 35
NUMBER 5
WWW.AJNR.ORG

THE JOURNAL OF DIAGNOSTIC AND INTERVENTIONAL NEURORADIOLOGY

Neuroimaging in patients with abnormal blood glucose levels

Cord injuries in blunt cervical spine trauma

Focused ultrasound for treatment of essential tremor

Official Journal ASNR • ASFNR • ASHNR • ASPNR • ASSR

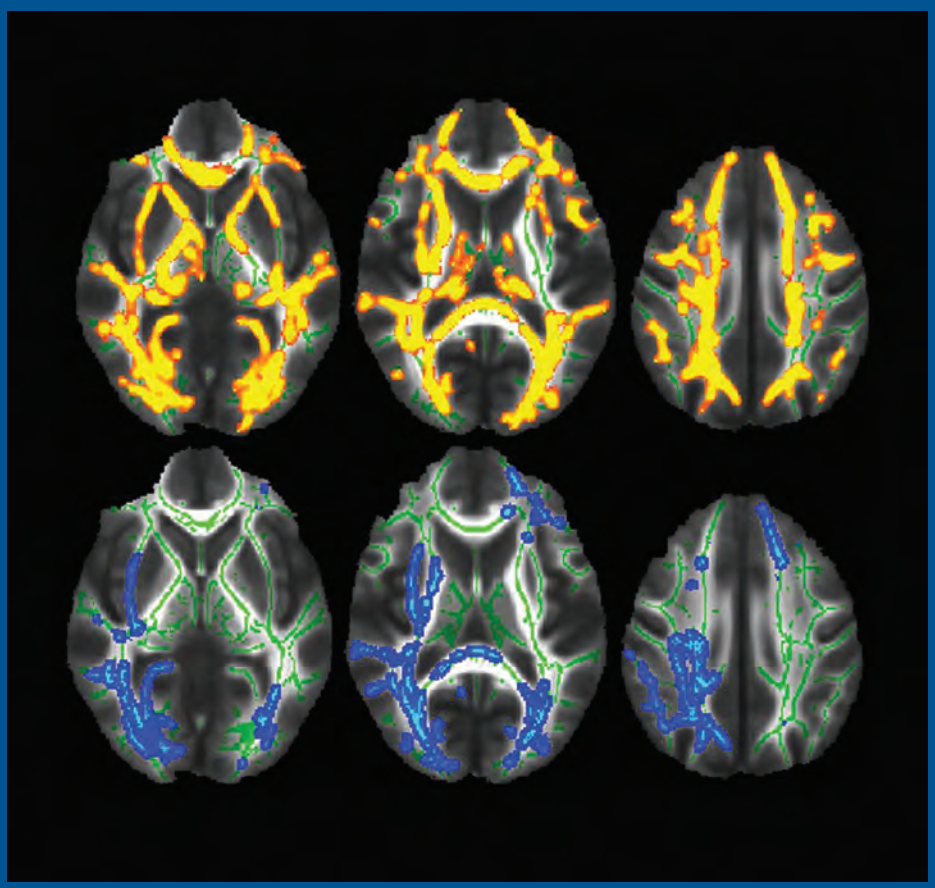

MicroVention® TERUMO

Dedicated to the development

The MicroVention family of neuroendovascular products:

DELIVERY & DETACHMENT SYSTEMS

V-Trak®

V-Trak® Soft

V-Grip®

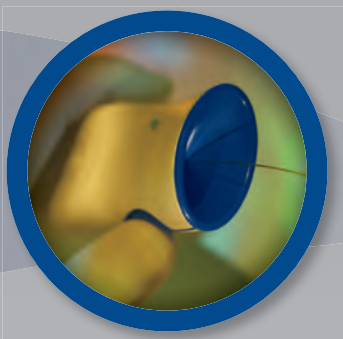

ACCESS PRODUCTS

Traxcess® Guidewire

Chaperon® Guiding Catheter

Headway® Microcatheter

Headway Duo microcatheter

Scepter Occlusion Balloon Catheter

microvention.com

CE 0297

# of innovative endovascular technologies

HYDROGEL COIL PRODUCTS

HydroFrame® HydroCoil® Embolic System

HydroSoft® HydroCoil® Embolic System

HydroFill® HydroCoil® Embolic System

PLATINUM COIL PRODUCTS

MICROPLEX® coil system

COSMOS® complex coil

VFC® Versatile Range Fill Coil

HYPERSOFT® finishing coil

Introducing…

HyperSoft® 3D complex coil

The softness of the HyperSoft® Coil available in Complex Form!

Now you can Frame, Fill and Finish with the softness
you need to match almost any aneurysm morphology.

MicroVention, Inc.
Worldwide Headquarters PH +1.714.247.8000
1311 Valencia Avenue
Tustin, CA 92780 USA
MicroVention UK Limited PH +44 (0) 191 258 6777
MicroVention Europe, S.A.R.L. PH +33 (1) 39 21 77 46
MicroVention Deutschland GmbH PH +49 211 210 798-0

BARRICADE™ COIL SYSTEM

PERFORMANCE AND VALUE DELIVERED

BLOCKADE MEDICAL

18 TECHNOLOGY DRIVE #169, IRVINE CA 92618 | **P** 949.788.1443
WWW.BLOCKADEMEDICAL.COM

MADE IN AMERICA

CE 0297

MKTG-020 REV. B

AJNR

AMERICAN JOURNAL OF NEURORADIOLOGY

MAY 2014
VOLUME 35
NUMBER 5
WWW.AJNR.ORG

Publication Preview at www.ajnr.org features articles released in advance of print. Visit www.ajnrblog.org to comment on AJNR content and chat with colleagues and AJNR's News Digest at http://ajnrdigest.org to read the stories behind the latest research in neuroimaging.

Indicates Editor's Choices selection

Indicates Fellows' Journal Club selection

Indicates open access to non-subscribers at www.ajnr.org

Indicates article with supplemental on-line table

Indicates article with supplemental on-line photo

Indicates article with supplemental on-line video

Indicates Evidence-Based Medicine Level 1

Indicates Evidence-Based Medicine Level 2

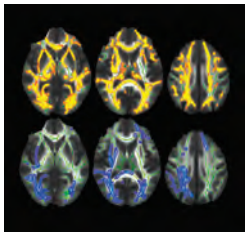

DTI maps show differences between controls and patients with subacute combined degeneration with proven vitamin B_{12} deficiency.

Target®
DETACHABLE COILS

Smooth and Stable

Whether you are framing, filling or finishing, Target Detachable Coils deliver consistently smooth deployment and exceptional microcatheter stability. Focused on design, Target Coils feature a host of advantages to ensure the high-powered performance you demand.

For more information, please visit www.strykerneurovascular.com/Target or contact your local Stryker Neurovascular sales representative.

stryker® Neurovascular

Stroke: *Our Only Focus. Our Ongoing Promise.*

American Society of Neuroradiology Future Annual Meetings

ASNR 2015 – 53rd ANNUAL MEETING

April 25-30 • Sheraton Chicago Hotel & Towers • Chicago, Illinois

ASNR 2016 – 54th ANNUAL MEETING

May 21-26 • Washington Marriott Wardman Park • Washington, DC

ASNR 2017 – 55th ANNUAL MEETING

April 22-27 • Long Beach Convention & Entertainment Center • Long Beach, California

ASNR 2018 – 56th ANNUAL MEETING

June 2-7 • Vancouver Convention Centre • Vancouver, B.C., Canada

ASNR 2019 – 57th ANNUAL MEETING

May 18-23 • Hynes Convention Center • Boston, Massachusetts

TO REQUEST MORE INFORMATION ON UPCOMING MEETINGS, CONTACT:

American Society of Neuroradiology
800 Enterprise Drive, Suite 205, Oak Brook, Illinois 60523-4216
Phone: 630-574-0220 • Fax: 630-574-0661
Website: www.asnr.org • Email: meetings@asnr.org

AJNR

Letter from the President-Elect – Search for New *AJNR* Editor

In June, 2015, Mauricio Castillo, MD, FACR, will complete an eight-year term as the Editor-in-Chief of the *AJNR*. He follows a short list of illustrious neuroradiologists, from Dr. Juan Taveras to Dr. Michael Huckman to Dr. Robert Quencer to Dr. Robert Grossman.

One only has to pick up any random issue of the *AJNR* to realize what a tremendous mark Mauricio has made on the journal. His imprint starts on the first page of content with his column, Perspectives. Probing, erudite, at times very witty, and always brilliant, Mauricio turns out a monthly commentary on the state of neuroradiology, the state of our profession, and, at times, the state of the world. His references and quotations demonstrate a mind not only scientific and exacting but also knowledgeable in realms far beyond medicine.

Having worked with Mauricio very closely at the ASNR for the past two years, I can also attest to the fact that Mauricio is totally dedicated to the journal. At times, it seemed his reason for being. And the journal has benefitted immensely, in turn. From its look to its organization to the quality of the articles, Mauricio has brought the journal into the forefront of all radiology journals and it now ranks #2 in Impact Factor of all radiology journals. *AJNR* is the premier clinical neuroimaging journal with the highest circulation among all imaging-related subspecialty journals, publishing about 350 articles in 12 issues per year. It receives over 1400 original submissions annually and its Web site is accessed over 10 million times a year. In addition to the print version of the Journal, Mauricio also initiated its biannual Special Collections and monthly *AJNR* Digest. Other electronic activities which he began include its popular Case Collection (Case of the Week, Case of the Month, Classic Case, and Clinical Correlation), podcasts (editor's and fellows' journal club selections, travelling journal club, and Special Collections), and Fellows' Portal. With his international background, Mauricio has also been the ideal person to spread the word of the *AJNR* across the world. Finally, he has done all this and kept the journal in sound financial health through a period of difficult economic times.

Mauricio took over leadership of the journal at a time when the concept of the journal was beginning to enter a state of flux. One only has to look at your neighborhood newsstand to realize that this has been a time when many publications have been unable to adjust and have disappeared. In the past eight years, the demands on the journal have changed. Our current expectations are for instant gratification, not a lag time before publication. We require our information in more bite-size pieces, directed at us and easily accessible.

The new editor will face an even more rapidly evolving world. What is the future of radiology journals? We know that the *AJNR* will survive but in what form? What will be the best digital format? There will be an increased demand for electronic access and a further migration to tablets and smartphones. Preserving the brand of the *AJNR* will become more challenging. While in the past, publication was the end point, increasingly, publication today is the starting point, the beginning of an interactive discussion. How will this impact on the financial state of the journal, with decreasing print advertising? How will the *AJNR* respond to the demands of social media?

To assist the Executive Committee in the search for a new editor in these changing times, I will chair a search committee comprised, in part, of Tina Young-Poussaint, Chair of the Publications Committee, Laurie Loevner, Vice-President, Howard Rowley, Robert Quencer, Robert D. Zimmerman, James Barkovich, Tabbassum Kennedy, and some of the Senior Editors of the *AJNR*, Harry J. Cloft, Nancy Fischbein, Pamela W. Schaefer, Jody Tanabe, and Charles M. Strother, as well as James Gantenberg, Karen Halm, and Angelo Artemakis from the ASNR headquarters. The appointment of the new Editor-in-Chief will be announced in the spring of 2015.

All interested physicians are invited to send their curriculum vitae and an introductory letter of intent to Dr. Gordon Sze, American Society of Neuroradiology, 800 Enterprise Drive, Suite 205, Oak Brook, IL, 60523 and via email to gordon.sze@yale.edu and jgantenberg@asnr.org. In addition, we welcome nominations of candidates from the ASNR membership. The deadline for receipt of submissions is August 1, 2014 but earlier submissions are welcome. A position description for the *AJNR* Editor and basic qualifications are posted at: www.ajnr.org/site/misc/eic-search-2015.xhtml.

Gordon Sze, MD, FACR
Chair, Editor-in-Chief Search Committee
President-Elect
American Society of Neuroradiology

Simplify
the MOC Process

Manage
your CME Credits Online

CMEgateway.org

It's Easy and Free!

Log on to CME Gateway to:

- View or print reports of your CME credits from multiple societies from a single access point.
- Print an aggregated report or certificate from each participating organization.
- Link to SAMs and other tools to help with maintenance of certification.

American Board of Radiology (ABR) participation!

By activating ABR in your organizational profile, your MOC–fulfilling CME and SAM credits can be transferred to your own personalized database on the ABR Web site.

Sign Up Today!

go to CMEgateway.org

Available to Members of Participating Societies

American Board of Radiology (ABR)
American College of Radiology (ACR)
American Roentgen Ray Society (ARRS)
American Society of Neuroradiology (ASNR)
Commission on Accreditation of Medical Physics Educational Programs, Inc. (CAMPEP)
Radiological Society of North America (RSNA)
Society of Interventional Radiology (SIR)
SNM
The Society for Pediatric Radiology (SPR)

AJNR

AMERICAN JOURNAL OF NEURORADIOLOGY

Publication Preview at www.ajnr.org features articles released in advance of print. Visit www.ajnrblog.org to comment on AJNR content and chat with colleagues and AJNR's News Digest at http://ajnrdigest.org to read the stories behind the latest research in neuroimaging.

MAY 2014 • VOLUME 35 • NUMBER 5 • WWW.AJNR.ORG

AJNR (Am J Neuroradiol ISSN 0195–6108) is a journal published monthly, owned and published by the American Society of Neuroradiology (ASNR), 800 Enterprise Drive, Suite 205, Oak Brook, IL 60523. Annual dues for the ASNR include $170.00 for journal subscription. The journal is printed by Cadmus Journal Services, 5457 Twin Knolls Road, Suite 200, Columbia, MD 21045; Periodicals postage paid at Oak Brook, IL and additional mailing offices. Printed in the U.S.A. POSTMASTER: Please send address changes to American Journal of Neuroradiology, P.O. Box 3000, Denville, NJ 07834, U.S.A. Subscription rates: nonmember $370 ($440 foreign) print and online, $300 online only; institutions $430 ($495 foreign) print and basic online, $850 ($915 foreign) print and extended online, $355 online only (basic), extended online $770; single copies are $35 each ($40 foreign). Indexed by PubMed/Medline, BIOSIS Previews, Current Contents (Clinical Medicine and Life Sciences), EMBASE, Google Scholar, HighWire Press, Q-Sensei, RefSeek, Science Citation Index, and SCI Expanded.

Pigeons and MRI: Tesla Vignettes

M. Castillo, *Editor-in-Chief*

Nikola Tesla's name is familiar to neuroradiologists, but few of us know why our profession and understanding of the brain are better because of him. His achievements were not universally recognized until 1960 (17 years after his death) when the *Conference Generale des Poids et Mesures* decided that the unit for measuring the magnetic field (B) should be called the "tesla." The strength of the magnetic field of the earth at the equator is 31 microteslas, and it is worth remembering that magnets found even in small speakers are as powerful as those found in our MR imaging units (1–2.4T).[1] His research also involved superconducting magnets cooled to a few degrees above absolute zero. Although Tesla was constantly on the verge of becoming rich, he died poor and alone at 86 years of age in a room at the Hotel New Yorker (still at 481 Eighth Avenue). After his death, unknown individuals and/or government forces removed his last inventions and papers from his apartment because they were thought to contain information regarding the "Death Ray," in which the military was interested.[2] This ray, presumably a particle beam, could repel armies and bring down airplanes. The list of Tesla's inventions is long and incredible in its breadth. During his life, Mr Tesla struggled for recognition, and it mostly eluded him, the Nobel Prize being one example. In this Perspectives, I mention some colorful aspects of Mr Tesla's life rather than recounting his incredible accomplishments.

Tesla and Edison

Tesla came to America after living in France for 2 years, and Mr Edison hired him to work at the Edison Machine Works in New York City. Edison's electric power generators producing direct current (DC) worked well only when electricity requirements were small. The power and output of DC are relatively weak, making its transmission over long distances impractical. Tesla solved this issue by perfecting alternating current (AC). Transformers decrease or increase the power of AC as needed, so if long-distance transmission is required, power is amplified, making it more efficient (with DC current, a generator every 3–4 km is needed). When Edison refused to pay him for his inventions, Tesla left and later sold them to Westinghouse. The War of Currents erupted, and Edison tried to instill fear in AC users by calling it extremely dangerous. He went as far as paying children to steal dogs, electrocute them with AC, then scatter their bodies together with flyers alerting the public to the dangers of AC. When killing dogs no longer shocked the public, he killed larger animals (sheep, cows, horses), eventually leading to the electrocution of Topsy the elephant (for a video of this see: http://tinyurl.com/mumu8mq and, for a good description of the process, I suggest reading Jean Echenoz's fictional Tesla biography *Des Eclairs*[3]).

http://dx.doi.org/10.3174/ajnr.A3675

Additionally, Edison promoted the first successful electrocution of a prisoner by using AC (DC was tried but was not powerful enough to kill a human being) to showcase the dangers of this type of electricity. The subsequent legal battles that erupted nearly caused Edison and Westinghouse to go broke and forced Tesla to forfeit royalties from his patents owned by the latter. When Edison died, Tesla wrote this bitter obituary: "He had no hobby, cared for no sort of amusement of any kind and lived in utter disregard of the most elementary rules of hygiene. . . . His method was inefficient in the extreme, for an immense ground had to be covered to get anything at all unless blind chance intervened and, at first, I was almost a sorry witness of his doings, knowing that just a little theory and calculation would have saved him 90% of the labor. But he had a veritable contempt for book learning and mathematical knowledge, trusting himself entirely to his inventor's instinct and practical American sense."[4] Just before dying, Edison acknowledged that ignoring Tesla's AC patent had been his biggest mistake.

Tesla and Roentgen

Before x-rays were officially named, Tesla investigated them by using single-terminal vacuum tubes (conventional ones use 2 terminals). We know that high-energy electrons emitted by a cathode hit the special material (tungsten, molybdenum) of the anode, "braking" them and secondarily emitting a very small percentage of high-energy x-rays. In Tesla's tube, no target existed. Energy left the electrons encountering a high-field electrical environment resulting from the oscillations of AC, and as they collided with the glass encasement, x-rays were generated. His experiment also worked well by using Geissler tubes that were filled with substances such as inert gasses (these were the forbearers of fluorescent light and the electron microscope). While in New York, he produced images of the bones in his hands and sent them to Roentgen, who ignored them. Tesla also claimed that his design produced x-rays much more powerful than Roentgen's. Because Tesla never published his findings and his research notes were lost during a fire of suspicious nature, he never received credit for the discovery of x-rays. Fortunately, he also became aware of Roentgen's health issues induced by radiation exposure and avoided them himself.

Tesla and Marconi

Although Guglielmo Marconi is credited with having invented the telegraph and received the Nobel Prize for the radio, Tesla discovered both years before Signore Marconi did. Tesla discovered that by using his coils, radio signals could be transmitted over great distances as long as the receiving coil was tuned to the resonant frequency of the transmitting one (sound familiar?). The receiving coil magnifies signals via resonance. Just before Tesla could demonstrate that his invention was able to transmit signal as far as 50 miles, his laboratory suspiciously burned down, causing him to lose his instruments and documents (note that Tesla demonstrated transmission at shorter distances in St. Louis 2 years before

Marconi showed his invention). About the same time as the aforementioned tragedy, Marconi developed a 2-way transmitter whose signals were too weak to cross even a small pond. He solved the problem by using Tesla coils. Marconi claimed ignorance about Tesla's coils when applying for a US patent, and the granting of patents to both inventors was delayed due to arguments on both sides claiming property rights. Aided by rich investors, Marconi's Wireless Telegraph Company thrived in the stock markets, and soon Andrew Carnegie and Thomas Edison became its 2 most important American investors. Shortly thereafter, Marconi amazed the world by transmitting signals wirelessly across the Atlantic Ocean. Because Marconi was using several of Tesla's patents to accomplish this, Nikola was not worried; but he should have been because 4 years later, the United States awarded the patents for the telegraph and radio to Marconi under political pressure from Carnegie and Edison. When Marconi received the Nobel Prize, Tesla was furious and sued Marconi for stealing his patents. Later, the Marconi Company sued the US government because the armed forces had used its patents for communications during World War I without permission or payment. The US Supreme Court eventually ruled that these patents belonged to Tesla (now dead and childless), thus avoiding any payments owed by the government to Marconi's company.[5] Tesla predicted that all of us would carry small, wireless telephones in our pockets; something Marconi did not.

Tesla and Twain

Exactly where Tesla and Samuel Clemens met is not clear; it could have been at the Player's Club (a bar in Manhattan) or in the laboratory. Although Tesla was familiar with Twain's writings, it was not until after the discovery of AC that Twain noticed Nikola. Both men shared friends in high society, including the Johnsons, Kipling, Roosevelt, and Muir. Tesla invited Twain to his laboratory, where the famous writer partook in some electrical experiments that reportedly filled him with vigor and vitality. While Twain was spending time in Austria, he heard about Tesla's experiments on destructive terror (the Death Ray) and wrote urging him to use these to make war impossible in the future by making it available to all (an idea akin to "assured mutual destruction").

Tesla and the FBI

While living in Colorado Springs, Tesla started developing the idea for a particle beam that could be used as a weapon, and though his idea never materialized, it was described in what is known as the "Tesla Papers." Immediately after his death, unknown persons raided his apartment in the New Yorker Hotel, stealing documents for fear that they would fall into Soviet hands. Two days after his death (when he was found by a maid), the FBI confiscated all that was left. The FBI appointed Dr John Trump of the National Research Committee to look into the documents, and he concluded that they were mostly speculative in nature. After World War II, interest in them was revived and the heavily funded "Project Nick" was started in Dayton, Ohio, only to be dropped later. Interest in a beam weapon waxed and waned until the late 1970s, when construction of a large beam weapon by the Soviets came to light. As a response, in the early 1980s, President Ronald Reagan proposed the Strategic Defense Initiative.[6] All attempts to build a Death Ray have failed, and many think that answers to the problems encountered were addressed in the missing "Tesla Papers " (some think that the US Government has them and is hiding them).

Tesla and Birds

No one knows why Tesla was interested in pigeons. This interest is nicely portrayed in *The Invention of Everything Else* by Samantha Hunt.[7] As an old man, Tesla walked every day to Bryant Park (located behind the New York Public Library between 6th Avenue and West 42nd Street, a scene again found in Paul Auster's *Moon Palace*[8]). At that time, pigeons were considered unmeritorious, and perhaps Tesla felt similarly about himself. On the night that he was awarded the Edison Medal (how ironic!), he suddenly disappeared from the banquet only to be found in Bryant Park covered by pigeons from head to evening pumps. Tesla said he considered pigeons to be his "sincere friends." He took sick ones into his apartment and caused cleaning crews to complain of dirt. Just days before his death, he became particularly attached to one and was able to recognize this particular bird and fed it every day (white wings with a touch of gray in their tips, photographs available at: http://www.teslauniverse.com/nikola-tesla-timeline-1922-tesla-pigeon-dies). When the pigeon became sick, Tesla took it with him to his apartment, but attempts to cure the bird failed and it died. Tesla died only a few days after the pigeon, it is said of a broken heart (this may be true because he died of heart failure); he previously stated that he had loved her as a man loves a woman (how sad is that?). Much has been made about the symbolism of the pigeon, comparing it with the dove in religion and its meaning in Tesla's life. Curiously, Tesla's favorite meal was squab.

Tesla, like Einstein, was a generalist, and like Edison, he was self-taught. His thoughts extended into many arenas of human enterprise without dwelling on details of how to accomplish them. Because he almost never published in scientific journals, many of his ideas are now lost. Some of his projects sounded like science fiction but are now reality; others are still within the realm of the impossible but are being reconsidered. Our knowledge has expanded so much that extrapolating what we now know into the world where Tesla lived is simply not possible, so it is hard for us to grasp his achievements. However, it is thanks to them that MR imaging and modern neuroimaging are possible.

Bonus

Two wonderful stories about Edison and Topsy, and Tesla and his pigeons can be found in *Love in Infant Monkeys* by Lydia Millet.[9]

REFERENCES

1. Tesla (unit). Wikipedia. http://en.wikipedia.org/wiki/Tesla_%28unit%29. Accessed June 5, 2013
2. Lost Tesla Papers about "Death Rays." Tesla Memorial Society of New York. http://www.teslasociety.com/deathray.htm. Accessed on June 5, 2013
3. Echenoz J. *Des Eclairs.* Paris: Les Editions de Minuit; 2010
4. Nikola Tesla. Wikipedia. http://en.wikipedia.org/wiki/Nikola_Tesla. Accessed on June 5, 2013
5. http://www.pbs.org/tesla/ll/ll_whoradio.html. Accessed on June 5, 2013
6. Tesla, Life and Legacy. The Missing Papers. PBS. http://www.pbs.org/tesla/ll/ll_mispapers.html. Accessed on June 5, 2013
7. Hunt S. *The Invention of Everything Else*. Boston: Mariner Books; 2008

8. Auster P. *Moon Palace.* New York: Viking Press; 1989
9. Millet L. *Love in Infant Monkeys.* New York: Soft Skull Press; 2009

EDITORIAL

In Memoriam: The Matrix Coil

W.J. van Rooij, M. Sluzewski, and J. Peluso

In this issue, the results of the Matrix and Platinum Science (MAPS) trial provide level 1 evidence that there is no beneficial effect of the polymer-modified Matrix detachable coil (Stryker, Kalamazoo, Michigan) over standard platinum coils in the recurrence rate of coiled intracranial aneurysms.[1] Although several previous studies indicated similar results,[2-4] this MAPS trial is the death blow for the "bioactive" coil. This is good news for patients and hospitals because the spilling of money by the excessive costs of these coils can now be avoided without compromising patient care.

It took the neurointerventional community more than 10 years (and many millions of dollars) to prove that a marketing concept launched by Boston Scientific (now Stryker) does not hold true in clinical practice. The history of the Matrix coil started in the beginning of this millennium. When the initial monopoly of Boston Scientific with the Guglielmi detachable coil ended with the introduction of similar coils by other manufacturers, Boston Scientific developed the concept of "bioactive" coils to regain market share. The Matrix coil was introduced, and this coil was coated with a bioabsorbable polyglycolic/polylactic acid (PGLA) polymer that was intended to accelerate neointimal healing at the neck of the aneurysm and thus was believed to provide a more stable occlusion at follow-up. The choice of this PGLA coating was primarily to get the device past regulatory hurdles and onto the market. Proof of efficacy of biologic activity was not a priority. PGLA is widely used in sutures as Vicryl (Ethicon, Cincinnati, Ohio) and has an excellent safety profile in humans. With this in mind, Boston Scientific managed to pass the regulatory process of the US Food and Drug Administration by claiming that Matrix was "substantially equivalent" to platinum coils. Although this obtained FDA approval was based on equivalency, marketing that followed was not. On the contrary, Matrix was marketed as a revolutionary new device.

After testing the coil in a few swine,[5] Matrix was launched as a new concept: Instead of aneurysm thrombosis following mechanical disruption of the intra-aneurysmal blood flow, Matrix would provide a durable biologic healing by improved neointimal proliferation and fibrosis. The marketing machine went off on full throttle, heavily supported by several of our peers. The concept of accelerated healing of aneurysms with significantly lower recurrence rates was very appealing, and many physicians started to treat their patients with the new Matrix coil, despite it being almost double the cost of standard coils.

In the meantime, a registry of 100 aneurysms was launched by Boston Scientific to provide extra arguments on sales (Acceleration of Connective Tissue Formation in Endovascular Aneurysm Repair [ACTIVE]). However, the results of this registry were not better than could have been expected from standard coils. On the contrary, many aneurysms were not immediately completely occluded, resulting in an alarmingly high early rebleeding rate of 7% (3 of 41 ruptured aneurysms). In sales meetings with potential Matrix users, the results of this registry were deliberately misinterpreted.[6] Even after published criticism on these misleading interpretations,[7] Moret and Viñuela persisted in peculiar explanations of the results in favor of the Matrix coil.[8] The disappointing findings of the ACTIVE registry have never been published. The marketing machine soon got overheated. At meetings and in scientific reports, the "proof of concept" was repeatedly illustrated: Many physicians reported a white band between the coil mesh and the parent artery called the "white collar sign," interpreted as a thick connective tissue barrier that prevented further aneurysmal filling.[9] Anyone with knowledge of imaging physics readily recognized that this band was caused by the Mach effect, a well-known optical illusion that occurs both with Matrix and platinum coils.[10,11] In a heterogeneous human autopsy study and in several experimental studies in swine and rabbits, the phenomenon of fibrous neck healing by the bioactive Matrix coils was enthusiastically claimed and communicated by Szikora et al[12] and Murayama and Viñuela,[13,14] though scientific evidence was lacking.

To overcome the initial criticism on the Matrix coil[15] and to reduce the reported high friction of the coated coils inside the microcatheter, Boston Scientific applied some minor modifications to the coil and the second-generation Matrix was introduced as Matrix2. After evaluation of this Matrix2 coil in a heterogeneous study including cases from the ACTIVE study, Murayama and Viňuela claimed without statistical evidence that use of Matrix2 coils resulted in improved mechanical performance and anatomic outcome compared with Matrix1 coils.[16] The marketing machine of Boston Scientific thus continued, and Matrix effectively survived the initial period, despite the publication of more clinical studies that failed to show a beneficial effect of the bioactive Matrix coils.[17] Even despite imposed scientific bias in a French registry design toward favorable results for Matrix, a beneficial effect of Matrix could not be shown.[18,19] Finally, the MAPS trial was announced in 2008; and now, 6 years later, the definitive results clearly indicate that Matrix coils are not better than standard platinum coils.

What can we learn from this Matrix saga, with Boston Scientific/Stryker supported by some of our overenthusiastic peers? How can we avoid large sums of public money being spilled on unproven devices to enhance the profits of device companies? We, as doctors, have to get back into the driver's seat, and we should take the lead from the industry in developing devices. Instead of selling our soul to the devil by using unproven devices at high costs from manufacturers with clever and possibly misleading marketing strategies, we should tell the industry what devices to make after adequate scientific hypotheses and clinical tests that convince regulatory bodies like the FDA. In addition, we should be more critical of our overenthusiastic peers involved in cutting-edge technology with a critical eye to the interpretation of their

http://dx.doi.org/10.3174/ajnr.A3928

first clinical results with new devices. In addition, device manufacturers should assume their public responsibility instead of mainly striving for financial profit and high stock prices.

Only then can scientific and financial blunders like the Matrix coil be averted. For now, finally, we hang out the flag for the burial of the Matrix coil.

REFERENCES

1. McDougall CG, Claiborne Johnston S, Gholkar A, et al. **Bioactive versus bare platinum coils in the treatment of intracranial aneurysms: the MAPS (Matrix and Platinum Science) Trial.** *AJNR Am J Neuroradiol* 2014;35:935–42
2. Rezek I, Mousan G, Wang Z, et al. **Coil type does not affect angiographic follow-up outcomes of cerebral aneurysm coiling: a systematic review and meta-analysis.** *AJNR Am J Neuroradiol* 2013;34:1769–73
3. Pierot L, Cognard C, Ricolfi F, et al. **Mid-term anatomic results after endovascular treatment of ruptured intracranial aneurysms with Guglielmi detachable coils and Matrix coils: analysis of the CLARITY series.** *AJNR Am J Neuroradiol* 2012;33:469–73
4. Smith MJ, Mascitelli J, Santillan A, et al. **Bare platinum vs Matrix detachable coils for the endovascular treatment of intracranial aneurysms: a multivariate logistic regression analysis and review of the literature.** *Neurosurgery* 2011;69:557–64
5. Murayama Y, Tateshima S, Gonzalez NR, et al. **Matrix and bioabsorbable polymeric coils accelerate healing of intracranial aneurysms: long-term experimental study.** *Stroke* 2003;34:2031–37
6. Matrix newsletter. Fremont, California: Boston Scientific; 2004
7. Sluzewski M, van Rooij WJ. **Questionable interpretation of results of ACTIVE study on Matrix coils by Boston Scientific.** *AJNR Am J Neuroradiol* 2005;26:2163–64
8. Sluzewski M, van Rooij WJ. **Reply to letter regarding interpretation of results of ACTIVE study.** *AJNR Am J Neuroradiol* 2005;26:2436–37
9. Gonzalez NR, Patel AB, Murayama Y, et al. **Angiographic evidence of aneurysm neck healing following endovascular treatment with bioactive coils.** *AJNR Am J Neuroradiol* 2005;26:912–14
10. Mach bands. http://en.wikipedia.org/wiki/Mach_bands. Accessed Feb 3, 2014
11. Kiyofuji S, Matsumaru Y, Tsuruta W, et al. **Emergence of the white-collar sign after coil embolization of cerebral aneurysms.** *Acta Neurochir (Wien)* 2014;156:11–16
12. Szikora I, Seifert P, Hanzely Z, et al. **Histopathologic evaluation of aneurysms treated with Guglielmi detachable coils or Matrix detachable microcoils.** *AJNR Am J Neuroradiol* 2006;27:283–88
13. Feng L, Vinuela F, Murayama Y. **Healing of intracranial aneurysms with bioactive coils.** *Neurosurg Clin N Am* 2005;16:487–99, v–vi
14. Lee D, Yuki I, Murayama Y, et al. **Thrombus organization and healing in the swine experimental aneurysm model. Part I. A histological and molecular analysis.** *J Neurosurg* 2007;107:94–108
15. Cloft HJ. **Have you been smoking something that is biologically active?** *AJNR Am J Neuroradiol* 2006;27:240–42
16. Ishii A, Murayama Y, Nien YL, et al. **Immediate and midterm outcomes of patients with cerebral aneurysms treated with Matrix1 and Matrix2 coils: a comparative analysis based on a single-center experience in 250 consecutive cases.** *Neurosurgery* 2008;63:1071–77
17. Murayama Y, Viñuela F, Ishii A, et al. **Initial clinical experience with Matrix detachable coils for the treatment of intracranial aneurysms.** *J Neurosurg* 2006;105:192–99
18. Pierot L, Bonafé A, Bracard S, et al, for the French Matrix Registry Investigators. **Endovascular treatment of intracranial aneurysms with Matrix detachable coils: immediate posttreatment results from a prospective multicenter registry.** *AJNR Am J Neuroradiol* 2006;27:1693–99
19. van Rooij WJ, Sluzewski M. **Registry on Matrix coils: bias in inclusion, exclusion, and publication.** *AJNR Am J Neuroradiol* 2007;28:398–99

EDITORIAL

Counterpoint—Response to "In Memoriam: The Matrix Coil"

A.S. Turk, D. Fiorella, J. Mocco, and C. Derdeyn

In this issue of the *American Journal of Neuroradiology* (*AJNR*), the Matrix and Platinum Science (MAPS) trial results are published.[1] The trial concluded that there was no superiority of the Matrix coil (Stryker, Kalamazoo, Michigan) over bare platinum coils. The MAPS investigators and sponsor should be congratulated on their willingness to test the efficacy of Matrix. The MAPS trial in no way negates the premise that the modification of coil surfaces or composition could potentially enhance coil performance and/or the long-term durability of coil embolization. To broadly extrapolate the MAPS results to all surface modified coils makes little sense.

While the approach taken by industry to promote the Matrix coil during the product launch certainly had serious flaws, this controversy should not cloud, or in any way diminish, the important clinical data provided by the MAPS study. With the benefit of hindsight, it appears that the coil vendor, as well as physician users, share responsibility for not demanding more robust data of improved efficacy over bare platinum coils before the routine use of Matrix in patients. Fortunately, our field continues to mature, and we have evolved past this to a large extent, as evidenced by the myriad industry-sponsored comparative coil trials that have been completed (Cerecyte trial, HydroCoil Endovascular Aneurysm Occlusion and Packing study) and those that are currently underway (Patients Prone to Recurrence After Endovascular Treatment, Hydrogel Endovascular Aneurysm Treatment trial, Framing Eighteen Coils in Cerebral Aneurysms trial).[1,2] These trials, like MAPS, represent real progress within our field and reflect recognition by physicians, as well as industry, that treatment decisions must be guided by reliable clinical trial data rather than marketing concepts that are based largely on preclinical studies.

Extensive preclinical studies were performed to better understand the results of coating bare platinum coils with a bioresorbable polymer. In retrospect, many of these studies were suboptimal in that they used an experimental aneurysm model that is now known to have low hemodynamic stresses and a high incidence of spontaneous thrombosis.[3]

The canine bifurcation model represents a better one for determining aneurysm coil performance, both angiographically and histologically.[4-9] In this model, the original version of Matrix was shown to undergo greater coil compaction and aneurysm neck recurrence compared with the conventional bare platinum Guglielmi detachable coil (GDC; Boston Scientific, Natick, Massachusetts), indicating that either the coil or the coating resulted in

http://dx.doi.org/10.3174/ajnr.A3929

reduced performance.[10] However, the addition of complex 360° shapes improved the angiographic outcomes for both Matrix and GDC coils—making the 2 more comparable.

In a detailed analysis, the actual benefit of Matrix surface modification was in the histopathologic results, which showed that Matrix-treated aneurysms showed improved endothelization, manifest as an absence of endothelialized clefts at the aneurysm neck (which are prevalent in GDC-treated aneurysms).[10] Endothelialized clefts have been proposed as the etiology for late angiographic recurrences.[5] Late recurrences have been reported at 3 years in up to 15% of aneurysms that had been completely occluded acutely and in short-term follow-up.[11] While the MAPS trial showed that in the short term, Matrix was essentially equivalent to platinum coils, the real benefits of surface modification may be manifest in the results at late (3- and 5-year) follow-up.

Furthermore, in subgroup analysis, when aneurysms were adequately occluded (Raymond-Roy scale 1 or 2), Matrix had significantly better outcomes with only 2.7% requiring retreatment compared with 9.6% ($P = .01$) with platinum coils.[12] However, aneurysms with residual flow (Raymond-Roy scale 3) demonstrated poor outcomes in both arms—Matrix (24.2%) and platinum (16.1%) ($P = .17$). These observations coincide well with the known polyglycolic/polylactic acid (PGLA) characteristics, the polymer coating on Matrix coils. When exposed to high-flow states, PGLA experiences an acceleration of breakdown, nullifying any potential gain due to the bioactive component of the coil. These results suggest that the short-term issues with Matrix were more likely related to the adequacy of mechanical occlusion rather than the efficacy of the bioactive coating.

We believe that collaborative doctor/industry relationships are an important synergistic dynamic that is essential for continued technologic advancement in our specialty. It is critical that high standards be set for new technologies, particularly for those designed to treat diseases with well-established safe therapies. Regimented postmarket data collection and evaluation should occur with all new technologies, ensuring that marketing claims are not confused with scientific evidence.[13] However, to mix concerns with technology marketing or limitations in the implementation of a technology with a perception of failure of the fundamental scientific premise would be a mistake.

In our opinion, the concept of platinum coil surface modification to stabilize or increase the rate of thrombus organization is still valid and continues to have promise for enhancing long-term aneurysm occlusion stability. Time will tell whether this benefit will be reflected in the late-term MAPS data; the current data do not negate the fundamental concepts of bioactive coatings. As such, continued innovation toward the development of better delivery mechanisms or more durable bioactive responses is entirely reasonable.

REFERENCES

1. Molyneux AJ, Clarke A, Sneade M, et al. **Cerecyte coil trial: angiographic outcomes of a prospective randomized trial comparing endovascular coiling of cerebral aneurysms with either cerecyte or bare platinum coils.** *Stroke* 2012;43:2544–50
2. White PM, Lewis SC, Nahser H, Sellar RJ, Goddard T, Gholkar A. **HydroCoil Endovascular Aneurysm Occlusion and Packing Study (HELPS trial): procedural safety and operator-assessed efficacy results.** *AJNR Am J Neuroradiol* 2008;29:217–23
3. Bouzeghrane F1, Naggara O, Kallmes DF, et al**. In vivo experimental intracranial aneurysm models: a systematic review.** *AJNR Am J Neuroradiol* 2010;31:418–23
4. Mawad ME, Mawad JK, Cartwright J, et al. **Long-term histopathological changes in canine aneurysms embolized with Guglielmi detachable coils.** *AJNR Am J Neuroradiol* 1995;16:7–13
5. Raymond J, Guilbert F, Metcalfe A, et al. **Role of the endothelial lining in recurrences after coil embolization: prevention of recanalization by endothelial denudation.** *Stroke* 2004;35:1471–75
6. Raymond J, Leblanc P, Morel F, et al. **Beta radiation and inhibition of recanalization after coil embolization of canine arteries and experimental aneurysms: how should radiation be delivered?** *Stroke* 2003;34:1262–68
7. Reul J, Weis J, Spetzger U, et al. **Long-term angiographic and histopathologic findings in experimental aneurysms of the carotid bifurcation embolized with platinum and tungsten coils.** *AJNR Am J Neuroradiol* 1997;18:35–42
8. Strother CM, Graves VB, Rappe AA. **Aneurysm hemodynamics: an experimental model.** *AJNR Am J Neuroradiol* 1992;13:1089–95
9. Turk AS, Aagaard-Kienitz B, Niemann DB, et al. **Natural history of the canine vein pouch aneurysm model.** *AJNR Am J Neuroradiol* 2007;28:531–32
10. Turk AS, Luty CM, Carr-Brendel V, et al. **Angiographic and histological comparison of canine bifurcation aneurysms treated with first generation Matrix and standard GDC coils.** *Neuroradiology* 2008;50:57–65
11. Raymond J, Guilbert F, Weill A, et al. **Long-term angiographic recurrences after selective endovascular treatment of aneurysms with detachable coils.** *Stroke* 2003;34:1398–403
12. McDougall CG, Claiborne Johnston S, Gholkar A, et al. **Bioactive versus bare platinum coils in the treatment of intracranial aneurysms: the MAPS (Matrix and Platinum Science) Trial.** *AJNR Am J Neuroradiol* 2014;35:935–42
13. Fargen KM, Frei D, Fiorella D, et al. **The FDA approval process for medical devices: an inherently flawed system or a valuable pathway for innovation?** *J Surg* 2013;5:269–75

EDITORIAL

MR-Guided, Focused Ultrasound: Applications to Essential Tremor and Other Neurologic Conditions

G. Suffredini and L.M. Levy

In this issue of the *American Journal of Neuroradiology,* a novel approach by means of MR-guided, focused sonography surgery (MRgFUS) is used to treat essential tremor.[1] The results indicate that clinical improvement is significantly related to total lesion size. No relationship was found between the imaging characteristics of the lesion and sonication number, power, or maximal temperature. Although the authors describe an important advance in the use of this procedure, the study also raises a number of questions regarding the broad application of this technique to various neurologic conditions.

The use of focused sonography to treat brain disorders has evolved over the past 70 years. In the 1950s, Francis and William Fry developed a system of converging sonography beams to pro-

http://dx.doi.org/10.3174/ajnr.A3800

duce focal ablations in the brains of pigs and cats when applied through a craniotomy acoustic window.[2] The major limitation of this technology was the inability to focus sufficient sonography energy through the bony skull because of attenuation of acoustic energy. By the 1970s, their lab described the acoustic properties of the human skull[3] and successfully achieved trans-skull transmission of an intensely focused ultrasonic beam.[4]

During the past decade, sonography therapy has emerged as a minimally invasive therapy for movement disorders, neuropathic pain, and malignancies. In combination with MR imaging and MR thermometry, MRgFUS can produce focused ablations in the brain by thermal and nonthermal effects with millimeter accuracy.[5] Thermal (ablative) effects of MRgFUS occur when tissue is heated above 57–60°C, resulting in coagulative necrosis and tissue destruction. The degree of tissue necrosis is related to the focused sonography beam and can be monitored in real time with MR thermometry. Nonthermal (nonablative) effects of focused sonography result from acoustically induced interactions of microscopic gas bubbles or "microbubbles" with the surrounding vascular endothelium, a process termed "cavitation." These interactions cause disruption of endothelial cell tight junctions and result in disruption of the blood-brain barrier. Because the sonography intensity needed to produce microbubble-induced cavitation is several orders of magnitude lower than the intensity needed for thermal ablation, this disruption of the blood-brain barrier is only temporary and has been shown to be safe and effective in an animal model.[6]

Both thermal and nonthermal mechanisms of MRgFUS can provide novel therapeutic opportunities for the treatment of brain disorders. Focused sonography is ideal for ablation therapy because it can target deep brain structures including the thalamus, subthalamus, and pallidum regions. However, it is limited in treatment of lesions near the calvaria because of the attenuation effects of the skull, which are more pronounced at locations nearer to bone. Ablative therapies have been investigated as suitable minimally invasive alternatives for glioblastoma,[7] neuropathic pain,[8] and essential tremor.[9,10] Investigations for the treatment of Parkinson disease are currently underway.[11]

The short-lived disruption of the blood-brain barrier by MRgFUS provides a means to target delivery of drugs, antibodies, and stem cells to brain tissue.[12-14] Sonography has also been used to enhance revascularization in a process termed "sonothrombolysis." A recent meta-analysis of the use of sonography in ischemic stroke showed the therapy to be safe and effective.[15] MRgFUS enables targeted delivery of sonography to the clot location and has the potential to improve the treatment of acute ischemic stroke. MR imaging can identify clot location and serve as a treatment map for immediate focused sonography therapy. Focused sonography sonothrombolysis has also been proposed for the treatment of intracerebral hemorrhage.[16] In this setting, sonothrombolysis is used to liquefy the clotted blood within the intracerebral hemorrhage with consequent minimally invasive MR imaging–guided drainage of the liquefied clot.

The effectiveness and utility of sonography therapy can be augmented with nanotechnology. Thermal ablation is being evaluated by use of multifunctional drug delivery systems capable of triggering local hyperthermia in the presence of low-frequency sonography.[17] These systems provide a unique synergistic combination of chemotherapy, thermal therapy, and real-time imaging and are being investigated for the treatment of CNS malignancies. The present study by Wintermark et al[1] demonstrates the importance of lesion size in achieving symptom relief. Although total lesion size was significantly correlated to clinical improvement, the value of the imaging findings remains unclear. The time-dependent imaging characteristics of MRgFUS-induced brain lesions on T2-weighted imaging consists of 3 concentric zones: zones I and II appear as a result of coagulation and necrosis, and zone III appears as the most peripheral of the concentric zones and represents transient edema.[18] A larger zone III area is correlated with clinical improvement, but some of this improvement is lost as the edema resolves. Of interest, 2 patients with limited clinical improvement had imaging characteristics that were not very different from those with clinical improvement. This raises the concern of difficulties associated with accurately locating therapeutic targets. The ventrointermediate nuclei (Vim) are the thalamic relays of the cerebellothalamocortical tract and are the principal targets of MRgFUS in the treatment of essential tremor. Two methods may be used to locate the Vim: image-based coordinate targeting (direct method) and atlas-based targeting (indirect method). The latter approach is subject to potential inaccurate localization of the anterior and posterior commissures, an error that can be >5 mm. Direct identification is considered to be more accurate in identifying Vim and may be achieved with fractional anisotropy and color-coded vector maps.[19] Lesion identification in the current study was determined by atlas coordinates and clinical parameters evaluated in real time with sublesional sonication. In the 2 patients with limited therapeutic benefit, the MRgFUS was not repositioned, and the patients did not show sensory symptoms during treatment. Future studies may incorporate direct methods of Vim location during sonication to confirm target identification. Diffusion tractography may also be useful in evaluating the integrity of these tracts over time and in correlating their integrity with clinical symptoms. This approach could potentially help to identify valuable imaging information and provide useful targets for repeat therapy. Last, in the current study, total lesion size appeared to be unrelated to sonication number, power, or maximal temperature, presumably because of the small effect size and underpowered study. Determining the optimal use of these variables may improve the clinical utility of MRgFUS.

REFERENCES

1. Wintermark M, Druzgal J, Huss D, et al. **Imaging findings in MR-guided focused ultrasound treatment for patients with essential tremor.** *AJNR Am J Neuroradiol* 2014;35:891–96.
2. Fry WJ, Mosberg WH Jr, Barnard JW, et al. **Production of focal destructive lesions in the central nervous system with ultrasound.** *J Neurosurg* 1954;11:471–78
3. Fry FJ, Barger JE. **Acoustical properties of the human skull.** *J Acoust Soc Am* 1978;63:1576–90
4. Fry FJ. **Transkull transmission of an intense focused ultrasonic beam.** *Ultrasound Med Biol* 1977;3:179–84
5. Colen RR, Jolesz FA. **Future potential of MRI-guided focused ultrasound brain surgery.** *Neuroimaging Clin North Am* 2010;20:355–66
6. McDannold N, Arvanitis CD, Vykhodtseva N, et al. **Temporary disruption of the blood-brain barrier by use of ultrasound and**

microbubbles: safety and efficacy evaluation in rhesus macaques. *Cancer Res* 2012;72:3652–63
7. McDannold N, Clement GT, Black P, et al. **Transcranial magnetic resonance imaging-guided focused ultrasound surgery of brain tumors: initial findings in 3 patients.** *Neurosurgery* 2010;66:323–32
8. Jeanmonod D, Werner B, Morel A, et al. **Transcranial magnetic resonance imaging-guided focused ultrasound: noninvasive central lateral thalamotomy for chronic neuropathic pain.** *Neurosurg Focus* 2012;32:E1
9. Lipsman N, Schwartz ML, Huang Y, et al. **MR-guided focused ultrasound thalamotomy for essential tremor: a proof-of-concept study.** *Lancet Neurol* 2013;12:462–68
10. Elias WJ, Huss D, Voss T, et al. **A pilot study of focused ultrasound thalamotomy for essential tremor.** *N Engl J Med* 2013;369:640–48
11. **InSightec. A Feasibility Study to Evaluate Safety and Initial Effectiveness of ExAblate Transcranial MR Guided Focused Ultrasound for Unilateral Thalamotomy in the Treatment of Medication-Refractory Tremor Dominant Idiopathic Parkinson's Disease.** In: ClinicalTrials.gov. Bethesda, Maryland: National Library of Medicine (US). 2000 [cited 2013 Sept 1]. http://clinicaltrials.gov/ct2/show/NCT01772693. 2013
12. Burgess A, Ayala-Grosso CA, Ganguly M, et al. **Targeted delivery of neural stem cells to the brain using MRI-guided focused ultrasound to disrupt the blood-brain barrier.** *PLoS One* 2011;6:e27877
13. Jordao JF, Thevenot E, Markham-Coultes K, et al. **Amyloid-beta plaque reduction, endogenous antibody delivery and glial activation by brain-targeted, transcranial focused ultrasound.** *Exp Neurol* 2013;248C:16–29
14. Arvanitis CD, Livingstone MS, McDannold N. **Combined ultrasound and MR imaging to guide focused ultrasound therapies in the brain.** *Phys Med Biol* 2013;58:4749–61
15. Saqqur M, Tsivgoulis G, Nicoli F, et al. **The role of sonolysis and sonothrombolysis in acute ischemic stroke: a systematic review and meta-analysis of randomized controlled trials and case-control studies.** *J Neuroimaging* 2013 Apr 22. [Epub ahead of print]
16. Monteith SJ, Harnof S, Medel R, et al. **Minimally invasive treatment of intracerebral hemorrhage with magnetic resonance-guided focused ultrasound.** *J Neurosurg* 2013;118:1035–45
17. Yang HW, Hua MY, Hwang TL, et al. **Non-invasive synergistic treatment of brain tumors by targeted chemotherapeutic delivery and amplified focused ultrasound-hyperthermia using magnetic nanographene oxide.** *Adv Mater* 2013;25:3605–11
18. Martin E, Jeanmonod D, Morel A, et al. **High-intensity focused ultrasound for noninvasive functional neurosurgery.** *Ann Neurol* 2009;66:858–61
19. Yamada K, Akazawa K, Yuen S, et al. **MR imaging of ventral thalamic nuclei.** *AJNR Am J Neuroradiol* 2010;31:732–35

EDITORIAL

Simple MRI Metrics Contribute to Optimal Care of the Patient with Multiple Sclerosis

J.H. Simon, R.A. Bermel, and R.A. Rudick

MR imaging has been a critical element in multiple sclerosis care because it has been the basis, along with clinical measures, for testing treatment efficacy. MR imaging serves as a primary outcome measure in phase II and a secondary outcome measure in phase III clinical trials in MS.[1] There are now 10 approved MS disease-modifying drugs, all showing measureable impact in population studies on inflammatory disease as indicated by new T2 hyperintense and/or gadolinium-enhancing lesions on MR imaging. MR imaging initially impacted the field as an important component of diagnostic criteria,[2] in part because MR imaging is much more sensitive to early MS than are clinical features. For similar reasons, clinicians have embraced the practice of monitoring subclinical MR imaging activity for treatment decisions, though formal criteria for an actionable response to MR imaging activity in an individual patient have been limited (On-line Table 1). MR imaging monitoring is also critical for detecting complications of therapy—for example, infection (progressive multifocal leukoencephalopathy) or inflammation (immune reconstitution inflammatory syndrome).[3]

Several recent initiatives by the MS community have addressed the concept of individualized, more tailored, and sometimes more aggressive early treatment. Treatment escalation has only recently become feasible with the introduction of new, potentially stronger MS treatments based on differing mechanisms and molecular targets.[4] As a result, MR imaging activity will be increasingly used in clinical practice to determine whether patients are responding to treatment or may benefit from a change in treatment or escalation to higher-risk therapy (On-line Table 1). For example, the Canadian MS Working Group guidelines were updated in 2013,[5] on the basis of combinations of relapse, disability, and MR imaging scores, for recommendations classified as low, medium, or high concern. The Rio score, developed in Barcelona, was modified recently on the basis of a validation study to include only MR imaging activity and relapse indicators.[6] Enhancing lesions, followed by relapses and new T2 lesions during the initial 2 years, were the best predictors of disability 15 years later in treated (distinct from placebo) patients in the interferon (IFN) β-1a trial,[7] suggesting that persistent inflammatory disease activity in patients on IFN reflected nonresponse to therapy. An analysis by Dobson et al[8] from 11 studies with IFN-β treatment found that those who develop new MR imaging lesions on IFN-β within 2 years of starting therapy are at significantly higher risk of future relapses and/or disability worsening and that these patients can be identified after just 6–12 months of treatment.

The simple MR imaging measures of focal T2 hyperintense and enhancing lesions seem to contribute strongly to relapse and disability outcomes and contribute significantly to brain atrophy, a surrogate of disability. This association is highlighted in a recent meta-analysis by Sormani et al,[9] based on >13,500 patients with relapsing MS in 13 clinical trials. The correlation coefficients (R^2) with downstream disability for new/enlarging T2 lesions and brain atrophy were 0.61 and 0.48, respectively, with both measures retained in a final model with a combined R^2 of 0.75, strongly supporting the use of these MR imaging outcomes as clinical surrogate measures when applied in an appropriate clinical-/treatment-specific context.[9]

It is likely that in the future, advanced quantitative and functional measures by MR imaging will assume far greater impor-

Indicates article with supplemental on-line tables.

http://dx.doi.org/10.3174/ajnr.A3937

tance in measuring aspects of neurodegeneration, de- and remyelination, and particularly in progressive stages of MS, including in individual patients. However, the currently recognized success of the existing MS therapies is thought to be predominantly based on the impact on the early inflammatory stages of disease, with a variable and lesser, perhaps only secondary, impact on neurodegeneration. Standardized brain volume (atrophy) measures are predictive of disability and, when applied serially, can be used to assess atrophy patterns, including in individual patients,[10] but these are not widely available or currently thought to be practical in clinical practice unless and until MR imaging manufacturers or other third parties support these measures.

There is an emerging consensus in the MS field that successful treatment results in no evident inflammatory disease activity (NEIDA), defined as the absence of new relapses or new MR imaging lesions. This was discussed at a recent international consensus workshop sponsored by the Cleveland Clinic (Las Vegas; December 12–14, 2013). Standardized MR imaging lesion reporting was identified by survey as a critical element for future implementation and testing of NEIDA. There have been prior initiatives to improve MS clinical care through standardized requests, MR imaging acquisition, and interpretation templates, including by the Consortium of MS Centers.[11] More recent revisions recognize the improved hardware, including the potential shift to a 3D acquisition technique (see www.mscare.org). MR imaging technology evolves rapidly, field strength is ever-increasing, and acquisition and processing techniques will continue to impact lesion counts, which will necessarily evolve as well. Nevertheless, well-planned 2D and 3D acquisition techniques and attention to detail in manual or computerized registration will provide a basis for accurate serial analyses.

While there is almost certain to be disagreement as to the optimal cut-point for lesion counts to support treatment for MS, standardized, high-quality MR imaging acquisition combined with reports that provide the essential elements for MS diagnosis or therapeutic decision-making (On-line Tables 2 and 3) can, no doubt, improve outcomes for patients with MS.

Disclosures: Jack H. Simon—*UNRELATED*: *Consultancy*: Cleveland Clinic Foundation, *Comments*: MS Experts Consensus Summit: No Evidence of Disease Activity as a Treatment Target in MS, Biogen Idec, *Comments:* MS Clinical Research Plan Advisory Board, *Grants/Grants Pending*: Biogen Idec,* *Comments*: CHAMPS/CHAMPIONS MS Trial research support (none current), manuscript preparation (editorial) support (no funds involved), Kinkel et al and Simon et al manuscripts of CHAMPS/CHAMPIONS outcomes, *Payment for Manuscript Preparation*: Biogen Idec, *Comments*: Manuscript preparation support continues (no money involved), *Royalties*: Cambridge University Press, *Comments*: Co-Editor of *Imaging Acute Neurologic Disease* (no royalties to date), *Travel/Accommodations/Meeting Expenses Unrelated to Activities Listed*: National Institutes of Health/National MS Society,* Canadian MS Society,* Guthy Jackson Foundation,* *Comments*: Study Section Work: National Institutes of Health/National MS Society/Canadian, no personal fees or honoraria accepted, travel reimbursement only (National Institutes of Health/National MS Society), Canadian MS/Italian MS/Ad Hoc (University of Washington Foundation), no fees or travel funds involved. Robert A. Bermel—*RELATED*: *Grant*: Biogen Idec,* Genzyme,* *Comments*: unrestricted educational grant in support of the 2014 No Evidence of Inflammatory Disease Activity as a Treatment Target Continuing Medical Education meeting, *Consultancy*: Biogen Idec, Novartis, Genzyme, Questcor, Astellas, *Comments*: in compliance with institutional conflict of interest policies, *Grants/Grants Pending*: Novartis.* Richard A. Rudick—*UNRELATED*: *Consultancy*: Biogen Idec, Novartis, Genzyme, *Comments*: consulting on MS drugs, *Grants/Grants Pending*: Novartis,* Genzyme,* *Comments*: grants to the Cleveland Clinic Foundation. *Money paid to the institution.

REFERENCES

1. Barkhof F, Simon JH, Fazekas F, et al. **MRI monitoring of immunomodulation in relapse-onset multiple sclerosis trials.** *Nat Rev Neurol* 2012;8:13–21
2. Polman CH, Reingold SC, Banwell B, et al. **Diagnostic criteria for multiple sclerosis: 2010 revisions to the McDonald criteria.** *Ann Neurol* 2011;69:292–302
3. Yousry TA, Pelletier D, Cadavid D, et al. **Magnetic resonance imaging pattern in natalizumab-associated progressive multifocal leukoencephalopathy.** *Ann Neurol* 2012;72:779–87
4. Kantarci OH, Pirko I, Rodriguez M. **Novel immunomodulatory approaches for the management of multiple sclerosis.** *Clin Pharmacol Ther* 2014;95:32–44
5. Freedman MS, Selchen D, Arnold DL, et al. **Treatment optimization in MS: Canadian MS Working Group updated recommendations.** *Can J Neurol Sci* 2013;40:307–23
6. Sormani MP, Rio J, Tintore M, et al. **Scoring treatment response in patients with relapsing multiple sclerosis.** *Mult Scler* 2013;19:605–12
7. Bermel RA, You X, Foulds P, et al. **Predictors of long-term outcome in multiple sclerosis patients treated with interferon beta.** *Ann Neurol* 2013;73:95–103
8. Dobson R, Rudick RA, Turner B, et al. **Assessing treatment response to interferon-β: is there a role for MRI?** *Neurology* 2014;21;82:248–54
9. Sormani MP, Arnold DL, De Stefano N. **Treatment effect on brain atrophy correlates with treatment effect on disability in multiple sclerosis.** *Ann Neurol* 2014;75:43–49
10. Fisher E, Lee, JC, Rudick, R. **Temporal patterns of brain atrophy in individual multiple sclerosis patients.** The American Academy of Neurology's 65th AAN Annual Meeting in San Diego, CA; March 16–23, 2013
11. Simon JH, Li D, Traboulsee A, et al. **Standardized MR imaging protocol for multiple sclerosis: Consortium of MS Centers Consensus Guidelines.** *AJNR Am J Neuroradiol* 2006;27:455–61

Neuroimaging in Patients with Abnormal Blood Glucose Levels

G. Bathla, B. Policeni, and A. Agarwal

ABSTRACT

SUMMARY: Smooth neuronal functioning requires an uninterrupted supply of energy that is provided by glucose under normal physiologic conditions. Significant variations in plasma glucose levels, be it hypoglycemia or hyperglycemia, can present with myriad clinical manifestations and may mimic stroke. At times, the diagnosis is either not apparent or not clinically suspected. Imaging can suggest the diagnosis in unsuspected cases and can help in the assessment of the extent of neuronal damage in known cases, making it vital for the neuroradiologist to be aware of both common and atypical neuroimaging findings in hypoglycemia and hyperglycemia.

ABBREVIATIONS: GABA = gamma aminobutyric acid; HC-HB = hemichorea-hemiballismus; NIDDM = non–insulin-dependent diabetes mellitus; NKHG = nonketotic hyperglycemia

The brain relies heavily on a continuous supply of glucose for optimal function. Because the neurons have a high metabolic rate and can neither generate nor store significant amounts of glucose, a rapid decline in plasma glucose can jeopardize neuronal homeostasis over a period of minutes.[1]

Relatively stable plasma glucose levels are therefore essential for survival and are maintained through a highly complex network of enzymes, hormones, and signaling mechanisms, with insulin playing a dominant role.[1] Enterically absorbed glucose is transported by the portal circulation to the liver, which is the primary organ involved in glucose homeostasis. Here, excess glucose is converted to glycogen and stored for subsequent use. A drop in plasma glucose level triggers a fall in plasma insulin levels, increased glucagon secretion, glycogenolysis, and gluconeogenesis (primarily in the liver) and helps to restore plasma glucose levels whenever needed.[1]

Uptake of glucose in most cells (except liver and brain) is dependent on insulin and is mediated through glucose transporters or occurs through a sodium-glucose co-transport mechanism (small bowel and renal tubules).[2] Neuronal uptake of glucose is independent of insulin and is mediated through glucose transporter 1. Absorbed glucose is then metabolized to carbon dioxide, thereby generating adenosine triphosphate in a process that is heavily oxygen-dependent. Under anaerobic conditions, however, glucose can only be metabolized to produce lactic acid, a process that is not only energy-inefficient but also leads to metabolic acidosis.[2]

Physiologic variations in plasma glucose levels occur during sleep, postprandial states, and as part of circadian rhythm.[3] Abnormal variations in plasma glucose levels may occur in neonates, diabetics, and patients with insulin-secreting tumors, sepsis, Addison disease, and hepatic or renal failure.[4-7]

Significant variations in glucose levels are often symptomatic. Hyperglycemic patients may present with HC-HB, weakness, hypotonia, pyramidal tract signs, and seizures.[8-10] Similar findings may occur in hypoglycemic patients, who can additionally present with chorea, ataxia, paresis, aphasia, and coma.[8,11-13] Neonates with hypoglycemia may show a constellation of symptoms that are usually nonspecific and include poor feeding, lip smacking, eye rolling, and seizures.[4,14]

In emergency settings, it is not uncommon for these symptoms be diagnosed and treated initially as stroke. Imaging in such cases can play a vital role by suggesting the correct diagnosis and ensuring early treatment. This is vital because delayed diagnosis affects morbidity and mortality.

In acute settings, these patients invariably undergo an NCCT of the head initially. It may be occasionally useful but is often nondiagnostic. MR imaging is the study of choice in these cases and is often used to determine diagnosis and prognosis.

As mentioned above, patients with hyperglycemia can present with various movement disorders. However, well-established

From the Department of Radiology (G.B., B.P.), University of Iowa Hospitals and Clinics, Iowa City, Iowa; and Penn State College of Medicine (A.A.), Milton S. Hershey Medical Center, Hershey, Pennsylvania.

Please address correspondence to Dr. Girish Bathla, Department of Radiology, University of Iowa Hospitals and Clinics, 20 Hawkins Dr, Iowa City, IA 52242; e-mail: Girish-bathla@uiowa.edu

Indicates open access to non-subscribers at www.ajnr.org

http://dx.doi.org/10.3174/ajnr.A3486

neuroimaging findings are only described in patients with NKHG who have either HC-HB or seizures. At times, patients with ketotic hyperglycemia can also present with movement disorder, though these cases lack any well-described imaging correlate.[9]

Similarly, adults and neonates with significant hypoglycemia can have varying symptoms. However, these are often a consequence of diffuse parenchymal involvement, and findings on imaging are often not correlated with specific symptoms, as seen with hyperglycemia. A notable exception to this is the development of hemiplegia in a subset of adult hypoglycemic patients that correlates with involvement of the contralateral internal capsule.[15]

The following discussion concentrates on hyperglycemic and hypoglycemic conditions that have well-established neuroimaging findings. In hyperglycemic patients, these conditions include HC-HB and seizures. This is followed by a review of imaging findings in neonatal and adult hypoglycemia, in which extensive involvement often precludes correlation with specific symptoms.

Hemichorea-Hemiballismus in Non-Ketotic Hyperglycemia

HC-HB refers to an involuntary, nonrhythmic, and poorly patterned movement disorder that involves one side of the body.[16,17] It most commonly results from a vascular insult involving the contralateral basal ganglia.[16-18] NKHG is the second most common cause for such presentation.[16] Occasionally, HC-HB may result from neoplastic or infective conditions involving the brain.[17,19]

HC-HB in association with hyperglycemia is well recognized.[8] It has been predominantly reported in elderly patients with NIDDM and is more common in Asians.[17,18,20]

Patients present with acute onset of HC-HB, which is often unilateral but may be generalized.[8,20] The abnormal movements may be continuous or intermittent and disappear during sleep.[8,21] Laboratory findings confirm poorly controlled diabetes with raised blood glucose and HbA1C levels and absence of blood and urinary ketones. The serum osmolality is often elevated.[19] Correction of underlying hyperglycemia is usually curative, leading to rapid cessation of abnormal movements within hours to a few days.[8,18] Occasionally, however, symptoms may persist for months and require additional suppressant therapy.[8]

The abnormal movements are thought to be secondary to reduced cerebral perfusion, presumably caused by hyperviscosity secondary to hyperglycemia.[16,19] This is supported by recent observations that raised plasma glucose levels directly correlate with cerebral hypoperfusion.[22] Ensuing anaerobic metabolism leads to depletion of GABA, which is used as a metabolite to generate energy.[19] Because GABA is an inhibitory neurotransmitter, its depletion causes increased thalamocortical drive, resulting in HC-HB.[16]

The pathogenesis of the imaging findings in these patients is controversial and is further compounded by variable histopathology results from different studies.[8,16] Focal hemorrhage and calcification were initially proposed to explain the imaging pattern on CT and MR imaging. However, these are not consistent features on histopathology studies.[8] The imaging patterns on MR imaging and resolution of findings on follow-up imaging in most cases also do not favor hemorrhage or calcification as a common finding.[16] Some authors have reported the presence of gliotic tissue with abundant gemistocytes (a form of reactive astrocytes), which may account for the T1 shortening on MR imaging. These usually appear during acute injury and can persist for years.[16,21] These astrocytes can accumulate manganese after periods of brief ischemia, which presumably results from a combination of underlying hyperviscosity and chronic vascular disease.[8,16,23,24] This is supported by similar signal changes in animals and humans after episodes of transient, nonlethal ischemia, unrelated to hyperglycemia.[25]

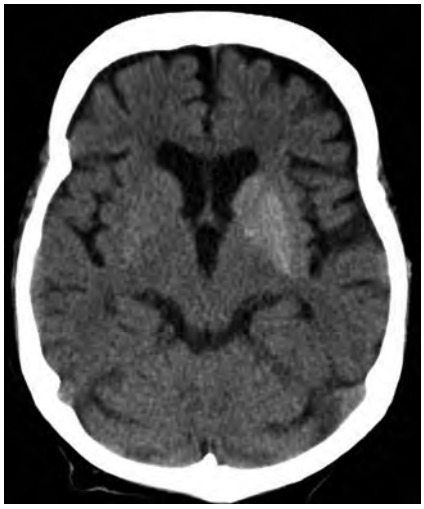

FIG 1. Axial NCCT image reveals asymmetric hyperattenuation involving the lentiform and caudate nuclei bilaterally, more pronounced on the left side.

The gemistocyte theory does not explain the changes seen on NCCT, leading some authors to speculate that the findings on CT, MR imaging, and associated HC-HB may reflect different pathologic mechanisms running in parallel.[21] It is possible that the pathogenesis of imaging findings in NKHG is more complex, and transient ischemia may not be the only factor. Hyperglycemia is known to cause endothelial dysfunction and increased oxidative stress in ischemic brain tissue.[26] These may also contribute to changes seen on imaging, though their precise role is yet to be established.

NCCT often reveals abnormal hyperattenuation, predominantly involving the putamen contralateral to the symptomatic side (Fig 1). The caudate and globus pallidus may be involved.[19] Patients with ballism may show bilateral abnormalities that can be asymmetric. There is no surrounding edema or mass effect.[8] Follow-up imaging may show resolution of changes after correction of hyperglycemia.[19] Occasionally, the initial scan may be normal.[8,19]

On NCCT, the findings are fairly characteristic in the appropriate context, though a similar appearance may occur with hemorrhage or asymmetric calcifications.[19] Patients receiving intra-arterial reperfusion therapy for stroke can also show transient hyperattenuation of the lentiform and insular cortex secondary to interstitial contrast extravasation.[27] Finally, because the hyperdensities in diabetic patients with HC-HB may resolve slowly or persist for years,[28] these may reflect previous hyperglycemia-induced injury.

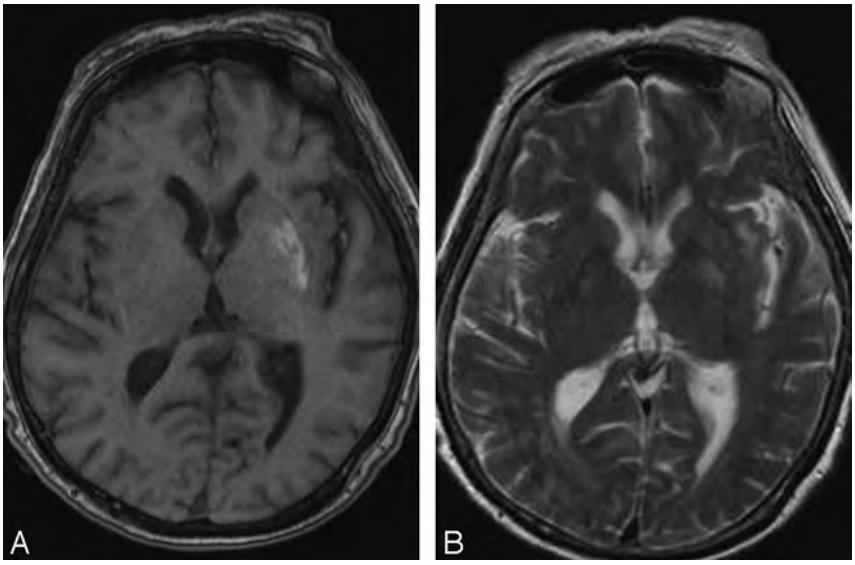

FIG 2. Axial *noncontrast T1WI in a patient with HC-HB reveals T1 shortening in the left lentiform. T2WI at the same level (B)* reveals mild T2 prolongation.

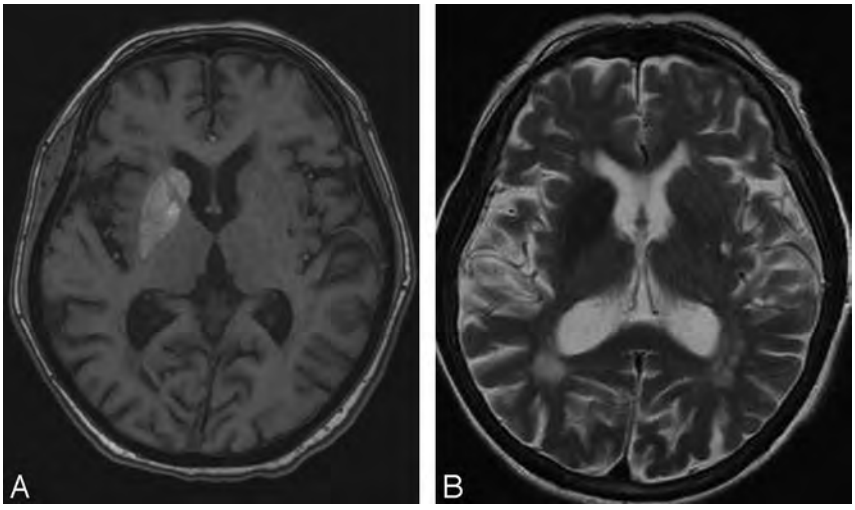

FIG 3. Axial T1WI *(A)* and T2WI *(B)* at the level of basal ganglia reveal T1 and T2 shortening involving the right corpus striatum.

MR imaging may also reveal abnormal putaminal signal with or without involvement of the caudate and globus pallidus.[8] As with CT, changes may be bilateral.[19] Sporadic cases with isolated involvement of subthalamic nuclei have been reported.[17] The involved regions show T1 shortening.[29] The signal changes on T2WI are variable, and the lesions may manifest either T2 shortening or prolongation (Figs 2 and 3).[17,19] Restricted diffusion and signal loss on gradient-echo images have been reported occasionally.[19,30,31] Some authors have reported abnormal mineral deposition in the affected regions on susceptibility-weighted MR imaging.[16] Additionally, dilated vessels over the affected side have been reported and are presumed to reflect underlying ischemia.[29]

Data are limited on 1H-MR spectroscopy findings, with the reported cases showing reduction of NAA/Cr ratio, elevation of Cho/Cr ratio, and presence of a lactate peak.[8,23] Similarly, sporadic case reports of SPECT show hypoperfusion within the basal ganglia, corresponding to the symptomatic side.[19]

The imaging findings are usually reversible, though they lag behind clinical improvement. Occasionally, the abnormalities persist and have been reported up to 6 years after the initial presentation.[28]

Besides HC-HB, T1 shortening of the basal ganglia may occur with chronic liver disease, manganese deposition, neurofibromatosis type 1, and calcifications.[32] However, a quick review of the patient chart usually excludes most of these considerations.

Seizures in Non-Ketotic Hyperglycemia

Seizures are relatively common in patients with NKHG.[33] These are often focal, with the most common subtype being focal motor seizure with or without secondary generalization.[34-36] Less frequently, occipital lobe seizures or epilepsia partialis continua may also occur.[10,33,35] MR imaging in these patients may show areas of transient T2 prolongation, which are thought to be secondary to the ictus and may be seen with seizures unrelated to hyperglycemia. However, some authors have reported subcortical areas of T2 shortening in a subset of patients with NKHG, which often correlate with localization of ictal focus on EEG studies and regress after normalization of hyperglycemia.[37] Therefore, these are more likely to be related to the underlying hyperglycemic state.

As with HC-HB, these patients also show evidence of poorly controlled diabetes and underlying hyperosmolality.[10] The HbA1C is often elevated, attesting to long-term hyperglycemia.[33,34] In some cases, the seizures may be the first presentation and uncover underlying diabetes.[34,35]

Similar to HC-HB, correction of underlying hyperglycemia is curative.[10,33] Anti-epileptic drugs are often not required because the seizures respond promptly to correction of hyperglycemia.[35] Occasional cases may require short-term phenobarbital or valproic acid.[35] Phenytoin is avoided because it worsens glycemic control and can aggravate seizures.[34]

A predilection for occipital lobe involvement exists.[34,36] Patients often present with visual symptoms such as blurring, field defects, and hallucinations. The parietal, temporal, and perirolandic cortex also may be involved.[33,37]

It is unclear how hyperglycemia precipitates seizures. Elevated blood glucose levels have a pro-convulsant effect and reduce seizure threshold.[34-36] As pointed out earlier, a hyperglycemic state also induces cellular anaerobic metabolism and depletes GABA, which is an inhibitory neurotransmitter.[35] The presence of con-

current ketoacidosis is thought to offer some protection against seizures because ketone bodies can serve as substrate for GABA generation.[36]

The reason for subcortical T2 shortening on imaging is also unclear. Postulated mechanisms include mineral deposition and ischemia.[33,34,38] A hypointense signal on the gradient-echo image would support free radical accumulation.[33]

NCCT is often negative, though rare cases with both HC-HB and seizures may show basal ganglia hyperattenuation.[38,39] On MR imaging, the involved regions are usually isointense on T1WI but may show focal T2 prolongation in the cortex and T2 shortening in the underlying WM.[33-35] Similar hypointense subcortical signal is also noted on gradient-echo images.[33] Associated cortical swelling is often appreciable on T2WI/ FLAIR images. Transiently reduced ADC values and focal cortical or leptomeningeal enhancement may occur.[33,35] These findings often completely resolve over a period of months, though some cases show focal gliosis.[33]

Sporadic reports of ^{1}H-MR spectroscopy have described reduced NAA in the involved regions.[38] There are few case reports of ictal hyperperfusion in the involved regions on technetium Tc99m hexamethylpropyleneamine oxime SPECT imaging, in contrast to HC-HB in a similar subgroup of patients, which shows hypoperfusion.[19,34,38]

Besides NKHG, subcortical T2 shortening may also be seen in viral encephalitis, meningitis, hypoxic insult, and Moyamoya disease.[33] Overlying leptomeningeal enhancement, if present, would add metastasis, sarcoidosis, and lymphoma to the list of differential considerations. However, a known hyperglycemic state and supportive EEG findings may help to clinch the diagnosis.

Neonatal Hypoglycemia

Transient hypoglycemia is relatively common in neonates as they transition from intrauterine to extrauterine environment.[5] The incidence of neonatal hypoglycemia is not clearly defined because there is no absolute consensus on the exact blood glucose value to define hypoglycemia.[4] The plasma glucose level used to define hypoglycemia varies between 25–46 mg/dL in different studies, though most researchers agree that a level $<$36 mg/dL within first 2–3 hours after birth requires intervention.[14,40,41]

Neuronal damage secondary to hypoglycemia is uncommon but may occur.[4,5] These children with this damage often present with nonspecific symptoms such as seizures, lip-smacking, poor feeding, hypotonia, cyanosis, and vomiting.[4,5,14,41]

Neonates often have development of hypoglycemia within hours to days of birth. Alkalay et al,[14] in their review of 23 patients, found that the mean age at presentation was 30 hours and varied between 1–72 hours. Because there is a broad list of differentials for seizures in this age group, these children often undergo a battery of tests to exclude metabolic, congenital, and infective causes before imaging is considered. Transcranial sonography is usually the initial imaging study and is performed to exclude hypoxic or hemorrhagic insults. However, it has low sensitivity for detecting hypoglycemic brain injury.[14] Because the clinical diagnosis of hypoglycemia can be made with a simple strip test, imaging with CT/MR is often performed to assess the extent of injury and prognosticate final recovery rather than to confirm the diagnosis.

Neuroimaging findings in neonatal hypoglycemia were first reported by Spar et al[42] in 1994. Since then, similar findings have been described in small patient cohorts by various authors.[4,14,43] A predilection for occipital and parietal lobe involvement exists, the exact reason for which is unclear.[4,5,14] Some authors have attributed it to relatively higher glucose utilization in this region from intensive axonal growth.[14] Others attribute the changes to a variable distribution of excitatory neurotransmitters in different parts of brain.[4,41] The remaining cerebral hemispheres, corticospinal tracts, corpus callosum, and deep gray nuclei also may be affected.[4,5,14,40] Posterior fossa involvement is rare.[5] The pattern of brain injury is independent of underlying etiology, essentially implicating hypoglycemia as the culprit.[4]

On CT, the involved regions appear hypoattenuated in the acute phase and are often bilateral. In fact, bilateral occipital involvement is considered by some to be specific for hypoglycemia-induced injury. The gray-white interface may be involved.[14,41,43] Lesions are often bilateral.[33,35] Hemorrhage has not been reported on CT studies. Follow-up imaging usually shows volume loss.[43]

On MR imaging, variable signal is noted on most sequences. The involved cortex is usually isointense on T1WI but may show focal T1 shortening. Similarly, the cortex usually shows T2 prolongation, but focal T2 shortening may occur.[4,14] Underlying WM involvement manifests as areas of T1 and T2 prolongation.[4] Follow-up imaging often shows parenchymal atrophy. Cystic encephalomalacia may occur.[4] Some patients may have transient abnormalities that resolve on follow-up.[14] Not surprisingly, these patients have less severe hypoglycemia and present early.[14]

DWI is most sensitive for identification of parieto-occipital injury, especially in the first 6 days after birth (Fig 4).[44] In the acute phase, there is restricted diffusion with correspondingly reduced ADC values.[14] Some authors think that the degree of restricted diffusion may correlate with parenchymal damage on follow-up.[45] Burns et al[5] described presence of focal WM hemorrhagic lesions in up to 30% of their cases. However, these findings have not been reported in other studies. The reason for this discrepancy is unclear.

Hypoglycemia potentiates hypoxia-induced damage, and a combination of the 2 leads to worse outcomes than hypoxia alone.[4,46,47] These children often present with nonspecific symptoms such as seizures, lip-smacking, poor feeding, hypotonia, cyanosis, and vomiting.[4]

There is scarce literature on perfusion imaging and spectroscopy findings in these patients. Kim et al[45] reported reduced NAA with the presence of a lactate peak in their patient, with further reduction in the NAA peak on follow-up 1H-MR spectroscopy on the 16th day.

On imaging, the most important differential consideration is hypoxic encephalopathy, either alone or in combination with hypoglycemia. When a predominantly posterior distribution is seen, the diagnosis of hypoglycemic injury is relatively straightforward. However, with diffuse bilateral involvement, it may be extremely difficult to exclude hypoxia or a combined insult. A review of the patient's Apgar score, plasma glucose, and arterial blood gas levels may provide important clues.

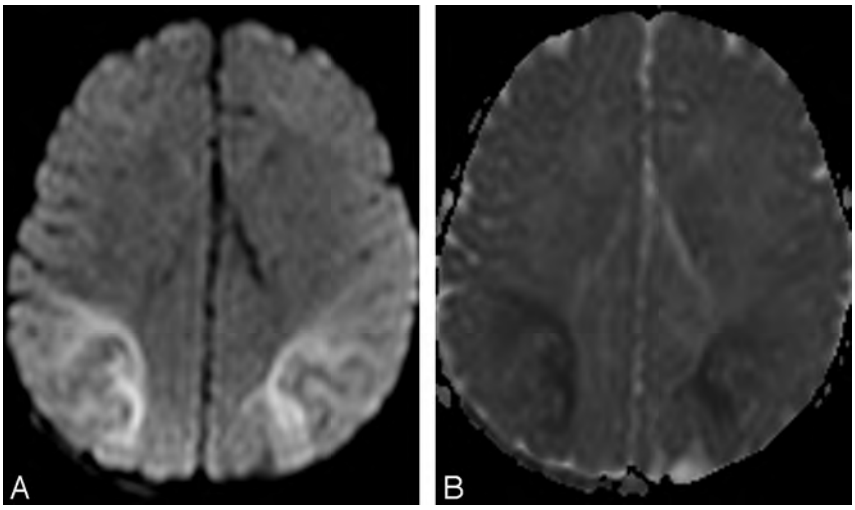

FIG 4. Axial DWI *(A)* and ADC image *(B)* in a hypoglycemic neonate reveal restricted diffusion involving predominantly the parietal and occipital regions with corresponding ADC hypointensity.

Prognosis in these children depends on prompt recognition and treatment of hypoglycemia. However, the long-term prognosis can be variable and correlates with WM damage at MR imaging.[5] The overall outcome may be complicated by occipital lobe epilepsy, visual disturbances, mental retardation, cerebral palsy, and microcephaly.[5,14,40]

Adult Hypoglycemia

According to the American Diabetes Association,[48] hypoglycemia and severe hypoglycemia are defined as plasma glucose levels <70 mg/dL (3.9 mmol/L) and 40 mg/dL (2.2 mmol/L), respectively. Hypoglycemia is more common in diabetic patients and can occur as a complication of therapy with insulin or long-acting sulfonylurea drugs. Symptomatic hypoglycemia is believed to affect 2% of diabetic patients annually and is associated with up to 4% of deaths in patients with type 1 diabetes.[6,11,49] Other causes include exogenous administration of insulin, which may be suicidal or accidental, insulin-secreting tumors, sepsis, Addison disease, and hepatic or renal failure.[6,7,11]

Hypoglycemic symptoms can be divided into autonomic, which include sweating, trembling, palpitations, and anxiety and neuroglycopenic, which include weakness, confusion, personality changes, seizures, and transient memory loss.[6,7,15,50,51] Severe hypoglycemia may present with altered mental state or coma.[6,52-54] Occasionally, patients may develop hemiparesis or quadriparesis and mimic a stroke.[12,51,53] In general, autonomic symptoms usually develop before neuroglycopenic symptoms. However, some diabetic patients may develop "hypoglycemic unawareness," and autonomic symptoms may not develop or may remain unrecognized.[11]

Energy failure leading to loss of cellular hemostasis is believed to be a key factor in hypoglycemia-induced brain damage.[6,52-54] Many authors have also pointed out the role of aspartate-induced injury in hypoglycemia, in contrast to hypoxia, in which the neuronal damage is secondary to glutamate.[15,52,55,56] Absence of glucose results in accumulation of oxaloacetate, which in turn leads to generation of excess aspartate. Aspartate is a known neurotoxin and has been shown to cause preferential neuronal necrosis in the cerebral cortex, neostriatum, and hippocampus.[6,11,15,50]

Hypoglycemia was initially reported to predominantly involve the cortex, neostriatum, and hippocampus.[6,11,12,54,57] However, many authors have also reported predominant WM involvement, mainly affecting the centrum semiovale, corona radiata, internal capsule, an splenium of the corpus callosum.[7,11,12,53,54,56] In fact, involvement of the WM is now thought to be earlier and more common than gray matter involvement.[52,53] Some cases may show diffuse gray matter and WM involvement.[6,7,53,54] The thalamus, brain stem, and cerebellum are invariably spared, and this may help to differentiate hypoglycemia from hypoxic injury, which often involves the thalamus.[6,52,55,56]

Because these patients often present in an altered mental state, underlying hypoglycemia may not be apparent. NCCT in these patients is often unremarkable.[15,49,50] Some cases may show nonspecific WM hypodensities or diffuse cerebral edema in the acute stage and parenchymal volume loss on follow-up.[15,49]

On MR imaging, the earliest changes are seen on DWI sequences.[52-54] The involved regions show restricted diffusion with corresponding ADC hypointensity.[6,7,12,15,53] The extent of these abnormalities depends on severity and duration of hypoglycemia.[6,49,52,57] Changes are usually bilateral, though bilaterally asymmetric, or, rarely, unilateral lesions, may occur.[11,52,57] Reduction in ADC values has been shown to follow establishment of cerebral isoelectricity, a process that may be asynchronous. This may explain asymmetric lesions in a given patient.[11,53,58]

Experimental studies on rats have shown that reduction in ADC values follows cerebral isoelectricity and may quickly normalize after glucose infusion.[51] It has also been shown that hypoglycemia-induced neuronal damage does not occur until the EEG becomes iso-electric and is independent of blood glucose level.[52] Establishment of cerebral isoelectricity may be asynchronous, and this may explain asymmetric lesions in a given patient.[9,46]

Contrary to the above observations, Schmidt et al[11] recently showed that short-term severe hypoglycemia by itself may not show any visible diffusion abnormalities. Although they reported findings in a small number of patients ($n = 10$), none of whom lost consciousness, the findings may lead one to speculate that individual susceptibility and associated comorbidities may also influence imaging findings and clinical outcomes.

Patients with hypoglycemia also may show T2 prolongation in both cortex and WM.[7] These regions are usually isointense on T1WI.[49] However, Fujioka et al[55] showed persistence of both T1 and T2 shortening in 4 patients who entered a persistent vegetative state. Hemorrhagic lesions have not been reported.[6,50,55] Post-contrast enhancement is usually absent but may occur.[6,49,50]

Sporadic reports on perfusion studies show either no significant change or slightly increased perfusion in affected re-

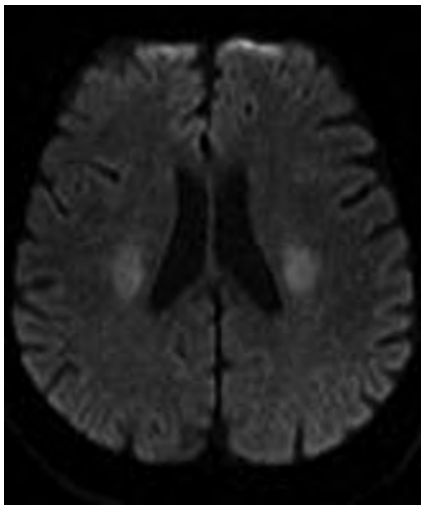

FIG 5. Axial DWI in a hypoglycemic patient reveals restricted diffusion involving the corona radiata bilaterally. The splenium was spared (not shown).

gions.[54,57,59] Similarly, only sporadic reports about ^{1}H-MR spectroscopy exist and show mildly reduced NAA and preservation of choline and creatine.[57] No lactate peak is seen, probably because of the absence of glucose.[55,60] This may help to distinguish hypoxic from hypoglycemic insults.

On the basis of the topographic distribution of the signal abnormalities, 3 imaging patterns have been described.[52] These include 1) predominant gray matter involvement affecting the cortex, neostriatum, and hippocampi; 2) predominant WM involvement affecting the periventricular WM, internal capsule, and splenium of corpus callosum (Fig 5); and 3) mixed pattern, involving both the gray matter and WM (Fig 6).

The division of patients on the basis of these imaging patterns is of unclear significance.[52,53] Patients with focal involvement of the internal capsule, corona radiata, or splenium usually have a good prognosis.[6,7,53,54] These lesions usually resolve promptly after restoration of blood glucose, though they tend to follow clinical symptom resolution.[6,7,12,15,54] Atay et al[56] reported near total resolution of DW abnormalities in their patient as early as 2 hours after blood glucose levels were restored.

Patients with extensive WM involvement show variable response.[52] The prognosis in these cases varies between complete recovery and persistent vegetative state.[53] Clinical improvement, if it occurs, is usually delayed by weeks.[6,17] Involvement of the neostriatum and diffuse cortical lesions often portend dismal outcome.[7,49,50,52,57] Failure of lesions to regress on follow-up imaging is also associated with poor prognosis.[6]

There is no satisfactory explanation as to why a subgroup of patients with hypoglycemia has hemiparesis and a good prognosis, whereas others show diffuse WM lesions and a variable prognosis, and still others have diffuse gray matter involvement and an invariably poor prognosis. Some authors believe that these probably represent a spectrum of injury and that focal WM changes usually result from transient hypoglycemia.[15,52] However, some other authors believe that they may be attributable to different pathophysiologies.[7,12,52] Regardless of the cause, imaging subgroups in hypoglycemia do exist, and DWI probably has some prognostic value.

Patients with extensive cortical and WM involvement often present a diagnostic challenge. Similar changes can also occur with hypoxia, hyperammonemia, encephalitis, after seizures, or may be drug-induced.[6,50] Splenial lesions have been reported in seizures, anti-epileptic drug withdrawal or toxicity, alcohol abuse, encephalitis, and electrolyte derangements.[30,61] The clinical context, along with a review of biochemical findings, should help narrow diagnostic considerations. Sparing of the thalamus, brain stem, and cerebellum is a useful clue. In select cases, 1H-MR spectroscopy may serve as a problem-solving technique.

CONCLUSIONS

Abnormal variations in plasma glucose levels are not uncommon and can show myriad imaging findings. The presentation is often nonspecific, and objective findings of HC-HB, memory loss, hemiparesis, and coma often clinically mimic stroke. A timely and accurate diagnosis would expedite correct treatment and limit neuronal injury in the early stage, when changes are potentially reversible.

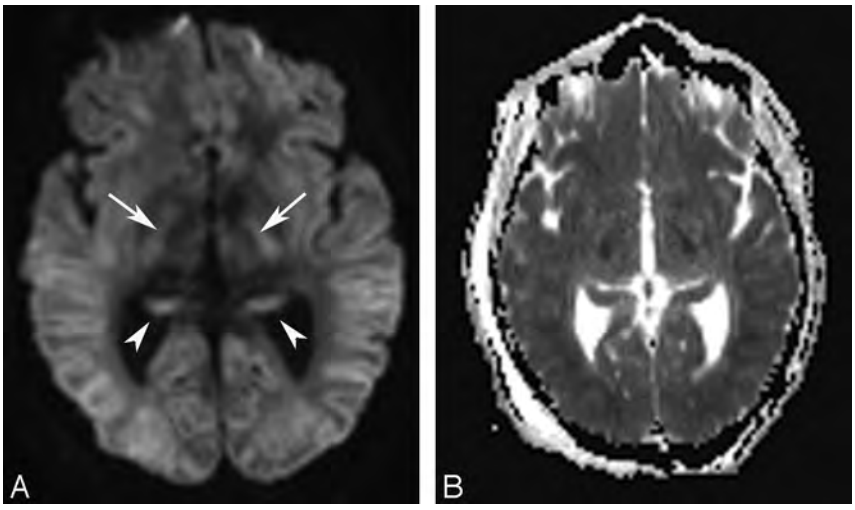

FIG 6. Axial DWI *(A)* and ADC image *(B)* in another hypoglycemic patient show restricted diffusion involving the cortex, hippocampi (*arrowheads* in *A*), and internal capsules (*arrows* in *A*) bilaterally with correspondingly reduced ADC values.

REFERENCES

1. Cryer PE, Davis SN. Hypoglycemia. In: Longo DL, Fauci AS, Kasper DL, et al, eds. *Harrison's Principles of Internal Medicine.* 18th ed. New York: McGraw-Hill Co; 2012:3003–09
2. Hall JE. *Guyton and Hall Textbook of Medical Physiology.* Philadelphia: Saunders Elsevier; 2011:809–18
3. Van Cauter E, Polonsky KS, Scheen AJ. **Roles of circadian rhythmicity and sleep in human glucose regulation.** *Endocr Rev* 1997;18:716–38
4. Barkovich AJ, Ali FA, Rowley HA, et al. **Imaging patterns of neonatal hypoglycemia.** *AJNR Am J Neuroradiol* 1998; 19:523–28

5. Burns CM, Rutherford MA, Boardman JP, et al. **Patterns of cerebral injury and neurodevelopmental outcomes after symptomatic neonatal hypoglycemia.** *Pediatrics* 2008;122:65–74
6. Kang EG, Jeon SJ, Choi SS, et al. **Diffusion MR imaging of hypoglycemic encephalopathy.** *AJNR Am J Neuroradiol* 2010;31:559–64
7. Lo L, Tan AC, Umapathi T, et al. **Diffusion-weighted MR imaging in early diagnosis and prognosis of hypoglycemia.** *AJNR Am J Neuroradiol* 2006;27:1222–24
8. Jagota P, Bhidayasiri R, Lang AE. **Movement disorders in patients with diabetes mellitus.** *J Neurol Sci* 2012;314:5–11
9. Bandyopadhyay SK, Dutta A. **Hemifacial spasm complicating diabetic ketoacidosis.** *J Assoc Physicians India* 2005;53:649–50
10. Sabitha KM, Girija AS, Vargese KS. **Seizures in hyperglycemic patients.** *J Assoc Physicians India* 2001;49:723–26
11. Schmidt P, Böttcher J, Ragoschke-Schumm A, et al. **Diffusion-weighted imaging in hyperacute cerebral hypoglycemia.** *AJNR Am J Neuroradiol* 2011;32:1321–27
12. Terakawa Y, Tsuyuguchi N, Nunomura K, et al. **Reversible diffusion-weighted imaging changes in the splenium of the corpus callosum and internal capsule associated with hypoglycemia: case report.** *Neurol Med Chir (Tokyo)* 2007;47:486–88
13. Kossoff EH, Ichord RN, Bergin AM. **Recurrent hypoglycemic hemiparesis and aphasia in an adolescent patient.** *Pediatric Neurol* 2001;24:385–86
14. Alkalay AL, Flores-Sarnat L, Sarnat HB, et al. **Brain imaging findings in neonatal hypoglycemia: case report and review of 23 cases.** *Clin Pediatr (Phila)* 2005;44:783–90
15. Albayram S, Ozer H, Gokdemir S, et al. **Reversible reduction of apparent diffusion coefficient values in bilateral internal capsules in transient hypoglycemia-induced hemiparesis.** *AJNR Am J Neuroradiol* 2006;27:1760–62
16. Cherian A, Thomas B, Baheti NN, et al. **Concepts and controversies in nonketotic hyperglycemia-induced hemichorea: further evidence from susceptibility-weighted MR imaging.** *J Magn Reson Imaging* 2009;29:699–703
17. Kim H-J, Moon WJ, Oh J, et al. **Subthalamic lesion on MR imaging in a patient with nonketotic hyperglycemia-induced hemiballism.** *AJNR Am J Neuroradiol* 2008;29:526–27
18. Shalini B, Salmah W, Tharakan J. **Diabetic non-ketotic hyperglycemia and the hemichorea-hemiballism syndrome: a report of four cases.** *Neurology Asia* 2010;15:89–91
19. Lai PH, Tien RD, Chang MH, et al. **Chorea-ballismus with nonketotic hyperglycemia in primary diabetes mellitus.** *AJNR Am J Neuroradiol* 1996;17:1057–64
20. Wintermark M, Fischbein NJ, Mukherjee P, et al. **Unilateral putaminal CT, MR, and diffusion abnormalities secondary to nonketotic hyperglycemia in setting of acute neurologic symptoms mimicking stroke.** *AJNR Am J Neuroradiol* 2004;25:975–76
21. Shan DE. **Hemichorea-hemiballism associated with hyperintense putamen on T1-weighted MR images: an update and a hypothesis.** *Acta Neurol Taiwan* 2004;13:170–77
22. Cosentino F, Battista R, Scuteri A, et al. **Impact of fasting glycemia and regional cerebral perfusion in diabetic subjects: a study with technetium-99m-ethyl cysteinate dimer single photon emission computed tomography.** *Stroke* 2009;40:306–08
23. Lai PH, Chen PC, Chang MH, et al. **In vivo proton MR spectroscopy of chorea-ballismus in diabetes mellitus.** *Neuroradiology* 2001; 43:525–31
24. Fujioka M, Taoka T, Matsou Y, et al. **Magnetic resonance imaging shows delayed ischemic striatal neurodegeneration.** *Ann Neurol* 2003;54:732–47
25. Baheti NN, Cherian A, Wattamwar PR, et al. **Ischemic hyperintensities on T1-weighted magnetic resonance imaging of patients with stroke: new insights from susceptibility weighted imaging.** *Neurol India* 2010;58:90–94
26. Bemeur C, Ste-Marie L, Montgomery J. **Increased oxidative stress during hyperglycemic cerebral ischemia.** *Neurochem Int* 2007; 50:890–904
27. Nakano S, Iseda T, Kawano H, et al. **Parenchymal hyperdensity on computed tomography after intra-arterial reperfusion therapy for acute middle cerebral artery occlusion: incidence and clinical significance.** *Stroke* 2001;32:2042–48
28. Shan DE, Ho DM, Chang C, et al. **Hemichorea-hemiballism: an explanation for MR signal changes.** *AJNR Am J Neuroradiol* 1998;19:863–70
29. Mittal P. **Hemichorea-hemiballism syndrome: a look through susceptibility weighted imaging.** *Ann Indian Acad Neurol* 2011;14:124–26
30. Massaro F, Palumbo P, Falcini M, et al, **Generalized chorea-ballism in acute non ketotic hyperglycemia: findings from diffusion-weighted magnetic resonance imaging**. *Parkinsonism Relat Disord* 2012;18:998–99
31. Chu K, Kang DW, Kim DE, et al. **Diffusion-weighted and gradient echo magnetic resonance findings of hemichorea-hemiballismus associated with diabetic hyperglycemia: a hyperviscosity syndrome?** *Arch Neurol* 2002;59:448–52
32. Rovira A, Alonso J, Córdoba J. **MR imaging findings in hepatic encephalopathy.** *AJNR Am J Neuroradiol* 2008;29:1612–21
33. Raghavendra S, Ashalatha R, Thomas SV, et al. **Focal neuronal loss, reversible subcortical focal T2 hypointensity in seizures with a nonketotic hyperglycemic hyperosmolar state.** *Neuroradiology* 2007;49:299–305
34. Hung WL, Hsieh PF, Lee YC, et al. **Occipital lobe seizures related to marked elevation of hemoglobin A1C: report of two cases.** *Seizure* 2010;19:359–62
35. Lin WS, Kao HW, Sung YF. **Reversible magnetic resonance imaging abnormality in a case of diabetic hyperglycemia related epilepsia partialis continua.** *J Intern Med Taiwan* 2011;22:438–43
36. Moien-Afshari F, Téllez-Zenteno JF. **Occipital seizures induced by hyperglycemia: a case report and review of literature.** *Seizure* 2009;18:382–85
37. Seo DW, Na DG, Na DL, et al. **Subcortical hypointensity in partial status epilepticus associated with nonketotic hyperglycemia.** *J Neuroimaging* 2003;13:259–63
38. Wang CP, Hsieh PF, Chen CC, et al. **Hyperglycemia with occipital seizures: images and visual evoked potentials.** *Epilepsia* 2005;46:1140–44
39. Chung SJ, Lee JH, Lee SA, et al. **Co-occurrence of seizure and chorea in a patient with nonketotic hyperglycemia.** *Eur Neurol* 2005;54:230–32
40. Tam EWY, Haeusslein BA, Bonifacio SL. **Hypoglycemia is associated with increased risk for brain injury and adverse neurodevelopmental outcome in neonates at risk for encephalopathy.** *J Pediatr* 2012;161:88–93
41. Karimzadeh P, Tabarestani S, Ghofrani M. **Hypoglycemia-occipital syndrome: a specific neurologic syndrome following neonatal hypoglycemia?** *J Child Neurol* 2010;26:152–59
42. Spar JA, Lewine JD, Orrison WW Jr. **Neonatal hypoglycemia: CT and MR findings.** *AJNR Am J Neuroradiol* 1994;15:1477–78
43. Traill Z, Squier M, Anslow P. B**rain imaging in neonatal hypoglycaemia.** *Arch Dis Child Fetal Neonatal Ed* 1998;79:F145–F147
44. Tam EWY, Widjaja E, Blaser SI, et al. **Occipital lobe injury and cortical visual outcomes after neonatal hypoglycemia.** *Pediatrics* 2008;122:507–12
45. Kim SY, Goo HW, Lim KH, et al. **Neonatal hypoglycaemic encephalopathy: diffusion-weighted imaging and proton MR spectroscopy.** *Pediatr Radiol* 2006;36:144–48
46. Basu P, Som S, Choudhuri N, et al. **Contribution of the blood glucose level in perinatal asphyxia.** *Eur J Pediatr* 2009;168:833–38
47. Nadeem M, Murray DM, Boylan GB, et al. **Early blood glucose profile and neurodevelopmental outcome at two years in neonatal hypoxic-ischaemic encephalopathy.** *BMC Pediatr* 2011;11:10
48. American Diabetes Association. **Standards of medical care in diabetes—2012.** *Diabetes Care* 2012;35(Suppl 1):S11–S63
49. Finelli PF. **Diffusion-weighted MR in hypoglycemic coma.** *Neurology* 2001;57:933

50. Chan R, Erbay S, Oljeski S, et al. **Case report: hypoglycemia and diffusion-weighted imaging.** *J Comput Assist Tomogr* 2003;27:420–23
51. Yoshino T, Meguro S, Soeda Y, et al. **A case of hypoglycemic hemiparesis and literature review.** *Ups J Med Sci* 2012;117:347–51
52. Ma JH, Kim YJ, Yoo WJ, et al. **MR imaging of hypoglycemic encephalopathy: lesion distribution and prognosis prediction by diffusion-weighted imaging.** *Neuroradiology* 2009;51:641–49
53. Johkura K, Nakae Y, Kudo Y, et al. **Early diffusion MR imaging findings and short-term outcome in comatose patients with hypoglycemia.** *AJNR Am J Neuroradiol* 2012;33:904–09
54. Böttcher J, Kunze A, Kurrat C, et al. **Localized reversible reduction of apparent diffusion coefficient in transient hypoglycemia-induced hemiparesis.** *Stroke* 2005;36:e20–e22
55. Fujioka M, Okuchi K, Hiramatsu K, et al. **Specific changes in human brain after hypoglycemic injury.** *Stroke* 1997;28:584–87
56. Atay M, Aralasmak A, Sharifov R, et al. **Transient cytotoxic edema caused by hypoglycemia: follow-up diffusion weighted imaging features.** *Emerg Radiol* 2012;19:473–75
57. Lim CC, Gan R, Chan CL, et al. **Severe hypoglycemia associated with an illegal sexual enhancement product adulterated with glibenclamide: MR imaging findings.** *Radiology* 2009;250:193-201
58. Hasegawa Y, Formato JE, Latour LL, et al. **Severe transient hypoglycemia causes reversible change in the apparent diffusion coefficient of water**. *Stroke* 1996;27:1648–56
59. Cordonnier C, Oppenheim C, Lamy C, et al. **Serial diffusion and perfusion-weighted MR in transient hypoglycemia.** *Neurology* 2005;65:175
60. Auer RN, Siesjo BK. **Biological differences between ischemia, hypoglycemia, and epilepsy.** *Ann Neurol* 1988;24:699–707
61. Gracia-Monco JC, Cortina IE, Ferreira E, et al. **Reversible splenial lesion syndrome (RESLES): what's in a name?** *J Neuroimaging* 2011;21:e1–e14

Optimal Timing of Cerebral MRI in Preterm Infants to Predict Long-Term Neurodevelopmental Outcome: A Systematic Review

A. Plaisier, P. Govaert, M.H. Lequin, and J. Dudink

ABSTRACT

SUMMARY: Advances in neonatal neuroimaging have improved detection of preterm brain injury responsible for abnormal neuromotor and cognitive development. Increasingly sophisticated MR imaging setups allow scanning during early preterm life. In this review, we investigated how brain MR imaging in preterm infants should be timed to best predict long-term outcome. Given the strong evidence that structural brain abnormalities are related to long-term neurodevelopment, MR imaging should preferably be performed at term-equivalent age. Early MR imaging is promising because it can guide early intervention studies and is indispensable in research on preterm brain injury.

ABBREVIATIONS: DEHSI = diffuse excessive high signal intensity; FA = fractional anisotropy; PLIC = posterior limb of the internal capsule; PMA = postmenstrual age; PWML = punctate white matter lesions

Preterm birth with subsequent brain injury is an increasing public health concern. Advances in neonatal intensive care have significantly improved survival rates among very-low-birthweight infants, but survivors are still at considerable risk to develop cognitive, behavioral, neurosensory, and motor disabilities.[1-5] The most common preterm brain injury patterns are the following: WM injury; germinal matrix-intraventricular hemorrhage and its correlates; and posthemorrhagic ventricular dilation and periventricular hemorrhagic venous infarction (Fig 1). Cystic periventricular leukomalacia is seen less often now, and diffuse noncystic types of WM injury, including punctate WM lesions and diffuse excessive high signal intensity, are therefore most frequent[6-10] and the leading cause of disturbed brain growth, connectivity, and functionality.[11-13]

Although MR imaging is superior to cranial sonography in detecting diffuse WM injury,[14-17] structural MR imaging studies fail to precisely predict outcome[6,8,18] because conventional MR imaging is not sensitive enough to measure changes in microstructure.[19] However, advanced MR imaging acquisition sequences and postprocessing techniques, such as DTI, volumetric MR imaging measurements, and proton MR spectroscopy (^{1}H-MR spectroscopy), may be a solution. For example, DTI allows quantification of WM at a microstructural level by measuring the diffusion of water molecules in tissues.[20,21]

DTI studies have shown increasing fractional anisotropy and decreasing ADC during brain maturation, which is ascribed to the decreased water content and increased WM complexity due to myelination.[20,22] Deviations from these developmental trends are considered diagnostic of perinatal WM injury.[23-25]

WM injury in preterm infants has been related to significantly reduced brain volume,[26,27] but brain growth in extremely preterm infants may also be disturbed in the absence of evident WM abnormalities. Volumes of brain regions and structures are correlated to perinatal complications and are inversely related to gestational age at birth.[28,29] Smaller volumes are often associated with impaired neuropsychological function at a later age.[29,30]

Assessment of cortical folding during early brain development, with the use of postprocessing software,[31] has provided insight into the underlying mechanisms of normal development, regional specialization, and functional lateralization.[32,33] Anomalous cortical folding, demonstrated in preterm infants, has been proposed as an early biomarker of neurocognitive impairment.[34,35]

Metabolic integrity of tissues can be measured in vivo with ^{1}H-MR spectroscopy. The NAA/Cho ratio is of special interest in neonatal neuroimaging because the ratio increases during brain maturation as an effect of synthesis by proliferating oligodendrocyte progenitor cells.[36]

Early MR imaging provides early biomarkers of preterm brain injury and enables early parental counseling. However, systematic

From the Division of Neonatology (A.P., P.G., J.D.), Department of Pediatrics, and Division of Pediatric Radiology (A.P., M.H.L., J.D.), Department of Radiology, Erasmus Medical Center-Sophia, Rotterdam, the Netherlands; and Department of Pediatrics (P.G.), Koningin Paola Children's Hospital, Antwerp, Belgium.

Please address correspondence to Annemarie Plaisier, MD, Division of Neonatology, Department of Pediatrics, Erasmus Medical Center-Sophia, Dr Molewaterplein 60, 3015 GJ Rotterdam, Netherlands; e-mail: a.plaisier.1@erasmusmc.nl

Indicates open access to non-subscribers at www.ajnr.org

Indicates article with supplemental on-line table.

http://dx.doi.org/10.3174/ajnr.A3513

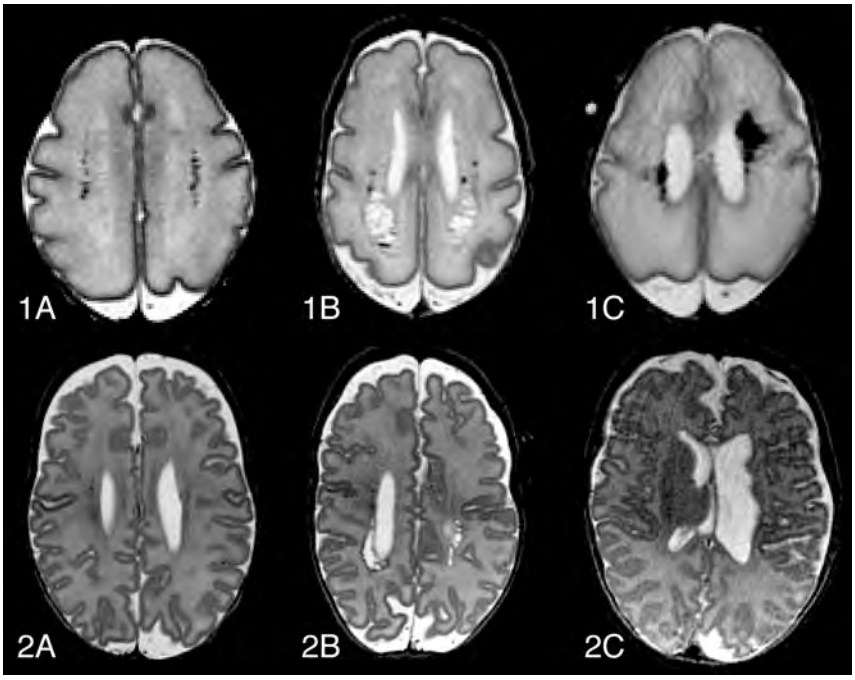

FIG 1. Evolution of common types of preterm brain injury, at 30 weeks' postmenstrual age (1) and at term-equivalent age (2). Transversal T2-FSE images of punctate white matter lesions (*A*), periventricular leukomalacia (*B*), and periventricular hemorrhagic venous infarction (*C*). Note that images 2*B* and 2*C* are slightly oblique.

use of such MR imaging has its limitations due to hemodynamic, respiratory, and thermodynamic instability seen in most preterm infants.[37] Moreover, technical aspects like smaller heads result in lower SNR.[38] As in most studies obtained at term-equivalent age,[18,30] less is known about the value of scanning at a lower postmenstrual age. Furthermore, brain injury can also occur in the late preterm period. MR imaging at term has the disadvantage of parents and caregivers not being fully informed until their child reaches term age. Furthermore, logistic issues may emerge in centers where infants are transferred to other hospitals once certain criteria are met.

Because there seems to be no consensus on the optimal timing of MR imaging, we reviewed the literature on the prediction of neurodevelopmental outcome with the use of brain MR imaging performed at either early preterm or term age.

MATERIALS AND METHODS

The Embase, MEDLINE OvidSP, Cochrane, and PubMed databases were systematically searched for relevant articles published between 1979 and November 2012. The strategy included synonyms and combinations of the following keywords: "prematurity, " "neuroimaging, " "brain, " and "MR imaging " (full research strategy is available on-line). The search was limited to human research that involved original patient data, and only articles written in English were included.

Studies were eligible under the following conditions: 1) they included preterm infants born at <32 week' gestation, 2) MR imaging was performed in the neonatal period, and 3) neurodevelopmental outcome was linked to MR imaging findings. To avoid large variations in MR imaging determinants, we only included structural MR imaging studies if they evaluated the findings according to a reproducible classification.

The initial search resulted in 2104 citations. Two reviewers (A.P., J.D.) screened all abstracts of these citations for relevance and reached a consensus after discussion in case of disagreement. Sixty-two articles were incorporated in this review. In the "Results " section, we present findings according to type of MR imaging technique: conventional structural MR imaging, such as T1- and T2-weighted scans, DTI, volumetric MR imaging, and proton MR spectroscopy. Further classification was based on the timing of MR imaging: serial, before 35 weeks', or after 35 weeks' PMA.

RESULTS

Conventional Structural MR Imaging

Serial MR Imaging. Three serial neuroimaging studies correlated injury to outcome (Table 1). One was a prospective consecutive MR imaging study by Dyet et al,[8] regarding 327 MR imaging scans of 119 preterm infants. Only major destructive cerebral and cerebellar lesions seen at the initial scan within 2 days after birth were related to poorer neurodevelopmental outcome. DEHSI and posthemorrhagic ventricular dilation at term-equivalent age were significantly related to adverse outcome. Isolated hemorrhage or PWML did not seem to predict adverse neurodevelopmental outcome. The second, by Miller et al,[39] demonstrated that moderately severe abnormalities, such as WM injury, ventriculomegaly, and intraventricular hemorrhage on early scans were associated with adverse neurodevelopmental outcome as strongly (or even more strongly) as abnormalities on the term-equivalent scans: The relative risk was 5.6 and 5.3, respectively. The third, a large serial MR imaging study by Tam et al,[40] demonstrated that not only large but also small cerebellar hemorrhages, not detected on cranial sonography, were associated with abnormal neurologic examination at 3–6 years of age. The presence of these small cerebellar hemorrhages was associated with a 5.0 odds ratio of abnormal neurologic examination findings at a mean age of 4.8 years.

MR Imaging at ≤35 Weeks' PMA. The presence of cystic periventricular leukomalacia and cerebellar hemorrhage at 35 weeks' gestation was significantly correlated to abnormal neurologic examination findings at 30 months in a retrospective neuroimaging study by Cornette et al.[41] Isolated PWML was not correlated to abnormal neurodevelopmental outcome at 30 months of age (Table 2).

MR Imaging at >35 Weeks' PMA. Twenty-six studies correlated brain injury or conventional MR imaging at 35 weeks' PMA with outcome (On-line Table).

Table 1: Details of included serial MRI studies

MRI Modality		Population	Timing of MRI (wk)	Main Findings
Structural conventional	Dyet et al[8]	119 Infants <30 wks	Serial	Abnormal outcome[a] at 18 mos was related to major destructive lesions, DEHSI, cerebellar hemorrhage, and posthemorrhagic ventricular dilation
	Miller et al[39]	89 Infants <34 wks	32 + 37	Abnormal outcome at 18 mos[b] was related to severity of WM injury, ventriculomegaly, and intraventricular hemorrhage on first (RR, 5.6) and second (RR, 5.3) MRIs
	Tam et al[40]	131 Infants <34 wks	32 + 37	Abnormal neurologic examination findings at 4.8 yrs were related to large and small cerebellar hemorrhage; OR for small hemorrhage was 5.0
DTI	Drobyshevsky et al[70]	24 Infants <32 wks	30 + 36	PDI[b] at 24 mos correlated to FA of the PLIC at 30 wks ($r = 0.55$), faster increase of FA/wk in internal capsule ($r = -0.63$), and occipital WM ($r = -0.59$)
	Glass et al[71]	9 Infants <34 wks	33 + 38	FA of the optic radiation was correlated with visual-evoked-potential amplitude ($r = 0.7$) at 10.5 mos
Volumetric	Dubois et al[81]	45 Infants <36 wks	32 + 41	Functional assessment at term was associated with inner cortical surface and sulcation index
	Kapellou et al[82] Rathbone et al[83]	119 Infants <30 wks	Serial	Growth of the cortical surface area was related to neurodevelopmental outcome[a] at 24 mos and full-scale IQ at 6 yrs

Note:—RR indicates relative risk; OR, odds ratio; PDI, Psychomotor Development Index.
[a] Griffiths Mental Developmental Scales.
[b] Bayley Scales of Infant Development.

Table 2: Details of included MRI studies, scanned at ≤35 weeks' postmenstrual age

MRI Modality		Population	Timing of MRI (wk)	Main Findings
Structural conventional	Cornette et al[41]	50 Infants <37 wks	35	Major cerebral abnormalities were correlated to abnormal outcome at 30 mos; isolated PWML were not related to neurodevelopmental impairment
Volumetric	Badr et al[84]	59 Infants <37 wks	31	WM volume was correlated significantly to PDI[a] ($r = 0.29$) and MDI[a] ($r = 0.31$) at 18 mos

Note:— PDI indicates Psychomotor Development Index; MDI, Mental Development Index.
[a] Bayley Scales of Infant Development.

The impact of overt WM lesions at term on neurodevelopment has been extensively investigated. The severity of WM abnormalities is often assessed according to a comprehensive scoring system[15] and is assumed to be directly associated with the incidence of neuromotor impairment until 5 years of age[9,10,15-17,42-49] and to be inversely correlated to the Bayley scales[50] until 30 months[15,16,43,51-54] and cognitive performance until 9 years of age.[55-60] The presence of WM injury has an odds ratio of 8.3 for low full-scale intelligence quotient (IQ < 70).[59] Moderate-to-severe WM abnormalities highly predict severe motor delay; odds ratios up to 10.0 and positive predictive values up to 100% have been demonstrated.[15,42,44,45,52,59]

The association between subtle diffuse WM injury and neurodevelopmental outcome is not clear.[61] Some research groups demonstrated a significant association between PWML and impaired neurodevelopmental outcome,[10,46,62] whereas others suggested the contrary, provided that no other major lesions were observed.[8,52] DEHSI was associated with adverse outcome in a large serial imaging study by Dyet et al,[8] but others could not confirm this finding.[10,42,51,59,62,63] The lack of clarity is thought to be due to the absence of objective definitions for these patterns of brain injury[24,48,64] and raises the importance of objective assessment of diffuse WM injury.

Extensive intraventricular hemorrhage and venous infarctions, according to Papile et al,[65] are associated with neurodevelopmental impairment.[16,17,48,53] Posthemorrhagic ventricular dilation is associated with neurologic impairment until 6 years of age.[66] In a study by De Vries et al,[67] asymmetric myelination of the PLIC at term age in preterm infants with venous infarction seemed to be an early predictor of future hemiplegia.

Although commonly described in cranial sonographic studies,[68] caudothalamic cysts were not related to cognitive and neuropsychological impairment in a MR imaging study by Lind et al.[69]

The impact of gray matter abnormalities remains unclear. They were significantly associated with abnormal neurobehavioral outcome at term in a study by Brown et al[47] and with decreased Bayley scales at 2 years in a study by Woodward et al,[15] but others[9,59] found no significant relationship between injury to the cerebral gray matter and neuromotor function at term[9] or cognitive outcome at 9 years of age.[59]

Diffusion Tensor Imaging

Serial MR Imaging. Two serial DTI studies found a significant correlation with cognitive and neurosensory outcome (Table 1). Drobyshevsky et al[70] demonstrated that the Bayley performance index at 24 months was correlated with FA of the PLIC at 30 weeks

($r = 0.55$) and faster increase of FA per week in the internal capsule ($r = -0.63$) and occipital WM ($r = -0.59$). Increased FA values in the optic radiation at 33 and 37 weeks were associated with increased visual-evoked-response amplitudes at 10.5 months ($r = 0.7$).[71] However, this may not necessarily mean that eventually visual function is better.

MR Imaging at ≤35 Weeks' PMA. None of the included studies related early DTI measurements to long-term outcome.

MR Imaging at >35 Weeks' PMA. In a tract-based spatial statistics study by van Kooij et al,[72] FA values of the corpus callosum were correlated to cognitive scores, gross motor scores were correlated with radial diffusion of the corpus callosum and internal and external capsules, and fine-motor scores were correlated to FA throughout the WM. Other DTI studies have demonstrated similar correlations: DTI parameters of the corpus callosum, PLIC, right orbital frontal cortex, and centrum semiovale were correlated to cognitive performance (On-line Table).[73-76] In other studies, DTI measurements of the corpus callosum, PLIC, and corona radiata were correlated to motor function.[74,77-79] Furthermore, FA values of the optic radiation were directly correlated to visual assessment scores at term-equivalent age.[80]

Volumetric MR Imaging

Serial MR Imaging. Three serial volumetric MR imaging studies demonstrated that early structural abnormalities are predictors of neurobehavioral outcome (Table 1). Dubois et al[81] concluded that at term-corrected age, neurobehavioral development was significantly associated with quantitative surrogates of cortical folding. Kapellou et al[82] found that the ratio between cortical surface area and cerebral volume was directly related to neurodevelopment at 24 months. The same group showed that growth of the cortical surface area was also significantly related to intelligence at 6 years: A faster growth of 0.032% per week resulted in an increase of 1 IQ point.[83]

MR Imaging at ≤35 Weeks' PMA. Badr et al[84] found that WM volume on MR imaging at a mean PMA of 31 weeks was significantly correlated to the Bayley Psychomotor Development Index ($r = 0.29$) and Mental Development Index ($r = 0.31$) at 18 months (Table 2).

MR Imaging at >35 Weeks' PMA. Volumetric MR imaging studies in preterm infants with neurodevelopmental impairment have demonstrated significantly smaller total brain volume[54,66,85] and volume of several cerebral structures or regions, including the cerebellum,[66,86-89] total WM,[90] total[28,91] and deep[66,76] gray matter, occipital lobes,[92] hippocampus,[93,94] and brain stem,[95] as well as significantly larger ventricles (On-line Table).[28,96] These findings were irrespective of the presence of overt brain injury. Simple linear metric assessment, such as biparietal and cerebellar diameter, on MR imaging also significantly correlated with neurocognitive function.[97,98] Impaired social-emotional development at 5 years was associated with decreased hippocampal volume in girls and decreased frontal lobe growth in boys.[75]

Proton MR Spectroscopy

MR Imaging at >35 Weeks' PMA. ^{1}H-MR spectroscopy is an accurate quantitative biomarker for the prediction of neurodevelopmental outcome after hypoxic-ischemic encephalopathy in term infants (On-line Table).[99] It is not clear whether this holds true for preterm infants. The cerebellar NAA/Cho ratio at term is suggested to correlate with cognitive outcome at 24 months.[89] However, Gadin et al[91] found no correlation between MR spectroscopy of the periventricular WM and motor development at 6 months.

DISCUSSIONS

This systematic review included 8 serial MR imaging studies, 2 MR imaging studies performed at ≤35 weeks, and 52 MR imaging studies performed at >35 weeks. The results of these studies made clear that the extent of structural abnormalities, microstructural deviations, and global reductions in brain volumes, both at preterm and term age, is directly related to the level of neuromotor and neurocognitive performance in childhood. Involvement of WM in preterm brain injury seems paramount. Accurate assessment of WM integrity, therefore, may help predict long-term outcome in preterm infants and is one of the challenging goals in the field of neonatal neurology.

These studies do not provide clear evidence on the optimal timing of MR imaging. Although an increasing number of neuroimaging studies used early MR imaging to show that brain abnormalities are often present during early preterm life,[22,100,101] only 2 of the studies linked these findings to outcome. Dyet et al[8] demonstrated that MR imaging within the first 2 days after birth was of limited additional value for predicting outcome. On the other hand, Miller et al[39] reported that early MR imaging findings at 32 weeks' gestation were as reliable for predicting neurodevelopment as MR imaging findings at term age. This finding suggests that predictive MR imaging may be performed well before term-equivalent age, provided it is after the first week of life.

Neonatal care would benefit from identifying brain injury early in preterm life, in terms of effective and timely parental counseling, tailored rehabilitation strategies, and better understanding of neuropathology. Currently, we have no efficacious therapy for preterm brain injury, but trials on possible neuroprotective agents, such as erythropoietin, melatonin, stem cell therapy, and magnesium sulfate are being conducted or planned for the near future.[102,103] Early MR imaging could provide early biomarkers that trials could target.

Image acquisition, processing, and interpretation are not as straightforward as with conventional MR imaging, though sophisticated techniques such as DTI allow objective and quantifiable assessment of cerebral tissue. Because measurement accuracy depends on various aspects, including scanner type, hardware setup, acquisition settings, and clinical characteristics, reproducibility of the same measurements in different imaging centers is low. Furthermore, the availability of normal ADC and FA values of specific WM structures is limited. In addition, DTI is especially sensitive to image artifacts and corruption.[104] Reliable conclusions can therefore only be drawn if quality assessment before postprocessing provided satisfactory data quality. In the included studies, quality assessment was often not performed.

MR imaging is expensive and time-consuming and requires great experience and dedication to ensure patient safety[37] as well as good quality data and interpretation.[105] These limitations should be especially taken into account with regard to the individual clinical care for patients with normal cranial sonography findings. This technique can reliably predict some aspects of the outcome of preterm infants and allows serial neuroimaging in a fast, convenient, and less-expensive manner.[106,107] Moreover, advanced applications, such as color Doppler sonography, also allow objective and quantitative brain assessment.

Several limitations of this systematic review need to be addressed. First, heterogeneity of the study populations was due to variation in age at MR imaging, acquisition settings, postprocessing methods for MR imaging evaluation and other technical aspects of MR imaging scanners, different ages at outcome measurement, and different measures of outcome. Second, follow-up periods were relatively short. Third, because the search was restricted to articles in the English language, possible relevant studies might not have been included.

CONCLUSIONS

MR imaging remains an outstanding method to predict long-term neurodevelopmental outcome, and cerebral MR imaging should be part of standard clinical care for preterm infants. Early MR imaging allows timely parental counseling, targeting of rehabilitation strategies, and availability of early biomarkers. However, the individual prognostic information provided by early scanning remains inferior to that provided by term scanning. As long as the correlation of brain injury from early MR imaging with outcome is not clear, we would argue that standard MR imaging should preferably be performed at term-equivalent age. On the other hand, early MR imaging yields important information about the pathogenesis of preterm brain injury and therefore is indispensable in research on preterm brain injury.

ACKNOWLEDGMENTS

We thank Wichor Bramer from the Erasmus Medical Center medical library for his help in devising the search strategy.

REFERENCES

1. Saigal S, Doyle LW. **An overview of mortality and sequelae of preterm birth from infancy to adulthood.** *Lancet* 2008;371:261–69
2. Bhutta AT, Cleves MA, Casey PH, et al. **Cognitive and behavioral outcomes of school-aged children who were born preterm: a meta-analysis.** *JAMA* 2002;288:728–37
3. Larroque B, Ancel PY, Marret S, et al. **Neurodevelopmental disabilities and special care of 5-year-old children born before 33 weeks of gestation (the EPIPAGE study): a longitudinal cohort study.** *Lancet* 2008;371:813–20
4. Marlow N, Wolke D, Bracewell MA, et al. **Neurologic and developmental disability at six years of age after extremely preterm birth.** *N Engl J Med* 2005;352:9–19
5. Williams J, Lee KJ, Anderson PJ. **Prevalence of motor-skill impairment in preterm children who do not develop cerebral palsy: a systematic review.** *Dev Med Child Neurol* 2010;52:232–37
6. Rutherford MA, Supramaniam V, Ederies A, et al. **Magnetic resonance imaging of white matter diseases of prematurity.** *Neuroradiology* 2010;52:505–21
7. Inder TE, Wells SJ, Mogridge NB, et al. **Defining the nature of the cerebral abnormalities in the premature infant: a qualitative magnetic resonance imaging study.** *J Pediatr* 2003;143:171–79
8. Dyet LE, Kennea N, Counsell SJ, et al. **Natural history of brain lesions in extremely preterm infants studied with serial magnetic resonance imaging from birth and neurodevelopmental assessment.** *Pediatrics* 2006;118:536–48
9. Spittle AJ, Brown NC, Doyle LW, et al. **Quality of general movements is related to white matter pathology in very preterm infants.** *Pediatrics* 2008;121:e1184–89
10. Jeon TY, Kim JH, Yoo SY, et al. **Neurodevelopmental outcomes in preterm infants: comparison of infants with and without diffuse excessive high signal intensity on MR images at near-term-equivalent age.** *Radiology* 2012;263:518–26
11. Volpe JJ. **Brain injury in premature infants: a complex amalgam of destructive and developmental disturbances.** *Lancet Neurol* 2009;8:110–24
12. Khwaja O, Volpe JJ. **Pathogenesis of cerebral white matter injury of prematurity.** *Arch Dis Child Fetal Neonatal Ed* 2008;93:F153–61
13. Hüppi PS, Murphy B, Maier SE, et al. **Microstructural brain development after perinatal cerebral white matter injury assessed by diffusion tensor magnetic resonance imaging.** *Pediatrics* 2001;107:455–60
14. Inder TE, Anderson NJ, Spencer C, et al. **White matter injury in the premature infant: a comparison between serial cranial sonographic and MR findings at term.** *AJNR Am J Neuroradiol* 2003;24:805–09
15. Woodward LJ, Anderson PJ, Austin NC, et al. **Neonatal MRI to predict neurodevelopmental outcomes in preterm infants.** *N Engl J Med* 2006;355:685–94
16. Mirmiran M, Barnes PD, Keller K, et al. **Neonatal brain magnetic resonance imaging before discharge is better than serial cranial ultrasound in predicting cerebral palsy in very low birth weight preterm infants.** *Pediatrics* 2004;114:992–98
17. Valkama AM, Paakko EL, Vainionpaa LK, et al. **Magnetic resonance imaging at term and neuromotor outcome in preterm infants.** *Acta Paediatr* 2000;89:348–55
18. Ment LR, Hirtz D, Huppi PS. **Imaging biomarkers of outcome in the developing preterm brain.** *Lancet Neurol* 2009;8:1042–55
19. Counsell SJ, Rutherford MA, Cowan FM, et al. **Magnetic resonance imaging of preterm brain injury.** *Arch Dis Child Fetal Neonatal Ed* 2003;88:F269–74
20. Hüppi PS, Dubois J. **Diffusion tensor imaging of brain development.** *Semin Fetal Neonatal Med* 2006;11:489–97
21. Jones DK. **Studying connections in the living human brain with diffusion MRI.** *Cortex* 2008;44:936–52
22. Dudink J, Lequin M, van Pul C, et al. **Fractional anisotropy in white matter tracts of very-low-birth-weight infants.** *Pediatr Radiol* 2007;37:1216–23
23. Miller SP, Vigneron DB, Henry RG, et al. **Serial quantitative diffusion tensor MRI of the premature brain: development in newborns with and without injury.** *J Magn Reson Imaging* 2002;16:621–32
24. Counsell SJ, Allsop JM, Harrison MC, et al. **Diffusion-weighted imaging of the brain in preterm infants with focal and diffuse white matter abnormality.** *Pediatrics* 2003;112:1–7
25. Counsell SJ, Shen Y, Boardman JP, et al. **Axial and radial diffusivity in preterm infants who have diffuse white matter changes on magnetic resonance imaging at term-equivalent age.** *Pediatrics* 2006;117:376–86
26. Inder TE, Huppi PS, Warfield S, et al. **Periventricular white matter injury in the premature infant is followed by reduced cerebral cortical gray matter volume at term.** *Ann Neurol* 1999;46:755–60
27. Thompson DK, Warfield SK, Carlin JB, et al. **Perinatal risk factors altering regional brain structure in the preterm infant.** *Brain* 2007;130:667–77
28. Inder TE, Warfield SK, Wang H, et al. **Abnormal cerebral structure is present at term in premature infants.** *Pediatrics* 2005;115:286–94
29. Keunen K, Kersbergen KJ, Groenendaal F, et al. **Brain tissue vol-**

umes in preterm infants: prematurity, perinatal risk factors and neurodevelopmental outcome—a systematic review. *J Matern Fetal Neonatal Med* 2012;25(suppl 1):89–100
30. Mathur A, Inder T. **Magnetic resonance imaging: insights into brain injury and outcomes in premature infants.** *J Commun Disord* 2009;42:248–55
31. Dubois J, Benders M, Cachia A, et al. **Mapping the early cortical folding process in the preterm newborn brain.** *Cereb Cortex* 2008;18:1444–54
32. Dubois J, Benders M, Lazeyras F, et al. **Structural asymmetries of perisylvian regions in the preterm newborn.** *Neuroimage* 2010;52:32–42
33. Dubois J, Hertz-Pannier L, Cachia A, et al. **Structural asymmetries in the infant language and sensori-motor networks.** *Cereb Cortex* 2009;19:414–23
34. Ajayi-Obe M, Saeed N, Cowan FM, et al. **Reduced development of cerebral cortex in extremely preterm infants.** *Lancet* 2000;356:1162–63
35. Hüppi PS, Schuknecht B, Boesch C, et al. **Structural and neurobehavioral delay in postnatal brain development of preterm infants.** *Pediatr Res* 1996;39:895–901
36. Hüppi PS, Lazeyras F. **Proton magnetic resonance spectroscopy ((1)H-MRS) in neonatal brain injury.** *Pediatr Res* 2001;49:317–20
37. Plaisier A, Raets MM, van der Starre C, et al. **Safety of routine early MRI in preterm infants**. *Pediatr Radiol* 2012;42:1205–11
38. Hillenbrand CM, Reykowski A. **MR imaging of the newborn: a technical perspective.** *Magn Reson Imaging Clin N Am* 2012; 20:63–79
39. Miller SP, Ferriero DM, Leonard C, et al. **Early brain injury in premature newborns detected with magnetic resonance imaging is associated with adverse early neurodevelopmental outcome.** *J Pediatr* 2005;147:609–16
40. Tam EW, Rosenbluth G, Rogers EE, et al. **Cerebellar hemorrhage on magnetic resonance imaging in preterm newborns associated with abnormal neurologic outcome.** *J Pediatr* 2011;158:245–50
41. Cornette LG, Tanner SF, Ramenghi LA, et al. **Magnetic resonance imaging of the infant brain: anatomical characteristics and clinical significance of punctate lesions.** *Arch Dis Child Fetal Neonatal Ed* 2002;86:F171–77
42. Skiöld B, Vollmer B, Bohm B, et al. **Neonatal magnetic resonance imaging and outcome at age 30 months in extremely preterm infants**. *J Pediatr* 2012;160:559–566.e1
43. Hnatyszyn G, Cyrylowski L, Czeszynska MB, et al. **The role of magnetic resonance imaging in early prediction of cerebral palsy.** *Turk J Pediatr* 2010;52:278–84
44. Spittle AJ, Boyd RN, Inder TE, et al. **Predicting motor development in very preterm infants at 12 months' corrected age: the role of qualitative magnetic resonance imaging and general movements assessments.** *Pediatrics* 2009;123:512–17
45. Spittle AJ, Cheong J, Doyle LW, et al. **Neonatal white matter abnormality predicts childhood motor impairment in very preterm children.** *Dev Med Child Neurol* 2011;53:1000–06
46. Nanba Y, Matsui K, Aida N, et al. **Magnetic resonance imaging regional T1 abnormalities at term accurately predict motor outcome in preterm infants.** *Pediatrics* 2007;120:e10–e19
47. Brown NC, Inder TE, Bear MJ, et al. **Neurobehavior at term and white and gray matter abnormalities in very preterm infants**. *J Pediatr* 2009;155:32–8, 38.e1
48. Aida N, Nishimura G, Hachiya Y, et al. **MR imaging of perinatal brain damage: comparison of clinical outcome with initial and follow-up MR findings.** *AJNR Am J Neuroradiol* 1998;19:1909–21
49. van Wezel-Meijler G, Van Der Knaap MS, Oosting J, et al. **Predictive value of neonatal MRI as compared to ultrasound in premature infants with mild periventricular white matter changes.** *Neuropediatrics* 1999;30:231–38
50. Bayley N. *Bayley Scales of Infant and Toddler Development,* 3rd ed. San Antonio, Texas: Harcourt Assessment; 2006
51. Hart A, Whitby E, Wilkinson S, et al. **Neuro-developmental outcome at 18 months in premature infants with diffuse excessive high signal intensity on MR imaging of the brain.** *Pediatr Radiol* 2011;41:1284–92
52. Sie LT, Hart AA, van Hof J, et al. **Predictive value of neonatal MRI with respect to late MRI findings and clinical outcome: a study in infants with periventricular densities on neonatal ultrasound.** *Neuropediatrics* 2005;36:78–89
53. Munck P, Haataja L, Maunu J, et al. **Cognitive outcome at 2 years of age in Finnish infants with very low birth weight born between 2001 and 2006.** *Acta Paediatr* 2010;99:359–66
54. Woodward LJ, Edgin JO, Thompson D, et al. **Object working memory deficits predicted by early brain injury and development in the preterm infant.** *Brain* 2005;128:2578–87
55. Spittle AJ, Treyvaud K, Doyle LW, et al. **Early emergence of behavior and social-emotional problems in very preterm infants.** *J Am Acad Child Adolesc Psychiatry* 2009;48:909–18
56. Edgin JO, Inder TE, Anderson PJ, et al. **Executive functioning in preschool children born very preterm: relationship with early white matter pathology.** *J Int Neuropsychol Soc* 2008;14:90–101
57. Woodward LJ, Clark CA, Pritchard VE, et al. **Neonatal white matter abnormalities predict global executive function impairment in children born very preterm.** *Dev Neuropsychol* 2011;36:22–41
58. Clark CA, Woodward LJ. **Neonatal cerebral abnormalities and later verbal and visuospatial working memory abilities of children born very preterm.** *Dev Neuropsychol* 2010;35:622–42
59. Iwata S, Nakamura T, Hizume E, et al. **Qualitative brain MRI at term and cognitive outcomes at 9 years after very preterm birth.** *Pediatrics* 2012;129:e1138–47
60. Reidy N, Morgan A, Thompson DK, et al. **Impaired language abilities and white matter abnormalities in children born very preterm and/or very low birth weight.** *J Pediatr* 2013;162:719–24
61. Iwata S, Iwata O, Bainbridge A, et al. **Abnormal white matter appearance on term FLAIR predicts neuro-developmental outcome at 6 years old following preterm birth.** *Int J Dev Neurosci* 2007;25:523–30
62. de Bruïne FT, Van Den Berg-Huysmans AA, Leijser LM, et al. **Clinical implications of MR imaging findings in the white matter in very preterm infants: a 2-year follow-up study.** *Radiology* 2011;261: 899–906
63. Kidokoro H, Anderson PJ, Doyle LW, et al. **High signal intensity on T2-weighted MR imaging at term-equivalent age in preterm infants does not predict 2-year neurodevelopmental outcomes.** *AJNR Am J Neuroradiol* 2011;32:2005–10
64. Hagmann CF, De Vita E, Bainbridge A, et al. **T2 at MR imaging is an objective quantitative measure of cerebral white matter signal intensity abnormality in preterm infants at term-equivalent age.** *Radiology* 2009;252:209–17
65. Papile LA, Burstein J, Burstein R, et al. **Incidence and evolution of subependymal and intraventricular hemorrhage: a study of infants with birth weights less than 1,500 gm.** *J Pediatr* 1978;92:529–34
66. Jary S, De Carli A, Ramenghi LA, et al. **Impaired brain growth and neurodevelopment in preterm infants with posthaemorrhagic ventricular dilatation**. *Acta Paediatr* 2012;101:743–48
67. De Vries LS, Groenendaal F, van Haastert IC, et al. **Asymmetrical myelination of the posterior limb of the internal capsule in infants with periventricular haemorrhagic infarction: an early predictor of hemiplegia.** *Neuropediatrics* 1999;30:314–19
68. Horsch S, Kutz P, Roll C. **Late germinal matrix hemorrhage-like lesions in very preterm infants.** *J Child Neurol* 2010;25:809–14
69. Lind A, Lapinleimu H, Korkman M, et al. **Five-year follow-up of prematurely born children with postnatally developing caudothalamic cysts.** *Acta Paediatr* 2010;99:304–07
70. Drobyshevsky A, Bregman J, Storey P, et al. **Serial diffusion tensor imaging detects white matter changes that correlate with motor outcome in premature infants.** *Dev Neurosci* 2007;29:289–301
71. Glass HC, Berman JI, Norcia AM, et al. **Quantitative fiber tracking of the optic radiation is correlated with visual-evoked potential**

amplitude in preterm infants. *AJNR Am J Neuroradiol* 2010;31:1424–29
72. van Kooij BJ, De Vries LS, Ball G, et al. **Neonatal tract-based spatial statistics findings and outcome in preterm infants.** *AJNR Am J Neuroradiol* 2012;33:188–94
73. Krishnan ML, Dyet LE, Boardman JP, et al. **Relationship between white matter apparent diffusion coefficients in preterm infants at term-equivalent age and developmental outcome at 2 years.** *Pediatrics* 2007;120:e604–09
74. van Kooij BJ, Van Pul C, Benders MJ, et al. **Fiber tracking at term displays gender differences regarding cognitive and motor outcome at 2 years of age in preterm infants.** *Pediatr Res* 2011;70:626–32
75. Rogers CE, Anderson PJ, Thompson DK, et al. **Regional cerebral development at term relates to school-age social-emotional development in very preterm children.** *J Am Acad Child Adolesc Psychiatry* 2012;51:181–91
76. Boardman JP, Craven C, Valappil S, et al. **A common neonatal image phenotype predicts adverse neurodevelopmental outcome in children born preterm.** *Neuroimage* 2010;52:409–14
77. Kaukola T, Perhomaa M, Vainionpaa L, et al. **Apparent diffusion coefficient on magnetic resonance imaging in pons and in corona radiata and relation with the neurophysiologic measurement and the outcome in very preterm infants.** *Neonatology* 2010;97:15–21
78. Rose J, Butler EE, Lamont LE, et al. **Neonatal brain structure on MRI and diffusion tensor imaging, sex, and neurodevelopment in very-low-birthweight preterm children.** *Dev Med Child Neurol* 2009;51:526–35
79. Arzoumanian Y, Mirmiran M, Barnes PD, et al. **Diffusion tensor brain imaging findings at term-equivalent age may predict neurologic abnormalities in low birth weight preterm infants.** *AJNR Am J Neuroradiol* 2003;24:1646–53
80. Bassi L, Ricci D, Volzone A, et al. **Probabilistic diffusion tractography of the optic radiations and visual function in preterm infants at term equivalent age.** *Brain* 2008;131:573–82
81. Dubois J, Benders M, Borradori-Tolsa C, et al. **Primary cortical folding in the human newborn: an early marker of later functional development.** *Brain* 2008;131:2028–41
82. Kapellou O, Counsell SJ, Kennea N, et al. **Abnormal cortical development after premature birth shown by altered allometric scaling of brain growth.** *PLoS Med* 2006;3:e265
83. Rathbone R, Counsell SJ, Kapellou O, et al. **Perinatal cortical growth and childhood neurocognitive abilities.** *Neurology* 2011;77:1510–17
84. Badr LK, Bookheimer S, Purdy I, et al. **Predictors of neurodevelopmental outcome for preterm infants with brain injury: MRI, medical and environmental factors.** *Early Hum Dev* 2009;85:279–84
85. Tan M, Abernethy L, Cooke R. **Improving head growth in preterm infants: a randomised controlled trial II: MRI and developmental outcomes in the first year.** *Arch Dis Child Fetal Neonatal Ed* 2008;93:f342–46
86. Lind A, Parkkola R, Lehtonen L, et al. **Associations between regional brain volumes at term-equivalent age and development at 2 years of age in preterm children.** *Pediatr Radiol* 2011;41:953–61
87. Lind A, Haataja L, Rautava L, et al. **Relations between brain volumes, neuropsychological assessment and parental questionnaire in prematurely born children.** *Eur Child Adolesc Psychiatry* 2010;19:407–17
88. Shah DK, Anderson PJ, Carlin JB, et al. **Reduction in cerebellar volumes in preterm infants: relationship to white matter injury and neurodevelopment at two years of age.** *Pediatr Res* 2006;60:97–102
89. van Kooij BJ, Benders MJ, Anbeek P, et al. **Cerebellar volume and proton magnetic resonance spectroscopy at term, and neurodevelopment at 2 years of age in preterm infants.** *Dev Med Child Neurol* 2012;54:260–66
90. Peterson BS, Anderson AW, Ehrenkranz R, et al. **Regional brain volumes and their later neurodevelopmental correlates in term and preterm infants.** *Pediatrics* 2003;111:939–48
91. Gadin E, Lobo M, Paul DA, et al. **Volumetric MRI and MRS and early motor development of infants born preterm.** *Pediatr Phys Ther* 2012;24:38–44
92. Shah DK, Guinane C, August P, et al. **Reduced occipital regional volumes at term predict impaired visual function in early childhood in very low birth weight infants.** *Invest Ophthalmol Vis Sci* 2006;47:3366–73
93. Thompson DK, Wood SJ, Doyle LW, et al. **Neonate hippocampal volumes: prematurity, perinatal predictors, and 2-year outcome.** *Ann Neurol* 2008;63:642–51
94. Beauchamp MH, Thompson DK, Howard K, et al. **Preterm infant hippocampal volumes correlate with later working memory deficits.** *Brain* 2008;131:2986–94
95. Valkama AM, Tolonen EU, Kerttula LI, et al. **Brainstem size and function at term age in relation to later neurosensory disability in high-risk, preterm infants.** *Acta Paediatr* 2001;90:909–15
96. Maunu J, Lehtonen L, Lapinleimu H, et al. **Ventricular dilatation in relation to outcome at 2 years of age in very preterm infants: a prospective Finnish cohort study.** *Dev Med Child Neurol* 2011;53:48–54
97. Tich SN, Anderson PJ, Hunt RW, et al. **Neurodevelopmental and perinatal correlates of simple brain metrics in very preterm infants.** *Arch Pediatr Adolesc Med* 2011;165:216–22
98. Spittle AJ, Doyle LW, Anderson PJ, et al. **Reduced cerebellar diameter in very preterm infants with abnormal general movements.** *Early Hum Dev* 2010;86:1–5
99. Thayyil S, Chandrasekaran M, Taylor A, et al. **Cerebral magnetic resonance biomarkers in neonatal encephalopathy: a meta-analysis.** *Pediatrics* 2010;125:e382–95
100. Nossin-Manor R, Chung AD, Whyte HEA, et al. **Deep gray matter maturation in very preterm neonates: regional variations and pathology-related age-dependent changes in magnetization transfer ratio.** *Radiology* 2012;263:510–17
101. Smyser CD, Inder TE, Shimony JS, et al. **Longitudinal analysis of neural network development in preterm infants.** *Cereb Cortex* 2010;20:2852–62
102. Doyle LW. **Antenatal magnesium sulfate and neuroprotection.** *Curr Opin Pediatr* 2012;24:154–59
103. Rees S, Harding R, Walker D. **The biological basis of injury and neuroprotection in the fetal and neonatal brain.** *Int J Dev Neurosci* 2011;29:551–63
104. Jones DK, Cercignani M. **Twenty-five pitfalls in the analysis of diffusion MRI data.** *NMR Biomed* 2010;23:803–20
105. Pannek K, Guzzetta A, Colditz PB, et al. **Diffusion MRI of the neonate brain: acquisition, processing and analysis techniques**. *Pediatr Radiol* 2012 42:1169–82
106. De Vries LS, Van Haastert IL, Rademaker KJ, et al. **Ultrasound abnormalities preceding cerebral palsy in high-risk preterm infants.** *J Pediatr* 2004;144:815–20
107. Horsch S, Skiold B, Hallberg B, et al. **Cranial ultrasound and MRI at term age in extremely preterm infants.** *Arch Dis Child Fetal Neonatal Ed* 2010;95:F310–14

Multivariate Classification of Blood Oxygen Level–Dependent fMRI Data with Diagnostic Intention: A Clinical Perspective

B. Sundermann, D. Herr, W. Schwindt, and B. Pfleiderer

ABSTRACT

SUMMARY: There has been a recent upsurge of reports about applications of pattern-recognition techniques from the field of machine learning to functional MR imaging data as a diagnostic tool for systemic brain disease or psychiatric disorders. Entities studied include depression, schizophrenia, attention deficit hyperactivity disorder, and neurodegenerative disorders like Alzheimer dementia. We review these recent studies which—despite the optimism from some articles—predominantly constitute explorative efforts at the proof-of-concept level. There is some evidence that, in particular, support vector machines seem to be promising. However, the field is still far from real clinical application, and much work has to be done regarding data preprocessing, model optimization, and validation. Reporting standards are proposed to facilitate future meta-analyses or systematic reviews.

ABBREVIATIONS: ADHD = attention deficit hyperactivity disorder; CV = cross-validation; LDA = linear discriminant analysis; MVPA = multivariate pattern analysis; SVM = support vector machine

Functional MR imaging based on blood oxygen level–dependent signal changes that are measured by using fast T2*-sensitive echo-planar imaging techniques provides an indirect measure of neural activity in the brain. It has an enormous impact on basic research in the field of cognitive neurosciences[1] and has been applied in numerous group studies with the aim of clarifying disease mechanisms in psychiatric and neurologic disorders, some of which do not exhibit obvious structural alterations (eg, Zhang and Raichle[2] and Chen et al[3]). However, the applicability of fMRI to single subjects in clinical settings has been limited to a few indications, mainly in the context of surgery planning.[4,5]

Although there has been a substantial effort to identify neuroimaging biomarkers for psychiatric disorders[6,7] (eg, schizophrenia,[8] depression,[9] and neurodegenerative disorders like Alzheimer dementia[10] with the goal of including biomarkers in official diagnostic criteria,[11]), to date capturing functional aspects in diagnostic imaging is almost limited to tracer studies in certain kinds of neurodegeneration.[6,12,13] In clinical practice, neuroradiologic MR imaging examinations are broadly confined to the exclusion of gross structural abnormalities, but normally, actual disease mechanisms are not used as further information in a majority of these individuals. Voxel-based morphometry, DTI, and fMRI have been proposed as potential MR imaging biomarkers that might help overcome this shortcoming in the future.[7,8]

A prime drawback of fMRI is the rather high inter- and intra-individual variability of measures in conventional analyses, even in healthy individuals,[14-16] that foils many such attempts. Conventional fMRI methods mainly comprise univariate activation or cofluctuation (functional-connectivity) analyses based on averaged signals in a few regions of interest or mass-univariate analyses across the whole brain,[1] which come along with high requirements to control for multiple comparisons.[17]

Overview of Machine-Learning-Based Classification Techniques for fMRI

In the case of intertrial variability in individual subjects, the problem of differentiating single trials has been overcome in recent years by the rise of multivariate supervised learning methods derived from the fields of machine learning and pattern recognition. Such methods, often termed multivariate or multivoxel pattern analyses (MVPAs), are increasingly adopted in psychologically motivated fMRI studies. The concept of such analyses is that at first an algorithm is used to derive a decision rule (classifier) on the basis of a set of labeled training data (eg, comprising ≥2 classes; eg, different stimuli categories or tasks). This rule is applied to classifying an independent set of test data as belonging to one of these classes in a second step. A general overview of this approach

Received May 31, 2013; accepted after revision June 19.

From the Department of Clinical Radiology (B.S., W.S., B.P.), University Hospital Münster, Münster, Germany; and Department of Psychiatry and Psychotherapy (D.H.), University of Cologne, Cologne, Germany.

Please address correspondence to Benedikt Sundermann, MD, Department of Clinical Radiology, University Hospital Münster, Albert-Schweitzer-Campus 1, Gebäude A1, 48149 Münster, Germany; e-mail: benedikt.sundermann@ukmuenster.de

Indicates article with supplemental on-line tables

http://dx.doi.org/10.3174/ajnr.A3713

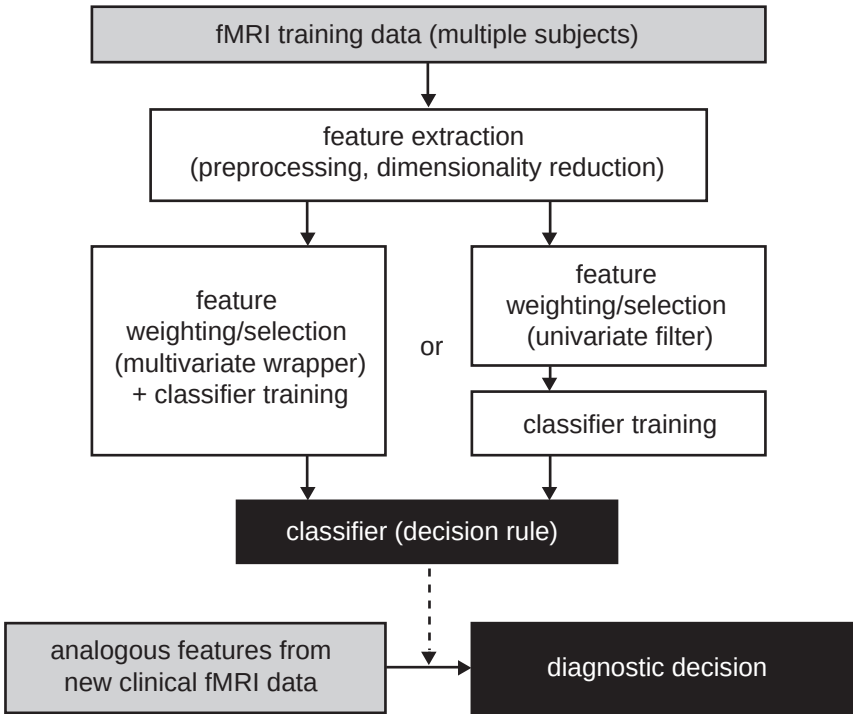

FIG 1. Illustration of the diagnostic workflow and data-processing pipeline proposed by most of the studies reviewed here.

is shown in Fig 1. In contrast to conventional analyses, these techniques are based on patterns of brain activation or connections not on individual regions or voxels.[18-20] Recently this concept has been extended to classifying individual subjects with a diagnostic purpose (for earlier, methodologically oriented reviews see Kloppel et al[21] and Orrù et al[22]). This article gives a comprehensive overview of MVPA applications to fMRI from a more clinical, particularly neuroradiologic, point of view.

Although there are a large number of supervised machine-learning techniques that can, in principle, be applied in this context,[23] 2 groups of methodologies are of particular importance: support vector machines (SVMs) and linear discriminant analyses (LDAs). In SVMs, the classification problem is operationalized as defining a hyperplane that best distinguishes groups of subjects. The classifier is trained by using a kernel by maximizing the margin of separation between 2 groups on the basis of the examples closest to the separating hyperplane.[22-24] In a typical LDA variant, all data points are projected to a 1D space with the aim of maximizing intergroup separation and minimizing intraclass variation.[22,23] LDA and support vector machines are very heterogeneous groups, depending on the actual operationalization or the kernel used. Certain kinds of SVMs are mathematically very similar to certain types of LDAs, while there can be important differences between different support vector machine formulations and parameter sets.[23] The distinction made is, therefore, somewhat artificial.

fMRI datasets usually comprise several thousand nonindependent voxels. Yet the number of subjects is usually limited to dozens. This difference poses a certain problem for MVPA because most methods cannot deal with a high dimensionality of the data compared with the number of samples. There is a high risk of overfitting. This means that the classifier is perfectly trained to separate the samples used for training but has a poor ability to generalize to the successful classification of new data. This issue can be dealt with by the selection of classification methods that are less sensitive to a high dimensionality, such as SVMs. In contrast, LDA is usually very sensitive to this. Still, a strict dimensionality reduction is necessary: Primary data are preprocessed to concatenate redundant information by feature extraction, and features that are decisive are identified before actual classifier training by feature selection or weighting. Filter approaches, partially by using conventional univariate statistics or wrapper-based approaches, are commonly applied for feature selection.[19]

An issue that has to be overcome in diagnostic classification is interindividual structural variability regarding the morphology of the cerebral sulci and gyri as well as their relation to histologically and functionally relevant brain areas.[25] Within-subject MVPA analyses often rely on fine-grained patterns on a single-voxel level.[18,19] In contrast, most diagnostic MVPA studies reviewed here focus on another spatial scale: larger functionally coherent brain areas.

A specific feature present in the design of most MVPA-based fMRI studies is that datasets are often small and that classification performance is assessed through cross-validation (CV). Here, feature selection and classifier training are repeated several times. Each time a different range of datasets, often exactly one in the case of leave-one-out CV, is excluded and used as a test set.[19]

Recent Diagnostic fMRI Approaches Based on MVPA

There has recently been a remarkable upsurge of scientific articles from the interdisciplinary functional neuroimaging community reporting successful applications of MVPA on fMRI data to various diagnostic problems, especially in the past 3 years. This constitutes a paradigm shift from comparative univariate to discriminative multivariate analyses of fMRI data. An exhaustive overview of these previous studies by using either task-based[26-63] or task-free[55,64-97] fMRI is given in On-line Tables 1 and 2. An overview of particularly reliable studies with above-average statistical power is presented in Fig 2.

Although they are promising at first glance, there is a high degree of methodologic heterogeneity of classification algorithms and data-preprocessing steps in these studies. Some of the reported results seem to be mostly add-ons to studies whose designs were primarily aimed at clarifying disease mechanisms or were focused on computational aspects, not primarily done with the aim of developing a diagnostic tool. Until now, no single effort in this field has provided sufficient large-scale validation and systematic optimization of methodologic choices leading to an application in a real medical diagnostic setting. Due to this

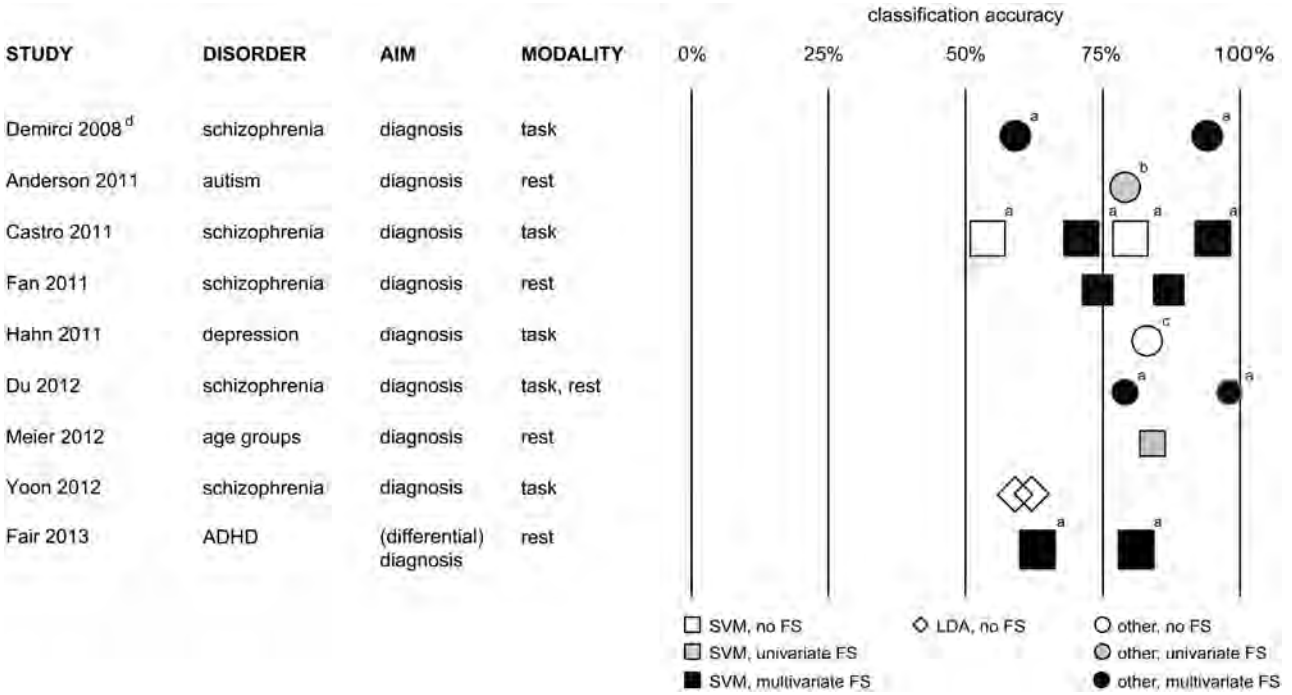

FIG 2. Overview of MVPA-based diagnostic fMRI studies with an above-average statistical power to detect successful models ($n \geq 25$ in every group of the training set; group size ratio ≤ 1.2 as a prerequisite for comparing the overall classification accuracies reported).[34,43,45,55,61,72,74,85,95] Symbol sizes represent average group sizes in the respective study. a, Only minimum and maximum classification accuracies are shown here. b, Study of cross-validation findings also reports results in a smaller independent validation set. c, Only Gaussian process classifier overall accuracy is shown here. d, High overlap with another study is not shown here. FS indicates feature selection. For a complete list of studies, see On-line Tables 1 and 2.

heterogeneity and because strategies to assess the statistical significance of diagnostic accuracy vary considerably between studies, we did not perform a formal meta-analytical comparison of these reports.

Data Acquisition and Preprocessing. By now a majority of reported approaches are based on conventional task-based fMRI.[26-63] This means that patients have to perform a specific, mainly neuropsychological task in the MR imaging scanner. Statistical models are designed to evaluate the amount of variance in the acquired EPI data caused by this task modification of brain activity. This corresponds to "brain activation" in conventional fMRI studies.[1] An advantage of this approach is a rather straightforward functional interpretability of such data. Yet in addition to mainly psychologically motivated studies in young healthy participants, patients' adherence to task instructions constitutes an important source of variability in real clinical settings and may even interfere with diagnostic decision-making.

Recently, a significant number of studies[55,64-97] have been based on task-free fMRI acquisitions, so-called resting-state fMRI, which focuses on the functional connectivity of distant brain regions in terms of signal cofluctuations and therefore on the integrity of large-scale brain networks.[98,99] A potential benefit of this method is that typical networks seem to be robustly identifiable in individual subjects. However, reports focusing on the reliability of typical resting-state fMRI measures highlight the problem that these are highly dependent on potentially confounding factors such as wakefulness or autonomic arousal.[100,101] Although most resting-state fMRI findings in basic neuroscience are based on short acquisitions of approximately 5 minutes, which seem to be sufficient for network detection,[102] there is recent evidence that retest reliability can be significantly improved by longer acquisitions.[103] Only a minority of resting-state functional connectivity–based MVPA approaches have used acquisitions lasting at least 7 minutes.[67,72,79,84,87,91]

As a common analysis step on a single subject level, feature-extraction methods are used to extract meaningful information from and simultaneously reduce the high dimensionality of the raw EPI time-series data. Prevailing approaches based on prior knowledge are activation modeling, based on general linear models for task-based acquisitions,[1] and seed-to-voxel or region-of-interest to region-of-interest correlation analyses for task-free acquisitions. In addition, recently more complex graph-theoretic approaches have been derived from the ROI–based methods. Another way of analyzing task-based and task-free studies relies on data-driven approaches such as independent component analyses.[98,104]

Recent further developments in diagnostic MVPA are not solely based on one of these methods. For example, Du et al[55] combined both task- and task-free fMRI in schizophrenia in a small study. Additionally, combinations of fMRI measures with volumetric data,[41,48-50,63,76,78-81,86,89] DTI,[46,49,92] as well as genetics[42] and behavioral data,[40,41,50,76] have been used as features in MVPA analyses. However, results reported so far do not allow verified statements about the benefit of such multimodal acquisitions.

Feature Selection, Classifier Training, and Assessment of Classification Accuracy. Figure 2 and On-line Tables 1 and 2 contain information about the multivariate classification methods in the studies included in this review. They also contain information about whether the selection of potentially decisive features was

based on conventional univariate analyses or whether it was also guided by multivariate information of distributed network patterns.

Apparently there are 2 groups of actual classification methods that have been applied successfully repeatedly: variants of LDA[26,53,59,61,65-67,70,73,79,81,82,94] and support vector machines.[35,36,38,40-49,51,52,54,58,60,62,67-71,74-78,80,81,83-85,88-90,92,93,95-97] Although a certain number of articles report on conceptually different machine-learning techniques[27-34,37,39,41,45,48,50,53-57,62,64,67,70,72,86-88,91] (eg, neural networks[31,39,64,67,70] and decision tree–based approaches[41,50,81,86,87,91]), each has only been applied occasionally, making reliable conclusions about their specific benefits and drawbacks in this context practically impossible.

With a few exceptions,[72,75-78,80,81,86,88,89,95] the small sample sizes in most studies did not allow testing the classification accuracy in datasets completely independent of those used for classifier training. As stated above, a trick makes approximative assessments of classification accuracy of a set of trained classifiers possible: Most studies use CV to show the generalizability of strongly overlapping classifiers to new test data. This means that in most reports only the diagnostic ability of 1 particular set of dependent classifiers[23] is proved. There is usually no formal test that allows conclusions regarding the ability of whole MVPA approaches (acquisition + feature extraction + feature selection + classifier training) to construct successful diagnostic tools in a particular clinical setting because CV is only used to assess classification of new data but not reliable classifier training independent from particular subjects. Additionally, setting up CV loops that do not strictly keep the test set and training set apart is a known source of error, leading to overoptimistic estimates of diagnostic accuracy. There is still some uncertainty regarding the most appropriate test of significance to be applied in the CV setting.[19]

Only a small subset of reports contains systematic comparisons and optimizations of larger sets of classification models used.[49,68,70,75-78,80,81,86,88,89,95]

Potential Clinical Applications and Integration in Diagnostic Workflows

To this point, most studies report applications to distinguish healthy controls and patients with a specific disease. These are a necessary step in developing and accessing diagnostic tools, but is it currently really clinically desirable to strive for such a tool?

In the context of practically illness-defining brain alterations, as in certain kinds of neurodegeneration, MVPA-fMRI methods might compete with radioactive tracer studies in the future. Regarding psychiatric diseases, it seems, for example, desirable to identify patients with a high risk of disease recurrence or progression. Especially in the case of major depressive disorders, there are a number of patients who do not respond to standard pharmacologic treatment; this outcome hints at potentially underlying divergent biologic mechanisms. Prediction of treatment response to a certain group of drugs seems to be a valuable objective as well.[9] To date, some MVPA-fMRI studies have already attempted to classify subjects regarding prognostically relevant subgroups.[36,38,40,46,49,50,52,53,56,58] Another important but overlapping clinical question may be how to distinguish patients with neurobiologically different disease entities but with a similar initial clinical presentation such as unipolar and bipolar depression. Such differential diagnostic aspects have been addressed in a few recent MVPA-fMRI studies as well.[32,39,51,54,57,71,73,75,78,80,81,88,89,94,95]

In this context, specific features of most psychiatric diseases should be taken into account when discussing the results of these analyses: The etiology and progression of disease are complex and only partly attributable to biologic causes. The biopsychosocial model of pathogenesis includes major influences of social and life event–related factors[105,106] that do not necessarily lead to correlates that are approachable by biologic measures such as fMRI.[107] Furthermore, many diagnostically relevant symptoms are, by definition, subjective (eg, depressed mood).[108] The burden of suffering is often decisive in terms of indications for treatment.[109] Therefore, fMRI-MVPA–based measures should not be expected to become the criterion standard in diagnostics and replace in-depth history-taking. The accuracies of the studies reviewed here support this theoretic argument. Still, imaging-based multivariate tools might be able to provide clinically useful additional information: When important information (eg, regarding prognosis) is, by definition, not deducible from the course of disease, these tools might provide the clinician with crucial hints,[7] unraveling the "biologic share" of disease.

In nearly all fMRI-MVPA studies, there was a significant amount of misclassifications (On-line Tables 1 and 2). Partially, they may be attributable to inherent noise in the data and remaining methodologic weaknesses in data analysis. However, misclassification might also be based on biologically and medically meaningful information like the effects of medication[110] and age.[69,85] Sex effects are a much-debated issue in fMRI as well.[111,112] Further investigation of misclassified subjects might even pose a starting point to identify biologically different disease subgroups. Supposedly, a practical problem is that the referring physician and the radiologist cannot easily grasp what leads to a single diagnostic decision by fMRI-MVPA. In comparison with other types of diagnostic imaging, it is therefore not directly possible to appreciate the extent of potentially biasing features in a specific subject. Only 5 recent studies have tried to overcome this issue by introducing individual confidence measures.[39,48,54,56,57]

As seen in Fig 2 and On-line Table 1, MVPA-fMRI has already been applied to a larger number of psychiatric disease entities. For depression,[35,36,38,45,47,48,54,57,68,84] schizophrenia,[26,32-34,37,39,42-44,55,58,61,62,64,66,70,74,90,91,96] and Alzheimer dementia,[26,27,41,50,53,65,71,73,79,82,94] there is now a larger body of independent work.

The diversity of scientific backgrounds of recent studies is reflected by a striking heterogeneity of reported methodologic details, sample characteristics, validation strategies, and performance measures. This heterogeneity limits effort to draw more reliable quantitative conclusions about the clinical benefits of MVPA-fMRI at this stage. More specifically designed studies with a sufficiently high statistical power and confounding factors of a real clinical setting in mind with a more standardized diagnostic end point should be performed to facilitate meta-analytic comparisons in the future. As a stimulus for further debate, we propose reporting standards and standards of study design that, in our opinion, may help overcome some of these issues. They are

Proposed reporting standards for future studies applying multivariate classification techniques to fMRI data with a diagnostic intention in addition to general reporting standards in fMRI research

Proposed Reporting Standards	Desirable Aspects of Study Design
Report of overall classification accuracies/generalization rate (in addition to sensitivity and specificity if applicable)	Sufficiently large, equally sized groups (25 subjects per group desirable, but depending on specific methodologies used and power analyses)
Rigorous statistical tests	Sufficiently long scan duration for resting state fMRI (at least 5 minutes, evaluation of a potential benefit of longer acquisitions desirable)
Report of all tested models (not only optimized/best models)	Systematic model optimization
Clearly identify inferential tests and explorative analyses	Well-chosen and well-defined clinical problem
Clearly identify feature extraction and feature selection/weighting strategies	Multisite/multiscanner studies
Denominate origin of classification algorithms if an independent toolbox is used for pipeline building	Evaluation of functionally/anatomically interpretable classifiers and methods with individual reliability measures
Good clinical characterization of the sample including demographic data (psychometric data if applicable)	Independent validation set

summarized in the Table. Before MVPA-fMRI could be applied in real clinical settings, potential interscanner variability[113] should also be taken into account.

CONCLUSIONS

Approximately 70 studies at the proof-of-principle level that use MVPA of fMRI data with a diagnostic intention have been reported. However, there is wide range of different methodologic decisions, from data-acquisition strategies through preprocessing and feature selection to actual diagnostic classification algorithms and parameter settings and, therefore, a high flexibility in study design. Results reported as yet are mainly based on small sets of subjects. Therefore, one has to be cautious in drawing reliable conclusions on the basis of this literature. Published results may just represent the tip of the iceberg, with a lot more unsuccessful unpublished attempts to apply this methodology. Therefore, there might be an important publication bias, and published results regarding the statistical significance of successful diagnostic classification should be interpreted in the light of a potential need to correct for multiple comparisons.[114] Nevertheless, it can be regarded meanwhile as an independently replicated finding that building on task-based and resting-state fMRI as well support vector machines as LDA approaches has the potential to differentiate patients from healthy subjects in psychiatric disorders with most repeated findings in dementia, schizophrenia, and depression.

In contrast, there is apparently more uncertainty regarding optimal strategies for data preprocessing and feature selection, advisable steps to allow the classification algorithm to work despite a very high dimensionality and noise level of the original data. Many of these methods are derived from conventional fMRI analysis methods. Hardly any effort seems to have been made to systematically compare and evaluate the influence of these different approaches and parameter-setting selections on diagnostic accuracy.

In conclusion, here is some evidence that MVPA-fMRI is promising for overcoming long-known reliability issues in fMRI and providing clinically important prognostic and differential diagnostic information in psychiatric disorders beyond pure exclusion of gross structural alterations. Despite the optimism coming from the recent discussion in the interdisciplinary functional neuroimaging community, this method is still rather new, and work has to be done to validate methodologic choices and identify those specific clinical settings that really allow a beneficial application. Moreover, a conceivable integration of MVPA-based fMRI into clinical workflow will depend critically on tackling diagnostic problems with a real clinical benefit and effects on therapeutic decision-making.

Disclosures: Wolfram Schwindt—*UNRELATED*: payment for manuscript preparation: *RöFo* (Executive Editor).

REFERENCES

1. Huettel SA, Song AW, McCarthy G. *Functional Magnetic Resonance Imaging.* Sunderland, Massachusetts: Sinauer Associates; 2009
2. Zhang D, Raichle ME. **Disease and the brain's dark energy.** *Nat Rev Neurol* 2010;6:15–28
3. Chen CH, Suckling J, Lennox BR, et al. **A quantitative meta-analysis of fMRI studies in bipolar disorder.** *Bipolar Disord* 2011;13:1–15
4. Bartsch AJ, Homola G, Biller A, et al. **Diagnostic functional MRI: illustrated clinical applications and decision-making.** *J Magn Reson Imaging* 2006;23:921–32
5. Pillai JJ. **The evolution of clinical functional imaging during the past 2 decades and its current impact on neurosurgical planning.** *AJNR Am J Neuroradiol* 2010;31:219–25
6. Gruber O. **Neuroimaging markers: their role for differential diagnosis and therapeutic decisions in personalized psychiatry** [in German]. *Nervenarzt* 2011;82:1404, 406, 408
7. Linden DE. **The challenges and promise of neuroimaging in psychiatry.** *Neuron* 2012;73:8–22
8. Oertel-Knöchel V, Bittner RA, Knochel C, et al. **Discovery and development of integrative biological markers for schizophrenia.** *Prog Neurobiol* 2011;95:686–702
9. Mössner R, Mikova O, Koutsilieri E, et al. **Consensus paper of the WFSBP task force on biological markers: biological markers in depression.** *World J Biol Psychiatry* 2007;8:141–74
10. Hampel H, Lista S, Khachaturian ZS. **Development of biomarkers to chart all Alzheimer's disease stages: the royal road to cutting the therapeutic gordian knot.** *Alzheimers Dement* 2012;8:312–36
11. Hyman SE. **Can neuroscience be integrated into the DSM-V?** *Nat Rev Neurosci* 2007;8:725–32
12. de Souza LC, Lehericy S, Dubois B, et al. **Neuroimaging in dementias.** *Curr Opin Psychiatry* 2012;25:473–79
13. Jack CR, Jr. **Alzheimer disease: new concepts on its neurobiology and the clinical role imaging will play.** *Radiology* 2012;263:344–61
14. Mueller S, Wang D, Fox MD, et al. **Individual variability in func-**

tional connectivity architecture of the human brain. *Neuron* 2013;77:586–95
15. Raemaekers M, du Plessis S, Ramsey NF, et al. **Test-retest variability underlying fMRI measurements.** *Neuroimage* 2012;60:717–27
16. Shehzad Z, Kelly AM, Reiss PT, et al. **The resting brain: unconstrained yet reliable.** *Cereb Cortex* 2009;19:2209–29
17. Nichols TE. **Multiple testing corrections, nonparametric methods, and random field theory.** *Neuroimage* 2012;62:811–15
18. Norman KA, Polyn SM, Detre GJ, et al. **Beyond mind-reading: multi-voxel pattern analysis of fMRI data.** *Trends Cogn Sci* 2006;10:424–30
19. Pereira F, Mitchell T, Botvinick M. **Machine learning classifiers and fMRI: a tutorial overview.** *Neuroimage* 2009;45:S199–209
20. Haynes JD, Rees G. **Decoding mental states from brain activity in humans.** *Nat Rev Neurosci* 2006;7:523–34
21. Klöppel S, Abdulkadir A, Jack CR Jr, et al. **Diagnostic neuroimaging across diseases.** *Neuroimage* 2012;61:457–63
22. Orrù G, Pettersson-Yeo W, Marquand AF, et al. **Using support vector machine to identify imaging biomarkers of neurological and psychiatric disease: a critical review.** *Neurosci Biobehav Rev* 2012;36:1140–52
23. Alpaydin E. *Introduction to Machine Learning.* Cambridge, Massachusetts: MIT Press; 2010
24. Vapnik VN. *The Nature of Statistical Learning Theory.* 2nd ed. New York: Springer-Verlag; 2000
25. Derrfuss J, Brass M, von Cramon DY, et al. **Neural activations at the junction of the inferior frontal sulcus and the inferior precentral sulcus: interindividual variability, reliability, and association with sulcal morphology.** *Hum Brain Mapp* 2009;30:299–311
26. Ford J, Farid H, Makedon F, et al. **Patient classification of fMRI activation maps.** In: Ellis R, Peters T, eds. *Medical Image Computing and Computer-Assisted Intervention - MICCAI 2003, Lecture Notes in Computer Science, Vol. 2879.* Berlin, Germany: Springer-Verlag; 2003:58
27. Kontos D, Megalooikonomou V, Pokrajac D, et al. **Extraction of discriminative functional MRI activation patterns and an application to Alzheimer's disease.** In: Barillot C, Haynor DR, Hellier P, eds. *Medical Image Computing and Computer-Assisted Intervention - MICCAI 2004, Lecture Notes in Computer Science, Vol. 3217.* Berlin, Germany: Springer-Verlag. 2004;727–35
28. Bogorodzki P, Rogowska J, Yurgelun-Todd DA. **Structural group classification technique based on regional fMRI BOLD responses.** *IEEE Trans Med Imaging* 2005;24:389–98
29. Zhang L, Samaras D, Tomasi D, et al. **Exploiting temporal information in functional magnetic resonance imaging brain data.** *Med Image Comput Comput Assist Interv* 2005;8:679–87
30. Shinkareva SV, Ombao HC, Sutton BP, et al. **Classification of functional brain images with a spatio-temporal dissimilarity map.** *Neuroimage* 2006;33:63–71
31. Chen R, Herskovits EH. **Clinical diagnosis based on bayesian classification of functional magnetic-resonance data.** *Neuroinformatics* 2007;5:178–88
32. Calhoun VD, Maciejewski PK, Pearlson GD, et al. **Temporal lobe and "default" hemodynamic brain modes discriminate between schizophrenia and bipolar disorder.** *Hum Brain Mapp* 2008;29:1265–75
33. Demirci O, Clark VP, Calhoun VD. **A projection pursuit algorithm to classify individuals using fMRI data: application to schizophrenia.** *Neuroimage* 2008;39:1774–82
34. Demirci O, Clark VP, Magnotta VA, et al. **A review of challenges in the use of fMRI for disease classification/characterization and a projection pursuit application from multi-site fMRI schizophrenia study.** *Brain Imaging Behav* 2008;2:147–226
35. Fu CH, Mourão-Miranda J, Costafreda SG, et al. **Pattern classification of sad facial processing: toward the development of neurobiological markers in depression.** *Biol Psychiatry* 2008;63:656–62
36. Marquand AF, Mourão-Miranda J, Brammer MJ, et al. **Neuroanatomy of verbal working memory as a diagnostic biomarker for depression.** *Neuroreport* 2008;19:1507–11
37. Michael AM, Calhoun VD, Andreasen NC, et al. **A method to classify schizophrenia using inter-task spatial correlations of functional brain images.** *Conf Proc IEEE Eng Med Biol Soc* 2008;2008:5510–13
38. Costafreda SG, Khanna A, Mourão-Miranda J, et al. **Neural correlates of sad faces predict clinical remission to cognitive behavioural therapy in depression.** *Neuroreport* 2009;20:637–41
39. Arribas JI, Calhoun VD, Adali T. **Automatic bayesian classification of healthy controls, bipolar disorder, and schizophrenia using intrinsic connectivity maps from fMRI data.** *IEEE Trans Biomed Eng* 2010;57:2850–60
40. Saur D, Ronneberger O, Kummerer D, et al. **Early functional magnetic resonance imaging activations predict language outcome after stroke.** *Brain* 2010;133:1252–64
41. Tripoliti EE, Fotiadis DI, Argyropoulou M, et al. **A six stage approach for the diagnosis of the Alzheimer's disease based on fMRI data.** *J Biomed Inform* 2010;43:307–20
42. Yang H, Liu J, Sui J, et al. **A hybrid machine learning method for fusing fMRI and genetic data: combining both improves classification of schizophrenia.** *Front Hum Neurosci* 2010;4:192
43. Castro E, Martinez-Ramon M, Pearlson G, et al. **Characterization of groups using composite kernels and multi-source fMRI analysis data: application to schizophrenia.** *Neuroimage* 2011;58:526–36
44. Costafreda SG, Fu CH, Picchioni M, et al. **Pattern of neural responses to verbal fluency shows diagnostic specificity for schizophrenia and bipolar disorder.** *BMC Psychiatry* 2011;11:18
45. Hahn T, Marquand AF, Ehlis AC, et al. **Integrating neurobiological markers of depression.** *Arch Gen Psychiatry* 2011;68:361–68
46. Hoeft F, McCandliss BD, Black JM, et al. **Neural systems predicting long-term outcome in dyslexia.** *Proc Natl Acad Sci U S A* 2011;108:361–66
47. Mourão-Miranda J, Hardoon DR, Hahn T, et al. **Patient classification as an outlier detection problem: an application of the one-class support vector machine.** *Neuroimage* 2011;58:793–804
48. Nouretdinov I, Costafreda SG, Gammerman A, et al. **Machine learning classification with confidence: application of transductive conformal predictors to MRI-based diagnostic and prognostic markers in depression.** *Neuroimage* 2011;56:809–13
49. Rizk-Jackson A, Stoffers D, Sheldon S, et al. **Evaluating imaging biomarkers for neurodegeneration in pre-symptomatic Huntington's disease using machine learning techniques.** *Neuroimage* 2011;56:788–96
50. Tripoliti EE, Fotiadis DI, Argyropoulou M. **A supervised method to assist the diagnosis and monitor progression of Alzheimer's disease using data from an fMRI experiment.** *Artif Intell Med* 2011;53:35–45
51. Weygandt M, Schaefer A, Schienle A, et al. **Diagnosing different binge-eating disorders based on reward-related brain activation patterns.** *Hum Brain Mapp* 2012;33:2135–46
52. Abdulkadir A, Ronneberger O, Wolf RC, et al. **Functional and structural MRI biomarkers to detect pre-clinical neurodegeneration.** *Curr Alzheimer Res* 2013;10:125–34
53. Andersen AH, Rayens WS, Liu Y, et al. **Partial least squares for discrimination in fMRI data.** *Magn Reson Imaging* 2012;30:446–52
54. Grotegerd D, Suslow T, Bauer J, et al. **Discriminating unipolar and bipolar depression by means of fMRI and pattern classification: a pilot study.** *Eur Arch Psychiatry Clin Neurosci* 2013;63:119–31
55. Du W, Calhoun VD, Li H, et al. **High classification accuracy for schizophrenia with rest and task fMRI data.** *Front Hum Neurosci* 2012;6:145
56. Mourão-Miranda J, Oliveira L, Ladouceur CD, et al. **Pattern recognition and functional neuroimaging help to discriminate healthy adolescents at risk for mood disorders from low risk adolescents.** *PLoS One* 2012;7:e29482
57. Mourão-Miranda J, Almeida JR, Hassel S, et al. **Pattern recognition analyses of brain activation elicited by happy and neutral faces in unipolar and bipolar depression.** *Bipolar Disord* 2012;14:451–60
58. Nejad AB, Madsen KH, Ebdrup BH, et al. **Neural markers of negative symptom outcomes in distributed working memory brain activity**

of antipsychotic-naive schizophrenia patients. *Int J Neuropsychopharmacol* 2013;16:1195–204
59. Ramezani M, Abolmaesumi P, Marble K, et al. **Classification of individuals based on sparse representation of brain cognitive patterns: a functional MRI study.** *Conf Proc IEEE Eng Med Biol Soc* 2012;2012:2688–91
60. Weygandt M, Blecker CR, Schafer A, et al. **fMRI pattern recognition in obsessive-compulsive disorder.** *Neuroimage* 2012;60:1186–93
61. Yoon JH, Nguyen DV, McVay LM, et al. **Automated classification of fMRI during cognitive control identifies more severely disorganized subjects with schizophrenia.** *Schizophr Res* 2012;135:28–33
62. Rish I, Cecchi G, Thyreau B, et al. **Schizophrenia as a network disease: disruption of emergent brain function in patients with auditory hallucinations.** *PLoS One* 2013;8:e50625
63. Kim J, Lee JH. **Integration of structural and functional magnetic resonance imaging improves mild cognitive impairment detection.** *Magn Reson Imaging* 2013;31:718–32
64. Jafri MJ, Calhoun VD. **Functional classification of schizophrenia using feed forward neural networks.** *Conf Proc IEEE Eng Med Biol Soc* 2006;(suppl):6631–34
65. Wang K, Jiang T, Liang M, et al. **Discriminative analysis of early Alzheimer's disease based on two intrinsically anti-correlated networks with resting-state fMRI.** *Med Image Comput Comput Assist Interv* 2006;9:340–47
66. Shi F, Liu Y, Jiang T, et al. **Regional homogeneity and anatomical parcellation for fMRI image classification: application to schizophrenia and normal controls.** *Med Image Comput Comput Assist Interv* 2007;10(pt 2):136–43
67. Zhu CZ, Zang YF, Cao QJ, et al. **Fisher discriminative analysis of resting-state brain function for attention-deficit/hyperactivity disorder.** *Neuroimage* 2008;40:110–20
68. Craddock RC, Holtzheimer PE 3rd, Hu XP, et al. **Disease state prediction from resting state functional connectivity.** *Magn Reson Med* 2009;62:1619–28
69. Supekar K, Musen M, Menon V. **Development of large-scale functional brain networks in children.** *PLoS Biol* 2009;7:e1000157
70. Shen H, Wang L, Liu Y, et al. **Discriminative analysis of resting-state functional connectivity patterns of schizophrenia using low dimensional embedding of fMRI.** *Neuroimage* 2010;49:3110–21
71. Zhou J, Greicius MD, Gennatas ED, et al. **Divergent network connectivity changes in behavioural variant frontotemporal dementia and Alzheimer's disease.** *Brain* 2010;133:1352–67
72. Anderson JS, Nielsen JA, Froehlich AL, et al. **Functional connectivity magnetic resonance imaging classification of autism.** *Brain* 2011;134:3742–54
73. Chen G, Ward BD, Xie C, et al. **Classification of Alzheimer disease, mild cognitive impairment, and normal cognitive status with large-scale network analysis based on resting-state functional MR imaging.** *Radiology* 2011;259:213–21
74. Fan Y, Liu Y, Wu H, et al. **Discriminant analysis of functional connectivity patterns on Grassmann manifold.** *Neuroimage* 2011;56:2058–67
75. Brown MR, Sidhu GS, Greiner R, et al. **ADHD-200 global competition: Diagnosing ADHD using personal characteristic data can outperform resting state fMRI measurements.** *Front Syst Neurosci* 2012;6:69
76. Bohland JW, Saperstein S, Pereira F, et al. **Network, anatomical, and non-imaging measures for the prediction of ADHD diagnosis in individual subjects.** *Front Syst Neurosci* 2012;6:78
77. Cheng W, Ji X, Zhang J, et al. **Individual classification of ADHD patients by integrating multiscale neuroimaging markers and advanced pattern recognition techniques.** *Front Syst Neurosci* 2012;6:58
78. Colby JB, Rudie JD, Brown JA, et al. **Insights into multimodal imaging classification of ADHD.** *Front Syst Neurosci* 2012;6:59
79. Dai Z, Yan C, Wang Z, et al. **Discriminative analysis of early Alzheimer's disease using multi-modal imaging and multi-level characterization with multi-classifier (M3).** *Neuroimage* 2012;59:2187–95
80. Dai D, Wang J, Hua J, et al. **Classification of ADHD children through multimodal magnetic resonance imaging.** *Front Syst Neurosci* 2012;6:63
81. Eloyan A, Muschelli J, Nebel MB, et al. **Automated diagnoses of attention deficit hyperactive disorder using magnetic resonance imaging.** *Front Syst Neurosci* 2012;6:61
82. Koch W, Teipel S, Mueller S, et al. **Diagnostic power of default mode network resting state fMRI in the detection of Alzheimer's disease.** *Neurobiol Aging* 2012;33:466–78
83. Long D, Wang J, Xuan M, et al. **Automatic classification of early Parkinson's disease with multi-modal MR imaging.** *PLoS One* 2012;7:e47714
84. Ma Q, Zeng LL, Shen H, et al. **Altered cerebellar-cerebral resting-state functional connectivity reliably identifies major depressive disorder.** *Brain Res* 2013;1495:86–94
85. Meier TB, Desphande AS, Vergun S, et al. **Support vector machine classification and characterization of age-related reorganization of functional brain networks.** *Neuroimage* 2012;60:601–13
86. Olivetti E, Greiner S, Avesani P. **ADHD diagnosis from multiple data sources with batch effects.** *Front Syst Neurosci* 2012;6:70
87. Richiardi J, Gschwind M, Simioni S, et al. **Classifying minimally disabled multiple sclerosis patients from resting state functional connectivity.** *Neuroimage* 2012;62:2021–33
88. Sato JR, Hoexter MQ, Fujita A, et al. **Evaluation of pattern recognition and feature extraction methods in ADHD prediction.** *Front Syst Neurosci* 2012;6:68
89. Sidhu GS, Asgarian N, Greiner R, et al. **Kernel principal component analysis for dimensionality reduction in fMRI-based diagnosis of ADHD.** *Front Syst Neurosci* 2012;6:74
90. Tang Y, Wang L, Cao F, et al. **Identify schizophrenia using resting-state functional connectivity: an exploratory research and analysis.** *Biomed Eng Online* 2012;11:50
91. Venkataraman A, Whitford TJ, Westin CF, et al. **Whole brain resting state functional connectivity abnormalities in schizophrenia.** *Schizophr Res* 2012;139:7–12
92. Wee CY, Yap PT, Zhang D, et al. **Identification of MCI individuals using structural and functional connectivity networks.** *Neuroimage* 2012;59:2045–56
93. Zeng LL, Shen H, Liu L, et al. **Identifying major depression using whole-brain functional connectivity: a multivariate pattern analysis.** *Brain* 2012;135:1498–507
94. Zhang Z, Liu Y, Jiang T, et al. **Altered spontaneous activity in Alzheimer's disease and mild cognitive impairment revealed by regional homogeneity.** *Neuroimage* 2012;59:1429–40
95. Fair DA, Nigg JT, Iyer S, et al. **Distinct neural signatures detected for ADHD subtypes after controlling for micro-movements in resting state functional connectivity MRI data.** *Front Syst Neurosci* 2012;6:80
96. Yu Y, Shen H, Zhang H, et al. **Functional connectivity-based signatures of schizophrenia revealed by multiclass pattern analysis of resting-state fMRI from schizophrenic patients and their healthy siblings.** *Biomed Eng Online* 2013;12:10
97. Zhang D, Liu B, Chen J, et al. **Determination of vascular dementia brain in distinct frequency bands with whole brain functional connectivity patterns.** *PLoS One* 2013;8:e54512
98. van den Heuvel MP, Hulshoff Pol HE. **Exploring the brain network: a review on resting-state fMRI functional connectivity.** *Eur Neuropsychopharmacol* 2010;20:519–34
99. Lee MH, Smyser CD, Shimony JS. **Resting-state fMRI: a review of methods and clinical applications.** *AJNR Am J Neuroradiol* 2013;34:1866–72
100. Fan J, Xu P, Van Dam NT, et al. **Spontaneous brain activity relates to autonomic arousal.** *J Neurosci* 2012;32:11176–86
101. De Havas JA, Parimal S, Soon CS, et al. **Sleep deprivation reduces default mode network connectivity and anti-correlation during rest and task performance.** *Neuroimage* 2012;59:1745–51
102. Van Dijk KR, Hedden T, Venkataraman A, et al. **Intrinsic func-**

tional connectivity as a tool for human connectomics: theory, properties, and optimization. *J Neurophysiol* 2010;103:297–321
103. Anderson JS, Ferguson MA, Lopez-Larson M, et al. **Reproducibility of single-subject functional connectivity measurements.** *AJNR Am J Neuroradiol* 2011;32:548–55
104. Margulies DS, Bottger J, Long X, et al. **Resting developments: a review of fMRI post-processing methodologies for spontaneous brain activity.** *MAGMA* 2010;23:289–307
105. Adler RH. **Engel's biopsychosocial model is still relevant today.** *J Psychosom Res* 2009;67:607–11
106. Engel GL. **The need for a new medical model: a challenge for biomedicine.** *Science* 1977;196:129–36
107. Smith RC, Fortin AH, Dwamena F, et al. **An evidence-based patient-centered method makes the biopsychosocial model scientific.** *Patient Educ Couns* 2013;91:265–70
108. Fuchs T. **Subjectivity and intersubjectivity in psychiatric diagnosis.** *Psychopathology* 2010;43:268–74
109. Büchi S, Sensky T, Sharpe L, et al. **Graphic representation of illness: a novel method of measuring patients' perceptions of the impact of illness.** *Psychother Psychosom* 1998;67:222–25
110. Marquand AF, De Simoni S, O'Daly OG, et al. **Pattern classification of working memory networks reveals differential effects of methylphenidate, atomoxetine, and placebo in healthy volunteers.** *Neuropsychopharmacology* 2011;36:1237–47
111. Biswal BB, Mennes M, Zuo XN, et al. **Toward discovery science of human brain function.** *Proc Natl Acad Sci U S A* 2010;107:4734–39
112. Gong G, He Y, Evans AC. **Brain connectivity: gender makes a difference.** *Neuroscientist* 2011;17:575–91
113. Friedman L, Glover GH, Krenz D, et al. **Reducing inter-scanner variability of activation in a multicenter fMRI study: role of smoothness equalization.** *Neuroimage* 2006;32:1656–68
114. Ioannidis JP. **Why most published research findings are false.** *PLoS Med* 2005;2:e124

Safety of Unilateral Endovascular Occlusion of the Cervical Segment of the Vertebral Artery without Antecedent Balloon Test Occlusion

G.H. Zoarski and R. Seth

ABSTRACT

BACKGROUND AND PURPOSE: Antecedent balloon test occlusion is often performed prior to vertebral artery sacrifice, but there is limited data to suggest this adds a significant clinical benefit, especially in the setting of trauma. Furthermore, balloon test occlusion can be time-consuming, add to the technical complexity of the procedure, and increase the overall cost of treatment. The purpose of this study was to determine the safety of unilateral vertebral artery occlusion without antecedent balloon test occlusion as part of the treatment regimen in patients with traumatic vertebral artery dissection, cervical tumor, or intracranial aneurysm.

MATERIALS AND METHODS: The medical records and imaging studies of 59 patients in whom unilateral endovascular cervical vertebral artery occlusion was performed were retrospectively reviewed. Procedure-related stroke was defined as imaging evidence of acute infarct in the vascular territories supplied by the occluded vertebral artery or new focal neurologic deficit developing in the first 30 days after vertebral artery occlusion attributable to infarction in the posterior circulation.

RESULTS: Fifty-nine patients underwent unilateral endovascular cervical vertebral artery occlusion to prevent potential thromboembolic complications of vertebral artery injury, for treatment of intracranial aneurysms, or for presurgical embolization of a cervical vertebral tumor. Unilateral occlusion was performed when endovascular reconstruction was considered impossible or deemed more risky than deconstruction. Fifty-eight of the 59 patients underwent vertebral artery occlusion without antecedent balloon test occlusion. None of the 59 patients had clinical or imaging evidence of a postprocedural infarct.

CONCLUSIONS: In this series, endovascular occlusion of a cervical segment of 1 vertebral artery was safely performed without antecedent balloon test occlusion. As long as both vertebral arteries were patent and converged at the vertebrobasilar junction, there was anatomic potential for retrograde filling of the distal intracranial vertebral artery to the level of the posterior inferior cerebellar artery origin, and there was no major vascular supply to the spinal cord arising from the target segment of the affected vessel. Dominant and nondominant vertebral arteries were safely occluded, and no infarcts were attributed to the treatment.

ABBREVIATIONS: BTO = balloon test occlusion; VA = vertebral artery

In most individuals, the basilar artery benefits from dual arterial inflow from the vertebral arteries (VAs). A rich cervical collateral network may further augment posterior circulation flow to a variable degree. This anatomic configuration is extremely effective in protecting the brain stem from ischemia in unilateral vertebral artery injury and allows therapeutic occlusion of the cervical segment of one of the vertebral arteries in most patients.

Received April 30, 2013; accepted after revision October 11.

From the Department of Neurointerventional Surgery (G.H.Z.), Christiana Care Health System, Newark, Delaware; and Department of Neuroradiology (R.S.), Radiology Associates of North Texas, Fort Worth, Texas.

Please address correspondence to Gregg H. Zoarski, MD, Neurointerventional Surgery, Christiana Care Health System, 4755 Ogletown-Stanton Rd, Suite 1E10, Newark, DE 19718; e-mail: gzoarski@gmail.com

http://dx.doi.org/10.3174/ajnr.A3885

Asymptomatic occlusion of the cervical vertebral artery, particularly at the level of its origin from the subclavian artery, is not unusual in patients with severe atherosclerosis. In many such cases, segmental cervical collaterals effectively reconstitute the vertebral artery below the level of the skull base. These collateral vessels often arise from muscular branches of the vertebral artery, the ascending cervical branch of the thyrocervical trunk, or the deep cervical branch of the costocervical trunk (Fig 1). Furthermore, segmental spinal arteries and the normal confluence of both vertebral arteries provide a rich collateral supply to the posterior fossa.

Due to the theoretic potential for significant morbidity from posterior circulation ischemia, intentional occlusion of even a severely compromised vertebral artery is undertaken with abundant concern for patient safety. There is little evidence that antecedent balloon test occlusion (BTO) of 1 vertebral artery is nec-

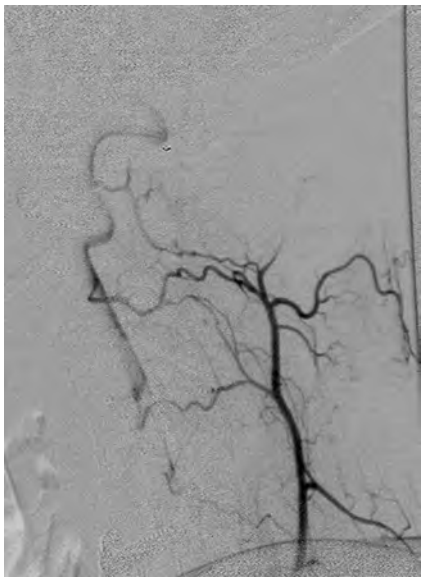

FIG 1. A 24-year-old man with C6–C7 fracture dislocation, spinal cord injury, and traumatic occlusion of the left vertebral artery following a motor vehicle collision. DSA of the left costocervical trunk demonstrates distal reconstitution of the occluded midcervical left VA from the posterior deep cervical branch of the costocervical trunk. The left VA is occluded proximally.

essary, or even reliable, in predicting ischemic deficits.[1,2] Additionally, balloon test occlusion can be time-consuming, add to the technical complexity of the procedure, and increase the overall cost of treatment. There are limited data to suggest that performing a BTO before vertebral artery sacrifice adds clinical benefit, especially in the setting of trauma, where patients are often intubated and sedated. To our knowledge, a large series of patients undergoing unilateral endovascular vertebral artery occlusion without antecedent BTO has not been previously published.

In a retrospective review of 28 treated dissecting vertebrobasilar aneurysms by Rabinov et al,[3] 7 of the 28 treated patients underwent an antecedent BTO. The authors speculated that "BTO may be of benefit to determine if the collateral circulation is limited anatomically or compromised by vasospasm," but provided no data to suggest that BTO changed management in any patients or led to improved outcome in the group that underwent BTO. A separate surgical report of 15 patients describes vertebral artery ligation before cervical tumor resection without antecedent BTO, performed only if the contralateral vertebral artery was larger or equal in diameter to the sacrificed vessel. No cases of cerebral or spinal cord ischemia were reported in this study.[4] Given this information and our own personal experience, we believe that unilateral therapeutic occlusion of a cervical vertebral artery is safe as long as the contralateral vertebral artery is patent to the level of the vertebrobasilar junction and there is no angiographic evidence of vascular supply to the spinal cord arising from the target segment of the affected vessel.

The purpose of this study was to review our experience in therapeutic occlusion of the cervical vertebral artery in the setting of traumatic injury, as part of distal vertebrobasilar aneurysm treatment, or to facilitate surgical resection of adjacent cervical tumors. Our rationale for therapeutic occlusion in the setting of VA injury was based on the belief that sudden recanalization of an occluded vertebral artery could result in thromboembolism and consequent stroke. However, the actual likelihood and incidence of such embolic events are unknown, and intentional vertebral artery occlusion should, therefore, only be performed if the risk of the procedure is determined to be small. Furthermore, we performed vertebral artery occlusion only when endovascular reconstruction was considered impossible or deemed more risky than deconstruction.

MATERIALS AND METHODS

Patients

The clinical records and imaging studies of 59 patients treated with unilateral endovascular vertebral artery occlusion between 1991 and 2006 were retrospectively reviewed following approval by our institutional review board. Patient clinical information was logged into a data base, and conventional and CT angiographic imaging was reviewed. Variables recorded included clinical presentation, diameter of the bilateral vertebral arteries, side of vertebral artery occlusion, endovascular techniques used, and the angiographic and clinical outcomes of treatment.

Occlusion Techniques

In most cases ($n = 55$), coils were used to achieve vertebral artery occlusion. Balloons, silk suture, or a combination of these devices were used for occlusion in the remaining 4 patients.

A successful BTO was performed before permanent occlusion in a single patient. In the remaining 58 patients, permanent vertebral artery occlusion was performed without BTO. The affected vertebral artery was only occluded when confluence of both vertebral arteries at the level of the vertebrobasilar junction was confirmed and the anatomic potential for retrograde filling of the vertebral artery down to the level of the posterior inferior cerebellar artery origin on the affected side was firmly established (Fig 2*B*). The potential for PICA filling was defined either by identification of antegrade opacification of the bilateral V4 segments and basilar artery, with or without opacification of the PICA on the affected side, or by retrograde opacification of the entire V4 segment of the affected vertebral artery on contralateral VA injection. Opacification of the PICA on the affected side was not necessary because opacification of the V4 segment of the affected vertebral artery suggested that the PICA would fill after ipsilateral vertebral artery occlusion.

Dominance of the affected vertebral artery or the presence or size of the posterior communicating arteries did not affect the decision to perform the occlusion. In many cases, the dominant vertebral artery was already completely or near completely occluded, or the need for occlusion of the dominant vertebral artery was clinically imperative. In cases of complete occlusion of the vertebral artery secondary to traumatic injury, coil embolization of the occluded stump (Fig 2*C*) was performed to prevent emboli in case of spontaneous recanalization.

In 55 patients, the vertebral artery was occluded only proximal to the site of injury. Arteriovenous fistulas were identified in 4 patients, and occlusion was performed both proximal and distal to the site of injury to eliminate arteriovenous flow in these 4 patients.

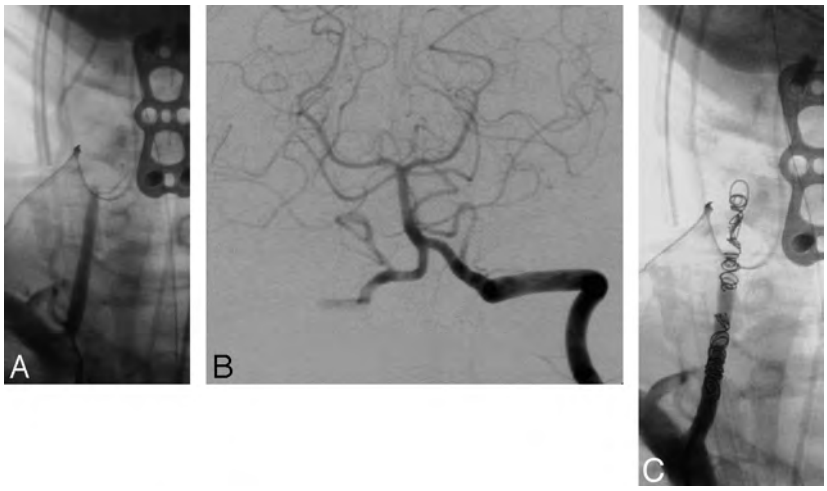

FIG 2. A 35-year-old man with a C5 burst fracture, right vertebral artery occlusion, and spinal cord injury following a motor vehicle collision. *A*, Anteroposterior digital subtraction angiography of the right vertebral artery shows occlusion at the level of C5 before endovascular treatment. *B*, Anteroposterior DSA of the intracranial left vertebral artery demonstrates backfilling of the occluded right vertebral artery down to the level of the right posterior inferior cerebellar artery. *C*, Anteroposterior angiographic image demonstrates occlusion of the right vertebral artery stump secured with fibered coils to avoid emboli in spontaneous recanalization.

When surgical comorbidities permitted, postprocedural systemic anticoagulation was administered to achieve a partial thromboplastin time of 40–50 seconds; and if clinically feasible, patients received antithrombotic treatment with aspirin, 81 or 325 mg for 90 days following endovascular occlusion.

Follow-Up

Follow-up CT or MR imaging of the brain was performed within 48 hours after treatment in all patients. Procedure-related stroke was defined as CT or MR imaging evidence of an acute infarct in the cerebral, cerebellar, or spinal cord vascular territories supplied by the occluded vertebral artery or a new focal neurologic deficit developing in the first 30 days after vertebral artery occlusion attributable to infarction in the posterior circulation.

RESULTS

Fifty-nine patients treated with endovascular unilateral vertebral artery occlusion between 1991 and 2006 were identified. Forty-four (74.6%) patients were male, and 15 (25.4%) were female. Patient age ranged from 14 to 73 years, with a mean age of 35.5 years.

Twenty-nine of 59 patients were treated due to traumatic vascular injury of the vertebral artery secondary to deceleration injury sustained during a motor vehicle collision or fall. Twenty-one patients were treated for penetrating trauma, most commonly gunshot wounds or stab injuries. Four patients were treated for vertebral artery injury during a surgical procedure or line placement. Unilateral vertebral artery occlusion was undertaken in the setting of vertebral artery injury with flow-limiting stenosis (>70%) in patients who were not candidates for traditional therapy of systemic anticoagulation or in cases in which intraluminal thrombus created concern for spontaneous embolization. In all cases, the contralateral vertebral artery was patent and without evidence of intimal injury. In 2 patients, proximal occlusion of a unilateral cervical vertebral artery was performed as part of the treatment plan for a distal aneurysm. In 3 cases, cervical vertebral artery occlusion was performed before surgical resection of tumors of the cervical vertebrae.

Fifty-eight (98.3%) of the 59 patients underwent vertebral artery occlusion without antecedent BTO. In 33 (55.9%) of 59 cases, the left vertebral artery was treated with endovascular occlusion; the right vertebral artery was treated in the remaining 26 (44.1%). Vascular measurements of the cervical vertebral artery were made on conventional angiographic or CT angiographic images in 35 (59.3%) of the 59 cases. Of these 35 cases, the dominant or codominant vertebral artery was treated in 29 (82.9%) patients, while the nondominant vertebral artery was treated in 6 (17.1%).

Complete angiographic occlusion of the target segment of the treated vertebral artery was achieved in all cases. Contralateral vertebral artery angiography after vessel occlusion demonstrated retrograde opacification of the intracranial V4 segment of the occluded vertebral artery in all cases. Of the 59 patients treated, none had a stroke attributed to intentional vertebral artery occlusion, and there were no instances of delayed ischemic events attributable to stump emboli or target vessel recanalization.

DISCUSSION

Safety of Unilateral Vertebral Artery Occlusion

Surgical ligation and endovascular deconstruction or segmental occlusion of the vertebral artery has long been used to facilitate resection of cervical spinal tumors and treat difficult intracranial aneurysms.[1,4-6] In some cases, surgical or endovascular vessel sacrifice can obviate complex skull base surgery. Dissecting aneurysms of the intracranial vertebral artery are particularly difficult to reconstruct surgically and have been treated successfully with proximal vertebral artery or endovascular segmental occlusion of the affected vessel.[7-10] Untreated, these lesions carry an inherent high risk of subarachnoid hemorrhage. Furthermore, untreated ruptured dissecting aneurysms have a high propensity for rehemorrhage, with rates ranging from 30% to 70%.[11,12]

Previous authors have demonstrated the feasibility and success of surgical or endovascular occlusion of the intracranial vertebral artery with low rates of ischemic or thromboembolic complications.[4,13] The favorable safety profile demonstrated in our study of 59 patients is consistent with these studies as well as a recent report by Kansagra et al,[14] in which 100 traumatic arterial cervicocerebral vascular injuries were endovascularly treated with a low rate of immediate or delayed neurovascular complications.

The potential adverse consequences of ligation of the vertebral artery are not insignificant. Symptoms of vertebrobasilar stroke include vertigo, nausea, vomiting, headache, visual field deficit, diplopia, pupillary abnormalities, ophthalmoplegia, agnosia, and alexia without agraphia. More significant deficits such as facial paralysis, dysarthria, sudden deafness, lower cranial nerve defi-

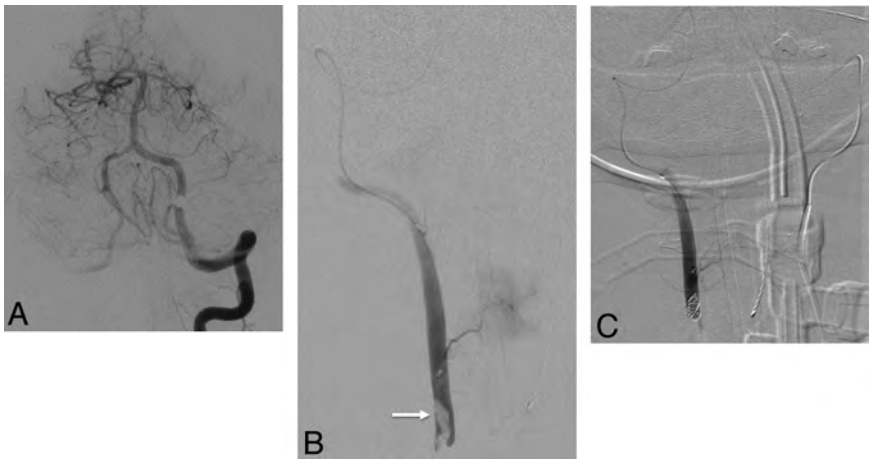

FIG 3. A 45-year-old man with fracture and diastasis of the right C4–C5 facet joint, with fracture extending through the right C5 transverse foramen, following a motorcycle collision. *A*, Anteropostior DSA of the left VA shows retrograde flow down the distal right VA due to proximal occlusion. *B*, A microcatheter was passed from the left VA to the vertebrobasilar junction, and retrograde microcatheterization of the right VA was performed. Hand-injection DSA demonstrates thrombus (*arrow*) in the lumen. *C*, Anteroposterior DSA with injection of the microcatheter following placement of coils above the thrombus to prevent embolization.

cits, altered awareness, Wallenberg syndrome, or Foville syndrome may also occur.[15,16]

Endovascular Occlusion

Demonstration of the confluence of both vertebral arteries at the level of the vertebral junction and the anatomic potential for retrograde filling of the PICA on the affected side was paramount in establishing the feasibility of unilateral therapeutic vertebral artery occlusion. Dominance of the affected vertebral artery did not affect our decision to perform the occlusion when the need for occlusion of the affected vertebral artery was clinically imperative. When the dominant vertebral artery was already occluded or near-occluded, intact neurologic examination findings demonstrated that the patient was already tolerating a functional test occlusion. In fact, it was our observation of several neurologically intact patients who presented with acute traumatic occlusion of the dominant vertebral artery that led us to believe that therapeutic occlusion of even the dominant vertebral artery could be performed safely on the basis of anatomic criteria without antecedent balloon test occlusion.

Preservation of flow into the PICA on the affected side is an essential component of therapy. Unlike reports describing endovascular treatment of dissecting intracranial vertebral artery aneurysms, most therapeutic occlusions in our series were performed for vertebral artery pathology located several cervical vertebral segments proximal to the origin of the PICA. In some cases, collaterals distal to the site of pathology already reconstituted the distal cervical vertebral artery and filled the PICA in an antegrade fashion before proximal or segmental vertebral artery occlusion. Without such cervical collaterals, the ipsilateral PICA was typically opacified by retrograde flow from the vertebrobasilar junction even before vertebral artery occlusion.

In the setting of a severe vascular injury, such as vertebral artery fistula or frank extravasation, proximal occlusion of the vertebral artery alone is insufficient treatment because the lesion will continue to derive flow from the patent distal cervical vertebral artery in retrograde fashion. Occlusion both proximal and distal to the lesion must be secured in such cases. In many instances, it is possible to advance a catheter or microcatheter beyond the level of the lesion in antegrade fashion to perform an initial distal occlusion. Proceeding in retrograde fashion, one can use coils, glue, particles, or balloons to occlude the vertebral artery at and below the level of the pathology.[17] In the case of a fistula or frank extravasation, embolic materials may also be placed outside the arterial lumen, as long as sufficient care is taken to avoid venous migration. When the proximal segment of the affected vertebral artery is already completely or near-completely occluded, coils can be placed distal to the level of injury by navigating a microcatheter through the contralateral vertebral artery, across the vertebrobasilar junction, and retrograde to the level of vascular injury (Fig 3).[18]

Regardless of the level or degree of vertebral artery pathology, the technique of occlusion must be designed to maintain the patency of the PICA origin and the vertebral artery contribution to the anterior spinal artery on the treatment side. Reconstruction of the injured segment should always be considered before vertebral artery occlusion, especially when the injured vessel is markedly dominant. However, neurologic sequelae from unilateral vertebral artery occlusion are unlikely in the presence of a normal contralateral vessel and in the absence of angiographic demonstration of branches to the spinal cord.[19]

Vertebral Artery Balloon Test Occlusion

While it is tempting to believe that balloon test occlusion of a vertebral artery may predict the possibility of posterior circulation stroke after permanent vertebral artery occlusion, the utility of vertebral artery balloon test occlusion has only been reported in small series,[1,2] none of which attest to the reliability or validity of vertebral artery test occlusion in predicting subsequent stroke after permanent vertebral artery occlusion. While it is clearly evident that a failed test occlusion predicts a poor outcome after permanent occlusion, there are no quantitative data to suggest that the converse is true and that passing a BTO before permanent vertebral artery occlusion diminishes the risk of subsequent posterior circulation stroke. Nevertheless, several authors prudently recommend that balloon test occlusion be performed before permanent occlusion in certain circumstances, including a contralateral vertebral artery that does not communicate with the vertebrobasilar junction, the presence of a markedly hypoplastic contralateral vertebral artery, or anticipated occlusion of a strongly dominant vertebral artery.

In a series of 23 patients with dissecting aneurysms of the vertebral artery, Albuquerque et al[13] suggested that "dominance of the affected artery complicates the treatment paradigm. In such cases, balloon test occlusion is helpful in assessing the risk of

stroke after vessel sacrifice." Only anecdotal references are provided to support this recommendation, and balloon test occlusion was only performed in a single patient in whom the affected artery was dominant. Hoshino et al[4] reported a series of 15 patients in whom no ischemic complications were demonstrated following ligation of the nondominant or codominant cervical vertebral artery. Although the authors suggested that angiographic test occlusion of the involved vertebral artery should be performed before permanent occlusion, only anecdotal support was provided for this recommendation. In their series, BTO was performed in a single patient who had a single vertebral artery, and the patient predictably became symptomatic during the BTO procedure.[4]

Luo et al[20] treated 10 patients with spontaneously ruptured vertebral dissecting aneurysms and proposed that sudden occlusion of the vertebral artery carries a risk of ischemia "particularly in patients who have a hypoplastic contralateral vertebral artery," and that "balloon occlusion test (BOT) is essential to determine the adequacy of collateral circulation from the contralateral vertebral artery or posterior communicating arteries." This determination was made despite any substantial evidence; however, the authors concede that "although BOT in the vertebrobasilar system is less effective in predicting future ischemia, it can indicate the extent of collateral circulation in the vertebrobasilar system." Similarly, Rabinov et al[3] described 26 patients with intracranial vertebrobasilar dissecting aneurysms who were treated by endovascular techniques. Although only 7 patients were evaluated with preprocedural BTO and no patients were reported to have failed BTO, the authors concluded that "BTO may be of benefit to determine if the collateral circulation is limited anatomically or compromised by vasospasm."[3] Despite the cautionary statements found in these articles, there are no published reports, to our knowledge, of a patient failing to tolerate vertebral BTO when the contralateral vertebral artery was documented to be patent to the level of the vertebrobasilar junction.

On the other hand, the literature demonstrates that patients who tolerate BTO of a unilateral vertebral artery may nevertheless experience ischemia and infarction after permanent vertebral artery occlusion. Sorteberg et al[2] have demonstrated the use of transcranial Doppler sonography to evaluate blood velocity and blood flow direction in the P1 segments during BTO to rapidly predict hemodynamic outcome at a risk comparable with that of conventional neuroangiography. Reversal of flow in the P1 segment following balloon inflation suggested that the patient was likely to tolerate permanent occlusion of the affected vertebral artery. Although all 7 patients who underwent unilateral VA BTO with transcranial Doppler in their study passed the test occlusion, a single patient developed Brown-Sequard syndrome due to medullary infarction after subsequent permanent occlusion of the intracranial VA just proximal to the origin of the PICA. The authors stated that spinal medullary branches may be too small to visualize during angiography and BTO cannot reliably exclude the risk of occlusion of a spinal medullary branch.[2] However, infarction in this case occurred subsequent to occlusion of the intracranial segment of the vertebral artery, where the potential for segmental cervical muscular collaterals to reconstitute the distal vertebral artery is absent. Delayed ischemic events, despite uneventful balloon test occlusion, have been described by other authors and may be related to hypoperfusion not predicted by BTO.[1]

Overall, BTO does not enhance the safety of subsequent occlusion of a unilateral vertebral artery, regardless of the reason or vessel size, if there is anatomic potential for filling of the ipsilateral PICA and there is no major vascular supply to the spinal cord arising from the target segment of the affected vessel.

Alternative Treatment Strategies/Conservative Therapy

Despite the lack of complications in our series, traditional alternatives to vertebral artery occlusion, such as systemic anticoagulation or antiplatelet therapy, are adequate treatment in many patients.[21-23] Biffl et al[24] reviewed the presentation, treatment, and outcome of 38 patients presenting with 47 blunt vertebral artery injuries during a 3.5-year period. The incidence of posterior circulation stroke was 24%, and death attributable to vertebral artery injury was 8%. They determined that systemic heparin therapy was effective in preventing stroke, neurologic deterioration, and progression to higher injury grade in patients both with and without established stroke. Additionally, dominance of the affected vertebral artery, the presence of bilateral injuries, or the initial injury grade did not appear to influence the incidence of stroke. While it has been speculated that nonocclusive injuries may be more dangerous than complete occlusions, this possibility was also not supported by their findings. The authors cautioned that anticoagulation may have resulted in complications, including hemorrhagic infarction; however, the overall benefit of systemic heparin therapy outweighed these potential complications. At our own institution, we evolved toward earlier and more frequent use of oral antiplatelet agents in patients with traumatic vascular injury in the absence of embolic sequelae. However, anticoagulation and antiplatelet therapies are not entirely benign and may still leave the patient at risk for thromboembolic events. Serious or fatal bleeding may occur, especially with multisystem trauma, and may be difficult or impossible to control.

CONCLUSIONS

Endovascular occlusion of the cervical segment of 1 vertebral artery can be safely performed without antecedent BTO as long as both vertebral arteries are patent and converge at the vertebrobasilar junction, there is anatomic potential for retrograde filling of the distal intracranial vertebral artery down to the level of the PICA origin, and there is no vascular supply to the spinal cord arising from the target segment of the affected vessel. Nondominant and dominant vertebral arteries were safely occluded following careful angiographic evaluation of posterior circulation anatomy in our series, and no infarcts were attributed to the treatment. We routinely perform unilateral cervical vertebral artery occlusion without prior balloon test occlusion in these circumstances, regardless of vertebral artery dominance, when endovascular reconstruction is considered impossible or deemed more risky than deconstruction.

REFERENCES

1. Graves VB, Perl J 2nd, Strother CM, et al. **Endovascular occlusion of the carotid or vertebral artery with temporary proximal flow**

arrest and microcoils: clinical results. *AJNR Am J Neuroradiol* 1997;18:1201–06
2. Sorteberg A, Bakke SJ, Boysen M, et al. **Angiographic balloon test occlusion and therapeutic sacrifice of major arteries to the brain.** *Neurosurgery* 2008;63:651–60
3. Rabinov JD, Hellinger FR, Morris PP, et al. **Endovascular management of vertebrobasilar dissecting aneurysms.** *AJNR Am J Neuroradiol* 2003;24:1421–28
4. Hoshino Y, Kurokawa T, Nakamura K, et al. **A report on the safety of unilateral vertebral artery ligation during cervical spine surgery.** *Spine* 1996;21:1454–57
5. Drake CG. **Ligation of the vertebral (unilateral or bilateral) or basilar artery in the treatment of large intracranial aneurysms.** *J Neurosurg* 1975;43:255–74
6. Barr JD, Lemley TJ. **Endovascular arterial occlusion accomplished using microcoils deployed with and without proximal flow arrest: results in 19 patients.** *AJNR Am J Neuroradiol* 1999;20:1452–56
7. Tanaka K, Waga S, Kojima T, et al. **Non-traumatic dissecting aneurysms of the intracranial vertebral artery: report of six cases.** *Acta Neurochir (Wien)* 1989;100:62–66
8. Iihara K, Sakai N, Murao K, et al. **Dissecting aneurysms of the vertebral artery: a management strategy.** *J Neurosurg* 2002;97:259–67
9. Leibowitz R, Do HM, Marcellus ML, et al. **Parent vessel occlusion for vertebrobasilar fusiform and dissecting aneurysms.** *AJNR Am J Neuroradiol* 2003;24:902–07
10. Halbach VV, Higashida RT, Dowd CF, et al. **Endovascular treatment of vertebral artery dissections and pseudoaneurysms.** *J Neurosurg* 1993;79:183–91
11. Aoki N, Sakai T. **Rebleeding from intracranial dissecting aneurysm in the vertebral artery.** *Stroke* 1990;21:1628–31
12. Mizutani T, Aruga T, Kirino T, et al. **Recurrent subarachnoid hemorrhage from untreated ruptured vertebrobasilar dissecting aneurysms.** *Neurosurgery* 1995;36:905–11, discussion 912–13
13. Albuquerque FC, Fiorella DJ, Han PP, et al. **Endovascular management of intracranial vertebral artery dissecting aneurysms.** *Neurosurg Focus* 2005;18:E3
14. Kansagra AP, Cooke DL, English JD, et al. **Current trends in endovascular management of traumatic cerebrovascular injury.** *J Neurointerv Surg* 2014;6:47–50
15. Shintani A, Zervas NT. **Consequence of ligation of the vertebral artery.** *J Neurosurg* 1972;36:447–50
16. Nakaso K, Nakayasu H, Isoe K, et al. **A case of dissecting aneurysm of the basilar artery presenting as a superior pons type of Foville syndrome** [in Japanese]. *Rinsho Shinkeigaku* 1995;35:1040–43
17. Herrera DA, Vargas SA, Dublin AB. **Endovascular treatment of traumatic injuries of the vertebral artery.** *AJNR Am J Neuroradiol* 2008;29:1585–89
18. Ji KY, Ahn JY, Song WS, et al. **Endovascular treatment for a penetrating vertebral artery injury.** *J Korean Neurosurg Soc* 2002;32:578–81
19. Golueke P, Sclafani S, Phillips T, et al. **Vertebral artery injury: diagnosis and management.** *J Trauma* 1987;27:856–65
20. Luo CB, Chang CY, Teng MM, et al. **Endovascular treatment of ruptured vertebral dissecting aneurysms with electrodetachable coils.** *J Chin Med Assoc* 2005;68:578–84
21. Cimini N, D'Andrea P, Gentile M, et al. **Cervical artery dissection: a 5-year prospective study in the Belluno district.** *Eur Neurol* 2004;52:207–10
22. Cervical Artery Dissection in Stroke Study Trial Investigators. **Antiplatelet therapy vs. anticoagulation in cervical artery dissection: rationale and design of the Cervical Artery Dissection in Stroke Study (CADISS).** *Int J Stroke* 2007;2:292–96
23. Menon R, Kerry S, Norris JW, et al. **Treatment of cervical artery dissection: a systematic review and meta-analysis.** *J Neurol Neurosurg Psychiatry* 2008;79:1122–27
24. Biffl WL, Moore EE, Elliott JP, et al. **The devastating potential of blunt vertebral arterial injuries.** *Ann Surg* 2000;231:672–81

Balloon Occlusion Tests and Therapeutic Vessel Occlusions Revisited: When, When Not, and How

The concept of therapeutic occlusion of arteries to and in the brain is old, with Cooper describing a carotid artery ligation performed in 1805,[1] and Matas, a vertebral artery sacrifice in 1893.[2] The potentially deleterious effect of losing a carotid artery was even known in ancient Greece, because they named this artery "karos," meaning to stupefy or plunge into deep sleep. Leonardo da Vinci (1452–1519) described the vessels of the neck and suggested that compression of the carotid artery, which at that time usually was called the "soporal artery," could rapidly lead to unconsciousness. Unselected carotid artery sacrifice without revascularization will lead to potentially lethal cerebral infarction in about two-thirds of individuals. Sacrifice or damage to the vertebral artery was earlier considered a "no man's land" as reflected in the citation by Sanson from 1836: "The vertebral artery cannot be ligated, on account of its great depth, nor compressed, because of the osseous canal which protects it; it can still less be cauterized. The wounds of this vessel are beyond the resources of art" (cited in Matas[2]).

The apprehension of the risk of therapeutic artery sacrifice has urged preprocedural risk evaluations, which, since Serbinenko's invention of balloon catheters in the early 70s,[3] usually are performed by angiographic balloon test occlusion (BTO). BTO with clinical surveillance considerably reduced the incidence of postoperative stroke compared with unselected carotid artery sacrifice but still carries a 5%–40% stroke rate.[4,5] In an attempt to enhance the prognostic validity of a BTO with clinical surveillance, a large battery of adjuvant assessments evolved. These include hypotensive challenges, stump pressure measurements, electroencephalography and evoked potentials monitoring, cerebral oximetry by using near-infrared spectroscopy, blood velocity measurements applying transcranial Doppler ultrasonography (TCD), evaluation of cerebral blood flow with technetium Tc99m hexamethylpropyleneamine oxime single-photon emission CT, positron-emission tomography, xenon-enhanced CT, and/or MR perfusion imaging.

This vast diversity of BTO protocols reflects the lack of a consensus as to a specified method clearly superior to others. This may be due to the persisting significant number of failures to predict hemodynamic stroke at carotid artery sacrifice, despite advanced but not necessarily adequate protocols. For instance, relative changes in CBF comparing the occluded with the nonoccluded hemisphere (qualitative evaluation) may introduce an error due to the nonoccluded side undergoing changes in CBF during the BTO as well (ie, the contralateral hemisphere cannot be used as a constant reference). Hence, up to 20% of patients may not tolerate ICA sacrifice, even though having symmetric BTO scan findings.[6-8] Quantitative CBF analysis during BTO using xenon-enhanced CT lowers the rate of false-negative BTO findings but they still remain between 3% and 10%.[5,9,10]

In addition to the imperfection of the predictive value of many BTO protocols, there is a procedural risk of 3%–4% in performing a BTO,[11-13] which needs to be addressed. Many complications are related to intimal damage, potentially resulting in arterial dissection and/or pseudoaneurysm formation and consecutive thromboembolism.[12] A common factor for most carotid artery BTO protocols is occlusion times ranging from 15 to 30 minutes along with the need for transporting the patient, with catheters in place, to a different suite. The rate of complications increases with the length of the angiographic procedure[12] or, in other words, the longer the BTO occlusion time, the higher the procedural risk.

In light of this reality, there is actually no good reason to still perform prolonged carotid artery occlusion tests because there are very swift BTO methods requiring no more than 60–90 seconds of occlusion time: The venous phase BTO,[14,15] with or without ultraswift TCD evaluation,[16] hence carries a very low procedural risk (0%–0.7%) (ie, it does not exceed the risk of diagnostic cerebral angiography per se). In addition, the positive predictive value of the latter method of BTO, ranging from 98% to 100%, is unsurpassed by any other protocol. Being nonclinical, this type of BTO does not lose any of its high predictive value when performed with the patient under general anesthesia. Venous phase BTO requires bilateral catheterization, but an increase in inguinal complications has yet not been reported. This method measures the synchronicity (not symmetry!) of venous filling between the occluded and nonoccluded hemispheres. A delay of <0.5 seconds in venous filling is considered safe for permanent vessel occlusion.[14] Carotid

artery sacrifice can actually be performed uneventfully in patients with a delay in venous filling of <2 seconds, whereas patients with a delay of 3 seconds may be prone to hemodynamic ischemia in conjunction with hypotensive episodes.[15]

The venous phase BTO can be further enhanced by concomitant TCD evaluation,[16] which can depict a subgroup of individuals who fail the venous phase test but still can safely undergo carotid artery sacrifice when passing the Doppler criteria.[16] Given the unexcelled level of safety and predictive value of TCD-guided venous phase BTO, this procedure should be considered "state of the art" in the preoperative evaluation of therapeutic carotid artery occlusion. It is good practice to perform a baseline TCD before the BTO, including a digital carotid compression test. If the ipsilateral middle cerebral artery velocity drops to <30% of baseline on carotid compression, an angiographic BTO can be omitted because it is obvious that the cerebral collateral capacity is insufficient. This does, though, not apply if the underlying pathology is a carotico-cavernous fistula or a highly vascularized neck or skull base tumor.

Regarding BTO in the vertebrobasilar circulation, there is not yet a reliable ultraswift protocol. This test is still clinical, in the 15- to 30-minute range. BTO in the vertebrobasilar circulation should only be performed with bilateral vertebral artery (VA) occlusion, unless the patient has merely 1 sole vertebral artery (ie, the contralateral vertebral artery is aplastic, occluded, or supplies its posterior inferior cerebellar artery [PICA] only). In other words, vertebral BTO should only be performed to test the collateral capacity of the circle of Willis, not to visualize retrograde ipsilateral vertebral filling alone. With 2 vertebral arteries joining at the vertebrobasilar junction, a unilateral vertebral BTO is obsolete, even if dominant vertebral artery sacrifice is planned. The article of Zoarski and Seth[17] in the present issue of the *American Journal of Neuroradiology* provides further evidence of the feasibility of permanent occlusion, even of a dominant vertebral artery, without a preceding BTO.

Bilateral VA BTO can be well-tolerated, even in the presence of 2 very slim posterior communicating arteries (PcomAs) or a single PcomA only (ie, the anatomy of the circle of Willis cannot always predict the feasibility of therapeutic bilateral vertebral [or basilar] occlusion). With TCD, insonation of the P1 segment will show an increase and reversal of flow velocity with a functional PcomA on bilateral VA BTO, whereas there is a drop in P2 velocity. The exact limit for this drop with respect to tolerance to bilateral VA or basilar artery occlusion is yet to be established. Nevertheless, concomitant insonation of the P1 or P2 segment during VA BTO is useful because it immediately detects possible slackening of the balloon. The risk of a false-negative test due to incomplete balloon occlusion can hence be reduced, and continuous Doppler surveillance would be superior to repeated contrast injections.

The most common indication for bilateral VA BTO is to test whether flow reversal for a large basilar tip aneurysm that cannot be treated otherwise at reasonable risk is possible. In that situation, the BTO may be performed at a different site (both VAs) than the one on which the actual permanent occlusion will be performed (either VAs pre-/post-PICA or clip ligation across the basilar artery). In general, a BTO should always be performed as close as possible to the point of intended permanent vessel closure. This is, in particular, important in the following situations:

1) Where the ophthalmic artery retrogradely fills the internal carotid artery and supraclinoid ICA occlusion is planned. BTO should then be performed beyond the ophthalmic artery.[18]

2) In carotico-cavernous fistulas that require balloon placement distal to the site of shunting. Ballon placement proximal to the fisula measures the compound effect of the capacity in the circle of Willis and the fistulous shunting.

3) In richly vascularized tumors of the neck or skull-base, the balloon must be placed distal to the tumor in order to prevent steal phenomena.[19] On common carotid artery occlusion, blood may flow in a retrograde fashion from the ICA to the bifurcation and supply the tumor through the external carotid artery. This will affect the BTO result significantly.

When it comes to therapeutic vessel occlusion, it should be considered as the integrated art of the optimal choice of the site of occlusion; mode of occlusion; risk assessment regarding hemodynamic and thromboembolic events; as precisely as possible, the estimation of success rate compared with other treatment modalities; and finally, postoperative surveillance and care. Such a procedure hence requires interdisciplinary cooperation among endovascular therapists, neurosurgeons, and neurointensive care staff, including those with expertise in cerebral hemodynamics.

The site of occlusion should be chosen from the perspective of maximal therapeutic effect and minimalization of a "blind stump," where thrombus may form in the artery and give raise to thromboembolism. The BTO can provide safety against hemodynamic events but cannot prevent or predict ischemia due to thromboembolism. This is, in particular, true regarding small perforating vessels. Therapeutic vessel occlusion requires antithrombotic prophylaxis with platelet inhibitors (75-mg acetylsalicylic acid) in conjunction with low-molecular heparin. Often, endovascular occlusion techniques may be chosen because they are less invasive than a neurosurgical approach. On the other hand, the latter provides a more precise and "cleaner" occlusion, which can be especially beneficial in therapeutic occlusion in the posterior circulation or whenever secondary thrombosis of perforating arteries is feared. Combined approaches may be chosen, like balloon or coil embolization of one VA proximal to the PICA and clip ligation of the other VA distal to the PICA for flow-reversal treatment of midbasilar or basilar junction aneurysms. Thus, inflow into the aneurysm may be maximally reduced, whereas the "blind stump" is kept at a minimum and the anterior circulation has a smaller additional vascular territory to supply.

The prevailing indications for therapeutic vessel occlusion are giant, fusiform dissecting, or very small (blister) aneurysms. The mode of action is either parent artery occlusion leading to immediate aneurysm flow stagnation and secondary thrombosis with consecutive shrinkage or flow reversal in the parent artery leading to changes in inflow into the aneurysm. In the latter, intra-aneurysmal flow is often preserved on flow reversal and intra-aneurysmal thrombosis may occur in a delayed fashion. An initial increase in intra-aneurysmal flow has been observed but can still result in a favorable long-term out-

come. Flow reversal in the parent artery is often chosen for giant untreated or failed basilar tip aneurysms. Thrombosis of giant aneurysms may lead to an initial increase in mass effect, which can be alleviated with steroids. Dissecting aneurysms at the PICA branching may respond well to flow reversal on proximal VA occlusion but may also require trap ligation, especially if ruptured. Likewise, the treatment of ruptured blister aneurysms represents a management conundrum. Preferably, these aneurysms should be repaired (surgically or endovascularly) or wrapped in the acute phase. Therapeutic occlusions performed in the acute phase of aneurysm rupture have the potential of vast hemodynamic infarction if complicated by vasospasm (even if the BTO was passed and the collateral circulation was deemed excellent).[20]

Postoperative treatment includes triple or double hypertensive, hypervolemia, hemodilution therapy. The level of hypertensive treatment is individualized in accordance with arterial blood pressures registered during the BTO. Surveillance of the hemodynamic status of the patient is performed with TCD, and both the triple H therapy and grade of postoperative mobilization can be tailor-made with the aid of Doppler sonography.[16] This approach allows therapeutic vessel occlusion even in patients with a BTO indicating a border zone for tolerance.

In general, whenever possible, a vessel-preservation approach is preferable over deconstructive solutions. Recently, low-porosity tubular stent-like implants, so-called flow diverters, have evolved. That type of stent may provide complete thrombosis of giant aneurysms without the need to fill the aneurysm with coils (and increase the mass effect) with preservation of the parent vessel. Flow diverters hence may represent another good treatment option for complex aneurysms that usually would be selected for treatment with therapeutic vessel occlusion. However, serious complications in the use of flow diverters have been reported, including stent and perforator occlusions, ipsilateral parenchymal hemorrhage (8.5%),[21] and delayed aneurysm rupture.[22,23]

The combined mortality/morbidity rate connected to the use of flow diverters is approximately 10% in unruptured aneurysms,[22,23] which represents a far higher risk than with therapeutic vessel occlusion. Delayed aneurysm rupture does not occur in therapeutic vessel occlusion. The efficacy of flow diverters in terms of total aneurysm occlusion is 73.6%[24] and hence lower than that of therapeutic vessel occlusion. The latter is extremely effective, both in terms of short- and long-term results. The fear of de novo aneurysm formation after therapeutic artery occlusion has sometimes been overemphasized.[16,22] Increased collateral flow and, hence, hemodynamic stress are present only in the acute phase after therapeutic vessel occlusion because the vessel diameter increases due to higher flow, thereby normalizing hemodynamic stress. Cerebral perfusion is not impaired during a prolonged time after ICA sacrifice in patients who passed the BTO.[25]

The evolution of new surgical and endovascular devices and skills in the future may change our treatment armamentarium and preferences, but at present, therapeutic vessel occlusion still is an efficient and safe treatment option, in particular when applying ultraswift venous phase TCD-guided BTO for preprocedural evaluation.

REFERENCES

1. Cooper A. **A case of aneurysm on the carotid artery.** *Med Chir Trans* 1809;1:1–10
2. Matas R. **Traumatisms and traumatic aneurysms of the vertebral artery and their surgical treatment with the report of a cured case.** *Ann Surg* 1893;18:477–521
3. Serbinenko FA. **Balloon catheterization and occlusion of major cerebral vessels.** *J Neurosurg* 1974;41:125–45
4. Gonzalez CF, Moret J. **Balloon occlusion of the carotid artery prior to surgery for neck tumors.** *AJNR Am J Neuroradiol* 1990;11:649–52
5. Linskey ME, Jungreis CA, Yonas H, et al. **Stroke risk after abrupt internal carotid artery sacrifice: accuracy of preoperative assessment with balloon test occlusion and stable xenon-enhanced CT.** *AJNR Am J Neuroradiol* 1994;15:829–34
6. Larson JJ, Tew JM Jr, Tomsick TA, et al. **Treatment of aneurysms of the internal carotid artery by intravascular balloon occlusion: long-term follow-up of 58 patients.** *Neurosurgery* 1995;36:23–30
7. Lorberboym M, Pandit N, Machac J, et al. **Brain perfusion imaging during preoperative temporary balloon occlusion of the internal carotid artery.** *J Nucl Med* 1996;37:415–19
8. Peterman SB, Taylor A Jr, Hoffman JC Jr. **Improved detection of cerebral hypoperfusion with internal carotid balloon test occlusion and 99m Tc-HMPAO cerebral perfusion SPECT imaging.** *AJNR Am J Neuroradiol* 1991;12:1035–41
9. de Vries EJ, Sekhar LN, Horton JA, et al. **A new method to predict safe resection of the internal carotid artery.** *Laryngoscope* 1990;100:85–88
10. Witt JP, Yonas H, Jungreis C. **Cerebral blood flow response pattern during balloon test occlusion of the internal carotid artery.** *AJNR Am J Neuroradiol* 1994;15:847–56
11. Tarr RW, Jungreis CA, Horton JA, et al. **Complications of preoperative balloon test occlusion of the internal carotid arteries: experience in 300 cases.** *Skull Base Surg* 1991;1:240–44
12. Mathis JM, Barr JD, Jungreis CA, et al. **Temporary balloon test occlusion of the internal carotid artery: experience in 500 cases.** *AJNR Am J Neuroradiol* 1995;16:749–54
13. Zhu W, Tian YL, Zhou LF, et al. **Treatment strategies for complex internal carotid artery (ICA) aneurysms: direct ICA sacrifice or combined with extracranial-to-intracranial bypass.** *World Neurosurg* 2011;75:476–84
14. van Rooij WJ, Sluzewski M, Slob MJ, et al. **Predictive value of angiographic testing for tolerance to therapeutic occlusion of the carotid artery.** *AJNR Am J Neuroradiol* 2005;26:175–78
15. Abud DG, Spelle L, Piotin M, et al. **Venous phase timing during balloon test occlusion as a criterion for permanent internal carotid artery sacrifice.** *AJNR Am J Neuroradiol* 2005;26:2602–09
16. Sorteberg A, Bakke SJ, Boysen M, et al. **Angiographic balloon test occlusion and therapeutic sacrifice of major arteries to the brain.** *Neurosurgery* 2008;63:651–60, discussion 660–61
17. Zoarski GH, Seth R. **Safety of unilateral endovascular occlusion of the cervical segment of the vertebral artery without antecedent balloon test occlusion.** *AJNR Am J Neuroradiol* 2014;35
18. Lesley WS, Rangaswamy R. **Balloon test occlusion and endosurgical parent artery sacrifice for the evaluation and management of complex intracranial aneurysmal disease.** *J NeuroInterv Surg* 2009;1:112–20
19. Sorteberg A, Sorteberg W, Bakke SJ, et al. **Varying impact of common carotid artery digital compression and internal carotid artery balloon test occlusion on cerebral hemodynamics.** *Head Neck* 1998;20:687–94
20. Meling TR, Sorteberg A, Bakke SJ, et al. **Blood blister-like aneurysms of the internal carotid artery trunk causing subarachnoid**

hemorrhage: treatment and outcome. *J Neurosurg* 2008; 108:662–71
21. Cruz JP, Chow M, O'Kelly C, et al. **Delayed ipsilateral parenchymal hemorrhage following flow diversion for the treatment of anterior circulation aneurysms.** *AJNR Am J Neuroradiol* 2012;33: 603–08
22. van Rooij WJ, Sluzewski M, van der Laak C. **Flow diverters for unruptured internal carotid artery aneurysms: dangerous and not yet an alternative for conventional endovascular techniques.** *AJNR Am J Neuroradiol* 2013;34:3–4
23. Kulcsár Z, Szikora I. **The ESMINT Retrospective Analysis of Delayed Aneurysm Ruptures after flow diversion (RADAR) study.** EJMINT Original Article, 2012: 1244000088. http://www.ejmint.org/original-article/1244000088. Accessed November 4, 2013
24. Becske T, Kallmes DF, Saatsci I, et al. **Pipeline for uncoilable or failed aneurysms: results from a multicenter trial.** *Radiology* 2013; 267:858–68
25. Gevers S, Heijtel D, Ferns SP, et al. **Cerebral perfusion long term after therapeutic occlusion of the internal carotid artery in patients who tolerated angiographic balloon test occlusion.** *AJNR Am J Neuroradiol* 2012;33:329–35

A. Sorteberg
Department of Neurosurgery
Oslo University Hospital
The National Hospital-Rikshospitalet
Oslo, Norway

http://dx.doi.org/10.3174/ajnr.A3852

CT Perfusion for Detection of Delayed Cerebral Ischemia in Aneurysmal Subarachnoid Hemorrhage: A Systematic Review and Meta-Analysis

D.I.A. Mir, A. Gupta, A. Dunning, L. Puchi, C.L. Robinson, H.-A.B. Epstein, and P.C. Sanelli

ABSTRACT

BACKGROUND AND PURPOSE: Delayed cerebral ischemia is a significant cause of morbidity and mortality after aneurysmal SAH, leading to poor outcomes. The purpose of this study was to evaluate the usefulness of CTP in determining delayed cerebral ischemia in patients with aneurysmal SAH.

MATERIALS AND METHODS: We conducted a systematic review evaluating studies that assessed CTP in patients with aneurysmal SAH for determining delayed cerebral ischemia. Studies using any of the following definitions of delayed cerebral ischemia were included in the systematic review: 1) new onset of clinical deterioration, 2) cerebral infarction identified on follow-up CT or MR imaging, and 3) functional disability. A random-effects meta-analysis was performed assessing the strength of association between a positive CTP result and delayed cerebral ischemia.

RESULTS: The systematic review identified 218 studies that met our screening criteria, of which 6 cohort studies met the inclusion criteria. These studies encompassed a total of 345 patients, with 155 (45%) of 345 patients classified as having delayed cerebral ischemia and 190 (55%) of 345 patients as not having delayed cerebral ischemia. Admission disease severity was comparable across all groups. Four cohort studies reported CTP test characteristics amenable to the meta-analysis. The weighted averages and ranges of the pooled sensitivity and specificity of CTP in the determination of delayed cerebral ischemia were 0.84 (0.7–0.95) and 0.77 (0.66–0.82), respectively. The pooled odds ratio of 23.14 (95% CI, 5.87–91.19) indicates that patients with aneurysmal SAH with positive CTP test results were approximately 23 times more likely to experience delayed cerebral ischemia compared with patients with negative CTP test results.

CONCLUSIONS: Perfusion deficits on CTP are a significant finding in determining delayed cerebral ischemia in aneurysmal SAH. This may be helpful in identifying patients with delayed cerebral ischemia before development of infarction and neurologic deficits.

ABBREVIATIONS: DCI = delayed cerebral ischemia; QUADAS = Quality Assessment of Diagnostic Accuracy Studies

Aneurysmal SAH is a devastating condition that occurs in up to 30,000 people in the United States annually and carries a 51% case mortality.[1,2] Delayed cerebral ischemia (DCI) is considered the most significant cause of morbidity and mortality in patients who survive the initial hemorrhage, with poor outcomes occurring in up to 30% despite aggressive therapy.[3,4] The definition of DCI is variable and has been described as a new onset of clinical deterioration, not explained by other causes.[5] However, recently it has been recommended to define DCI on the basis of its primary outcome measures, such as cerebral infarction and functional disability.[6] Therefore, DCI is a challenging diagnosis to make prospectively, before its poor outcomes, particularly in comatose or sedated patients, thus limiting initiation of pre-emptive therapy.[5] Despite these difficulties, DCI is used to complement older clinicoradiographic terminology such as angiographic vasospasm and symptomatic vasospasm because DCI has been shown to have the strongest associations with poor outcomes, including cognitive impairment and reduced quality of life after aneurysmal SAH.[6] Furthermore, it has become clear that the pathogenesis of DCI is not fully attributable to large-vessel vasospasm alone and

Received July 30, 2013; accepted after revision September 19.

From the Departments of Radiology (D.I.A.M., A.G., L.P., C.L.R., P.C.S.), and Public Health (A.D., P.C.S.), and the Samuel J. Wood Library and C.V. Starr Biomedical Information Center (H.-A.B.E.), Weill Cornell Medical College, New York, NY.

This publication was supported by Grant Number 5K23NS058387 from the National Institute of Neurological Disorders and Stroke (NINDS), a component of the National Institutes of Health (NIH). Its contents are solely the responsibility of the authors and do not necessarily represent the official view of NINDS or NIH.

Please address correspondence to Pina C. Sanelli, MD, MPH, Department of Radiology, Weill Cornell Medical College/New York Presbyterian Hospital, 525 E. 68th St, Starr 8A, New York, NY 10065; e-mail: pcs9001@med.cornell.edu

Indicates open access to non-subscribers at www.ajnr.org

Indicates article with supplemental on-line appendix.

Evidence-Based Medicine Level 2.

http://dx.doi.org/10.3174/ajnr.A3787

may, in fact, be the result of several independent processes acting in concert.[7] The common denominator, however, seems to be hemodynamic alterations in cerebral perfusion leading to ischemia and/or infarction.

Cerebral perfusion can be assessed by use of CT, MR, PET, and SPECT imaging. Specifically, CTP is a technique that allows for rapid, noninvasive assessment of CBF, MTT, and CBV. CTP has had an increasing role in the evaluation of patients with aneurysmal SAH, as it can be performed in conjunction with traditional noncontrast CT and CTA, requiring little extra examination time.[8] Many initial studies have evaluated the diagnostic accuracy of CTP for vasospasm compared with DSA- and CTA-defined vasospasm. However, CTP remains a relatively new technique for the evaluation of DCI, and it remains unclear how well CTP can detect DCI.[9] Given the limitations of relying on the conclusions of individual studies in the literature, particularly when relatively small cohorts are used and findings are not entirely conclusive, we aimed to perform a systematic review and meta-analysis to evaluate CTP in the detection of DCI in patients with aneurysmal SAH.

MATERIALS AND METHODS

We have implemented the methods described in the Preferred Reporting Items for Systematic Reviews and Meta-Analyses statement.[10]

Eligibility Criteria

To be more inclusive in identifying studies in the literature that evaluated CTP for DCI in patients with aneurysmal SAH, we included any of the following definitions of DCI in our inclusion criteria: 1) clinical deterioration not explained by other causes and sufficiently judged to be the result of DCI, 2) cerebral infarction identified on follow-up CT or MR imaging, and 3) functional disability related to DCI. If any one of these criteria was positive, DCI was considered to have occurred. We limited our selection to include manuscripts published in English only. In cases of duplicated cohorts, we included the study with the largest number of patients.

Information Sources and Search

An experienced medical librarian performed a systematic search to identify studies in accordance with the eligibility criteria. Potential articles were found by a search of the electronic data bases of Ovid MEDLINE, EMBASE, and Web of Knowledge. Additional records were identified by use of the Related Articles feature in PubMed and the Cited Reference Search in the ISI Web of Science. All studies included in these data bases through March 2013 were searched. Further details of the search strategy are described in the On-line Appendix.

Study Selection and Data Collection Process

After removal of duplicate articles, search results were preliminarily screened via title and abstract information by a single reader. Shortlisted manuscripts were independently reviewed in full by 2 additional readers to determine conformity to the eligibility criteria. Disagreements were resolved by consensus.

With use of a standardized data collection template, study characteristics including baseline patient demographics, CTP test characteristics, and detailed DCI outcome data were collected by 2 independent readers, with disagreements resolved by a third reader. All eligible studies were included in the qualitative systematic review. Of these, studies reporting test characteristics or data from which they could be tabulated were included in the meta-analysis.

Validity Assessment

To assess the validity of each study, we implemented the Quality Assessment of Diagnostic Accuracy Studies (QUADAS) tool.[11] This tool assesses bias in each study according to 14 criteria, with possible answers as "Yes," "No," or "Unknown." Two reviewers scored each study with disagreements resolved by consensus. The full QUADAS tool is available in the On-line Appendix.

Statistical Analysis

A meta-analysis was performed on those studies in which test characteristics could be extracted and/or tabulated. Pooled sensitivity, specificity, and odds ratios with corresponding 95% CIs were calculated. The pooled sensitivity and specificity were calculated by use of weighted averages derived from the sample size of each study. The pooled odds ratio was calculated by use of a random-effects model. We chose this statistical method rather than the less conservative fixed-effects model because of the wide variation in these studies, including the definitions of DCI, different CTP protocols, and postprocessing software, as well as differences in what constituted an abnormal CTP result. Furthermore, study heterogeneity was assessed by calculating the I^2 statistic. All analyses were conducted by using StataVersion 12 software (StataCorp, College Station, Texas).

RESULTS

Study Selection

After removal of duplicated citations, search results yielded 218 manuscripts. Of these, 25 articles were selected for full review on the basis of screening the titles and abstracts, with 14 meeting the eligibility criteria. Seventy-one percent (10/14) of these studies were suspected to contain at least partially overlapping cohorts; therefore, their authors were contacted for further clarification.[12-21] One group replied to our request (authors of[14,16,20,21]) and indicated that duplicate cohorts were used; in this case, the study with the largest number of included patients was included in our review.[14] No reply was received from the other groups; therefore, only those with the largest cohorts were included.[12,13] One study was also excluded for not providing the number of patients in the DCI and non-DCI groups.[22] Finally, 6 studies were included in the systematic review.[12-14,23-25] The study selection is summarized in Fig 1.

Qualitative Assessment and Study Characteristics

The 6 studies that met our final eligibility criteria were all prospective, with 3 completed in the United States,[14,23,24] 2 in the Netherlands,[12,13] and 1 study in Germany.[25] Together, these studies encompassed 345 patients, of which 155 (45%) were classified as having DCI and 190 (55%) as not having DCI. Although admission disease severity, demographics, and median day of DCI onset were comparable across groups, large

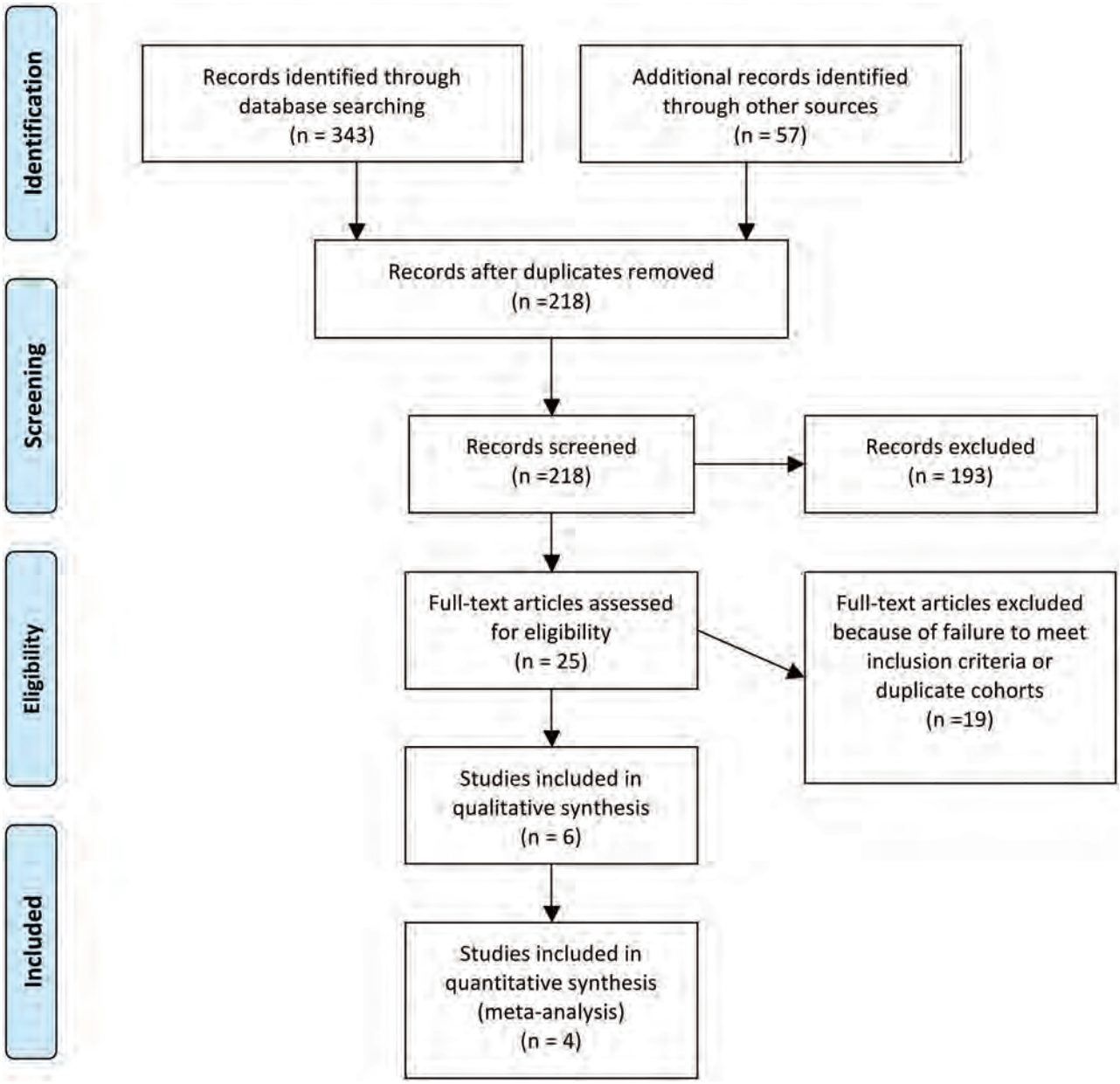

FIG 1. Study selection flow diagram. Figure adapted from the Preferred Reporting Items for Systematic Reviews and Meta-Analyses Group Statement.[10]

differences existed in the cohort sizes with a range from 10–97 patients (On-line Table 1). Studies tended to implement CTP imaging either at the onset of symptomatic vasospasm or before; however, for 2 studies this information was not reported.[12,24] Studies had variable CTP methodology and postprocessing algorithms, variation in the definition of a positive CTP test result, and variability in the definition of DCI used as an outcome measure (On-line Table 2).

Validity Assessment

The percentage of studies scoring "Yes," "No," or "Unknown" for each of the 14 items on the QUADAS tool is displayed in Fig 2. All of the studies scored "Yes" on items 1 and 8 of the QUADAS tool, indicating an absence of spectrum bias (presence of a cohort representative of patients who would receive the index test in practice) and the presence of a clear description of the definition of DCI. In addition, 80% of studies scored "Yes" on items 2, 3, 5–7, 9, and 12 on the QUADAS tool, indicating that a clear description of selection criteria was provided; appropriate reference standards were chosen; and that there was an absence of primary selection bias (whole or part of the study population received verification by the reference standard), differential verification bias (study population received verification by the same reference standard), and incorporation bias (the reference standard was independent of the index test) among most studies. Last, most studies scored "No" or "Unknown" on items 4, 11, 13, and 14, indicating the presence of disease progression bias (unsure if the time between implementation of the reference standard and the index test is short enough to ensure that the target condition did not change between the 2 tests), test classification bias (the reference standard results were interpreted without

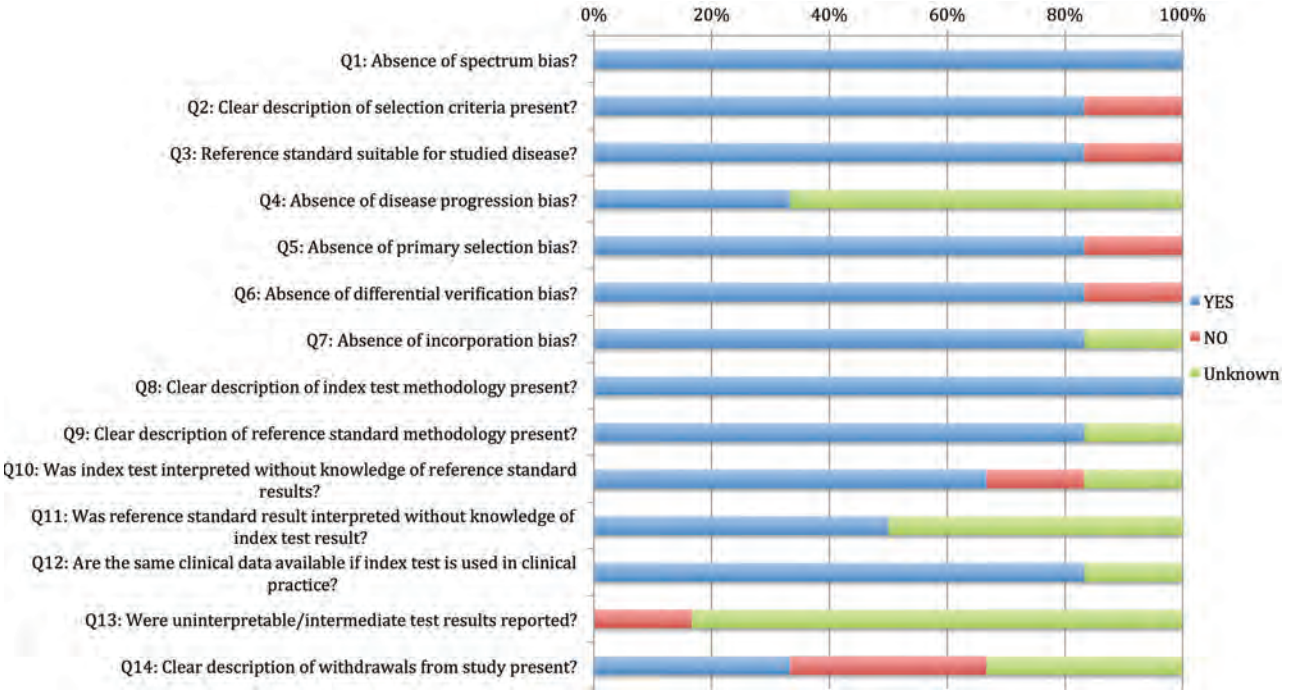

FIG 2. Percentage of studies included in the systematic review scoring "Yes," "No," or "Unknown" on QUADAS tool criteria. Questions truncated in figure according to information provided from previously published work.[11]

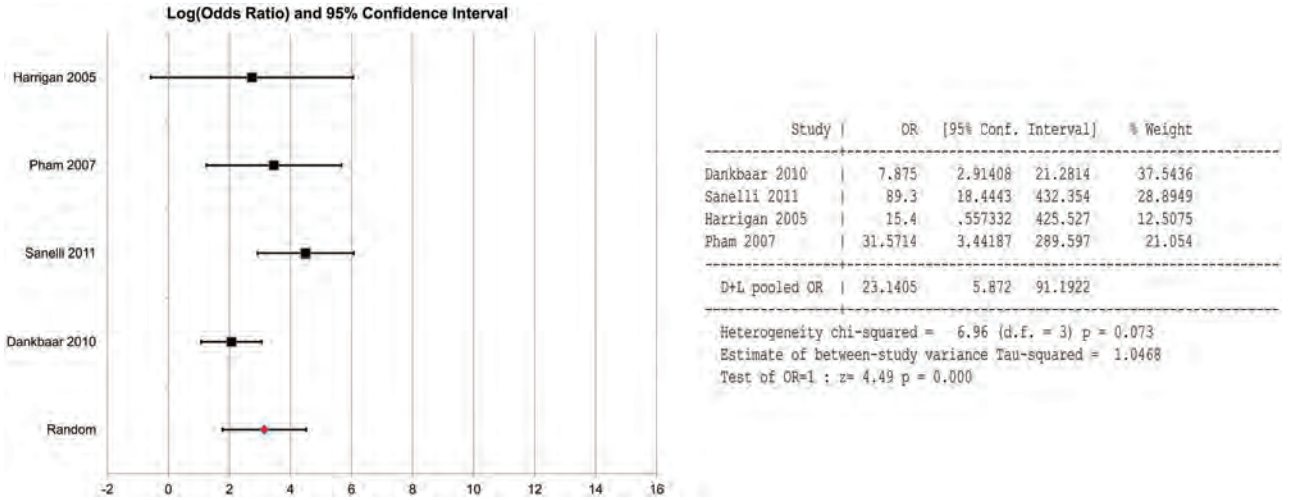

FIG 3. Forest plot of data used to tabulate the pooled odds ratios for studies included in the meta-analysis.

knowledge of the results of the index test and vice versa), and a lack of explanation for patient withdrawals.

Statistical Analysis

In 4 (67%) of the 6 studies, CTP test characteristics and DCI were reported in a way that could be tabulated for a meta-analysis.[13,14,23,25] This number included studies attempting to determine optimal CTP characteristics and thresholds to detect DCI; in these cases, we used the best single test characteristic to tabulate the odds ratio for the meta-analysis (On-line Table 2). The weighted averages and ranges of the extracted/tabulated sensitivities and specificities with corresponding ranges of CTP in the detection of DCI from these studies were 0.84 (0.7–0.95) and 0.77 (0.66–0.82), respectively. The meta-analysis also revealed a pooled odds ratio of 23.14 (95% CI, 5.87 – 91.19) (Fig 3), suggesting that the patients with aneurysmal SAH with a positive CTP test were approximately 23 times more likely to experience DCI compared with those patients with aneurysmal SAH without a positive CTP test. The study heterogeneity ($I^2 = 6.96$) in these data was not significant ($P = .073$).

DISCUSSION

The pathogenesis of DCI is now thought to be multifactorial, with an alteration of cerebral perfusion and reduced CBF leading to ischemia and/or infarction.[7] CTP can noninvasively evaluate cerebral perfusion and can often be combined with other CT-based examinations, thereby minimizing examina-

tion time. Few studies, however, have assessed the ability of CTP to detect DCI.[9]

DCI is considered a diagnosis of exclusion and is often difficult to make prospectively, especially in sedated and/or comatose patients, as physical examinations may not be reliable.[5] Furthermore, defining DCI by its primary outcomes measures only allows its detection after irreversible damage has already occurred, thus limiting the timely delivery of efficacious therapy. Because DCI involves perturbations in CBF, it is thought that CTP may be able to detect DCI before its primary outcomes of cerebral infarction or functional disability manifest, thus allowing pre-emptive therapy.[13]

Our systematic review and meta-analysis indicates that patients with aneurysmal SAH with positive CTP test results demonstrating perfusion deficits are approximately 23-fold more likely to experience DCI compared with patients with normal CTP results, suggesting that CTP has the potential to be a useful tool in clinical practice. Compared with other imaging measures used to detect DCI, such as intraventricular hemorrhage and Fisher scores, hydrocephalus, and transcranial Doppler flow prolongation, which have reported odds ratios ranging from 0.5–2.7,[26] CTP has demonstrated a higher odds ratio in this meta-analysis. Moreover, CTP had a superior odds ratio, even at the lower limit of the 95% CI, compared with other nonimaging-derived parameters, such as an admission mean arterial pressure $>$ 112 mm Hg, which has a reported odds ratio of 3.3.[26] This result was achieved despite variation in the patient populations studied, CTP protocols and software used, and the various definitions of DCI implemented in the studies included in this meta-analysis.

By applying the QUADAS tool, we found that among the studies included in our systematic review, most were free of spectrum bias, primary selection bias, differential verification bias, and incorporation bias (see "Results" section for description). They each also clearly described the definition of DCI implemented and patient selection criteria used. In most cases, the choice of a reference standard was considered appropriate. Most studies, however, contained signs of disease progression bias and test classification bias (see "Results" section for description). Last, most studies did not explain patient withdrawals from the study, nor did they report uninterpretable or intermediate test results. These shortcomings represent areas of future improvement in diagnostic accuracy studies assessing the role of CTP in detecting DCI in aneurysmal SAH.

Our analysis also revealed other limitations of the existing literature on CTP for the detection of DCI. These primarily arose from the nonuniform definitions for DCI used in the literature, interinstitutional differences in the CTP protocol and postprocessing software programs used, and the lack of consistency among the definitions of an abnormal CTP test result (On-line Table 2). Given such variability, our analysis combined the various definitions of DCI used in each study. Specific subanalyses to determine if a particular definition of DCI was better detected by CTP could not be performed given the limited sample size of the studies that met eligibility criteria in this investigation. Other subanalyses examining the best time to perform CTP to detect DCI (hospital admission, during symptoms, or both) could also not be performed because of the variability of when CTP was performed among the studies that met our eligibility criteria. Furthermore, those studies that assessed CTP test results quantitatively reported test characteristics for different CTP hemodynamic parameters (MTT, CBF, CBV, and TTP), often by using various thresholds. In these cases, we chose the CTP parameter and threshold with the greatest overall diagnostic value for DCI because we were evaluating CTP as a single test and not by its individual components. These limitations, and the fact that the studies that met our eligibility criteria also had variable CTP methodology and postprocessing algorithms with evaluation of the results limited to the anterior circulation, may be sources of bias and must be considered when the results of our meta-analysis are interpreted. However, despite these differences among studies, our meta-analysis revealed a statistically significant odds ratio and no statistically detectable heterogeneity, suggesting that a strong association exists between CTP deficits and DCI, across variations in DCI definition and CTP technique used.

It is noteworthy to mention that CTP itself has limitations. The amount of brain volume coverage may be limited in the clinical setting, and the amount of radiation exposure to the patient is higher compared with standard noncontrast CT of the head.[27] Furthermore, accurate quantification is dependent on an intact blood-brain barrier, which may not be normally functioning in ischemic events, such as DCI.[27] Last, different postprocessing software vendors may quantify CTP data differently, which may introduce undue variation in the results. Despite these shortcomings, however, because CTP uses ubiquitous technology, it has the potential to be quickly and widely implemented. CTP, therefore, may find a place in the clinical setting for better and earlier detection of DCI and its devastating outcomes.

CONCLUSIONS

Our meta-analysis revealed a strong association between CTP perfusion deficits and the development of DCI in patients with aneurysmal SAH. Because DCI is challenging to diagnose prospectively, treatment is often of limited efficacy when initiated after morbidity has already occurred. CTP may aid in the detection of DCI earlier and with more accuracy, allowing for pre-emptive therapy and/or closer monitoring to prevent potentially devastating outcomes of cerebral infarction and functional disability.

Disclosures: Ajay Gupta—*UNRELATED: Grants/Grants Pending:* AUR GE Radiology Research and Academic Fellowship. Pina Sanelli—*RELATED: Grant:* This publication was made possible by Grant Number 5K23NS058387 from the National Institute of Neurological Disorders and Stroke (NINDS), a component of the National Institutes of Health (NIH). Its contents are solely the responsibility of the authors and do not necessarily represent the official view of NINDS or NIH.* **Money paid to institution.*

REFERENCES

1. Graf CJ, Nibbelink DW. **Cooperative study of intracranial aneurysms and subarachnoid hemorrhage. Report on a randomized treatment study. 3. Intracranial surgery.** *Stroke* 1974;5:557–601
2. Hop JW, Rinkel GJ, Algra A, et al. **Case-fatality rates and functional outcome after subarachnoid hemorrhage: a systematic review.** *Stroke* 1997;28:660–64
3. Kassell NF, Torner JC, Haley EC Jr, et al. **The International Cooperative Study on the Timing of Aneurysm Surgery. Part 1: Overall management results.** *J Neurosurg* 1990;73:18–36

4. Mayberg MR. **Cerebral vasospasm.** *Neurosurg Clin N Am* 1998;9:615–27
5. Vergouwen MD, Vermeulen M, van Gijn J, et al. **Definition of delayed cerebral ischemia after aneurysmal subarachnoid hemorrhage as an outcome event in clinical trials and observational studies: proposal of a multidisciplinary research group.** *Stroke* 2010;41:2391–95
6. Frontera JA, Fernandez A, Schmidt JM, et al. **Defining vasospasm after subarachnoid hemorrhage: what is the most clinically relevant definition?** *Stroke* 2009;40:1963–68
7. Hansen-Schwartz J, Vajkoczy P, Macdonald RL, et al. **Cerebral vasospasm: looking beyond vasoconstriction.** *Trends Pharmacol Sci* 2007;28:252–56
8. Hoeffner EG, Case I, Jain R, et al. **Cerebral perfusion CT: technique and clinical applications.** *Radiology* 2004;231:632–44
9. Greenberg ED, Gold R, Reichman M, et al. **Diagnostic accuracy of CT angiography and CT perfusion for cerebral vasospasm: a meta-analysis.** *AJNR Am J Neuroradiol* 2010;31:1853–60
10. Liberati A, Altman DG, Tetzlaff J, et al. **The PRISMA statement for reporting systematic reviews and meta-analyses of studies that evaluate health care interventions: explanation and elaboration.** *PLoS Med* 2009;6:e1000100
11. Whiting P, Rutjes AW, Reitsma JB, et al. **The development of QUADAS: a tool for the quality assessment of studies of diagnostic accuracy included in systematic reviews.** *BMC Med Res Methodol* 2003;3:25
12. van der Schaaf I, Wermer MJ, van der Graaf Y, et al. **Prognostic value of cerebral perfusion-computed tomography in the acute stage after subarachnoid hemorrhage for the development of delayed cerebral ischemia.** *Stroke* 2006;37:409–13
13. Dankbaar JW, de Rooij NK, Rijsdijk M, et al. **Diagnostic threshold values of cerebral perfusion measured with computed tomography for delayed cerebral ischemia after aneurysmal subarachnoid hemorrhage.** *Stroke* 2010;41:1927–32
14. Sanelli PC, Ugorec I, Johnson CE, et al. **Using quantitative CT perfusion for evaluation of delayed cerebral ischemia following aneurysmal subarachnoid hemorrhage.** *AJNR Am J Neuroradiol* 2011; 32:2047–53
15. Dankbaar JW, de Rooij NK, Velthuis BK, et al. **Diagnosing delayed cerebral ischemia with different CT modalities in patients with subarachnoid hemorrhage with clinical deterioration.** *Stroke* 2009;40: 3493–98
16. Sanelli PC, Anumula N, Johnson CE, et al. **Evaluating CT perfusion using outcome measures of delayed cerebral ischemia in aneurysmal subarachnoid hemorrhage.** *AJNR Am J Neuroradiol* 2013;34: 292–98
17. van der Schaaf I, Wermer MJ, van der Graaf Y, et al. **CT after subarachnoid hemorrhage: relation of cerebral perfusion to delayed cerebral ischemia.** *Neurology* 2006;66:1533–38
18. Dankbaar JW, de Rooij NK, Smit EJ, et al. **Changes in cerebral perfusion around the time of delayed cerebral ischemia in subarachnoid hemorrhage patients.** *Cerebrovasc Dis* 2011;32:133–40
19. Rijsdijk M, van der Schaaf IC, Velthuis BK, et al. **Global and focal cerebral perfusion after aneurysmal subarachnoid hemorrhage in relation with delayed cerebral ischemia.** *Neuroradiology* 2008;50: 813–20
20. Sanelli PC, Jou A, Gold R, et al. **Using CT perfusion during the early baseline period in aneurysmal subarachnoid hemorrhage to assess for development of vasospasm.** *Neuroradiology* 2011;53:425–34
21. Killeen RP, Mushlin AI, Johnson CE, et al. **Comparison of CT perfusion and digital subtraction angiography in the evaluation of delayed cerebral ischemia.** *Acad Radiol* 2011;18:1094–100
22. Lagares A, Cicuendez M, Ramos A, et al. **Acute perfusion changes after spontaneous SAH: a perfusion CT study.** *Acta Neurochir (Wien)* 2012;154:405–11;discussion 411–12
23. Harrigan MR, Magnano CR, Guterman LR, et al. **Computed tomographic perfusion in the management of aneurysmal subarachnoid hemorrhage: new application of an existent technique.** *Neurosurgery* 2005;56:304–17
24. Sviri GE, Britz GW, Lewis DH, et al. **Dynamic perfusion computed tomography in the diagnosis of cerebral vasospasm.** *Neurosurgery* 2006;59:319–25
25. Pham M, Johnson A, Bartsch AJ, et al. **CT perfusion predicts secondary cerebral infarction after aneurysmal subarachnoid hemorrhage.** *Neurology* 2007;69:762–65
26. Claassen J, Bernardini GL, Kreiter K, et al. **Effect of cisternal and ventricular blood on risk of delayed cerebral ischemia after subarachnoid hemorrhage: the Fisher scale revisited.** *Stroke* 2001;32: 2012–20
27. Latchaw RE, Yonas H, Hunter GJ, et al. **Guidelines and recommendations for perfusion imaging in cerebral ischemia: A scientific statement for healthcare professionals by the writing group on perfusion imaging, from the Council on Cardiovascular Radiology of the American Heart Association.** *Stroke* 2003;34:1084–104
28. Reichman MB, Greenberg ED, Gold RL, et al. **Developing patient-centered outcome measures for evaluating vasospasm in aneurysmal subarachnoid hemorrhage.** *Acad Radiol* 2009;16:541–45
29. Reichman M, Gold R, Greenberg E, et al. **Validation of a new reference standard for the diagnosis of vasospasm.** *Acad Radiol* 2010; 17:1083–89

DTI Correlates of Cognition in Conventional MRI of Normal-Appearing Brain in Patients with Clinical Features of Subacute Combined Degeneration and Biochemically Proven Vitamin B_{12} Deficiency

P.K. Gupta, R.K. Gupta, R.K. Garg, Y. Rai, B. Roy, C.M. Pandey, H.S. Malhotra, and P.A. Narayana

ABSTRACT

BACKGROUND AND PURPOSE: Vitamin B_{12} deficiency may cause neural injury that results in cognitive deficits. The main purpose of our study was to evaluate morphometric and microstructural changes in the brain and relate them to cognition in subacute combined degeneration of the spinal cord and patients with biochemically deficient vitamin B_{12}.

MATERIALS AND METHODS: Fifty-one patients were recruited and underwent nerve-conduction velocity tests and routine hematologic examinations. Serum vitamin B_{12} and homocystine levels were also measured. All patients and 46 age- and sex-matched controls underwent cervical spine and brain MR imaging along with cognition tests. MR imaging included conventional scans and DTI. Voxel-based morphometry was performed for determining the WM and GM volumes, based on T1-weighted images. DTI measures that included fractional anisotropy, ADC, radial diffusivity, and axial diffusivity were determined by using tract-based statistics.

RESULTS: None of the patients showed any abnormality on conventional MR imaging. No significant changes in GM and WM volumes were observed in patients compared with controls. Significant reductions in the fractional anisotropy and an increase in ADC and radial diffusivity values were observed in multiple brain regions in patients compared with controls. These changes were confirmed on the region-of-interest analysis. Neuropsychological scores were significantly different in patients compared with controls and showed significant correlation with fractional anisotropy and radial diffusivity in a few brain regions.

CONCLUSIONS: Microstructural changes are seen in WM regions on DTI in patients with vitamin B_{12} deficiency and correlate with cognition scores. DTI can be used for objective assessment of microstructural changes in the brain in vitamin B_{12} deficiency.

ABBREVIATIONS: AD = axial diffusivity; FA = fractional anisotropy; MNI = Montreal Neurological Institute; RD = radial diffusivity; SACD = subacute combined degeneration; TBSS = tract-based spatial statistics

B vitamins contribute to CNS development and proper functioning by acting as a cofactor in numerous catalytic reactions in the human body that are required for the synthesis and functioning of neurotransmitters and myelination. A deficiency of vitamin B_{12} may result in injury to the neural tissue. A limited number of clinical studies in children demonstrated a correlation between vitamin B_{12} deficiency and cognition.[1,2] Studies in elderly subjects suggest that vitamin B_{12} deficiency is associated with cognitive decline and may contribute to Alzheimer dementia,[3,4] whereas others have failed to demonstrated an increased risk.[5,6]

Subjects with B_{12} deficiency may also show changes in the posterolateral column of the spinal cord on MR imaging. Clinical symptoms relating to neuropathy and spinal cord involvement, referred to as subacute combined degeneration (SACD) of the spinal cord, are common in adult subjects with B_{12} deficiency. Changes in the brain parenchyma on MR imaging have been sporadically reported, with poor sensitivity.[7,8] In a cross-sectional study on an elderly population, a reduction in brain volume was observed with B_{12} deficiency.[9] There are isolated reports of brain demyelination in patients with SACD, which may or may not show resolution following vitamin B_{12} replacement.[10,11]

Elderly populations with vitamin B_{12} deficiency are reported to show whole-brain atrophy and white matter damage.[12,13] On

Received August 19, 2013; accepted after revision September 9.

From the Department of Neurology (P.K.G., R.K.Garg, H.S.M.), King George's Medical University, Lucknow, Uttar Pradesh, India; Department of Radiology and Imaging (R.K.Gupta, B.R.), Fortis Memorial Research Institute, Gurgaon, Haryana, India; Department of Radiodiagnosis (Y.R.) and Biostatistics (C.M.P.), Sanjay Gandhi Postgraduate Institute of Medical Sciences, Lucknow, Uttar Pradesh, India; and Department of Diagnostic and Interventional Imaging (P.A.N.), University of Texas Medical School at Houston, Houston, Texas.

This work was supported by grant BT/IN/German/04/RKG/2010 from the Department of Biotechnology, Ministry of Science and Technology, Government of India.

Please address correspondence to Rakesh K. Gupta, MD, Department of Radiology and Imaging, Fortis Memorial Research Institute, Gurgaon, Haryana-122002; e-mail: rakeshree1@gmail.com

Evidence-Based Medicine Level 2.

http://dx.doi.org/10.3174/ajnr.A3785

the basis of a number of case reports, brain atrophy is also a pathologic feature in infants with vitamin B_{12} deficiency.[14-16] Advanced MR imaging–based modalities such as DTI and MR spectroscopy showed abnormalities in a variety of diffuse neurologic disorders, whereas conventional MR imaging findings appeared normal. We hypothesized that patients with clinical symptoms of SACD and biochemical evidence of vitamin B_{12} deficiency will have an associated cognitive decline and microstructural alterations in brain WM on DTI, even when conventional MR imaging findings appear normal. To verify this hypothesis, we performed whole-brain DTI and cognitive assessment in patients who presented with clinical signs of SACD and a biochemical deficiency of vitamin B_{12}. The DTI measures were correlated with neuropsychological test scores. We also performed voxel-based morphometry analysis for volumetric changes in GM and WM. To the best of our knowledge, this is the first study to quantify the microstructural changes in normal-appearing brain on MR imaging in patients with SACD and biochemically confirmed vitamin B_{12} deficiency.

MATERIALS AND METHODS

Patients with clinical features of peripheral neuropathy suspected of having spinal cord involvement and clinically labeled as having SACD were included in this study. Fifty-one patients who met the above criteria were recruited (38 men, 13 women; mean age, 34.6 ± 12.2 years; age range, 18–58 years). Forty-six age- and sex-matched healthy controls (not on any medication and not known to have any disease) were also included in the study (33 men and 13 women; mean age, 31.1 ± 8.0 years; age range, 18–53 years). No significant differences in age and sex were observed between the patient group and healthy controls.

Clinical Assessment

Neurologic examinations were performed by a neurologist to assess the severity of impairment in patients with vitamin B_{12} deficiency. The patients had detailed nerve-conduction velocity tests and biochemical analysis for serum vitamin B_{12} and homocysteine levels. The diagnosis of vitamin B_{12} deficiency was based on low serum vitamin B_{12} levels (<200 pg/mL).[17] The serum homocysteine level was measured by an enzymatic method.[18] Routine hematologic examinations that included hemoglobin levels and red cell mean corpuscular volume were also performed. Healthy controls were evaluated for serum vitamin B_{12} levels and neurologic and cognitive status; however, they did not undergo nerve-conduction velocity tests and other biochemical analyses. All patients who showed vitamin B_{12} deficiency and had clinical features of SACD underwent MR imaging of both the cervical spine and brain. All patients with normal brain MR imaging findings with or without imaging changes in the cervical spine underwent cognitive testing.

Neuropsychological tests were performed on both patients and controls by an experienced neuropsychologist. This battery included the Trail-Making test, number connection tests A and B, and figure connection tests A and B as well as the performance subset of the modified Wechsler Adult Intelligence Scale (modified for the population), which included picture completion, digit symbol, block design, picture arrangement, and object assembly. These tests evaluate visuospatial capacity and visuomotor speed. The Trail-Making test assesses the visual motor coordination, concentration, attention, mental speed, and memory alteration.[19] In the number connection and figure connection tests A and B, lower scores represent better performance, whereas in the Wechsler Adult Intelligence Scale, a higher score represents a better performance.

This study protocol was approved by the Institutional Ethics Committee. Informed written consent was obtained from each subject.

MR Imaging

All MR imaging studies were performed on a 3T MR imaging scanner (Signa Hdxt; GE Healthcare, Milwaukee, Wisconsin). An 8-channel head coil was used for brain MR imaging. T2-weighted axial images were acquired with TR = 9200 ms, TE = 72 ms, NEX = 1, section thickness = 3 mm, flip angle = 90°, acquisition matrix = 512 × 256, FOV = 240 mm, reconstructed matrix = 1024 × 1024. Parameters of FLAIR imaging were TR = 9000 ms, TE = 128 ms, TI = 2400 ms, NEX = 1, section thickness = 3 mm, flip angle = 90°, acquisition matrix = 320 × 256, FOV = 240 mm, reconstructed matrix = 512 × 512. 3D T1-weighted inversion-recovery-prepared fast-spoiled gradient-echo imaging was performed by using the following parameters: TR = 8.4 ms, TE = 3.3 ms, number of sections = 184, section thickness = 1 mm, intersection gap = 0, FOV = 240 mm, image matrix = 512 × 512, NEX = 1, TI = 400 ms, and flip angle = 13°. DTI data were acquired by using dual spin-echo single-shot echo-planar sequences with 30 uniformly distributed directions with ramp sampling. The acquisition parameters were the following: TR = 17 sec, TE = 88.7 ms, number of sections = 62, section thickness = 3 mm, intersection gap = 0, FOV = 240 × 240 mm, image matrix = 256 × 256, NEX = 1, diffusion-weighting b factor = 1000 s/mm^2.

MR imaging of the cervical spine was performed on a 12-channel head-neck-spine coil by using T1 FLAIR and T2 fast recovery FSE in the sagittal and axial planes. Imaging parameters for T1 FLAIR were the following: TR = 2496 ms, TE = 25 ms, TI = 1013 ms, NEX = 1, section thickness = 3 mm, flip angle = 90°, acquisition matrix = 384 × 256, FOV = 259.99 mm, reconstructed matrix = 512 × 512. T2 fast recovery FSE in the sagittal plane had the following parameters: TR = 2080 ms, TE = 87.17 ms, NEX = 2, section thickness = 3 mm, flip angle = 90°, acquisition matrix = 384 × 256, FOV = 260 mm, reconstructed matrix = 512 × 512. Imaging parameters for T2 fast recovery FSE in the axial plane were the following: TR = 3120 ms, TE = 124 ms, NEX = 2, section thickness = 3 mm, flip angle = 90°, acquisition matrix = 320 × 224, FOV = 180 mm, reconstructed matrix = 512 × 512.

MR Imaging Analysis

Structural Analysis. Voxel-based morphometry analysis was performed by using SPM8 (Wellcome Department of Imaging Neuroscience, London, UK; http://www.fil.ion.ucl.ac.uk/spm) to determine possible changes in the GM and WM volumes. Before processing, the images were visually inspected for possible artifacts. For tissue segmentation, a customized template was built from the sample by using a nonlinear registration

algorithm (DARTEL toolbox in SPM8).[20] This template was registered to the Montreal Neurological Institute (MNI) template for group comparisons. The Jacobian determinants from the normalization procedure were used to modulate the voxel-based morphometry data to preserve the WM and GM volumes. Individual GM and WM images were smoothed with an isotropic Gaussian kernel of 6-mm full width at half maximum before statistical analysis. Global volumes of GM and WM were assessed from segmented images by using the VBM8 toolbox in SPM8 after correcting for age and sex.

Comparison of various neuropsychological parameters among patients presenting with vitamin B_{12} deficiency and age- and sex-matched controls

Test	Subject	Mean	*P* Value
Digit symbol	Control	11.19 ± 2.04	<.001
	Patient	7.22 ± 2.79	
Number connection test A	Control	39.63 ± 9.4	<.001
	Patient	61.67 ± 25.09	
Number connection test B	Control	64.59 ± 16.61	<.001
	Patient	101.59 ± 43.37	
Picture completion	Control	14.89 ± 1.23	<.001
	Patient	12.04 ± 1.89	
Block designing	Control	12.74 ± 1.1	<.001
	Patient	9.08 ± 2.31	
Picture arrangement	Control	13.35 ± 11.53	<.001
	Patient	11.53 ± 2.22	
Object assembling	Control	11.19 ± 1.26	<.001
	Patient	9.88 ± 1.90	
Figure connection test A	Control	56.37 ± 21.72	<.001
	Patient	80.49 ± 41.64	
Figure connection test B	Control	77.85 ± 23.92	<.001
	Patient	125.61 ± 40.99	

Diffusion Tensor Image Processing

The Diffusion Toolbox software tool in the FMRIB Software Library (FSL; http://www.fmrib.ox.ac.uk/fsl/fdt/index.html) was used for calculating the DTI indices fractional anisotropy (FA), ADC, axial diffusivity (AD), and radial diffusivity (RD). The DWI was corrected for eddy current–induced distortions and minor head movements by using affine registration to the reference B0 images. The Brain Extraction Tool was used for extracting the brain.[21]

Tract-Based Spatial Statistics and Voxelwise Analysis

Voxelwise analysis of FA was performed by using tract-based spatial statistics (TBSS),[22] part of the FSL package.[23] Individual skeletonized FA maps were aligned to the MNI 152 template by using the Nonlinear Registration Tool in FMRIB.[24] Each subject's aligned FA map was then projected onto this skeleton, and the voxelwise general linear model was applied by using permutation-based nonparametric testing, corrected for multiple comparisons. Using the same registration parameters from the FA maps, we also spatially transformed ADC, RD, and AD maps to the MNI space.

Region-of-Interest Analysis

In addition to the TBSS analysis, the region-of-interest analysis was also performed on those regions that were observed to be significantly different on the TBSS analysis. Elliptic regions of interest of sizes varying from 25 to 50 mm^2 were placed on different regions in the FA maps of patients and controls.

Statistical Analysis

The differences in the neuropsychological scores between patients and controls were analyzed with independent *t* tests by using the

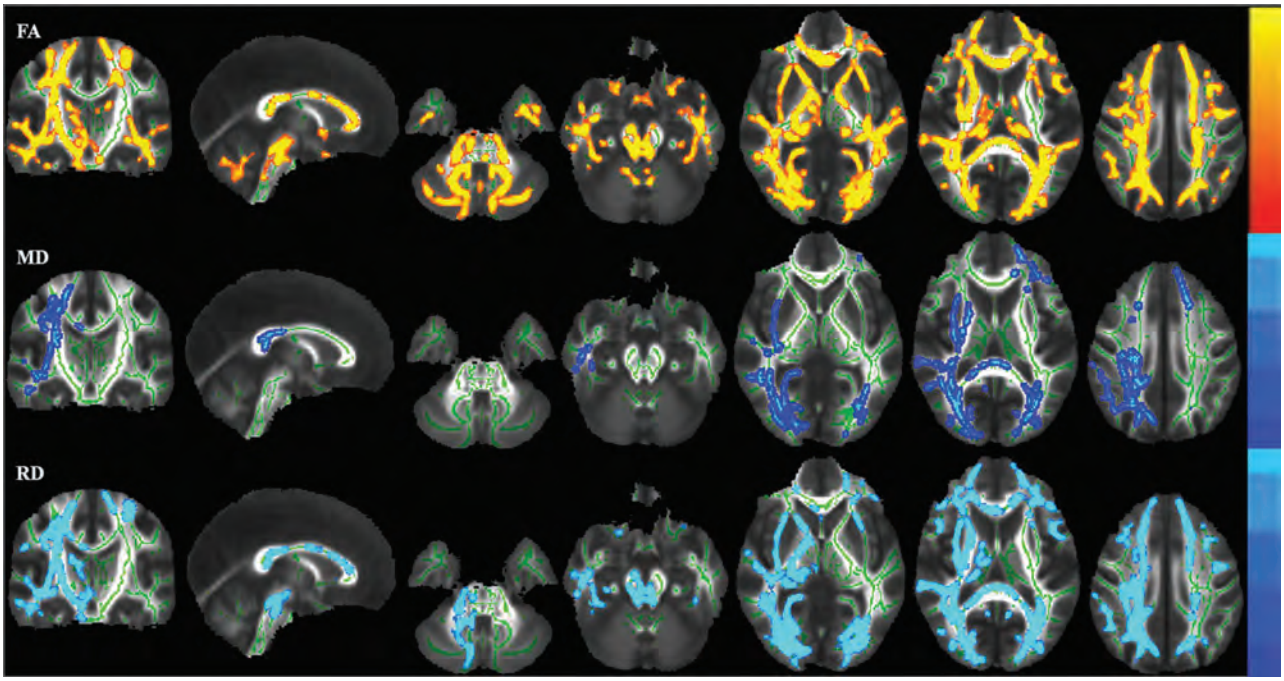

FIG 1. Differences in DTI measures between patients and controls. Statistical maps show voxels that exhibit differences in DTI parameters in patients versus controls (red and yellow colors, according to the lower and higher significance, respectively; dark blue and light blue colors, according to the lower and higher significance, respectively). FA is significantly decreased, and ADC and RD are increased in the patient group compared with controls. Differences are widespread and evident in various WM regions. All WM tracts are overlaid on a 1-mm standard image in MNI 152 (TBSS analysis, 2-sample, $P < .05$, threshold-free cluster enhancement corrected).

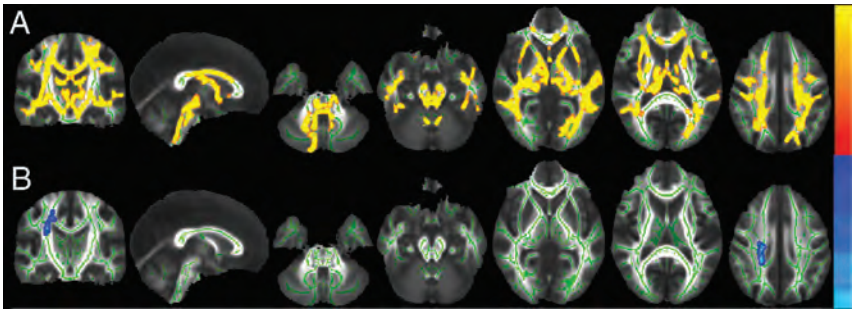

FIG 2. Correlation between FA and neuropsychological scores. The statistical map shows voxels that correlate with neuropsychological scores. *A*, FA positively correlates with Digit Symbol score in various WM regions. *B*, Negative correlation between FA and the number connection test score was observed. All WM tracts are overlaid on a 1-mm standard image in MNI 152 (TBSS analysis, $P < .05$, threshold-free cluster enhancement corrected).

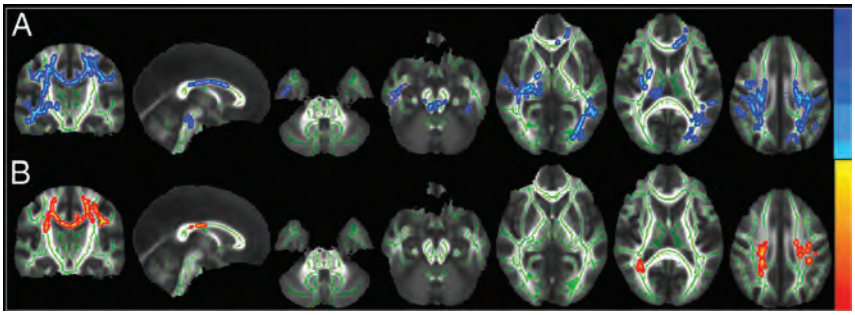

FIG 3. Correlation between RD and neuropsychological scores. Statistical map shows voxels that correlate with neuropsychological scores. *A*, RD negatively correlates with the Digit Symbol score in various WM regions. *B*, A positive correlation between RD and the number connection test score was observed. All WM tracts are overlaid on a 1-mm standard image in MNI 152 (TBSS analysis, $P < .05$, threshold-free cluster enhancement corrected).

Statistical Package for Social Sciences software, Version 16.0l (IBM, Armonk, New York). The correlation between the neuropsychological score and DTI-derived indices of WM was based on the Pearson coefficient. All statistical analyses were based on a 2-tailed test with an α level of $<.05$ for statistical significance.

Morphologic differences between the patients and control subjects were estimated by using an independent-samples *t* test at the voxel level within the general linear model framework of statistical parametric mapping. Comparison between patients and control subjects was made for 2 different contrasts, corresponding to an increase (patient > controls) or decrease (patient < controls) in GM and WM volumes. A false discovery rate at $P < .05$ was used. Differences were considered significant if the cluster size was >15.[25]

The general linear model was applied across all subjects to identify the brain regions in which the patient group showed significant differences in FA, ADC, AD, and RD relative to the healthy control group. The correlation analyses were performed to study the relationship between neuropsychological scores and each of the DTI-derived indices FA, ADC, AD, and RD in the WM by using neuropsychological scores as regressors in the framework of a general linear model. The effects of age and sex were regressed out in these models. DTI-derived maps were included in a nonparametric permutation-based group model by using "Randomize" in FSL. An independent *t* test was used to determine the differences in FA, ADC, RD, and AD values obtained from the region-of-interest analysis between patient and control groups.

RESULTS

Clinical Assessment

The mean hemoglobin level in patients with vitamin B_{12} deficiency was 10.95 ± 2.28 g/dL (range, 6.8–16 g/dL), the mean serum vitamin B_{12} concentration was 145.26 ± 42.07 pg/mL (range, 26–199 pg/mL), the mean cell volume was 103.6 ± 12.26 fL (range, 81.3–122.3 fL), and the serum homocysteine level was 19.84 ± 7.32 μmol/L (range, 7.9–41.29 μmol/L). The mean serum vitamin B_{12} concentration in healthy controls was 330.22 ± 135.22 pg/mL (range, 255–678 pg/mL). All patients had gait disturbance, sensory disturbance, mental impairment, and neuropathy. A total of 11.8% of patients presented clinically with pyramidal tract damage. Differences were observed in all the neuropsychological scores between patients and controls (Table).

Conventional MR Imaging

MR imaging of the cervical spine showed T2 hyperintensity in the posterior spinal cord in 7 patients and diffuse hyperintensity of the cervical cord in 1 patient. The remaining 43 patients did not show any abnormality in the cervical cord on conventional MR imaging.

Voxel-Based Morphometry Analysis

The voxel-based morphometry analysis of the 3D-T1WI did not show a significant difference in the cerebral GM and WM volumes between patients and controls.

TBSS Analysis

TBSS analysis showed significantly reduced FA values in patients compared with controls in a number of WM regions, which included the frontal, parietal, and temporal lobes and the entire corpus callosum and its associated fibers (Fig 1). The patient group also had a widespread increase in ADC and RD values, predominantly in the right hemisphere tracts (right > left) and the corpus callosum.

Correlation Analysis of DTI Indices with Neuropsychological Scores

Correlation maps showed a significant positive correlation between the Digit Symbol scores and FA values (Fig 2*A*) and a significant negative correlation between the number connection test and FA values (Fig 2*B*) in many WM bundles (*P* corrected < .05). RD values were found to correlate negatively with Digit Symbol scores (Fig 3*A*) and positively with number connection test scores (Fig 3*B*). ADC and AD did not show any significant correlation

with neuropsychological scores. The mean FA and RD values were extracted subject by subject from correlation maps from regions showing significant correlation between DTI indices and neuropsychological scores. Thereafter, Pearson correlation coefficients were obtained by using SPSS in the Digit Symbol test, with FA ($r = 0.63$, $P < .001$ in patients; $r = 0.56$, $P < .001$ controls) and RD ($r = -0.54$, $P < .001$ in patients; $r = -0.53$, $P < .001$ in controls); and the number connection test with FA ($r = -0.56$, $P < .001$ in patients; $r = -0.22$, $P = .14$ in controls) and RD ($r = 0.57$, $P < .001$ in patients; $r = 0.403$, $P < .005$ in controls) to verify the results obtained on correlation maps.

Region-of-Interest Analysis

Region of interest–based analysis confirmed the TBSS results. The results are summarized in Fig 4. AD values did not show a significant change between patients and controls either on the TBSS or region-of-interest analysis.

DISCUSSION

This study shows widespread changes in the cerebral WM in patients with vitamin B_{12} deficiency in all the DTI metrics, except AD, indicating altered WM microstructure in multiple regions in these patients. These results were confirmed in the region-of-interest analysis. In addition, all these patients showed significant cognitive decline over the controls. The cognitive scores correlated with DTI measures in various brain regions. Our findings suggest that the microstructure changes in WM are quite widespread in the brain, even when patients showed clinical symptoms related to the spinal cord. We did not observe any volume changes in WM and GM on voxel-based morphometry analysis, suggesting that atrophy is not a major pathologic component in these patients.

FA is widely considered a robust measure of WM organization, and a number of studies have reported abnormalities in FA across both psychotic and affective illnesses.[26] Disruptions in WM organization (reflected in reductions in FA) can result from various mechanisms, including demyelination as well as axonal loss and lacks pathologic specificity. However, the other DTI-derived measures, such as RD and AD, are thought to reflect myelin and axonal integrity, respectively.[27] While still controversial, some published literature suggests that RD is a more sensitive measure of myelin integrity, while AD reflects axonal integrity.[28,29] In the current study, we observed increased RD and unchanged AD, suggesting that demyelination, not axonal loss, is the major pathologic substrate in B_{12} deficiency. Scalabrino and Veber[30] have demonstrated, in the rat model, that vitamin B_{12} deficiency damages myelin and causes myelin vacuolation and reactive astrocytosis in the CNS. In a recent study, Minn et al[31] reported that patients with SACD have progressive degeneration in the following sequential order: lower spinal cord, cervical spinal cord, peripheral nerve/optic nerve, and, finally, the brain. Our data do not support this view and show that B_{12} deficiency causes demyelination in the brain even when it may manifest clinically with SACD.

In a prospective study on 50 patients with vitamin B_{12} deficiency, Reynolds[32] has shown cognitive impairment or an affective disorder in one-third of patients. Minn et al[31] did not find any symptoms of dementia in any of their patients who presented with SACD. However, in the current study, all 51 patients showed sig-

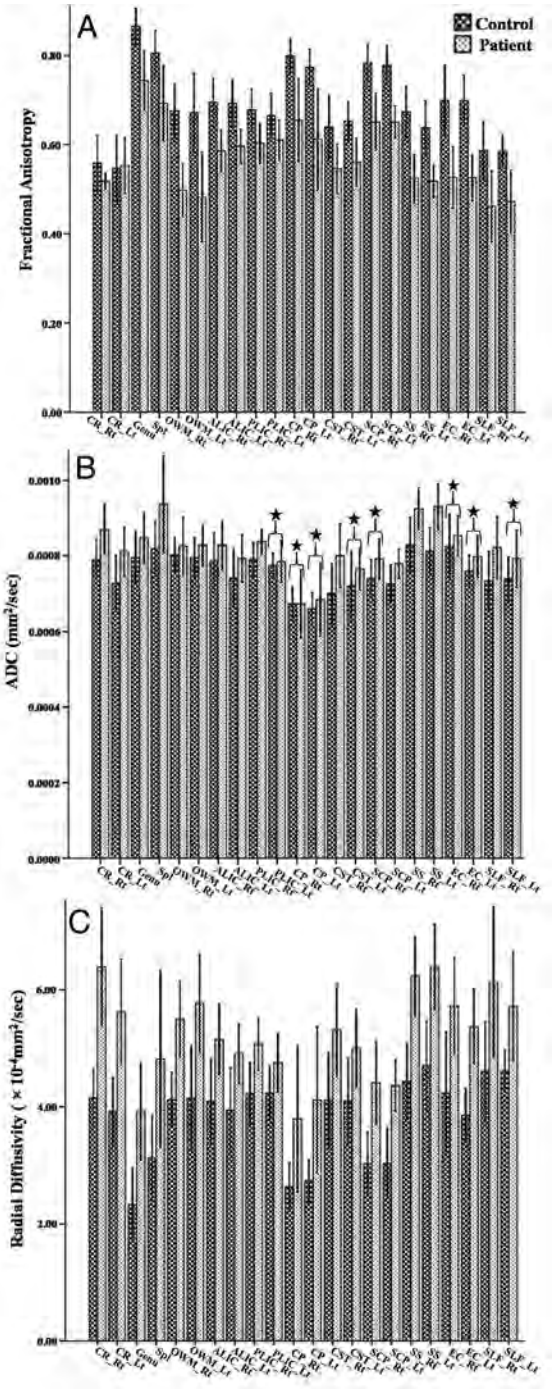

FIG 4. Bar diagram showing significant differences in various white matter regions on DTI metrics in patients compared with controls on region-of-interest analysis. Bars show a significant difference in FA (*A*), ADC (the asterisk indicates regions with nonsignificant differences) (*B*), and RD (*C*) in the specified regions. CR_Rt & CR_Lt indicates corona radiata right and left; Spl, splenium; OWM_Rt & OWM_Lt, occipital white matter right and left; ALIC_Rt & ALIC_Lt, anterior limb of the internal capsule right and left; PLIC_Rt & PLIC_Lt, posterior limb of the internal capsule right and left; CP_Rt & CP_Lt, cerebellar peduncle right and left; CST_Rt & CST_Lt, corticospinal tract right and left; SCP_Rt & SCP_Lt, superior cerebellar peduncle right and left; SS_Rt & SS_Lt, sagittal stratum right and left; EC_Rt & EC_Lt, external capsule right and left; SLF_Rt & SLF_Lt, superior longitudinal fasciculus right and left.

nificant cognitive deficits on neuropsychological tests compared with the age- and sex-matched controls, suggesting that a complete battery of tests may be needed to detect cognitive impairment in these patients. Dementia and cognitive changes have been typically reported in elderly subjects with B_{12} deficiency. In contrast, we detected cognitive deficits in our relatively young patient cohort.

Cognitive decline has been observed at all age groups in patients with vitamin B_{12} deficiency. Sensitive neuropsychological tests have shown an association with vitamin deficiency.[33] In the current study, we also observed a decline in visuospatial and performance skills in these patients. Another group has reported cognitive decline in patients between 35 and 50 years of age with vitamin B_{12} deficiency, which improved following its supplementation.[34]

Most studies in the geriatric population show conflicting results. Some authors have found a strong causal relationship between cognitive decline and vitamin B_{12} deficiency, while others have described the relationship as mere coincidence in the geriatric population.[3,5,12] The mechanism for cognition decline is the accumulation of methylmalonic acid secondary to nonactivation of methylmalonyl-CoA mutase, which is myelinotoxic.[35] We also observed a strong correlation of the neuropsychological scores with FA, ADC, and RD changes in some brain regions on DTI.

CONCLUSIONS

Microstructural changes in various brain regions are demonstrated on DTI metrics in patients with SACD, and these are associated with abnormal neuropsychological scores and show a correlation with various specific brain regions. The imaging technique may be of value in the objective assessment of the brain changes in B_{12} deficiency.

Disclosures: Ponnada Narayana—*UNRELATED*: *Grants/Grants Pending*: National Institutes of Health,* Department of Defense. **Money paid to the institution.

REFERENCES

1. Strand TA, Taneja S, Ueland PM, et al. **Cobalamin and folate status predicts mental development scores in North Indian children 12–18 mo of age.** *Am J Clin Nutr* 2013;97:310–17
2. Black MM. **Effects of vitamin B12 and folate deficiency on brain development in children.** *Food Nutr Bull* 2008;29:S126–31
3. Clarke R, Birks J, Nexo E, et al. **Low vitamin B-12 status and risk of cognitive decline in older adults.** *Am J Clin Nutr* 2007;86:1384–91
4. Kivipelto M, Annerbo S, Hultdin J, et al. **Homocysteine and holotranscobalamin and the risk of dementia and Alzheimers disease: a prospective study.** *Eur J Neurol* 2009;16:808–13
5. Lachner C, Steinle NI, Regenold WT. **The neuropsychiatry of vitamin B12 deficiency in elderly patients.** *J Neuropsychiatry Clin Neurosci* 2012;24:5–15
6. Ford AH, Flicker L, Thomas J, et al. **Vitamins B12, B6, and folic acid for onset of depressive symptoms in older men: results from a 2-year, placebo-controlled, randomized trial.** *J Clin Psychiatry* 2008:69:1203–09
7. Crawford JR, Say D. **Vitamin B12 deficiency presenting as acute ataxia.** *BMJ Case Rep* 2013;pii
8. Gürsoy AE, Kolukısa M, Babacan-Yıldız G, et al. **Subacute combined degeneration of the spinal cord due to different etiologies and improvement of MRI findings.** *Case Rep Neurol Med* 2013;2013:159649
9. Tangney CC, Aggarwal NT, Li H, et al. **Vitamin B12, cognition, and brain MRI measures.** *Neurology* 2011;77:1276–82
10. Silva MT, Cavalcanti JL, Moreira DM. **Neuroradiological features of the brain in subacute combined spinal cord degeneration: case report** [in Portuguese]. *Arq Neuropsiquiatr* 2000;58:752–55
11. Katsaros VK, Glocker FX, Hemmer B, et al. **MRI of spinal cord and brain lesions in subacute combined degeneration.** *Neuroradiology* 1998;40:716–19
12. Smith AD, Refsum H. **Vitamin B-12 and cognition in the elderly.** *Am J Clin Nutr* 2009;89:707S–11S
13. Vogiatzoglou A, Refsum H, Johnston C, et al. **Vitamin B12 status and rate of brain volume loss in community-dwelling elderly.** *Neurology* 2008;71:826–32
14. Biancheri R, Cerone R, Schiaffino MC, et al. **Cobalamin (Cbl) C/D deficiency: clinical, neurophysiological and neuroradiologic findings in 14 cases.** *Neuropediatrics* 2001;32:14–22
15. Lövblad K, Ramelli G, Remonda L, et al. **Retardation of myelination due to dietary vitamin B12 deficiency: cranial MRI findings.** *Pediatr Radiol* 1997;27:155–58
16. Taskesen M, Yaramis A, Pirinccioglu AG, et al. **Cranial magnetic resonance imaging findings of nutritional vitamin B12 deficiency in 15 hypotonic infants.** *Eur J Paediatr Neurol* 2012;16:266–70
17. Remacha AF, Souto JC, Piñana JL, et al. **Vitamin B12 deficiency, hyperhomocysteinemia and thrombosis: a case and control study.** *Int J Hematol* 2011;93:458–64
18. Clarke R, Refsum H, Birks J, et al. **Screening for vitamin B-12 and folate deficiency in older persons.** *Am J Clin Nutr* 2003;77:1241–47
19. Dhiman RK, Saraswat VA, Verma M, et al. **Figure connection test: a universal test for assessment of mental state.** *J Gastroenterol Hepatol* 1995;10:14–23
20. Ashburner J. **A fast diffeomorphic image registration algorithm.** *Neuroimage* 2007:38:95–113
21. Smith SM. **Fast robust automated brain extraction.** *Hum Brain Mapp* 2002;17:143–55
22. Smith SM, Jenkinson M, Johansen-Berg H, et al. **Tract-based spatial statistics: voxelwise analysis of multi-subject diffusion data.** *Neuroimage* 2006;31:1487–505
23. Smith SM, Jenkinson M, Woolrich MW, et al. **Advances in functional and structural MR image analysis and implementation as FSL.** *Neuroimage* 2004;23:S208–19
24. Andersson JL, Jenkinson M, Smith S. Non-linear optimisation. FMRIB Analysis Group Technical Reports. TR07JA1. www.fmrib.ox.ac.uk/analysis/techrep. Accessed 2007
25. Margariti PN, Astrakas LG, Tsouli SG, et al. **Investigation of unmedicated early onset restless legs syndrome by voxel-based morphometry, T2 relaxometry, and functional MR imaging during the nighttime hours.** *AJNR Am J Neuroradiol* 2012;33:667–72
26. Domen PA, Michielse S, Gronenschild E, et al. **Microstructural white matter alterations in psychotic disorder: a family-based diffusion tensor imaging study.** *Schizophr Res* 2013;146:291–300
27. Inano S, Takao H, Hayashi N, et al. **Effects of age and gender on white matter integrity.** *AJNR Am J Neuroradiol* 2011;32:2103–09
28. Song SK, Sun SW, Ramsbottom MJ, et al. **Dysmyelination revealed through MRI as increased radial (but unchanged axial) diffusion of water.** *Neuroimage* 2002;17:1429–36
29. Bockhorst KH, Narayana PA, Dulin J, et al. **Normobaric hyperoximia increases hypoxia-induced cerebral injury: DTI study in rats.** *J Neurosci Res* 2010;88:1146–56
30. Scalabrino G, Veber D. **Normal prions as a new target of cobalamin (vitamin B12) in rat central nervous system.** *Clin Chem Lab Med* 2013;51:601–06
31. Minn YK, Kim SM, Kim SH, et al. **Sequential involvement of the nervous system in subacute combined degeneration.** *Yonsei Med J* 2012;53:276–78
32. Reynolds E. **Vitamin B12, folic acid, and the nervous system.** *Lancet Neurol* 2006;5:949–60
33. Morris MS. **The role of B vitamins in preventing and treating cognitive impairment and decline.** *Adv Nutr* 2012;3:801–12
34. Aaron S, Kumar S, Vijayan J, et al. **Clinical and laboratory features and response to treatment in patients presenting with vitamin B12 deficiency-related neurological syndromes.** *Neurol India* 2005;53:55–58
35. Selhub J, Morris MS, Jacques PF, et al. **Folate-vitamin B-12 interaction in relation to cognitive impairment, anemia, and biochemical indicators of vitamin B-12 deficiency.** *Am J Clin Nutr* 2009;89:702S–06S

Role of EPI-FLAIR in Patients with Acute Stroke: A Comparative Analysis with FLAIR

A. Meshksar, J.P. Villablanca, R. Khan, R. Carmody, B. Coull, and K. Nael

ABSTRACT

BACKGROUND AND PURPOSE: Further improvement in acquisition speed is needed, if MR imaging is to compete with CT for evaluation of patients with acute ischemic stroke. The purpose of this study was to evaluate the feasibility of implementing an echo-planar fluid-attenuated inversion recovery (EPI-FLAIR) sequence into an acute MR stroke protocol with potential reduction in scan time and to compare the results with conventional FLAIR images.

MATERIALS AND METHODS: Fifty-two patients (28 men and 24 women; age range, 32–96 years) with acute ischemic stroke were prospectively evaluated with an acute stroke MR protocol, which included both conventional FLAIR and EPI-FLAIR imaging with integration of parallel acquisition. The image acquisition time was 52 seconds for EPI-FLAIR and 3 minutes for conventional FLAIR. FLAIR and EPI-FLAIR studies were assessed by 2 observers independently for image quality and conspicuity of hyperintensity in correlation with DWI and were rated as concordant or discordant. Coregistered FLAIR and EPI-FLAIR images were evaluated for signal intensity ratio of the DWI-positive lesion to contralateral normal white matter.

RESULTS: An estimated 96% of all FLAIR and EPI-FLAIR studies were rated of diagnostic image quality by both observers, with interobserver agreements of $\kappa = 0.82$ and $\kappa = 0.63$ for FLAIR and EPI-FLAIR, respectively. In 36 (95%) of 38 patients with acute infarction, FLAIR and EPI-FLAIR were rated concordant regarding DWI lesion. The mean ± standard deviation of the signal intensity ratio values on EPI-FLAIR and FLAIR for DWI-positive lesions were 1.28 ± 0.16 and 1.25 ± 0.17, respectively ($P = .47$), and demonstrated significant correlation ($r = 0.899$, z value $= 8.677$, $P < .0001$).

CONCLUSIONS: In patients with acute stroke, EPI-FLAIR is feasible with comparable qualitative and quantitative results to conventional FLAIR and results in reduced acquisition time.

ABBREVIATIONS: AIS = acute ischemic stroke; GRE = gradient recalled-echo; SD = standard deviation; SIR = signal intensity ratio

Neuroimaging plays a central role in the evaluation of patients with acute ischemic stroke (AIS). With improved technology during the last decade, imaging now provides information beyond the mere presence or absence of intracranial hemorrhage. Multimodal cerebrovascular CT and MR can now provide information about tissue viability, site of occlusion, and collateral status. The success of CT in the initial evaluation of AIS is due, in part, to fast acquisition time, widespread availability, and ease of interpretation in the emergency department setting.

MR imaging has been demonstrated to be more sensitive for the detection of acute ischemia and more specific for delineation of infarction core volume compared with CT.[1,2] However, because of longer acquisition time and limited availability, it has been mainly used in large institutions and comprehensive stroke centers. With recent advances in MR technology, a comprehensive MR protocol including parenchymal imaging (DWI, gradient recalled-echo [GRE], FLAIR), MRA, and MR perfusion can now be adequately obtained in 20 minutes as demonstrated in several clinical trials.[3-7] In a likewise fashion, the introduction of multisection technology has dramatically increased the speed and simplicity of CT techniques and has set a high standard for alternative imaging techniques. A comprehensive CT stroke algorithm including parenchymal imaging (noncontrast head CT), CTA, and perfusion/penumbral imaging by CT perfusion can now be ac-

Received May 10, 2013; accepted after revision September 8.

From the Departments of Medical Imaging (A.M., R.K., R.C., K.N.), and Neurology (B.C.), University of Arizona; Tucson, Arizona; and Department of Radiological Sciences (J.P.V.), University of California at Los Angeles, Los Angeles, California.

Abstract previously presented at: Annual Meeting of the American Society of Neuroradiology, May 22, 2013; San Diego, California.

Please address correspondence to Kambiz Nael, MD, Assistant Professor of Radiology, Director of Neuroradiology MRI, Department of Medical Imaging, Neuroradiology Section, University of Arizona Medical Center, 1501 N. Campbell, PO Box 245067, Tucson, AZ; e-mail: kambiz@radiology.arizona.edu

http://dx.doi.org/10.3174/ajnr.A3786

quired and processed in a comparable period.[8,9] If MR imaging is to compete with CT for evaluation of acute stroke, there is need for further improvements in acquisition speed.

FLAIR imaging as a part of an acute MR stroke protocol has several advantages including detection of subtle cerebral subarachnoid hemorrhage; added diagnostic value to GRE images for the detection of intra-arterial clot[10-12]; and, most important, helping to determine the age of infarction in patients with both known and unknown time of onset of neurologic deficit (wake-up stroke).[13] The latter advantage has a major impact on the treatment planning because FLAIR hyperintensity is usually indicative of a completed stroke, thereby excluding these patients from most therapeutic interventions.[14,15]

Introduction of fast imaging techniques such as parallel acquisition[16] and EPI[17,18] has significantly enhanced the performance of MR imaging in acquisition speed. The main advantage of EPI, as in the case of DWI, is rapid acquisition time, which is made possible by rapid gradient switching, which allows the acquisition of all frequency and phase-encoding steps during a single pulse cycle. The addition of parallel imaging can further enhance the acquisition speed and may also serve to mitigate the geometric distortion and susceptibility artifacts commonly associated with long echo-train sequences such as EPI.[19,20] If their potential is realized, the application of EPI and parallel imaging techniques to the FLAIR sequence can result in a reduction of image acquisition time of the entire brain to less than a minute, a 3-fold reduction in scan time compared with conventional FLAIR imaging. The purpose of this study was to evaluate the feasibility of implementing an EPI-FLAIR sequence into an acute MR stroke protocol with its potential reduction in scan time, and to compare the result with conventional FLAIR imaging.

MATERIALS AND METHODS

This prospective study was conducted between May and September 2012. All examinations were performed in accordance with institutional review board guidelines with an approved study protocol. Our inclusion criteria included 1) patients with clinical suspicion of AIS who presented within the first 24 hours from the onset of neurologic deficits, and 2) acquisition of MR imaging as the initial imaging study. Exclusion criteria included ferromagnetic or MR incompatible implants, glomerular filtration rate < 30 mL/min/1.73 m^2, and severe claustrophobia. The baseline NIHSS scores and median time from stroke onset to MR imaging were documented for each patient when available.

Image Acquisition

All patients were studied on a 1.5T MR system (Avanto; Siemens, Erlangen, Germany). The imaging protocol included DWI, conventional FLAIR, EPI-FLAIR, GRE, MRA, and dynamic susceptibility contrast perfusion imaging. A combination of head and neck coil with up to 12 channels was used for radiofrequency signal reception. A spin-echo and an EPI sequence were used for FLAIR and EPI-FLAIR, respectively, with the following parameters: TR, 9000 ms (10,000 ms for EPI-FLAIR); TE, 88 ms (106 ms for EPI-FLAIR); inversion time, 2500 ms; flip angle, 150° (90° for EPI-FLAIR). Other imaging parameters, including field of view of 22 cm, matrix size of 256 mm (192 mm for EPI-FLAIR), and 26 total sections each 5-mm thick, were kept constant between the 2 sequences. Integration of generalized autocalibrating partially parallel acquisition with an acceleration factor of 2 resulted in an acquisition time of 3 minutes for conventional FLAIR and 52 seconds for EPI-FLAIR, respectively.

Image Analysis

Conventional FLAIR and EPI-FLAIR images were reviewed independently by 2 experienced neuroradiologists and in separate reading sessions. The observers were able to adjust image contrast and size. A 4-scale imaging score was used to evaluate the image quality with respect to susceptibility-mediated distortion at tissue interfaces, noise, and motion: 1) poor image quality, not interpretable; 2) impaired image quality with significant distortion and noise, limiting delineation of major structures; 3) good image quality with minimal distortion, diagnostic image quality; and 4) excellent image quality with delineation of all structures.

In addition to image quality, the observers were asked to correlate the FLAIR and EPI-FLAIR images with DWI-ADC maps, determine the presence of hyperintense signal corresponding to the area of restricted diffusion, and categorize the image pairs as concordant or discordant. This comparison was performed during different reading sessions for both conventional FLAIR and EPI-FLAIR, to avoid recall bias. The observers were also asked to localize the FLAIR/EPI-FLAIR lesions to 3 anatomic regions: 1) supratentorial, 2) infratentorial, or 3) both. Finally, and again in a different reading session, any discrepancy between readers for lesion location or FLAIR/EPI-FLAIR DWI correlation was resolved by consensus agreement. These scores were then used to perform comparative analysis between conventional FLAIR and EPI-FLAIR.

DWI, FLAIR, and EPI-FLAIR images for each patient were coregistered by a commercially available FDA-approved software (Olea Sphere; Olea Medical SAS, La Ciotat, France) by use of a 12 degrees-of-freedom transformation and a mutual information cost function. This was followed by visual inspection to ensure adequate alignment. The segmentation was performed by a single neuroradiologist. The ROIs were placed over the region of infarction (DWI+) in 1 section to extract the corresponding FLAIR and EPI-FLAIR signal intensity values. ROIs were then mirrored onto the contralateral hemisphere, and the SIR values with respect to contralateral, normal-appearing white matter were calculated by use of the mean SI values. Manual restriction of the ROIs was applied when necessary to avoid regions with prior infarction or chronic microvascular ischemic changes.

In patients who did not have a DWI abnormality, a 1-cm ROI was placed in the centrum semiovale and automatically mirrored onto the contralateral hemisphere to calculate the SIR.

The volume of lesions on FLAIR and EPI-FLAIR studies was calculated by use of Olea Sphere software. ROIs were created on the basis of the signal intensity subsuming the entire region of hyperintensity, and the volume and standard deviation (SD) was calculated. The range included was the interval of pixel values to

Table 1: Correlation of FLAIR and EPI-FLAIR compared with DWI ($n = 50$)

N	DWI	FLAIR (Signal)	EPI-FLAIR (Signal)	Conclusion
12	−	−	−	No ischemic infarction
10	+	−	−	Concordant FLAIR–EPI-FLAIR, early stage of ischemic infarction
26	+	+	+	Concordant FLAIR–EPI-FLAIR, completed infarction
2	+	+	−	EPI-FLAIR discordant with FLAIR

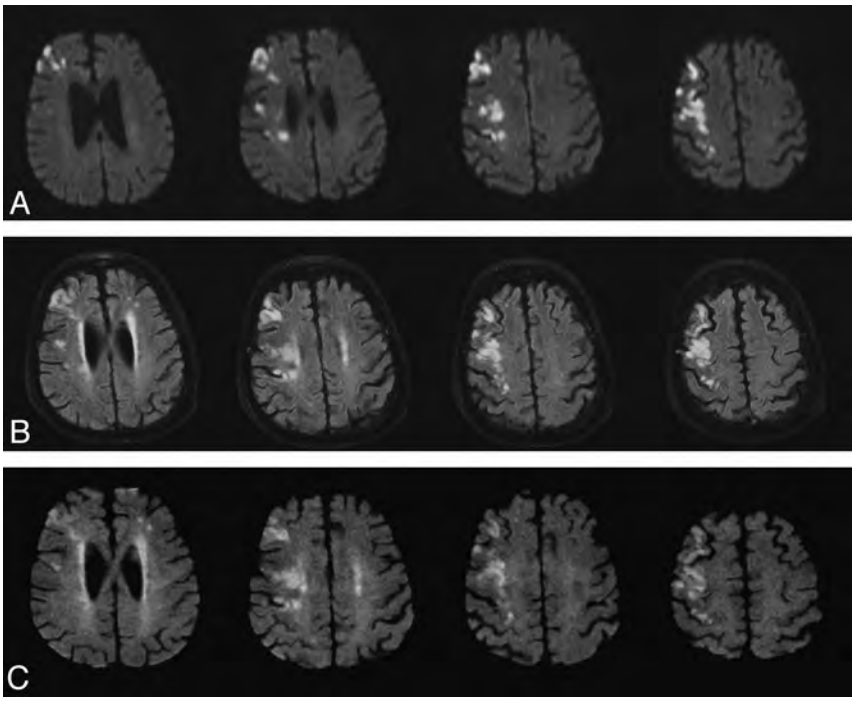

FIG 1. An 86-year-old man with acute onset left-sided weakness after elective cardiac surgery, NIHSS:8. Axial DWI (4500/90, $b = 1000$ s/mm^2) (*A*), FLAIR (9000/88/2500) (*B*), and EPI-FLAIR (10,000/106/2500) (*C*) images obtained 4.5 hours after the onset of symptoms. Watershed infarctions are noted along the right cerebral hemisphere deep white matter zones. Note the comparable image quality between FLAIR and EPI-FLAIR, both demonstrating increased signal intensity in the region of DWI abnormality, indicative of completed infarctions. Acquisition time for FLAIR was 3 minutes; for EPI-FLAIR, it was 52 seconds.

include the central value of the initial seed-voxel. Manual restriction of the ROIs was applied when necessary. The largest lesion in a single section was selected for the volume measurement. For patients with multiple or embolic infarction, the largest lesion was selected for volume analysis.

Finally, the patients with acute infarction were categorized in 2 groups based on time from onset to MR imaging of ≥4.5 hours as the cutoff value for thrombolysis. The mean ± SD of the SIR values on EPI-FLAIR and FLAIR correlated in these 2 groups.

Statistical Analysis

Statistical analysis was performed by use of MedCalc Version 12.2.1 (MedCalc Software, Mariakerke, Belgium).The Wilcoxon signed rank test was used to compare the mean ratings of FLAIR and EPI-FLAIR. A weighted κ test with a calculation of 95% CI was used to evaluate the interobserver and intermodality agreement. The Spearman correlation coefficient was calculated for the comparative analysis of DWI with FLAIR/EPI-FLAIR. The quantitative SIR values between FLAIR and EPI-FLAIR were tested with a *t* test and a correlation coefficient (*r*). The significance level was defined as $P < .05$ (2-sided).

RESULTS

A total of 52 consecutive patients (28 men and 24 women; age range, 32–96 years) met our inclusion criteria. The median and interquartile ranges of the baseline NIHSS scores were 11 and 10.75, respectively. The median and interquartile ranges of the time from presentation to MR imaging was 6 and 7.5 hours, respectively, in 34 of 38 patients with acute ischemic infarction. In 4 patients with acute infarction, the time from the onset of symptoms was unknown.

Two studies (4%) were deemed nondiagnostic and were excluded from the study, one because of susceptibility artifacts caused by dental braces and the other because of significant motion artifacts. In 50 (96%) of 52 studies, FLAIR and EPI-FLAIR studies were rated of diagnostic image quality (image quality ≥3) by both observers. The median and ranges of image quality scores were 4 and 3–4, respectively, for FLAIR by both observers, with no statistically significant difference ($P = .54$) and with an interobserver agreement of $\kappa = 0.82$; 95% CI, 0.67–0.90. The median and ranges of image quality scores were 3 and 3–4, respectively, for EPI-FLAIR by both observers with no statistically significant difference ($P = .4$) and an interobserver agreement of $\kappa = 0.63$ (95% CI, 0.37–0.80).

Twelve patients did not have restricted diffusion on DWI; therefore, results were negative on both FLAIR and EPI-FLAIR with complete concordance. There were 38 patients who had acute infarction (+DWI lesion). The infarctions were supratentorial in 32 patients, infratentorial in 2 patients, and both supratentorial and infratentorial in 4 patients. In 36 (95%) of 38 patients with acute infarction, FLAIR and EPI-FLAIR concurred and demonstrated good correlation: $r = 0.88$; 95% CI, 0.80–0.93 (Table 1). In 26 patients in whom both FLAIR and EPI-FLAIR were positively concordant with DWI (Fig 1), the time from onset to MR imaging ranged from 2.5–18 hours. In 10 patients for whom both FLAIR and EPI-FLAIR were negatively concordant with DWI hyperintensity, the time from presentation to MR imaging ranged from 50 minutes to 3 hours. In only 2 patients (5%), EPI-FLAIR was discordant with FLAIR and was unable to show subtle FLAIR hyperintensity corresponding to a DWI lesion. In 1 case, there was a punctate small thalamic infarction. The other discordant case was a hyperacute ischemic infarction in a patient who

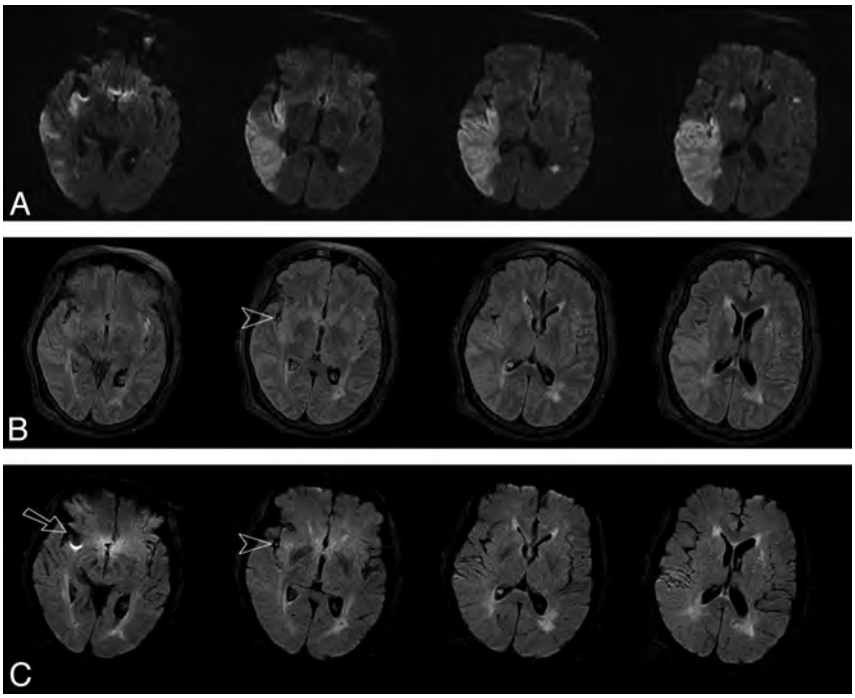

FIG 2. A 60-year-old man with sudden-onset left-sided weakness after an aneurysm coil was placed for a proximal supraclinoid ICA aneurysm. Axial DWI (4500/90, b = 1000 s/mm^2) (*A*), FLAIR (9000/88/2500) (*B*), and EPI-FLAIR (10,000/106/2500) (*C*) obtained approximately 60 minutes after onset of symptoms. Acute infarction along the right MCA territory is noted. The signal intensity ratio of the lesion to the contralateral hemisphere was elevated and measured 1.19 for FLAIR and 1.15 for EPI-FLAIR. Qualitatively, however, very subtle increased hyperintensity corresponding to the region of DWI abnormality is evident on FLAIR but is not clearly seen on EPI-FLAIR. Note the susceptibility artifacts related to the dislodged coil in the MCA bifurcation, which is more pronounced on EPI-FLAIR (*arrow*) and likely contributed to field inhomogeneity and may have explained the qualitative discrepancy with FLAIR. Note the hyperintense vessel sign (*arrowheads*) on both FLAIR and EPI-FLAIR caused by sluggish flow or clot in the sylvian MCA branches.

Table 2: Comparison of SIR values between FLAIR and EPI-FLAIR studies (n = 50)

	FLAIR SIR	EPI-FLAIR SIR	*T* Test (*P* Value)
DWI negative			
(−) FLAIR, (−) EPI-FLAIR (n = 12)	1.02 ± 0.005	1.02 ± 0.006	.2
DWI positive			
<4.5 hours of time from onset to MR imaging (n = 12)	1.14 ± 0.08	1.10 ± 0.06	.22
>4.5 hours of time from onset to MR imaging (n = 22)	1.36 ± 0.16	1.33 ± 0.17	.83
(+) FLAIR, (−) EPI-FLAIR (n = 2)	1.15 ± 0.03	1.13 ± 0.05	/A[a]

Note:—Data are mean ± standard deviation.

[a] In 2 discrepant cases, the SIR values were comparable. The sample was too small for evaluation with the *t* test. In 4 patients with unknown time of presentation, the SIR values were concordant between FLAIR and EPI-FLAIR (SIR > 1.3, n = 3; SIR < 1.3, n = 1).

underwent imaging only 1 hour after endovascular aneurysm coiling (Fig 2). There were no discrepancies between FLAIR and EPI-FLAIR in identification of the anatomic location of infarctions. A hyperintense vascular sign, which was suggestive of a blood clot or sluggish flow, was identified in 5 cases on both FLAIR and EPI-FLAIR (supraclinoid internal carotid artery [n = 2], basilar artery [n = 1], and proximal MCA [n = 2]).

The volume (mean ± SD) of lesions on FLAIR and EPI-FLAIR were 15.4 ± 12.7 and 17.5 ± 15.8, respectively (P = .3).The mean ± SD of the SIR values for EPI-FLAIR and FLAIR are detailed in Table 2. In 12 patients with no infarction, the mean SIR values were 1.02 for both FLAIR and EPI-FLAIR (P = .2). The overall mean ± SD of the SIR values on EPI-FLAIR and FLAIR for DWI-positive lesions were 1.28 ± 0.16 and 1.25 ± 0.17, respectively (P = .47).

The mean (1.33) of EPI-FLAIR SIR values for patients who presented > 4.5 hours from the onset was statistically higher (t value, 7.959; P < .0001) than for those who presented < 4.5 hours from the onset (1.10). In a similar fashion, the mean (1.36) of FLAIR SIR values for patients who presented > 4.5 hours from the onset was statistically higher (t value, 7.491; P < .0001) than for those who presented < 4.5 hours (1.14).

There was significant correlation for the SIR values between FLAIR and EPI-FLAIR (r = 0.899; z value = 8.677; P < .0001). Fig 3 shows the scatterplots and Bland-Altman plots of the SIR between FLAIR and EPI-FLAIR. In 2 discordant cases, despite visual discordancy between FLAIR and EPI-FLAIR for the detection of hyperintensity corresponding to a DWI lesion, the SIR values were comparable (Table 2). In 4 patients with an unknown time of presentation, the FLAIR and EPI-FLAIR values were concordant, with SIR values > 1.3 in 3 patients and SIR < 1.3 in 1 patient.

DISCUSSION

There are 2 different schools of thought on neuroimaging for AIS. Although CT is the most widely available method and is a faster imaging technique, some larger institutions and many comprehensive stroke centers favor streamlined MR protocols compared with CT in the acute stroke setting because of the higher specificity and superior tissue characterization afforded by MR imaging.

Our results demonstrate that the described EPI-FLAIR sequence is feasible for use in the acute stroke setting, with comparable qualitative and quantitative results to a conventional FLAIR sequence, and has the potential for saving valuable acquisition time in patients with AIS. For such patients within the therapeutic time window, it has been estimated that for every minute during which ischemic stroke is left untreated, approximately 1.9 million neurons are lost.[21] Therefore, an interest prevails in enhancing image acquisition and postprocessing speed for both CT- and MR-based imaging protocols, with the goal of identifying the optimal balance between the concepts of "time is brain" and "imaging is brain."[22,23]

The MR imaging treatment scheme for AIS at our institution includes a rapid imaging plan including DWI, GRE, and FLAIR.

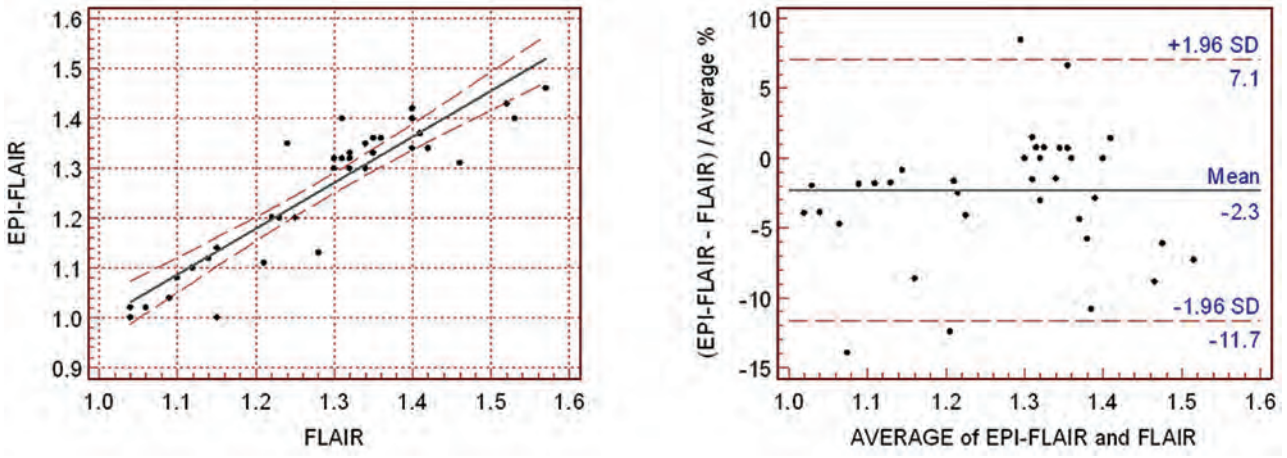

FIG 3. Bland-Altman plots and scatterplot show significant correlation ($r = 0.899$; z value $= 8.677$; $P < .0001$) for the SIR values between FLAIR and EPI-FLAIR in patients with acute infarction (DWI-positive lesions [$n = 38$]).

The images are then reviewed by neuroradiologists and neurologists on-line. On the basis of clinical deficits and imaging findings, a decision is made to give or withhold thrombolysis by IV tPA. It should be noted that saving 2 minutes of acquisition time is a step forward in improved total MR image time. This is particularly relevant because the time reduction occurs before the thrombolysis decision point in our imaging treatment scheme.

In general, magnetic field inhomogeneity and susceptibility artifacts are problematic for imaging sequences such as EPI, because of long acquisition intervals and long echo trains.[17] As a consequence, prior reports on the use of EPI-FLAIR sequences to evaluate intracranial processes such as brain tumors[24,25] and stroke[26] have produced mixed results, with susceptibility artifacts being a major limiting factor. We postulate that the improved image quality of our EPI-FLAIR technique can be partly explained by the integration of parallel imaging and its complementary effects with EPI.

Parallel imaging results in faster acquisition speed and also helps to mitigate the distortion and susceptibility artifacts associated with the EPI technique.[19,20] Integration of parallel imaging with the EPI sequence and undersampling of *k*-space can result in shortening of the echo-train length and an increase in blip gradients. Accordingly, the pixel bandwidth in the phase-encoding direction increases, which leads to a reduction in susceptibility artifacts. In addition, the shortened echo train provides the opportunity to reduce the echo time and hence the T2 decay, which in turn can lead to a significant SNR gain, offsetting the SNR penalty incurred by use of the parallel imaging technique. In this study, the complementary effects of integration of parallel imaging with EPI has resulted in a FLAIR sequence with diagnostic image quality that avoids the potential EPI-related susceptibility artifacts, when compared with conventional FLAIR.

The main clinical use of FLAIR imaging in the setting of acute stroke is to identify acute ischemic infarcts within the thrombolytic time window. Use of only time from symptom onset can result in exclusion of potentially treatable ischemic stroke cases when the time of onset is uncertain, such as patients with symptoms first noted on awakening, or those with unwitnessed onset, who are unable to provide an accurate history. As a rule, the prevalence of lesion visibility on FLAIR increases as time passes from the stroke onset. Recent reports have demonstrated that approximately 27%–50% of patients with stroke have positive FLAIR findings within 3 hours and 93% at > 6 hours,[13-14,27] indicating the development of cytotoxic edema, and corresponding to completed tissue infarction. Although our study goals did not include the aging of infarcts, we found that the described EPI-FLAIR sequence is comparable to conventional FLAIR in the detection of FLAIR hyperintensity corresponding to DWI abnormality, agreeing with conventional FLAIR in 92% of patients with AIS.

It is more important to note that our results indicate that the SIR values of the EPI-FLAIR technique are concordant with FLAIR in patients with time of onset to MR imaging of < 4.5 hours, an important timeline for IV thrombolysis treatment planning. Our values are concordant with the results of a recently published clinical trial by Song et al.[28]

In 2 cases, EPI-FLAIR was unable to show subtle FLAIR hyperintensity corresponding to the area of infarction. However, the SIR values of these lesions were comparable (Table 2). In 1 case, the infarction was too small. The other discrepant case was a hyperacute infarction that occurred approximately 1 hour after aneurysm coil placement and consequently had very subtle FLAIR hyperintensity (Fig 2). In addition, the aneurysm coil mass in the MCA bifurcation near the vicinity of the infarction probably resulted in added susceptibility artifacts and may have caused incomplete water suppression, hence reduced lesion to background contrast ratio and a decrease in sensitivity of EPI-FLAIR. It is important to note that the SIR values of these lesions were comparable on both FLAIR and EPI-FLAIR (Table 2), suggesting that the detection of a hyperintense signal may be a null point for practical purposes if the SIR values are comparable.

This study had several limitations. The first was a relatively small sample size possibly introducing a size selection bias. The second limitation was the inherent susceptibility artifacts associated with EPI techniques. Although susceptibility artifacts were mitigated by integration of parallel imaging and did not affect the diagnostic image quality of our study, we anticipate that this could be more problematic at higher magnetic fields such as 3T, especially at tissue interfaces and near the skull base. Third, we noted

that the EPI-FLAIR sequence exhibits a reduced white-gray matter contrast ratio, likely caused by incomplete, or inhomogeneous, water suppression. This could diminish the conspicuity of the EPI-FLAIR sequence to small white matter abnormalities, a possibility not specifically addressed in our study. Larger clinical studies will likely be needed to more fully determine the clinical usefulness of the described EPI-FLAIR technique in a broader setting.

CONCLUSIONS

The described EPI-FLAIR technique is feasible, with comparable qualitative and quantitative results to conventional FLAIR images for evaluation of patients with AIS. EPI-FLAIR can be implemented in the acute stroke MR protocol, resulting in a valuable reduction in scan time.

REFERENCES

1. Jauch EC, Saver JL, Adams HP Jr, et al. **Guidelines for the early management of patients with acute ischemic stroke: a guideline for healthcare professionals from the American Heart Association/American Stroke Association.** *Stroke* 2013;44:870–947
2. Chalela JA, Kidwell CS, Nentwich LM, et al. **Magnetic resonance imaging and computed tomography in emergency assessment of patients with suspected acute stroke: a prospective comparison.** *Lancet* 2007;369:293–98
3. Kang DW, Chalela JA, Dunn W, et al. **MRI screening before standard tissue plasminogen activator therapy is feasible and safe.** *Stroke* 2005;36:1939–43
4. Hjort N, Butcher K, Davis SM, et al. **Magnetic resonance imaging criteria for thrombolysis in acute cerebral infarct.** *Stroke* 2005;36:388–97
5. Schellinger PD, Jansen O, Fiebach JB, et al. **A standardized MRI stroke protocol: comparison with CT in hyperacute intracerebral hemorrhage.** *Stroke* 1999;30:765–68
6. Albers GW, Thijs VN, Wechsler L, et al. **Magnetic resonance imaging profiles predict clinical response to early reperfusion: the diffusion and perfusion imaging evaluation for understanding stroke evolution (DEFUSE) study.** *Ann Neurol* 2006;60:508–17
7. Davis SM, Donnan GA, Parsons MW, et al. **Effects of alteplase beyond 3 h after stroke in the Echoplanar Imaging Thrombolytic Evaluation Trial (EPITHET): a placebo-controlled randomised trial.** *Lancet Neurol* 2008;7:299–309
8. Zhu G, Michel P, Aghaebrahim A, et al. **Computed tomography workup of patients suspected of acute ischemic stroke: perfusion computed tomography adds value compared with clinical evaluation, noncontrast computed tomography, and computed tomography angiogram in terms of predicting outcome.** *Stroke* 2013;44:1049–55
9. Schaefer PW, Roccatagliata L, Ledezma C, et al. **First-pass quantitative CT perfusion identifies thresholds for salvageable penumbra in acute stroke patients treated with intra-arterial therapy.** *AJNR Am J Neuroradiol* 2006;27:20–25
10. Flacke S, Urbach H, Keller E, et al. **Middle cerebral artery (MCA) susceptibility sign at susceptibility-based perfusion MR imaging: clinical importance and comparison with hyperdense MCA sign at CT.** *Radiology* 2000;215:476–82
11. Assouline E, Benziane K, Reizine D, et al. **Intra-arterial thrombus visualized on T2* gradient echo imaging in acute ischemic stroke.** *Cerebrovasc Dis* 2005;20:6–11
12. Noguchi K, Ogawa T, Seto H, et al. **Subacute and chronic subarachnoid hemorrhage: diagnosis with fluid-attenuated inversion-recovery MR imaging.** *Radiology* 1997;203:257–62
13. Thomalla G, Rossbach P, Rosenkranz M, et al. **Negative fluid-attenuated inversion recovery imaging identifies acute ischemic stroke at 3 hours or less.** *Ann Neurol* 2009;65:724–32
14. Thomalla G, Cheng B, Ebinger M, et al. **DWI-FLAIR mismatch for the identification of patients with acute ischaemic stroke within 4.5 h of symptom onset (pre-FLAIR): a multicentre observational study.** *Lancet Neurol* 2011;10:978–86
15. Aoki J, Kimura K, Iguchi Y, et al. **FLAIR can estimate the onset time in acute ischemic stroke patients.** *J Neurol Sci* 2010;293:39–44
16. Griswold MA, Jakob PM, Heidemann RM, et al. **Generalized autocalibrating partially parallel acquisitions (GRAPPA).** *Magn Reson Med* 2002;47:1202–10
17. Mansfield P. **Real-time echo-planar imaging by NMR.** *Brit Med Bull* 1984;40:187–90
18. DeLaPaz RL. **Echo-planar imaging.** *Radiographics* 1994;14:1045–58
19. Pruessmann KP. **Parallel imaging at high field strength: synergies and joint potential.** *Top Magn Reson Imaging* 2004;15:237–44
20. Wiesinger F, Van de Moortele PF, Adriany G, et al. **Potential and feasibility of parallel MRI at high field.** *NMR Biomed* 2006;19:368–78
21. Saver JL. **Time is brain–quantified.** *Stroke* 2006;37:263–66
22. Michel P, Bogousslavsky J. **Penumbra is brain: no excuse not to perfuse.** *Ann Neurol* 2005;58:661–63
23. González RG. **Imaging-guided acute ischemic stroke therapy: from "time is brain" to "physiology is brain".** *AJNR Am J Neuroradiol* 2006;27:728–35
24. Tomura N, Kato K, Takahashi S, et al. **Multi-shot echo-planar FLAIR imaging of brain tumors: comparison of spin-echo T1-weighted, fast spin-echo T2-weighted, and fast spin-echo FLAIR imaging.** *Comput Med Imaging Graph* 2002;26:65–72
25. Korogi Y, Sugahara T, Shigematsu Y, et al. **Ultrafast FLAIR imaging with single-shot echo-planar technique in evaluation of intracranial lesions.** *Comput Med Imaging Graph* 1999;23:119–26
26. Matoba M, Tonami H, Yokota H, et al. [**Echo-planar FLAIR imaging in patients with brain disorders: comparative studies with turbo-SE T2WI and turbo-FLAIR**]. [in Japanese] *Nihon Igaku Hoshasen Gakkai Zasshi* 1998;58:129–36
27. Petkova M, Rodrigo S, Lamy C, et al. **MR imaging helps predict time from symptom onset in patients with acute stroke: implications for patients with unknown onset time.** *Radiology* 2010;257:782–92
28. Song SS, Latour LL, Ritter CH, et al. **A pragmatic approach using magnetic resonance imaging to treat ischemic strokes of unknown onset time in a thrombolytic trial.** *Stroke* 2012;43:2331–35

CTA Collateral Status and Response to Recanalization in Patients with Acute Ischemic Stroke

V. Nambiar, S.I. Sohn, M.A. Almekhlafi, H.W. Chang, S. Mishra, E. Qazi, M. Eesa, A.M. Demchuk, M. Goyal, M.D. Hill, and B.K. Menon

ABSTRACT

BACKGROUND AND PURPOSE: Collateral status at baseline is an independent determinant of clinical outcome among patients with acute ischemic stroke. We sought to identify whether the association between recanalization after intra-arterial acute stroke therapy and favorable clinical response is modified by the presence of good collateral flow assessed on baseline CTA.

MATERIALS AND METHODS: Data are from the Keimyung Stroke Registry, a prospective cohort study of patients with acute ischemic stroke from Daegu, South Korea. Patients with M1 segment MCA with or without intracranial ICA occlusions on baseline CTA from May 2004 to July 2009 who also had baseline MR imaging were included. Two readers blinded to all clinical information assessed baseline and follow-up imaging. Leptomeningeal collaterals on baseline CTA were assessed by consensus by use of the regional leptomeningeal score.

RESULTS: Among 84 patients (mean age, 65.2 ± 13.2 years; median NIHSS score, 14; interquartile range, 8.5), median time from stroke onset to initial MR imaging was 164 minutes. TICI 2b–3 recanalization was achieved in 38.1% of patients and mRS 0–2 at 90 days in 35.8% of patients. In a multivariable model, the interaction between collateral status and recanalization was significant. Only patients with intermediate or good collaterals who recanalized showed a statistically significant association with good clinical outcome (rate ratio = 3.8; 95% CI, 1.2–12.1). Patients with good and intermediate collaterals who did not achieve recanalization and patients with poor collaterals, even if they achieved recanalization, did not do well.

CONCLUSIONS: Patients with good or intermediate collaterals on CTA benefit from intra-arterial therapy, whereas patients with poor collaterals do not benefit from treatment.

ABBREVIATIONS: IAT = intra-arterial therapy; rLMC = regional leptomeningeal collateral score; SD = standard deviation

Leptomeningeal collaterals are pre-existing anastomoses that connect a small number of distal-most arterioles within the crowns of the cerebral artery trees.[1,2] During an acute stroke, ischemic brain depends on blood flow from these collaterals to survive until the occluded artery is opened.[3-8] This collateral circulation is highly variable and potentially influences the rate at which an infarct grows.[4,8-10] Collateral status at baseline is an independent determinant of clinical outcome among patients with acute ischemic stroke.[3,5,7,8,11] Nonetheless, "effect modification" by collateral status measured noninvasively by use of CTA of the relationship between recanalization and clinical outcome has not been demonstrated before. This tool can be used to select patients for intra-arterial therapy (IAT) through demonstration of a differential clinical response to recanalization by collateral status.

In this study, we first demonstrate the concept of validity of collateral status measured by use of CTA among patients presenting with acute ischemic stroke by correlating it with infarct volume on baseline MR DWI and infarct growth over 24 hours. We then demonstrate "effect modification" by collateral status of the relationship between recanalization and clinical outcome in patients with acute ischemic stroke undergoing IAT, thus justifying the use of baseline collateral status on CTA as a patient selection tool for IAT.

MATERIALS AND METHODS

The Keimyung Stroke Registry is an ongoing, single-center, prospective cohort study of patients with acute ischemic stroke presenting to the Keimyung University, Dongsan Hospital in Daegu, South Korea. All patients undergo an NCCT of the head at admission followed by CTA of the head and neck. For the study (time period, May 2004 to

Received July 19, 2013; accepted after revision September 29.

From the Calgary Stroke Program, Departments of Clinical Neurosciences (V.N., M.A.A., S.M., E.Q., M.E., A.M.D., M.G., M.D.H., B.K.M.), Radiology (M.E., A.M.D., M.G., M.D.H., B.K.M.), and Community Health Sciences (M.D.H., B.K.M.), University of Calgary, Calgary, Alberta, Canada; Departments of Neurology (S.I.S.) and Radiology (H.W.C.), Brain Research Institute, Keimyung University, Daegu, South Korea; Department of Internal Medicine (M.A.A.), King Abdulaziz University, Jeddah, Saudi Arabia; and Hotchkiss Brain Institute (A.M.D., M.G., M.D.H., B.K.M.), University of Calgary, Calgary, Alberta, Canada.

Please address correspondence to Bijoy K. Menon, MD, 1079 A, 29th Street NW, Calgary, AB, Canada T3H4J2; e-mail: docbijoymenon@gmail.com

http://dx.doi.org/10.3174/ajnr.A3817

July 2009), we included only patients presenting with acute ischemic stroke with M1 segment MCA with or without ICA occlusion on baseline CTA with witnessed stroke symptom onset who were treated with IAT and had a pretreatment brain MR imaging and 24-hour posttreatment MR imaging. During this time period, there were 286 patients with documented anterior circulation occlusions on baseline CTA. We excluded 202 patients (43 patients with a documented MCA occlusion beyond the M1 MCA segment, 28 patients with isolated ICA without M1 MCA occlusion, 7 patients with simultaneously detected occlusions in the posterior circulation or contralateral ICA territory, 71 patients with unknown stroke onset time, 16 patients with baseline MR imaging obtained after treatment, 29 patients with poor-quality MR imaging at baseline, and 8 patients without 24-hour MR imaging). Finally, 84 patients were included in these analyses. Stroke severity was assessed by use of the NIHSS at baseline, immediately after treatment, at discharge, and at 90 days. Interval times from stroke symptom onset to presentation in the emergency department, imaging, and endovascular procedures were collected. Functional status was assessed at baseline and 90 days by use of the mRS. We collected data on mRS by clinical review in a face-to-face interview at 3 months (in approximately 70% of patients) and by telephone interview at 3 months (in approximately 25% of patients). For 5% of patients, we obtained the 3-month mRS information at 5–9 months. The study was approved by the local institutional review board.

Imaging Protocol

Standard nonhelical NCCT was performed on a multisection scanner (Sensation 16; Siemens, Erlangen, Germany) by use of 120 kV, 170 mAs, with 5-mm section thickness. NCCT was followed by CTA with the use of a helical scan technique. Coverage was from arch to vertex, with continuous axial sections parallel to the orbitomeatal line with 0.6–1.25-mm section thickness. Acquisitions were obtained after a single bolus intravenous contrast injection of 90–120 mL nonionic contrast media into an antecubital vein at 3–5 mL/s, auto-triggered by appearance of contrast in a region of interest manually placed in the ascending aorta. This was followed by a baseline MR imaging (3T Signa Excite; GE Healthcare, Milwaukee, Wisconsin) consisting of DWI, time-of-flight MRA, and gradient recalled-echo as a part of a stroke protocol. Follow-up MR imaging was performed within 24 hours by use of the same protocol.

Intra-Arterial Therapy

Intravenous tPA was given to all eligible patients within 3 hours of stroke onset as per accepted guidelines. MR imaging was primarily used to assess intracerebral hemorrhage on gradient recalled-echo and recanalization status on MR TOF. Patients were taken to the angiography suite from the MR imaging suite for IAT. Patients with MCA occlusions with or without ICA occlusions who did not show recanalization on MRA or rapid clinical improvement after IV tPA were considered for IAT. IAT included local urokinase (10,000–20,000 IU/min; maximum permissible dose, 300,000 IU; Green Cross Pharm, Seoul, Republic of Korea), balloon angioplasty, or wire manipulation. Glycoprotein IIb/IIIa receptor antagonists were given in a small number of patients. For clots not manageable by the above methods, we used off-label stent placement (with the use of coronary stents). Recanalization was assessed by means of angiography in all cases. Successful recanalization was defined as TICI 2b/3 flow on final angiogram. Penumbra Stroke System aspiration catheters (Penumbra, Alameda, California) and stent retriever devices (eg, Solitaire FR [Covidien, Irvine, California], Trevo [Stryker, Kalamazoo, Michigan]) were not available during this period.

Imaging Analyses

Baseline and follow-up images were analyzed at the imaging core lab of the Calgary Stroke Program. OsiriX version 3.5 (http://www.osirix-viewer.com), an image-processing software designed for multiplanar reconstruction, was used to reconstruct 2D multiplanar reconstruction images of CTA in axial, coronal, and sagittal planes by use of 24-mm-thick slabs. Leptomeningeal collaterals were assessed on baseline CTA by consensus (B.K.M., S.I.S.) by use of the regional leptomeningeal score (rLMC), a previously published ordinal scoring system that is based on the Alberta Stroke Program Early CT Score template that has excellent interrater reliability[3] (Fig 1). Infarct volumes were measured on baseline and 24-hour MR DWI by use of an in-house–validated software, Quantomo (Cybertrial, Calgary, Canada). Infarct growth over 24 hours was calculated by subtracting initial infarct volume from the 24-hour volume measurement. Quantomo has been previously validated and has good interrater and intrarater agreement.[12] Readers were blinded to all clinical information and follow-up data at the time of scan reading.

Statistical Analyses

Continuous variables are summarized as means (±1 SD) or medians (interquartile range or range) as appropriate. Collateral status by use of the rLMC score (0–20) was trichotomized into 3 groups: good (17–20), intermediate (11–16), and poor (0–10), according to previously published literature.[3] Differences between these 3 groups were assessed by means of the Fisher exact test for proportions, 1-way ANOVA for parametric data, and a rank sum test for nonparametric data. We adjusted for multiple comparisons by use of the Bonferroni method. We tested for trend in outcome measure (infarct growth and mRS 0–2 at 90 days) by collateral status in the recanalizers (TICI 2b–3) and in the non-recanalizers (TICI 0–1) by use of the Cuzick test of trends. We then built a multivariable model by use of generalized linear modeling with a log link, with mRS 0–2 versus 3–6 at 90 days as the outcome and collateral status (good, intermediate, and poor), recanalization status (TICI 2b–3 versus 0–2a), and age (by decile) as independent variables. Because there was no significant association of sex, baseline NIHSS, or onset to imaging time with mRS at 90 days, these variables were not included in the model. We specifically included a multiplicative interaction term between collateral status and recanalization status. All hypothesis tests were 2-sided, with a value of $P < .05$ considered statistically significant. In multivariable analysis, interaction effects were considered significant at a value of $P < .10$.[13] Analyses were performed with the use of STATA/SE 12.1 software (StataCorp, College Station, Texas).

RESULTS

Among 84 patients, the mean age was 65.2 ± 13.2 years, median NIHSS score was 14 (interquartile range, 8.5), and median time

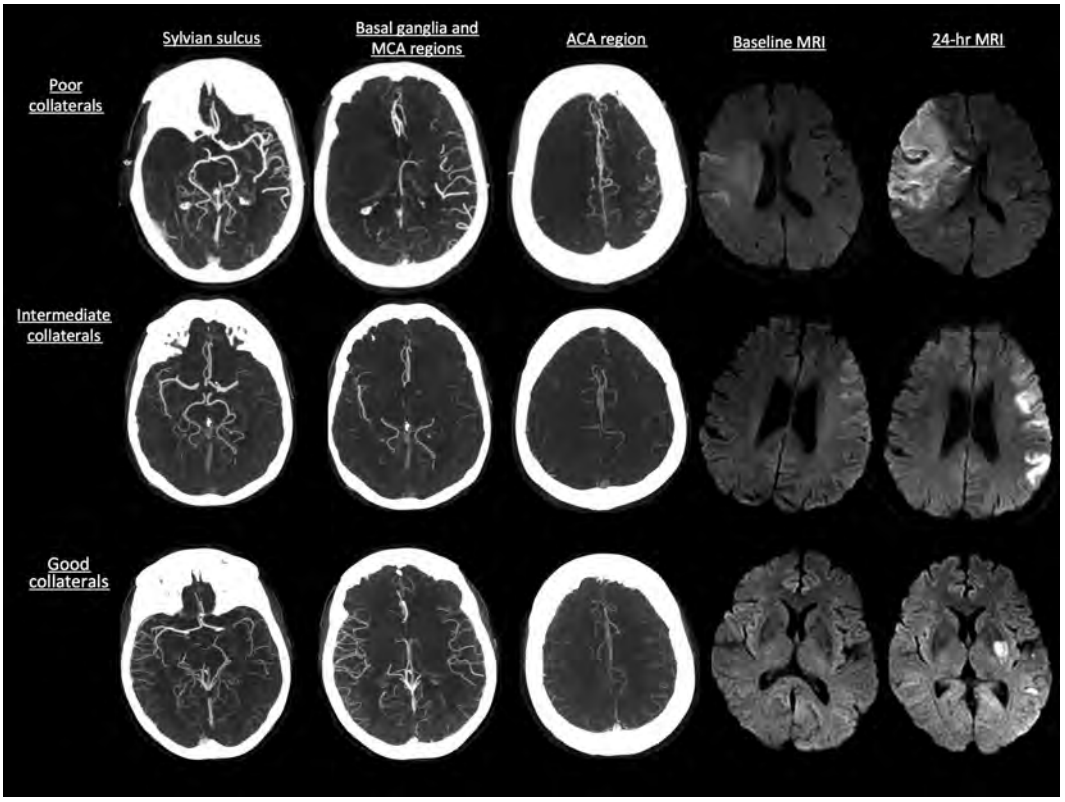

FIG 1. Collateral status on CTA as measured by the rLMC score with baseline and 24-hour infarct volume on MR DWI.

Table 1: Baseline characteristics of patients in study stratified by collateral status ($n = 84$)

	Good Collaterals (rLMC Score 17–20, $n = 19$)	Intermediate Collaterals (rLMC Score 11–16, $n = 34$)	Poor Collaterals (rLMC Score 0–10, $n = 31$)	*P* Value
Age, y, median (range)	63 (26–78)	66 (40–85)	70 (45–89)	.15
Sex, male, %	52.6%	58.8%	45.2%	.55
Baseline NIHSS score, median (range)	10 (5–25)	13 (4–23)	18 (8–25)	<.01
Baseline ASPECTS, median (range)	8 (3–10)	8 (3–10)	5 (1–10)	<.01
Onset to baseline MRI time, min, median (range)	166 (68–724)	176.5 (55–493)	148 (36–334)	.06
Baseline infarct volume, mL (±1 SD)	12.6 (13.2)	37.1 (32.1)	110.1 (75.1)	<.01
IV tPA (%)	52.6%	55.9%	48.4%	.72
Recanalization, %, TICI 2b–3	31.6%	50%	29%	.2
Onset to recanalization, min,[a] $n = 32$, median (range)	400 (295–766)	360 (160–620.5)	290 (157–323)	.01
Infarct growth, mL (±1 SD)	42.1 (52.1)	37.6 (54.8)	90.9 (86.7)	<.01

[a] In recanalizers alone ($n = 32$).

from stroke onset to initial MR imaging was 164 minutes. Successful recanalization (TICI 2b–3) was achieved in 38.1% of patients and good clinical outcome (mRS 0–2 at 90 days) in 35.8% of patients. Mean baseline infarct volume was 58.5 mL (±1 SD, 64.4 mL) and mean infarct growth over 24 hours was 58.3 mL (±1 SD, 72 mL). There were 19 patients with good, 34 with intermediate, and 31 with poor collateral scores at baseline. Baseline characteristics stratified by good, intermediate, and poor collateral status are described in Table 1. Patients with good collateral status had lower baseline NIHSS score, higher baseline ASPECTS on NCCT, smaller baseline infarct volume on MR imaging, and lesser infarct growth over 24 hours (Table 1).

Infarct growth over 24 hours was significantly lower in patients with good collateral status at baseline who achieved recanalization (7.0 mL; ±1 SD = 11.7 mL) when compared with those with intermediate collateral status who achieved recanalization (26.6 mL; ±1 SD = 43.4 mL) and those with poor collaterals who recanalized (67.7 mL; ±1 SD = 75.1 mL) ($P = .05$; between group difference). There was no difference in infarct growth in the non-recanalizers stratified by collateral status (good collaterals: 58.4 mL, ±1 SD = 58.6 mL; intermediate collaterals: 48.6 mL, ±1 SD = 63.7 mL; poor collaterals: 100.4 mL, ±1 SD = 91 mL; $P = .09$, between-group difference) (Fig 2). Similarly, good clinical outcome (mRS 0–2 at 90 days) was higher among patients with good collateral status who achieved recanalization (100%) when compared with those with intermediate collateral status who recanalized (58.8%) and those with poor collaterals who recanalized (33.3%) ($P = .04$). There was no statistically significant difference in good clinical outcome in the non-recanalizers stratified by collateral status (30.8% in those with good collaterals, 17.6% in those with intermediate collaterals, and 18.2% in those with poor collaterals; $P = .67$). The Cuzick test of trend by collateral status was statistically significant for good clinical outcome (mRS 0–2 at 90 days, $P = .01$) in the recanalizers. There was no statistically significant trend by collateral status for good clinical outcome ($P = .08$) in the non-recanalizers (Fig 3).

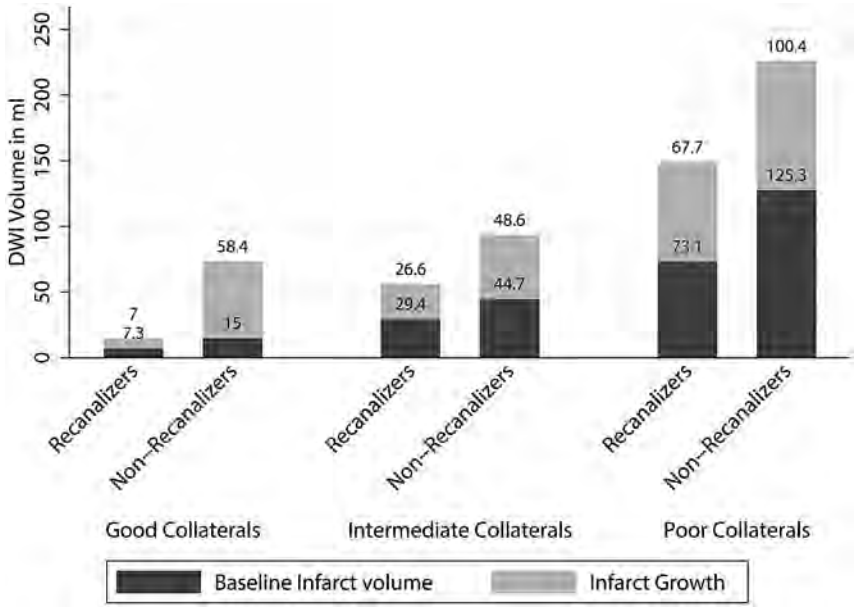

FIG 2. Mean baseline infarct volume and infarct growth over 24 hours stratified by baseline collateral status on CTA and final recanalization (TICI score 2b–3 versus 0–2a).

In the multivariable model, the interaction between collateral status and recanalization was relevant ($P = .08$). This final model also included age as a significant independent predictor of good clinical outcome. Given the presence of a statistically significant interaction in the model, we report age- and sex-adjusted rate ratios for patients in 4 groups, namely, group 1 (poor collaterals who do not recanalize, $n = 22$), group 2 (poor collaterals who recanalize, $n = 9$), group 3 (intermediate or good collaterals who do not recanalize, $n = 30$), and group 4 (intermediate or good collaterals who recanalize, $n = 23$). Patients with intermediate and good collaterals were collapsed into 1 group for ease of reporting interaction effects. Only patients with intermediate or good collaterals who recanalize showed a statistically significant association with good clinical outcome (rate ratio = 3.8; 95% CI, 1.2–12.1). None of the other groups did as well clinically (Table 2). Fig 3 shows the unadjusted mRS scores at 90 days in these 4 groups stratified by recanalization status.

DISCUSSION

Our results show that collateral status measured at baseline by use of CTA among patients with acute ischemic stroke correlates with baseline infarct volume and with infarct growth over 24 hours. Furthermore, we demonstrated effect modification by collateral status of the relationship between recanalization and good clinical outcome. Patients with good and intermediate collaterals who achieve recanalization with IAT do well when compared with those who do not achieve recanalization. Patients with poor collaterals do not do well even if recanalization is achieved with IAT (Table 2).

Several imaging paradigms propose to "select" patients most suitable for IAT.[14-18] MR imaging–based diffusion/perfusion mismatch is one such paradigm. MR imaging, however, takes time to screen, perform, and interpret.[19] Many patients do not tolerate it as well as CT; image quality is affected by patient motion. MR imaging also has limited availability "after hours."[20] Moreover, the recent MR Rescue Trial showed that the tool may not help in selecting patients for IAT.[21] NCCT ASPECTS has moderate interrater reliability, even among experts.[22-25] Reliability is less in the early presenters (within 90 minutes from stroke symptom onset).[26] In addition, ASPECTS interpretation is affected by patient motion and in the aged.[27] CT perfusion needs algorithms for postprocessing images that are vendor-specific, not standardized, and therefore variable across centers.[28-31] Trained personnel are sometimes needed to process these images. In addition, image quality is affected to some extent by patient motion.[29] Additional radiation dose is also a concern.[32] Collateral assessment on CTA has good interrater reliability.[3,4,33] Good correlation with baseline infarct volume and infarct growth on MR DWI in our study demonstrates the tool's content validity. Furthermore, by demonstrating "effect modification" by collateral status among patients undergoing IAT, we demonstrate for the first time that this tool can be used to select patients for this therapy. Collateral assessment on CTA does not need any sophisticated algorithm or trained personnel for postprocessing images and is relatively resistant to patient motion–induced artifacts. It is available 24 hours a day in most centers. We therefore propose the use of this tool for patient selection within future endovascular trials.

Despite the variability in measuring collaterals at baseline in patients with acute ischemic stroke, our study further reinforces evidence from previous literature that patients with good collaterals at baseline have small baseline infarcts when compared with patients with intermediate and poor baseline collaterals.[34,35] Recanalization helps reduce further infarct growth, thus limiting size of final infarct.[8] Our study also shows that the rate of infarct growth is quicker in patients with intermediate collaterals; these patients may only benefit if recanalization is achieved quickly. Patients with poor collaterals at baseline grow their infarcts the quickest; the likelihood that they will benefit from recanalization is the least. Nonetheless, the fact that some patients with poor collaterals in our study achieved good clinical outcome raises the possibility that routine CTA may have underestimated good and intermediate collaterals in some patients, misclassifying these collaterals as poor. Routine CTA is a single snapshot of contrast-filled blood vessels. Early timing of image acquisition with respect to that of bolus injection could potentially result in underestimation of true collateral status by use of this technique.[3] The 4 patients who achieved good clinical outcome despite having poor collaterals at baseline and not achieving recanalization had a mean baseline infarct volume of 63.1 mL (range, 13.3–133.5 mL)

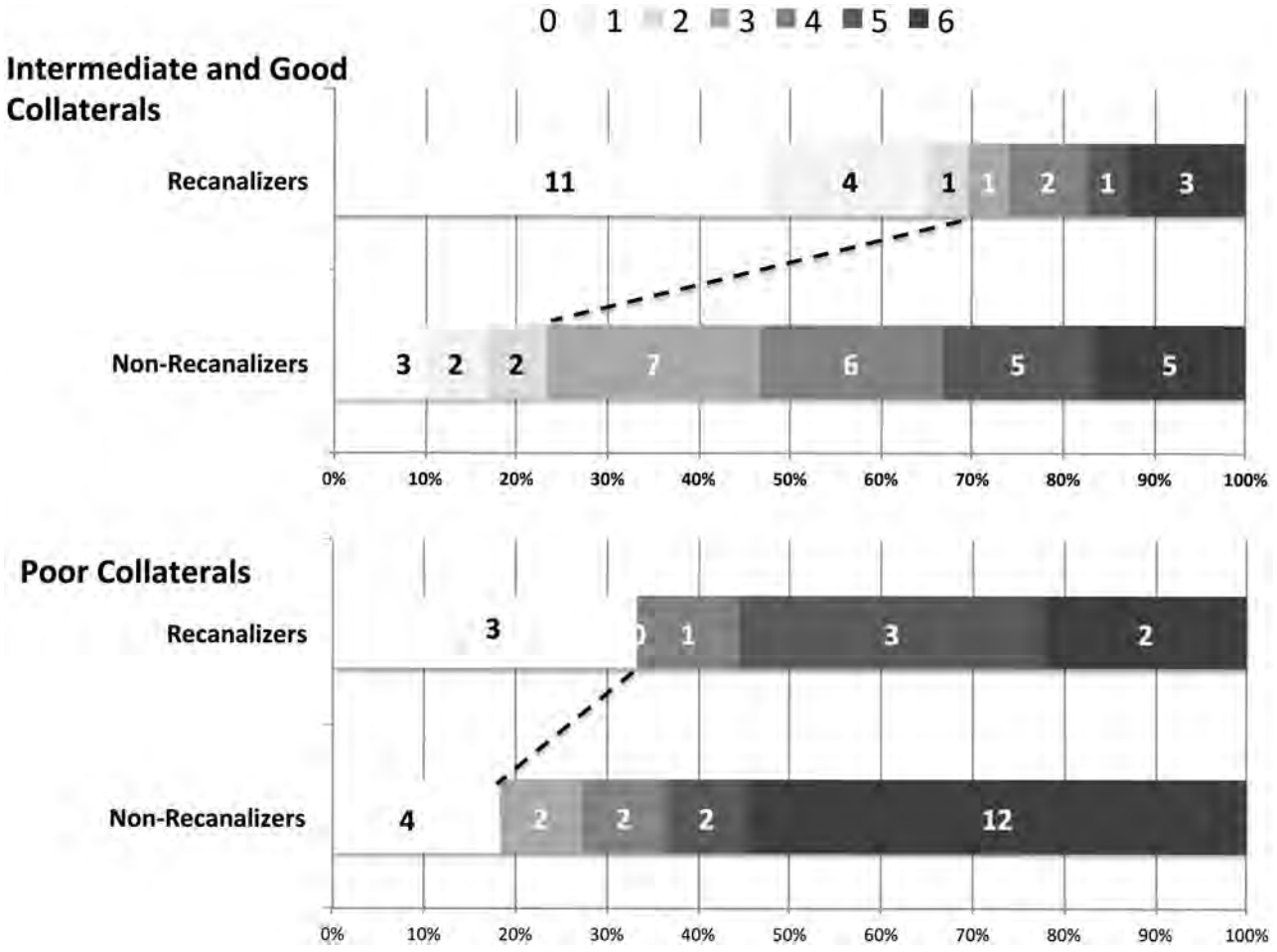

FIG 3. Ninety-day clinical outcome according to the mRS stratified by baseline collateral status on CTA and final recanalization (TICI score, 2b–3).

Table 2: Generalized linear model with the use of log link showing rate ratios for good clinical outcome (mRS 0–2 at 90 days) by collateral status and recanalization status adjusted for age and sex

Group	Rate Ratio	95% CI	mRS 0–2 at 90 Days, %	*P* Value
Poor collaterals, non-recanalizers ($n = 22$)	1	–	18.2%	–
Poor collaterals, recanalizers ($n = 9$)	2	0.5–8.3	33.3%	.34
Intermediate and good collaterals, non-recanalizers ($n = 30$)	1.6	0.5–5.5	23.3%	.44
Intermediate and good collaterals, recanalizers ($n = 23$)	3.8	1.2–12.1	70%	.02
Age (for every 10 y below 80)	1.2	1.1–1.4	–	.01
Sex, male	0.6	0.4–1.1		.12

Note:—Reference group is patients with poor collaterals who do not recanalize.

compared with a mean baseline infarct volume of 110 mL for all patients with poor collaterals in the study, thus suggesting possible misclassification of good and intermediate collateral status as poor by use of routine CTA in at least those patients with small or intermediate baseline infarct volume.[36] The rLMC score used in our study, being more liberal when defining poor collaterals in comparison with stricter definitions used in other studies, could also explain why some patients with poor collaterals did well in our study.[34] Finally, variability in brain eloquence or possible misclassification of 90-day clinical outcome as the result of telephone follow-up in approximately 25% of patients could potentially explain why 2 patients with poor baseline collaterals and baseline infarct volumes >80 mL in our study did well clinically.[36] Both these patients had right hemisphere infarcts. Our study, however, is able to show with a degree of statistical certainty that the patients most likely to benefit from recanalization are those with good and intermediate baseline collaterals; patients with poor collaterals do not show a differential response to recanalization.

Reperfusion-related edema and injury has been postulated to be a cause for increased infarct growth among patients without mismatch who achieve reperfusion.[18] In our study, patients with poor collateral status who did not recanalize had more infarct growth than did patients with poor collateral status who recanalized. Our results do not support the reperfusion injury hypothesis. On the contrary, we speculate that early recanalization, even among patients with poor collaterals, may reduce the risk of death.[37]

Our study is not a randomized, controlled trial. Similar to previous studies supporting the use of a "mismatch"-based para-

digm on perfusion imaging, our study provides evidence for the use of a "CTA collateral assessment–based paradigm" in selecting patients for IAT.[18] We did not have data on every procedural time metric; approximately 30% of follow-up clinical data (mRS at 90 days) was ascertained by telephone. We were also underpowered to do a secondary analysis on the effect of time to recanalization on clinical outcomes stratified by collateral status. Our recanalization rates are modest and reflective of the time period when patients were recruited; nonetheless, our study is unique in that we were able to show a statistically significant interaction between collateral status and recanalization. With the advent of stent retrievers that achieve recanalization rates in excess of 80%, future demonstration of such statistically significant "effect modification" may need very large cohorts.[37] Our study is thus timely in being able to demonstrate the utility of this tool in patient selection for IAT.

CONCLUSIONS

The results from our study suggest a differential clinical and imaging response to recanalization by IAT in patients with good and intermediate collaterals. Patients with poor collaterals show no such differential response. Collateral assessment on CTA can potentially help aid patient selection for acute intra-arterial stroke treatment and for potential inclusion in endovascular stroke trials.

Disclosures: Emmad Qazi—*UNRELATED: Employment:* The Calgary Stroke Program, Comments: I work at the Calgary Stroke Program as a part-time employee. Mayank Goyal—*UNRELATED: Consultancy:* Covidien/ev3, Comments: For designing and conducting trial; *Grants/Grants Pending:* Covidien/ev3,* Comments: Funding for ESCAPE trial; *Payment for Lectures (including service on speakers bureaus):* Covidien/ev3, Comments: For speaking engagements related to acute stroke treatment. Michael Hill—*UNRELATED: Board Membership:* DSMB Aldagen trial; *Grants/Grants Pending:* Covidien,* Comments: Grant for a clinical trial; *Stock/Stock Options:* Calgary Scientific Inc. (stock). Bijoy Menon—*UNRELATED: Grants/Grants Pending:* Heart and Stroke Foundation of Canada,* CIHR*. Andrew Demchuk (*UNRELATED*): *Grant support and lecture fees*: Covidien,* Heart and Stroke Foundation of Canada,* CIHR*. (**money paid to institution*).

REFERENCES

1. Liebeskind DS. **Collateral circulation.** *Stroke* 2003;34:2279–84
2. Shuaib A, Butcher K, Mohammad AA, et al. **Collateral blood vessels in acute ischaemic stroke: a potential therapeutic target.** *Lancet Neurol* 2011;10:909–21
3. Menon BK, Smith EE, Modi J, et al. **Regional leptomeningeal score on CT angiography predicts clinical and imaging outcomes in patients with acute anterior circulation occlusions.** *AJNR Am J Neuroradiol* 2011;32:1640–45
4. Menon BK, O'Brien B, Bivard A, et al. **Assessment of leptomeningeal collaterals using dynamic CT angiography in patients with acute ischemic stroke.** *J Cereb Blood Flow Metab* 2013;33:365–71
5. Miteff F, Levi CR, Bateman GA, et al. **The independent predictive utility of computed tomography angiographic collateral status in acute ischaemic stroke.** *Brain* 2009;132:2231–38
6. Maas MB, Lev MH, Ay H, et al. **Collateral vessels on CT angiography predict outcome in acute ischemic stroke.** *Stroke* 2009;40:3001–05
7. Lima FO, Furie KL, Silva GS, et al. **The pattern of leptomeningeal collaterals on CT angiography is a strong predictor of long-term functional outcome in stroke patients with large vessel intracranial occlusion.** *Stroke* 2010;41:2316–22
8. Christoforidis GA, Mohammad Y, Kehagias D, et al. **Angiographic assessment of pial collaterals as a prognostic indicator following intra-arterial thrombolysis for acute ischemic stroke.** *AJNR Am J Neuroradiol* 2005;26:1789–97
9. Bang OY, Saver JL, Kim SJ, et al. **Collateral flow predicts response to endovascular therapy for acute ischemic stroke**. *Stroke* 2011; 42:693–99
10. Menon BK, Smith EE, Coutts SB, et al. **Leptomeningeal collaterals are associated with modifiable metabolic risk factors**. *Ann Neurol* 2013;74:241–48
11. Kim JJ, Fischbein NJ, Lu Y, et al. **Regional angiographic grading system for collateral flow: correlation with cerebral infarction in patients with middle cerebral artery occlusion.** *Stroke* 2004;35:1340–44
12. Steffenhagen N, Campos CR, Poppe AY, et al. **Reliability of measuring lesion volumes in transient ischemic attack and minor stroke.** *Stroke* 2010;41:814–16
13. The NINDS t-PA Stroke Study Group. **Generalized efficacy of t-PA for acute stroke: subgroup analysis of the NINDS t-PA Stroke Trial.** *Stroke* 1997;28:2119–25
14. Demchuk AM, Menon B, Goyal M. **Imaging-based selection in acute ischemic stroke trials: a quest for imaging sweet spots.** *Ann N Y Acad Sci* 2012;1268:63–71
15. Campbell BC, Christensen S, Levi CR, et al. **Cerebral blood flow is the optimal CT perfusion parameter for assessing infarct core.** *Stroke* 2011;42:3435–40
16. Ebinger M, Iwanaga T, Prosser JF, et al. **Clinical-diffusion mismatch and benefit from thrombolysis 3 to 6 hours after acute stroke.** *Stroke* 2009;40:2572–74
17. Kakuda W, Lansberg MG, Thijs VN, et al. **Optimal definition for PWI/DWI mismatch in acute ischemic stroke patients.** *J Cereb Blood Flow Metab* 2008;28:887–91
18. Lansberg MG, Straka M, Kemp S, et al. **MRI profile and response to endovascular reperfusion after stroke (DEFUSE 2): a prospective cohort study.** *Lancet Neurol* 2012;11:860–67
19. Sheth KN, Terry JB, Nogueira RG, et al. **Advanced modality imaging evaluation in acute ischemic stroke may lead to delayed endovascular reperfusion therapy without improvement in clinical outcomes**. *J Neurointervent Surg* 2013;5 suppl 1:i62–65
20. Hand PJ, Wardlaw JM, Rowat AM, et al. **Magnetic resonance brain imaging in patients with acute stroke: feasibility and patient related difficulties.** *J Neurol Neurosurg Psychiatry* 2005;76:1525–27
21. Kidwell CS, Jahan R, Gornbein J, et al. **A trial of imaging selection and endovascular treatment for ischemic stroke**. *N Engl J Med* 2013;368:914–23
22. Gupta AC, Schaefer PW, Chaudhry ZA, et al. **Interobserver reliability of baseline noncontrast CT Alberta Stroke Program Early CT Score for intra-arterial stroke treatment selection.** *AJNR Am J Neuroradiol* 2012;33:1046–49
23. Wardlaw JM, Mielke O. **Early signs of brain infarction at CT: observer reliability and outcome after thrombolytic treatment–systematic review.** *Radiology* 2005;235:444–53
24. Patel SC, Levine SR, Tilley BC, et al. **Lack of clinical significance of early ischemic changes on computed tomography in acute stroke.** *JAMA* 2001;286:2830–38
25. Coutts SB, Hill MD, Demchuk AM, et al. **ASPECTS reading requires training and experience**. *Stroke* 2003;34:e179
26. Bal S, Bhatia R, Menon BK, et al. **Time dependence of reliability of noncontrast computed tomography in comparison to computed tomography angiography source image in acute ischemic stroke.** *Int J Stroke* 2012 Sep 13. [Epub ahead of print]
27. Barber PA, Demchuk AM, Zhang J, et al. **Validity and reliability of a quantitative computed tomography score in predicting outcome of hyperacute stroke before thrombolytic therapy: ASPECTS Study Group: Alberta Stroke Programme Early CT Score.** *Lancet* 2000;355:1670–74
28. Kudo K, Sasaki M, Yamada K, et al. **Differences in CT perfusion maps generated by different commercial software: quantitative analysis by using identical source data of acute stroke patients.** *Radiology* 2010;254:200–09
29. Goyal M, Menon BK, Derdeyn CP. **Perfusion imaging in acute ischemic stroke: let us improve the science before changing clinical practice.** *Radiology* 2013;266:16–21
30. Zussman BM, Boghosian G, Gorniak RJ, et al. **The relative effect of**

vendor variability in CT perfusion results: a method comparison study. *AJR Am J Roentgenol* 2011;197:468–73
31. Bivard A, Levi C, Spratt N, et al. **Perfusion CT in acute stroke: a comprehensive analysis of infarct and penumbra.** *Radiology* 2012;267:543–50
32. Mnyusiwalla A, Aviv RI, Symons SP. **Radiation dose from multidetector row CT imaging for acute stroke.** *Neuroradiology* 2009;51:635–40
33. McVerry F, Liebeskind DS, Muir KW. **Systematic review of methods for assessing leptomeningeal collateral flow.** *AJNR Am J Neuroradiol* 2012;33:576–82
34. Souza LC, Yoo AJ, Chaudhry ZA, et al. **Malignant CTA collateral profile is highly specific for large admission DWI infarct core and poor outcome in acute stroke**. *AJNR Am J Neuroradiol* 2012;33:1331–36
35. Tan IY, Demchuk AM, Hopyan J, et al. **CT angiography clot burden score and collateral score: correlation with clinical and radiologic outcomes in acute middle cerebral artery infarct.** *AJNR Am J Neuroradiol* 2009;30:525–31
36. Yoo AJ, Verduzco LA, Schaefer PW, et al. **MRI-based selection for intra-arterial stroke therapy: value of pretreatment diffusion-weighted imaging lesion volume in selecting patients with acute stroke who will benefit from early recanalization.** *Stroke* 2009;40:2046–54
37. Saver JL, Jahan R, Levy EI, et al. **Solitaire flow restoration device versus the Merci retriever in patients with acute ischaemic stroke (SWIFT): a randomised, parallel-group, non-inferiority trial.** *Lancet* 2012;380:1241–49

Imaging Findings in MR Imaging–Guided Focused Ultrasound Treatment for Patients with Essential Tremor

M. Wintermark, J. Druzgal, D.S. Huss, M.A. Khaled, S. Monteith, P. Raghavan, T. Huerta, L.C. Schweickert, B. Burkholder, J.J. Loomba, E. Zadicario, Y. Qiao, B. Shah, J. Snell, M. Eames, R. Frysinger, N. Kassell, and W.J. Elias

ABSTRACT

BACKGROUND AND PURPOSE: MR imaging–guided focused sonography surgery is a new stereotactic technique that uses high-intensity focused sonography to heat and ablate tissue. The goal of this study was to describe MR imaging findings pre- and post-ventralis intermedius nucleus lesioning by MR imaging–guided focused sonography as a treatment for essential tremor and to determine whether there was an association between these imaging features and the clinical response to MR imaging–guided focused sonography.

MATERIALS AND METHODS: Fifteen patients with medication-refractory essential tremor prospectively gave consent; were enrolled in a single-site, FDA-approved pilot clinical trial; and were treated with transcranial MR imaging–guided focused sonography. MR imaging studies were obtained on a 3T scanner before the procedure and 24 hours, 1 week, 1 month, and 3 months following the procedure.

RESULTS: On T2-weighted imaging, 3 time-dependent concentric zones were seen at the site of the focal spot. The inner 2 zones showed reduced ADC values at 24 hours in all patients except one. Diffusion had pseudonormalized by 1 month in all patients, when the cavity collapsed. Very mild postcontrast enhancement was seen at 24 hours and again at 1 month after MR imaging–guided focused sonography. The total lesion size and clinical response evolved inversely compared with each other (coefficient of correlation = 0.29, *P* value = .02).

CONCLUSIONS: MR imaging–guided focused sonography can accurately ablate a precisely delineated target, with typical imaging findings seen in the days, weeks, and months following the treatment. Tremor control was optimal early when the lesion size and perilesional edema were maximal and was less later when the perilesional edema had resolved.

ABBREVIATIONS: CRST = Clinical Rating Scale for Tremor; Vim = ventralis intermedius nucleus

MR imaging–guided focused sonography surgery is a new stereotactic technique that uses high-intensity focused sonography to heat and ablate tissue rapidly under closed-loop image guidance and control throughout all steps of the intervention process. MR imaging allows precise intraprocedural localization of the ablation target, verification of safety margins for the sonography treatment, and real-time monitoring of thermal ablation dynamics.[1-7] MR imaging–guided focused sonography is now accepted in the treatment of soft-tissue disorders, including prostate cancer and uterine fibroids. Intracranial applications for brain tumors[8,9] and neuropathic pain syndromes[10,11] are currently under investigation. More recently, MR imaging–guided focused sonography was tested in a clinical trial as a treatment for essential tremor.

Essential tremor is a common and disabling movement disorder with an estimated prevalence of 0.3%–5.55%.[12-17] Patients with essential tremor may suffer more from the mental effects on quality of life, such as lower perceived health status,[18] than from actual physical symptoms.[19] Essential tremor may be medically refractory: up to 30% of patients do not respond to first-line therapy and may consider surgical options.[20] Improved imaging and refined electrophysiologic localization have demonstrated that the ventralis intermedius nucleus (Vim) of the thalamus is the most effective target. The ventralis intermedius nucleus was the target for the MR imaging–guided focused sonography treatment in the clinical trial mentioned above.

The goal of this study was to describe findings on MR imaging

Received July 5, 2013; accepted after revision August 20.

From the Departments of Radiology, Neuroradiology Division (M.W., J.D., P.R., T.H., L.C.S., B.B., Y.Q.), Neurosurgery (D.S.H., M.A.K., S.M., J.J.L., R.F., N.K., W.J.E.), and Neurology (B.S.), University of Virginia, Charlottesville, Virginia; Focused Ultrasound Surgery Foundation (J.S., M.E.), Charlottesville, Virginia; and Insightec Ltd (E.Z.), Haifa, Israel.

This work was supported by a grant of the Focused Ultrasound Surgery Foundation (http://www.fusfoundation.org). The content of the article is solely the responsibility of the authors and does not necessarily represent the official views of the Focused Ultrasound Surgery Foundation.

Please address correspondence to Max Wintermark, MD, Department of Radiology, Neuroradiology Division, University of Virginia, PO Box 800170, (FedEx: 1215 Lee St-New Hospital, 1st Floor, Room 1011), Charlottesville, VA 22908-0170; e-mail: Max.Wintermark@virginia.edu

http://dx.doi.org/10.3174/ajnr.A3808

both pre- and post-Vim lesioning by MR imaging–guided focused sonography as a treatment for essential tremor in the 15 patients enrolled in the trial and to determine whether there was an association between these imaging features, the number and/or energy of sonications, and the clinical response to MR imaging–guided focused sonography.

MATERIALS AND METHODS

Study Population

Under the auspices of our institutional review board, 15 patients with medication-refractory essential tremor prospectively gave consent; were enrolled in a single-site, FDA-approved pilot clinical trial; and were treated with MR imaging–guided focused sonography targeting the Vim of the thalamus contralateral to the hand-dominant side. A complete medical history was obtained for each patient, along with a detailed physical and neurologic examination. Assessment of the patient's tremor was performed by using a validated Clinical Rating Scale for Tremor (CRST),[21] which has been shown to be reliable among examiners.[22] Inclusion and exclusion criteria are reported elsewhere.[23]

Procedure

The MR imaging–guided focused sonography thalamotomies were performed in a clinical 3T MR imaging system (HD750; GE Healthcare, Milwaukee, Wisconsin) by using a clinical system for focused sonography surgery (ExAblate 4000; InSightec, Haifa, Israel) featuring a hemispheric 1024-element phased array transducer.

The patient's head was fully shaven and then was immobilized within a MR imaging–compatible frame placed by using a local anesthetic. The patient's head rigidly affixed in the frame was carefully positioned in the helmet-like cavity of the sonography transducer. A flexible membrane filled with degassed water for sonography sealed the coupling space between the transducer and head surface. The water circulated at 16°C for continuous scalp cooling. The ablation target (ie, the Vim of the thalamus) was localized on 3D T1-weighted MR images by using the anterior/posterior commissure line as a reference. The Vim of the thalamus was initially targeted with standard indirect measurements from the anterior/posterior commissure line.

The first portion of the procedure consisted of several pretreatment test sonications to confirm that the thermal hot spot was centered in the target location. Several low-power sonications of 10–20 seconds' duration were applied to induce peak temperatures of <45°C. These brief temperatures are unlikely to cause lesioning but are easily visualized on MR thermometry images to validate the exact position and size of the hot spot, which typically measures 6 mm in height and 4 mm in diameter (75 μL).

The treatment itself consisted of several high-power sonications applied in an iterative process guided by MR imaging and MR thermometry. To induce local tissue ablation, we stepwise increased the acoustic power from sonication to sonication to finally achieve a peak temperature between 55°C and 60°C at the target. Typically, continuous wave sonications of 10–20 seconds duration, up to a maximum acoustic power of 1200 W and 800 W, respectively, were applied.

Patients were fully awake and responsive during all stages of the intervention. They were monitored and questioned repeatedly to ensure their neurologic integrity and to assess changes in tremor intensity or other sensations experienced during the treatment.

Clinical Outcome Assessment

All patients were monitored in the hospital for at least 24 hours. Postoperative assessments were performed at 24 hours, 1 week, 1 month, and 3 months and included tremor evaluation,[21] neurologic examination, and gait testing.[24,25] The contralateral appendicular tremor was evaluated by using the Clinical Rating Scale for Tremor (having a total of 160 points), which includes 3 parts: 1) observed tremor location and severity, 92 points; 2) motor tasks: drawing, handwriting, pouring, 36 points; and 3) disabilities related to speaking, feeding, drinking hygiene, dressing, writing, working, and social activities, 32 points.[21]

Imaging Studies

Preprocedural imaging included a noncontrast head CT, which was used during the procedure to provide a skull-correction algorithm for transcranial sonication. MR imaging studies were performed on a 3T scanner before the procedure and 24 hours, 1 week, 1 month, and 3 months following the procedure. The MR imaging protocol was the same at all 5 time points and included the following sequences: sagittal MPRAGE (TR = 1900 ms, TE = 1.94 ms, TI = 900 ms, flip angle = 9°, 3D, 240 sections per slab, section thickness = 0.9 mm, distance factor = 50%, base resolution = 256, phase resolution = 96%, acceleration factor = 2, whole-brain coverage); axial T1 spin-echo (TR = 600 ms, TE = 8.5 ms, flip angle = 90°, 30 sections, section thickness = 5.0 mm, distance factor = 20%, base resolution = 256, phase resolution = 100%, whole-brain coverage); axial T2 FSE (TR = 5410 ms, TE = 102 ms, flip angle = 50°, 30 sections, section thickness = 2.0 mm, distance factor = 0%, base resolution = 384, phase resolution = 85%, acceleration factor = 2, whole-brain coverage angled with the anterior/posterior commissure line and centered over the thalami); axial FLAIR (TR = 9000 ms, TE = 110 ms, TI = 2500 ms, flip angle = 180°, 30 sections, section thickness = 5.0 mm, distance factor = 20%, base resolution = 256, phase resolution = 100%, whole-brain coverage); axial SWI (TR = 27 ms, TE = 20 ms, flip angle = 15°, 3D, 104 sections per slab, section thickness = 1.5 mm, distance factor = 20%, base resolution = 256, phase resolution = 95%, acceleration factor = 2, whole-brain coverage); axial and coronal DWI (TR = 6200 ms, TE = 99 ms, 30 sections, section thickness = 5.0 mm, distance factor = 20%, base resolution = 178, phase resolution = 100%, acceleration factor = 2, whole-brain coverage); and axial T1 spin-echo postcontrast (TR = 600 ms, TE = 8.5 ms, flip angle = 90°, 30 sections, section thickness = 5.0 mm, distance factor = 20%, base resolution = 256, phase resolution = 100%, whole-brain coverage).

Data Analysis

Using a mixed model, we assessed whether the imaging pattern observed after treatment depended on the number of sonications, power used for the last sonication, and maximal temperature during the MR imaging–guided focused sonography treatment. Using correlation analysis, we evaluated whether the imaging fea-

tures observed after MR imaging–guided focused sonography treatment for essential tremor were associated with the clinical response to the treatment.

RESULTS

Patients

Fifteen patients (10 men and 5 women; age, 67 ± 8 years) were prospectively enrolled in this trial. Twelve were right-handed, and 3, left-handed. The target of the MR imaging–guided focused sonography treatment was the Vim of the thalamus on the contralateral side of the patient's hand dominance.

Procedures

Patients received an average of 18 sonications (minimum, 11; maximum, 26), with gradual increase in the energy of each sonication. The power used for the last sonication was 845 ± 243 W (minimum, 600 W; maximum, 1300 W). The duration of the last sonication was between 10 and 16 seconds. The maximal temperature reached during the MR imaging–guided focused sonography treatment was 59 ± 3°C (minimum, 55°C; maximum, 63°C).

Clinical Outcome

Clinical outcome in the 15 patients enrolled in the trial is reported in Table 1.

Imaging Findings

On T2-weighted imaging, we found a lesion pattern at the site of the focal spot with features similar to those previously found in a trial of MR imaging–guided focused sonography treatment of neuropathic pain.[10] There were 3 concentric zones: a hypointense zone I at the center; a strongly hyperintense zone II demarcated by a hypointense rim; and finally, a fuzzy, slightly hyperintense zone III at the periphery (Fig 1). The diameters of zone I and the thicknesses of zones II and III and their evolution with time are reported in Table 2 and Fig 2.

The focused sonography lesion in the axial plane, defined by the outline of zone II, was round in 10 patients, a vertical (anteroposterior) oval in 2 patients, and a horizontal (left-right) oval in 3 patients. In the 3 patients who required anterior repositioning of the focus, the observed shape was a vertical (anteroposterior) oval in 2 and a horizontal (left-right) oval in 1. The lesion had an elongated oval shape along the z-axis.

A cavity had developed in the location of zones I and II by 24 hours in 13 patients and by 1 week in the remaining 2 patients. This cavity collapsed by 1 month in 12 patients and by 3 months in the remaining 3 patients (Fig 3).

The inner 2 zones, zones I and II, showed reduced ADC values ($0.52 \pm 0.18 \times 10^{-3}$ mm^2/s) at 24 hours in all patients except 1. Diffusion had pseudonormalized by 1 week in 10 patients and by 1 month in the remaining 5 patients, when the cavity collapsed (Fig 3). T1 shortening in the location of the MR imaging–guided focused sonography lesion was present in 9 patients by 1 month and in 1 additional patient by 3 months posttreatment (Fig 3). Very mild postcontrast enhancement was seen in 6 patients at 24 hours after the MR imaging–guided focused sonography treatment. Enhancement appeared (or re-appeared) by 1 week in 6

Table 1: Clinical outcome in the 15 patients enrolled in the trial, measured in terms of the Clinical Rating Scale for Tremor[a]

Time Point	Mean	SD	Minimum	Maximum
Baseline CRST	54.9	14.4	38	87
24-Hour CRST	19.3	10.8	5	43
1-Week CRST	18.5	11.0	6	43
1-Month CRST	18.7	12.0	2	39
3-Month CRST	20.3	11.0	6	37
Outcomes (difference between baseline and 3-month CRST)	34.6	10.4	13	50

[a] Lower score is favorable; higher score is unfavorable.

Table 2: Diameters of zone I and thicknesses of zones II and III (mean in millimeters) after MR imaging–guided focused ultrasound treatment

T2 Imaging	Zone I	Zone II	Zone III
24 Hours	2.7 ± 1.4	2.2 ± 1.0	3.0 ± 1.1
1 Week	4.0 ± 1.6	1.8 ± 0.8	2.7 ± 1.8
1 Month	2.1 ± 1.4	1.2 ± 0.9	0.1 ± 0.3
3 Months	0.5 ± 0.7	0.1 ± 0.4	0.0 ± 0.0

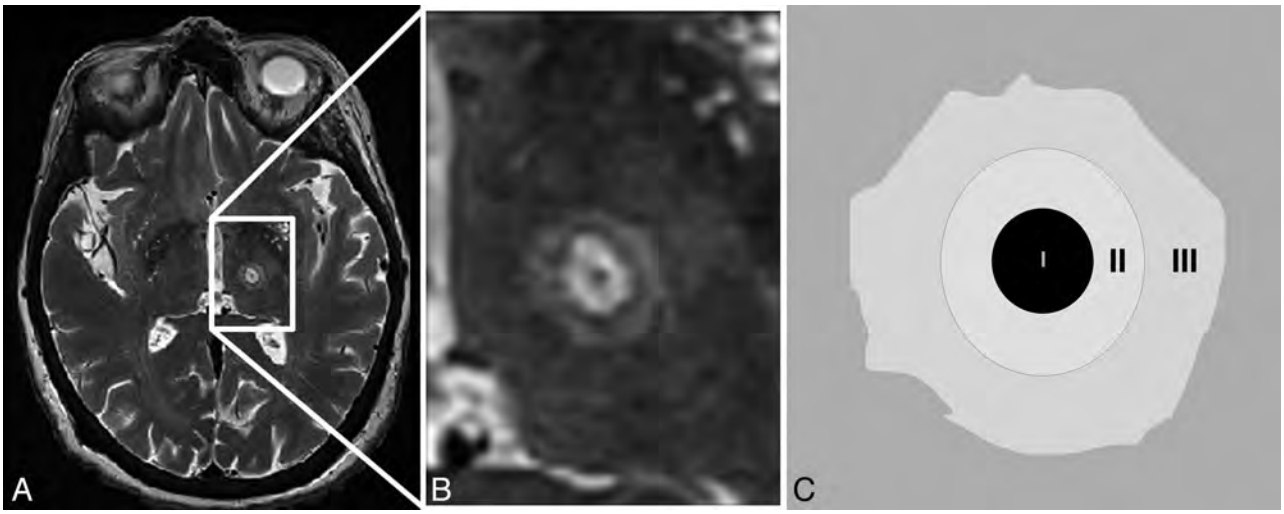

FIG 1. Schematic representation of zones I, II, and III visualized on T2-weighted imaging and the corresponding T2-weighted image of the lesion. On T2-weighted imaging, the patient developed 3 concentric zones at the site of lesioning: a hypointense zone I at the center; a strongly hyperintense zone II demarcated by a hypointense rim; and finally, a fuzzy, slightly hyperintense zone III at the periphery.

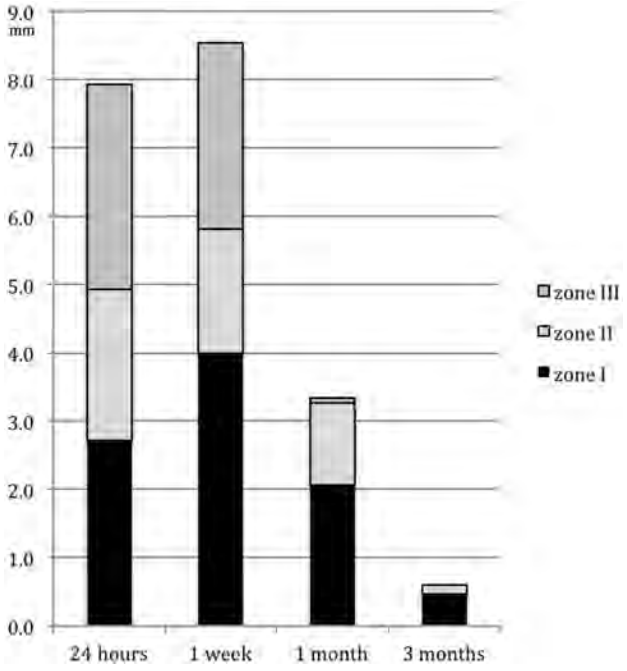

FIG 2. Average diameters of zone I and thicknesses of zones II and III, as seen on T2-weighted imaging, at 24 hours, 1 week, 1 month, and 3 months after the MR imaging–guided focused sonography treatment, all expressed in millimeters.

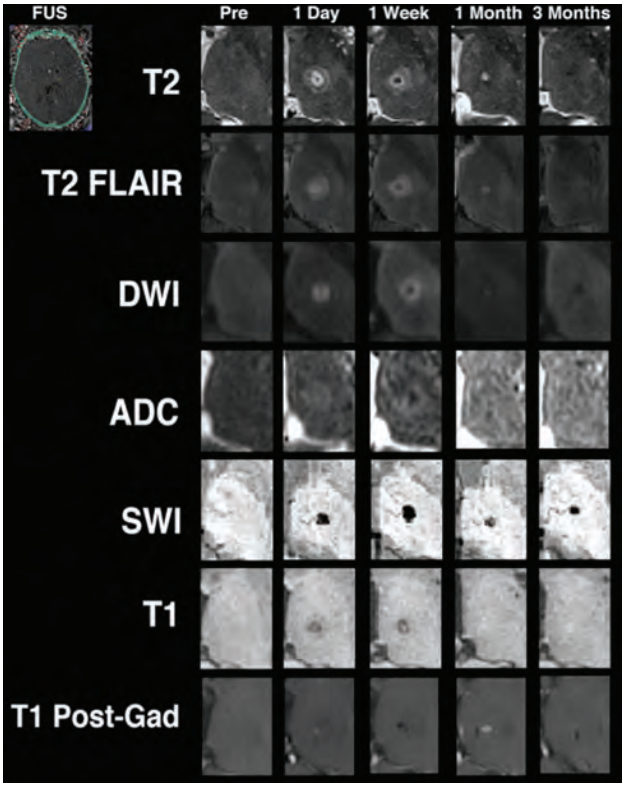

FIG 3. A 76-year-old, right-handed woman with essential tremor treated with MR imaging–guided focused sonography lesioning of the left Vim of the thalamus (thermography image obtained during the treatment is in the left upper corner). On T2-weighted imaging, the patient developed 3 concentric zones at the site of lesioning. Zone II corresponds to vasogenic edema and was seen at 24 hours and 1 week and then resolved. Zones I and II evolved into a round cavity in which diffusion was restricted by 24 hours after treatment. Diffusion pseudonormalized by 1 month when the cavity collapsed. T1 shortening was observed at 1 month and 3 months. Very mild enhancement was seen at 24 hours, likely resulting from the reversible alteration of the blood-brain barrier caused by the focused sonography treatment. Enhancement reappeared by 1 week and peaked at 1 month, by then likely representing neoangiogenesis. No major bleed occurred at any time point, but blood products responsible for susceptibility artifacts were seen within zones I and II at all time points.

patients, was present in all patients by 1 month, and had resolved by 3 months in all except 3 patients (Fig 3).

No intracerebral hemorrhage occurred, but blood products responsible for artifacts on susceptibility-weighted imaging were seen within zones I and II at all time points (Fig 3).

Relationship between the Imaging Pattern after Treatment and Characteristics of the MR Imaging–Guided Focused Sonography Treatment

We could not find any significant relationship between the imaging characteristics of the lesions and the number of sonications (P values ranging from .13 to .94), the final power (P values ranging from .29 to .98), or the maximal temperature reached (P values ranging from .13 to .99).

Relationship between the Imaging Pattern after Treatment and the Clinical Response to the MR Imaging–Guided Focused Sonography Treatment

We observed that the total lesion size (including zone III) and the clinical response measured based on the CRST score, especially its part B, evolved inversely compared with each other (coefficient of correlation = 0.29, P value = .02). Tremor control was optimal at 1 week when the lesion size and the perilesional edema were maximal, and it was less at 1 or 3 months when the perilesional edema had resolved and the total lesion size was smaller. On the other hand, adverse effects were most prominent during the first postoperative week and tended to resolve with the resolution of perilesional edema. Lesion collapse did not mean loss of tremor control. In addition, in the 2 patients who were outliers in terms of tremor control (ie, in the 2 patients who responded less well to the treatment), the imaging characteristics were not significantly different from those in the other patients. More specifically, the total lesions were not smaller, and these 2 patients did not show less perilesional edema.

DISCUSSION

Typical imaging findings following the MR imaging–guided focused sonography treatment for essential tremor consisted of 3 concentric zones at the site of lesioning. These findings were consistent with those previously reported in a trial of MR imaging–guided focused sonography lesioning of the contralateral thalamus for neuropathic pain.[10] Zone III was consistent with vasogenic edema[26,27]; it was typically seen at 24 hours and 1 week and then resolved. This appearance of lesions and their evolution with time was similar to the imaging findings observed for stereotactic radiofrequency thalamotomies but quite different from those observed with gamma knife radiosurgery.[28] Direct comparison between the different treatment modalities in terms of imaging is available in pigs,[29] and further studies comparing MR imaging–guided focused sonogra-

phy with radiofrequency ablation should be conducted in humans.

Zones I and II showed restricted diffusion at 24 hours that pseudonormalized by 1 week or 1 month, when the cavity developing in the location of zones I and II collapsed. Therefore, zones I and II likely represent areas of coagulation necrosis and cytotoxic edema.[8,26]

T1 shortening at the site of lesioning was seen in a little more than half of patients, typically starting at 1 month. Very mild enhancement was seen at 24 hours, likely resulting from the reversible alteration of the blood-brain barrier caused by the focused sonography treatment.[30] This alteration of the blood-brain barrier typically happens within the first 24 hours and then resolves,[31] explaining that enhancement was captured at 24 hours in only 6 patients. Enhancement reappeared by 1 week and peaked at 1 month. Further investigation in animal models is needed to elucidate the exact nature of this enhancement, which might be related to neovascularization.[32] Of note, in the previous application of MR imaging–guided focused sonography for neuropathic pain syndromes,[10] enhancement was seen at 24 hours and had resolved by 48 hours. Patients were not imaged beyond 48 hours. As such, the 1-month enhancement we are reporting could not be assessed in the neuropathic pain trial.

The focused sonography lesion was round or a horizontal or vertical oval. In patients in whom the focus was repositioned, the lesion was oval; however, the oval shape was also observed in patients for whom the focus was not repositioned.

We found a relationship between the size of the lesion on imaging and the response of the tremor to the treatment, suggesting that tremor control is influenced not only by the lesion size and the amount of perilesional edema but also, most likely, by lesion location.

As a limitation to our study, we acknowledge the limited sample size of our study population. The lack of significance of most of our analyses may reflect the fact that our study was underpowered. Further studies with larger sample size are needed for additional characterization of imaging findings in MR imaging–guided focused ultrasound treatment.

CONCLUSIONS

High-intensity focused sonography can accurately produce controlled heating to a precise intracranial target, with typical imaging findings seen in the days, weeks, and months following the treatment. Tremor control was optimal early when the lesion size and perilesional edema were maximal and was less later when the perilesional edema had resolved and the total lesion size was smaller. Further studies should be conducted to better understand the value of imaging findings either as a guidance for improving the treatment procedure or as a prediction for long-term clinical outcome.

Disclosures: Max Wintermark—*RELATED*: *Grant*: Focused Ultrasound Surgery Foundation*; *UNRELATED*: *Board Membership*: Bayer,* St. Jude Medical*; *Grants/Grants Pending*: GE Healthcare,* Philips Healthcare.* Johanna J. Loomba—*RELATED*: *Grant*: Focused Ultrasound Surgery Foundation,* *Comments*: This nonprofit provided institutional grant funding for the ET001 study. Eyal Zadicario is an employee of InSightec Ltd. Neal Kassell is a founding member of the board of the Focused Ultrasound Surgery Foundation, as well as a director and shareholder of InSightec Ltd. *RELATED*: *Board Membership*: InSightec. William Jeff Elias receives research support from the Focused Ultrasound Surgery Foundation for clinical and preclinical studies,* as well as an honorarium for serving on the movement disorder steering committee of the Focused Ultrasound Surgery Foundation. *Money paid to the institution.

REFERENCES

1. Jolesz FA, McDannold N. **Current status and future potential of MRI-guided focused ultrasound surgery.** *J Magn Reson Imaging* 2008;27:391–99
2. Moonen CT, Quesson B, Salomir R, et al. **Thermal therapies in interventional MR imaging: focused ultrasound.** *Neuroimaging Clin N Am* 2001;11:737–47
3. Salomir R, Delemazure AS, Palussiere J, et al. **Image-based control of the magnetic resonance imaging-guided focused ultrasound thermotherapy.** *Top Magn Reson Imaging* 2006;17:139–51
4. Cline HE, Schenck JF, Hynynen K, et al. **MR imaging-guided focused ultrasound surgery.** *J Comput Assist Tomogr* 1992;16:956–65
5. Jolesz FA, Bleier AR, Lauter RS. **Laser surgery benefits from guidance by MR.** *Diagnostic Imaging* 1990;12:103–08
6. Jolesz FA, Blumenfeld SM. **Interventional use of magnetic resonance imaging.** *Magn Reson Q* 1994;10:85–96
7. Jolesz FA, Moore GJ, Mulkern RV, et al. **Response to and control of destructive energy by magnetic resonance.** *Invest Radiol* 1989;24:1024–27
8. Ram Z, Cohen ZR, Harnof S, et al. **Magnetic resonance imaging-guided, high-intensity focused ultrasound for brain tumor therapy.** *Neurosurgery* 2006;59:949–55, discussion 955–56
9. McDannold N, Clement GT, Black P, et al. **Transcranial magnetic resonance imaging-guided focused ultrasound surgery of brain tumors: initial findings in 3 patients.** *Neurosurgery* 2010;66:323–32, discussion 332
10. Martin E, Jeanmonod D, Morel A, et al. **High-intensity focused ultrasound for noninvasive functional neurosurgery.** *Ann Neurol* 2009;66:858–61
11. Jeanmonod D, Werner B, Morel A, et al. **Transcranial magnetic resonance imaging-guided focused ultrasound: noninvasive central lateral thalamotomy for chronic neuropathic pain.** *Neurosurg Focus* 2012;32:E1
12. Bharucha NE, Bharucha EP, Bharucha AE, et al. **Prevalence of essential tremor in the Parsi community of Bombay, India.** *Arch Neurol* 1988;45:907–08
13. Haerer AF, Anderson DW, Schoenberg BS. **Prevalence of essential tremor. Results from the Copiah County study.** *Arch Neurol* 1982;39:750–51
14. Hornabrook RW, Nagurney JT. **Essential tremor in Papua, New Guinea.** *Brain* 1976;99:659–72
15. Rajput AH, Offord KP, Beard CM, et al. **Essential tremor in Rochester, Minnesota: a 45-year study.** *J Neurol Neurosurg Psychiatry* 1984;47:466–70
16. Rautakorpi I, Takala J, Marttila RJ, et al. **Essential tremor in a Finnish population.** *Acta Neurologica Scandinavica* 1982;66:58–67
17. Nguyen HV, Ngian V, Cordato D, et al. **Quality of life in a random sample of community dwelling older patients with essential tremor.** *Acta Neurol Scand* 2007;116:289–92
18. Woods SP, Scott JC, Fields JA, et al. **Executive dysfunction and neuropsychiatric symptoms predict lower health status in essential tremor.** *Cogn Behav Neurol* 2008;21:28–33
19. Lorenz D, Schwieger D, Moises H, et al. **Quality of life and personality in essential tremor patients.** *Mov Disord* 2006;21:1114–18
20. Zesiewicz TA, Elble R, Louis ED, et al. **Practice parameter: therapies for essential tremor: report of the quality standards subcommittee of the American Academy of Neurology.** *Neurology* 2005;64:2008–20
21. Fahn S, Tolosa E, Marin C. **Clinical rating scale for tremor.** In: Jankovic J, Tolosa E, eds. *Parkinson's Disease and Movement Disorders.* Baltimore: Urban & Schwarzenberg; 1988
22. Stacy MA, Elble RJ, Ondo WG, et al. **Assessment of interrater and intrarater reliability of the Fahn-Tolosa-Marin tremor rating scale in essential tremor.** *Mov Disord* 2007;22:833–38

23. Elias J, Huss D, Voss T, et al. **A pilot study of focused ultrasound thalamotomy for essential tremor.** *N Engl J Med* 2013;369:640–48
24. Herman T, Inbar-Borovsky N, Brozgol M, et al. **The dynamic gait index in healthy older adults: the role of stair climbing, fear of falling and gender.** *Gait Posture* 2009;29:237–41
25. Wrisley DM, Marchetti GF, Kuharsky DK, et al. **Reliability, internal consistency, and validity of data obtained with the functional gait assessment.** *Phys Ther* 2004;84:906–18
26. Chen L, Bouley DM, Harris BT, et al. **MRI study of immediate cell viability in focused ultrasound lesions in the rabbit brain.** *J Magn Reson Imaging* 2001;13:23–30
27. Hynynen K, McDannold N, Clement G, et al. **Pre-clinical testing of a phased array ultrasound system for MRI-guided noninvasive surgery of the brain: a primate study.** *Eur J Radiol* 2006;59:149–56
28. Tomlinson FH, Jack CR Jr, Kelly PJ. **Sequential magnetic resonance imaging following stereotactic radiofrequency ventralis lateralis thalamotomy.** *J Neurosurg* 1991;74:579–84
29. Elias WJ, Khaled M, Hilliard JD, et al. **A magnetic resonance imaging, histological, and dose modeling comparison of focused ultrasound, radiofrequency, and gamma knife radiosurgery lesions in swine thalamus.** *J Neurosurg* 2013;119:307–17
30. Hynynen K, McDannold N, Vykhodtseva N, et al. **Non-invasive opening of BBB by focused ultrasound.** *Acta Neurochir Suppl* 2003;86:555–58
31. Hynynen K, McDannold N, Vykhodtseva N, et al. **Noninvasive MR imaging-guided focal opening of the blood-brain barrier in rabbits.** *Radiology* 2001;220:640–46
32. Smirniotopoulos JG, Murphy FM, Rushing EJ, et al. **Patterns of contrast enhancement in the brain and meninges.** *Radiographics* 2007; 27:525–51

Changes in the Thalamus in Atypical Parkinsonism Detected Using Shape Analysis and Diffusion Tensor Imaging

C.P. Hess, C.W. Christine, A.C. Apple, W.P. Dillon, and M.J. Aminoff

ABSTRACT

BACKGROUND AND PURPOSE: The thalamus is interconnected with the nigrostriatal system and cerebral cortex and has a major role in cognitive function and sensorimotor integration. The purpose of this study was to determine how regional involvement of the thalamus differs among Parkinson disease, progressive supranuclear palsy, and corticobasal syndrome.

MATERIALS AND METHODS: Nine patients with Parkinson disease, 5 with progressive supranuclear palsy, and 6 with corticobasal syndrome underwent 3T MR imaging along with 12 matched, asymptomatic volunteers by using a protocol that included volumetric T1 and diffusion tensor imaging. Acquired data were automatically processed to delineate the margins of the motor and nonmotor thalamic nuclear groups, and measurements of ADC were calculated from the DTI data within these regions. Thalamic volume, shape, and ADC were compared across groups.

RESULTS: Thalamic volume was smaller in the progressive supranuclear palsy and corticobasal syndrome groups compared with the Parkinson disease and control groups. Shape analysis revealed that this was mainly due to the diminished size of the lateral thalamus. Overall, ADC measurements were higher in the progressive supranuclear palsy group compared with both the Parkinson disease and control groups, and anatomic subgroup analysis demonstrated that these changes were greater within the motor regions of the thalamus in progressive supranuclear palsy and corticobasal degeneration.

CONCLUSIONS: Reduced size and increased ADC disproportionately involve the lateral thalamus in progressive supranuclear palsy and corticobasal syndrome, consistent with selective neurodegeneration and atrophy in this region. Because these findings were not observed in Parkinson disease, they may be more specific markers of tau-related neurodegeneration.

ABBREVIATIONS: CBD = corticobasal degeneration; CBS = corticobasal syndrome; PD = Parkinson disease; PSP = progressive supranuclear palsy; VLa = ventral lateral anterior; VLp = ventral lateral posterior

The neurodegenerative movement disorders Parkinson disease (PD), progressive supranuclear palsy (PSP), and corticobasal degeneration (CBD) are distinguished postmortem by differing histologic abnormalities and regional patterns of neuropathologic changes. PSP and corticobasal syndrome (CBS) exhibit neuronal and glial cytoplasmic inclusions from accumulation of highly phosphorylated microtubule-associated tau protein, which is not evident in PD.[1-3] Paralleling these differences, typical clinical phenotypes help to distinguish these disorders. However, classic presentations are consistent only in advanced disease, and misdiagnosis is frequent in patients with early symptoms.[4,5] The diagnosis of CBD is particularly problematic[6]; for this reason, the term "corticobasal syndrome" is applied in lieu of CBD to convey the fact that disorders including Alzheimer disease, certain variants of frontotemporal lobar degeneration, and prion disease can present similarly.

Various observations on MR imaging have been reported to differentiate PD, PSP, and CBD. Alterations in the shape or volume of several subcortical brain regions correlate with gross inspection of the brain in pathologically confirmed cases.[7] However, such changes are subject to observer bias and are reliably found only in late disease. Unbiased approaches by using voxel-based morphometry and automated segmentation have also been applied with some success.[8-13] DTI studies have revealed increased diffusivity within the superior cerebellar peduncles in

Received July 24, 2013; accepted after revision October 2.

From the Departments of Radiology and Biomedical Imaging (C.P.H., A.C.A., W.P.D.) and Neurology (C.W.C., W.P.D., M.J.A.), University of California, San Francisco, San Francisco, California.

This work was supported by the UCSF Department of Radiology and Biomedical Imaging. C.P.H. was supported in part by the GE-AUR Radiology Research Academic Fellowship.

Please address correspondence to Christopher P. Hess, MD, PhD, University of California, San Francisco, 505 Parnassus Ave, Room L-358, Box 0628, San Francisco, CA 94143-0628; e-mail: Christopher.Hess@ucsf.edu

Indicates article with supplemental on-line table.

http://dx.doi.org/10.3174/ajnr.A3832

PSP,[14-16] along with more widespread changes within supratentorial white matter.[17,18] A number of groups have also described alterations in deep gray matter diffusion. For example, measurements of ADC are elevated within the putamen in up to 90% of patients with atypical parkinsonism but not significantly different from controls in patients with PD.[16,19]

The shared anatomic involvement of the basal ganglia and other brain regions in these disorders likely contributes to their frequent clinical overlap. Few studies have focused specifically on the thalamus, which, through the nigrostriatal system and thalamocortical circuits, plays a major role in cognition and sensorimotor integration. Alterations in thalamic volume have not been shown in prior studies of CBS, but significantly lower thalamic volume has been observed in PSP compared with both patients with PD[20] and controls.[10,20] Diminished volume by itself does not provide insight into how separate nuclear groups within the thalamus are selectively affected, however. One study suggested that thalamic shape differs between subjects with PD and healthy elders, though these changes were challenging to interpret because there was multifocal involvement over the entire surface of the thalamus without a corresponding difference in volume.[21] Using DTI, Erbetta et al[22] measured higher ADC within the anterior and lateral thalami in PSP and CBS compared with controls, but their analysis was based on relatively imprecise atlas-based estimates of nuclear boundaries.[22]

We hypothesized that regional thalamic morphology and tissue microstructure, measured with volumetric T1-weighted MR imaging and DTI, respectively, would be different in patients with PSP and CBS compared with patients with PD and controls. Using fully automated analysis of 3T T1 and DTI data, we evaluated thalamic shape and diffusion within motor and nonmotor thalamic nuclear groups and compared these measurements in patients with CBS, PSP, and PD and in healthy control subjects.

MATERIALS AND METHODS

Subject Recruitment

The University of California, San Francisco Committee on Human Research approved this study. Subjects with PD ($n = 9$), PSP ($n = 5$), or CBS ($n = 6$) were prospectively recruited from the UCSF Parkinson's Disease and Movement Disorders Clinic. Two movement disorder specialists (M.J.A., C.W.C.) independently assigned a diagnosis to all patients based on history, neurologic examination, and prior response to levodopa therapy. Patients were included only if there was agreement between the 2 clinicians. Data abstracted during patient interviews included the initial symptom and laterality (if present) at disease onset, age at diagnosis, response to levodopa therapy, and the presence or absence of cognitive symptoms. Patients with PSP met the criteria for clinically probable PSP[23] and patients with PD met the criteria for probable PD,[24] except for one who had not been previously treated with dopaminergic medication and therefore met the criteria for possible PD. Patients diagnosed with CBS also met accepted criteria.[25] Twelve healthy control subjects without any history of neurologic illness and normal neurologic examination findings were also recruited and imaged for comparison with patients.

Data Acquisition

After providing written consent, subjects were imaged on a 3T Signa HDx 14.x scanner (GE Healthcare, Milwaukee, Wisconsin) with an 8-channel head coil. To delineate thalamic boundaries, 3D T1 inversion recovery spoiled gradient-echo images were acquired in the sagittal plane with 1-mm isotropic voxel resolution and TR/TE/TI = 7.2/2.3/400 ms, flip angle = 15°, matrix size = 256 × 192, slab thickness = 1.0 mm, FOV = 256 × 192 mm (scan time 5 minutes 54 seconds). In the same session, DTI was performed at 2-mm isotropic resolution by using a single-shot axial echo-planar acquisition with TR/TE = 17 seconds/68.4 ms, FOV = 256 × 256 mm, matrix = 128 × 128 zero-filled to 256 × 256 (scan time 8 minutes 47 seconds). Diffusion-weighting of $b = 1000$ s/mm^2 was applied along 30 noncollinear directions. A single $b = 0$ s/mm^2 image was acquired, and array spatial sensitivity encoding technique parallel imaging was used with R = 2 to reduce susceptibility artifacts. Axial T2 FLAIR images were also acquired and visually inspected to exclude significant white matter disease and lesions within the thalami such as lacunar infarctions that might interfere with volumetric analysis, tractography, or ADC quantitation. Although some subjects in each group had a few punctate foci of nonspecific white matter T2 signal, no abnormality was evident within the thalami of any subject.

Thalamic Morphology

Before morphometric analysis, T1-weighted images were corrected for multichannel coil-related nonuniformities in intensity by using vendor software on the scanner. Six-parameter rigid-body registration to the isotropic 1-mm T1-weighted version of the Montreal Neurological Institute International Consortium for Brain Mapping 152 atlas was used to obtain gross alignment of coordinate axes among subjects. Standard space masking to remove neck and eye tissue was then performed and followed by skull stripping by using the Brain Extraction Tool, included in the FSL software package (http://www.fmrib.ox.ac.uk/fsl).[26]

Shape analysis relied on automated thalamic parcellation within each hemisphere by using the FIRST subcortical segmentation tool in FSL.[27] Thalamic volumes were calculated from the resulting binary masks. Estimated total intracranial volume was computed for each subject by using in-house software implementing the atlas-based method developed by Buckner et al.[28] Differences in thalamic morphology between groups were assessed by using the heat kernel smoothing approach for structure modeling developed by Kim et al.[29] This technique allows robust, point-by-point evaluation of the displacement vector fields that map the study-specific normal template for each structure of interest onto the estimated boundaries of the same structure in each subject's brain.

Two steps were implemented to calculate surface deformation data: 1) normal template construction for each thalamus, and 2) estimation of deformation fields between the normal template and individual subject surfaces. In the first step, the group-average brain volume was derived from the images of healthy controls by using the nonlinear iterative template construction tool in the Advanced Normalization Tools software package (http://software.incf.org/software/advanced-normalization-tools).[30] The deformation fields warping each normal brain to the template were then applied to the binary subcortical masks from FIRST, and the

Baseline characteristics for study participants

	NC	PD	PSP	CBD	*P* Value
No.	12	9	5	6	
Age (yr)	68.6 ± 5.5	66.3 ± 7.9	69.2 ± 3.0	70.5 ± 4.8	.67
Sex (F/M)	4:8	2:7	3:2	5:1	.09
Disease duration (yr)	N/A	8.6 ± 4.2	3.8 ± 1.4	5.5 ± 1.4	.03[a]
Side of main symptoms	N/A	5 left; 4 right	N/A	3 left; 3 right	.24
eTIV (L)	1.59 ± 0.18	1.53 ± 0.10	1.43 ± 0.27	1.58 ± 0.32	.24

Note:—NC indicates healthy control; L, liters; NA, not applicable; eTIV, estimated total intracranial volume.
[a] Statistically significant ($P < .05$).

masks were averaged in template space to obtain mean thalamic volumes. Isosurfaces were constructed from these volumes by using the marching cubes algorithm in Matlab (MathWorks, Natick, Massachusetts).

In the second step, the deformation field for warping the template to each subject's T1-weighted images was calculated by using the diffeomorphic shape and averaging technique with cross-correlation as the similarity metric in Advanced Normalization Tools. Because the field is defined on voxels, deformation fields were interpolated onto the mesh vertices for the surfaces obtained in the first step. For each subject, the length of the displacement vector at each point on the surface mesh was computed. Finally, the resulting displacement lengths were smoothed by using the Laplace-Beltrami eigenfunctions.[29]

Thalamic Diffusion

DTI data were skull-stripped and corrected for motion and eddy current artifacts by using FSL, and ADC maps were calculated by using in-house code implementing standard diffusion reconstruction. To account for the possibility of slight misregistration between the diffusion and T1-weighted data, we aligned each T1 volume with the corresponding $b=0$ diffusion volume by using linear registration in FSL with mutual information as the registration metric.

Thalamic nuclear groups corresponding to the conglomerate ventral anterior, VLa, and VLp nuclei were delineated by using the probabilistic tractography technique described by Behrens et al[31] and implemented in FMRIB Diffusion toolbox in FSL (http://www.fmrib.ox.ac.uk/fsl/fdt/index.html). Regions corresponding to primary motor, premotor, and supplementary motor area cortices were delineated as a single region of motor thalamic projections distinct from the remainder of the cortex within each hemisphere on the standard International Consortium for Brain Mapping 152 template. By first registering the template brain to each subject's T1-weighted scan, cortical ROIs were defined in each subject and used as classification targets for seed-based tractography. The resulting segmentations were used to construct motor and nonmotor masks for calculation of ADC for the entire, motor, and nonmotor thalami on each side of the brain.

Statistical Analysis

Differences in sex among groups were evaluated by using χ^2 tests for equivalence. One-way analysis of variance was used to compare age at the time of MR imaging, disease duration (defined as the time between approximate initial symptom onset and MR imaging), and estimated total intracranial volume. Thalamic volumes were assessed for asymmetry across hemispheres in subjects with PD and CBS by using paired *t* tests and were subsequently compared across groups by using multivariate analysis of covariance with age, sex, and estimated total intracranial volume as covariates. Kruskal-Wallis nonparametric tests were used to identify intergroup differences in mean thalamic ADC, with the significance threshold at $P < .05$, followed by post hoc 1-way ANOVA with unequal variances between groups in which differences were found. For all pair-wise comparisons, differences were considered significant at a false discovery rate of $q < 0.05$.

The above statistical tests were performed by using R (http://www.r-project.org/).[32] The SurfStat toolbox (http://www.math.mcgill.ca/keith/surfstat/),[33] a platform-designed surface mesh and volume data analysis, was used for group comparisons of thalamic shape. This package permits multivariate shape analysis with linear mixed-effects models, including multiple-comparisons correction by using random field theory.

RESULTS

Subjects

Baseline characteristics for the 4 study groups are summarized in the Table and On-line Table, respectively. There were 4 female and 8 male controls, ranging from 61.6 to 80.6 years of age. Patient age, sex, and estimated total intracranial volume were not significantly different between groups. Disease duration was longer in the PD group than in both the CBS and PSP groups ($P = .026$).

Thalamic Volume and Shape

There was no difference in right or left thalamic volume between healthy controls and patients with PD (Fig 1*A*). However, both volumes were smaller in the PSP and CBS groups compared with the healthy control and PD groups. Comparisons within groups after ordering volumes by size revealed no interhemispheric asymmetry in thalamic volume within any group. This included PD and CBS groups, in which asymmetric symptom onset was noted in all patients.

Using multivariate analysis with age and estimated total intracranial volume as covariates, while correcting for multiple comparisons, the study was not adequately powered to detect changes in thalamic shape specific to each group. However, on the basis of the statistical equivalence of the volumes in the CBS and PSP groups and on previously noted neuropathologic overlap between the disorders, these 2 groups were pooled for shape analysis. Figure 1*B* illustrates the results of this comparison for the 3 groups (healthy control, PD, and CBS+PSP). There were no differences in shape on the medial aspect of the thalamus. However, differences were present bilaterally for the group with atypical parkinsonism in both the ventral anterior and ventral lateral thalamus, corresponding to the location of the thalamic motor nuclei (Fig 2). The lateral surface of the conglomerate motor nuclei was involved when considering all voxels with a trend ($P < .25$) toward significance.

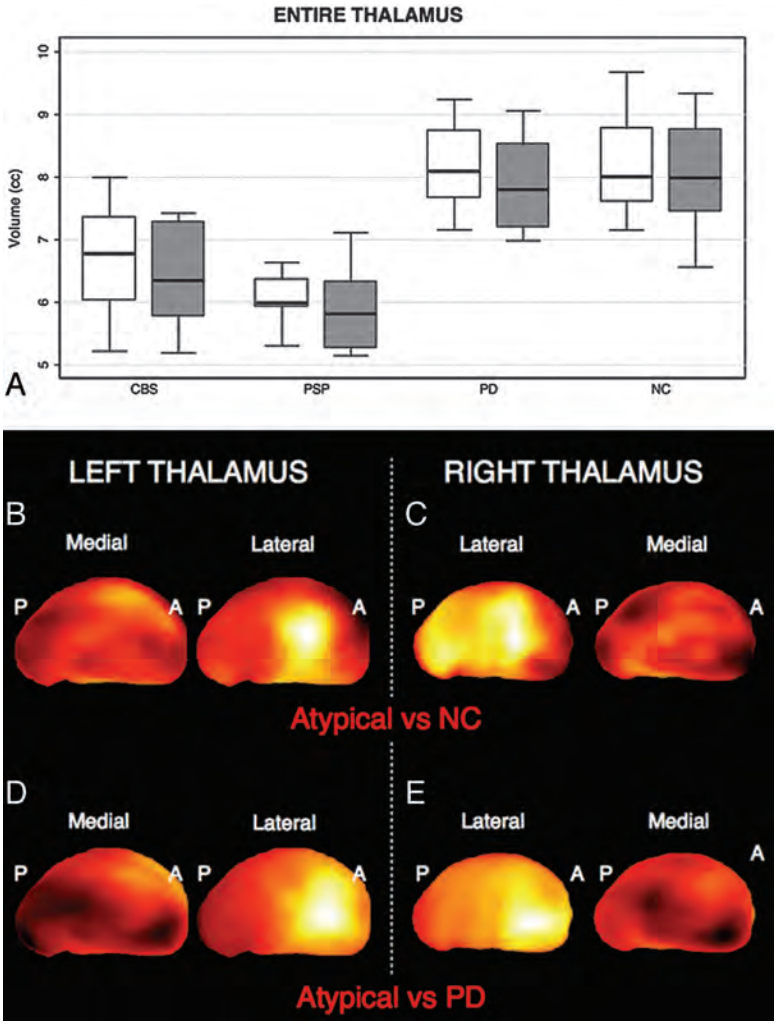

FIG 1. *A*, Boxplots of left (white) and right (gray) thalamic volumes in milliliters in healthy controls and patients with PD, CBS, and PSP. Vertical lines illustrate the range in calculated volume for each group, and upper and lower box boundaries correspond to 75th and 25th percentiles for volumes, respectively. Dark horizontal lines represent median values. *B–E*, Statistical maps of shape difference displayed on the average left (*B* and *D*) and right (*C* and *E*) thalami. Note relatively the symmetric shape difference in the lateral thalamus, with relative sparing of the medial thalamus. Only white met statistical significance. Yellow indicates areas with trends toward significance ($P < .25$), seen clustered more extensively around regions in the expected location of the ventral anterior and ventral lateral thalamic nuclei. A similar pattern of difference in shape is observed when the atypical group (CBD+PSP) is compared with the healthy control group (*B* and *C*) and patients with PD (*D* and *E*).

Thalamic Mean Diffusivity

Mean ADC values within the right and left thalami are shown in Fig 3*A*. Because there was no interhemispheric asymmetry in ADC values in any group, ADCs for the left and right thalami were averaged in each patient. Group differences were detected in mean ADC ($P = .037$) across the 4 groups (healthy control, PD, CBS, PSP), and post hoc between-group ANOVAs revealed differences in ADC between the PSP and healthy control groups ($P = .033$) and between the PSP and PD groups ($P = .0081$). Pair-wise comparisons between other groups showed no additional differences.

For analysis of ADC within thalamic nuclei, the CBS and PSP groups were combined, in analogy with the pooling of subjects used for volumetric analysis. No interhemispheric asymmetry in ADC was observed, so values were averaged for these regions in all 3 groups (healthy control, PD, and CBS+PSP). There was no difference in ADC within nonmotor thalamic regions ($P = .31$), but the ADC values differed within the motor thalamic regions ($P < .001$, Fig 3*B*). Post hoc pair-wise ANOVAs showed that motor thalamic ADC in the CBS+PSP group was significantly greater than the motor thalamic ADC in both the healthy control and PD groups ($P < .001$).

DISCUSSION

Our results show that patients diagnosed with the atypical parkinsonian disorders CBS and PSP exhibit not only global differences in thalamic volume but also localized alterations in shape and ADC within thalamic motor nuclear regions (ventral anterior, VLa, and VLp) compared with patients with PD and controls. These changes are spatially concordant, supporting the concept of disproportionate motor thalamus involvement in these 2 disorders. Furthermore, similar changes were not found in patients with PD; this finding suggests that the differences may be specific to tau neurodegeneration. These results provide imaging evidence for alterations in thalamic substructure in atypical parkinsonism and corroborate existing histopathologic data showing motor thalamus degeneration in postmortem-confirmed cases of these disorders.[1-3,6]

In contrast to most prior studies that included the thalamus, we used fully automated analysis of images from a single 3T MR imaging scanner instead of manual region-of-interest analysis of 1.5T T1 and diffusion data. Because the analysis was performed in the native measurement space for each subject, the methods are inherently more sensitive than voxel-based morphometry; registration of subjects to a common template and spatial smoothing to reduce misregistration errors in voxel-based morphometry can obscure group differences within small structures like the thalamus. This limitation may account for the absence of regional thalamic changes in prior studies using voxel-based morphometry.

Our work differs in several respects from the related work of Saini et al,[13] who applied a different technique for shape analysis in a number of subcortical structures in PSP, including the thalamus. First, nonlinear registration in this work provided more precise estimates for deformation at each surface point, thereby allowing vertex-wise comparison without multivariate Gaussian assumptions. Second, the random field technique for multiple comparisons provides a smoother and more robust approach (on the mesh surface) than the false discovery rate method. Finally, changes in morphology were studied together with changes in diffusivity, helping to confirm the veracity of spatially concordant changes in both thalamic tissue microstructure and shape.

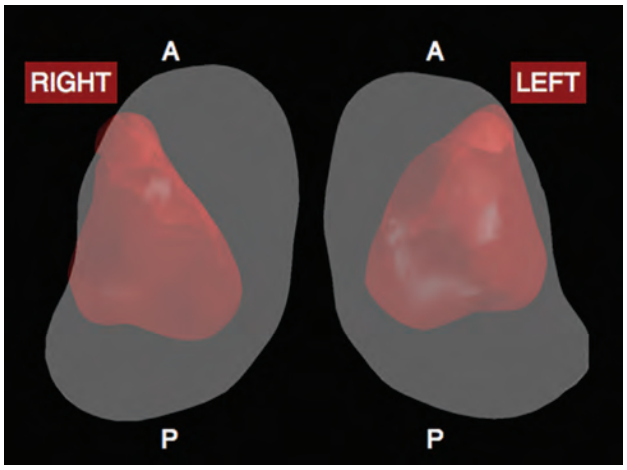

FIG 2. Correspondence between thalamic surface templates and DTI estimates of the location of thalamic nuclei, as viewed from a level superior to the thalami. The right and left thalamic motor nuclear groups, parcellated from the nonmotor regions of the thalamus by using probabilistic DTI tractography, are depicted in red. The contours of the thalami, shaded gray, were delineated automatically from the T1-weighted anatomic images. A indicates anterior; P, posterior.

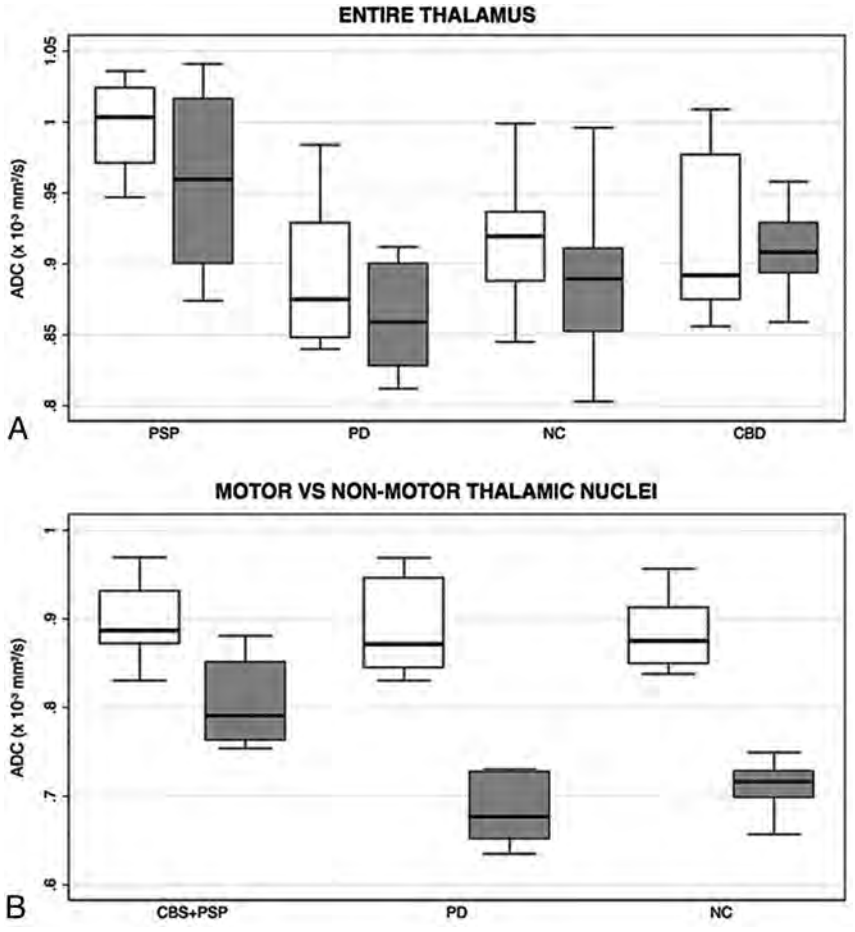

FIG 3. *A*, Boxplots of left (white) and right (gray) thalamic ADC in mm^2/s ($\times 10^{-3}$) in control, PD, CBS, and PSP groups. Nonparametric tests of intergroup equivalence demonstrate significant differences in thalamic ADC in the PSP group compared with both healthy controls and patients with PD (see text). *B*, Boxplots of mean ADC in mm^2/s ($\times 10^{-3}$) within nonmotor (white) and motor (gray) thalamic nuclei in healthy controls and patients with PD and atypical PD (CBS+PSP).

In this study, the most striking differences in thalamic shape and ADC were evident in the PSP group, and a more intermediate difference was found in the CBS group (Figs 1 and 3). This intermediate effect suggests greater disease heterogeneity in the CBS group because patients with CBS due to Alzheimer disease or other pathologies may exhibit different degrees of thalamic injury than those with tau pathology. Pathologic confirmation of diagnosis was lacking in our study, however, making it difficult to discriminate among the disorders with absolute certainty. Although it was necessary to combine patients with CBS and PSP into a single group to improve statistical power, we justify this approach on the basis of the pathologic overlap between PSP and many cases of CBS, especially with respect to tau deposition within the thalamus.[1]

Neuropathologic studies have shown thalamic atrophy in both CBS and PSP.[2,3] Although thalamic involvement has also been described in the caudal intralaminar nuclei in PD,[34] the central location of these nuclei makes their selective atrophy difficult to detect by using surface morphometry as applied in this study. In the absence of longitudinal data and pathology, is it impossible to distinguish whether the differences that we observed in the motor thalamus reflect primary neurodegeneration in this region or secondary "downstream" degeneration related to abnormalities arising in the basal ganglia or cortical gray matter and secondarily involving the thalamus.

Selective involvement of thalamic motor nuclei in CBS and PSP is consistent with disruption of normal thalamocortical motor connectivity. The primary motor cortex receives thalamic input from the VLp nucleus, and the ventral anterior and VLa regions are more broadly connected to the premotor cortex and supplementary motor areas. The anatomic interruption of these pathways has been associated with dystonia, alien hand syndrome, apraxia, and other clinical features evident in both CBS and PSP.[35] The observation of involvement of frontoparietal white matter by using hypothesis-free whole-brain analysis of ADC in patients with PSP[18] further corroborates the idea that PSP preferentially affects these pathways. Along similar lines, Whitwell et al[36] used fMRI, DTI, and voxel-based morphometry to support their hypothesis that PSP causes disruption of the long, polysynaptic dentatorubrothalamic tract. The results of our work support this concept and further suggest that the overlapping phenotypes of CBS and PSP might reflect selective involvement of different segments of this pathway, with both disorders involving the motor thalamus, but with cerebellar disconnection predominating in PSP and cortical disconnection predominating in CBS.

The present work has several limitations. First, the number of subjects was small, necessitating the combination of the PSP and CBS groups for our statistical analyses. There was a difference in disease duration between groups, and this could be relevant if the observed higher values of ADC in PSP or CBS later normalize in the disease course. Third, the boundary estimates for the thalamic nuclei derived by using probabilistic tractography are inherently imprecise, and as such, the derived ADC values may have been subject to partial volume effects between nuclear groups. Finally, we used clinical criteria for diagnosis and did not have pathologic confirmation.

CONCLUSIONS

Reduced size and increased ADC are disproportionately found in the motor thalamus in the atypical parkinsonian disorders PSP and CBS, consistent with selective neurodegeneration in these regions. The absence of similar changes in PD suggests that these differences may be specific to tau-related neurodegeneration.

ACKNOWLEDGMENTS

The authors are grateful to Seung-Goo Kim for helpful discussions regarding the implementation of deformation tensor morphometry.

Disclosures: Christopher Hess—*RELATED*: *Grant*: GE Radiology Research Academic Fellowship,* *Comments*: salary support, *UNRELATED*: *Consultancy*: Imaging Endpoints Inc, *Comments*: clinical trial consulting, *Expert Testimony*: medicolegal, *Grants/Grants Pending*: GE.* Chadwick W. Christine—*UNRELATED*: *Consultancy*: Transcept Pharmaceuticals, *Comments*: consulting for new Parkinson disease drug development, *Grants/Grants Pending*: Kinemed Inc,* *Comments*: support of an ongoing biomarker study for Parkinson disease, *Other*: National Institutes of Health/National Institute of Neurological Disorders and Stroke,* *Comments*: support of ongoing clinical studies, in neuroprotection in Parkinson Disease. William P. Dillon—*UNRELATED*: *Expert Testimony*: medicolegal. Michael J. Aminoff—*UNRELATED*: *Grants/Grants Pending*: National Parkinson's Foundation,* National Institutes of Health,* Fox Foundation,* *Comments*: I direct the UCSF Parkinson's Disease Center, which is a National Parkinson Foundation Center of Excellence. I also have a grant through the Parkinson's Study Group and the National Institutes of Health to participate in a multicenter study of creatine in slowing the course of Parkinson disease. Finally, I have a grant funded by the Michael J. Fox Foundation to study CSF in Parkinson disease. None of this is related to the present work, *Royalties*: Elsevier, McGraw Hill, Oxford University Press, Wolters Kluwer Health, *Comments*: for books on neurology or biography. No relation whatsoever to the present work, *Payment for Development of Educational Presentations*: TEVA Corp, *Comments*: to help support an annual course on Parkinson disease for patients and caregivers. No relation to the present work. *Money paid to the institution.

REFERENCES

1. Feany MB, Dickson DW. **Widespread cytoskeletal pathology characterizes corticobasal degeneration.** *Am J Pathol* 1995;146:1388–96
2. Dickson DW. **Neuropathologic differentiation of progressive supranuclear palsy and corticobasal degeneration.** *J Neurol* 1999; 246 (suppl 2):II6–15
3. Dickson DW, Berferon C, Chin SS, et al. **Office of Rare Diseases neuropathologic criteria for corticobasal degeneration syndrome from progressive supranuclear palsy.** *J Neuropathol Exp Neurol* 2002;61:935–46
4. Litvan I, Grimes, DA, Lang AE, et al. **Clinical features differentiating patients with postmortem confirmed progressive supranuclear palsy and corticobasal degeneration.** *J Neurol* 1999;246(suppl 2):II1–5
5. Scaravilli T, Tolosa E, Ferrer I. **Progressive supranuclear palsy and corticobasal degeneration: lumping versus splitting.** *Mov Disord* 2005;20:S21–28
6. Ling H, O'Sullivan SS, Holton JL, et al. **Does corticobasal degeneration exist? A clinicopathological re-evaluation.** *Brain* 2010;133: 2045–57
7. Savoiardo M. **Differential diagnosis of Parkinson's disease and atypical parkinsonian disorders by magnetic resonance imaging.** *Neurol Sci* 2003;24(suppl 1):S35–37
8. Gröschel K, Hauser T-K, Luft A, et al. **Magnetic resonance imaging-based volumetry differentiates progressive supranuclear palsy from corticobasal degeneration.** *Neuroimage* 2004;21:714–24
9. Price S, Paviour D, Scahill R, et al. **Voxel-based morphometry detects patterns of atrophy that help differentiate progressive supranuclear palsy and Parkinson's disease.** *Neuroimage* 2004;23:663–69
10. Boxer AL, Geschwind MD, Belfor N, et al. **Patterns of brain atrophy that differentiate corticobasal degeneration syndrome from progressive supranuclear palsy.** *Arch Neurol* 2006;63:81–86
11. Josephs KA, Whitwell JL, Dickson DW, et al. **Voxel-based morphometry in autopsy proven PSP and CBD.** *Neurobiol Aging* 2008;29: 280–89
12. Whitwell JL, Jack CR, Boeve BF, et al. **Imaging correlates of pathology in corticobasal syndrome.** *Neurology* 2010;75:1879–87
13. Saini J, Bagepally BS, Sandya M, et al. **Subcortical structures in progressive supranuclear palsy: vertex-based analysis.** *Eur J Neurol* 2013;20:493–501
14. Blain CR, Barker GJ, Jarosz JM, et al. **Measuring brain stem and cerebellar damage in parkinsonian syndromes using diffusion tensor MRI.** *Neurology* 2006;67:2199–205
15. Nicoletti G, Tonon C, Lodi R, et al. **Apparent diffusion coefficient of the superior cerebellar peduncle differentiates progressive supranuclear palsy from Parkinson's disease.** *Mov Disord* 2008;23:2370–76
16. Rizzo G, Martinelli P, Manners D, et al. **Diffusion-weighted brain imaging study of patients with clinical diagnosis of corticobasal degeneration, progressive supranuclear palsy and Parkinson's disease.** *Brain* 2008;131:2690–700
17. Knake S, Belke N, Menzler K, et al. **In vivo demonstration of microstructural brain pathology in progressive supranuclear palsy: a DTI study using TBSS.** *Mov Disord* 2010;25:1232–38
18. Saini J, Bagepally BS, Sandhya M, et al. **In vivo evaluation of white matter pathology in patients of progressive supranuclear palsy using TBSS.** *Neuroradiology* 2012;54:771–80
19. Seppi K, Schocke MF, Esterhammer R, et al. **Diffusion-weighted imaging discriminates progressive supranuclear palsy from PD, but not from the Parkinson variant of multiple system atrophy.** *Neurology* 2003;60:922–27
20. Messina D, Cerasa A, Condino F, et al. **Patterns of brain atrophy in Parkinson's disease, progressive supranuclear palsy and multiple system atrophy.** *Parkinsonism Relat Disord* 2011;17:172–76
21. McKeown MJ, Uthama A, Abugharbieh R, et al. **Shape (but not volume) changes in the thalami in Parkinson disease.** *BMC Neurol* 2008;8:8
22. Erbetta A, Mandelli ML, Savoiardo, et al. **Diffusion tensor imaging shows different topographic involvement of the thalamus in progressive supranuclear palsy and corticobasal degeneration.** *AJNR Am J Neuroradiol* 2009;30: 1482–87
23. Litvan I, Agid Y, Calne D, et al. **Clinical research criteria for the diagnosis of progressive supranuclear palsy (Steele-Richardson-Olszewski syndrome): report of the NINDS-SPSP international workshop.** *Neurology* 1996;47:1–9
24. Gelb DJ, Oliver E, Gilman S. **Diagnostic criteria for Parkinson's disease.** *Arch Neurol* 1999;56:33–39
25. Riley DE, Lang AE. **Clinical diagnostic criteria.** *Adv Neurol* 2000;82:29–34
26. Jenkinson M, Beckmann CF, Behrens TE, et al. **FSL.** *Neuroimage* 2012;62:782–90
27. Patenaude B, Smith SM, Kennedy D, et al. **A Bayesian model of shape and appearance for subcortical brain.** *Neuroimage* 2011;56:907–22
28. Buckner RL, Head D, Parker J, et al. **A unified approach for morphometric and functional data analysis in young, old, and demented adults using automated atlas-based head size normalization: reliability and validation against manual measurement of total intracranial volume.** *Neuroimage* 2004;23:724–38
29. Kim SG, Chung MK, Schaefer SM, et al. **Sparse shape representation using the Laplace-Beltrami eigenfunctions and its application to**

modeling subcortical structures. *Proc Workshop Math Methods Biomed Image Analysis* 2012:25–32
30. Avants BB, Tustison NJ, Song G, et al. **A reproducible evaluation of ANTs similarity metric performance in brain image registration.** *Neuroimage* 2011;54:2033–44
31. Behrens TE, Johansen-Berg H, Woolrich MW, et al. **Non-invasive mapping of connections between human thalamus and cortex using diffusion imaging.** *Nat Neurosci* 2003;6:750–57
32. R Development Core Team. *R: A Language and Environment for Statistical Computing.* Vienna, Austria: R Foundation for Statistical Computing; 2005
33. Worsley KJ. A Matlab toolbox for the statistical analysis of univariate and multivariate surface and volumetric data using linear mixed effects models and random field theory. SurfStat. http://www.math.mcgill.ca/keith/surfstat. Accessed October 1, 2013
34. Halliday GM, Macdonald V, Henderson JM. **A comparison of degeneration in the motor thalamus and cortex between progressive supranuclear palsy and Parkinson's disease.** *Brain* 2005;128:2272–80
35. Schmahmann JD, Pandya DN. **Disconnection syndromes of the basal ganglia, thalamus and cerebrocerebellar systems.** *Cortex* 2008;44:1037–66
36. Whitwell JL, Avula R, Master A, et al. **Disrupted thalamocortical connectivity in PSP: a resting state fMRI, DTI, VBM study.** *Parkinsonism Relat Disord* 2011;17:599–605

The Thalamus: A Small but Precious Window on τ-Related Neurodegeneration?

Progressive supranuclear palsy (PSP) and corticobasal degeneration (CBD) are pathologically distinct causes of progressive atypical parkinsonism, poorly responsive or not responsive to levodopa.[1] Both diseases are characterized by hyperphosphorylated τ aggregates in the brain, accompanied by neuronal loss and gliosis in a characteristic distribution.[1] The large majority of patients with PSP present with Richardson syndrome, also known as PSP syndrome,[2] characterized by postural instability, leading to backward falls within the first year of symptom onset; axial rigidity; progressive vertical ophthalmoplegia; dementia; and personality changes. CBD pathology can cause multiple different neurologic syndromes, including corticobasal syndrome, PSP syndrome, frontotemporal dementia, or primary progressive aphasia. Corticobasal syndrome includes a mixed movement disorder (eg, levodopa-unresponsive rigidity associated with apraxia, dystonia, myoclonus, and alien limb) and impaired cognition.[3] An early and accurate diagnosis of tauopathies in vivo is becoming increasingly important with the advent of clinical trials of drugs aimed at modifying the underlying τ pathology. However, outside specialized centers and especially in the early stage of the diseases, differential diagnosis among atypical parkinsonian syndromes and with Parkinson disease (PD) is challenging because of the similarity of symptoms and lack of preclinical markers of the disease.

The thalamus is a major conduit for the bidirectional flow of neuronal signals between cortical and subcortical regions and links different cortical regions via transthalamic pathways. It comprises numerous nuclei, which receive a specific set of afferent connections and project primarily within the confines of specific cortical areas. Thalamic degeneration is known to occur in PSP and CBD, though the topographic distribution of thalamic lesions differs between the 2 pathologies.[4-6] A recent [^{18}F]2-(1-{6-[2-[fluorine-18]fluoroethyl)(methyl)amino]-2-naphthyl}-ethylidene)-malononitrile positron-emission tomography study showed the presence of τ fibrillar aggregates in the thalamus of patients with PSP syndrome.[7] Thalamic damage occurs also in patients with PD; however, it is less severe and is likely to occur later in the course of the disease compared with PSP and CBD.[5,8] Thus, measures of thalamic involvement may be useful in the differential diagnosis of these neurodegenerative conditions.

It is technically very difficult to assess accurately the thalamic subnuclei in vivo by using imaging technology. Previous studies of PD and atypical parkinsonisms demonstrated thalamic abnormalities by using region-of-interest or voxelwise approaches.[9-13] MR imaging–based analysis of the shape of the subcortical structures provides useful pieces of information about the location and pattern of structural abnormalities associated with these pathologic conditions. Using such an approach, several studies reported regional thalamic damage in patients with schizophrenia, obsessive-compulsive disorders, Alzheimer disease, and Tourette syndrome.[14-16] However, only a few MR imaging studies so far have used this approach in patients with parkinsonian syndromes and have focused their attention on the differences between disease groups and healthy controls, and not among different patient groups.[17,18]

Against this background, the preliminary study by Hess et al[19] published in the present issue of the *American Journal of Neuroradiology* has investigated thalamic degeneration in a small sample of patients with PSP syndrome, corticobasal syndrome, and PD by using an approach that combines shape analysis and diffusion tensor imaging. The aim of the study[19] was to evaluate whether the regional patterns of thalamic atrophy and microstructural damage differ in patients with atypical parkinsonian syndromes compared with those with idiopathic PD. By contrasting the volumes of the thalamus among different patient groups, the authors demonstrated that this structure undergoes more atrophy in patients with PSP syndrome and corticobasal syndrome than in those with PD. Shape analysis also provided insight into the topography of thalamic tissue loss, which was driven by a diminished size of the ventral anterior and ventral lateral portions of the structure. The DTI-based analysis showed that mean apparent diffusion coefficient values were higher in patients with PSP syndrome compared with those with PD and control groups, and shape analysis revealed that microstructural abnormalities were greater within the motor regions of the thalamus in both PSP syndrome and corticobasal syndrome groups relative to PD and controls.

Overall this article provides new evidence for thalamic damage occurring in atypical parkinsonisms, highlighting the preferential

involvement of lateral (motor) nuclei that are, instead, relatively spared in patients with PD. The selective involvement of thalamic motor nuclei and, as a consequence, of motor thalamocortical circuits in PSP syndrome and corticobasal syndrome may be interpreted as a regionally specific vulnerability to τ-related neurodegeneration. Therefore, in the near future, structural and diffusion tensor MR imaging is likely to provide useful markers to distinguish patients with atypical parkinsonisms not only from healthy individuals but also from patients with PD, which is the actual clinical dilemma.

The study by Hess et al[19] is hampered by a number of limitations, as acknowledged by the authors. The small number of subjects and the inclusion of cases not pathologically confirmed limit the generalizability of their findings and transferability to clinical practice. In addition, thalamic networks are involved in motor behavior, but they are also related to emotional, motivational, associative, and cognitive abilities. As a consequence, future studies should explore the relationship between regional thalamic damage and cognitive and behavioral findings in subjects with PSP syndrome and corticobasal syndrome.

Although the approach of this study requires further work to assess its consistency and reproducibility, the results reported by Hess et al[19] provide a solid justification to use a combination of shape analysis and structural and/or functional connectivity to study the pattern of thalamic degeneration in larger populations with pathologically proved PSP syndrome and corticobasal syndrome. Such studies could enable researchers to improve knowledge on these pathologic processes and overhaul the way we approach drug discovery for these devastating conditions.

REFERENCES

1. Dickson DW, Kouri N, Murray ME, et al. **Neuropathology of frontotemporal lobar degeneration-tau (FTLD-tau).** *J Mol Neurosci* 2011;45:384–89
2. Litvan I, Agid Y, Calne D, et al. **Clinical research criteria for the diagnosis of progressive supranuclear palsy (Steele-Richardson-Olszewski syndrome): report of the NINDS-SPSP international workshop.** *Neurology* 1996;47:1–9
3. Armstrong MJ, Litvan I, Lang AE, et al. **Criteria for the diagnosis of corticobasal degeneration.** *Neurology* 2013;80:496–503
4. Hattori M, Hashizume Y, Yoshida M, et al. **Distribution of astrocytic plaques in the corticobasal degeneration brain and comparison with tuft-shaped astrocytes in the progressive supranuclear palsy brain.** *Acta Neuropathol* 2003;106:143–49
5. Halliday GM, Macdonald V, Henderson JM. **A comparison of degeneration in motor thalamus and cortex between progressive supranuclear palsy and Parkinson's disease.** *Brain* 2005;128:2272–80
6. Ling H, O'Sullivan SS, Holton JL, et al. **Does corticobasal degeneration exist? A clinicopathological re-evaluation.** *Brain* 2010;133:2045–57
7. Kepe V, Bordelon Y, Boxer A, et al. **PET imaging of neuropathology in tauopathies: progressive supranuclear palsy.** *J Alzheimers Dis* 2013;36:145–53
8. Henderson JM, Carpenter K, Cartwright H, et al. **Loss of thalamic intralaminar nuclei in progressive supranuclear palsy and Parkinson's disease: clinical and therapeutic implications.** *Brain* 2000;123(pt 7):1410–21
9. Erbetta A, Mandelli ML, Savoiardo M, et al. **Diffusion tensor imaging shows different topographic involvement of the thalamus in progressive supranuclear palsy and corticobasal degeneration.** *AJNR Am J Neuroradiol* 2009;30:1482–87
10. Agosta F, Pievani M, Svetel M, et al. **Diffusion tensor MRI contributes to differentiate Richardson's syndrome from PSP-parkinsonism.** *Neurobiol Aging* 2012;33:2817–26
11. Boxer AL, Geschwind MD, Belfor N, et al. **Patterns of brain atrophy that differentiate corticobasal degeneration syndrome from progressive supranuclear palsy.** *Arch Neurol* 2006;63:81–86
12. Padovani A, Borroni B, Brambati SM, et al. **Diffusion tensor imaging and voxel based morphometry study in early progressive supranuclear palsy.** *J Neurol Neurosurg Psychiatry* 2006;77:457–63
13. Messina D, Cerasa A, Condino F, et al. **Patterns of brain atrophy in Parkinson's disease, progressive supranuclear palsy and multiple system atrophy.** *Parkinsonism Relat Disord* 2011;17:172–76
14. Kang DH, Kim SH, Kim CW, et al. **Thalamus surface shape deformity in obsessive-compulsive disorder and schizophrenia.** *Neuroreport* 2008;19:609–13
15. Zarei M, Patenaude B, Damoiseaux J, et al. **Combining shape and connectivity analysis: an MRI study of thalamic degeneration in Alzheimer's disease.** *Neuroimage* 2010;49:1–8
16. Wang L, Lee DY, Bailey E, et al. **Validity of large-deformation high dimensional brain mapping of the basal ganglia in adults with Tourette syndrome.** *Psychiatry Res* 2007;154:181–90
17. McKeown MJ, Uthama A, Abugharbieh R, et al. **Shape (but not volume) changes in the thalami in Parkinson disease.** *BMC Neurol* 2008;8:8
18. Saini J, Bagepally BS, Sandhya M, et al. **Subcortical structures in progressive supranuclear palsy: vertex-based analysis.** *Eur J Neurol* 2013;20:493–501
19. Hess CP, Christine CW, Apple AC, et al. **Changes in the thalamus in atypical parkinsonism detected using shape analysis and diffusion tensor imaging.** *AJNR Am J Neuroradiol* 2014;35:897–903

M. Filippi
F. Agosta
F. Caso
Neuroimaging Research Unit
Institute of Experimental Neurology
Division of Neuroscience
San Raffaele Scientific Institute
Vita-Salute San Raffaele University
Milan, Italy

http://dx.doi.org/10.3174/ajnr.A3930

Clinical Application of 3D Arterial Spin-Labeled Brain Perfusion Imaging for Alzheimer Disease: Comparison with Brain Perfusion SPECT

H. Takahashi, K. Ishii, C. Hosokawa, T. Hyodo, N. Kashiwagi, M. Matsuki, R. Ashikaga, and T. Murakami

ABSTRACT

BACKGROUND AND PURPOSE: Alzheimer disease is the most common neurodegenerative disorder with dementia, and a practical and economic biomarker for diagnosis of Alzheimer disease is needed. Three-dimensional arterial spin-labeling, with its high signal-to-noise ratio, enables measurement of cerebral blood flow precisely without any extrinsic tracers. We evaluated the performance of 3D arterial spin-labeling compared with SPECT, and demonstrated the 3D arterial spin-labeled imaging characteristics in the diagnosis of Alzheimer disease.

MATERIALS AND METHODS: This study included 68 patients with clinically suspected Alzheimer disease who underwent both 3D arterial spin-labeling and SPECT imaging. Two readers independently assessed both images. Kendall W coefficients of concordance (*K*) were computed, and receiver operating characteristic analyses were performed for each reader. The differences between the images in regional perfusion distribution were evaluated by means of statistical parametric mapping, and the incidence of hypoperfusion of the cerebral watershed area, referred to as "borderzone sign" in the 3D arterial spin-labeled images, was determined.

RESULTS: Readers showed $K = 0.82/0.73$ for SPECT/3D arterial spin-labeled imaging, and the respective areas under the receiver operating characteristic curve were 0.82/0.69 for reader 1 and 0.80/0.69 for reader 2. Statistical parametric mapping showed that the perisylvian and medial parieto-occipital perfusion in the arterial spin-labeled images was significantly higher than that in the SPECT images. Borderzone sign was observed on 3D arterial spin-labeling in 70% of patients misdiagnosed with Alzheimer disease.

CONCLUSIONS: The diagnostic performance of 3D arterial spin-labeling and SPECT for Alzheimer disease was almost equivalent. Three-dimensional arterial spin-labeled imaging was more influenced by hemodynamic factors than was SPECT imaging.

ABBREVIATIONS: AD = Alzheimer disease; ASL = arterial spin-labeling; ROC = receiver operating characteristic; HMPAO = hexamethylpropyleneamine oxime

Alzheimer disease (AD) is the most common neurodegenerative disorder with dementia and is becoming a social problem in most developed countries. A practical and economic biomarker for diagnosis of AD is needed. CBF is commonly accepted as a physiologic correlate of brain function.[1] AD is associated with regional decreases in CBF, so the ability of CBF to differentiate between individuals affected by AD and healthy individuals has been evaluated with the use of SPECT.[2]

Arterial spin-labeling (ASL) enables measurement of CBF without any extrinsic tracers by use of magnetically labeled arterial blood water as a diffusible tracer. ASL MR imaging has 2 major modalities: pulsed ASL[3] and continuous ASL.[4] The continuous ASL technique uses continuous adiabatic inversion, whereas pulsed ASL uses a single inversion pulse. The recently developed pulsed-continuous ASL imaging protocol based on 3D stack-of-spirals readouts[5] is an intermediate method between the conventional pulsed ASL and continuous ASL methods, in that pulsed-continuous offers a longer tag bolus than does pulsed ASL and a higher labeling efficiency than does the amplitude-modulated continuous ASL.[6,7] Each section acquired with 2D ASL experiences a slightly different inflow time; thus, it is difficult to estimate a precise transit time when multiple sections are acquired. The use of 3D acquisition techniques overcomes many of these limitations, allowing both whole-brain coverage and simultaneous acquisition to ensure a unified mean transit time. The SNR of 3D acquisitions can be greater than that of 2D multisection methods. Although ASL has inherently low SNR, mainly because of the relatively small amount of labeled spins in the tissue, pulsed-continuous can provide a better balance between labeling efficiency

Received July 8, 2013; accepted after revision September 10.

From the Department of Radiology, Kinki University Faculty of Medicine, Osaka-Sayama, Japan.

Please address correspondence to H. Takahashi, MD, Kinki University Faculty of Medicine 377-2 Ohno-Higashi, Osaka-Sayama, Japan; e-mail: hiroto.takahashi07@gmail.com

http://dx.doi.org/10.3174/ajnr.A3780

and SNR than conventional ASL methods. This can improve the accuracy of quantified CBF estimates. Many AD studies by use of ASL have been reported, which indicates that ASL MR imaging is an indispensable technique for studying AD.[8-12] CBF measured with ASL MR imaging can detect regional hypoperfusion in the AD precuneus and bilateral parietal cortex and discriminate individuals with AD from normal subjects. Recent research with the use of pulsed-continuous reported that 3D ASL can evaluate the severity of cognitive impairment as measured by the correlation of CBF with cognition.[13]

SPECT is now commonly used for CBF assessment in the diagnosis of AD, so we considered that it was important to evaluate the differences in CBF distribution in perfusion images obtained with both SPECT and ASL by use of similarly behaved diffusible tracers and to demonstrate the characteristics of ASL in comparison with SPECT. To the best of our knowledge, the evaluation of brain perfusion imaging by use of both ASL and SPECT in the same subjects with clinically suspected AD to discriminate the AD group from the non-AD group has not been reported. We used whole-brain 3D ASL MR imaging with pulsed-continuous labeling for CBF measurement in the diagnosis of AD because of its high SNR and the possibilities for improving image quality.

In this study, we evaluated the detectability of reduced regional cerebral perfusion in AD by use of 3D ASL compared with brain perfusion SPECT and demonstrated the characteristics of perfusion images obtained by means of 3D ASL.

MATERIALS AND METHODS

Our institutional review board approved this study. The requirement for participant informed consent was waived because of the retrospective nature of the study.

Patients

We retrospectively selected 68 consecutive patients with clinically suspected AD from the period between May 2011 and December 2012. Patients included 21 men and 47 women (age range: 53–93 years; mean, 77 years). All patients received the Japanese version of the Mini-Mental State Examination,[14] and their scores ranged from 6–29 points (mean, 21 points). MR examinations were performed as part of the patients' routine clinical care. All patients underwent brain perfusion imaging both with 3D ASL on a 1.5T clinical MR scanner and with technetium Tc99m-hexamethylpropylene amine oxime (HMPAO) SPECT within a 1-month period. Structural MR imaging was performed in addition to brain perfusion imaging to confirm that there was no other structural abnormality that could explain the patient's symptoms. Patients had no history of cerebrovascular disease, brain tumor, head trauma, or other causes of dementia. Thirty-six patients were diagnosed with AD and 32 patients were diagnosed as non-AD by experienced neurologists and psychiatrists, by use of the criteria of the National Institute of Neurologic and Communicative Disorders and Stroke in concert with the Alzheimer Disease and Related Disorders Association,[15] and the *Diagnostic and Statistical Manual of Mental Disorders,* 4th edition.[16] Four patients with mild cognitive impairment who later converted to AD were included in the AD group. Among patients diagnosed as non-AD, 5 patients had dementia with Lewy bodies, 3 patients had vascular dementia, and 24 were cognitively normal. The diagnosis of dementia with Lewy bodies was based on the criteria of the DLB Consortium.[17] Vascular dementia was diagnosed according to the criteria of the National Institute of Neurologic Disorders and Stroke–Association Internationale pour la Recherche et l'Enseignement en Neuroscience.[18] A summary of the demographic characteristics and neuropsychological test results for the patients is shown in Table 1.

Table 1: Demographic characteristics of the subjects

	Patients with AD	Patients with Non-AD
Numbers	36	32
Age, y	Mean, 78 (range: 55–93)	Mean, 72 (range: 53–92)
Sex: male:female	9:27	12:20
MMSE scores	Mean, 19 (range: 6–26)	Mean, 23 (range: 13–29)
Included patients	AD = 32; MCI due to AD = 4	DLB = 5; VaD = 3; CN = 24

Note:—MMSE indicates Mini-Mental State Examination; DLB, dementia with Lewy bodies; VaD, vascular dementia; CN, cognitively normal.

MR Imaging

All MR imaging was performed with a 1.5T unit (Signa; GE Healthcare, Milwaukee, Wisconsin) and an 8-channel head array receiving coil. Pulsed-continuous imaging (3D fast spin-echo acquisition with background suppression, a labeling period of 1450 ms, postlabeling delay of 1525 ms, echo time of 10.47 ms, repetition time of 4546 ms, spiral readout of 8 arms × 512 samples, 30 × 4.0-mm axial sections, 3.2 × 3.2-mm in-plane resolution, reconstructed pixel size of 1.7 × 1.7 mm, acquisition time of 4 minutes, 30 seconds) was performed with the labeling plane at the level of the foramen magnum. Labeled and reference images were then subtracted to obtain perfusion-weighted imaging data. In addition to ASL imaging, all patients underwent axial diffusion-weighted (repetition time of 6000 ms, echo time of 70 ms, b factor of 1000 ms/mm^2, 3 directions) and axial T2-weighted fast spin-echo (repetition time of 4717 ms, echo time of 85 ms) imaging to confirm that there was no other structural abnormality. All of these examinations were performed with a 5-mm section thickness, 1.5-mm skip, and 24-cm field of view. In addition, high-resolution 3D T1-weighted whole-brain images (repetition time of 8.3 ms, echo time of 3.8 ms, inversion time of 240 ms, 8° flip angle, matrix of 256 × 256, 176 sections, voxel size of 1.0 × 0.9 × 0.9 mm, imaging time of 4 minutes, 50 seconds) were obtained by use of the magnetization-prepared rapid acquistion of gradient echo (spoiled gradient-echo) sequence for anatomic information. The images were obtained in sagittal planes and were reconstructed into 1-mm-thick consecutive transverse images.

SPECT

Patients were directed to lie down for 20 minutes in the supine position with their eyes closed in a dim, quiet room. SPECT was performed by use of a double-head gamma camera (Forte; ADAC Laboratories, Milpitas, California) equipped with a Vertex general purpose collimator (VXGP; ADAC Laboratories) and converging collimators with a focal length of 65 cm. The acquisition began 7 minutes after the injection of 740 MBq of HMPAO, and projection data were obtained at 25 seconds/step × 32 views, resulting in a total acquisition time of approximately 20 minutes. A Butterworth filter (cutoff: 0.25, order: 8) was used for filtered back-projection reconstruction of the SPECT image, yielding a

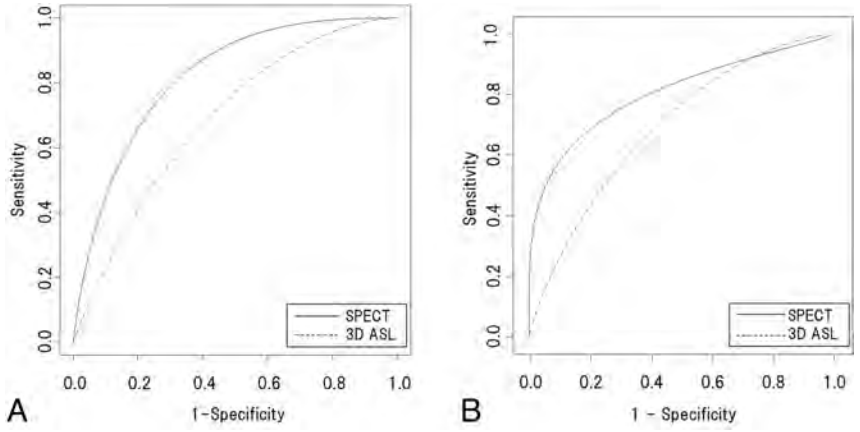

FIG 1. *A*, Average ROC curves for SPECT and 3D ASL for reader 1. *B*, Average ROC curves for SPECT and 3D ASL for reader 2. Smoothed curves were adjusted by calculation with a bootstrap test. Area under the ROC curve of 3D ASL was not significantly different ($P > .05$) from that of SPECT.

reconstructed pixel size of 2.5 mm within the transverse plane and a section thickness of 3.6 mm; attenuation correction was performed by use of the Chang method (JETStream Workspace 3.0. Philips Healthcare, Best, The Netherlands). No scatter compensation was available on the SPECT system.

Image Analysis

The ASL and SPECT data were evaluated with visual inspection and 3D stereotactic surface projection *z* score maps. The normal control data base for 3D stereotactic surface projection of ASL perfusion images was constructed with the newly prepared ASL images of 30 cognitively normal subjects: 11 men and 19 women (age range: 64–84 years; mean age, 73 years) who underwent brain MR imaging because of indefinite complaints and who had no structural abnormalities such as cerebrovascular disease, brain tumor, head trauma, or neurodegenerative disorder. The preset normal data base for HMPAO SPECT in the iSSP program (Nihon Medi-Physics, Tokyo, Japan) was used for this study. Two readers (C.H., K.I.) other than the study coordinator independently reviewed the SPECT images and 3D ASL images. These 2 readers were radiologists with 22 and 25 years of experience in nuclear medicine and were blinded to the results of the examination for AD. In both SPECT images and 3D ASL images, they assessed focal hypoperfusion in areas over the bilateral precunei and posterior cingulate gyri. They recorded their confidence levels regarding the presence of focal hypoperfusion as an indicator of AD by use of the following 5-point rating system: 1, definitely absent; 2, probably absent; 3, presence equivocal; 4, probably present; 5, definitely present. Kendall W coefficients of concordance (K) were computed to compare the assessment of the level of confidence of the 2 readers. Kendall W coefficients (K) of 0.5–0.8 were considered to indicate good agreement, and coefficients higher than 0.8 were considered to indicate excellent agreement. A value of $P < .05$ was considered to indicate a significant difference. Receiver operating characteristic (ROC) analysis to compare the diagnostic performance was performed with the aid of R software (Version 2.12.1; http://www.r-project.org/).[19] The area under the ROC curve was calculated to compare the diagnostic performance for both the 3D ASL images and SPECT images for each of the 2 readers. A confidence level of 4 or 5 was considered a positive finding for the calculation of sensitivity and specificity of AD diagnosis, but the readers were not informed of this. The area under the ROC curve, sensitivity, and specificity were statistically compared between the readers by use of the bootstrap test for 2 correlated ROC curves. In addition, a paired *t* test was performed to evaluate the differences in regional perfusion distribution between the 2 imaging methods, by use of voxel-based analysis with statistical parametric mapping. Both 3D ASL and SPECT image preprocessing were implemented by use of SPM 8 software (Wellcome Department of Imaging Neuroscience, London, United Kingdom) and code written in Matlab (MathWorks, Natick, Massachusetts). For each subject, images were preprocessed as follows: 1) individual 3D ASL images were coregistered with individual SPECT images; 2) the SPECT images were spatially normalized to the Montreal Neurological Institute space by the SPM program; 3) the 3D ASL images were then spatially normalized to the Montreal Neurological Institute space by using the individual parameter obtained from SPECT normalization; 4) the spatially normalized images were smoothed by use of an isotropic Gaussian kernel with a 12-mm full width for 3D ASL and 8 mm for SPECT images at half maximum to reduce the noise and residual anatomic differences among the brains and to match the spatial resolution of 3D ASL and SPECT images; and 5) a paired *t* test was performed by using both preprocessed 3D ASL and SPECT images. To control for family-wise errors resulting from multiple comparisons, the initial significance threshold was set at $P < .001$.

In a recent report, hypoperfusion of the watershed area on 3D ASL imaging in many healthy subjects was referred to as the "borderzone sign."[20] We considered that this sign might have an effect on the performance of AD diagnosis; therefore we evaluated the frequency of this sign in the diagnostic discrepancy group. The patients with a discrepancy between clinical diagnosis and 3D ASL results and with a diagnostic discrepancy for reader 1 by use of SPECT–3D ASL were assessed. The borderzone sign was evaluated on the simple criterion that the signal defect of the watershed area in the 3D ASL images was positive by consensus between the 2 readers (C.H., K.I.).

RESULTS

The 2 readers showed excellent agreement for the diagnosis of AD on the SPECT images ($K = 0.82$, $P = .00087$) and good agreement for that on the 3D ASL images ($K = 0.73$, $P = .0083$). The ROC curves for 3D ASL and SPECT images obtained by each reader are shown in Fig 1*A*, -*B*. For reader 1, the area under the ROC curve distinguishing AD from non-AD was 0.82 for SPECT images alone and 0.69 for 3D ASL images alone. A bootstrap test for the 2 correlated ROC curves showed that there was no significant difference ($P = .08$) between the 2 images. For reader 2, the area under the ROC curve distinguishing

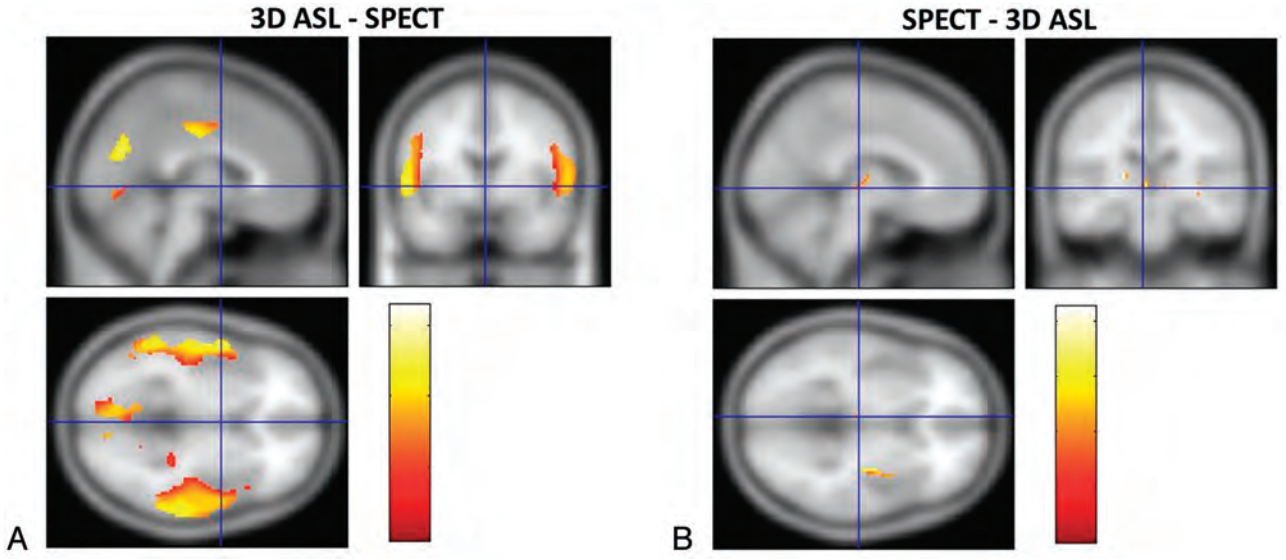

FIG 2. SPM analysis revealed that the perfusion images of 3D ASL were delineated by areas of higher CBF (red-to-yellow areas) in the middle cerebral artery region and in the posterior cerebral artery region than those observed on SPECT images (*A*), whereas small areas of higher CBF (red-to-yellow areas) were scattered in the SPECT perfusion images compared with those on 3D ASL (*B*).

Table 2: Clinical diagnosis and 3D ASL diagnosis

	3D ASL	
	Correct	Incorrect
Patients with AD, $n = 36$	17	19
Borderzone sign (+: −)	(6: 11)	(6: 13)
Patients with non-AD, $n = 32$	22	10
Borderzone sign (+: −)	(5: 17)	(7: 3)

Table 3: Clinical diagnosis, SPECT diagnosis, and 3D ASL diagnosis

	SPECT/3D ASL	SPECT/3D ASL
	Correct/Incorrect	Incorrect/Correct
Patients with AD, $n = 19$	14	5
Borderzone sign (+: −)	(4: 10)	(2: 3)
Patients with non-AD, $n = 9$	5	4
Borderzone sign (+: −)	(4: 1)	(0: 4)

AD from non-AD was 0.80 for SPECT images alone and 0.69 for 3D ASL images alone. A bootstrap test for the 2 correlated ROC curves showed that there was no significant difference ($P = .20$) between the 2 images.

SPM analysis showed that in the 3D ASL image, the perisylvian and medial parieto-occipital perfusion was significantly higher than in the SPECT image ($P < .001$) (Fig 2*A*). In contrast, the area of hypoperfusion was barely detected in the 3D ASL image in comparison with the SPECT image ($P < .001$) (Fig 2*B*).

The results for the frequency of the borderzone sign and the discrepancy between clinical diagnosis and 3D ASL diagnosis are described in Table 2. The borderzone sign was observed in 6 of 17 patients (35%) with AD correctly diagnosed by 3D ASL and in 7 of 10 patients (70%) with non-AD incorrectly diagnosed by 3D ASL. The results for the frequency of the borderzone sign and the diagnostic discrepancy between SPECT and 3D ASL are described in Table 3. Diagnostic discrepancy between SPECT and 3D ASL was observed for 28 of 68 patients (41%). In the 9 patients without AD, 1 patient had dementia with Lewy bodies, 1 patient had vascular dementia, and 7 were cognitively normal. More detailed analysis of these results was not performed because the small number of patients precluded statistical analysis. In the patients with SPECT–3D ASL diagnostic discrepancy, the borderzone sign was observed in 2 of 5 patients (40%) with AD correctly diagnosed by 3D ASL and in 4 of 5 patients (80%) with non-AD incorrectly diagnosed by 3D ASL. Representative images of the borderzone sign in patients with diagnostic discrepancy are shown in Fig 3.

DISCUSSION

CBF assessment by SPECT is established as an indispensable clinical tool in the diagnosis of AD.[21,22] HMPAO SPECT and FDG-PET showed hypoperfusion and decreased metabolism in the temporoparietal and posterior cingulate gyrus in AD, which indicates a direct coupling in AD between these 2 effects.[23] In addition, a recent study to compare 3D ASL MR imaging with FDG-PET in the same subjects showed similar degrees of functional deficits in the affected areas,[24] which indicates that 3D ASL MR imaging may be a more easily accessible alternative perfusion technique than SPECT in the diagnosis of AD.

Voxelwise comparison of the ASL images can be useful to help discriminate patients with AD from healthy subjects.[12] A more recent study indicated that CBF maps obtained with 3D ASL can be a marker for disease severity ranging from mild cognitive impairment to advanced AD.[13] Although many recent ASL perfusion studies were performed on 3T MR imaging, it has been shown in other studies that ASL with 1.5T MR imaging could detect regional hypoperfusion, mainly in the temporoparietal association cortex and the posterior cingulate gyrus.[8,10,25] Another study suggested that CBF mapping by ASL may perform better than MR morphologic analysis by using voxel-based morphometry in discriminating patients with AD from healthy control subjects and that the combination of the 2 methods was more effective than either method alone.[26] This result may support our proposal for the combination of structural MR imaging and ASL MR perfusion imaging. Three-dimensional ASL acquisition in our study required 4.5 minutes, which is short enough to be included in a clinical protocol.

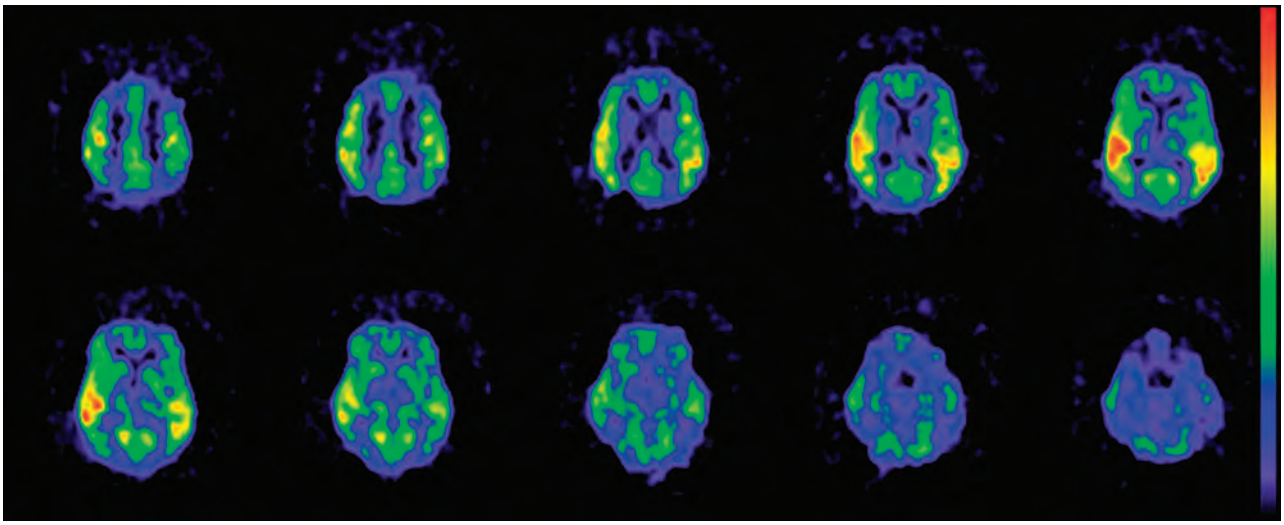

FIG 3. Three-dimensional ASL images frequently show the borderzone sign (watershed area), which indicates bilateral signal deficiency in the middle cerebral artery–anterior cerebral artery and middle cerebral artery–posterior cerebral artery borderzones, with a high signal intensity in the surrounding cortex.

In our study, interobserver agreement for both SPECT and 3D ASL revealed a statistically significant difference (SPECT: $K = 0.82$, $P = .00087$; and 3D ASL: $K = 0.73$, $P = .0083$), which may indicate that there were differences between the 2 readers in the accuracy of AD diagnosis. However, interobserver agreement was excellent for the SPECT images and good for the ASL images. In addition, the result of each reader's ROC analysis showed no significant difference between the image types, so we concluded that the diagnostic performance of 3D ASL on a 1.5T MR scanner is slightly but not significantly inferior to that of SPECT in the differential diagnosis of AD and non-AD.

Our results identified regional variability in the reliability of perfusion assessment by ASL. SPM analysis of 3D ASL and SPECT revealed some regional differences in perfusion distribution. In most of the participants, the distribution of perfusion was almost symmetric in the 2 hemispheres. Three-dimensional ASL perfusion images showed higher signal intensities than SPECT images in the MCA region and in the posterior cerebral artery region. We consider that this was because the MCA and posterior cerebral artery have high flow rates and because perfusion images of 3D ASL are influenced more than SPECT by hemodynamics, so the 3D ASL images can identify hypoperfusion of the watershed area. This is associated with aging and is related to a combination of increased arterial transit time and reduced CBF. Diagnostic discrepancies between 3D ASL and SPECT images were observed for 28 patients. We suggest that the misdiagnosis of cases of non-AD as AD by 3D ASL may result from this effect and that the borderzone sign has major effects on AD diagnosis as a false-positive finding because of its high incidence (70% and 80%) in these cases (Tables 2 and 3). Zaharchuk et al[20] reported that about half of the patients with normal imaging findings on bolus perfusion-weighted imaging performed by use of gadolinium enhancement had abnormal ASL findings, most commonly the borderzone sign. The patients included in that study were also older (mean age, 71 ± 11 years). These findings suggest that perfusion imaging with 3D ASL is influenced more than SPECT by hemodynamic factors such as arterial transit time, especially in older people. We used a postlabeling delay of 1525 ms, which in previous reports has been suggested to be too short for quantitative CBF measurements in older patients, in whom arterial transit time could potentially be longer.[27] Our patients with suspected AD were all older (mean, 77 ± 8 years). The reason for the use of a postlabeling delay of 1525 ms is that a longer postlabeling delay causes a decrease in SNR because of T1 relaxation, so there is a trade-off between a longer postlabeling delay and decreased SNR.

SPM analysis revealed the same perfusion of the frontal brain regions on 3D ASL images as on SPECT images, so we believe that the effect of the difference of perfusion distribution between 3D ASL images and SPECT images is of minor importance in evaluation of the function of frontal brain regions (eg, the diagnosis of frontotemporal lobar degeneration). We judged that the result shown in Fig 2*B* of hypoperfusion on 3D ASL was within the limits of statistical error, because hypoperfusion on the 3D ASL image was visible as small scattered areas and its distribution was not related to cerebral hemodynamics.

Given these limitations, this study can be regarded as a pilot investigation to identify the most suitable ASL images for evaluating CBF distribution, which must be more rigorously examined in future studies. There are 2 factors important in obtaining an accurate CBF map: arterial arrival time and postlabeling delay. In addition, our results indicate that a high magnetic field will be valuable because of its high label efficiency and slower label decay.

CONCLUSIONS

Perfusion imaging with 3D ASL was influenced to a greater extent than SPECT by hemodynamic factors such as arterial transit time. Statistical analysis revealed that 3D ASL MR imaging can be an alternative perfusion imaging method to SPECT in the diagnosis of AD and indicates that 3D ASL is an appropriate method for diagnosing AD and will allow a "one-stop shop" MR routine examination.

REFERENCES

1. Villringer A, Dirnagl U. **Coupling of brain activity and cerebral blood flow: basis of functional neuroimaging.** *Cerebrovasc Brain Metab Rev* 1995;7:240–76
2. Soininen H, Helkala EL, Kuikka J, et al. **Regional cerebral blood flow measured by 99mTc-HMPAO SPECT differs in subgroups of Alzheimer's disease.** *J Neural Transm Park Dis Dement Sect* 1995; 9:95–109
3. Golay X, Stuber M, Pruessmann KP, et al. **Transfer insensitive labeling technique (TILT): application to multislice functional perfusion imaging.** *J Magn Reson Imaging* 1999;9:454–61
4. Alsop DC, Detre JA. **Multisection cerebral blood flow MR imaging with continuous arterial spin labeling.** *Radiology* 1998;208:410–16
5. Dai W, Garcia D, de Bazelaire C, et al. **Continuous flow-driven inversion for arterial spin labeling using pulsed radio frequency and gradient fields.** *Magn Reson Med* 2008;60:1488–97
6. Wang J, Zhang Y, Wolf RL, et al. **Amplitude-modulated continuous arterial spin-labeling 3.0-T perfusion MR imaging with a single coil: feasibility study.** *Radiology* 2005;235:218–28
7. Wu WC, Fernández-Seara M, Detre JA, et al. **A theoretical and experimental investigation of the tagging efficiency of pulsed-continuous arterial spin labeling.** *Magn Reson Med* 2007;58:1020–27
8. Alsop DC, Detre JA, Grossman M. **Assessment of cerebral blood flow in Alzheimer's disease by spin-labeled magnetic resonance imaging.** *Ann Neurol* 2000;47:93–100
9. Du AT, Jahng GH, Hayasaka S, et al. **Hypoperfusion in frontotemporal dementia and Alzheimer disease by arterial spin labeling MRI.** *Neurology* 2006;67:1215–20
10. Johnson NA, Jahng GH, Weiner MW, et al. **Pattern of cerebral hypoperfusion in Alzheimer disease and mild cognitive impairment measured with arterial spin-labeling MR imaging: initial experience.** *Radiology* 2005;234:851–59
11. Sandson TA, O'Connor M, Sperling RA, et al. **Noninvasive perfusion MRI in Alzheimer's disease: a preliminary report.** *Neurology* 1996;47:1339–42
12. Yoshiura T, Hiwatashi A, Noguchi T, et al. **Arterial spin labelling at 3-T MR imaging for detection of individuals with Alzheimer's disease.** *Eur Radiol* 2009;19:2819–25
13. Binnewijzend MA, Kuijer JP, Benedictus MR, et al. **Cerebral blood flow measured with 3D pulsed-continuous arterial spin-labeling MR imaging in Alzheimer disease and mild cognitive impairment: a marker for disease severity.** *Radiology* 2013;267:221–30
14. Ideno Y, Takayama M, Hayashi K, et al. **Evaluation of a Japanese version of the Mini-Mental State Examination in elderly persons.** *Geriatr Gerontol Int* 2012;12:310–16
15. McKhann G, Drachman D, Folstein M, et al. **Clinical diagnosis of Alzheimer's disease: report of the NINCDS-ADRDA Work Group under the auspices of Department of Health and Human Services Task Force on Alzheimer's Disease.** *Neurology* 1984;34:939–44
16. American Psychiatric Association. *Diagnostic and Statistical Manual of Mental Disorders: DSM-IV*. 4th ed. Washington: American Psychiatric Association; 1994
17. McKeith IG, Dickson DW, Lowe J, et al. **Diagnosis and management of dementia with Lewy bodies: third report of the DLB Consortium.** *Neurology* 2005;65:1863–72
18. Román GC, Tatemichi TK, Erkinjuntti T, et al. **Vascular dementia: diagnostic criteria for research studies: Report of the NINDS-AIREN International Workshop.** *Neurology* 1993;43:250–60
19. R Development Core Team. **R: A language and environment for statistical computing.** Vienna, Austria: R Foundation for Statistical Computing; 2010
20. Zaharchuk G, Bammer R, Straka M, et al. **Arterial spin-label imaging in patients with normal bolus perfusion-weighted MR imaging findings: pilot identification of the borderzone sign.** *Radiology* 2009;252:797–807
21. Johnson KA, Jones K, Holman BL, et al. **Preclinical prediction of Alzheimer's disease using SPECT.** *Neurology* 1998;50:1563–71
22. El Fakhri G, Kijewski MF, Albert MS, et al. **Quantitative SPECT leads to improved performance in discrimination tasks related to prodromal Alzheimer's disease.** *J Nucl Med* 2004;45:2026–31
23. Herholz K, Schopphoff H, Schmidt M, et al. **Direct comparison of spatially normalized PET and SPECT scans in Alzheimer's disease.** *J Nucl Med* 2002;43:21–26
24. Chen Y, Wolk DA, Reddin JS, et al. **Voxel-level comparison of arterial spin-labeled perfusion MRI and FDG-PET in Alzheimer disease.** *Neurology* 2011;77:1977–85
25. Asllani I, Habeck C, Scarmeas N, et al. **Multivariate and univariate analysis of continuous arterial spin labeling perfusion MRI in Alzheimer's disease.** *J Cereb Blood Flow Metab* 2008;28:725–36
26. Dashjamts T, Yoshiura T, Hiwatashi A, et al. **Simultaneous arterial spin labeling cerebral blood flow and morphological assessments for detection of Alzheimer's disease.** *Acad Radiol* 2011;18:1492–99
27. Campbell AM, Beaulieu C. **Pulsed arterial spin labeling parameter optimization for an elderly population.** *J Magn Reson Imaging* 2006; 23:398–403

Subcortical Deep Gray Matter Pathology in Patients with Multiple Sclerosis Is Associated with White Matter Lesion Burden and Atrophy but Not with Cortical Atrophy: A Diffusion Tensor MRI Study

R. Cappellani, N. Bergsland, B. Weinstock-Guttman, C. Kennedy, E. Carl, D.P. Ramasamy, J. Hagemeier, M.G. Dwyer, F. Patti, and R. Zivadinov

ABSTRACT

BACKGROUND AND PURPOSE: The association between subcortical deep gray matter, white matter, and cortical pathology is not well understood in MS. The aim of this study was to use DTI to investigate the subcortical deep gray matter alterations and their relationship with lesion burden, white matter, and cortical atrophy in patients with MS and healthy control patients.

MATERIALS AND METHODS: A total of 210 patients with relapsing-remitting MS, 75 patients with progressive MS, and 110 healthy control patients were included in the study. DTI metrics in whole brain, normal-appearing white matter, normal-appearing gray matter, and subcortical deep gray matter structures were compared. The association between DTI metrics of the subcortical deep gray matter structures with lesion burden, normalized white matter volume, and normalized cortical volume was investigated.

RESULTS: DTI measures were significantly different in whole brain, normal-appearing white matter, and normal-appearing gray matter among the groups ($P < .01$). Significant differences in DTI diffusivity of total subcortical deep gray matter, caudate, thalamus, and hippocampus ($P < .001$) were found. DTI diffusivity of total subcortical deep gray matter was significantly associated with normalized white matter volume ($P < .001$) and normalized cortical volume ($P = .033$) in healthy control patients. In both relapsing and progressive MS groups, the DTI subcortical deep gray matter measures were associated with the lesion burden and with normalized white matter volume ($P < .001$), but not with normalized cortical volume.

CONCLUSIONS: These findings suggest that subcortical deep gray matter abnormalities are associated with white matter lesion burden and atrophy, whereas cortical atrophy is not associated with microstructural alterations of subcortical deep gray matter structures in patients with MS.

ABBREVIATIONS: AD = axial diffusivity; FA = fractional anisotropy; HC = healthy control; MD = mean diffusivity; PMS = progressive MS; RD = radial diffusivity; RRMS = relapsing-remitting MS; SDGM = subcortical deep gray matter

Although in the past MS has been considered an inflammatory demyelinating disease affecting primarily the white matter of the central nervous system, currently, a substantial number of studies have established that gray matter is also involved in different stages of the disease.[1-5] Cortical and subcortical deep gray matter (SDGM) atrophy occurs also in the early stages of MS, and disability progression is significantly influenced by the neuronal loss of the gray matter.[6-8]

Atrophy of the SDGM structures is associated with disability progression and cognitive dysfunctions and can also predict the conversion to clinically definite MS.[9-12] An increasing body of evidence suggests that the atrophy of cortical and SDGM structures is associated with white matter lesion burden,[13] but the underlying pathophysiologic processes remain poorly understood. Secondary Wallerian degeneration is certainly implicated in neuronal damage of gray matter structures; however, it seems unlikely to be the sole cause of gray matter pathology.[4,14]

DTI is an advanced MR imaging technique that has been used in a number of in vivo and ex vivo studies.[15,16] DTI measures are

Received July 26, 2013; accepted after revision September 18.

From the Buffalo Neuroimaging Analysis Center (R.C., N.B., C.K., E.C., D.P.R., J.H., M.G.D., R.Z.), and Jacobs Neurological Institute, Department of Neurology (B.W.-G., R.Z.), State University of New York, Buffalo, New York; and Department GF Ingrassia, Section of Neurosciences (R.C., F.P.), University of Catania, Catania, Italy.

Please address correspondence to Robert Zivadinov, MD, PhD, FAAN, Department of Neurology, School of Medicine and Biomedical Sciences, The Jacobs Neurological Institute, 100 High St, Buffalo, NY 14203; e-mail: rzivadinov@bnac.net

Indicates open access to non-subscribers at www.ajnr.org

Indicates article with supplemental on-line tables.

http://dx.doi.org/10.3174/ajnr.A3788

able to identify alterations outside the focal lesions in the so-called normal-appearing white matter and normal-appearing gray matter that remain largely undetected with conventional MR imaging in patients with MS.[17]

There is a growing interest in studying the DTI alterations of the SDGM in the different stages of the MS disease process. Previous studies suggested that SDGM DTI abnormalities are also present in patients with clinically isolated syndrome[18,19] and are associated with disability progression as well as cognitive dysfunctions in patients with MS.[20-23]

Although different studies have investigated the associations between white matter lesions, brain atrophy, and DTI alteration in patients with MS,[24-26] the same relationships were not extensively investigated in healthy people whose pathophysiologic alteration of the brain cannot be attributable to the inflammatory process in the central nervous system. Therefore, in the current study, we aimed to investigate volumetric and DTI global, tissue-specific, and regional brain differences in a large cohort of healthy control (HC) patients, patients with relapsing-remitting MS (RRMS), and patients with progressive MS (PMS). We hypothesized that microstructural abnormalities of SDGM structures detected by DTI techniques are associated with lesion burden, and with white matter and gray matter volume alterations in patients with MS. Another aim was to explore the same associations in the HC group.

MATERIALS AND METHODS

Patients

A total of 285 patients with MS according to the McDonald criteria[27] and 110 HC patients were recruited and underwent scanning by use of the same MR imaging protocol. They were classified as having RRMS, secondary-progressive MS, and primary-progressive MS. Participants were excluded if they had contraindications to MR imaging, had any pre-existing medical conditions known to be associated with brain pathology, had relapse (patients with MS), or were treated with steroids within the month preceding study entry. All patients underwent neurologic examination, and an Expanded Disability Status Scale assessment was obtained by an examiner blinded to their MR imaging characteristics. All HC patients also underwent both neurologic and clinical examinations. Moreover, we collected previous medical history, demographic, and physical data to evaluate the vascular risk factors. The internal Institutional Review Board approved the study protocol, and written informed consent was obtained from all participants.

MR Imaging Acquisition

All patients were examined on a 3T Signa Excite HD 12.0 Twin Speed 8-channel scanner (GE Healthcare, Milwaukee, Wisconsin) by use of an 8-channel head and neck coil. MR imaging sequences included multiplanar dual FSE proton attenuation and T2WI, FLAIR, 3D T1WI by use of a fast-spoiled gradient echo with magnetization-prepared inversion recovery pulse and spin-echo T1WI both with and without a single dose of an intravenous bolus of 0.1 mMol/kg of gadolinium with diethylene triamine pentaacetic acid. Pulse sequence characteristics for 3T MR imaging were as follows: All scans were acquired with a 256 × 256 matrix and a 25.6-cm FOV for an in-plane resolution of 1 × 1 mm^2 with a phase FOV of 75% and 1 average. Sequence specific parameters were as follows: for the proton attenuation/T2: 3-mm-thick sections with no gap; TE1, 12 ms; TE2, 95 ms; TR, 3000 ms; echo-train length, 14; flip angle, 90°; for the FLAIR scans: 3-mm thick sections with no gap; TE, 120 ms; TI, 2100 ms; TR, 8500 ms; flip angle, 90°; for 3D T1WI: 1-mm thick sections with no gap; TE, 2.8 ms; TI, 900 ms; TR, 5.9 ms; flip angle, 10°; and for spin-echo T1WI: 3-mm-thick sections with no gap; TE, 16 ms; TR, 600 ms; flip angle, 90°.

An echo-planar DTI sequence was acquired as part of the MR imaging protocol. The sequence was acquired with 3-mm-thick sections with no gap, a 96 × 96 matrix, a 32-cm FOV, and a 75% phase FOV, resulting in a voxel size of 3.33 mm × 3.33 mm × 3.00 mm. The sequence used a TE of 81.8 ms, TR of 8200 ms, 1 average, and an array spatial sensitivity encoding technique (parallel imaging) factor of 2. DTI parameters were 15 noncollinear directions with a b-value of 800 s/mm^2.

MR Imaging Analysis

Initial DTI processing was performed by use of the FMRIB Diffusion Toolbox (FSL; http://www.fmrib.ox.ac.uk/fsl).[28,29] In brief, raw diffusion tensor images were eddy corrected to minimize gradient-related geometric distortions. Then, "dtifit" was used to fit a tensor model at each voxel, and scalar maps of fractional anisotropy (FA), mean diffusivity (MD), radial diffusivity (RD), and axial diffusivity (AD) were created. Subsequently, these maps were coregistered and resampled into the high-resolution 3D T1WI space by use of the B0 image as a reference. In this space, tissue segmentation and parcellation data were overlaid, and summary measures for each DTI metric were calculated on a region-by-region basis. The FSL registration tool FLIRT (http://www.fmrib.ox.ac.uk/) was used with nearest-neighbor interpolation to bring the FIRST (version 1.2; http://fsl.fmrib.ox.ac.uk/fsl/fslwiki/FIRST) masks and DWI data into a common space.

The SIENAX Cross-Sectional Software Tool (version 2.6; http://fsl.fmrib.ox.ac.uk/fsl/fslwiki/SIENA) was used to estimate normalized gray matter volume, normalized white matter volume, normalized brain parenchymal volume, normalized lateral ventricular volume, and normalized cortical volume. Before segmentation, the 3D T1WI was modified by use of an in-house developed inpainting tool to avoid the impact of T1 hypointensities.[2] To segment SDGM structures, the FIRST tool on 3D T1WI was used. Specifically, the thalamus, caudate, putamen, globus pallidus, hippocampus, amygdala, and accumbens nucleus were identified in this way.

T2-weighted hyperintense and T1-weighted hypointense precontrast and postcontrast lesion volume were assessed by use of a semiautomated edge detection contouring/thresholding technique.[2] T2 lesions were delineated on FLAIR images and were confirmed on proton attenuation and T2 images. T1-hypointense lesions were delineated on T1-spin-echo images, and T1-Gd lesions were delineated on postcontrast T1-spin-echo images.

Statistical Analysis

Analyses were conducted by PASW Statistics, version 18.0 (IBM, Armonk, New York). Distributions of volume and DTI data were

Table 1: Demographic, clinical, and conventional MRI characteristics of healthy control patients and patients with MS

	HC (n = 110)	MS (n = 285)		RRMS (n = 210)	PMS (n = 75)	P Value
Age (y), mean (SD) median	47.0 (12.9) 50	46.9 (8.2) 48	0.965	46.1 (8.5) 46	49.2 (6.5) 50	.006*
Sex, female, n (%)	76 (69.1)	206 (72.3)	0.329	149 (70.9)	57 (78)	.496
Disease duration (y), mean (SD) median	NA	14.4 (9.1) 13		13.2 (8.8) 12	17.9 (9.2) 18	<.001*
EDSS, mean (SD) median	NA	3.4 (1.9) 3.0		2.6 (1.5) 2.5	5.4 (1.5) 6.0	<.001*
T2-LV, mean (SD) median	0.3 (1.2) 0	13.5 (16.1) 7.3	<.001*	11.0 (13.5) 6.7	20.4 (20.4) 13.2	.001*
T1-LV, mean (SD) median	0	3.3 (6.5) 1.0	NA	2.7 (6.1) 0.8	5.1 (7.2) 1.7	.037*
T1-Gd-LV mean (SD) median	NA	0.05 (0.02) 0	NA	0.06 (0.4) 0	0.01 (0.02) 0	.046*

Note:—EDSS indicates Expanded Disability Status Scale; LV, lesion volume; NA, not available; SD, standard deviation.
Statistical analysis among groups was performed with the Student t test, test, the Mann-Whitney U test and the χ^2 test. All P values were corrected for multiple comparisons with use of Benjamini-Hochberg correction.
The volumes are expressed in milliliters.
* indicates significant P values ($P < .05$) after correction.

Table 2: Structural brain volume measures in patients with MS and healthy control patients

	HC (n = 110)	MS (n = 285)	P Value
Global and tissue-specific brain structures			
NGMV, mean (SD) median	762.4 (53.0) 759.8	726.4 (66.0) 729	<.001*
NWMV, mean (SD) median	757.1 (41.2) 757.6	749.2 (73.1) 740.1	.054
NBPV, mean (SD) median	1519.5 (82.7) 1515.6	1475.7 (93.5) 1474.4	<.001*
NLVV, mean (SD) median	33.0 (12.6) 28.8	49.4 (22.4) 43.9	<.001*
NCV, mean (SD) median	622.0 (45.6) 621.2	587.8 (55.1) 590.8	<.001*
Subcortical deep gray matter structures			
Total SDGM, mean (SD) median	44.9 (5.4) 45.3	42.0 (5.4) 42.2	<.001*
Caudate, mean (SD) median	6.7 (1.1) 6.7	6.2 (1.0) 6.2	<.001*
Putamen, mean (SD) median	9.4 (1.4) 9.5	8.9 (1.3) 8.9	.001*
Globus pallidus, mean (SD) median	3.5 (0.5) 3.5	3.2 (0.5) 3.2	<.001*
Thalamus, mean (SD) median	14.9 (1.76) 14.9	13.8 (2.0) 13.9	<.001*
Hippocampus, mean (SD) median	7.1 (0.9) 7.1	6.8 (0.9) 6.8	.001*
Amygdala, mean (SD) median	2.4 (0.4) 2.4	2.4 (0.4) 2.4	.355
Nucleus accumbens, mean (SD) median	0.8 (0.2) 0.8	0.7 (0.2) 0.7	.042*

Note:—NBPV indicates normalized brain parenchymal volume; NCV, normalized cortical volume; NGMV, normalized gray matter volume; NLVV, normalized lateral ventricular volume; NWMV, normalized white matter volume.
Statistical analysis between groups was performed with use of the Mann-Whitney test for nonparametric data and the Student t test for parametric data. All P values were corrected for multiple comparisons using Benjamini-Hochberg correction.
The volumes are expressed in milliliters.
* indicates significant P values ($P < .05$) after correction.

tested for normality by use of the Shapiro-Wilk test. Demographic, clinical, and MR imaging differences between the groups were tested by use of the χ^2 test, the Student t test, and the Mann-Whitney U test in pair-wise comparisons, and ANOVA and the Kruskal-Wallis test for 3-way analyses, where appropriate.

We also performed linear regression analysis to evaluate the relationships between DTI variables and MR imaging metrics. In each analysis, DTI variables were the dependent variable. The analyses were age and sex adjusted in the HC group, and age, sex, disability level, and disease duration adjusted in the MS groups.

All P values were corrected for multiple comparisons by use of Benjamini-Hochberg correction. Nominal P values $< .05$ were regarded as significant, by 2-tailed testing.[30]

RESULTS

Demographic, Clinical, and Conventional MR Imaging Characteristics

Demographic, clinical, and conventional MR imaging characteristics of HC patients and patients with MS are shown in Table 1. Patients did not significantly differ from the HC group in sex, age, or cardiovascular risk factors. The mean age of the patients with MS was 46.9 years (standard deviation, 8.2), 206 (72.3%) were women, the mean disease duration was 14.4 years (standard deviation, 9.1), and median Expanded Disability Status Scale score was 3.0. Of the 285 patients with MS in the study, 225 were receiving disease-modifying treatment, which included interferon-beta ($n = 94$), glatiramer acetate ($n = 59$), natalizumab ($n = 44$), intravenous immunoglobulin ($n = 4$), and combination therapy ($n = 24$).

Demographic, clinical, and MR imaging characteristics were also compared between 210 patients with RRMS and 75 patients with progressive MS. The progressive MS group consisted of 58 patients with secondary-progressive MS and 17 with primary-progressive MS. As expected, the mean age, disease duration, Expanded Disability Status Scale score, and MR imaging measures were significantly different between the RRMS and PMS groups.

As expected, patients with MS showed significantly increased T2 lesion volume compared with HC patients ($P < .001$, Table 1). Patients with PMS showed significantly increased T2 lesion volume ($P = .001$) and T1 lesion volume ($P = .037$) compared with those in the RRMS group, whereas the RRMS group presented with significantly increased T1 gadolinium lesion volume ($P = .046$).

Brain Volume Differences among Study Groups

Table 2 shows the differences between HC patients and patients with MS in global, tissue-specific, and regional brain volume structures. Global and tissue-specific brain volumetric assessment showed a significant decrease of normalized gray matter volume, normalized brain parenchymal volume, normalized cortical volume, and a significant increase of normalized lateral ventricular volume (all $P < .001$) in the MS group. These patients also showed decreased total SDGM, caudate, globus pallidus, thalamus (all $P < .001$), putamen and hippocampus (both $P = .001$), and nucleus accumbens ($P = .042$). This is referenced in On-line Tables 1 and 2.

Differences in DTI Measures among the Study Groups

DTI differences are shown in Table 3. DTI FA, MD, AD, and RD differences in global and tissue-specific brain structures were in-

vestigated among the HC, RRMS, and PMS groups. Significant differences were found in FA, MD, and RD in the global brain measures ($P < .01$), particularly in the normal-appearing brain tissue FA ($P < .001$), normal-appearing white matter FA ($P < .001$), normal-appearing brain tissue RD ($P = .001$), and normal-appearing white matter RD ($P < .001$). Only the normal-appearing gray matter AD was significantly different ($P = .011$) among the groups.

Table 3: Linear regression analysis including diffusion tensor imaging measures, T2 lesion burden, and white matter and cortical volumes in the healthy control group

	T2-LV	NWMV	NCV
FA, Total SDGM	0.024	−0.103	−0.136
β, *P* value	.864	.493	.451
Caudate	0.049	0.114	−0.102
β, *P* value	.674	.360	.553
Thalamus	0.057	0.090	0.121
β, *P* value	.626	.481	.480
Hippocampusr	−0.024	−0.152	−0.063
β, *P* value	.862	.211	.728
MD, Total SDGM	0.154	−0.348*	−0.318*
β, *P* value	.135	.001*	.033*
Caudate	0.010	−0.226*	−0.337*
β, *P* value	.936	.033*	.015*
Thalamus	0.159	−0.325*	−0.376*
β, *P* value	.099	.001*	.006*
Hippocampus	0.165	−0.250*	−0.130
β, *P* value	.141	.037*	.466
AD, Total SDGM	0.152	−0.336*	−0.321*
β, *P* value	.140	.002*	.033*
Caudate	0.024	−0.224*	−0.371*
β, *P* value	.847	.034*	.008*
Thalamus	0.157	−0.313*	−0.369*
β, *P* value	.100	.002*	.006*
Hippocampus	0.149	−0.253*	−0.134
β, *P* value	.190	.034*	.451
RD, Total SDGM	0.157	−0.349*	−0.315*
β, *P* value	.130	.001*	.036*
Caudate	0.007	−0.206	−0.318
β, *P* value	.958	.051	.237
Thalamus	0.141	−0.329*	−0.377*
β, *P* value	.141	<.001*	.006*
Hippocampus	0.174	−0.244*	−0.126
β, *P* value	.122	.042*	.483

Note:—NCV indicates normalized cortical volume; NWMV, normalized white matter volume; T2-LV, T2 lesion volume.
Regression analysis was adjusted for the effects of age and sex. All *P* values were corrected for multiple comparisons using Benjamini-Hochberg correction.
* indicates significant *P* values ($P < .05$) after correction.

The DTI MD, AD, and RD measures for total SDGM, caudate, thalamus, and hippocampus were significantly increased ($P < .001$) in patients with MS. FA was significantly decreased only in the thalamus ($P = .002$) and hippocampus ($P = .047$), and it was increased in the putamen ($P = .025$) and nucleus accumbens ($P = .006$).

Linear Regression between SDGM DTI and MR Imaging Measures

Linear regression analysis included only DTI variables of SDGM regions, which were significantly different among the 3 study groups from the ANOVA analyses. Associations of these significant SDGM DTI measures were then used to find associations with lesion volume, normalized white matter volume, and normalized cortical volume. The associations between SDGM DTI measures and MR imaging metrics in HCs are described in Table 3 and Figs 1–3. Significant associations were identified between the MD, AD, and RD of SDGM structures but not FA, and a decrease in normalized white matter volume ($P < .001$) and normalized cortical volume ($P = .033$) with the exception of hippocampus. No significant associations were detected between DTI measures and T2 lesion volume.

Linear regression analysis in the RRMS and PMS groups is shown in Tables 4 and 5 as well as Figs 1–3, respectively. Increased MD, AD, and RD variables were strongly associated with decreased normalized white matter volume in the RRMS and PMS groups (all $P < .001$), but no significance was detected for the normalized cortical volume. The FA showed fewer significant results. T1 lesion volume and T2 lesion volume were associated with most of the examined SDGM structure DTI measures.

DISCUSSION

Understanding the pathophysiology of gray matter degeneration and the relationship between focal lesions and distant tissue alterations in the gray matter is important to determine the right treatment strategies that can prevent clinical progression in patients with MS. It has been shown that development of gray matter pathology is associated with the progression of physical and cognitive disability in both cross-sectional and longitudinal studies.[1-4,8-12,20,31]

In this study, we used DTI on 3T MR imaging to investigate structural brain changes in a large cohort of HC patients and patients with MS. Then, we focused on the SDGM structures to

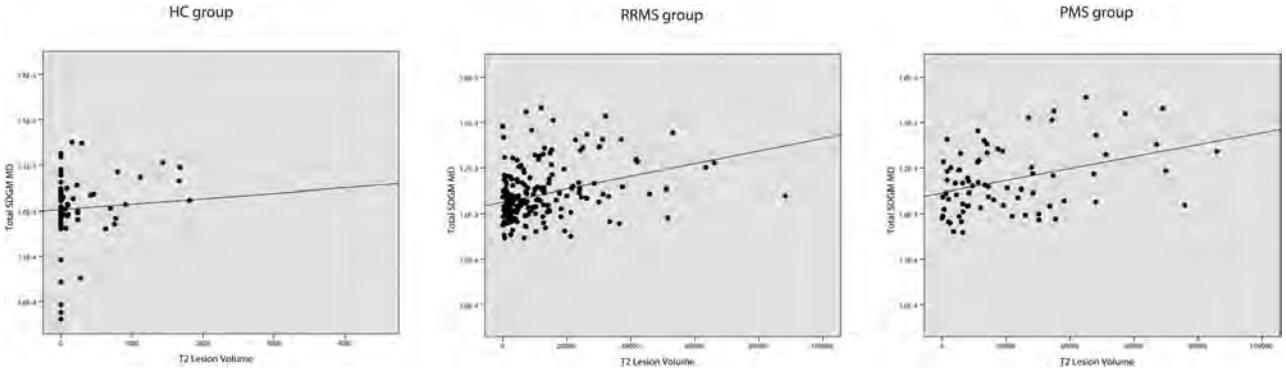

FIG 1. Linear regression analysis between MD of total SDGM and T2 lesion volume in HC patients ($\beta = 0.154$, $P = .135$), patients with RRMS ($\beta = 0.206$, $P = .015$), and in patients with PMS ($\beta = 0.449$, $P < .001$).

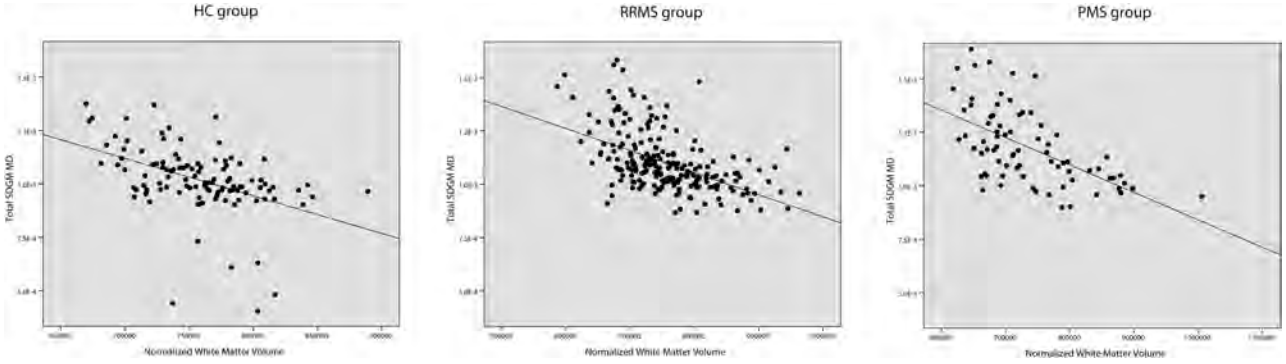

FIG 2. Linear regression analysis between MD of total SDGM and normalized white matter volume in HC patients ($\beta = -0.348$, $P = .001$), patients with RRMS ($\beta = -0.415$, $P < .001$), and patients with PMS ($\beta = -0.551$, $P < .001$).

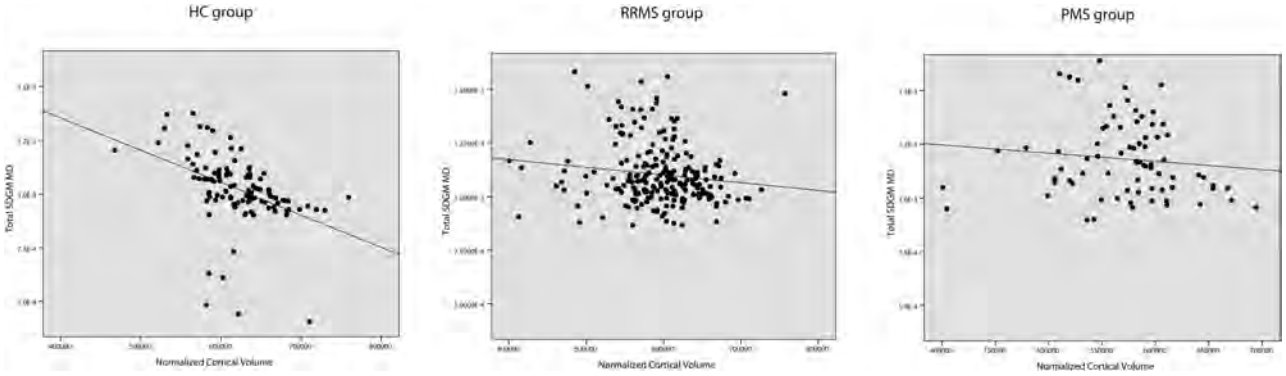

FIG 3. Linear regression analysis between MD of total SDGM and normalized cortical volume in HC patients ($\beta = -0.318$, $P = .033$), patients with RRMS ($\beta = 0.003$; $P = .979$), and patients with PMS ($\beta = -0.009$; $P = .964$).

investigate the association between their DTI alterations and lesion burden, white matter, and cortical atrophy among the study groups. To better evaluate the microstructural damage of SDGM structures, we studied the diffusivity in the axial and radial directions to detect differences that may be underestimated by the MD measures. The findings confirmed that brain gray matter is not spared by the MS pathologic process.[3] We found widespread DTI alterations in the global and tissue-specific brain structures among patients in the RRMS and PMS groups. In agreement with previous studies, the FA, MD, and RD were found to be significantly different in the normal-appearing brain tissue, normal-appearing white matter, and normal-appearing gray matter.[32-34] In line with another study,[35] the AD was significantly different in the normal-appearing gray matter but not in the normal-appearing white matter or the normal-appearing brain tissue. In accordance with a prior study, normal-appearing white matter MD was increased and was dominated by increased RD with no significant change in AD among the 3 groups.[36] Also, in alignment with the results from previous studies,[21,23] we detected a significant increase of MD, AD, and RD in the total SDGM, caudate, thalamus, and hippocampus in patients with RRMS and particularly in patients with PMS. FA was significantly decreased in the thalamus and hippocampus of patients with MS as reported previously[21,37] and significantly increased in the putamen and nucleus accumbens. Despite the extensive investigation of DTI abnormalities in the thalamus and other SDGM structures, FA has limitations in the study of gray matter structures; therefore, anisotropic findings remain conflicting.[38-40] Our present study supports results from previous studies, which point toward the thalamus as one of the most affected SDGM structures.[21,37]

A significant issue to be clarified is related to the pathophysiology of the SDGM involvement and its associations with inflammatory and degenerative pathology. The inflammatory process seems to be an important contributor to the atrophy of gray matter, and previous studies have already established the spatial and temporal relationship between T2 lesion burden and gray matter volume loss.[13,26] The main objective of this study was to further investigate this issue, which included a large cohort of HC patients and patients with MS. To the best of our knowledge, this has not been previously studied in the HC patients. Our results suggest that lesion burden is related to SDGM diffusivity in patients with MS and particularly in the progressive type, where we found modest associations. However, at best, these associations explained 25%–30% of the variance. In support of this, other studies showed that an increase in thalamic DTI diffusivity and in myo-Inositol also correlated with T2 lesion volume in patients with MS.[23] On the contrary, we did not detect a significant correlation among SDGM DTI measures and lesion burden in the HC group, as expected. These results support the hypothesis that the structural damage of white matter connections could lead to trans-synaptic axonal degeneration and retrograde degeneration of neurons with alteration of the microstructural architecture of SDGM structures.

To better understand the differences in SDGM DTI abnormalities between patients with MS and HC patients, we investigated the relationship between white matter and cortical atrophy, to

Table 4: Linear regression analysis including diffusion tensor imaging measures, T2 lesion burden, white matter, and cortical volumes in relapsing-remitting MS

	T1-LV	T2-LV	NWMV	NCV
FA, Total SDGM	−0.180	−0.094	0.096	0.221*
β, *P* value	.052	.331	.273	.013*
Caudate	−0.118	0.056	0.291*	−0.147
β, *P* value	0.230	0.583	0.001*	0.120
Thalamus	−0.130	0.068	0.101	0.176
β, *P* value	.177	.496	.250	.054
Hippocampus	−0.242*	−0.295*	0.084	0.376*
β, *P* value	.010*	.001*	.360	<.001*
MD, Total SDGM	0.270*	0.206*	−0.415*	0.003
β, *P* value	.002*	.015*	<.001*	.979
Caudate	0.282*	0.142	−0.471*	0.050
β, *P* value	.002*	.115	<.001*	.605
Thalamus	0.268*	0.125	−0.370*	−0.058
β, *P* value	.003*	.167	<.001*	.553
Hippocampus	0.227*	0.304*	−0.230*	−0.063
β, *P* value	.014*	<.001*	.006*	.526
AD, Total SDGM	0.225*	0.179*	−0.389*	0.050
β, *P* value	.010*	.037*	<.001*	.591
Caudate	0.280*	0.156	−0.458*	0.043
β, *P* value	.002*	.076	<.001*	.653
Thalamus	0.246*	0.131	−0.361*	−0.018
β, *P* value	.006*	.139	<.001*	.867
Hippocampus	0.175	0.240*	−0.226*	0.026
β, *P* value	.058	.006*	.006*	.807
RD, Total SDGM	0.296*	0.222*	−0.428*	−0.028
β, *P* value	<.001*	.008*	<.001*	.785
Caudate	0.282*	0.133	−0.476*	0.053
β, *P* value	.002*	.140	<.001*	.583
Thalamus	0.280*	0.120	−0.372*	−0.081
β, *P* value	.002*	.190	<.001*	.408
Hippocampus	0.252*	0.334*	−0.227*	−0.113
β, *P* value	.006*	<.001*	.006*	.230

Note:—NCV indicates normalized cortical volume; NWMV, normalized white matter volume; T1-LV, T1 lesion volume; T2-LV, T2 lesion volume.
Regression analysis was adjusted for the effects of age, sex, disability level, and disease duration. All *P* values were corrected for multiple comparisons using Benjamini-Hochberg correction.
* indicates significant *P* values ($P < .05$) after correction.

Table 5: Linear regression analysis including diffusion tensor imaging measures, T2 lesion burden, white matter, and cortical volumes in progressive MS

	T1-LV	T2-LV	NWMV	NCV
FA, Total SDGM	−0.152	−0.091	0.005	−0.179
β, *P* value	.361	.581	.978	.237
Caudate	0.103	0.160	0.377*	−0.352*
β, *P* value	.551	.327	.008*	.014*
Thalamus	0.029	0.026	0.053	−0.089
β, *P* value	.883	.888	.756	.582
Hippocampus	−0.363*	−0.396*	−0.002	0.211
β, *P* value	.011*	.003*	.984	.131
MD, Total SDGM	0.289*	0.449*	−0.551*	−0.009
β, *P* value	.038*	<.001*	<.001*	.964
Caudate	0.223	0.335*	−0.543*	0.065
β, *P* value	.133	.016*	<.001*	.672
Thalamus	0.198	0.346*	−0.387*	−0.087
β, *P* value	.174	.010*	.003*	.559
Hippocampus	0.404*	0.569*	−0.529*	−0.096
β, *P* value	.006*	<.001*	<.001*	.553
AD, Total SDGM	0.268*	0.434*	−0.546*	−0.028
β, *P* value	.050*	<.001*	<.001*	.866
Caudate	0.240	0.366*	−0.523*	0.033
β, *P* value	.097	.008*	<.001*	.850
Thalamus	0.214	0.374*	−0.403*	−0.109
β, *P* value	.128	.006*	.001*	.464
Hippocampus	0.342*	0.516*	−0.566*	−0.051
β, *P* value	.023*	<.001*	<.001*	.765
RD, Total SDGM	0.30*	0.455*	−0.549*	0.003
β, *P* value	.036*	<.001*	<.001*	.985
Caudate	0.213	0.317*	−0.539*	0.082
β, *P* value	.158	.025*	<.001*	.592
Thalamus	0.187	0.328*	−0.375*	−0.076
β, *P* value	.208	.017*	.003*	.611
Hippocampus	0.426*	0.582*	−0.496*	−0.117
β, *P* value	<.001*	<.001*	<.001*	.469

Note:—NCV indicates normalized cortical volume; NWMV, normalized white matter volume; T1-LV, T1 lesion volume; T2-LV, T2 lesion volume.
Regression analysis was adjusted for the effects of age, sex, disability level, and disease duration. All *P* values were corrected for multiple comparisons using Benjamini-Hochberg correction.
* indicates significant P values ($P < .05$) after correction.

evaluate if the DTI alterations are also associated with atrophy in these structures. Some studies have recently demonstrated that thalamic DTI alterations are related to aging in HC patients.[41,42] Linear regression analysis in the present study, adjusted for age and sex, demonstrated significant associations among increased diffusivity of the SDGM structures and white matter and cortical atrophy in the HC group. Indeed, these are important findings that have not been previously reported in healthy patients. These findings suggest that neuronal and axonal loss leading to white matter and cortical atrophy is modestly related to microstructural changes of the SDGM in HC patients. In contrast, we found SDGM DTI diffusivity associations with white matter atrophy in MS groups but not with cortical atrophy. DTI alterations of the SDGM structures seem to be more influenced by degeneration of the white matter network exemplified by accumulation of lesion burden, but not by the neuronal loss of the cortical gray matter. A previous study also did not detect a relationship between normal-appearing gray matter diffusivity changes and gray matter volume.[43] Taken together, these results suggest that SDGM DTI alterations are not associated with gray matter atrophy.

Although we detected uniformly consistent associations in regression analyses for MD, AD, and RD measures, those for FA measures were not particularly consistent in both groups.

A limitation of our current study concerns the absence of longitudinal investigations that could better explain the relationship among accumulation of lesion burden, development of white matter, and cortical and DTI alterations of the SDGM in patients with MS and in healthy patients. In addition, we performed DTI acquisition with larger voxel sizes that could lead to some potential bias of acquisition data of the normal-appearing gray matter measures, especially in the cortical structures with a thickness < 3 mm. Moreover, we did not investigate clinical correlation with DTI measures, as these were considered out of the current scope of our study. However, our present study confirmed that SDGM DTI alterations were present in different MS clinical phenotypes of the disease and were more pronounced in patients with PMS.

CONCLUSIONS

DTI alterations of the SDGM in patients with MS are related to white matter lesion burden and atrophy but not to cortical atrophy. On the contrary, there was an association of SDGM DTI metrics with white matter and cortical atrophy in the HC group.

Further longitudinal and postmortem studies need to shed light on the pathogenesis of SDGM and cortical degeneration in patients with MS.

Disclosures: Bianca Weinstock-Guttman received honoraria as a speaker and as a consultant for Biogen Idec, Teva Pharmaceuticals, EMD Serono, Pfizer, Novartis, and Acorda. Dr. Weinstock-Guttman received research funds from Biogen Idec, Teva Pharmaceuticals, EMD Serono, Pfizer, Novartis, Acorda, and Cyberonics. ADDITIONAL DISCLOSURES* (ICMJE): *UNRELATED: Consultancy:* Teva Neuroscience, Genzyme & Sanofi, Novartis Mylan; *Grants/Grants Pending:* Teva Neuroscience, Genzyme & Sanofi, Questcor, Novartis; *Payment for Lectures (including service on speaker bureaus):* Biogen Idec, Teva Neuroscience, EMD Serono, Genzyme &Sanofi, Novartis; *Payment for Manuscript Preparation:* Novartis. Francesco Patti received honoraria for speaking and consultant activities by Bayer, Biogen Idec, Merck Serono, Novartis, Sanofi-Aventis, and Teva Pharmaceuticals. He also received research grant by FISM (Fondazione Italiana Sclerosi Multipla) and MIUR (Ministero Italiano della Università e della Ricerca). ADDITIONAL DISCLOSURES* (ICMJE): *RELATED: Consulting Fee or Honorarium:* Genzyme, Comments: I served as an advisory board member and speaking activity for the mentioned companies; *UNRELATED: Board Membership:* Bayer Schering, Biogen Idec, Merck Serono, Novartis, Sanofi-Genzyme, Comments: Advisory board; *Payment for Lectures (including service on speaker bureaus):* Bayer Schering, Biogen Idec, Merck Serono, Novartis, Sanofi-Genzyme, Teva, Comments: Travel grants/honoraria. Robert Zivadinov received personal compensation from Teva Pharmaceuticals, Biogen Idec, EMD Serono, Novartis, and Sanofi-Genzyme for speaking and consultant fees. Dr. Zivadinov received financial support for research activities from Biogen Idec, Teva Pharmaceuticals, EMD Serono, Novartis, and Sanofi-Genzyme. ADDITIONAL DISCLOSURES* (ICMJE): *UNRELATED: Payment for Lectures (including service on speaker bureaus):* Biogen Idec, EMD Serono, Teva Pharmaceuticals, Genzyme-Sanofi, Novartis. **If not disclosed previously.*

REFERENCES

1. De Stefano N, Matthews PM, Filippi M, et al. **Evidence of early cortical atrophy in MS: relevance to white matter changes and disability.** *Neurology* 2003;60:1157–62
2. Zivadinov R, Heininen-Brown M, Schirda CV, et al. **Abnormal subcortical deep-gray matter susceptibility-weighted imaging filtered phase measurements in patients with multiple sclerosis: a case-control study.** *Neuroimage* 2012;59:331–39
3. Hulst HE, Geurts JJ. **Gray matter imaging in multiple sclerosis: what have we learned?** *BMC Neurol* 2011;11:153
4. Lucchinetti CF, Popescu BF, Bunyan RF, et al. **Inflammatory cortical demyelination in early multiple sclerosis.** *N Engl J Med* 2011;365:2188–97
5. Ceccarelli A, Rocca MA, Pagani E, et al. **A voxel-based morphometry study of grey matter loss in MS patients with different clinical phenotypes.** *Neuroimage* 2008;42:315–22
6. Calabrese M, Rinaldi F, Mattisi I, et al. **The predictive value of gray matter atrophy in clinically isolated syndromes.** *Neurology* 2011;77:257–63
7. Minagar A, Barnett MH, Benedict RH, et al. **The thalamus and multiple sclerosis: modern views on pathologic, imaging, and clinical aspects.** *Neurology* 2013;80:210–19
8. Fisher E, Lee JC, Nakamura K, et al. **Gray matter atrophy in multiple sclerosis: a longitudinal study.** *Ann Neurol* 2008;64:255–65
9. Zivadinov R, Havrdová E, Bergsland N, et al. **Thalamic atrophy is associated with development of clinically definite multiple sclerosis.** *Radiology* 2013;268:831–41
10. Zivadinov R, Bergsland N, Dolezal O, et al. **Evolution of cortical and thalamus atrophy and disability progression in early relapsing-remitting MS during 5 years.** *AJNR Am J Neuroradiol* 2013;34:1931–39
11. Benedict RH, Zivadinov R, Carone DA, et al. **Regional lobar atrophy predicts memory impairment in multiple sclerosis.** *AJNR Am J Neuroradiol* 2005;26:1824–31
12. Bakshi R, Benedict RH, Bermel RA, et al. **T2 hypointensity in the deep gray matter of patients with multiple sclerosis: a quantitative magnetic resonance imaging study.** *Arch Neurol* 2002;59:62–68
13. Bendfeldt K, Blumhagen JO, Egger H, et al. **Spatiotemporal distribution pattern of white matter lesion volumes and their association with regional grey matter volume reductions in relapsing-remitting multiple sclerosis.** *Hum Brain Mapp* 2010;31:1542–55
14. Bö L, Geurts JJ, van der Valk P, et al. **Lack of correlation between cortical demyelination and white matter pathologic changes in multiple sclerosis.** *Arch Neurol* 2007;64:76–80
15. Schmierer K, Wheeler-Kingshott CA, Boulby PA, et al. **Diffusion tensor imaging of post mortem multiple sclerosis brain.** *Neuroimage* 2007;35:467–77
16. Filippi M, Rocca MA. **MR imaging of multiple sclerosis.** *Radiology* 2011;259:659–81
17. Rovaris M, Gass A, Bammer R, et al. **Diffusion MRI in multiple sclerosis.** *Neurology* 2005;65:1526–32
18. Raz E, Cercignani M, Sbardella E, et al. **Clinically isolated syndrome suggestive of multiple sclerosis: voxelwise regional investigation of white and gray matter.** *Radiology* 2010;254:227–34
19. Raz E, Cercignani M, Sbardella E, et al. **Gray- and white-matter changes 1 year after first clinical episode of multiple sclerosis: MR imaging.** *Radiology* 2010;257:448–54
20. Benedict RH, Hulst HE, Bergsland N, et al. **Clinical significance of atrophy and white matter mean diffusivity within the thalamus of multiple sclerosis patients.** *Mult Scler* 2013;19:1478–84
21. Mesaros S, Rocca MA, Pagani E, et al. **Thalamic damage predicts the evolution of primary-progressive multiple sclerosis at 5 years.** *AJNR Am J Neuroradiol* 2011;32:1016–20
22. Senda J, Watanabe H, Tsuboi T, et al. **MRI mean diffusivity detects widespread brain degeneration in multiple sclerosis.** *J Neurol Sci* 2012;319:105–10
23. Tovar-Moll F, Evangelou IE, Chiu AW, et al. **Thalamic involvement and its impact on clinical disability in patients with multiple sclerosis: a diffusion tensor imaging study at 3T.** *AJNR Am J Neuroradiol* 2009;30:1380–86
24. Jehna M, Langkammer C, Khalil M, et al. **An exploratory study on the spatial relationship between regional cortical volume changes and white matter integrity in multiple sclerosis.** *Brain Connect* 2013;3:255–64
25. Henry RG, Shieh M, Amirbekian B, et al. **Connecting white matter injury and thalamic atrophy in clinically isolated syndromes.** *J Neurol Sci* 2009;282:61–66
26. Mühlau M, Buck D, Forschler A, et al. **White-matter lesions drive deep gray-matter atrophy in early multiple sclerosis: support from structural MRI.** *Mult Scler* 2013;19:1485–92
27. Polman CH, Reingold SC, Banwell B, et al. **Diagnostic criteria for multiple sclerosis: 2010 revisions to the McDonald criteria.** *Ann Neurol* 2011;69:292–302
28. Behrens TE, Johansen-Berg H, Woolrich MW, et al. **Non-invasive mapping of connections between human thalamus and cortex using diffusion imaging.** *Nat Neurosci* 2003;6:750–57
29. Behrens TE, Woolrich MW, Jenkinson M, et al. **Characterization and propagation of uncertainty in diffusion-weighted MR imaging.** *Magn Reson Med* 2003;50:1077–88
30. Benjamini Y, Hochberg Y. **Controlling the false discovery rate—a practical and powerful approach to multiple testing.** *J Roy Stat Soc B Met* 1995;57:289–300
31. Batista S, Zivadinov R, Hoogs M, et al. **Basal ganglia, thalamus and neocortical atrophy predicting slowed cognitive processing in multiple sclerosis.** *J Neurol* 2012;259:139–46
32. Bozzali M, Cercignani M, Sormani MP, et al. **Quantification of brain gray matter damage in different MS phenotypes by use of diffusion tensor MR imaging.** *AJNR Am J Neuroradiol* 2002;23:985–88
33. Liu Y, Duan Y, He Y, et al. **Whole brain white matter changes revealed by multiple diffusion metrics in multiple sclerosis: a TBSS study.** *Eur J Radiol* 2012;81:2826–32
34. Akbar N, Lobaugh NJ, O'Connor P, et al. **Diffusion tensor imaging abnormalities in cognitively impaired multiple sclerosis patients.** *Can J Neurol Sci* 2010;37:608–14

35. Hasan KM, Walimuni IS, Abid H, et al. **Human brain atlas-based multimodal MRI analysis of volumetry, diffusimetry, relaxometry and lesion distribution in multiple sclerosis patients and healthy adult controls: implications for understanding the pathogenesis of multiple sclerosis and consolidation of quantitative MRI results in MS.** *J Neurol Sci* 2012;313:99–109
36. Yu HJ, Christodoulou C, Bhise V, et al. **Multiple white matter tract abnormalities underlie cognitive impairment in RRMS.** *Neuroimage* 2012;59:3713–22
37. Bozzali M, Spanò B, Parker G, et al. **Anatomical brain connectivity can assess cognitive dysfunction in multiple sclerosis.** *Mult Scler* 2013;19:1161–68
38. Ciccarelli O, Werring DJ, Wheeler-Kingshott CA, et al. **Investigation of MS normal-appearing brain using diffusion tensor MRI with clinical correlations.** *Neurology* 2001;56:926–33
39. Hannoun S, Durand-Dubief F, Confavreux C, et al. **Diffusion tensor-MRI evidence for extra-axonal neuronal degeneration in caudate and thalamic nuclei of patients with multiple sclerosis.** *AJNR Am J Neuroradiol* 2012;33:1363–68
40. Zhao DD, Zhou HY, Wu QZ, et al. **Diffusion tensor imaging characterization of occult brain damage in relapsing neuromyelitis optica using 3.0T magnetic resonance imaging techniques.** *Neuroimage* 2012;59:3173–77
41. Hasan KM, Walimuni IS, Abid H, et al. **Multimodal quantitative magnetic resonance imaging of thalamic development and aging across the human lifespan: implications to neurodegeneration in multiple sclerosis.** *J Neurosci* 2011;31:16826–32
42. Hughes EJ, Bond J, Svrckova P, et al. **Regional changes in thalamic shape and volume with increasing age.** *Neuroimage* 2012;63:1134–42
43. Oreja-Guevara C, Rovaris M, Iannucci G, et al. **Progressive gray matter damage in patients with relapsing-remitting multiple sclerosis: a longitudinal diffusion tensor magnetic resonance imaging study.** *Arch Neurol* 2005;62:578–84

Can Diffusion Tensor Imaging Noninvasively Detect *IDH1* Gene Mutations in Astrogliomas? A Retrospective Study of 112 Cases

W.L. Tan, W.Y. Huang, B. Yin, J. Xiong, J.S. Wu, and D.Y. Geng

ABSTRACT

BACKGROUND AND PURPOSE: *IDH1* mutational status probably plays an important role in the predictive response for patients with astroglioma. This study explores whether DTI metrics are able to noninvasively detect *IDH1* status in astrogliomas.

MATERIALS AND METHODS: The DTI data of 112 patients with pathologically proven astroglioma (including 25, 12, and 10 cases with *IDH1* mutation and 11, 11, and 43 cases without mutation in grades II, III, and IV, respectively) were retrospectively reviewed. The maximal fractional anisotropy, minimal ADC, ratio of maximal fractional anisotropy, and ratio of minimal ADC in the tumor body were measured. In the same World Health Organization grading, the imaging parameters of patients with and without *IDH1* R132H mutation were compared by means of optimal metrics for detecting mutations. Receiver operating characteristic curve analysis was performed.

RESULTS: The maximal fractional anisotropy and ratio of maximal fractional anisotropy values had statistical significance between patients with *IDH1* R132H mutation and those without mutation in astrogliomas of grades II and III. The areas under the curve for maximal fractional anisotropy and ratio of maximal fractional anisotropy were both 0.92 in grade II and 0.80 and 0.82 in grade III. The minimal ADC value and ratio of minimal ADC value also demonstrated statistical significance between patients with mutation and those without mutation in all astroglioma grades. The areas under the curve for minimal ADC were 0.94 (II), 0.76 (III), and 0.66 (IV), and the areas under the curve for ratio of minimal ADC were 0.93 (II), 0.83 (III), and 0.70 (IV).

CONCLUSIONS: Fractional anisotropy and ADC from DTI can noninvasively detect *IDH1* R132H mutation in astrogliomas.

ABBREVIATIONS: *IDH1* = *isocitrate dehydrogenase 1*; FA = fractional anisotropy; rmFA = ratio of maximal fractional anisotropy; rmADC = ratio of minimal ADC; AUC = area under the curve; WHO = World Health Organization

Mutations in *isocitrate dehydrogenase 1 (IDH1)* exist in a large percentage of gliomas.[1,2] The value of detecting *IDH1* mutational status has been reported in diagnostic and prognostic studies, and it might also be useful as a predictive indicator. *IDH1* mutations are not found in nonneoplastic conditions thus far.[3-5] Mutations in the *IDH1* gene were associated with improved outcomes in patients with anaplastic astrocytomas and glioblastomas.[2] Furthermore, Juratli et al[6] suggested that early radiation therapy appeared to be beneficial only in patients with low-grade astrocytoma with *IDH* mutations. SongTao et al[7] reported that *IDH* mutations were correlated with a higher rate of objective response to temozolomide.

Thus far, the reference standard for testing the status of *IDH1* is gene sequencing. Immunohistochemical analysis by use of the mouse monoclonal *IDH1* R132H antibody is commonly applied in clinical examinations with high sensitivity.[8] However, both sequencing and immunohistochemical examinations require tumoral tissues, and neither method can offer preoperative detection of *IDH1* gene status. Some patients will not or cannot undergo operations (such as patients with brain stem gliomas or with poor physical condition). Therefore, we need a noninvasive method to detect *IDH1* mutational status before surgery or biopsy. Metellus et al[9] reported morphologic changes in *IDH1* mutant gliomas but lack of a quantitative indicator. Glioma-associated *IDH1* mutations result in overproduction of the oncometabolite R(–)-2-hydroxyglutarate.[10,11] Although the concentration of 2-hydroxyglutarate in serum cannot be used to judge the status of *IDH1* mutations, these mutations are associated with the accumulation of R(–)-2-hydroxyglutarate within the tumor.[12,13] Pope et al[14] suggested that MR spectroscopy could detect 2-hy-

Received August 1, 2013; accepted after revision October 1.

From the Departments of Radiology (W.L.T., W.Y.H., B.Y., D.Y.G.), Neuropathology (J.S.X.), and Neurosurgery (J.W.), Huashan Hospital, Fudan University, Shanghai, Peoples Republic of China.

This work was supported by the National Natural Science Foundation of China (81071132) and by the Natural Science Foundation of Shanghai (10411952100).

Please address correspondence to Daoying Geng, MD, No. 12, Middle Rd Wu Lu Mu Qi, Shanghai, PR China; e-mail: gengdy@163.com

http://dx.doi.org/10.3174/ajnr.A3803

droxyglutarate in patients with *IDH1*-mutant glioma and provide a noninvasive measurement of 2-hydroxyglutarate in gliomas. However, the measurement of 2-hydroxyglutarate through MR spectroscopy is performed by special software and is inconvenient for clinical application.

DTI has been used to detect the genetic characteristics of gliomas.[15] In the current study, we explore whether the metrics determined from DTI can help to detect *IDH1* gene status of astrogliomas noninvasively.

MATERIALS AND METHODS

Clinical Data and Groupings

A total of 112 patients with pathologically proven astroglioma and preoperatively performed DTI were retrospectively reviewed from January 2011 to June 2012 in our hospital. Clinical data, including age and sex, were collected. According to the 2007 World Health Organization (WHO) classification of tumors of the central nervous system,[16] there were 36 cases of grade II astrocytoma, 23 cases of grade III anaplastic astrocytoma, 46 cases of grade IV primary glioblastoma, and 7 cases of grade IV secondary glioblastoma.

IDH1 R132H immunohistochemical results were also reviewed. *IDH1* R132H protein expression was determined in paraffin-embedded tumor specimens after surgery by use of anti-mIDH1R132H antibody (internal clone H09; Dianova, Hamburg, Germany). The expression of *IDH1* R132H was determined by use of the methods of Takano et al.[17] Cases with ≥10% positive cells were rated positive, and cases with <10% positive cells were rated negative. There were 25 (69.44%), 12 (52.17%), and 10 (18.87%) cases showing positive results in grades II, III, and IV, respectively. Six of 10 cases of grade IV glioblastoma with positive results were primary glioblastomas.

All of the patients were divided into 6 groups according to immunochemical results and WHO grades as follows: 1) group 1: grade II with *IDH1* R132H mutation; 2) group 2: grade II without *IDH1* R132H mutation; 3) group 3: grade III with *IDH1* R132H mutation; 4) group 4: grade III without *IDH1* R132H mutation; 5) group 5: grade IV with *IDH1* R132H mutation; and 6) group 6: grade IV without *IDH1* R132H mutation.

This study was approved by the local research ethics committee. Patient informed consent was waived for this retrospective study.

MR Technique

MR scanning was performed with the use of a 3T scanner (MAGNETOM Verio; Siemens, Erlangen, Germany), with an 8-channel head coil. All of the patients underwent preoperative DTI. Parameters were as follows: TR = 7600 ms; TE = 91 ms; FOV = 23.0 cm × 23.0 cm; acquisition matrix of 128 × 128; section thickness = 3 mm; no intersection separation; b = 0/1000 seconds/mm^2; number of excitations = 2; bandwidth = 1502 Hz/Px. Twenty directions were acquired. A single-shot echo-planar imaging diffusion tensor sequence was used. Other sequences including T2WI (TR = 4000 ms, TE = 96 ms, number of excitations = 1, echo trains per section = 8, bandwidth = 221 Hz/Px), and T1WI and postcontrast T1WI (TR = 2000 ms, TE = 17 ms, number of excitations = 1, echo trains per section = 17, bandwidth = 260 Hz/Px). Parallel imaging was used in all the sequences mentioned above with acceleration factor = 2.

Image Analysis

According to the DTI data, the workstation automatically generated the fractional anisotropy (FA) and ADC mapping. All of the FA and ADC maps were retrospectively interpreted by 2 experienced neuroradiologists (W. Tan and W. Huang, with 10 and 6 years of brain MR imaging experience, respectively) who did not know the pathologic results. The maximal FA was measured by manually placing ROIs in the most solid and highest signal-intensity part of the tumoral regions on the FA mapping by visual inspection. The size of every ROI was between 15–20 pixels. The mean value of small ROIs drawn to encompass the voxels with maximal FA values was recorded. Each neuroradiologist drew 3 ROIs to obtain the maximal FA, according to the gray-scale map. The maximal FA value among these values was chosen as the result. An average of the results of 2 neuroradiologists was used as the patient's maximal FA. If the value for one reader varied by >20% from the second reader,[18] a third reader, a neuroradiologist with 22 years of experience (D. Geng), would measure the maximal FA value. The average of Dr Geng's result and the result closer to her result from the other 2 neuroradiologists was used as the patient's maximal FA, and 22 (19.6%) patients required the third reader method. Cystic and hemorrhage areas were excluded according to T2WI and enhanced T1WI, when the ROI was drawn. The minimal ADC was obtained by the same method, and 17 (15.2%) patients required the third reader method.

The FA and ADC values were also measured in the peritumoral regions. The peritumoral area is defined as a region containing nonenhanced and higher signal intensity outside the tumoral solid area on T2WI and ADC images. If there was not different signal noticed from T2WI and ADC mapping, especially in grade II tumors, the ROI was manually drawn in the peritumoral area adjoining to the tumoral area (<1 cm). Forty-five (40.18%) and 36 (32.14%) patients required the third reader method in the measurement of peritumoral FA and ADC, respectively. Because of regional variation of the FA and ADC absolute values,[19] the contralateral normal posterior limb of the internal capsule was measured as the control to normalize FA and ADC values. The ratio of maximal FA (rmFA), ratio of peritumoral FA or ratio of minimal ADC (rmADC), and ratio of peritumoral ADC were equal to the maximal FA, peritumoral FA or minimal ADC, and peritumoral ADC divided by the contralateral FA or contralateral ADC.

Statistics

All of the statistical analyses were performed with the use of the Statistical Package for the Social Sciences software (version 13.0; IBM, Armonk, New York). The Kolmogorov-Smirnov test was performed on the age and imaging data to analyze whether they were normally distributed. Statistical significance was set at the $P < .05$ level. The interobserver intraclass correlations were calculated for the maximal FA, minimal ADC, peritumoral FA, peritumoral ADC, contralateral FA, and contralateral ADC, respectively. Receiver operating characteristic curves of the parameters with statistical significance were obtained to seek the cutoff value

Table 1: Results of clinical and imaging data

	Group 1	Group 2	Group 3	Group 4	Group 5	Group 6
No. of patient cases	25	11	12	11	10	43
Sex, M/F	15/10	5/6	9/3	7/4	8/2	27/16
Age, y	39.68 ± 7.22	42.45 ± 18.38	41.92 ± 8.71	42.64 ± 17.90	41.70 ± 11.39	54.42 ± 12.63
Edema FA	0.26 ± 0.12	0.28 ± 0.14	0.18 ± 0.09	0.24 ± 0.11	0.18 ± 0.06	0.20 ± 0.09
Ratio of edema FA	0.37 ± 0.17	0.40 ± 0.20	0.24 ± 0.12	0.34 ± 0.16	0.25 ± 0.07	0.27 ± 0.13
Contralateral FA	0.72 ± 0.03	0.72 ± 0.03	0.74 ± 0.04	0.72 ± 0.04	0.70 ± 0.05	0.73 ± 0.04
Edema ADC ($\times 10^{-3}$ mm^2/s)	1.15 ± 0.37	1.13 ± 0.27	1.35 ± 0.31	1.33 ± 0.42	1.57 ± 0.22	1.53 ± 0.33
Ratio of edema ADC	1.63 ± 0.56	1.58 ± 0.46	1.93 ± 0.50	1.84 ± 0.62	2.12 ± 0.30	2.11 ± 0.47
Contralateral ADC	0.71 ± 0.03	0.72 ± 0.04	0.71 ± 0.05	0.74 ± 0.04	0.74 ± 0.04	0.73 ± 0.03

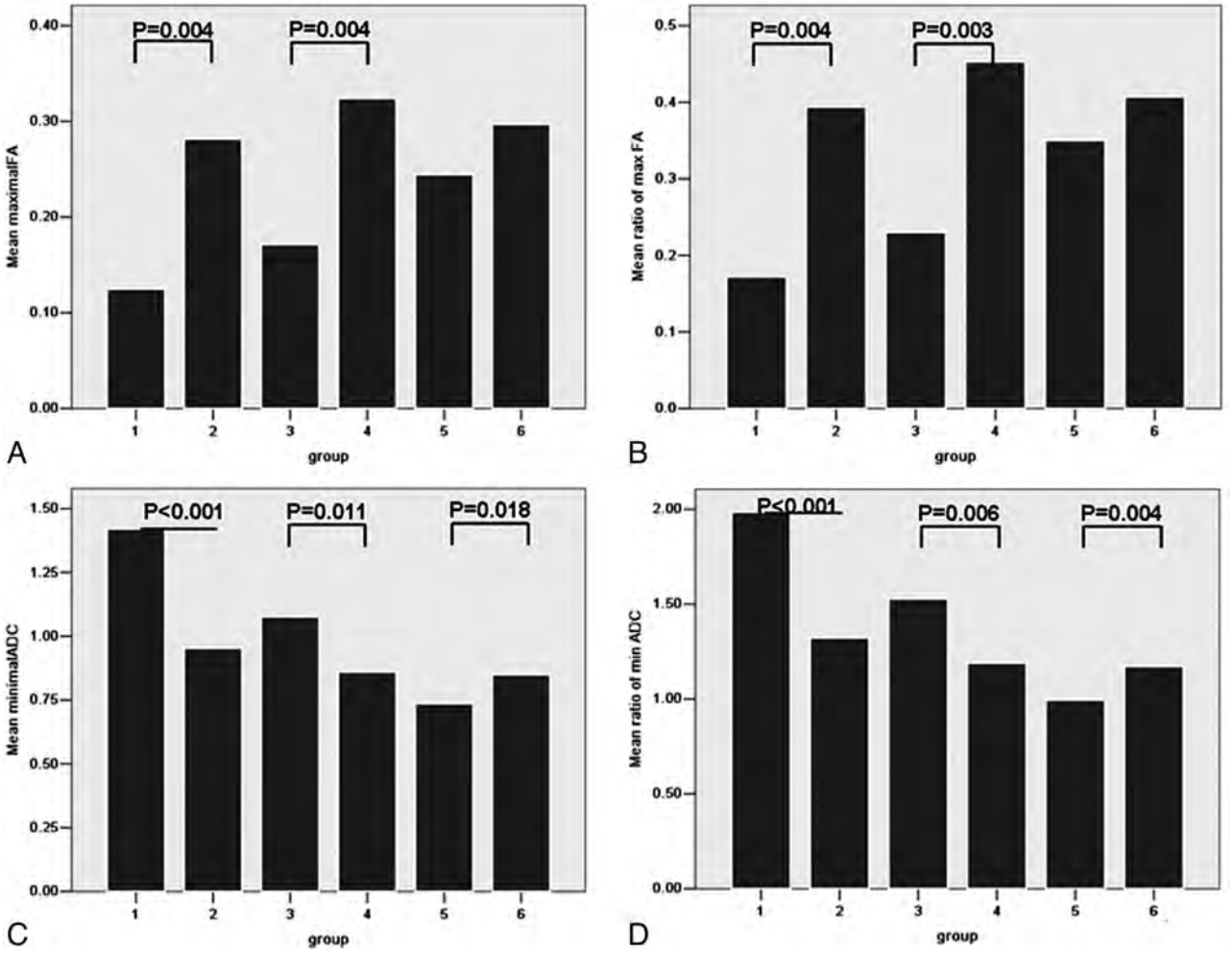

FIG 1. Bar graph of maximal fractional anisotropy (FA) (*A*), ratio of maximal FA (rmFA) (*B*), minimal ADC (*C*), and ratio of minimal ADC (rmADC) (*D*) in different groups. *P* values with statistical significance are shown. Maximal FA and rmFA could differentiate group 1 from group 2 and group 3 from group 4. Minimal ADC (unit: $\times 10^{-3}$ mm^2/s) and rmADC showed statistical significance in groups 1 and 2, in groups 3 and 4, and in groups 5 and 6.

for distinguishing between groups with and without *IDH1* R132H mutation. The sensitivity and specificity of these parameters were calculated. Sex differences were tested by means of the χ^2 test.

RESULTS

The age and imaging data were normally distributed. The age and imaging parameters in the different groups are shown as mean ± standard deviation. Sex was shown as the ratio of men to women. The interobserver intraclass correlations were 0.73, 0.84, 0.65, 0.70, 0.87, and 0.86 for the maximal FA, minimal ADC, peritumoral FA, peritumoral ADC, contralateral FA, and contralateral ADC, respectively.

Group 1 and Group 2

One case in group 2 was recurrent glioma. The differences in age and sex between groups 1 and 2 were not statistically significant (Table 1). The maximal FA (0.25 ± 0.16) and rmFA (0.35 ± 0.22) values in group 2 were higher than those (0.14 ± 0.07 and

Table 2: Cutoff value, sensitivity, specificity, and AUC of imaging parameters in the differentiation of astroglioma with and without *IDH1* R132H mutations

	Cutoff Value	Sensitivity	Specificity	AUC
Maximal FA				
Groups 1 and 2	0.18	90.90%	96.00%	0.92
Groups 3 and 4	0.27	81.80%	83.30%	0.80
Ratio of maximal FA				
Groups 1 and 2	0.25	90.90%	96.00%	0.92
Groups 3 and 4	0.37	81.80%	83.30%	0.82
Minimal ADC ($\times 10^{-3}$ mm^2/s)				
Groups 1 and 2	1.07	100.00%	90.90%	0.94
Groups 3 and 4	0.99	75.00%	81.80%	0.76
Groups 5 and 6	0.81	53.50%	90.00%	0.66
Ratio of minimal ADC				
Groups 1 and 2	1.47	100.00%	81.80%	0.93
Groups 3 and 4	1.31	91.70%	81.80%	0.83
Groups 5 and 6	1.10	53.50%	90.00%	0.70

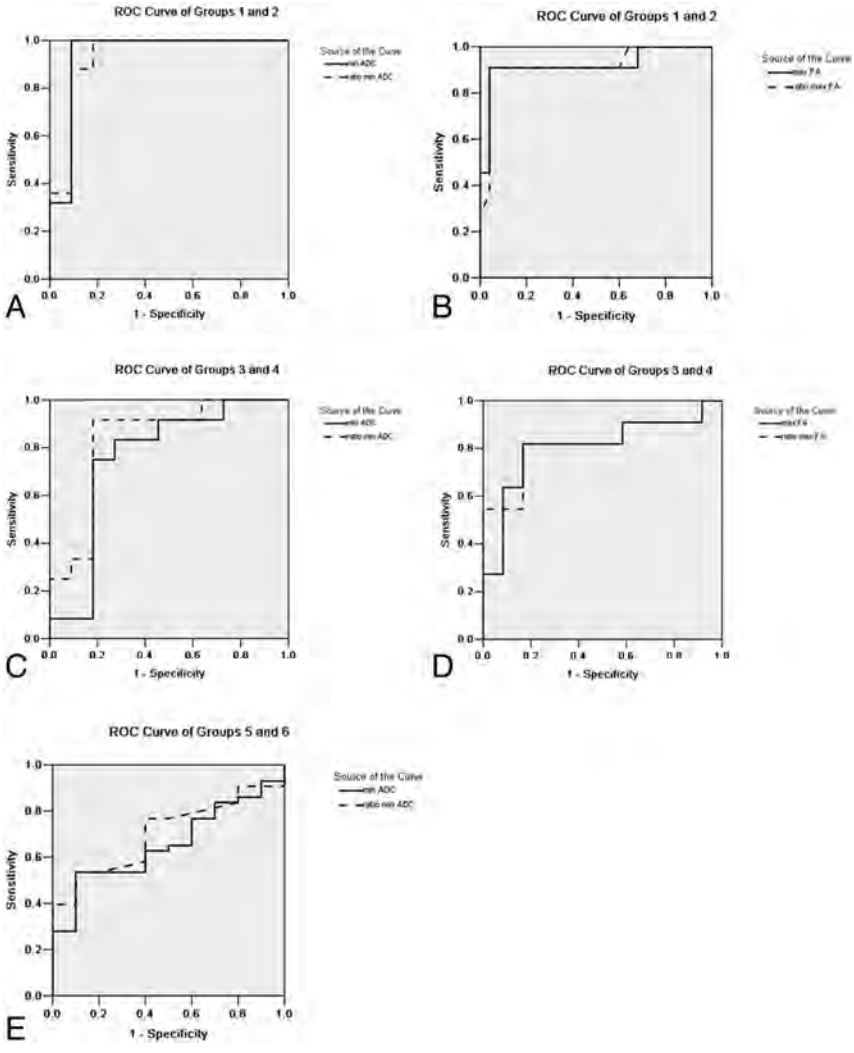

FIG 2. Receiver operating characteristic curves with statistical significance are shown. The area under the curve (AUC) showed a decreasing trend in imaging parameters from grade II to grade IV. Minimal ADC showed the largest AUC in group 1 and group 2, and the second largest parameter was the ratio of minimal ADC (rmADC). In groups 3, 4, 5, and 6, the largest AUC was rmADC.

0.20 ± 0.09) in group 1 (both $P = .004$) (Fig 1). In receiver operating characteristic curve analysis, when the cutoffs were, respectively, 0.18 and 0.25 (Table 2), the maximal FA and rmFA had the same sensitivity (90.90%), specificity (96%), and area under the curve (AUC) (0.92) (Table 2 and Fig 2). Regarding minimal ADC and rmADC, the values ($1.02 \pm 0.29 \times 10^{-3}$ mm^2/s and 1.42 ± 0.43) in group 2 were lower than those ($1.39 \pm 0.34 \times 10^{-3}$ mm^2/s and 1.95 ± 0.43) in group 1 (both $P < .001$) (Figs 1 and 3). When the cutoff values were, respectively, 1.07×10^{-3} mm^2/s and 1.47 (Fig 2), the sensitivity of both parameters was 100%, and specificities and AUC were, respectively, 90.90%, 81.80%, and 0.94, 0.93 (Table 2).

Group 3 and Group 4

Two cases in group 4 were recurrent glioma. The differences in age and sex between groups 3 and 4 were not statistically significant. The maximal FA value (0.32 ± 0.13) and rmFA (0.45 ± 0.18) in group 4 were higher than those (0.17 ± 0.10 and 0.23 ± 0.13) in group 3 ($P = .004$ and 0.003, respectively) (Figs 1 and 4). When the cutoffs were, respectively, 0.27 and 0.37, the AUC of the rmFA (0.82) was larger than that of maximal FA (0.80) (Fig 2). Regarding minimal ADC value and rmADC value, the values ($0.86 \pm 0.21 \times 10^{-3}$ mm^2/s and 1.19 ± 0.30) in group 4 were lower than those ($1.08 \pm 0.15 \times 10^{-3}$ mm^2/s and 1.53 ± 0.23) in group 3 ($P = .011$ and $P = .006$, respectively) (Figs 1 and 4). The cutoffs for minimal ADC and rmADC were 0.99×10^{-3} mm^2/s and 1.31 (Table 2), respectively. The AUC of rmADC (0.83) was larger than that of minimal ADC (0.76) (Fig 2).

Group 5 and Group 6

In group 5 and group 6, the differences in age and sex were statistically significant. In group 5, the patients were younger than those in group 6, and male subjects were more common in group 5 (8 male to 2 female subjects). There was no statistical significance for maximal FA value or rmFA (Figs 1 and 5). Regarding minimal ADC value and rmADC value, the values ($0.74 \pm 0.11 \times 10^{-3}$ mm^2/s and 0.99 ± 0.13) in group 5 were lower than those ($0.85 \pm 0.20 \times 10^{-3}$ mm^2/s and 1.17 ± 0.26) in group 6 ($P = .018$ and $P = .004$, respectively) (Figs 1 and 5). The cutoffs for minimal ADC and rmADC were 0.81×10^{-3} mm^2/s and 1.10 with the AUC equal to 0.66 and 0.70, respectively (Table 2 and Fig 2).

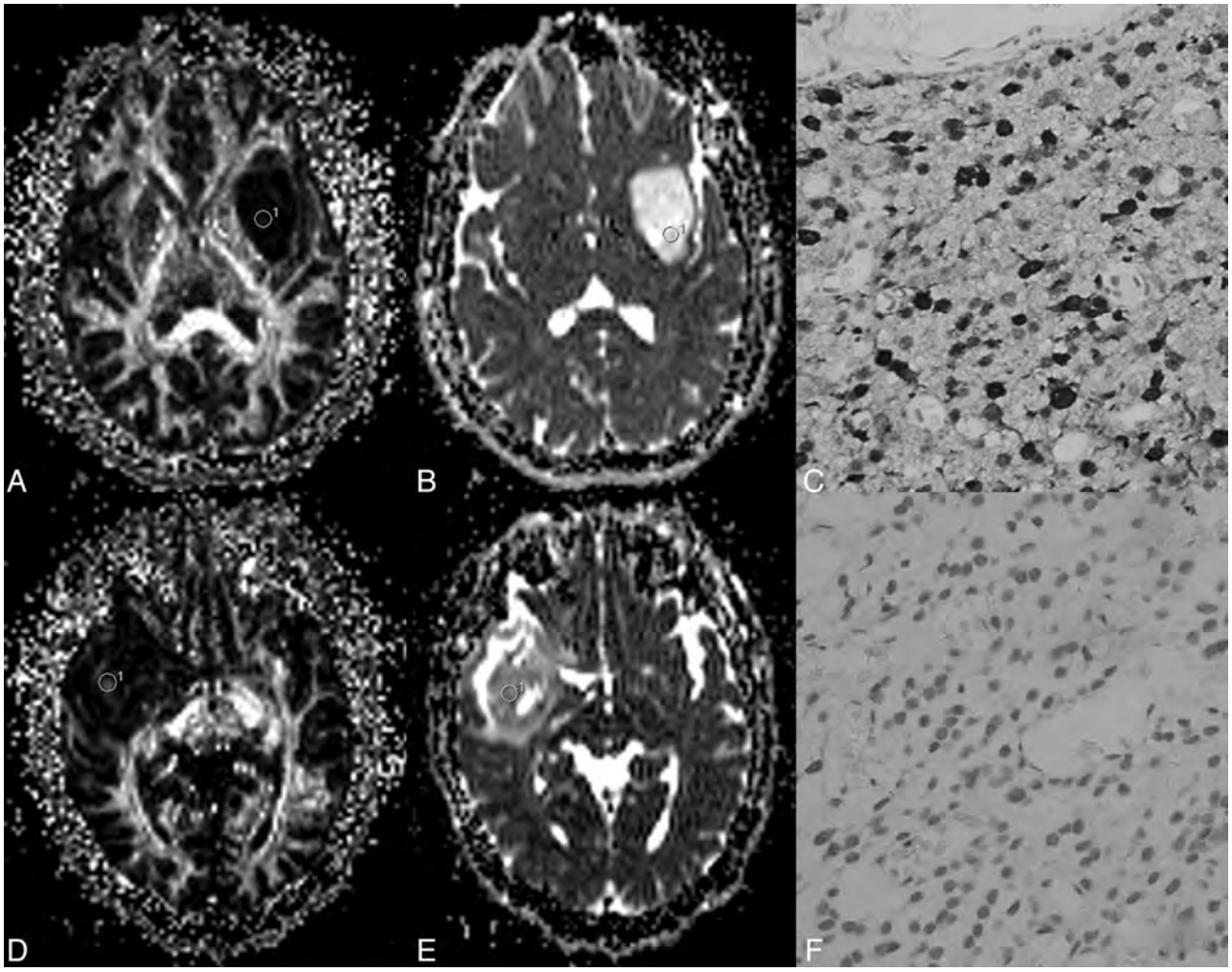

FIG 3. *A–C*, A 43-year-old man with a grade II astrocytoma and *IDH1* R132H antibody examination expressed positively. *D–F*, A 28-year-old woman with a grade II astrocytoma and *IDH1* R132H expressed negatively. In *A*, the fractional anisotropy gray-scale mapping shows a homogeneous low signal; in *D*, a heterogeneous image is shown with a dotted high signal. The signal of ADC mapping in *B* was higher than that in *E*. *C* shows diffuse positivity on immunochemistry; *F* shows negativity on immunochemistry.

Other imaging parameters, including peritumoral FA, ratio of peritumoral FA, contralateral FA, peritumoral ADC, ratio of peritumoral ADC, and contralateral ADC, had no statistical differences between 2 groups with the same WHO grades.

DISCUSSION

Several studies have suggested that gene expression might be a better predictor of key outcomes than histologic classification.[20] Thus, noninvasively detecting the genetic characteristics before surgery is important for predicting the outcome and choosing the best therapy. In the current study, we suggested that DTI could be a useful tool for detecting *IDH1* R132H mutation in astrogliomas, and, on the basis of receiver operating characteristic curve analysis, we believe that rmADC is the best metric for detecting *IDH1* R132H mutation in astrogliomas.

Diffusion imaging is a method that provides direct insight into the microscopic physical properties of tissues[21]; it has the ability to detect the genetic characteristics of gliomas. Jenkinson et al[22] reported that tumors with intact 1p/19q had higher maximum ADC value on DWI. Khayal et al[15] reported that ADC determined from DTI showed promising value for distinguishing oligoastrocytomas with codeletions in chromosomes 1p and 19q from those with intact 1p/19q chromosomes.

In the present study, we investigated the possibility that ADC and FA from DTI might be used to distinguish astrogliomas with *IDH1* R132H mutation from those without mutation. In grade II tumors, minimal ADC had the largest AUC, and the second was rmADC. In grade III and grade IV tumors, rmADC had the largest AUC in the ROC analysis. Thus, we believe that rmADC is the best metric for detecting *IDH1* R132H mutation, regardless of the grades. In *IDH1* R132H–mutant astrogliomas, maximal FA and rmFA showed an increasing trend from grade II to grade IV, and the minimal ADC and rmADC presented a decreasing tendency. However, this tendency was not so distinct in *IDH1* wild-type astrogliomas.

The role of *IDH1* R132H mutation in tumorigenic processes of glioma remains unclear. The FA and ADC values are largely affected by cellularity and/or vascularity.[21-24] Zhao et al[25] showed that *IDH1* appears to function as a tumor suppressor that when mutationally inactivated, contributes to tumorigenesis partially through induction of the HIF-1 pathway. HIF-1α promotes angiogenesis. This may be one of the reasons for higher FA values

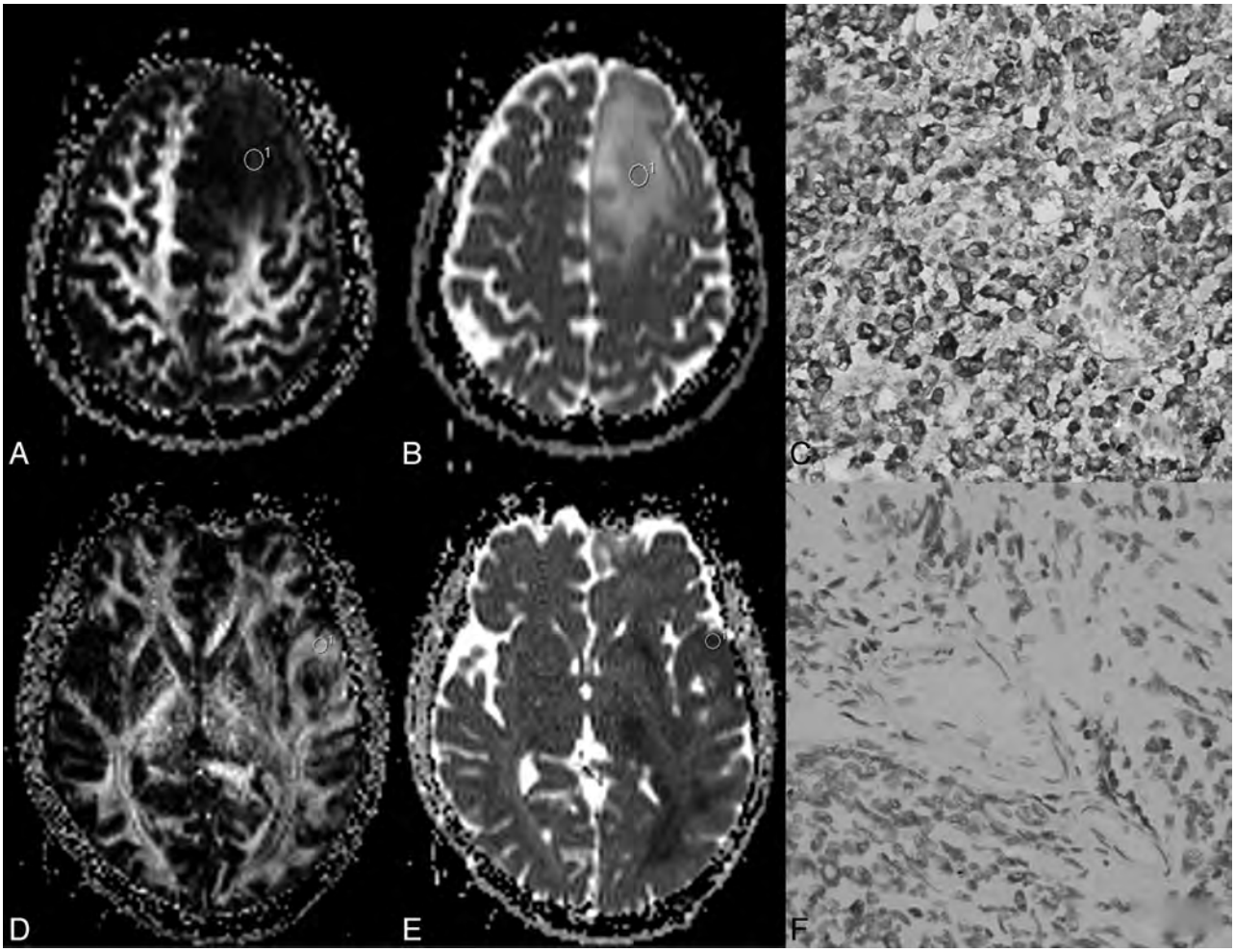

FIG 4. *A–C*, A 35-year-old woman with a grade III anaplastic astrocytoma and *IDH1* R132H antibody examination expressed positively. *D–F*, A 17-year-old young man with grade III anaplastic astrocytoma and *IDH1* R132H antibody examination expressed negatively. In *A*, fractional anisotropy gray-scale mapping showed a heterogeneous low signal with some iso- and hyper-signals; in *D*, a high signal was seen, except for the middle necrosis area. The signal of ADC mapping in *B* is higher than that in *E*. *C* and *F*, Immunochemistry results are shown.

and lower ADC values in the wild-type group than the mutation group in grade II and III tumors. According to our results, we suggest that future studies should be performed to observe the differences in cellularity and angiogenesis between astrogliomas with and without *IDH1* R132H mutation.

Furthermore, it is unusual that neither maximal FA nor rmFA demonstrated statistically significant differences in grade IV tumors because they were in grade II and grade III astrogliomas. The minimal ADC and rmADC values in group 5 were less than those in group 6. The sensitivity and specificity of minimal ADC and rmADC were less in grade IV glioblastoma. These phenomena might have 2 reasons. One is that the tumorigenesis in glioblastoma multiforme is a complicated polygene-related process. Many studies have reported that secondary glioblastomas had different subsets of genetic abnormalities from primary glioblastomas.[3] Even in primary glioblastoma, there are different genes taking part in tumorigenesis. In the present study, grade IV tumors mostly consisted of both primary and secondary glioblastomas, and *IDH1* R132H was the only analyzed genetic mutation type. Moreover, *IDH* mutations are considered as early events in astrocytoma tumorigenesis.[26] Therefore, we suggest that the prevalence and role of *IDH1* mutations in different grades of astrogliomas result in these phenomena. The small sample size in group 5 might be another reason for these findings.

In some studies, mean FA and ADC have been measured to grade gliomas. However, it is well known that diffuse infiltrating astrocytomas have different grades within the same tumor.[27] If the diffusion tensor metrics are calculated from whole tumor, there is a theoretic possibility of missing the small foci of high-grade tumors within otherwise low-grade tumors.[28] If mean FA and ADC were measured in any focal area within tumors, they could not represent the cellular attenuation or the arrangement of cells for the entire tumors. Such a mistake would therefore be magnified. In the present study, maximal FA and minimal ADC were used as diffusion tensor metrics. This method avoided the aforementioned error. In addition, maximal FA and minimal ADC could better reflect the difference between the *IDH1*-R132H–mutant and nonmutant groups. This also explains why the maximal FA value in the current study was a little greater than the mean FA values reported in the literature.[23,29-31]

Currently, immunohistochemical analysis and gene sequencing are the main available methods for detecting *IDH* mutations

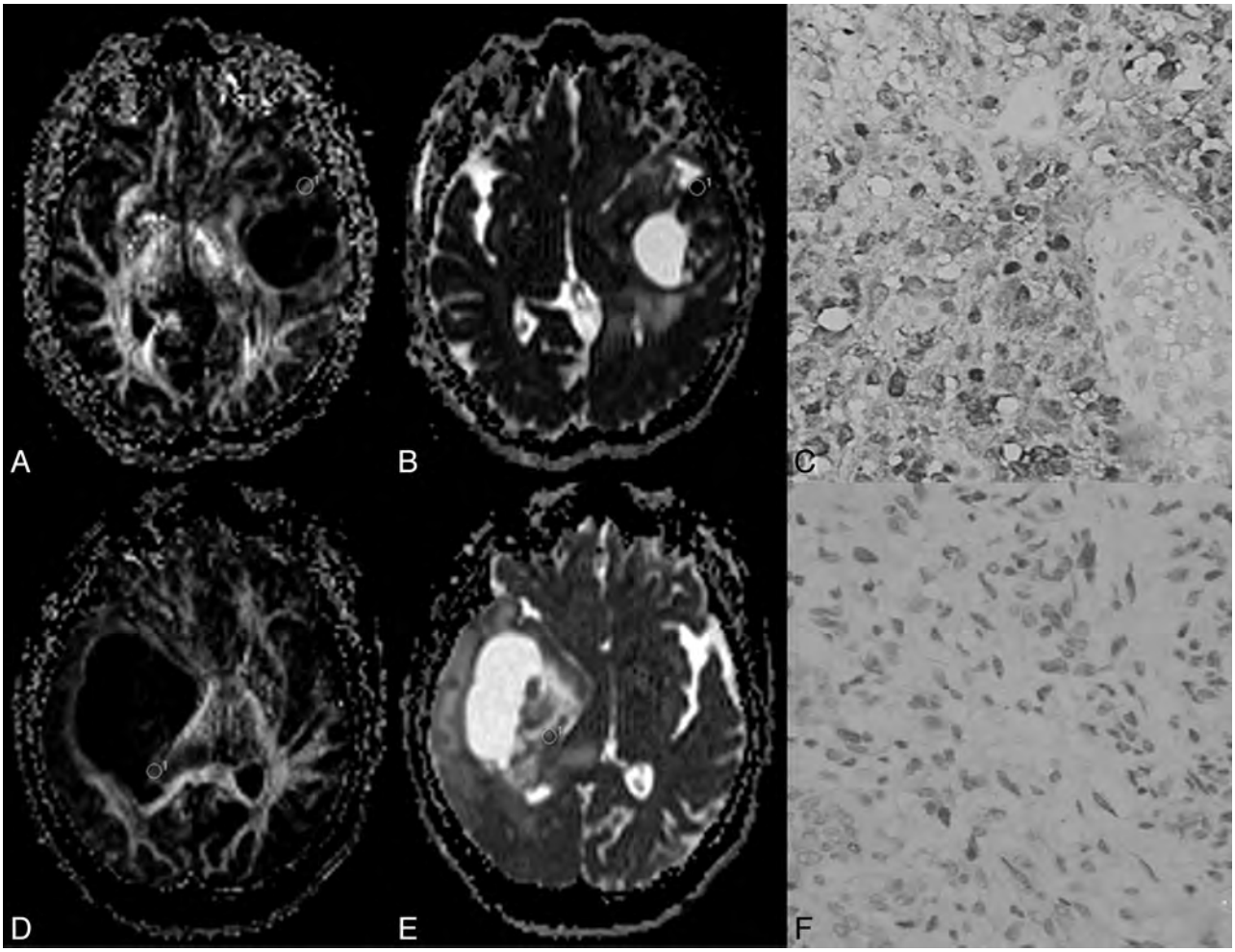

FIG 5. *A–C*, A 33-year-old woman with a grade IV primary glioblastoma and *IDH1* R132H antibody examination expressed positively. *D–F*, A 48-year-old man with a grade IV primary glioblastoma and *IDH1* R132H antibody examination expressed negatively. In *A* and *D*, fractional anisotropy mappings show heterogeneous images with scattered high signals. The signal of ADC mapping in *B* is lower than that in *E*. Immunohistochemistry results of these patients are shown.

in gliomas. Gene sequencing is considered the reference standard for detecting all types of *IDH* mutations.[32] A monoclonal antibody, H09, has been developed for detecting the most common mutation, *IDH1* R132H. The sensitivity and specificity of this antibody for detecting *IDH1* R132H reportedly approached 100%.[33] The accuracy of gene sequencing could be affected by highly contaminated tumor samples or by the quantity of tumor cell in the sample. Capper et al[33] reported that *IDH1* sequencing missed 8 of 112 cases of *IDH1* R132H mutation in the first round of sequencing. The predominant amino acid sequence alteration in *IDH1* mutation was R132H, accounting for 92.7% of the detected mutations in 1010 cases of WHO grade II and III gliomas, whereas *IDH2* mutations were much less common.[34] Hartmann et al[34] reported that astrocytoma grades II and III carried only 0.9% *IDH2* mutations. Because of the high accuracy of monoclonal antibody H09 and the lower frequency of other *IDH1* mutation types and *IDH2* mutations in glioma, we chose immunochemical examination as the reference standard for detecting *IDH1* R132H mutation.

There were some important limitations to our study. Our study classified astrogliomas from grade II to grade IV, according to pathologic results. The data show some overlap between group 2 and group 3 and between group 4 and group 5. Therefore, imaging techniques with high accuracy to grade astrogliomas must be combined with this technique in the future. Although the patients with brain stem or thalamic astrogliomas would benefit most from *IDH1* status by avoiding biopsy, all the cases included in the current study were lobar tumors. Therefore, the results in this study should be applied carefully to particular location astrogliomas. Because this was a retrospective study, there was no precise point-to-point biopsy guided by maximal FA and minimal ADC information. Thus, the correlation of maximal FA and minimal ADC with histopathologic change could not be assessed, which is especially important for the evaluation of grades III and IV tumors because these tumors display more heterogeneity. Future prospective studies with point-to-point biopsy design will be necessary to verify our findings of optimal parameters for accurate preoperative detection of *IDH1* R132H mutation.

CONCLUSIONS

We demonstrate that DTI metrics, including maximal FA, rmFA, minimal ADC, and rmADC from the tumor body have potential ability to distinguish astrogliomas with *IDH1* R132H mutation

from those without mutation in grade II and grade III tumors. Minimal ADC and rmADC in grade IV tumors are helpful to differentiate glioblastomas with *IDH1* R132H mutation from those without mutation. The rmADC is the best metric for the noninvasive detection of such mutation across different tumor grades. Nonetheless, these results are preliminary, and further investigation with histologic validation will be necessary to prove the difference between astrogliomas with *IDH1* R132H mutation and those without mutation.

REFERENCES

1. Parsons DW, Jones S, Zhang X, et al. **An integrated genomic analysis of human glioblastoma multiforme.** *Science* 2008;321:1807–12
2. Yan H, Parsons DW, Jin G, et al. **IDH1 and IDH2 mutations in gliomas.** *N Engl J Med* 2009;360:765–73
3. Nikiforova MN, Hamilton RL. **Molecular diagnostics of gliomas.** *Arch Pathol Lab Med* 2011;135:558–68
4. Horbinski C, Kofler J, Kelly LM, et al. **Diagnostic use of IDH1/2 mutation analysis in routine clinical testing of formalin-fixed, paraffin-embedded glioma tissues.** *J Neuropathol Exp Neurol* 2009;68:1319–25
5. Capper D, Sahm F, Hartmann C, et al. **Application of mutant IDH1 antibody to differentiate diffuse glioma from nonneoplastic central nervous system lesions and therapy-induced changes.** *Am J Surg Pathol* 2010;34:1199–204
6. Juratli TA, Kirsch M, Robel K, et al. **IDH mutations as an early and consistent marker in low-grade astrocytomas WHO grade II and their consecutive secondary high-grade gliomas.** *NeuroOncol* 2012;108:403–10
7. SongTao Q, Lei Y, Si G, et al. **IDH mutations predict longer survival and response to temozolomide in secondary glioblastoma.** *Cancer Sci* 2012;103:269–73
8. Loussouarn D, Le Loupp AG, Frenel JS, et al. **Comparison of immunohistochemistry, DNA sequencing and allele-specific PCR for the detection of IDH1 mutations in gliomas.** *Int J Oncol* 2012;40:2058–62
9. Metellus P, Coulibaly B, Colin C, et al. **Absence of IDH mutation identifies a novel radiologic and molecular subtype of WHO grade II gliomas with dismal prognosis.** *Acta Neuropathol* 2010;120:719–29
10. Dang L, White DW, Gross S, et al. **Cancer-associated IDH1 mutations produce 2-hydroxyglutarate.** *Nature* 2009;462:739–44
11. Ward PS, Patel J, Wise DR, et al. **The common feature of leukemia-associated IDH1 and IDH2 mutations is a neomorphic enzyme activity converting alpha-ketoglutarate to 2-hydroxyglutarate.** *Cancer Cell* 2010;17:225–34
12. Capper D, Simon M, Langhans CD, et al. **2-Hydroxyglutarate concentration in serum from patients with gliomas does not correlate with IDH1/2 mutation status or tumor size.** *Int J Cancer* 2012;131:766–68
13. Choi C, Ganji SK, DeBerardinis RJ, et al. **2-hydroxyglutarate detection by magnetic resonance spectroscopy in IDH-mutated patients with gliomas.** *Nat Med* 2012;18:624–29
14. Pope WB, Prins RM, Albert Thomas M, et al. **Non-invasive detection of 2-hydroxyglutarate and other metabolites in IDH1 mutant glioma patients using magnetic resonance spectroscopy.** *J NeuroOncol* 2012;107:197–205
15. Khayal IS, Vandenberg SR, Smith KJ, et al. **MRI apparent diffusion coefficient reflects histopathologic subtype, axonal disruption, and tumor fraction in diffuse-type grade II gliomas.** *NeuroOncol* 2011;13:1192–201
16. Louis DN, Ohgaki H, Wiestler OD, et al. **The 2007 WHO classification of tumours of the central nervous system.** *Acta Neuropathol* 2007;114:97–109
17. Takano S, Tian W, Matsuda M, et al. **Detection of IDH1 mutation in human gliomas: comparison of immunohistochemistry and sequencing.** *Brain Tumor Pathol* 2011;28:115–23
18. Khalid L, Carone M, Dumrongpisutikul N, et al. **Imaging characteristics of oligodendrogliomas that predict grade.** *AJNR Am J Neuroradiol* 2012;33:852–57
19. Brander A, Kataja A, Saastamoinen A, et al. **Diffusion tensor imaging of the brain in a healthy adult population: normative values and measurement reproducibility at 3 T and 1.5 T.** *Acta Radiol* 2010;51:800–07
20. Nutt CL, Mani DR, Betensky RA, et al. **Gene expression-based classification of malignant gliomas correlates better with survival than histological classification.** *Cancer Res* 2003;63:1602–07
21. Le Bihan D. **Looking into the functional architecture of the brain with diffusion MRI.** *Nat Rev Neurosci* 2003;4:469–80
22. Jenkinson MD, Smith TS, Brodbelt AR, et al. **Apparent diffusion coefficients in oligodendroglial tumors characterized by genotype.** *J Magn Reson Imaging* 2007;26:1405–12
23. Beppu T, Inoue T, Shibata Y, et al. **Measurement of fractional anisotropy using diffusion tensor MRI in supratentorial astrocytic tumors.** *J NeuroOncol* 2003;63:109–16
24. Mikkelsen T. **Predicting survival in glioblastomas using diffusion tensor imaging metrics.** *J Magn Reson Imaging* 2010;32:788–95
25. Zhao S, Lin Y, Xu W, et al. **Glioma-derived mutations in IDH1 dominantly inhibit IDH1 catalytic activity and induce HIF-1alpha.** *Science* 2009;324:261–65
26. Liu Y, Jiang W, Liu J, et al. **IDH1 mutations inhibit multiple α-ketoglutarate-dependent dioxygenase activities in astroglioma.** *J Neurooncol* 2012;109:253–60
27. Graham DI, Lantos PL. *Greenfield's Neuropathology*. London: Hodder Arnold Publisher; 2002:767–1052
28. Jolapara M, Patro SN, Kesavadas C, et al. **Can diffusion tensor metrics help in preoperative grading of diffusely infiltrating astrocytomas? A retrospective study of 36 cases.** *Neuroradiology* 2011;53:63–68
29. Byrnes TJ, Barrick TR, Bell BA, et al. **Diffusion tensor imaging discriminates between glioblastoma and cerebral metastases in vivo.** *NMR Biomed.* 2011;24:54–60
30. Jakab A, Molnár P, Emri M, et al. **Glioma grade assessment by using histogram analysis of diffusion tensor imaging-derived maps.** *Neuroradiology* 2011;53:483–91
31. Zou QG, Xu HB, Liu F, et al. **In the assessment of supratentorial glioma grade: the combined role of multivoxel proton MR spectroscopy and diffusion tensor imaging.** *Clin Radiol* 2011;66:953–60
32. Gupta R, Webb-Myers R, Flanagan S, et al. **Isocitrate dehydrogenase mutations in diffuse gliomas: clinical and aetiological implications.** *J Clin Pathol* 2011;64:835–44
33. Capper D, Weissert S, Balss J, et al. **Characterization of R132H mutation-specific IDH1 antibody binding in brain tumors.** *Brain Pathol* 2010;20:245–54
34. Hartmann C, Meyer J, Balss J, et al. **Type and frequency of IDH1 and IDH2 mutations are related to astrocytic and oligodendroglial differentiation and age: a study of 1,010 diffuse gliomas.** *Acta Neuropathol* 2009;118:469–74

Diagnostic Utility of Diffusion Tensor Imaging in Differentiating Glioblastomas from Brain Metastases

S. Wang, S.J. Kim, H. Poptani, J.H. Woo, S. Mohan, R. Jin, M.R. Voluck, D.M. O'Rourke, R.L. Wolf, E.R. Melhem, and S. Kim

ABSTRACT

BACKGROUND AND PURPOSE: Differentiation of glioblastomas and solitary brain metastases is an important clinical problem because the treatment strategy can differ significantly. The purpose of this study was to investigate the potential added value of DTI metrics in differentiating glioblastomas from brain metastases.

MATERIALS AND METHODS: One hundred twenty-eight patients with glioblastomas and 93 with brain metastases were retrospectively identified. Fractional anisotropy and mean diffusivity values were measured from the enhancing and peritumoral regions of the tumor. Two experienced neuroradiologists independently rated all cases by using conventional MR imaging and DTI. The diagnostic performances of the 2 raters and a DTI-based model were assessed individually and combined.

RESULTS: The fractional anisotropy values from the enhancing region of glioblastomas were significantly higher than those of brain metastases ($P < .01$). There was no difference in mean diffusivity between the 2 tumor types. A classification model based on fractional anisotropy and mean diffusivity from the enhancing regions differentiated glioblastomas from brain metastases with an area under the receiver operating characteristic curve of 0.86, close to those obtained by 2 neuroradiologists using routine clinical images and DTI parameter maps (area under the curve = 0.90 and 0.85). The areas under the curve of the 2 radiologists were further improved to 0.96 and 0.93 by the addition of the DTI classification model.

CONCLUSIONS: Classification models based on fractional anisotropy and mean diffusivity from the enhancing regions of the tumor can improve diagnostic performance in differentiating glioblastomas from brain metastases.

ABBREVIATIONS: AUC = area under the curve; ER = enhancing region; FA = fractional anisotropy; IPR = immediate peritumoral region; LRM = logistic regression model; MD = mean diffusivity

Differentiation of glioblastomas and solitary brain metastases is an important clinical problem because the treatment strategy can significantly differ depending on the tumor type.[1,2] In some cases, clinical history and/or multiplicity of enhancing brain lesions makes the diagnosis of brain metastases relatively straightforward. However, a solitary brain metastasis on MR imaging can have a nonspecific appearance. Similarly confounding the issue is the fact that glioblastomas can also occasionally present as multiple enhancing lesions. Moreover, although a glioblastoma typically presents as a solitary mass, a solitary brain metastasis may be the first manifestation of disease in approximately 30% of patients with systemic cancer.[3] Hence, accurate distinction between glioblastomas and brain metastases can be challenging, often necessitating an invasive surgical biopsy for a definitive diagnosis.

DTI has been used to differentiate glioblastomas from brain metastases, but with conflicting results. Some reports have suggested that mean diffusivity (MD)[4-6] is helpful for the differentiation, while others indicated the limited use of MD in the differentiation of neoplasms.[7-9] Wang et al[10] and Reiche et al[11] reported lower fractional anisotropy (FA) from the enhancing regions (ERs) of glioblastomas compared with brain metastases. In contrast, another study reported that glioblastomas have higher FA in the enhancing regions than metastases.[12] The potential reasons for these conflicting results may include differ-

Received July 8, 2013; accepted after revision September 13.

From the Departments of Radiology (S.W., H.P., J.H.W., S.M., M.R.V., R.L.W.) and Neurosurgery (D.M.O.), Hospital of the University of Pennsylvania, Philadelphia, Pennsylvania; Department of Radiology (S.J.K.), University of Ulsan, Asan Medical Center, Seoul, Republic of Korea; Medical Data Research Center (R.J.), Providence Health and Services, Portland, Oregon; Department of Diagnostic Radiology and Nuclear Medicine (E.R.M.), University of Maryland Medical Center, Baltimore, Maryland; and Department of Radiology (S.K.), New York University School of Medicine, New York, New York.

Paper previously presented in part at: Annual Meetings of the International Society for Magnetic Resonance in Medicine, May 5–11, 2012; Melbourne, Victoria, Australia; and April 20–26, 2013; Salt Lake City, Utah.

Please address correspondence to Sumei Wang, MD, Department of Radiology, Division of Neuroradiology, Hospital of the University of Pennsylvania, 219 Dulles Building, 3400 Spruce St, Philadelphia, PA 19104; e-mail: Sumei.Wang@uphs.upenn.edu

http://dx.doi.org/10.3174/ajnr.A3871

ences in analysis methods, particularly in defining the region of interest, as well as the relatively small size of cohorts used in individual studies ($n = 24–66$).[4,5,7,10,13] Hence, a primary objective of this study was to investigate the DTI characteristics of glioblastomas and brain metastases in a substantially larger cohort of patients, in order to determine whether they may have diagnostic utility.

Restricted water diffusion in solid tumors has been reported by many groups.[7,14-17] It is generally assumed that a solid tumor does not have any microstructural orientation by itself and its growth induces structural disorder in the tissue, which leads to decreased FA.[18] However, although the association between FA and tumor cellularity has been studied, the relationship remains unclear because both positive[12,14,19] and negative[16] correlations have been reported. Our previous study[12] showing higher FA in glioblastomas than in brain metastases also found a negative linear trend between FA and MD in glioblastomas, which was not seen in metastases, perhaps indicating a tumor-dependent relationship between these 2 parameters. While promising results with DTI have been published in the diagnosis of brain tumors, to date, its clinical value in improving the diagnostic accuracy of radiologists has not been evaluated.

Hence, the objectives of the present study were to investigate the potential of DTI in differentiation of glioblastomas from solitary brain metastases in a relatively large cohort of 221 patients and to compare its diagnostic accuracy in comparison with that of 2 experienced neuroradiologists.

MATERIALS AND METHODS

Patients

Patients with solitary enhancing lesions ($n = 221$), based on contrast-enhanced T1-weighted images, were retrospectively recruited from our institutional data base between June 2006 and February 2012. Patients with nonenhancing or multiple enhancing tumors or a clinical history of any prior therapy to the brain were not included. The study was approved by the institutional review board and was compliant with the Health Insurance Portability and Accountability Act.

Histopathologic diagnosis of the tumor was available for all patients through surgical resection or biopsy. The final diagnoses included 128 glioblastomas (78 men, 50 women; age, 60.5 ± 12.3 years; range, 24–90 years) and 93 brain metastases (46 men, 47 women; age, 58.8 ± 11.6 years; range, 44–88 years). Of the 93 metastases, the primary sites for cancer included lung ($n = 56$), breast ($n = 16$), skin ($n = 8$), colon ($n = 3$), renal ($n = 2$), neck ($n = 1$), arm ($n = 1$), parotid ($n = 1$), esophagus ($n = 2$), thyroid ($n = 1$), peritoneum ($n = 1$), and endometrium ($n = 1$).

Data Acquisition

MR imaging studies were performed on a Tim Trio 3T whole-body scanner (Siemens, Erlangen, Germany) by using a 12-channel phased-array head coil. Routine MR imaging pulse sequences included axial T1-weighted 3D MPRAGE (TR/TE/TI = 1760/3.1/950 ms, matrix size = 192 × 256, section thickness = 1 mm) and axial FLAIR (TR/TE/TI = 9420/141/2500 ms, section thickness = 3 mm). DTI data were acquired by using a single-shot spin-echo EPI sequence with parallel imaging by using generalized autocalibrating partially parallel acquisition and an acceleration factor of 2. The DTI data from 55 patients (40 glioblastomas, 15 metastases) were acquired by using 12 diffusion-weighting directions (TR/TE = 4900/83 ms, NEX = 6); and in the remaining 166 patients, DTI data were acquired with 30 directions (TR/TE = 5000/86 ms, NEX = 3). Other sequence parameters were as follows: FOV = 22 × 22 cm^2, b=0, 1000 s/mm^2, section thickness = 3 mm, total scanning time = 8 minutes. All our 12- and 30-direction DTI data were acquired by using the same imaging parameters with the same scanning times at the same scanner. On the basis of previous studies,[20-22] we assume that there is no significant difference in mean or median MD and FA values from the 12- and 30-direction DTI datasets, particularly when FA is mostly <0.3 as in the solid tumors included in this study[21] and we combined the data from all the patients in this study.

Image Processing

The diffusion-weighted images were coregistered to the non-diffusion-weighted (b=0) images by using the methods described in another work.[12] The corrected raw images were combined to estimate rotationally invariant DTI parameter maps, including FA and MD, by using in-house software.[12,23,24]

The DTI parameter maps and FLAIR images were then coregistered to contrast-enhanced T1-weighted images. A semiautomatic segmentation approach was used to subdivide each lesion into 3 regions: enhancing region, immediate peritumoral region (IPR), and distant peritumoral region by using contrast-enhanced T1 and FLAIR images.[12] ER was the region with enhancement higher than the mean +3 SDs of the signal intensity from the WM. IPR was chosen as a 4-mm-wide band around the enhancing region. The remaining region of FLAIR abnormality, outside of the IPR, was the distant peritumoral region.[12,23,25] The median FA and MD values were measured from the 3 regions. Data analysis tools, including image coregistration and segmentation, were implemented by using IDL (Exelis Visual Information Solutions, Boulder, Colorado).

Data Analysis

A Mann-Whitney U test was used for the difference in the median MD and FA values between glioblastomas and brain metastases from the 3 regions. A P value < .05 was considered significant. Linear regression analysis was used to investigate the association between 2 continuous measures, FA and MD. A multivariate logistic regression analysis was used to determine the best classification model of DTI parameters, namely the logistic regression model (LRM). Bootstrapping validation was applied to estimate the accuracy of the LRM. Specifically, 70% of the full dataset was randomly selected with replacement and was used as an independent validation set; this process was repeated 500 times.[26] Means and SDs of the area under the receiver operating characteristic curves (AUCs) were computed. The cutoff lines for separating glioblastomas from metastases were determined by maximizing the sum of specificity and sensitivity (ie, Youden index).

Two neuroradiologists with 10 and 9 years of experience independently reviewed the cases on the basis of contrast-enhanced

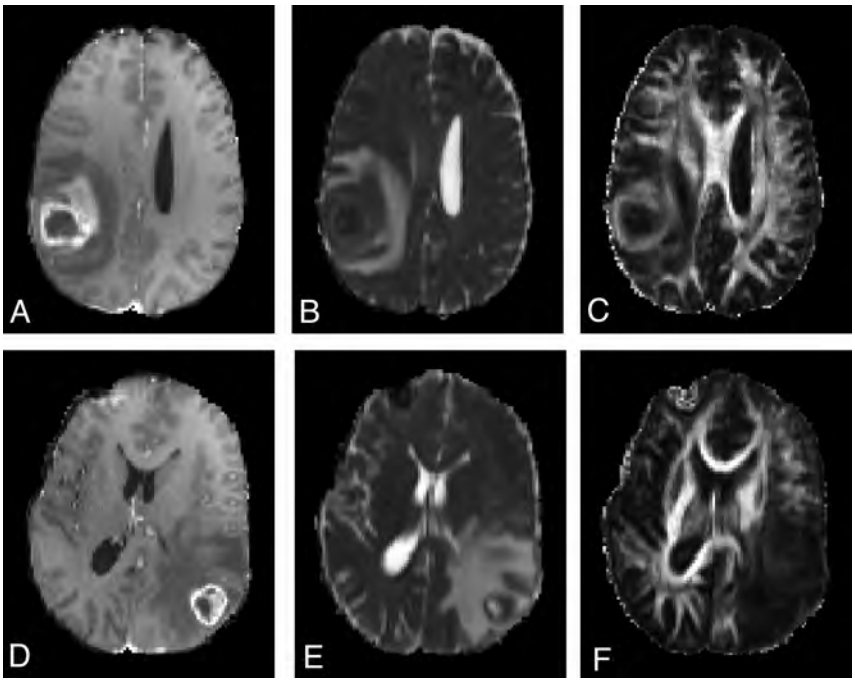

FIG 1. Comparison of imaging features between glioblastomas (*A–C*) and brain metastases (*D–F*). Both show ring enhancement and extensive edema on axial contrast-enhanced TI-weighted images (*A* and *D*) and restricted diffusion of the enhancing part on MD maps (*B* and *E*). However, for the FA map, the glioblastoma case demonstrates high FA values from the enhancing region. The high FA starts from the enhancing region and extends to the immediate peritumoral region, making an FA rim.

T1, FLAIR, DWI, FA, and MD maps. The radiologists were asked to rate their level of confidence for each case, whether the tumor was metastasis or glioblastoma. A rating was classified into 5 scales based on the following 5 confidence levels: level 1, 90% metastasis; level 2, 70% metastasis; level 3, 50%; level 4, 70% glioblastoma; and level 5, 90% glioblastoma. The diagnostic performances of the 2 raters and LRM were evaluated by using the receiver operating characteristic analysis curves. The AUCs were compared by using the method of DeLong et al.[27] The weighted κ was used to assess the interobserver agreement between the 2 raters and LRM. All data analysis was conducted by using the Statistical Package for the Social Sciences for Windows, Version 15.0 (IBM, Armonk, New York). R software (Version 2.15.0; http://www.r-project.org) was used for the bootstrapping validation.

RESULTS

Comparison of Imaging Parameters

Representative MR images of patients with glioblastoma and metastasis are shown in Fig 1. The MD maps in both cases showed similar levels of restricted diffusion in the enhancing parts. In contrast, the FA maps showed that the glioblastoma had higher FA than the brain metastasis. The high FA rim extended to the immediate peritumoral regions in glioblastomas. Similar observation was made with most cases as summarized by the boxplots shown in Fig 2*A*, -*B*. The median FA value of glioblastomas from the ER and IPR was significantly higher than that of brain metastases ($P < .01$). There was no significant difference in the median values of MD from all the regions. None of the parameters showed significant differences from the distant peritumoral regions.

Diffusion Tensor Logistic Regression Model

FA from the ER and IPR and MD from the ER were evaluated for their diagnostic performance by using receiver operating characteristic analysis (Table). The single best predictor for the discrimination is FA from the ER with a sensitivity of 0.80, a specificity of 0.76, and an AUC of 0.84. The logistic regression analysis indicated that the best model included FA and MD from the ER as follows:

$$1)\quad f(MD, FA) = \frac{1}{1 + \exp[-(\beta 0 + \beta 1 MD + \beta 2 FA)]},$$

where $\beta 0 = -7.79$, $\beta 1 = 2.14$, and $\beta 2 = 43.30$. This model was validated by using the bootstrapping procedure described above (repeated 500 times) with a mean AUC of 0.86 and SD of 0.03.

The scatterplots of FA and MD from the ER in Fig 2*C* demonstrate how LRM can have a higher AUC than FA alone, though MD itself is a poor predictor (AUC = 0.50). The cutoff line of LRM shown in Fig 2*C* was slanted and positioned between the linear regression lines for glioblastomas and brain metastases, shown separately in Fig 2*D*, -*E*, respectively. The linear negative regression between FA and MD in the glioblastoma group was significant ($R^2 = 0.26$, $P < .05$).

Comparison between Diffusion Tensor and Raters

The results of diagnostic reading by 2 expert neuroradiologists by using the 5-point rating scale and LRM output are presented as scatterplots in Fig 3*A*, -*B*. If one assumes that the LRM output is equivalent to the reader confidence level, confidence level 1 of the raters (90% metastasis) corresponds to 0–0.2 of the LRM output; confidence level 2, to 0.2–0.4 of the LRM output; and so forth. The weighted κ values between the 2 raters, rater 1 and LRM, and rater 2 and LRM, were 0.63, 0.40. 0.43, respectively, indicating moderate agreement. The receiver operating characteristic analysis curves in Fig 3*C* demonstrate that the diagnostic performances of the 2 raters and LRM are similar; the AUC values were 0.90, 0.85, and 0.86, for rater 1, rater 2, and LRM, respectively. There was a significant difference between the AUCs of rater 1 and rater 2 ($P = .03$).

Figure 3*A*, -*B* indicates that approximately half of the cases had low confidence levels (levels 2–4 for the raters and 0.2–0.8 for the LRM): 43% for rater 1, 56% for rater 2, and 50% for the LRM. Fig 3*D* shows the receiver operating characteristic analysis curves only for the cases with confidence levels between 2 and 4 by both raters ($n = 72$). The AUC of the LRM (0.87) for these challenging cases was higher than those of rater 1 (0.70) and rater 2 (0.64), suggesting that the LRM can be helpful in improving the classification of the cases with low rater confidence levels.

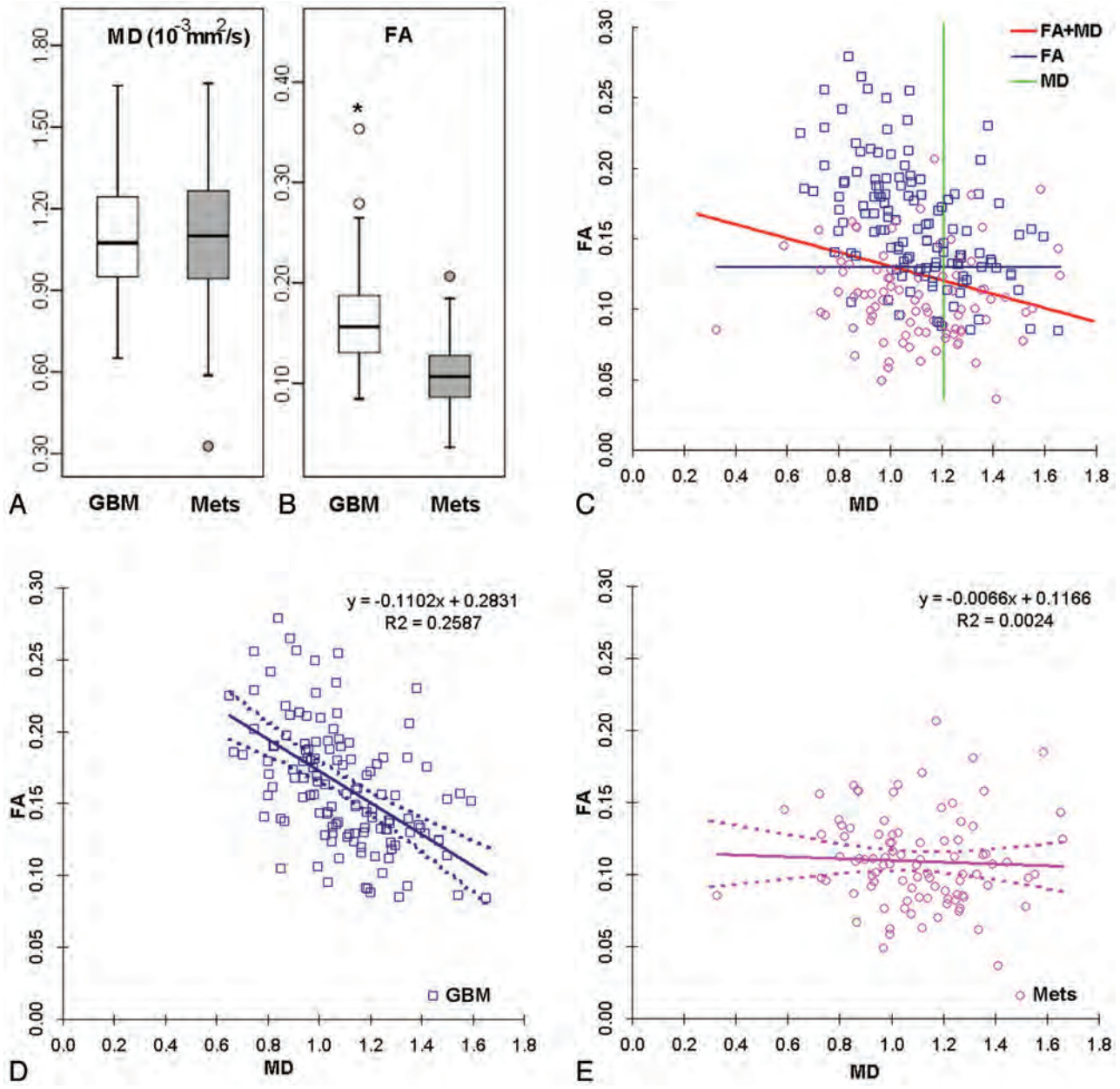

FIG 2. Boxplot of FA and MD from the enhancing region in glioblastomas (white) and brain metastases (gray) (*A* and *B*). The outliers are represented by circles. Asterisks indicate significant differences ($P < .01$). A scatterplot of FA and MD from the enhancing region of glioblastomas (*blue square*) and brain metastases (*purple circle*) (*C*) is shown. The green line represents the cutoff line of MD; the blue line, the cutoff line of FA; and the red line, the cutoff line of the combined model of FA and MD, which can successfully separate the glioblastomas and brain metastases. FA and MD regression lines for glioblastomas (*D*), FA and MD regression lines for brain metastases (*E*), and the dotted line indicate 95% confidence intervals. There is a negative correlation of FA and MD in glioblastomas ($R = 0.51$, $P < .05$).

Diagnostic performance of 2 raters and the logistic regression model of DTI parameters for all the cases

	Sensitivity	Specificity	PPV	NPV	AUC	Cutoff Value
FA_{ER}	0.80	0.76	0.80	0.73	0.84	0.13
MD_{ER} (10^{-3} mm^2/s)	0.73	0.34	0.60	0.47	0.51	1.21
FA_{IPR}	0.65	0.68	0.73	0.58	0.69	0.17
LRM	0.84	0.77	0.83	0.78	0.86	0.50
Rater 1	0.70	0.93	0.75	0.94	0.90	4.5
LRM + rater 1	0.93	0.88	0.92	0.90	0.96	0.54
Rater 2	0.76	0.85	0.94	0.54	0.85	2.5
LRM + rater 2	0.85	0.85	0.88	0.81	0.93	0.54

Note:—PPV indicates positive predictive value; NPV, negative predictive value.

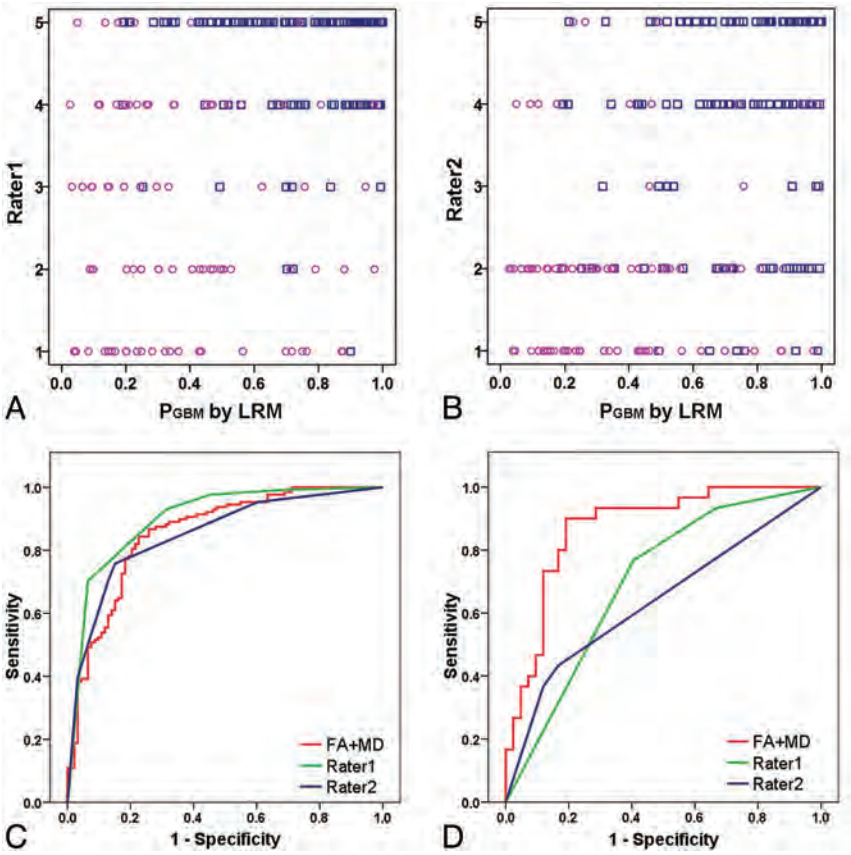

FIG 3. Scatterplot of 2 raters and the logistic regression model for glioblastomas (*blue square*) and brain metastases (*purple circles*) (*A* and *B*). Approximately half of cases were with low confidence levels (levels 2–4 for the raters and 0.2–0.8 for the LRM). P_{GBM} represents the probability, predicted by the model, for glioblastoma (GBM). Receiver operative characteristic curve analysis from 2 raters and the LRM for the whole cases (*C*) and challenging cases for the raters with confidence level of 2–4 (*D*) are shown. The performance of the LRM is close to that of both raters. For challenging cases, the performance of the LRM remains at about the same level as those for all cases.

DTI and Rater Combined Classifier

Figure 4 illustrates the improvement in the diagnostic accuracy of each rater by combining with the LRM. A logistic regression model was generated by using LRM output and rater 1:

$$2) \quad f(Rater1, LRM) = \frac{1}{1 + \exp[-(\beta 0 + \beta 1 Rater\ 1 + \beta 2 LRM)]}$$

where $\beta 0 = -9.54$, $\beta 1 = 1.70$, and $\beta 2 = 6.25$. The scatterplot in Fig 4*A* demonstrates that most of the glioblastomas are above the diagonal line and most of the brain metastases are below the diagonal line. LRM plus rater 1 had an AUC of 0.96 compared with 0.9 by rater 1 alone. We tested the model by using rater 2. Figure 4*B*, -*D* shows that the combined model with LRM plus rater 1 can also improve the results of rater 2. The AUC was 0.93, compared with 0.85 by rater 2 alone. The combined model significantly improved the AUC of both rater 1 ($P < .001$) and rater 2 ($P < .001$). This model can be applied to all raters.

A summary of diagnostic performance of individual readers and combined schemes of DTI parameters, including sensitivity, specificity, positive predictive value, negative predictive value, and AUC, is shown in the Table.

DISCUSSION

In this study, the diagnostic performance of DTI based on FA and MD was compared with those of 2 experienced neuroradiologists. Our results demonstrated that the diagnostic accuracy of the classifier was as good as those of experienced neuroradiologists and that LRM could be used to further improve the diagnostic performance of the readers. Our previous studies in a smaller sample population ($n = 63$) have shown that FA and MD from the enhancing part are very useful for differentiating glioblastomas from brain metastases.[12,23] Results from the present study with a substantially larger sample size ($n = 221$) confirmed that FA and MD from the enhancing part can be used to generate a robust model for the classification between glioblastomas and brain metastases.

Our study demonstrated that FA from the enhancing regions of glioblastomas was significantly higher than that of brain metastases. Toh et al[28,29] reported similar findings and interpreted them as the influence of gliosis surrounding the glioblastomas. We speculate that the high FA in glioblastomas may be due to the orientation of overproduced extracellular matrix.[30,31] The extracellular space and matrix play an important role in tumor growth and infiltration. Glioblastoma cells produce large amounts of tumor-specific extracellular matrix components, which serve as a substrate for adhesion and subsequent migration of the cells through the enlarged extracellular space.[30] These molecules accumulate and are oriented in extracellular matrix,[32] resulting in high anisotropy. Our previous study in meningiomas demonstrated high FA and planar anisotropy coefficient in fibroblastic meningiomas compared with other subtypes.[26] These findings can be explained by the presence of a large amount of collagen in fibroblastic subtypes.[25,33] It has been reported that the structure and orientation of extracellular matrix affect the anisotropy, but not the mean diffusivity[34]; these results are consistent with ours. On the other hand, in brain metastases, neoplasm cells grow into the brain parenchyma in an expansive, noninfiltrating pattern. In contrast to glioblastoma, degradation of the extracellular matrix begins the process of metastasis.[35,36]

We did not observe a significant difference in MD values from the enhancing region between glioblastomas and metastases, indicating a limited sensitivity and specificity of this parameter in tumor differentiation. However, MD was still an important parameter for LRM because FA in glioblastomas varied depending on MD, but did not in metastases. If one assumes that MD reflects

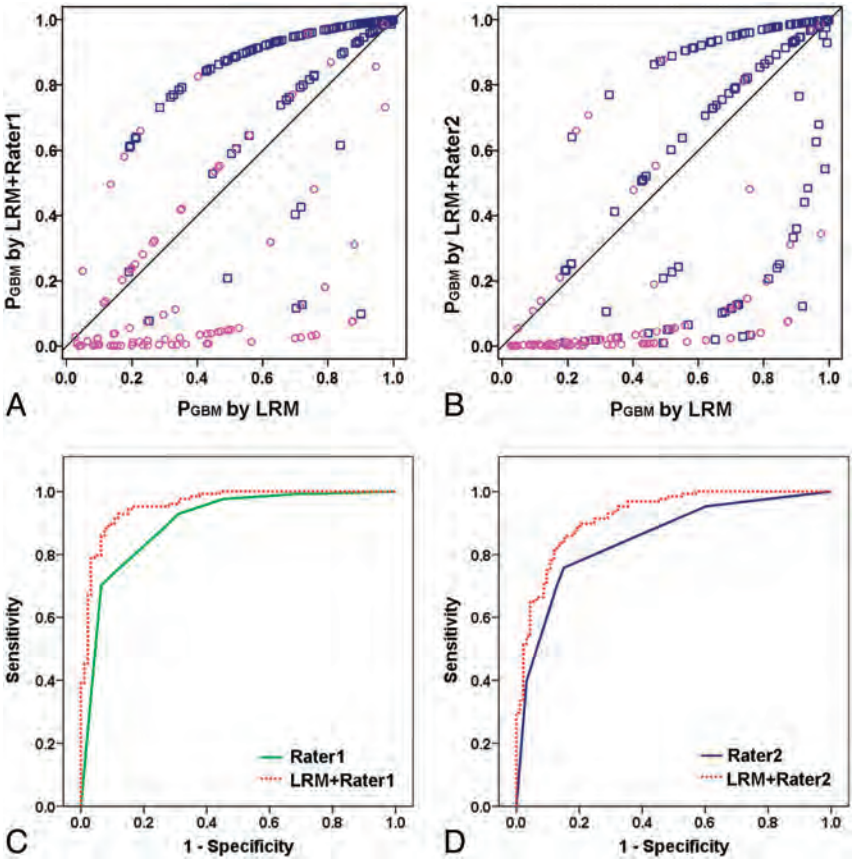

FIG 4. The diagnostic performance of rater 1 improves by combining the DTI logistic regression model (*A* and *C*). Most of the glioblastomas (*blue squares*) are above the diagonal line, and most of the brain metastases (*purple circles*) are below the diagonal line. P_{GBM} represents the probability, predicted by the model, for glioblastoma (GBM). AUC improves from 0.90 to 0.960 for rater 1. The combined model with LRM plus rater 1 can also improve the results of rater 2 (*B* and *D*). AUC improves from 0.85 to 0.93 for rater 2.

cellularity, our findings from in vivo data substantiate previous reports on the positive correlation between FA and tumor cellularity.[12,14,19] Furthermore, our study shows, for the first time, that such association between FA and MD is found only in glioblastomas, but not in brain metastases. The underlying mechanism for such discrepancy between these 2 types of tumors is not fully understood, but it may help in improving the diagnostic accuracy as demonstrated in this study.

In this study, the AUC values are similar between the raters (0.90 and 0.85) and LRM (0.86). This result indicates that the 2 raters and LRM had differences in their confidence levels for individual cases, but overall the performance of LRM was close to that of both raters. Furthermore, with the use of the DTI classification model, the diagnostic performance of each radiologist improved noticeably, with high sensitivity, specificity, positive predictive values, and negative predictive values. The AUC increased from 0.90 to 0.96 for rater 1 and from 0.85 to 0.93 for rater 2. The model is easy to use in clinical practice. Specifically, the readers first interpreted the case on the basis of the 5-scale confidence levels. Then they put the FA and MD values from the enhancing part into equation 1 and calculated the probability. Finally they used equation 2 to get the final interpretation. Alternatively, on the basis of the promising results of the current study, the LRM output can be provided to the radiologists as complementary information to consider when reading the case. A future study is warranted to test whether the availability of the LRM output can improve the diagnostic performance of radiologists with different levels of experience. We also evaluated challenging cases for the readers with lower confidence levels. The AUC remained at about the same level as that in all the cases. This finding was in accordance with several previous studies[5,12,17] and indicates that the model is very helpful for readers, even for experienced radiologists.

A potential limitation of our study is its retrospective design. To further validate our results, a prospective study with similar or larger cohort size is warranted. Water diffusivity is affected by many factors including cellularity, extracellular volume, viscosity, and membrane permeability. The mean diffusivity and directionality changes measured by DTI are the sum of all the microstructural changes. Hence, a thorough pathologic investigation would be necessary to elucidate the underlying tissue structure responsible for higher FA in glioblastomas and the association with MD. In this retrospective study, image-guided biopsy was not available. Future study with pathologic validation is required. Furthermore, we may further improve the DTI-based model by using histogram analysis of FA and MD values in voxels. Future study is warranted to fully use the vast voxelwise information collected through DTI for better diagnosis.

CONCLUSIONS

The classification model based on FA and MD from the enhancing region is a robust one for differentiating glioblastomas from brain metastases. The model performed as well as experienced neuroradiologists. The diagnostic performance of radiologists in differentiating glioblastomas from brain metastases can be improved by adding a DTI classification model.

Disclosures: Harish Poptani—*UNRELATED*: *Consultancy*: American College of Radiology Image Metrix, *Grants/Grants Pending:* National Institutes of Health.* Donald M. O'Rourke—*UNRELATED*: *Expert Testimony*: neurosurgery medicolegal expert review, *Grants/Grants Pending*: Celldex Therapeutics,* Philanthropy,* *Patents (planned, pending or issued)*: US Patents, University of Pennsylvania.* Ronald L. Wolf—*UNRELATED*: *Other*: ACRIN "tie-breaker" reads for glioblastoma study, *Comments*: unrelated to publication. *Money paid to the institution.

REFERENCES

1. Giese A, Westphal M. **Treatment of malignant glioma: a problem beyond the margins of resection.** *J Cancer Res Clin Oncol* 2001;127:217–25
2. Soffietti R, Ruda R, Mutani R. **Management of brain metastases.** *J Neurol* 2002;249:1357–69

3. Schiff D. **Single brain metastasis.** *Curr Treat Options Neurol* 2001;3:89–99
4. Lu S, Ahn D, Johnson G, et al. **Peritumoral diffusion tensor imaging of high-grade gliomas and metastatic brain tumors.** *AJNR Am J Neuroradiol* 2003;24:937–41
5. Lu S, Ahn D, Johnson G, et al. **Diffusion-tensor MR imaging of intracranial neoplasia and associated peritumoral edema: introduction of the tumor infiltration index.** *Radiology* 2004;232:221–28
6. Morita K, Matsuzawa H, Fujii Y, et al. **Diffusion tensor analysis of peritumoral edema using lambda chart analysis indicative of the heterogeneity of the microstructure within edema.** *J Neurosurg* 2005;102:336–41
7. Yamasaki F, Kurisu K, Satoh K, et al. **Apparent diffusion coefficient of human brain tumors at MR imaging.** *Radiology* 2005;235:985–91
8. Calli C, Kitis O, Yunten N, et al. **Perfusion and diffusion MR imaging in enhancing malignant cerebral tumors.** *Eur J Radiol* 2006;58:394–403
9. Oh J, Cha S, Aiken AH, et al. **Quantitative apparent diffusion coefficients and T2 relaxation times in characterizing contrast enhancing brain tumors and regions of peritumoral edema.** *J Magn Reson Imaging* 2005;21:701–08
10. Wang W, Steward CE, Desmond PM. **Diffusion tensor imaging in glioblastoma multiforme and brain metastases: the role of p, q, L, and fractional anisotropy.** *AJNR Am J Neuroradiol* 2009;30:203–08
11. Reiche W, Schuchardt V, Hagen T, et al. **Differential diagnosis of intracranial ring enhancing cystic mass lesions–role of diffusion-weighted imaging (DWI) and diffusion-tensor imaging (DTI).** *Clin Neurol Neurosurg* 2010;112:218–25
12. Wang S, Kim S, Chawla S, et al. **Differentiation between glioblastomas and solitary brain metastases using diffusion tensor imaging.** *Neuroimage* 2009;44:653–60
13. Chen XZ, Yin XM, Ai L, et al. **Differentiation between brain glioblastoma multiforme and solitary metastasis: qualitative and quantitative analysis based on routine MR imaging.** *AJNR Am J Neuroradiol* 2012;33:1907–12
14. Kinoshita M, Hashimoto N, Goto T, et al. **Fractional anisotropy and tumor cell density of the tumor core show positive correlation in diffusion tensor magnetic resonance imaging of malignant brain tumors.** *Neuroimage* 2008;43:29–35
15. Murakami R, Hirai T, Sugahara T, et al. **Grading astrocytic tumors by using apparent diffusion coefficient parameters: superiority of a one- versus two-parameter pilot method.** *Radiology* 2009;251:838–45
16. Stadlbauer A, Ganslandt O, Buslei R, et al. **Gliomas: histopathologic evaluation of changes in directionality and magnitude of water diffusion at diffusion-tensor MR imaging.** *Radiology* 2006;240:803–10
17. Al-Okaili RN, Krejza J, Woo JH, et al. **Intraaxial brain masses: MR imaging-based diagnostic strategy–initial experience.** *Radiology* 2007;243:539–50
18. Kim S, Pickup S, Hsu O, et al. **Diffusion tensor MRI in rat models of invasive and well-demarcated brain tumors.** *NMR Biomed* 2008;21:208–16
19. Beppu T, Inoue T, Shibata Y, et al. **Fractional anisotropy value by diffusion tensor magnetic resonance imaging as a predictor of cell density and proliferation activity of glioblastomas.** *Surg Neurol* 2005;63:56–61
20. Hope T, Westlye LT, Bjornerud A. **The effect of gradient sampling schemes on diffusion metrics derived from probabilistic analysis and tract-based spatial statistics.** *Magn Reson Imaging* 2012;30:402–12
21. Jones DK. **The effect of gradient sampling schemes on measures derived from diffusion tensor MRI: a Monte Carlo study.** *Magn Reson Med* 2004;51:807–15
22. Landman BA, Farrell JA, Jones CK, et al. **Effects of diffusion weighting schemes on the reproducibility of DTI-derived fractional anisotropy, mean diffusivity, and principal eigenvector measurements at 1.5T.** *Neuroimage* 2007;36:1123–38
23. Wang S, Kim S, Chawla S, et al. **Differentiation between glioblastomas, solitary brain metastases, and primary cerebral lymphomas using diffusion tensor and dynamic susceptibility contrast-enhanced MR imaging.** *AJNR Am J Neuroradiol* 2011;32:507–14
24. Westin CF, Maier SE, Mamata H, et al. **Processing and visualization for diffusion tensor MRI.** *Med Image Anal* 2002;6:93–108
25. Wang S, Kim S, Zhang Y, et al. **Determination of grade and subtype of meningiomas by using histogram analysis of diffusion-tensor imaging metrics.** *Radiology* 2012;262:584–92
26. Rutter CM. **Bootstrap estimation of diagnostic accuracy with patient-clustered data.** *Acad Radiol* 2000;7:413–19
27. DeLong ER, DeLong DM, Clarke-Pearson DL. **Comparing the areas under two or more correlated receiver operating characteristic curves: a nonparametric approach.** *Biometrics* 1988;44:837–45
28. Toh CH, Wei KC, Ng SH, et al. **Differentiation of tumefactive demyelinating lesions from high-grade gliomas with the use of diffusion tensor imaging.** *AJNR Am J Neuroradiol* 2012;33:846–51
29. Toh CH, Wei KC, Ng SH, et al. **Differentiation of brain abscesses from necrotic glioblastomas and cystic metastatic brain tumors with diffusion tensor imaging.** *AJNR Am J Neuroradiol* 2011;32:1646–51
30. Zamecnik J. **The extracellular space and matrix of gliomas.** *Acta Neuropathol* 2005;110:435–42
31. Vargova L, Homola A, Zamecnik J, et al. **Diffusion parameters of the extracellular space in human gliomas.** *Glia* 2003;42:77–88
32. Pope WB, Mirsadraei L, Lai A, et al. **Differential gene expression in glioblastoma defined by ADC histogram analysis: relationship to extracellular matrix molecules and survival.** *AJNR Am J Neuroradiol* 2012;33:1059–64
33. Tropine A, Dellani PD, Glaser M, et al. **Differentiation of fibroblastic meningiomas from other benign subtypes using diffusion tensor imaging.** *J Magn Reson Imaging* 2007;25:703–08
34. Stylianopoulos T, Diop-Frimpong B, Munn LL, et al. **Diffusion anisotropy in collagen gels and tumors: the effect of fiber network orientation.** *Biophys J* 2010;99:3119–28
35. Preusser M, Capper D, Ilhan-Mutlu A, et al. **Brain metastases: pathobiology and emerging targeted therapies.** *Acta Neuropathol* 2012;123:205–22
36. Varga I, Hutoczki G, Petras M, et al. **Expression of invasion-related extracellular matrix molecules in human glioblastoma versus intracerebral lung adenocarcinoma metastasis.** *Cent Eur Neurosurg* 2010;71:173–80

Bioactive versus Bare Platinum Coils in the Treatment of Intracranial Aneurysms: The MAPS (Matrix and Platinum Science) Trial

C.G. McDougall, S. Claiborne Johnston, A. Gholkar, S.L. Barnwell, J.C. Vazquez Suarez, J. Massó Romero, J.C. Chaloupka, A. Bonafe, A.K. Wakhloo, D. Tampieri, C.F. Dowd, A.J. Fox, S.J. Imm, K. Carroll, and A.S. Turk, for the MAPS Investigators

ABSTRACT

BACKGROUND AND PURPOSE: The ability of polymer-modified coils to promote stable aneurysm occlusion after endovascular treatment is not well-documented. Angiographic aneurysm recurrence is widely used as a surrogate for treatment failure, but studies documenting the correlation of angiographic recurrence with clinical failure are limited. This trial compares the effectiveness of Matrix^2 polyglycolic/polylactic acid biopolymer–modified coils with bare metal coils and correlates the angiographic findings with clinical failure (ie, target aneurysm recurrence), a composite end point that includes any incident of posttreatment aneurysm rupture, retreatment, or unexplained death.

MATERIALS AND METHODS: This was a multicenter randomized noninferiority trial with blinded end point adjudication. We enrolled 626 patients, divided between Matrix^2 and bare metal coil groups. The primary outcome was target aneurysm recurrence at 12 ± 3 months.

RESULTS: At 455 days, at least 1 target aneurysm recurrence event had occurred in 14.6% of patients treated with bare metal coils and 13.3% of Matrix^2 ($P = .76$, log-rank test) patients; 92.8% of target aneurysm recurrence events were re-interventions for aneurysms that had not bled after treatment, and 5.8% of target aneurysm recurrence events resulted from hemorrhage or rehemorrhage, with or without retreatment. Symptomatic re-intervention occurred in only 4 (0.6%) patients. At 455 days, 95.8% of patients with unruptured aneurysms and 90.4% of those with ruptured aneurysms were independent (mRS ≤ 2). Target aneurysm recurrence was associated with incomplete initial angiographic aneurysm obliteration, presentation with rupture, and a larger aneurysmal dome and neck size.

CONCLUSIONS: Tested Matrix^2 coils were not inferior to bare metal coils. Endovascular coiling of intracranial aneurysms was safe, and the rate of technical success was high. Target aneurysm recurrence is a promising clinical outcome measure that correlates well with established angiographic measurements.

ABBREVIATIONS: BMC = bare metal coil; HELPS = HydroCoil Endovascular Aneurysm Occlusion and Packing Study; ISAT = International Subarachnoid Aneurysm Trial; MAPS = Matrix and Platinum Science; TAR = target aneurysm recurrence

Treatment of ruptured intracranial aneurysms with endovascular coiling is widely accepted, but incomplete or impermanent aneurysm occlusions are common.[1,2] Although failure to achieve durable angiographic occlusion is frequent, delayed hemorrhage after coiling is infrequent.[3] Because large sample sizes are required to detect treatment effects on infrequent events, many trials use angiographic aneurysm residuals and/or recurrence as a surrogate for the much less frequent outcome of clinical failure, even though the correlation between angiographic failure and clinical failure is not well-characterized. While hemorrhage after treatment is the most concerning form of clinical failure, retreatment is also a significant negative clinical event for the patient

Received June 5, 2013; accepted after revision October 2.

From the Department of Neurosurgery (C.G.M.), Barrow Neurological Institute, St. Joseph's Hospital and Medical Center, Phoenix, Arizona; Clinical and Translational Science Institute (S.C.J.) and Department of Radiology (C.F.D.), University of California, San Francisco, San Francisco, California; Department of Neuroradiology (A.G.), Regional Neurosciences Center, Royal Victoria Infirmary, Newcastle Upon Tyne, UK; Departments of Neurological Surgery and Diagnostic Radiology (S.L.B.), Oregon Health and Science University, Portland, Oregon; Therapeutic Neuroradiology Unit (J.C.V.S.), University General Hospital of Alicante, Alicante, Spain; Department of Interventional Neuroradiology (J.M.R.), Hospital Donostia, San Sebastián, Spain; Department of Neurosurgery and Radiology (J.C.C.), Mount Sinai Medical Center, Miami Beach, Florida; Service de Neuroradiologie (A.B.), Hôspital Gui de Chauliac, Montpellier Cedex, France; Division of Neuroimaging and Intervention (A.K.W.), Department of Radiology, University of Massachusetts Medical School, Worcester, Massachusetts; Department of Diagnostic and Interventional Neuroradiology (D.T.), Montreal Neurological Institute, Montreal, Canada; Department of Neuroradiology (A.J.F.), Sunnybrook Health Sciences Center, Toronto, Ontario, Canada; Stryker Corporation (S.J.I., K.C.), Fremont, California; and Departments of Neurointerventional Surgery, Radiology, and Neurosurgery (A.S.T.), Medical University of South Carolina, Charleston, South Carolina.

This work was sponsored by Stryker Corporation (Formerly Boston Scientific Corporation). Clinical Trial Registration-URL is http://www.clinicaltrials.gov/ct2/show/NCT00396981?term = MAPS&rank = 3. The unique identifier is NCT00396981.

Please address correspondence to Cameron G. McDougall, MD, c/o Neuroscience Publications; Barrow Neurological Institute, St. Joseph's Hospital and Medical Center, 350 W. Thomas Rd, Phoenix, Arizona 85013; e-mail: neuropub@dignityhealth.org

Indicates article with supplemental on-line tables.

Indicates article with supplemental on-line figure.

Evidence-Based Medicine Level 1.

http://dx.doi.org/10.3174/ajnr.A3857

and, as such, requires consideration. From the patient's perspective, it is the clinical, not the angiographic, outcome that is important, and it is, therefore, critical that the relationship between imaging and clinical outcomes be better understood.

Several varieties of polymer-modified coils have been developed with the goal of achieving more durable aneurysm occlusion. Matrix^2 (Stryker, Kalamzoo, Michigan) is a platinum coil modified with a polyglycolic/polylactic acid braid. Although multiple studies of this coil and of a previous iteration of this coil have been conducted,[4-19] this trial was initiated because no randomized trial had been conducted and the benefits of Matrix^2 remained unproven.

The goals of this study were to compare Matrix^2 with its bare metal counterpart the Guglielmi detachable coil (Stryker) and to use this trial to validate a composite clinical outcome measure created for the trial. The clinical outcome was designated as "target aneurysm recurrence" (TAR) and was defined as occurring when a patient experienced any of the following conditions after his or her initial aneurysm coiling:

1) Target aneurysm hemorrhage
2) Target aneurysm retreatment
3)Death from unknown cause.

MATERIALS AND METHODS

This randomized multicenter trial was conceived and designed by the investigators, with advice provided by the sponsor. This study was approved by all local institutional review boards. The study was conducted in accordance with the relevant parts of the International Conference on Harmonization Good Clinical Practice: Consolidated Guideline; the Declaration of Helsinki, EN ISO14155 Clinical Investigations of Medical Devices for Human Subjects; and the applicable regulations from the US Food and Drug Administration. Study centers were invited to participate; high-volume centers with broad geographic representation were selected for invitation.

Study Subjects

The study population included subjects 18–80 years of age with a single untreated, intracranial saccular aneurysm (4–20 mm; Hunt and Hess scale score, I–III; mRS score, 0–3), ruptured or unruptured, for which both polymer-modified coils and bare metal coils (BMCs) were treatment options and for which primary coiling treatment was planned to be completed during a single procedure.

Twenty-six of the 43 investigational sites were located in the United States. Due to the wide variability in the rate of patient recruitment among centers, large-volume centers were closed to enrollment after 60 patients were recruited to avoid having the recruitment dominated by a small number of large-volume centers. On-line Table 1 details enrollment by participating centers. Subjects were seen at the time of treatment and again 12 ± 3 months after the procedure. Preprocedural neurologic scores consisted of an independent assessment of the mRS score for all subjects plus a Hunt and Hess scale assessment for subjects with ruptured aneurysms. Long-term follow-up is to occur by telephone annually to 5 years post-index procedure.

All enrolled Matrix and Platinum Science (MAPS) Trial subject data are included in the intent-to-treat analysis except for 4 excluded subjects. One subject did not have an aneurysm, and 3 subjects were excluded at the request of the local institutional review board due to noncompliance with good clinical practice in obtaining informed consent. Overall, 626 MAPS Trial subjects were included in the intent-to-treat analyses.

Procedures

Patients were randomized in blocks of 2 and 4, stratified by target aneurysm rupture status and hospital site, to ensure equal distribution of those elements between the trial arms. Patients randomized to Matrix^2 were to be treated with ≥75% total length of coils composed of Matrix^2 and the remainder, of BMCs, while those randomized to BMCs were to be treated entirely with BMCs. To minimize confounding variables related to mechanical properties of different coil types, we allowed no other coil types or coils by different manufacturers in the index procedure. The use of adjunctive devices, specifically the use of the Neuroform stent (Stryker Neurovascular, Fremont, California), was at the operators' discretion.

As defined above, the primary outcome measure was TAR. Secondary outcome measures, all defined a priori, included angiographic assessment by site and core laboratory; assessments of mRS scores at 12 ± 3 months and direction of change from baseline, whether it improved or worsened, performed in person by an independent certified practitioner at a scheduled clinic visit; and technical procedural success, defined as the successful delivery and deployment of coils in the target aneurysm. Target aneurysm reintervention was defined as any further treatment of the aneurysm with the retreatment decision being at the discretion of the operator.

All sites graded their own angiographic outcomes on the basis of the modified 3-point Raymond scale postprocedurally and at follow-up. All sites also recorded an assessment of perceived change from baseline (same, better, worse) at follow-up. Digitized copies of the angiograms were created for all cases and were stored at an independent angiographic core laboratory located at the University of California, San Francisco. The core laboratory assessed all treatment and 1-year follow-up angiograms blinded to the treatment technique. Core laboratory evaluations were performed by using the same angiographic scales as the self-assessed outcomes.

An independent steering committee was responsible for overall oversight of the science and execution of the trial. Patient safety data were reviewed at regular intervals by an independent Data-Monitoring Committee. An independent Clinical Events Committee was responsible for reviewing and adjudicating all deaths and neurologic events. Monitoring and source document verification were performed by an external monitoring clinical research organization, Geelen and Geelen. On-site monitoring and source document verification of Case Report Forms against original patient records were completed for >40% of patients at the completion of the 1-year follow-up.

Statistical Methods

This study used a noninferiority design to evaluate whether Matrix^2 coils are noninferior to BMCs, with a clinically acceptable noninferiority margin set at 10%, at a 1-sided significance level of $\alpha = .05$. Noninferiority was used to establish the baseline estimate from which future superiority studies could be conducted. Based on a literature review, the estimated 1-year TAR rate for aneurysms treated with BMCs was 20%. Powering to noninferiority required

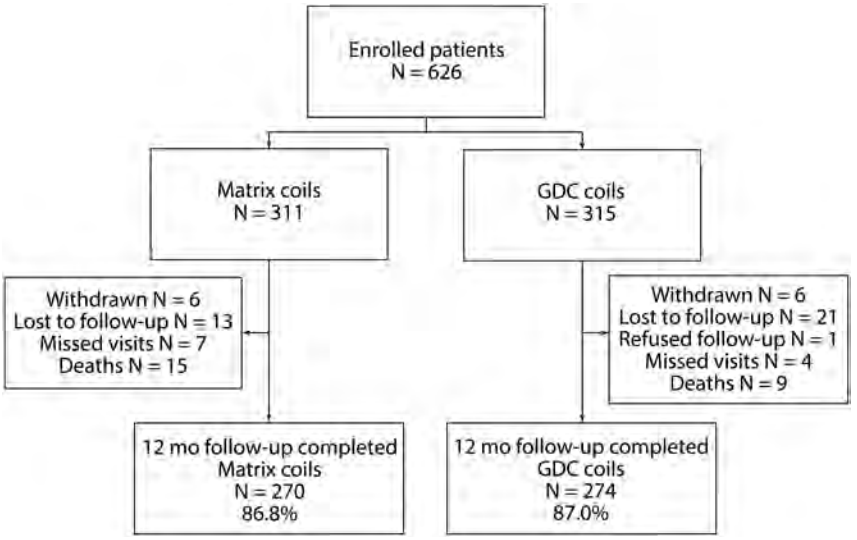

FIG 1. Subject flow through 455 days.

250 patients in each arm, with 87% power if the Matrix^2 was equivalent to the BMC. Assuming 20% lost to follow-up increased the sample size to 315 patients in each arm.

The primary end point (TAR) rate was calculated by using Kaplan-Meier estimates in each group at the end of a window of 12 ± 3 months (455 days). Time to event was based on the real time to rupture/rerupture, retreatment, or unknown cause of death, whichever happened first for each subject. Subjects who had not experienced an event were censored at their last clinical visit or 455 days, whichever came earlier. Noninferiority was to be claimed if the upper limit of the 1-sided 95% confidence interval of the treatment difference was less than the prespecified 10% noninferiority margin. After showing noninferiority, a test for superiority was also to be conducted. Superiority was to be claimed if the upper limit of the 2-sided 95% confidence interval of the treatment difference was <0.

The protocol prespecified additional subgroup analyses of TAR, modified Raymond scale, changes in mRS score from baseline to the 12-month assessment, and univariate and multivariate regression models to analyze TAR.

Logistic regression models were fitted to find baseline predictors for TAR, including baseline clinical and angiographic findings. The stepwise method was used with $P = .1$ entry and exit criteria for model selection.

A Student t test was used for distributions of continuous variables between the groups. Either the χ^2 or Fisher exact test was used to analyze binary variables according to standard statistical practice. For ordinal variables, such as the modified Raymond Scale, recanalization, and mRS scores, the Wilcoxon rank sum test was used to test the distribution between the groups. The differences between the groups were presented with the 95% confidence interval estimated by the normal approximation. For the binary outcomes, the relative risks as well as the 95% confidence intervals were also presented.

All statistical analyses were performed by using SAS, Version 9.2 (SAS Institute, Cary, North Carolina).

RESULTS

Between March 29, 2007, and October 20, 2009, six hundred twenty-six patients were enrolled in the MAPS trial (Fig 1). Thirty-three subjects received nonstudy coils, received no coils, or experienced a violation of the prespecified ratio of coil length. Nine subjects received excluded stents in addition to the randomized coil type. All 626 enrolled subjects were included in this intent-to-treat analysis.

Baseline Characteristics

Baseline demographics were relatively evenly distributed between the 2 groups (Table 1). More patients had diabetes ($P = .0401$) and a worse neurologic status at baseline in the Matrix^2 arm than in the BMC arm. BMC patients with unruptured aneurysms had worse mRS scores ($P = .0457$), and BMC patients with ruptured aneurysms had poorer Hunt and Hess scale scores ($P = .0136$). Approximately 87% (543/626) of aneurysms treated were located in the anterior circulation; the most common location was the anterior communicating artery (On-line Table 2). There were no differences among aneurysm locations based on treatment group (On-line Table 2). Of the 228 (36%) subjects who presented with acutely ruptured aneurysms, 218 (96%) were treated within 14 days of rupture. Of the 626 subjects enrolled in the study, 509 (81%) had wide-neck aneurysms based on study site measurements. The use of stents in wide-neck aneurysms was evenly distributed in both arms.

Procedural Outcomes

The procedural success rate was high in both treatment arms (97.5% [307/315] for BMCs versus 96.8% [301/311] for Matrix^2). The inability to access the target aneurysm was the most common reason for technical failure. The rate of device malfunction was low in both groups (3.9% [12/308] for BMCs versus 3.9% [12/309] for Matrix^2; On-line Table 3). The periprocedural complication rates (15.0% [47/313] for BMCs versus 14.8% [46/311] for Matrix^2) were consistent with other reports.[13] On average, 6.9 coils were implanted per patient in the BMC arm compared with 5.5 coils in the Matrix^2 arm. The packing attenuation of Matrix^2 (26.4%) was significantly greater ($P = .0013$) compared with that of BMCs (23.3%). Although the protocol allowed up to 25% of coil length in the Matrix^2 arm to be BMCs, 71.1% (221/311) of patients in the Matrix^2 arm received 100% Matrix^2.

Primary End Point

The Kaplan-Meier estimates of TAR at 455 days were 13.3% for the Matrix^2 treatment group and 14.6% for BMC group (Fig 2). Noninferiority was shown with the upper limit (3.9%) of a 1-sided 95% confidence interval of the difference that was less than the prespecified 10% margin. However, the difference in TAR rates was not large enough to demonstrate superiority: The upper limit (4.9%) of a 2-sided 95% confidence interval of the

Table 1: Summary of subject baseline characteristics[a]

Variable	BMC (n = 315)	Matrix^2 (n = 311)
Male	104 (33.0%)	82 (26.4%)
Age (yr)	54.4 ± 13.2	55.7 ± 11.6
Ethnicity and race		
Caucasian/white	259 (82.2%)	249 (80.1%)
Black or African American	13 (4.1%)	12 (3.9%)
Asian	11 (3.5%)	13 (4.2%)
Hispanic or Latino	13 (4.1%)	16 (5.1%)
Other	19 (6.0%)	21 (6.8%)
Current use of illicit drugs and/or alcohol abuse	25 (8.4%)	25 (8.6%)
Hypertension	143 (45.5%)	153 (49.5%)
Coronary disease	29 (9.4%)	44 (14.5%)
Hyperlipidemia/hypercholesterolemia	70 (22.5%)	85 (28.0%)
Intracranial atherosclerosis	7 (2.3%)	4 (1.3%)
Current smoking	124 (42.6%)	117 (41.6%)
Diabetes	19 (6.1%)	33 (10.7%)
Prior stroke or TIA	35 (11.2%)	31 (10.2%)

[a] Values are presented as mean ± SD for continuous variables and No. (%) for categoric variables. The denominator used for rates (%) can be smaller than the number of subjects in each group due to missing values.

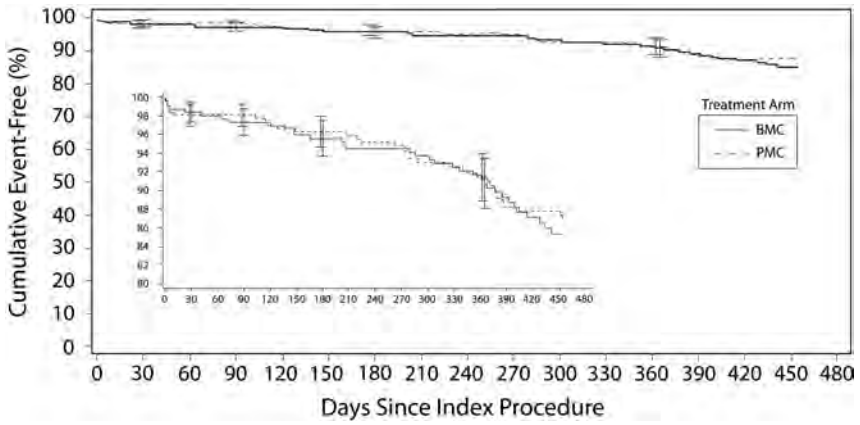

FIG 2. Kaplan-Meier curve showing freedom from TAR to 455 days in the intent-to-treat population (n = 626).

difference was >0. A Kaplan-Meier curve of per protocol analysis is shown in On-line Fig 1. Overall, 93% (64/69) of TARs resulted from re-intervention of aneurysms that had not bled after treatment. Symptomatic re-intervention occurred in 4 of 626 patients (0.6%, Table 2), 3 of whom had aneurysmal hemorrhage. One TAR event occurred due to an unexplained death. Subgroup analysis of the primary end point is given in On-line Table 4.

Secondary End Points

The immediate postprocedural angiographic assessment was similar between the 2 coil groups (P = .9894, Table 3). There was no difference in angiographic outcomes at 12 months between the 2 groups (P = .8297). There was no significant difference in the 2 groups with respect to changes in the immediate post-index treatment and 12-month neurologic assessments compared with the preprocedural assessments.

The immediate postprocedural independent neurologic assessment demonstrated that 91% (524/579) of the subjects had the same or better mRS scores compared with their pretreatment neurologic assessment. The results were similar for both treatment groups (P = .4220). There also was no difference between the treatment groups with respect to worsening mRS scores from before the procedure to the 12-month follow-up (11.7% [33/281]for BMCs versus 9.9% [28/284] for Matrix^2, P = .4705).

Principal Safety Outcomes

The Clinical Events Committee–adjudicated principal safety outcomes up to 455 days including all deaths, strokes, and ruptures/reruptures are presented in On-line Table 5. During the study, there were 837 safety events reported: 279 (33%) as serious adverse events and 558 (67%) as nonserious adverse events. Four (0.6%, 4/626) aneurysms, 2 in each arm, ruptured or reruptured within 455 days of the index treatment. Twenty-four deaths were reported post-index treatment through 455 days. No unanticipated adverse device events were identified during the study. No cases of hydrocephalus were associated with unruptured aneurysms in either arm.

For all causes of death at 30 days, 3 patients died in the BMC arm and 12 in the Matrix^2 arm (P = .0174, On-line Table 5). At 30 days, there was 1 neurologic death in the BMC arm and 11 in the Matrix^2 arm (P = .0033). By 12 months, 9 patients (5 with ruptured aneurysms, 56%) in the BMC arm had died compared with 15 (11 presented ruptured, 73%) in the Matrix^2 arm (P = .2002). At 12 months, there was 1 neurologic death in the BMC arm versus 13 in the Matrix^2 arm (P = .0011). There was no significant difference in the nonneurologic deaths at any time point.

All neurologic deaths were independently reviewed by the Clinical Events Committee. Deaths of known cause, unrelated to the target aneurysm or to potential neurologic etiologies (eg, pancreatic cancer, colon cancer, liver failure), were counted as non-neurologic and were not further evaluated. Neurologic deaths were adjudicated as related or not to the underlying disease, the procedure, and/or the study device, with the probability of the relationship being noted.

Of the 13 neurologic deaths in the Matrix^2 group, 7 were ruled the result of the presenting hemorrhage, unrelated to either the procedure or the device. One death of unknown cause was automatically adjudicated as a TAR event, with unknown deaths being conservatively defined in the protocol as neurologic in cause and related to the study device. Two additional deaths occurred in patients with ruptured aneurysms for whom it was adjudicated that the procedure and or device may have played a role in addition to the effects of the presenting hemorrhage, and 3 procedural complications in patients with unruptured aneurysms (1 procedure-related ischemic stroke and 2 procedural hemorrhages) led to deaths. By contrast, of the 9 deaths occurring in the bare coil group, only 1 was neurologic in nature and was adjudicated as related to the procedure and study device.

Based on the Clinical Events Committee adjudication, there were no statistically significant differences in neurologic deaths related to the study device, index procedure, or both. At both 30 days and 12 months, significantly more neurologic deaths in the Matrix^2 arm were adjudicated as unrelated to the study device and index procedure ($P = .0147$ and $P = .0072$, respectively).

There were 14 site-reported intraprocedural perforations: 8 (2.5%, 8/315) in the BMC arm and 6 (1.9%, 6/311) in the Matrix^2 arm ($P = .6056$). None of the perforations resulted in death.

Table 2: Number of TAR events at 455 days

Subjects	BMC (No.) (%)	Matrix^2 (No.) (%)	All Subjects (No.) (%)
Overall	315	311	626
Subjects who met primary end point	35 (11.1)	34 (10.9)	69 (11.0)
Re-intervention only	33 (10.5)	31 (10.0)	64 (10.2)
Ruptures or reruptures	2 (0.6)	2 (0.6)	4 (0.6)[a]
Unknown causes of death	0	1 (0.3)	1 (0.2)
Symptomatic TAR	3 (1.0)	4 (1.3)	7 (1.1)
Symptomatic retreatment	2 (0.6)	2 (0.6)	4 (0.6)
Unruptured	196	202	398
Subjects who met primary end point	18 (9.2)	19 (9.4)	37 (9.3)
Re-intervention only	18 (9.2)	18 (8.9)	36 (9.0)
Ruptures or reruptures	0	1 (0.5)	1 (0.3)[b]
Unknown causes of death	0	0	0
Symptomatic TAR	1 (0.5)	2 (1.0)	3 (0.8)
Symptomatic retreatment	1 (0.5)	2 (1.0)	3 (0.8)
Ruptured	119	109	228
Subjects who met primary end point	17 (14.3)	15 (13.8)	32 (14.0)
Re-intervention only	15 (12.6)	13 (11.9)	28 (12.3)
Ruptures or reruptures	2 (1.7)	1 (0.9)	3 (1.3)[c]
Unknown causes of death	0	1 (0.9)	1 (0.4)
Symptomatic TAR	2 (1.7)	2 (1.8)	4 (1.8)
Symptomatic retreatment	1 (0.8)	0	1 (0.4)

[a] Three patients (2 BMC, 1 Matrix^2) with a rupture/rerupture also had a subsequent re-intervention.
[b] One patient (Matrix^2) with a rupture also had a subsequent re-intervention.
[c] Two patients (BMC) with a rerupture also had a subsequent re-intervention.

Subgroup Analysis of the Primary End Point (TAR)

There were no significant differences between the groups based on aneurysm location, dome size, neck width, dome-to-neck ratio, rupture status, flow orientation, or use of adjunctive devices.

Association between Primary and Secondary End Points

The angiographic characteristics at treatment were assessed as predictors of TAR (Table 4). Incomplete aneurysm obliteration immediately after treatment tended to be associated with a greater likelihood of TAR at 455 days. Multivariate modeling of 12-month TAR predictors (Table 5) included the rupture status of the aneurysm, the dome and neck size of the aneurysm, and the initial quality of the aneurysm occlusion (Raymond 3 versus Raymond 1). Among patients whose aneurysms were more completely occluded at the time of initial treatment (Raymond 1 or 2), TAR rates were lower in the Matrix^2-treated patients (2.7%, 4/147) than in the BMC-treated patients (9.6%, 15/157) ($P = .01$). However, for patients with residual dome filling after initial treatment (Raymond 3), the TAR rate for the Matrix^2-treated patients tended to be higher (24.2%, 22/91) than that observed in the BMC-treated patients (16.1%, 15/93) ($P = .17$).

DISCUSSION

The MAPS Trial has shown Matrix^2 to be noninferior to BMCs. The composite end point of TAR—aneurysm hemor-

Table 3: Secondary end points[a]

Assessment	BMC (n = 315)	Matrix^2 (n = 311)	Relative Risk (95% CI)	Difference (95% CI)	*P* Value
Angiographic assessment by core laboratory					
Modified Raymond Scale after procedure					
1) Complete obliteration	89 (35.6%)	87 (36.6%)	0.97 (0.77–1.23)	−1.0% (−9.5–7.6)	.9894
2) Residual neck/dog ear	68 (27.2%)	60 (25.2%)	1.08 (0.80–1.45)	2.0% (−5.8–9.8)	
3) Residual aneurysm	93 (37.2%)	91 (38.2%)	0.97 (0.77–1.22)	−1.0% (−9.6–7.6)	
Modified Raymond Scale at 455-day FU or re-intervention					
1) Complete obliteration	99 (39.9%)	105 (44.3%)	0.90 (0.73–1.11)	−4.4% (−13.2–4.4)	.8297
2) Residual neck/dog ear	69 (27.8%)	48 (20.3%)	1.37 (1.00–1.90)	7.6% (0.0–15.1)	
3) Residual aneurysm	80 (32.3%)	84 (35.4%)	0.91 (0.71–1.17)	−3.2% (−11.6–5.2)	
Aneurysm change					
Better	81 (32.7%)	60 (25.4%)	1.28 (0.97–1.70)	7.2% (−0.8–15.3)	.1225
Same	82 (33.1%)	85 (36.0%)	0.92 (0.72–1.17)	−3.0% (−11.4–5.5)	
Worse	85 (34.3%)	91 (38.6%)	0.89 (0.70–1.13)	−4.3% (−12.9–4.3)	
Neurologic assessment					
Worse[b] mRS score					
At post-index procedure	25 (8.5%)	30 (10.5%)	0.81 (0.49–1.35)	−2.0% (−6.7–2.8)	.4220
At 455 days follow-up[c]	33 (11.7%)	28 (9.9%)	1.19 (0.74–1.92)	1.9% (−3.2–7.0)	.4705
Technical success					
Technical procedure success[d]	307 (97.5%)	301 (96.8%)	1.01 (0.98–1.03)	0.7% (−1.9–3.3)	.6130

Note:—FU indicates follow-up.
[a] Values are presented as mean ± SD for continuous variables and No. (%) for categoric variables. The denominator used for rates (%) can be smaller than the number of subjects in each group due to missing values.
[b] Compared with the pre-index procedure.
[c] All causes of deaths within 455 days were incorporated as a follow-up mRS score of 6.
[d] Technical success evaluated at the patient level.

Table 4: 455-Day TAR rate by the Modified Raymond Scale at immediate postprocedure[a]

Modified Raymond Scale	BMC	Matrix[2]	Relative Risk (95% CI)	Difference (95% CI)	*P* Value
1) Complete obliteration	7.9% (7/89)	3.4% (3/87)	2.28 (0.61–8.54)	4.4% (−2.4–11.2)	.3297
2) Residual neck/dog ear	11.8% (8/68)	1.7% (1/60)	7.06 (0.91–54.81)	10.1% (1.8–18.4)	.0358
3) Residual aneurysm	16.1% (15/93)	24.2% (22/91)	0.67 (0.37–1.20)	−8.0% (−19.6–3.5)	.1733

[a] Values are presented as % (x/N).

Table 5: 455-Day TAR predictors by logistic regression models[a]

Variable	Coefficient	Standard Error	OR (95% CI)	*P* Value
Rupture status (ruptured vs unruptured)	1.4	0.3	4.0 (2.1–7.9)	<.0001
Core lab postproc Raymond Scale (2 vs 1)	0.3	0.5	1.4 (0.5–3.7)	.4917
Core lab postproc Raymond Scale (3 vs 1)	1.6	0.4	5.0 (2.2–11.0)	<.0001
Dome size[a] (≥10 vs <10 mm)	1.6	0.4	5.0 (2.2–11.5)	.0001
Neck size (≥4 vs <4 mm)	0.8	0.3	2.3 (1.2–4.4)	.0140

Note:—postproc indicates postprocedural; AP, anteroposterior.

[a] Dome size is calculated as a minimum of the 2 widths (AP plane, lateral plane).

rhage after treatment, target aneurysm retreatment, and/or death from unknown cause—was reached in 13.3% of the Matrix[2]-treated patients and in 14.6% of the BMC-treated patients as Kaplan-Meier estimates at 455 days. While this study does not suggest any benefit from Matrix[2] at 1 year, the 5-year follow-up results are not yet known.

Most of the TAR events were the result of asymptomatic target aneurysm retreatment. The significant baseline predictors of TAR included aneurysm size of >10 mm, neck size of >4 mm, pretreatment rupture status, and core laboratory adjudication of modified Raymond Scale 3 residual aneurysm filling on the immediate postprocedural angiogram. The immediate postprocedural Raymond Scale 3 versus 1 was a strong predictor of future TAR for Matrix[2]-treated patients (OR, 8.9; 95% confidence interval, 2.6–31.1; $P = .0006$) and tended to be so for the BMC-treated patients (OR, 2.3; 95% confidence interval, 0.9–5.8; $P = .0935$) in a univariate fashion. Aneurysm retreatment strongly correlated with core laboratory adjudication of modified Raymond Scale 3 residual aneurysm filling at 455 days.

The primary end point of TAR is a practical, efficient, unequivocal end point that measures the clinical events that are important to patients. TAR can easily be applied in future trials and correlates well with angiographic benchmarks already in common use. Most TAR events were due to asymptomatic retreatments, given that the other elements of TAR (ie, hemorrhage and unexplained death) are relatively uncommon. Even though the association with angiographic aneurysm remnants and recurrent hemorrhage is not well-characterized,[20] this poorly characterized threat drives most retreatments. In fact, 63 of 67 (94%) retreatments occurred in asymptomatic subjects. By contrast, not all recurrences were retreated, again, not surprising, because the clinically important event of retreatment is based on additional factors beyond the angiographic findings. Retreatment cannot occur without residual aneurysm, but it is evident that treating physicians do not believe that all aneurysm residuals need to be treated. It is also likely that the clinicians making these retreatment decisions are selecting clinical and angiographic features that they believe place one patient at higher risk for hemorrhage than another.

The primary limitation of this study is that TAR most often resulted from the retreatment of asymptomatic angiographic aneurysm remnants. This limitation naturally raises the question of whether TAR is a better outcome measure than core laboratory angiographic measurements. Additionally, although the core laboratory adjudicators were blinded to the coil type, the treating physicians were not. It can similarly be argued that the decision to retreat an aneurysm based on an asymptomatic angiographic recurrence is arbitrary. Indeed, different practitioners may have widely disparate thresholds for making the decision to retreat. While many residuals or recurrences may be innocuous, it is certain that some are not. Still, compared with an asymptomatic angiographic finding of residual aneurysm, retreatment is a much more important event to the patient, as are the other components of TAR. This relative importance of retreatment compared with purely angiographic end points is no less true even if the urgency of retreatment is uncertain and the risk is low. Additionally, while different practice patterns may make it difficult to compare TAR rates among trials, this difficulty does not diminish the applicability of TAR within a trial comparing 2 treatment modalities. With the 5-year follow-up that is ongoing in MAPS and additional long-term follow-up from other trials such as International Subarachnoid Aneurysm Trial (ISAT), whether an aggressive strategy of retreatment is warranted may become more apparent.

The impact of differing thresholds for retreatment is exemplified when MAPS is compared with the HydroCoil Endovascular Aneurysm Occlusion and Packing Study (HELPS) trial. Although the rates of major recurrence reported in the 2 "per protocol" treatment arms of HELPS were 24% and 34%, respectively, the retreatment rate was only 3% in both groups.[21] It is not clear why the retreatment rates in the 2 arms were the same despite a 10% difference in the rate of major recurrence between the 2 groups.

How well TAR correlates with angiographic outcomes and recurrent SAH will become clearer with the ongoing long-term follow-up occurring in MAPS and other trials. Although TAR correlated well with the angiographic occlusion scales, the core laboratory adjudication of immediate post-procedural occlusion correlated better with TAR at 455 days than did the local investigators' assessment. In 36% of cases, the local investigators reported a better degree of occlusion than did the core laboratory.

The correlation of TAR with the Raymond Scale of occlusion immediately after the procedure is a particularly useful finding. This correlation is important because the Raymond Scale is easily measured and is well-accepted. It is even more important, however, because unlike aneurysm size or rupture status, it is potentially modifiable at the time of initial aneurysm treatment. In other words, aggressive occlusion of the aneurysm at the first treatment is important in preventing a recurrence and in reducing

the need for retreatment. Should long-term follow-up confirm a significant link between Raymond 3 aneurysm residuals and future hemorrhage, the clinical relevance of TAR will be enhanced.

The comparatively lower rate of TAR in the Matrix^2-treated patients with an immediate Raymond 1 or 2 category occlusion is an interesting but inconclusive finding that requires replication. For patients with immediate posttreatment aneurysm occlusion scores of Raymond 1 or 2, the TAR rate was only 2.7%. For patients with Raymond occlusion scores of 3, the TAR rate for Matrix^2 was higher than that seen in the BMC patients. This finding is biologically consistent with previous animal studies suggesting that an initially mechanically stable occlusion must be achieved to allow the biologic effect of clot stabilization to occur before the external polymer is absorbed.

The increased incidence of deaths in the Matrix^2 arm was driven primarily by neurologic causes. It may be partially explained by differences in the comorbidities at the time of the index procedure (increased incidence of coronary artery disease, diabetes, and poor preprocedural neurologic status related to worse mRS or Hunt and Hess scale scores at admission). The much higher death rate in the Matrix^2 patients was mostly the result of deaths adjudicated as unrelated to the study device or index procedure. However, 5 of the 13 deaths were adjudicated as being possibly related to the procedure and/or device, and 3 of these 5 deaths were in patients presenting with unruptured aneurysms.

An additional important finding of MAPS is that aneurysm coiling has become a remarkably safe procedure. Because of the sample size, a mix of patients with ruptured and unruptured aneurysms, prospective design, rigorous independent evaluations, and consistency with the findings of the HELPS and Cerecyte Coil Trials,[21,22] important benchmarks with respect to the safety of endovascular aneurysm treatment are now confidently established. Regarding patients with ruptured aneurysms, at 455 days only 20 of 208 (9.6%) were dead or disabled (mRS >2); this outcome compares favorably with the 1-year ISAT outcome of 23.5% by using the same outcome scale.[1] Similarly, of the patients treated for unruptured aneurysms, only 15 of 360 patients (4.2%) were dead or disabled at 455 days. This finding compares favorably with the International Study of Unruptured Intracranial Aneurysms, which reported (after excluding non-treatment-related deaths) a dead or disabled rate of 6.2% for the endovascular treatment of unruptured aneurysms.[23] Both of these favorable comparisons are no doubt the result of improvements in technology and increased experience since these 2 landmark studies were completed.

More contemporary, higher quality comparisons are available. In HELPS,[21] outcomes were adjudicated at 18 months. Poor outcomes (mRS > 2) were seen in 24 of 214 patients (11.2%) available for follow-up who had originally presented without recent hemorrhage and in 47 of 253 patients (18.6%) who had originally presented with SAH. Most interesting, in the HELPS trial, only 3% of patients were retreated, though major angiographic recurrences were adjudicated in 27%–36% of the aneurysms at follow-up. Similar excellent procedural safety results have recently been reported in the Aneurysms Treated by Endovascular Approach registry and the Cerecyte Coil Trial.[22,24] The Aneurysms Treated by Endovascular Approach study reported 1-month morbidity and mortality rates of 1.7% and 1.6%, respectively. Likewise, the Cerecyte Coil Trial reported exceptionally good clinical outcomes in both treatment arms with only 2.7% of patients with unruptured aneurysms experiencing procedure-related neurologic deterioration.

Perhaps most reassuring in MAPS is that the posttreatment hemorrhage rate at 455 days was very low: 1 of 398 patients (0.25%) for unruptured aneurysms and 3 of 228 patients (1.32%) for previously ruptured aneurysms. These outcomes compare favorably with those in the ISAT trial, in which the rehemorrhage rate for aneurysms randomized to coiling after recent rupture was 28/1073 (2.6%) within the first year after coiling,[1] and with those in the Cerebral Aneurysm Rerupture After Treatment Trial, with its 3% rate at 1 year.[25]

CONCLUSIONS

The MAPS Trial demonstrates that after 1 year of follow-up, Matrix^2 is not inferior to BMCs. Pending the results after 5 years of follow-up, in the absence of a finding of superiority for either coil type, cost and other factors may be important in choosing Matrix^2 versus BMCs for clinical practice.

In addition, MAPS has shown TAR to be a practical clinical outcome measure that relates well to widely used angiographic assessments. Again, longer term follow-up should help clarify the utility of TAR as an outcome measurement.

Finally, MAPS provides additional evidence that coiling of intracranial aneurysms can be done with reliably excellent outcomes as evidenced by a very high rate of technical success, low treatment-related morbidity and mortality rates, and low posttreatment hemorrhage rates. These findings suggest continued improvement in the endovascular treatment of intracranial aneurysms, compared with earlier trials.[9] The broad geographic nature of this multicenter trial and broad inclusion criteria suggest widespread generalizability of the study results.

Disclosures: Cameron G. McDougall—*UNRELATED*: *Consultancy*: Covidien, MicroVention, *Comments*: scientific advisory board for Covidien and proctor for ev3, consultant to MicroVention. S. Claiborne Johnston—*RELATED*: *Grant*: Stryker Neurovascular.* Anil Gholkar—*RELATED*: *Grant*: My hospital trust received a small grant for recruiting patients in the MAPS Trial. This was for collection of data for the study,* *Support for Travel to Meetings for the Study or Other Purposes*: Stryker, *Comments*: I received support for travel to investigator meetings, *UNRELATED*: *Consultancy*: Codman Neurovascular, Stryker Neurovascular, Johnson & Johnson; *Comments*: I work as a consultant and was paid an honorarium for educational activities sponsored by device companies. The activities are around training of interventional neuroradiology trainees, *Travel/Accommodations/Meeting Expenses Unrelated to Activities Listed*: MicroVention, *Comments*: travel support to attend World Federation of Interventional and Therapeutic Neuroradiology and Society of Neurointerventional Surgery meetings from various device-manufacturing companies, *Other*: In the past, an interventional neuroradiology trainee at my hospital was partly supported by Stryker Neurovascular. As far as I am aware, this has not been the case for at least several years.* Stanley L. Barnwell—*Consultancy*: Stryker Neurovascular. Javier Massó Romero—*RELATED*: *Grant*: Stryker Neurovascular,* *Consulting Fee or Honorarium*: Stryker Neurovascular. John C. Chaloupka—*RELATED*: *Grant*: Stryker Neurovascular,* *Comments*: administrative support for data collection and follow-up for the trial, *UNRELATED*: *Consultancy*: Stryker Neurovascular, *Comments*: expert clinical and technical advice on various research and development projects, *Payment for Lectures (including service on Speakers Bureaus)*: received payment from Stryker Neurovascular for sponsored lectures, *Comments*: educational lecturing on various topics involving the use of stenting in neuroendovascular practice. Alain Bonafe—*RELATED*: *Grant*: Stryker,* *Support for Travel to Meetings for the Study or Other Purposes*: Stryker, *UNRELATED*: *Consultancy*: Stryker. Ajay K. Wakhloo— *UNRELATED*: *Board Membership*: Surpass Medical Ltd, *Consultancy*: Stryker Neurovascular, Codman Johnson & Johnson Neurovascular, Philips Health-

care, Boston Biomedical Associates, Soteira, *Expert Testimony*: Hugsland and Knopf, LLC, New Jersey, *Grants/Grants Pending*: National Institutes of Health,* Philips Healthcare,* *Payment for Lectures (including service on Speakers' Bureaus)*: Harvard postgraduate course, *Stock/Stock Options*: Stryker Neurovascular, *Travel/Accommodations/Meeting Expenses Unrelated to Activities Listed*: Stryker Neurovascular, Codman Johnson & Johnson Neurovascular, Surpass Medical Ltd. Christopher F. Dowd—*RELATED*: *Fees For Participation in Review Activities such as Data Monitoring Boards, Statistical Analysis, Endpoint Committees, and the Like*: Stryker Neurovascular, *Comments*: I served as Chief Adjudicator for the MAPS Trial. I also served as a Medical Advisor to Neuro Vasx Inc. Allan J. Fox—*RELATED*: *Grant*: core laboratory for the Cerecyte Trial, *Support for Travel to Meetings for the Study or Other Purposes*: Micrus Endovascular,* *Comments*: for meetings of Cerecyte; *OTHER RELATIONSHIPS*: Chair of Adverse Events Committee for the MAPS Trial, payment per hour for work done, organized by Stryker Neurovascular. So Jung Imm—*RELATED*: I worked for Stryker Neurovascular, which sponsored this study. I did not receive compensation beyond my normal salary for working on this project. *UNRELATED*: *Employment*: Stryker Neurovascular, *Comments*: At the time of this study, I was an employee of Stryker Neurovascular. Kirsten Carroll—*RELATED*: *Grant*: I work for Stryker, which sponsored the study. I did not receive compensation beyond my normal salary for working on this project. I did not receive third-party funding outside of Stryker for my work on the project, *UNRELATED*: *Employment*: Stryker Neurovascular, *Comments*: I am an employee of Stryker Neurovascular; *Stock/Stock Options*: Stryker Neurovascular, *Comments*: I receive stock grants as part of my annual compensation at Stryker Neurovascular. Aquilla S. Turk—*RELATED*: *Consulting Fee or Honorarium*: Stryker, *Comments*: consultation work, honoraria, research funding from Stryker, *UNRELATED*: *Consultancy*: Covidien, MicroVention, Penumbra, Stryker (other projects), Siemens, Codman, *Comments*: consultation work, honoraria, research funding, *Grants/Grants Pending*: Medical University of South Carolina,* *Comments*: for the clinical trial LARGE, *Payment for Lectures (including service on Speakers Bureaus)*: Covidien, MicroVention, Penumbra, Stryker (other projects), Siemens, Codman. *Money paid to the institution.

REFERENCES

1. Molyneux AJ, Kerr RS, Yu LM, et al. **International subarachnoid aneurysm trial (ISAT) of neurosurgical clipping versus endovascular coiling in 2143 patients with ruptured intracranial aneurysms: a randomised comparison of effects on survival, dependency, seizures, rebleeding, subgroups, and aneurysm occlusion.** *Lancet* 2005;366:809–17
2. McDougall CG, Spetzler RF, Zabramski JM, et al. **The Barrow Ruptured Aneurysm Trial.** *J Neurosurg* 2012;116:135–44
3. Molyneux AJ, Kerr RS, Birks J, et al. **Risk of recurrent subarachnoid haemorrhage, death, or dependence and standardised mortality ratios after clipping or coiling of an intracranial aneurysm in the International Subarachnoid Aneurysm Trial (ISAT): long-term follow-up.** *Lancet Neurol* 2009;8:427–33
4. Kang HS, Han MH, Kwon BJ, et al. **Short-term outcome of intracranial aneurysms treated with polyglycolic acid/lactide copolymer-coated coils compared to historical controls treated with bare platinum coils: a single-center experience.** *AJNR Am J Neuroradiol* 2005;26:1921–28
5. Taschner CA, Leclerc X, Rachdi H, et al. **Matrix detachable coils for the endovascular treatment of intracranial aneurysms: analysis of early angiographic and clinical outcomes.** *Stroke* 2005;36:2176–80
6. Lubicz B, Leclerc X, Gauvrit JY, et al. **Endovascular treatment of intracranial aneurysms with Matrix coils: a preliminary study of immediate post-treatment results.** *AJNR Am J Neuroradiol* 2005;26:373–75
7. Raymond J, Guilbert F, Weill A, et al. **Long-term angiographic recurrences after selective endovascular treatment of aneurysms with detachable coils.** *Stroke* 2003;34: 1398–1403
8. Heros RC, Zauner A. **Early experience with Matrix detachable coils.** *J Neurosurg* 2006;105:190–91, discussion 191
9. Murayama Y, Vinuela F, Ishii A, et al. **Initial clinical experience with Matrix detachable coils for the treatment of intracranial aneurysms.** *J Neurosurg* 2006;105:192–99
10. Fiorella D, Albuquerque FC, McDougall CG. **Durability of aneurysm embolization with Matrix detachable coils.** *Neurosurgery* 2006;58: 51–59
11. Niimi Y, Song J, Madrid M, et al. **Endosaccular treatment of intracranial aneurysms using Matrix coils: early experience and midterm follow-up.** *Stroke* 2006;37:1028–32
12. Katsaridis V, Papagiannaki C, Violaris C. **Guglielmi detachable coils versus Matrix coils: a comparison of the immediate posttreatment results of the embolization of 364 cerebral aneurysms in 307 patients—a single-center, single-surgeon experience.** *AJNR Am J Neuroradiol* 2006;27:1841–48
13. Pierot L, Bonafe A, Bracard S, et al. **Endovascular treatment of intracranial aneurysms with Matrix detachable coils: immediate post-treatment results from a prospective multicenter registry.** *AJNR Am J Neuroradiol* 2006;27:1693–99
14. Rivet DJ, Moran CJ, Mazumdar A, et al. **Single-institution experience with Matrix coils in the treatment of intracranial aneurysms: comparison with same-center outcomes with the use of platinum coils.** *AJNR Am J Neuroradiol* 2007;28:1736–42
15. Pierot L, Leclerc X, Bonafe A, et al. **Endovascular treatment of intracranial aneurysms using Matrix coils: short- and mid-term results in ruptured and unruptured aneurysms.** *Neurosurgery* 2008;63:850–57
16. Pierot L, Leclerc X, Bonafe A, et al. **Endovascular treatment of intracranial aneurysms with Matrix detachable coils: midterm anatomic follow-up from a prospective multicenter registry.** *AJNR Am J Neuroradiol* 2008;29:57–61
17. Ishii A, Murayama Y, Nien YL, et al. **Immediate and midterm outcomes of patients with cerebral aneurysms treated with Matrix1 and Matrix2 coils: a comparative analysis based on a single-center experience in 250 consecutive cases.** *Neurosurgery* 2008;63:1071–77
18. Smith MJ, Mascitelli J, Santillan A, et al. **Bare platinum vs Matrix detachable coils for the endovascular treatment of intracranial aneurysms: a multivariate logistic regression analysis and review of the literature.** *Neurosurgery* 2011;69:557–64
19. Pierot L, Cognard C, Ricolfi F, et al. **Mid-term anatomic results after endovascular treatment of ruptured intracranial aneurysms with Guglielmi detachable coils and Matrix coils: analysis of the CLARITY series.** *AJNR Am J Neuroradiol* 2012;33:469–73
20. Johnston SC, Dowd CF, Higashida RT, et al. **Predictors of rehemorrhage after treatment of ruptured intracranial aneurysms: the Cerebral Aneurysm Rerupture After Treatment (CARAT) study.** *Stroke* 2008;39:120–25
21. White PM, Lewis SC, Gholkar A, et al. **Hydrogel-coated coils versus bare platinum coils for the endovascular treatment of intracranial aneurysms (HELPS): a randomised controlled trial.** *Lancet* 2011;377:1655–62
22. Coley S, Sneade M, Clarke A, et al. **Cerecyte Coil Trial: procedural safety and clinical outcomes in patients with ruptured and unruptured intracranial aneurysms.** *AJNR Am J Neuroradiol* 2012;33:474–80
23. Wiebers DO, Whisnant JP, Huston J III, et al. **Unruptured intracranial aneurysms: natural history, clinical outcome, and risks of surgical and endovascular treatment.** *Lancet* 2003;362:103–10
24. Pierot L, Spelle L, Vitry F. **Immediate clinical outcome of patients harboring unruptured intracranial aneurysms treated by endovascular approach: results of the ATENA study.** *Stroke* 2008;39:2497–504
25. The CARAT Investigators. **Rates of delayed rebleeding from intracranial aneurysms are low after surgical and endovascular treatment.** *Stroke* 2006;37:1437–42

Endovascular Treatment of Anterior Communicating Artery Aneurysms: A Systematic Review and Meta-Analysis

S. Fang, W. Brinjikji, M.H. Murad, D.F. Kallmes, H.J. Cloft, and G. Lanzino

ABSTRACT

BACKGROUND AND PURPOSE: Endovascular therapy has become an acceptable alternative to traditional clipping for the management of intracranial aneurysms. However, a limited number of studies have examined outcomes and complications specific to embolization of anterior communicating artery aneurysms.

MATERIALS AND METHODS: A systematic review of the literature was conducted with the use of multiple data bases to identify reports on endovascular treatment of anterior communicating artery aneurysms between 1994 and 2012. Angiographic results, clinical outcomes, and complication rates were pooled across studies by using random-effects meta-analysis with subgroup analysis of outcomes by rupture status and time trend stratification.

RESULTS: Fourteen studies, consisting of 1552 treated anterior communicating artery aneurysms, were included in this meta-analysis. The rate of immediate and long-term complete and near-complete angiographic occlusion was 88% (95% CI = 81–93%) and 85% (95% CI = 78–90%), respectively. Intraprocedural rupture rate was 4% (95% CI = 3–6%). The re-bleeding rate was 2% (95% CI = 1–4%) and the retreatment rate was 7% (95% CI = 5–12%). Morbidity or mortality caused by perioperative stroke occurred at a 3% (95% CI = 2–6%) rate. Overall procedure-related morbidity and mortality were 6% (95% CI = 4–8%) and 3% (95% CI = 2–4%), respectively. Outcomes did not differ between ruptured and unruptured aneurysms, nor did outcomes change over time, though these latter subanalyses were relatively underpowered.

CONCLUSIONS: Endovascular therapy for anterior communicating artery aneurysms is associated with a high rate of complete angiographic occlusion. However, the procedure-related permanent morbidity and mortality are not negligible for aneurysms in this location.

ABBREVIATION: AcomA = anterior communicating artery; ISAT = International Subarachnoid Aneurysm Trial; CARAT = Cerebral Aneurysm Rerupture After Treatment

The anterior communicating artery (AcomA) is the most common location for intracranial aneurysms in most series, and rupture of aneurysms in this location accounts for approximately 40% of aneurysmal subarachnoid hemorrhages in adults.[1-5] Aneurysms of the AcomA can be technically challenging from a surgical perspective because of complex regional flow dynamics, frequent anatomic variations, variable geometry, and the presence of critical perforators.[1,6-10] In the past 2 decades, the inherently less invasive endovascular approach has emerged as a feasible and acceptable treatment option for AcomA aneurysms.[11-14] Continual advancements in endovascular technique and adjuvant devices have led to an enlarging proportion of patients with AcomA aneurysms who are successfully treated with coil embolization.[10,11,15,16] A limited number of case series have detailed the clinical outcomes, angiographic results, and procedure-related complications specific for endovascular treatment in this location.[10-13,15-24] We performed a systematic review of the published literature to better define safety and efficacy profiles for coil embolization of AcomA aneurysms beyond single-center experiences.

Received May 15, 2013; accepted after revision October 2.

From Mayo Medical School (S.F.), Department of Radiology (W.B., D.F.K., H.J.C.), Division of Preventive Medicine (M.H.M.), and Department of Neurologic Surgery (G.L.), Mayo Clinic, Rochester, Minnesota.

Please address correspondence to Giuseppe Lanzino, MD, Department of Neurological Surgery, Mayo Clinic, 200 First St SW, Rochester, MN 55905; e-mail: lanzino.giuseppe@mayo.edu

Indicates article with supplemental on-line tables.

EBM 1 Evidence-Based Medicine Level 1.

http://dx.doi.org/10.3174/ajnr.A3802

MATERIALS AND METHODS

Systematic Literature Search

We performed a comprehensive review of the literature between January 1994 to December 2012 through the use of the key words "anterior communicating artery," "intracranial aneurysm," "en-

Table 1: Studies included in meta-analysis

Author (year)	Study Design	No. of Patients with AcomA Aneurysms	AcomA Aneurysms Treated	Patients with Ruptured AcomA Aneurysms	Patients with Unruptured AcomA Aneurysms
Birknes et al (2006)	Retrospective	123	123	113	10
Cherian et al (2001)	Prospective	103	103	103	0
Choi et al (2011)	Retrospective	45	45	45	0
Elias et al (2003)	Prospective	30	30	30	0
Finitsis et al (2010)	Prospective	280	281	239	42
Guglielmi et al (2009)	Retrospective	306	306	236	70
Huang et al (2011)	Retrospective	20	20	20	0
Johnson et al (2012)	Retrospective	64	64	–	–
Leclerc et al (2002)	Prospective	20	20	20	0
Moret et al (1996)	Prospective	36	36	30	6
Proust et al (2003)	Prospective	37	37	36	1
Raslan et al (2011)	Retrospective	44	44	43	1
Schuette et al (2011)	Retrospective	347	347	277	70
Songsaeng et al (2010)	Retrospective	96	96	7	89

Note:—Studies are from References 10–13 and 15–24. AcomA indicates anterior communicating artery.

dovascular," "coil," and "embolization" in the PubMed, Ovid MEDLINE, Ovid EMBASE, Scopus, and Web of Science data bases. Studies reporting on the endovascular treatment of AcomA aneurysms were selected. All case reports, reviews, and articles not published in English were excluded. The search strategy for the electronic data bases was developed and conducted by a reference librarian with expertise in systematic reviews.

Identified studies were reviewed for inclusion in the meta-analysis on the basis of these criteria: 1) studies reporting on endovascular treatment of consecutive series of AcomA intracranial aneurysms comprising ≥20 patients, 2) studies providing rates of aneurysmal occlusion and data on intra- and postoperative complications, and 3) studies reporting the rupture status of treated aneurysms. For multiple series from the same institution or authors, only the most recent (usually larger) series was included to avoid including the same patients in the analysis.

For each included study, information was extracted with regard to aneurysm rupture status, immediate angiographic outcomes, long-term angiographic outcomes, and retreatment rate. Long-term angiographic outcomes were only included for those studies with 6 months or more of angiographic follow-up. Complete occlusion was defined as absence of angiographic filling in aneurysm neck or sac, and near-complete occlusion was defined as small residual neck filling without any filling of the sac. For procedure-related complications, we extracted information regarding intraoperative rupture, vasospasm, perioperative thromboembolic complications resulting in morbidity and mortality, re-hemorrhage, and procedure-related mortality and permanent morbidity. Procedure-related mortality and morbidity were defined as permanent morbidity and mortality resulting from intraoperative rupture, cerebral ischemia, new neurologic deficits, aneurysmal re-bleeding, sepsis, and myocardial infarction during the perioperative period.

Statistical Analysis

We estimated the cumulative incidence (event rate at the end of study follow-up) and 95% CI for every outcome. Event rates were pooled across studies by means of random-effects meta-analysis.[25] We considered outcomes of ruptured and unruptured AcomA aneurysms separately, as well as a combined outcome. We also performed subgroup analysis comparing outcomes of studies published from the years 2007–2012 and those published before 2007. Interaction of covariates with the log of event rate was performed as described by Altman.[26] The I^2 statistic was used to evaluate the extent of heterogeneity across studies and represents the proportion of heterogeneity in study results that is not attributable to chance or random error.[27] Values of <25%, 25–50%, and >50% are consistent with small, moderate, and substantial heterogeneity, respectively. We conducted Begg and Mazumdar rank correlation to evaluate publication bias. All statistical analyses were performed with the use of Comprehensive Meta-Analysis Version 2.0 (www.meta-analysis.com).

RESULTS

Study Selection

Data base search led to the retrieval of 488 articles, 14 of which fulfilled the criteria for inclusion. These included 8 retrospective consecutive series and 6 prospective studies. A summary of the studies included in this meta-analysis is provided in Table 1. Five of these studies included outcomes of patients with ruptured aneurysms only, whereas 9 studies included outcomes of patients with both ruptured and unruptured AcomA aneurysms. Information on angiographic outcomes, perioperative complications, and procedure-related morbidity and mortality was not consistently provided in every study. Furthermore, not all studies that included both ruptured and unruptured AcomA aneurysms described stratified outcomes with regard to rupture status. In total, this meta-analysis included 1551 patients, with 1552 treated AcomA aneurysms. In the 13 articles reporting numbers of patients presenting with ruptured or unruptured status, there was a total of 1488 patients with AcomA aneurysms. These consisted of 1199 patients presenting with ruptured aneurysms and 289 patients presenting with unruptured aneurysms.

Study Outcomes

Immediate and Long-Term Angiographic Outcomes. The overall rate of complete and near-complete occlusion (>95%) immediately after procedure was 88% (95% CI = 81–93%). At follow-up, at least 6 months after the procedure, the complete and near-complete occlusion was 85% (95% CI = 78–90%). Occlusion rates for ruptured and unruptured aneurysms were similar for

Table 2: Overall complication rates

Outcome	No. of Studies	Raw No. of Events in All Aneurysms[a]	Meta-Analysis Percentage (95% CI)	I^2
Intraoperative rupture	11	57/1387	4% (3–6%)	0
Vasospasm	6	182/1091	13% (5–28%)	95
Re-bleeding event	11	16/1065	2% (1–4%)	0
Aneurysm retreatment	10	73/777	7% (5–12%)	60
Morbidity or mortality due to stroke <30 days	10	21/771	3% (2–6%)	32
Permanent procedure-related morbidity	11	53/1077	6% (4–8%)	47
Procedure-related mortality	11	25/1077	3% (2–4%)	15

[a] Discordances between the raw event percentages and the percentages calculated from the meta-analysis are caused by greater weights assigned to outcomes of studies with larger sample sizes.

both the immediate ($P = .13$) and long-term follow-up ($P = .39$). The overall rate of retreatment as the result of re-bleeding, recanalization, or aneurysmal growth was 7% (95% CI = 5–12%). Ruptured and unruptured aneurysms did not show significantly different rates of retreatment after the procedure ($P = .61$). These results are shown in On-line Table 1.

Procedure-Related-Complications. The intraprocedural rupture rate in all aneurysms was 4% (95% CI = 3–6%). The rupture rate was not significantly different between ruptured and unruptured aneurysms ($P = .87$). Vasospasm was reported at an overall rate of 13% (95% CI = 5–28%). The rate of vasospasm was 11% (95% CI = 3–30%) in ruptured aneurysms and 1% (95% CI = 3–30%) in unruptured aneurysms. Aneurysmal re-bleeding occurred in 2% of patients (95% CI = 1–4%), with similar rates of postprocedure bleeding in ruptured and unruptured aneurysms ($P = .50$). These results are shown in Table 2. Outcome event rates from overall and ruptured/unruptured aneurysms are compared in On-line Table 2.

Morbidity and Mortality From Endovascular Treatment. Overall procedure-related permanent morbidity and mortality was 6% (95% CI = 4–8%) and 3% (95% CI = 2–4%), respectively. Permanent morbidity was 7% (95% CI = 4–12%) for ruptured aneurysms and 8% (95% CI = 3–20%) for unruptured aneurysms ($P = .90$). Mortality as the result of the procedure was 4% (95% CI = 3–7%) in ruptured aneurysms and 2% (95% CI = 1–9%) for unruptured aneurysms ($P = .40$). Among ruptured aneurysms, the rate of death attributed to the presenting SAH was 7% (95% CI = 4–13%). No difference was observed in the morbidity or mortality rates as the result of perioperative stroke between ruptured and unruptured aneurysms ($P = .49$).

Time-Trend Analysis of Angiographic Results and Complication Rates. We analyzed the outcomes for studies published before 2007 as compared with studies published between 2007 and 2012. The rate of aneurysm occlusion and procedure-related complications did not differ significantly over time. The results are shown in On-line Table 3.

Heterogeneity and Publication Bias. Analysis of the statistical heterogeneity across the studies included in this meta-analysis was low to moderate for most outcomes. Outcomes associated with significant heterogeneity (I^2>50%) were the angiographic outcomes immediately after surgery ($I^2 = 82$) and in long-term follow-up ($I^2 = 69$), vasospasm ($I^2 = 95$), and aneurysm retreatment ($I^2 = 60$). Information provided in the studies was not sufficient for further analysis of possible causes for the observed differences in patient populations or in treatments, including any effect of subgroup analysis on heterogeneity.

The results of the Begg and Mazumdar rank correlation test do not suggest publication bias ($P > .05$) for study outcomes with minimal or moderate heterogeneity (I^2 <50%). For analyses associated with heterogeneity, evaluation of publication bias was not possible because statistical testing for funnel asymmetry assumes a fixed-effect model with no heterogeneity.

DISCUSSION

In this meta-analysis, we combined data from 14 studies to analyze the representative outcomes for angiographic occlusion, procedure-related complications, and morbidity as well as mortality associated with endovascular treatment of AcomA aneurysms. Our results demonstrated that AcomA aneurysms can be successfully treated with endovascular embolization and maintain a high rate of complete or near-complete occlusion at follow-up. However, complications associated with coil embolization of AcomA aneurysms are not negligible, with a permanent morbidity rate of 6% and mortality rate of 3%.

Since the introduction of Guglielmi Detachable Coils in 1991, endovascular technique has dramatically changed the management of these aneurysms and established coiling as an acceptable alternative option to traditional clip ligation.[13,18,28,29] Large, randomized trials such as the International Subarachnoid Aneurysm Trial (ISAT) and the Barrow Ruptured Aneurysm Trial have shown that patients with ruptured aneurysms have significant advantages in disability independent survival and functional outcome when compared with those treated surgically.[30,31] However, one of the major limitations of endovascular treatment continues to be the risk of postprocedure re-bleeding. Data from ISAT and the Cerebral Aneurysm Rerupture After Treatment (CARAT) studies show significantly higher risks of re-bleeding after endovascular treatment as compared with surgical therapy.[4,32] In our meta-analysis, we found that the rate of periprocedural re-bleeding for AcomA aneurysms with endovascular retreatment was 2%, which is consistent with rates reported in CARAT and ISAT. However, recurrence or rupture of aneurysms after the initial treatment requiring retreatment by secondary coiling or clipping occurred in 7% of cases.

With the advances made in endovascular technology in recent years, the characteristics of complicated AcomA aneurysms that previously precluded treatment by coiling are increasingly challenged. The inherent small diameter of the AcomA from which the aneurysm rises as well as the propensity for AcomA aneurysms to be small in size or wide-neck are the features that can make

endovascular treatment difficult.[11,13,17] Since the mid-1990s, advances in technology such as 3D rotational angiography and newer microguidewire/catheters, in combination with adjunctive devices such as balloon-assisted or stent-assisted coiling, have revolutionized treatment of aneurysms once deemed unfeasible to coil. Newer studies are beginning to examine the effects of these adjunctive devices on long-term angiographic stability and complications and recurrence rates associated with endovascular treatment; however, this is not yet well characterized for coiling therapy in AcomA aneurysms.[10,20,23]

To determine any effect of advancements in technology and operator experience on the safety and efficacy of AcomA embolization, we looked at the angiographic and complication outcomes of patients in studies published before 2007 as compared with those published between 2007 and 2012. No statistically significant differences were found in our analysis of angiographic results or complications, which might be caused by underpowering. However, there was a trend suggesting decreased overall procedure-related permanent morbidity and mortality in the studies published from 2007–2012. This trend of decreased morbidity and mortality observed in patients with AcomA aneurysm over time is consistent with the finding that morbidity and mortality rates have increasingly been reduced across time among a sample of patients treated with endovascular coiling in the United States (Nationwide Inpatient Sample).[28,33,34] These studies showed that morbidity rates decreased from 7.6–4.9% in the analysis of patients treated with endovascular therapy in 1996–2000 compared with 2001–2008. Mortality rates of overall patients treated with endovascular coiling decreased from 1.7% in 1996–2000 to 0.6% in 2001–2008.

Across this time period stratification, our meta-analysis also showed that the overall aneurysm retreatment rate doubled from 5–10% when comparing studies published before and after 2007; however, the trend toward an increase was not statistically significant. Given the consistently smaller number of studies included in the "before 2007" time period stratification group, along with nationally increased use of embolization therapy over time, this increased trend found in retreatment rate may reflect a larger and more representative sample size in the 2007–2012 stratification group. Alternatively, this trend may be a result of endovascular coil embolization applied to a subset of aneurysms that are not necessarily considered "ideal" for endovascular treatment due to higher risks of recanalization.

There are several limitations to this study. Because of the highly selected cases available for analysis, this systematic review does not provide information on the proportion of all AcomA aneurysms that met the criteria for endovascular treatment. Many published studies collected data retrospectively; therefore, stratification of outcomes by rupture status and other variables such as previous rupture and number or types of adjunctive devices used was not provided in every study. The studies that were performed prospectively were not randomized studies and did not include control groups. Many of the studies included in this meta-analysis ranged in sample size, and several of the studies did not provide complete follow-up data in terms of clinical outcome or angiographic results. The included studies covered consecutive patients over many years; however, the different time periods covered largely limited our ability to stratify and scrutinize outcomes over time. Further temporal stratification of outcomes may reveal variations in complication rates over time as a result of increased experience or improvements in technology.

An important limitation of this meta-analysis is the variability inherent in assessment of angiographic outcomes for endovascular treatment of aneurysms. Multiple studies have shown only "fair" interobserver and intra-observer agreement on interpretation of the completeness of occlusion after coiling, with improvement to "moderate" agreement with follow-up angiography.[35,36] However, judgment and adjudicating aneurysms into a residual aneurysms category remain poor and can vary among observers to range from 20–60%.[36] The interobserver and intra-observer variability is inherent to the assessment scales used for extent of occlusion and can result in decreased variability in scales with fewer response options, though this can be less ideal for assessing effects of occlusion completeness on important outcomes such as recurrence or re-hemorrhage.[35,37] Although we were unable to individually validate the extent of occlusion for each aneurysm, many studies used the Raymond-Roy classification system[38] for categorization of angiographic outcomes, and we adhered to this scale as best we could, given the descriptors used in the methods for included studies. Despite this, caution is warranted when interpreting the results of this meta-analysis. It is important to consider the effects of the interobserver and intra-observer variability because the data used are gathered from case series from different institutions with the use of various technologies and equipment and conducted by specialists with ranging levels of experience and techniques.

CONCLUSIONS

The results of this meta-analysis suggest that the endovascular treatment of AcomA aneurysms is feasible and effective and can maintain high rates of complete and near-complete occlusion at long-term follow-up. However, the procedure-related morbidity and mortality associated with this treatment technique are not negligible and should be considered when deciding the best management approach to AcomA aneurysms.

ACKNOWLEDGMENTS

This study was supported by the Center for the Science of Health care Delivery and the Center for Translational Science Activities, Mayo Clinic, Rochester, Minnesota. The authors thank Sherry Kallies for assistance in editing and preparing the manuscript for submission.

Disclosures: David F. Kallmes—*UNRELATED: Consultancy:* General Electric, ev3, Codman,* Comments: General consulting regarding planning and implementation of clinical trials; serving as investigator in ongoing trials; *Grants/Grants Pending:* Sequent, Codman, ev3, Benvenue,* MicroVention; *Royalties:* UVA Patent Foundation, Comments: License fees for spine fusion technology; *Travel/Accommodations/Meeting Expenses Unrelated to Activities Listed:* MicroVention,* ev3*; Comments: Presentation at meetings. Harry J. Cloft—*UNRELATED: Grants/Grants Pending:* Cordis Endovascular,* Comments: Site PI at enrolling site for SAPPHIRE (Stenting and Angioplasty with Protection in Patients and HIgh Risk for Endarterectomy) registry sponsored by Cordis Endovascular. Giuseppe Lanzino—*UNRELATED: Consultancy:* ev3/Covidien*; *OTHER:* Unrelated educational grants to the institution.

REFERENCES

1. Hernesniemi J, Dashti R, Lehecka M, et al. **Microneurosurgical management of anterior communicating artery aneurysms.** *Surg Neurol* 2008;70:8–28
2. Kassell NF, Torner JC, Haley EC Jr, et al. **The International Cooperative Study on the Timing of Aneurysm Surgery, part 1: overall management results.** *J Neurosurg* 1990;73:18–36
3. Le Roux PD, Elliott JP, Downey L, et al. **Improved outcome after rupture of anterior circulation aneurysms: a retrospective 10-year review of 224 good-grade patients.** *J Neurosurg* 1995;83:394–402
4. Molyneux AJ, Kerr RS, Birks J, et al. **Risk of recurrent subarachnoid haemorrhage, death, or dependence and standardised mortality ratios after clipping or coiling of an intracranial aneurysm in the International Subarachnoid Aneurysm Trial (ISAT): long-term follow-up.** *Lancet Neurol* 2009;8:427–33
5. Brisman JL, Song JK, Newell DW. **Cerebral aneurysms.** *N Engl J Med* 2006;355:928–39
6. Riina HA, Lemole GM Jr, Spetzler RF. **Anterior communicating artery aneurysms.** *Neurosurgery* 2002;51:993–96
7. Nathal E, Yasui N, Sampei T, et al. **Intraoperative anatomical studies in patients with aneurysms of the anterior communicating artery complex.** *J Neurosurg* 1992;76:629–34
8. Kirgis HD, Fisher WL, Llewellyn RC, et al. **Aneurysms of the anterior communicating artery and gross anomalies of the circle of Willis.** *J Neurosurg* 1966;25:73–78
9. Sekhar LN, Natarajan SK, Britz GW, et al. **Microsurgical management of anterior communicating artery aneurysms.** *Neurosurgery* 2007;61(5 Suppl 2):273–90
10. Huang QH, Wu YF, Xu Y, et al. **Vascular geometry change because of endovascular stent placement for anterior communicating artery aneurysms.** *AJNR Am J Neuroradiol* 2011;32:1721–25
11. Moret J, Pierot L, Boulin A, et al. **Endovascular treatment of anterior communicating artery aneurysms using Guglielmi detachable coils.** *Neuroradiology* 1996;38:800–05
12. Birknes JK, Hwang SK, Pandey AS, et al. **Feasibility and limitations of endovascular coil embolization of anterior communicating artery aneurysms: morphological considerations.** *Neurosurgery* 2006;59:43–52
13. Guglielmi G, Vinuela F, Duckwiler G, et al. **Endovascular treatment of 306 anterior communicating artery aneurysms: overall, perioperative results.** *J Neurosurg* 2009;110:874–79
14. Proust F, Martinaud O, Gerardin E, et al. **Quality of life and brain damage after microsurgical clip occlusion or endovascular coil embolization for ruptured anterior communicating artery aneurysms: neuropsychological assessment.** *J Neurosurg* 2009;110:19–29
15. Cherian MP, Pranesh MB, Mehta P, et al. **Outcomes of endovascular coiling of anterior communicating artery aneurysms in the early post-rupture period: a prospective analysis.** *Neurol India* 2001;59:218–23
16. Schuette AJ, Hui FK, Spiotta AM, et al. **Endovascular therapy of very small aneurysms of the anterior communicating artery: five-fold increased incidence of rupture.** *Neurosurgery* 2011;68:731–37
17. Choi JH, Kang MJ, Huh JT. **Influence of clinical and anatomic features on treatment decisions for anterior communicating artery aneurysms.** *J Korean Neurosurg Soc* 2011;50:81–88
18. Elias T, Ogungbo B, Connolly D, et al. **Endovascular treatment of anterior communicating artery aneurysms: results of clinical and radiological outcome in Newcastle.** *Br J Neurosurg* 2003;17:278–86
19. Finitsis S, Anxionnat R, Lebedinsky A, et al. **Endovascular treatment of ACom intracranial aneurysms: report on series of 280 patients.** *Interv Neuroradiol* 2010;16:7–16
20. Johnson AK, Munich SA, Heiferman DM, et al. **Stent assisted embolization of 64 anterior communicating artery aneurysms.** *J Neurointerv Surg* 2012;5:Suppl 3 iii62–iii65
21. Leclerc X, Navez JF, Gauvrit JY, et al. **Aneurysms of the anterior communicating artery treated with Guglielmi detachable coils: follow-up with contrast-enhanced MR angiography.** *AJNR Am J Neuroradiol* 2002;23:1121–27
22. Proust F, Debono B, Hannequin D, et al. **Treatment of anterior communicating artery aneurysms: complementary aspects of microsurgical and endovascular procedures.** *J Neurosurg* 2003;99:3–14
23. Raslan AM, Oztaskin M, Thompson EM, et al. **Neuroform stent-assisted embolization of incidental anterior communicating artery aneurysms: long-term clinical and angiographic follow-up.** *Neurosurgery* 2011;69:27–37
24. Songsaeng D, Geibprasert S, Willinsky R, et al. **Impact of anatomical variations of the circle of Willis on the incidence of aneurysms and their recurrence rate following endovascular treatment.** *Clin Radiol* 2010;65:895–901
25. DerSimonian R, Laird N. **Meta-analysis in clinical trials.** *Control Clin Trials* 1986;7:177–88
26. Altman DG, Bland JM. **Interaction revisited: the difference between two estimates.** *BMJ* 2003;326:219
27. Higgins JP, Thompson SG, Deeks JJ, et al. **Measuring inconsistency in meta-analyses.** *BMJ* 2003;327:557–60
28. Brinjikji W, Rabinstein AA, Nasr DM, et al. **Better outcomes with treatment by coiling relative to clipping of unruptured intracranial aneurysms in the United States, 2001–2008.** *AJNR Am J Neuroradiol* 2011;32:1071–75
29. Cowan JA Jr, Ziewacz J, Dimick JB, et al. **Use of endovascular coil embolization and surgical clip occlusion for cerebral artery aneurysms.** *J Neurosurg* 2007;107:530–35
30. Molyneux A, Kerr R, Stratton I, et al. **International Subarachnoid Aneurysm Trial (ISAT) of neurosurgical clipping versus endovascular coiling in 2143 patients with ruptured intracranial aneurysms: a randomized trial.** *J Stroke Cerebrovasc Dis* 2002;11:304–14
31. McDougall CG, Spetzler RF, Zabramski JM, et al. **The Barrow Ruptured Aneurysm Trial.** *J Neurosurg* 2012;116:135–44
32. Carat Investigators. **Rates of delayed rebleeding from intracranial aneurysms are low after surgical and endovascular treatment.** *Stroke* 2006;37:1437–42
33. Alshekhlee A, Mehta S, Edgell RC, et al. **Hospital mortality and complications of electively clipped or coiled unruptured intracranial aneurysm.** *Stroke* 2010;41:1471–76
34. Hoh BL, Rabinov JD, Pryor JC, et al. **In-hospital morbidity and mortality after endovascular treatment of unruptured intracranial aneurysms in the United States, 1996–2000: effect of hospital and physician volume.** *AJNR Am J Neuroradiol* 2003;24:1409–20
35. Cloft HJ, Kaufmann T, Kallmes DF. **Observer agreement in the assessment of endovascular aneurysm therapy and aneurysm recurrence.** *AJNR Am J Neuroradiol* 2007;28:497–500
36. Tollard E, Darsaut TE, Bing F, et al. **Outcomes of endovascular treatments of aneurysms: observer variability and implications for interpreting case series and planning randomized trials.** *AJNR Am J Neuroradiol* 2012;33:626–31
37. Raymond J, White PM, Molyneux AJ. **Scales, agreement, outcome measures, and progress in aneurysm therapy.** *AJNR Am J Neuroradiol* 2007;28:501–02
38. Raymond J, Guilbert F, Weill A, et al. **Long-term angiographic recurrences after selective endovascular treatment of aneurysms with detachable coils.** *Stroke* 2003;34:1398–403

Treatment of Cavernous Sinus Aneurysms with Flow Diversion: Results in 44 Patients

R.C. Puffer, M. Piano, G. Lanzino, L. Valvassori, D.F. Kallmes, L. Quilici, H.J. Cloft, and E. Boccardi

ABSTRACT

BACKGROUND AND PURPOSE: Aneurysms of the cavernous segment of the ICA are difficult to treat with standard endovascular techniques, and ICA sacrifice achieves a high rate of occlusion but carries an elevated level of surgical complications and risk of de novo aneurysm formation. We report rates of occlusion and treatment-related data in 44 patients with cavernous sinus aneurysms treated with flow diversion.

MATERIALS AND METHODS: Patients with cavernous segment aneurysms treated with flow diversion were selected from a prospectively maintained data base of patients from 2009 to the present. Demographic information, treatment indications, number/type of flow diverters placed, outcome, complications (technical or clinical), and clinical/imaging follow-up data were analyzed.

RESULTS: We identified 44 patients (37 females, 7 males) who had a flow diverter placed for treatment of a cavernous ICA aneurysm (mean age, 57.2; mean aneurysm size, 20.9 mm). The mean number of devices placed per patient was 2.2. At final angiographic follow-up (mean, 10.9 months), 71% had complete occlusion, and of those with incomplete occlusion, 40% had minimal remnants (<3 mm). In symptomatic patients, complete resolution or significant improvement in symptoms was noted in 90% at follow-up. Technical complications (which included, among others, vessel perforation in 4 patients, groin hematoma in 2, and asymptomatic carotid occlusion in 1) occurred in approximately 36% of patients but did not result in any clinical sequelae immediately or at follow-up.

CONCLUSIONS: Our series of flow-diversion treatments achieved markedly greater rates of complete occlusion than coiling, with a safety profile that compares favorably with that of carotid sacrifice.

ABBREVIATION: PED = Pipeline Embolization Device

Aneurysms originating from the cavernous segment of the internal carotid artery are thought to have a more benign natural history than intracranial aneurysms in other vascular territories, with a substantially lower risk of rupture.[1-3] Treatment is indicated when these aneurysms are symptomatic and/or reach very large and giant size. Due to the dysplastic nature of these aneurysms and typically difficult morphology, achieving complete aneurysm occlusion by using endovascular "reconstructive" techniques is difficult. "Deconstructive" ICA sacrifice for cavernous ICA aneurysms with or without bypass achieves remarkably high rates of complete aneurysm occlusion.[4] However, ICA sacrifice is associated with several potential disadvantages because many of these patients have contralateral mirror ICA aneurysms and ipsilateral ICA occlusion limits therapeutic options for those contralateral aneurysms in the future. Concerns have been raised about long-term hemodynamic effects of ICA sacrifice in young patients, with resultant de novo aneurysm formation in 4%–11% of patients thought to result from increased flow in the anterior and posterior communicating artery regions.[5-8] Finally, the need for either low- or high-flow bypass in patients who do not tolerate balloon test occlusion may add risk to the overall procedure.

Endoluminal flow-diversion devices have been associated with high rates of complete aneurysm occlusion, even in giant aneurysms.[9] Cavernous ICA aneurysms appear well-suited to treatment by flow diversion, given the sidewall morphology and lack of critical perforating side branches of the aneurysm in the region of the aneurysm cavity. However, given the relatively benign natural history of these aneurysms and the excellent results reported with ICA sacrifice, it remains critical to assess the risk-benefit ratio for treatment by flow diversion compared with alternative approaches. While there are multiple studies demonstrating a single

Received June 17, 2013; accepted after revision September 26.

From the Departments of Neurosurgery (R.C.P.) and Radiology (G.L., D.F.K., H.J.C.), Mayo Clinic, Rochester, Minnesota; and Division of Neuroradiology (M.P., L.V., L.Q., E.B.), Ospedale Niguarda, Milano, Italy.

Please address correspondence to Giuseppe Lanzino, MD, Department of Neurosurgery, Mayo Clinic, 200 1st St SW, Rochester, MN 55905; e-mail: lanzino.giuseppe@mayo.edu

Indicates article with supplemental on-line tables.

http://dx.doi.org/10.3174/ajnr.A3826

institutional experience treating intracranial aneurysms with flow diverters, to our knowledge, there has been no previous case series published focusing specifically on treatment of cavernous ICA aneurysms by flow diversion. In the current study, we detail the safety and efficacy of flow diversion in 44 patients with cavernous ICA aneurysms.

MATERIALS AND METHODS

This study was approved by the institutional review board at both institutions where data were collected. From prospectively maintained data bases of patients treated with flow diverters, those who underwent treatment for a cavernous ICA aneurysm from 2009 to the present were selected and retrospectively reviewed. Some of the patients reported were enrolled in the Pipeline for Uncoilable or Failed Aneurysms Study[9] or were reported as part of a large series on flow diversion.[10] Demographic information, indication for treatment, type and number of flow diverters placed, treatment outcome, complications (technical or clinical, with 1-sided confidence intervals), and clinical/imaging follow-up data were collected and analyzed. The 5 main operators performing these procedures each had at least 10 years of independent practice, and many of the procedures were performed with 2 experienced operators present.

All patients undergoing treatment were premedicated with aspirin and clopidogrel, and full anticoagulation was maintained during the procedure (target activated clotting time between 250 and 300 seconds). Following the procedure, patients were maintained on dual antiplatelet therapy for 3 months (institution 1) and for 1 month (institution 2). After these time intervals, clopidogrel was discontinued and aspirin was continued indefinitely (institution 1) and for a total of 3 months (institution 2). No patient underwent testing for clopidogrel response. The shorter duration of the dual antiplatelet therapy is related to our belief that if flow diverters are adequately sized, they oppose better against the vessel wall; therefore, after an initial period of potential higher thrombogenicity, the risk of late thromboembolic complications when these devices are used in the proximal ICA is very low and is outweighed by the risk of continuing dual antiplatelet therapy akin to a proximal carotid stent.[11]

All procedures were performed with the patient under general endotracheal anesthesia. Patients were treated with a Pipeline Embolization Device (PED; Covidien, Irvine, California), a Silk flow-diverting stent (Balt Extrusion, Montmorency, France), a Surpass Stent (Stryker Neurovascular, Fremont, California), or, in some cases, a combination of 2 separate devices. There were 2 patients in the series in whom a Liberté stent (Boston Scientific, Natick, Massachusetts) was used to correct a persistent stenosis related to compression from the aneurysm mass; in 1 patient, a LEO stent (Balt Extrusion) was used as a scaffold for the flow diverter to bridge a wide aneurysm neck. Flow diverters were sized to match the maximum diameter of the target vessel, and 1 or multiple devices were used at the discretion of the operators to maximize the chance of complete aneurysm occlusion and/or to ensure adequate coverage of the aneurysm neck and of a segment of the parent artery proximal and distal to it. Digital subtraction angiography was performed at 2 frames per second before and following placement of the flow diverter. Flow diverters were placed under fluoroscopy with a frame rate of 12.5 frames per second.

RESULTS

We identified 44 patients (37 females and 7 males) who had a flow diverter placed for treatment of a cavernous ICA aneurysm. Their clinical and demographic information is included in On-line Table 1. The mean age for the cohort was 57.2 ± 14.3 years (range, 17–81 years), and the mean aneurysm size was 20.9 ± 6.9 mm (range, 4–40). Of note, 48% of patients (21/44) in this series had giant cavernous sinus aneurysms (>25 mm). The most frequent presenting symptoms included cavernous cranial neuropathy/diplopia in 52% (23/44), headache/retro-orbital pain in 30% (13/44), and incidental discovery after an unrelated symptom with or without interval growth in 23% (10/44). Adjacent aneurysms were present in 27% of patients (12/44), and in 4 of the patients with adjacent aneurysms, the flow diverter also covered the neck of the adjacent aneurysm, resulting in treatment of multiple aneurysms simultaneously.

Aneurysms were previously treated with coils in only 1 patient. The PED was the only flow diverter used in 64% of patients (27/42), 24% (10/42) were treated with the Silk device only, 2% (1/42) were treated with the Surpass flow diverter, and 4/42 patients (10%) were treated with a combination of flow diverters and scaffold stents placed telescopically. Multiple devices were required in the initial procedure in 48% (20/42) of patients to achieve adequate coverage of the aneurysm neck. The mean number of flow diverters placed in this cohort was 2.2 ± 2.0 (range, 1–10).

Adequate angiographic and clinical follow-up was available in 36 patients, and their angiographic and clinical outcomes are demonstrated in On-line Table 2. One patient was excluded from occlusion analysis due to subsequent transvenous coiling of the cavernous sinus for treatment of a carotid cavernous fistula. At final angiographic follow-up (3–36 months; mean, 10.9 months), 71% (25/35) had complete occlusion, and of the 10 patients with incomplete occlusion, 40% (4/10) had minimal remnants present on angiography. In patients who had incomplete occlusion noted on 6-month angiograms and also had a follow-up angiogram at 12 months or later, 50% (4/8) were found to have progressed to complete occlusion at final follow-up (Fig 1).

There were 29 patients who were symptomatic at presentation and had adequate clinical follow-up. Complete resolution or significant improvement of their presenting symptoms was noted in 90% of patients (26/29). Persistent, pre-existing symptoms included continued cranial neuropathy in 2 patients and minor headache in 1 patient. New clinical symptoms developed in 23% (10/29) of patients periprocedurally, mostly 2–5 days after the treatment, and included localized retro-orbital pain in 5, worsening of pre-existing diplopia in 3, chemosis in 2, and a complete cavernous sinus syndrome in 1 patient with a giant cavernous aneurysm. This periprocedural pain resolved completely within the first month in all these patients with medical treatment (pain medications and/or short steroid taper). The patients with worsening or new-onset diplopia experienced resolution of their clinical symptoms by the time of the first clinical follow-up (usually 1 month after treatment), and the patient with a delayed, complete cavernous sinus syndrome had almost complete resolution of

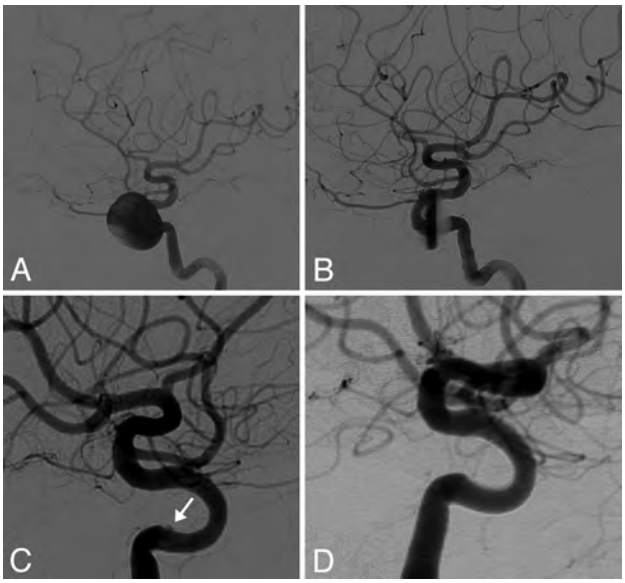

FIG 1. *A*, Lateral digital subtraction angiography of the left ICA in a 67-year-old woman demonstrates a large (20 mm) aneurysm originating from the cavernous segment of the ICA. *B*, Immediate postplacement image of 3 PEDs demonstrates stasis of contrast within the aneurysm. *C*, Follow-up lateral DSA at 6 months demonstrates a minimal remnant (*white arrow*). *D*, Final angiographic follow-up demonstrates complete aneurysm occlusion at 36 months.

these new symptoms at 6-month follow-up but continues to have slight upgaze limitation. A small, asymptomatic distal hematoma in the frontal lobe was identified on postprocedural CT in 1 patient (2%, 1/42).

Intraprocedural technical complications were encountered in 36% of procedures (16/44), including minor catheter-induced vasospasm (4.5%, 2/44), incomplete opening of the device requiring angioplasty (16%, 7/44), inability to pass the catheter across the aneurysm due to difficult anatomy (2%, 1/44), and vessel perforation (9%, 4/44). Access complications (groin hematoma requiring repair by vascular surgery) occurred in 2 patients (4.5%). Delayed, in-stent stenosis of ≥50% was found in 1 patient (2%) at follow-up, and in this patient, a Liberté stent was later placed to prevent progression of the stenosis. Asymptomatic ICA occlusion was found in 1 patient (2%) at follow-up angiography. No patients who experienced intraprocedural or delayed complications had any clinical sequelae either immediately postprocedure or at follow-up (95% confidence interval, 0%–9.6%).

DISCUSSION

In this study, we demonstrated that flow diverters are an effective treatment technique for cavernous aneurysms, not only for achieving aneurysm closure but also for resolution of presenting clinical symptoms. Remarkably high rates of complete or near-complete occlusion were achieved (83%), even though the mean aneurysm size was approximately 21 mm and almost 50% of the cohort had giant aneurysms. Furthermore, >90% of cranial neuropathies, either pre-existing or developing soon after treatment, resolved with time in all except 1 patient. These findings are similar to those in a recently published multicenter study on flow-diversion with a subset analysis of 26 cavernous sinus aneurysms. In that study, the authors achieved a complete or near-complete occlusion rate of 100%, with resolution or significant improvement in symptoms in 72% of patients.[12] Symptom resolution in these patients was related to decreased pulsation of the aneurysm and to regression of the sac, which follows successful exclusion of the aneurysm with flow diversion as eloquently demonstrated by Szikora et al.[13] Perianeurysmal inflammation can cause patients to have initial worsening of their presenting symptoms, new-onset headache, or cranial neuropathy. This occurred in 23% of our patients, and mostly resolved with time, sometimes after a short steroid taper. Overall, these results suggest that flow diversion should be considered a viable treatment for symptomatic, cavernous ICA aneurysms in selected patients.

Traditional methods for treatment of cavernous sinus aneurysms, such as carotid sacrifice with or without bypass, have been very effective. Carotid sacrifice achieves a 98.7% rate of complete aneurysm occlusion and an 81% resolution of diplopia but is associated with a 5% risk of procedure-related neurologic deficits.[4] Furthermore, carotid sacrifice may lead to changes in the hemodynamics of cerebral blood flow and increased stress on arterial walls of the contralateral carotid circulation.[7,14-20] This hemodynamic issue is of particular importance in patients with large, cavernous sinus aneurysms because they are often young females who can have an intrinsic weakness of the carotid vessel wall.[21] This may predispose to the formation and growth of aneurysms contralateral to carotid sacrifice (estimated incidence, 4%–11% in a previous review[5]) and also may hinder treatment choices of contralateral mirror aneurysms in the future. Unlike carotid sacrifice, endovascular coiling is a "reconstructive" technique that has been used in the treatment of cavernous sinus aneurysms. However, because these aneurysms are often very large or giant with a wide neck, standard endovascular coiling achieved a complete aneurysm occlusion rate of only 43% in a systematic review from 2002.[4]

Flow diversion may provide a valid alternative to these more traditional endovascular techniques by preserving the parent artery while achieving high complete occlusion rates. A recent publication of the results from the Pipeline for Uncoilable or Failed Aneurysms multicenter trial of flow diversion for intracranial aneurysms of the ICA proximal to the origin of the posterior communicating artery demonstrated an overall 5% morbidity, similar to that in ICA sacrifice, though subset analysis of morbidity in patients treated for cavernous ICA aneurysms was not performed.[9]

Another review and meta-analysis of flow diversion demonstrated an all-comer late complication rate of 2.4%.[22] Few studies have subset analyses specific to cavernous segment aneurysms, but in a multicenter Italian study, Briganti et al[23] reported a 4% mortality rate for treatment of cavernous segment aneurysms with flow diverters, but this comprised 3 total cases (of 76): Two patients experienced fatal ICA thrombosis, and the other experienced a fatal ICA perforation, all during treatment of giant cavernous aneurysms. The mortality rate reported in the Italian study differs from that in both the subset analysis in the recent Canadian study[12] and in this series (both with 0% overall morbidity and mortality, 70 total combined cavernous aneurysms).

However, despite the very low incidence of permanent neurologic symptoms in patients in this series, technical complications were not uncommon. These were mostly related to vasospasm, incomplete device opening, and difficulty passing the catheter

through the segment harboring the aneurysm. There were 4 instances of vessel perforation while attempting to obtain adequate catheter positioning for treatment. With further improvement of implant construction and delivery techniques, the incidence of these complications may decrease. Nevertheless, these issues underscore the fact that many of these procedures are not always smooth and straightforward. Keeping in mind these issues, we have slightly modified our approach, and after a phase of probably "overenthusiasm" for a novel technology, we now tend to be more cautious, especially in elderly patients. For elderly patients with challenging aneurysms, in whom issues with traversing the aneurysm or excessive proximal tortuosity can be anticipated, we include balloon test occlusion at the outset of the procedure, and in the presence of adequate collateral circulation, treatment via ICA sacrifice may be preferred.

This study is limited by its small sample size and the fact that multiple, different, flow-diverting stents were used, making it difficult to attribute these data to any particular device with its associated specifications. Timelines for radiographic follow-up were different between the 2 institutions, and not all patients in the cohort adhered to strict radiographic follow-up schedules, so it is difficult to determine which patients with incomplete occlusion at final follow-up in this series will eventually demonstrate complete occlusion. We did not perform any comparison of flow diversion with standard endovascular coiling techniques or carotid occlusion in this series; thus, we must be careful in comparing our results with those of other independent series. The patients in this cohort were highly selected, treated at 2 centers, both having very extensive experience with treatment of intracranial aneurysms; due to the relative novelty of flow diversion, the patients were carefully followed with adequate clinical and radiographic follow-up in nearly every case.

CONCLUSIONS

Flow-diverting stents represent a highly effective treatment technique for aneurysms of the cavernous ICA and may be a safer choice than carotid sacrifice with or without surgical bypass, given the ideal vessel characteristics of the cavernous ICA for flow diversion. Technical issues are not uncommon, occurring in just more than 1 in 3 cases, some of which were serious complications, though none resulted in any permanent neurologic morbidity in this series. Nevertheless, these technical issues, combined with the often advanced age of these patients and their relative vessel fragility, require a careful analysis to choose the procedure best indicated in each individual case.

Disclosures: Giuseppe Lanzino—*UNRELATED*: *Board Membership*: Edge Therapeutics,* *Consultancy*: ev3/Covidien,* Stryker.* Luca Piero Valvassori—*UNRELATED*: *Consultancy*: Covidien, AB Medica, *Travel/Accommodations/Meeting Expenses Unrelated to Activities Listed*: Covidien, MicroVention, *Other*: Covidien/ev3, *Comments*: fees for participation in review activities such as data monitoring boards, statistical analysis, end point committees, and the like. David F. Kallmes—*UNRELATED*: *Consultancy*: ev3,* Codman,* Medtronic,* *Comments*: planning and implementation of clinical trials, *Grants/Grants Pending*: MicroVention,* ev3,* Sequent,* Codman,* *Comments*: preclinical and clinical research, *Royalties*: University of Virginia Patent Foundation, *Comments*: spine fusion. Harry J. Cloft—*UNRELATED: Grants/Grants Pending*: Cordis Endovascular,* *Comments*: Site principal investigator at enrolling site for Stenting and Angioplasty with Protection in Patients and HIgh Risk for Endarterectomy registry sponsored by Cordis Endovascular. Edoardo Boccardi—*UNRELATED*: *Consultancy*: Balt, Covidien. *Money paid to the institution.

REFERENCES

1. Kupersmith MJ, Stiebel-Kalish H, Huna-Baron R, et al. **Cavernous carotid aneurysms rarely cause subarachnoid hemorrhage or major neurologic morbidity.** *J Stroke Cerebrovasc Dis* 2002;11:9–14
2. Kupersmith MJ, Hurst R, Berenstein A, et al. **The benign course of cavernous carotid artery aneurysms.** *J Neurosurg* 1992;77:690–93
3. van Rooij WJ. **Endovascular treatment of cavernous sinus aneurysms.** *AJNR Am J Neuroradiol* 2012;33:323–26
4. van der Schaaf IC, Brilstra EH, Buskens E, et al. **Endovascular treatment of aneurysms in the cavernous sinus: a systematic review on balloon occlusion of the parent vessel and embolization with coils.** *Stroke* 2002;33:313–18
5. Dyste GN, Beck DW. **De novo aneurysm formation following carotid ligation: case report and review of the literature.** *Neurosurgery* 1989;24:88–92
6. Arambepola PK, McEvoy SD, Bulsara KR. **De novo aneurysm formation after carotid artery occlusion for cerebral aneurysms.** *Skull Base* 2010;20:405–08
7. Tomsick T. **Long-term clinical follow-up of therapeutic internal carotid artery occlusion.** *AJNR Am J Neuroradiol* 2007;28:1626
8. Arnaout OM, Rahme RJ, Aoun SG, et al. **De novo large fusiform posterior circulation intracranial aneurysm presenting with subarachnoid hemorrhage 7 years after therapeutic internal carotid artery occlusion: case report and review of the literature.** *Neurosurgery* 2012;71:E764–71
9. Becske T, Kallmes DF, Saatci I, et al. **Pipeline for uncoilable or failed aneurysms: results from a multicenter clinical trial.** *Radiology* 2013;267:858–68
10. Piano M, Valvassori L, Quilici L, et al. **Midterm and long-term follow-up of cerebral aneurysms treated with flow diverter devices: a single-center experience.** *J Neurosurg* 2013;118:408–16
11. Lanzino G. **Editorial: ophthalmic segment aneurysms.** *J Neurosurg* 2013;118:935, discussion 935–36
12. O'Kelly CJ, Spears J, Chow M, et al. **Canadian experience with the pipeline embolization device for repair of unruptured intracranial aneurysms.** *AJNR Am J Neuroradiol* 2013;34:381–87
13. Szikora I, Marosfoi M, Salomvary B, et al. **Resolution of mass effect and compression symptoms following endoluminal flow diversion for the treatment of intracranial aneurysms.** *AJNR Am J Neuroradiol* 2013;34:935–39
14. Gurdjian ES, Lindner DW, Thomas LM. **Experiences with ligation of the common carotid artery for treatment of aneurysms of the internal carotid artery.** *J Neurosurg* 1965;23:311–18
15. Drapkin AJ, Rose WS. **Serial development of 'de novo' aneurysms after carotid ligation: case report.** *Surg Neurol* 1992;38:302–08
16. Klemme WM. **Hemorrhage from a previously undemonstrated intracranial aneurysm as a late complication of carotid artery ligation: case report.** *J Neurosurg* 1977;46:654–58
17. Niiro M, Shimozuru T, Nakamura K, et al. **Long-term follow-up study of patients with cavernous sinus aneurysm treated by proximal occlusion.** *Neurol Med Chir (Tokyo)* 2000;40:88–96, discussion 96–87
18. Ostergaard JR. **A long-term follow-up study of juvenile aneurysm patients.** *Acta Neurochir (Wien)* 1985;77:103–09
19. Parekh HC, Prabhu SS, Keogh AJ. **De novo development of saccular aneurysms: report of two cases.** *Br J Neurosurg* 1995;9:695–98
20. Winn HR, Richardson AE, Jane JA. **Late morbidity and mortality of common carotid ligation for posterior communicating aneurysms: a comparison to conservative treatment.** *J Neurosurg* 1977;47:727–36
21. Brisman JL, Song JK, Newell DW. **Cerebral aneurysms.** *N Engl J Med* 2006;355:928–39
22. Arrese I, Sarabia R, Pintado R, et al. **Flow-diverter devices for intracranial aneurysms: systematic review and meta-analysis.** *Neurosurgery* 2013;73:193–99, discussion 199–200
23. Briganti F, Napoli M, Tortora F, et al. **Italian multicenter experience with flow-diverter devices for intracranial unruptured aneurysm treatment with periprocedural complications: a retrospective data analysis.** *Neuroradiology* 2012;54:1145–52

Transverse Sinus Stenting for Pseudotumor Cerebri: A Cost Comparison with CSF Shunting

R.M. Ahmed, F. Zmudzki, G.D. Parker, B.K. Owler, and G.M. Halmagyi

ABSTRACT

BACKGROUND AND PURPOSE: Transverse sinus venous stent placement has been shown to lower intracranial pressure in patients with venogenic pseudotumor cerebri and to reverse, or at least stabilize, its symptoms and signs. There have been no studies comparing the cost of venous stenting with the time-honored treatment for pseudotumor cerebri–CSF shunting. The purpose of this study was to compare the cost of trasverse sinus stenting versus CSF shunting for the treatment of pseudotumor cerebri.

MATERIALS AND METHODS: This work was a retrospective cost analysis of individual resource use in 86 adults who were stented for pseudotumor cerebri during a 12-year period compared with resource use in 110 children who were shunted for hydrocephalus during a 3-year period.

RESULTS: There was no significant difference between the cost of inserting an initial venous stent ($13,863 ± 4890) versus inserting an initial CSF shunt ($15,797 ± 5442) ($P = .6337$) or between inserting an additional venous stent ($9421 ± 69) versus revising a CSF shunt ($10,470 ± 1245) ($P = .4996$). There were far fewer additional venous stent insertions per patient than there were subsequent CSF shunt revisions; 87% of stents placed required just 1 stent procedure, whereas only 45% of shunts required 1 shunt procedure. The main cause of the cost difference was the need for repeated revisions of the shunts, especially when they became infected—24 instances of a total 143 shunt procedures (16.8%) at an average cost of $84,729, approximately 5 times the cost of an initial shunt insertion.

CONCLUSIONS: Venous stenting costs significantly less per 100 procedures than does CSF shunting, due largely to the high cost of treating shunt infections and the need for repeated shunt revisions.

ABBREVIATIONS: PTC = pseudotumor cerebri; TSS = transverse sinus stenting

Transverse sinus venous stent placement is an effective treatment for pseudotumor cerebri (PTC)[1-3]; however, its cost has not been assessed or compared with the cost of the traditional alternative—CSF shunting. The annual cost of treating PTC in the United States exceeds US $444 million, and the annual cost of all CSF shunts—not just for PTC—exceeds $1 billion.[4,5] We wanted to estimate the cost of transverse sinus venous stenting and compare it with the cost of CSF shunting. Because pediatric hydrocephalus typically requires CSF shunt insertion, this pediatric group was the most suitable one available for cost comparison. Since the advent of venous sinus stenting for PTC, no patient has undergone CSF shunting at our institution for PTC. We reviewed the cost per patient for stent-versus-shunt insertion and reviewed the cost in terms of failed procedures, infection, and the need for revision, representing the full cost of these procedures.

MATERIALS AND METHODS

We reviewed the costs of treatment of 86 adult patients who had transverse sinus stenting (TSS) for PTC at Royal Prince Alfred Hospital between 2001 and 2012 and of 110 pediatric patients who had CSF shunting for hydrocephalus at Westmead Children's Hospital between 2007 and 2009. Each procedure was classified as "new" (first time) or as "subsequent," and details of complications were identified.

For each patient, a total annual cost was estimated on the basis of the individual patient's resource use for that year. The cost comparison was undertaken from the perspective of the Sydney hospitals that provided the treatment, focusing on detailed, direct medical costs. Ethics approval was not required by Royal Prince

Received June 7, 2013; accepted after revision September 23.

From the Departments of Neurology (R.A., G.M.H.) and Radiology (G.P.), Royal Prince Alfred Hospital, Sydney Australia; Époque Consulting (F.Z.), Sydney, Australia; TY Nelson Department of Neurology and Neurosurgery (B.O.), Children's Hospital at Westmead, Sydney, Australia; and Discipline of Pediatrics and Child Health, and Surgery (B.O.), University of Sydney, Sydney, Australia.

Please address correspondence to Michael Halmagyi, MD, Department of Neurology, Royal Prince Alfred Hospital, Missenden Rd, Camperdown NSW, Australia 2050; e-mail: gmh@icn.usyd.edu.au

http://dx.doi.org/10.3174/ajnr.A3806

Alfred Hospital because TSS is offered as a treatment. Ethics approval was separately provided by the Children's Hospital Westmead Human Research Ethics Committee. All costs have been adjusted to 2012 levels in Australian dollars (AUD). The Australian dollar at the time of writing was roughly equivalent to 0.94 US dollars.

Transverse Sinus Venous Stenting

The 86 patients with PTC underwent 99 procedures during the 12-year period, with follow-up from 6 months to 10 years, with a mean of 4 years. All details of resource usage were collated for each stage of diagnosis and treatment. For preadmission, the main costs comprised the following: 1) consultations with a neurologist, ophthalmologist, radiologist, and anesthetist; 2) MR imaging; 3) lumbar puncture; 4) diagnostic direct retrograde cerebral venography and manometry; and 5) dual antiplatelet medication for 1 week before stenting and platelet function studies. The main hospital treatment costs comprised the following: 1) therapeutic diagnostic direct retrograde cerebral venography; 2) general anesthesia; 3) the stent; 4) medication during the procedure, primarily heparin; and 5) postprocedure accommodation, usually 1 night in a high-dependency unit. One-third of patients stayed an additional night in a general hospital bed for further observation.

This information provided measurement of all resource use, length of stay, and revision rates. Valuation of resources was then incorporated by using published service schedules and unit costs, principally from the Australian Medical Benefits Scheme and published *Diagnostic Related Groups*; and specific costs, when necessary, were provided by the Royal Prince Alfred Radiology Department. The approach and costing sources used in this study are consistent with Australian government guidelines for preparing health economic analyses.[6]

CSF Shunting

The 110 patients had 143 procedures during the 3 years, for shunt insertion, shunt revision, and shunt infection, with no subsequent follow-up beyond the study period. Actual hospital costs were provided by the Children's Hospital Westmead by using the Power Performance system. This is a clinical inpatient costing system linking resource cost inputs and allocation to each individual patient on the basis of actual use. Allocation algorithms are applied to relevant source feeds from each system, including imaging, pathology, pharmacy, operating theater, and physiotherapy. Resource use is captured by the time used, so costs reflect the duration of surgical procedures, the number of nurses, the duration of anesthesia, and so forth.

Following extraction of the detailed costing data from the Power Performance Manager, review of records was undertaken to classify each episode. This was to exclude non-hydrocephalus primary diagnoses and to categorize patients as having a new shunt or a shunt revision. Patients with CSF shunts were additionally classified if they developed infection, to assess separately the cost of treatment. Patients with hydrocephalus secondary to trauma, malignancy, or other complex conditions (except myelomeningocele) were excluded. Figures from the Power Performance Manager were adjusted to the 2012 AUD by using the total health price index published by the Australian Institute of Health and Welfare 2012.[7]

Statistics

The mean costs of each group were analyzed by using the Student *t* test, and a χ^2 test was used for demographic independence with a P value $< .05$ considered statistically significant. Several 1-way sensitivity analyses were performed to establish whether the comparative results were sensitive to cost, infection, or revision rate variables. These included using costs, infection, and revision rates and the total number of revisions per patient from studies of equivalent adult shunt cohorts to validate comparable age-matched scenarios. Statistical analysis was undertaken by using STATA statistical software (Special Edition, Version 12.1 2011; StataCorp, College Station, Texas).

RESULTS

Patient Groups

The baseline demographic characteristics for transverse sinus stent and CSF shunt patients are presented in Table 1.

A χ^2 test of independence confirmed the difference between the 2 demographic groups ($P < .001$).

Table 1: Baseline demographics of patients with transverse sinus stents and CSF shunts

Age and Sex	No. of Patients (%)		*P* Value
	Transverse Sinus Stent (*n* = 86)	CSF Shunt (*n* = 110)	
Mean age (yr)	36.9 ± 13.6	6.6 ± 6.0	<.001
Sex			
Male	10 (11.6)	78 (70.9)	<.001
Female	76 (88.4)	32 (29.1)	

Number of Procedures

Most stented patients had just 1 stent at 1 procedure (Table 2); in contrast, many patients with CSF shunts needed further procedure revisions and treatment of infections (Table 3). The stented patient group, during the 12-year period, underwent 99 stent procedures, 78 of 86 patients receiving a single procedure (90.7%) and the remaining 8 having additional stents: 5 patients, just 1 more; 1 patient, 2 more; and 2 patients, 3 more.

In contrast, the CSF shunt group had 143 procedures, only 40 of which (28%) were first-shunt insertions (Table 3).

Table 2: Venous stents: number of patients by initial and repeat procedures

No. of Stent Procedures per Patient	No. of Patients	Stent Procedures per Patient	No. of Stent Procedures	% Total Patients
New stent procedure	78	1	78	90.7%
1 Subsequent procedure	5	2	10	5.8%
2 Subsequent procedures	1	3	3	1.2%
3 Subsequent procedures	2	4	8	2.3%
Total	86		99	100.0%

Average Cost

There was no significant difference between the average cost of an initial venous stenting ($13,863 ± 4890) and an initial CSF shunting ($15,797 ± 5442) ($P = .6337$); any difference is attributable to a few serious high-cost complications that

Table 3: Cost summary by procedure: stent versus shunt

	No. of Procedures	% of Total Procedures	Total Cost ($AUD)	% of Total Cost	Average Cost ($AUD)	SD	Total LOS (Days)	Average LOS (Days)
Transverse sinus stent								
First transverse sinus stent	86	86.9%	$1,192,219	90.7%	$13,863	22,809	324	3.8
Subsequent transverse sinus stents	13	13.1%	$122,468	9.3%	$9421	114	15	1.2
Transverse sinus stent infection	0	0.0%	–	0.0%	–	–		
Grand total	99	100.0%	$1,314,687	100.0%	$13,280	21,296	339	3.4
CSF shunt								
First CSF shunt	40	28.0%	$631,888	18.1%	$15,797	17,015	340	8.5
CSF shunt revision	79	55.2%	$827,145	23.7%	$10,470	5557	437	5.5
CSF shunt infection	24	16.8%	$2,033,485	58.2%	$84,729	141,948	1060	44.2
Grand total	143	100.0%	$3,492,518	100.0%	$24,423	64,062	1837	12.8

Note:—$AUD indicates Australian dollars; LOS, length of hospital stay.

Table 4: Transverse sinus stenting versus CSF shunting: average cost comparison per 100 cases

Procedure	Infection Rate	Average Cost per Infection	Average Cost of Infection	Average Cost of New (Non-Infected) Cases	Average Cost per Revision	Revision Rate	Average Cost of Revisions	Total Cost per 100 Procedures
Transverse sinus stent	0.0%	0	–	$1,204,261	$9421	13.1%	$123,705	$1,327,967
CSF shunt[a]	16.8%	$84,729	$1,422,017	$441,880	$10,470	55.2%	$578,423	$2,442,320

Note:— – indicates no infection in TSS patients.

[a] Average cost figures for new and revised shunts presented as separately categorized noninfection cases.

occurred during the initial shunting. The influence of these complication outliers on the mean is reflected in the even closer median for each initial procedure at $9374 for venous stenting and $9535 for CSF shunting. The CSF shunting average costs for first procedures and revisions excluded infection, which was classified separately to evaluate its cost implications. This infection component was combined with other classification group average figures in the cost per 100 cases presented below.

Similarly, there was no significant difference between the average cost of a subsequent venous stenting ($9421 ± 69) and of a CSF shunt revision ($10,470 ± 1245) ($P = .4996$), and there was no difference in the median cost, $9374 for venous stenting versus $9029 for CSF shunting.

With resource usage for venous stenting similar to that for CSF shunting, the average cost of each first and subsequent procedure was not significantly different. The lower average cost of subsequent compared with new procedures is largely due to high-cost complications occurring in only new stent procedures, as well as high-cost shunt complications being separately categorized as infection cases, so there were no high-cost outliers increasing the average revision cost. The average costs for CSF shunting reported here are in line with previous data.[8,9]

Additional Stents versus Revised Shunts

The main cause of the cost difference between stenting and shunting is the need for subsequent procedures: 79/143 (55.2%) for shunting but only 13/99 (13.1%) for stenting. While the average cost per procedure is similar, the proportional cost in terms of the total number of subsequent procedures is higher for shunting.

Infection

An important difference between shunts and stents is that stents do not get infected. Infection necessitated 24 shunt revisions (16.8%), often incurring the additional cost of removing and eventually replacing the shunt and all the associated costs of medical treatment to eradicate the infection. This is reflected in the higher average cost of treating an infected shunt ($84,729 ± 59,939) rather than inserting a new shunt ($15,797 ± 17,015) or just revising a shunt ($10,470 ± 5557), as well as in the longer average length of stay of 44 days, compared with 9 days for an initial shunt and 6 days for a revised shunt. Therefore, shunt infections are a major cost component; although they represent only 16.8% of cases, they account for 58.2% of the total cost, $2 million for the 3-year shunt group. Similar rates of shunt infection from 7.2%–15% and comparable 5-fold average cost increases in hospital charges have already been reported.[9,10] Previous research has also shown that patients with adult PTC shunts similarly experience complications in this range with a 9% shunt infection rate.[11]

Cost per 100 Procedures

To allow for the different study and follow-up periods of the shunted and stented patients and for the presence of infection, the average costs per procedure, both new and subsequent, are calculated in terms of cost per 100 procedures (Table 4). These results reflect the high revision rate for CSF shunts, multiplied by the average procedure cost in each group, as well as the cost of managing infected CSF shunts.

In these terms, the cost per 100 cases is significantly higher for CSF shunting, almost double that for venous stenting (Fig 1). The reason for this is the higher proportion of CSF shunt revisions and the higher cost of shunt complications, not the average cost per procedure.

The cost per 100 cases, however, underestimates the true comparable long-term cost of ongoing revisions. Because the stented group continued for 12 years, it is reasonable to view the absolute number of additional stentings as representative; >90% of patients had just a single stenting, with a maximum 3 additional stentings in only 2 patients. The shunting study period by comparison, covering only 3 years, was sufficient to provide an estimate of the average cost per revision but cannot provide an adequate follow-up period to verify the total number of shunt revisions needed by each patient.

Thus, a literature review was undertaken to verify revision rates and, in particular, the total number of revisions per patient;

this indicated revision rates resulting from complications such as blockage and infection between 25% and 55%.[12,13] The pattern of ongoing shunt complications has also been reported in adult PTC shunt groups, with similarly high revision rates of 51%–63%.[14,15]

Furthermore, some "shunt-intolerant" patients can require ≥10 ventriculoperitoneal shunt revisions and >30 lumboperitoneal shunt revisions.[16] As for the infection and revision rates, previous research has also reported cases of ≥10 revisions per patient in adult PTC shunt groups.[14] In contrast, the highest number of stent procedures recorded for 1 patient was 4.[1]

Total Cost per Patient

These results provide the average cost per procedure and separately indicate the revision and infection rates, which in turn determine the total cost per patient for each group. There are many more high-cost shunt patients than stent patients (Fig 2). The relative difference is in higher cost shunt patients overall and, in particular, the scale of costs required to manage the top 2% of patients with severe complications. Stent and shunt patients in the lower 40% by cost have similar, single procedures with no infection. Above 40%, the shunt patient costs increase consistently to the highest cost, 4%, around $100,000, 3-fold the comparable highest cost of stent patients. While both groups include extreme outliers in the highest cost 2% of patients, the scale of the shunted patients continues to be at least 3-fold higher than the stented patients, again reflecting the higher rates of infection and ongoing shunt revisions. Length-of-stay figures are also presented for each percentile group.

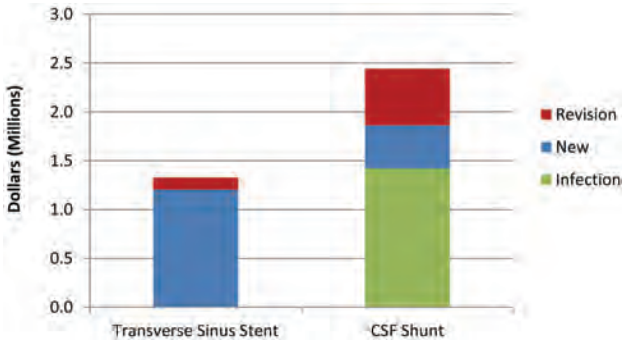

FIG 1. Stent versus shunt. Cost comparison per 100 procedures. Graph shows the average cost per 100 procedures of transverse sinus stenting versus CSF shunting. The total cost is shown, plus an individual breakdown of costs based on revision and infection rates of each group.

Complications

Complications after stenting included headache, transient hearing loss, and allergic reactions to aspirin or clopidogrel and, in one case, an anaphylactic reaction to the anesthetic. Apart from these cases, there were 3 patients from the total of 86 in the transverse sinus stent group (3.5%) who had major neurologic complications during stenting, largely vein perforation causing subdural, subarachnoid, or intracerebral bleeding. All 3 patients made a full recovery; 2 needed an urgent craniotomy for evacuation of a hematoma.

From a resource use and cost perspective, the 3 severe-complication cases required extended inpatient stays and ongoing rehabilitation. From a cost perspective, these patients are extreme outliers with a total individual cost of $119,468, $135,440, and $143,272. In comparison, severe complications for the 3 highest cost shunt patients resulted in individual patient costs of $170,850, $411,619, and $641,824.

Total Revisions per Patient

To explore the potential cost implications of subsequent procedures, especially shunt revisions, a series of scenarios were developed on the basis of average costs from the 2 datasets supported by evidence from previous studies.[9,10] These provided cross-validated estimates of the average cost of initial stenting or shunting, as well as of subsequent procedures, infection risk, and associated

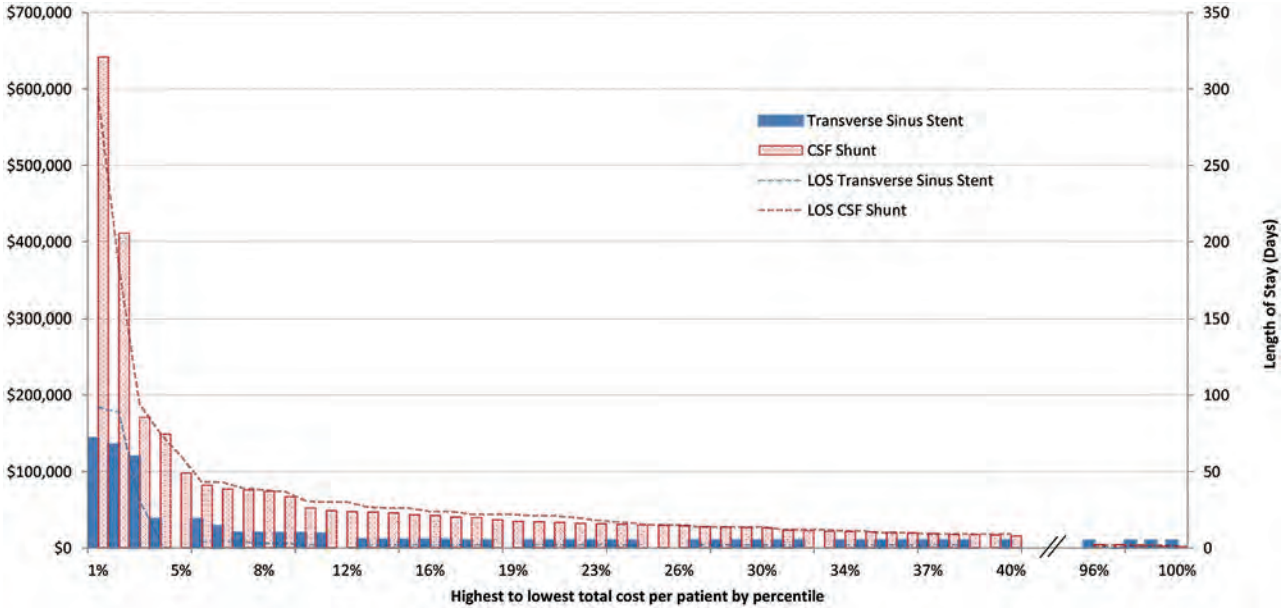

FIG 2. Stent versus shunt. Cost (AUD) per patient by percentile of the group and the length of stay. Graph shows highest-to-lowest cost per patient by percentile for transverse sinus stenting (blue) and CSF shunting (red). The length of hospital stay (LOS) is also shown for each group.

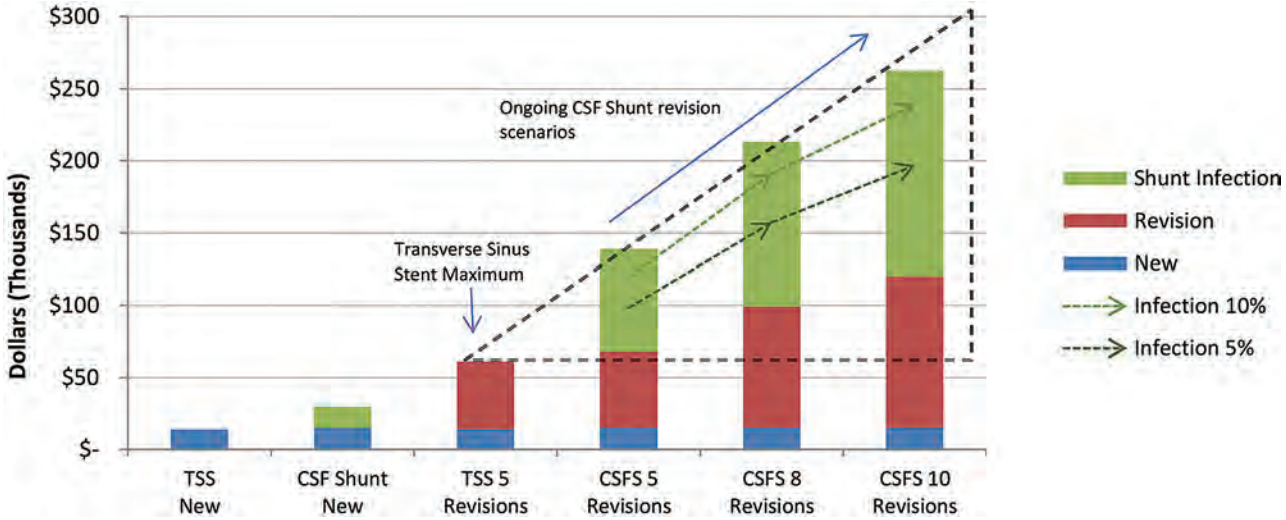

FIG 3. Stents versus shunts by the total number of shunt revisions or additional stents per patient. Graph shows the cost of transverse sinus stenting versus CSF shunting for both new procedures versus a variable number of revisions. Ongoing CSF shunt revision costs are compared with the maximum reported TSS cases of 5 (dotted triangle). Predicted costs for CSF shunting are also shown, with reduced infection rate scenarios of 5% and 10% for the variable number of revisions.

average infection cost. These scenarios are consistent with studies of adult patients with PTC shunts, as referenced in previous sections, which have shown infection and revision rates and the total number of shunt revisions per patient to be similar to those of our pediatric study group.

These findings then support a series of scenarios based on the total number of additional procedures per patient as presented in Fig 3. The maximum number of subsequent stentings in the 12-year group was 3, and additional stenting beyond 5 have not been reported, so 5 is considered the maximum upper limit. In this context, the first scenario illustrates the relative comparison of 5 subsequent stentings and 5 subsequent shunt revisions, with the slightly higher total cost of shunting due to the additional cost of managing infections.

Additional scenarios were prepared to investigate a reduced infection rate for CSF shunting with use of antibiotic-impregnated shunts, which included infection rates below those reported in previous adult study groups.[17]

In the scenarios of 8 and then 10 revisions, shown only for shunts, the trend is further established. While 10 revisions are presented as an extreme scenario, there have been reports of adult patients with PTC needing even more, which extends the increasing cost trend for patients with higher revision shunts.[14,18]

Previous modeling suggests that the cost of shunting in pediatric hydrocephalus is more sensitive to the revision rate, particularly in the first year after shunting, than to the decreased infection rate or length of hospital stay.[19] Also long-term investigations of shunted children have confirmed that 81% need at least 1 revision and often several, requiring repeated procedures and hospitalizations.[13]

The shunt infection column bars in Fig 3 report the shunt infection rate of the study group (16.8%), which is shown against 2 reduced-infection-rate sensitivity scenarios of 10% and 5%. These scenarios indicate that even with an infection rate of only 5%, a patient receiving 10 shunt revisions is estimated to cost $196,771, almost a 4-fold increase in the highest cost of inserting 5 additional stents. Despite reported examples of reduced shunt infection rates, rates of 10% still occur even with antibiotic-impregnated shunts.[20] As described previously, adult patient groups with PTC shunts have been reported as having a similar 9% infection rate. Here, the estimated cost of $239,136 is close to 5-fold the highest cost for a stented patient. In all scenarios with >5 subsequent procedures, an increasing upward cost trend resulted for shunts, in line with the number of procedures, shown as the dotted triangle in Fig 3.

In summary, the average cost per 100 patients, the total cost per patient, and the skewed upside risk of additional costs through ongoing shunt revisions and infections show stenting costing less than shunting, while nonetheless providing patients with PTC with effective long-term treatment.

DISCUSSION

In the first part of this study, we calculated the average cost of venous stenting and CSF shunting and found no significant difference between the 2, either as initial or subsequent procedures. This finding reflects similar resource use, operating theater time, and medical-surgical team composition for each procedure and provides the underlying base-cost component to the calculation of total cost per patient. The main cause for the cost difference between stenting and shunting is, therefore, not the difference in average cost for each routine procedure but problems and complications with CSF shunting, leading to a high revision rate, up to 30% for ventriculoperitoneal shunts and 60% for lumboperitoneal shunts and an infection rate of 5%–15%. These cost drivers are consistent with similar shunt revision and infection rates previously reported in adult PTC study groups.[21]

It follows that ongoing additional stents and shunt revisions are simple multiples of the average cost; the key difference between stenting and shunting is that shunts not only need frequent revisions, they also can become infected and this outcome results in higher total costs. The analysis scenarios in this study have taken the conservative case of 10 revisions for shunts, though even

more can occur in both pediatric and adult PTC cases.[19] There remains, therefore, an unbounded upside risk for a few shunt-intolerant patients, which will potentially add substantially to total cost per patient.

Venous stenting, by comparison, has been shown to require significantly fewer repeat procedures, with >90% of patients successfully receiving just a single stent. Also, the need for additional venous stenting, while low, has been further lowered with time, due to a better understanding of the mechanism by which stents lower intracranial pressure and the availability of longer stents. We have proposed[1] that stenting prevents compression of the transverse sinuses by intracranial hypertension itself, breaking a positive feedback cycle. A stent creates a rigid, noncollapsible transverse sinus, one no longer vulnerable to compression from intracranial hypertension so that CSF absorption is improved, lowering intracranial pressure. With time, longer stents have been inserted so that fewer extrinsic stenoses develop at the distal end of the stent, reducing the need for second or third stenting procedures. In some cases, the entire transverse sinus has been stented.[1]

Given this significant difference in the repeat rates of the 2 procedures, the cost per 100 cases does not represent the total longer term cost per patient of ongoing revisions. Because the venous stent group was followed up to 12 years, it is reasonable to view the absolute number of repeat procedures as representative. During the 12 years of data, >90% of patients received only a single stent, with a maximum of 3 revisions in 2 cases. The shunt study period by comparison, covering 3 years, is sufficient to provide an estimate of average cost per revision but cannot provide an adequate follow-up period to verify the lifetime total number of shunt revisions per patient.

Revision rates resulting from shunt complications, such as blockage and infection, range from 25% to 50% or more, suggesting that the long-term costs of CSF shunting could be even higher than we found here.[13]

In addition to high-cost cases of ongoing revisions, infection is also an important factor in the overall higher total cost per shunt patient. A few infected shunts result in a disproportionately high shunting cost increase, typically 4- to 5-fold higher than a noninfected case. In our shunt group, the 16.8% of infections accounted for 58.2% of total cost, over $2 million.

The rate and costs of infection are being reduced with the wider use of antimicrobial impregnated sutures, shunts, and catheters to below 5% in some cases, though this level of reduction would depend on using impregnated devices in all shunt procedures, and there is some reluctance to use them because of their increased cost.[22,23]

Given the variation in shunt infection rates and potentially reduced rates resulting from the more widespread use of antibiotic-impregnated shunt components, our scenario analyses included reduced infection rates of 10% and 5%, to investigate the impact on total cost. The scenarios demonstrate that reduced rates of infection, while reducing the magnitude of the cost difference, nonetheless confirm the substantially lower cost of venous stenting in all cases. Because the infection component has been isolated and analyzed separately, even if infection cases were reduced to zero, venous stenting would still cost substantially less than CSF shunting.

The benefit of venous stenting in PTC is now clear,[1-3] and a lower complication rate (9.3% of patients in our own study) compared with shunting has been reported in all studies. We have now shown that the cost of stenting is also significantly less than that of shunting. Finding a therapeutically effective and cost-effective treatment for PTC is of growing importance, given the increasing cost of PTC and the growing rates of obesity.[4]

Study Limitations

Our study has 1 noteworthy limitation: Our CSF shunting group was composed of pediatric patients with hydrocephalus, and it is often suggested that the complications of shunting are more common in pediatric than in adult patients. The ideal comparison group would have been adult shunted patients with PTC. Unfortunately these data were not available because new adult patients at our institution, and in fact in our state, who have PTC with venous stenosis have been so rarely shunted since stenting became available. Therefore, we decided to choose as a comparison group to our stented patients a group of pediatric patients from a prospective registry of cases kept at the Westmead Children's Hospital. To balance this limitation, we reviewed the literature on complications of shunting for adult PTC and verified that the key cost drivers of infection and revision rates and the total number of revisions per patient have been reported at levels similar to those in our pediatric hydrocephalus study group.

In this context, we are confident that our work is valid and adds significantly to the debate on the role of stenting versus shunting in the treatment of venogenic PTC.

The study is also limited by its retrospective nature, and ideally a prospective study comparing the cost of stenting versus shunting is needed in a group of adult patients with PTC.

CONCLUSIONS

In treating PTC, transverse sinus stenting costs less than CSF shunting in the long term, not because of the average cost of the procedure itself but as a result of a relatively lower revision rate, fewer total revisions per patient, and no infections to date.

REFERENCES

1. Ahmed RM, Wilkinson M, Parker GD, et al. **Transverse sinus stenting for idiopathic intracranial hypertension: a review of 52 patients and of model predictions.** *AJNR Am J Neuroradiol* 2011;32:1408–14
2. Kumpe DA, Bennett JL, Seinfeld J, et al. **Dural sinus stent placement for idiopathic intracranial hypertension.** *J Neurosurg* 2012;116:538–48
3. Radvany MG, Solomon D, Nijjar S, et al. **Visual and neurological outcomes following endovascular stenting for pseudotumor cerebri associated with transverse sinus stenosis.** *J Neuroophthalmol* 2013;33:117–22
4. Friesner D, Rosenman R, Lobb BM, et al. **Idiopathic intracranial hypertension in the USA: the role of obesity in establishing prevalence and healthcare costs.** *Obes Rev* 2011;12:e372–80
5. Simon TD, Riva-Cambrin J, Srivastava R, et al. **Hospital care for children with hydrocephalus in the United States: utilization, charges, comorbidities, and deaths.** *J Neurosurg Pediatr* 2008;1:131–37
6. Department of Health and Aging. *Manual of Resource Items and Their Associated Costs, for Use in Major Submissions to the Pharmaceutical Benefits Advisory Committee Involving Economic Analyses.* Version 4.0.

Australian Government, Department of Health and Aging, Canberra, Australia, December 2009
7. Australian Institute of Health and Welfare 2012. *Health Expenditure Australia 2010–11: Health and Welfare Expenditure Series No. 47.* Cat. No. HWE 56. Canberra, Australia: Australian Institute of Health and Welfare, 2012
8. Pham AC, Fan C, Owler BK. **Treating pediatric hydrocephalus in Australia: a 3-year hospital-based cost analysis and comparison with other studies.** J *Neurosurg Pediatr* 2013;11:398–401
9. Stone J, Gruber TJ, Rozzelle CJ. **Healthcare savings associated with reduced infection rates using antimicrobial suture wound closure for cerebrospinal fluid shunt procedures.** *Pediatr Neurosurg* 2010; 46:19–24
10. Patwardhan RV, Nanda A. **Implanted ventricular shunts in the United States: the billion-dollar-a-year cost of hydrocephalus treatment.** *Neurosurgery* 2005;56:139–44, discussion 144–45
11. El-Saadany WF, Farhoud A, Zidan I. **Lumboperitoneal shunt for idiopathic intracranial hypertension: patients' selection and outcome.** *Neurosurg Rev* 2012;35:239–43, discussion 243–44
12. Del Bigio MR. **Epidemiology and direct economic impact of hydrocephalus: a community based study.** *Can J Neurol Sci* 1998;25:123–26
13. Appelgren T, Zetterstrand S, Elfversson J, et al. **Long-term outcome after treatment of hydrocephalus in children.** *Pediatr Neurosurg* 2010;46:221–26
14. Sinclair AJ, Kuruvath S, Sen D, et al. **Is cerebrospinal fluid shunting in idiopathic intracranial hypertension worthwhile? A 10-year review.** *Cephalalgia* 2011;31:1627–33
15. Tarnaris A, Toma AK, Watkins LD, et al. **Is there a difference in outcomes of patients with idiopathic intracranial hypertension with the choice of cerebrospinal fluid diversion site: a single centre experience.** *Clin Neurol Neurosurg* 2011;113:477–79
16. Wang VY, Barbaro NM, Lawton MT, et al.: **Complications of lumboperitoneal shunts.** *Neurosurgery* 2007;60:1045–48, discussion 1049
17. Attenello FJ, Garces-Ambrossi GL, Zaidi HA, et al. **Hospital costs associated with shunt infections in patients receiving antibiotic-impregnated shunt catheters versus standard shunt catheters.** *Neurosurgery* 2010;66:284–89, discussion 289
18. Burgett RA, Purvin VA, Kawasaki A. **Lumboperitoneal shunting for pseudotumor cerebri.** *Neurology* 1997;49:734–39
19. Cochrane D, Kestle J, Steinbok P, et al. **Model for the cost analysis of shunted hydrocephalic children.** *Pediatr Neurosurg* 1995;23:14–19
20. Farber SH, Parker SL, Adogwa O, et al. **Cost analysis of antibiotic-impregnated catheters in the treatment of hydrocephalus in adult patients.** *World Neurosurg* 2010;74:528–31
21. Abubaker K, Ali Z, Raza K, et al. **Idiopathic intracranial hypertension: lumboperitoneal shunts versus ventriculoperitoneal shunts: case series and literature review.** *Br J Neurosurg* 2011;25:94–99
22. Rozzelle CJ, Leonardo J, Li V. **Antimicrobial suture wound closure for cerebrospinal fluid shunt surgery: a prospective, double-blinded, randomized controlled trial.** *J Neurosurg Pediatr* 2008;2: 111–17
23. Sciubba DM, Lin LM, Woodworth GF, et al. **Factors contributing to the medical costs of cerebrospinal fluid shunt infection treatment in pediatric patients with standard shunt components compared with those in patients with antibiotic impregnated components.** *Neurosurg Focus* 2007;15:22:E9

Mechanical Thrombectomy with Stent Retrievers in Acute Basilar Artery Occlusion

M. Möhlenbruch, S. Stampfl, L. Behrens, C. Herweh, S. Rohde, M. Bendszus, C. Hametner, S. Nagel, P.A. Ringleb, and M. Pham

ABSTRACT

BACKGROUND AND PURPOSE: Basilar artery occlusion remains one of the most devastating subtypes of ischemic stroke. The prognosis is poor if early recanalization is not achieved. The purpose of this study was to evaluate the safety and technical feasibility of self-expanding retrievable stents in the endovascular treatment of acute basilar artery occlusion.

MATERIALS AND METHODS: Twenty-four patients with acute basilar artery occlusion were treated with Solitaire FR or Revive SE devices between December 2009 and May 2012. Additional treatment included intravenous and/or intra-arterial thrombolysis (21/24) and percutaneous transluminal angioplasty/permanent stent placement (7/24). Recanalization was assessed by means of the TICI score. Clinical outcome was determined at discharge (NIHSS), and at 3 months (mRS).

RESULTS: Median NIHSS score on admission was 24; median duration of symptoms was 254 minutes. Successful recanalization (TICI 2b +3) by thrombectomy only was achieved in 18 patients (75%). Intracranial stent deployment after thrombectomy caused by underlying atherosclerotic stenosis was performed in 7 patients. If these patients with intracranial stent placement are included, successful recanalization was achieved in 21 of 24 patients (87.5%). NIHSS improvement ≥10 points was reached in 54% of patients (n = 13/24). Mortality during the first 3 months was 29% (7/24). After 3 months, 8 patients (33%) had a favorable clinical outcome (mRS 0–2).

CONCLUSIONS: In our series, application of self-expanding retrievable stents in acute basilar artery occlusion resulted in a high recanalization rate without procedural complications and good clinical outcome in one-third of patients.

ABBREVIATIONS: BAO = basilar artery occlusion; IAT = intra-arterial thrombolysis; MT = mechanical thrombectomy

Basilar artery occlusion (BAO), representing 20% of all ischemic strokes occurring in the posterior circulation, remains the stroke subtype with the highest mortality rate by far.[1] Severe neurologic and non-neurologic sequelae are caused by ischemic infarction of brain stem parenchyma, cranial nerve nuclei, and autonomic centers, with death and dependency rates exceeding 70% even after treatment.[2]

Regardless of treatment, recanalization of an occluded basilar artery is the single greatest predictor of good outcome.[3] The likelihood of a good outcome in nonrecanalized patients is approximately 13%.[4] There exists only limited data on the efficacy of different recanalization strategies to achieve complete recanalization of the occluded vessel segment.[1] Either intravenous or local intra-arterial administration of thrombolytics has shown low rates of recanalization in approximately 60% of cases and consequently has been associated with poor clinical outcome. Given the poor results in achieving complete vessel recanalization by pharmacologic intravenous or local intra-arterial thrombolysis (IAT), more effective recanalization strategies are highly desirable, and many centers favor additional mechanical thrombectomy (MT). A variety of intra-arterial devices intended to disrupt, stent, or aspirate the thrombus has been reported for recanalization of basilar artery occlusions.[5-10] Recently, the appearance of self-expanding retrievable stents (stent retriever), which have increased recanalization rates to >90% in the anterior circulation,[11-14] has brought up a promising alternative to all other therapeutic strategies. While an increasing number of studies has investigated the use of stent retrievers in anterior circulation, employment in acute BAO has been reported infrequently and in most studies with <20 patients (Table 1).

We investigated a series of 24 patients with acute BAO thus far treated by stent retrievers and analyzed safety and efficacy data as well as clinical results.

Received June 10, 2013; accepted after revision September 13.

From the Departments of Neuroradiology (M.M., S.S., L.B., C.H., S.R., M.B., M.P.) and Neurology (C.H., S.N., P.A.R.), University of Heidelberg Medical Center, Heidelberg, Germany.

Please address correspondence to Markus Möhlenbruch, MD, Department of Neuroradiology, University of Heidelberg Medical Center, Im Neuenheimer Feld 400, 69120 Heidelberg, Germany; e-mail: markus.moehlenbruch@med.uni-heidelberg.de

http://dx.doi.org/10.3174/ajnr.A3796

Table 1: Comparison of baseline stroke severity and outcome variables between this study and others with the use of a stent retriever in acute basilar artery occlusion

	N(BAO)/N (Total)	NIHSS Initial	Successful Recanalization (TICI 2b–3), %	sICH, %	mRS 0–2 After 90 Days, %	90-Day Mortality, %
Roth et al[23]	8/22	19	87.5	12.5	37.5	50
Miteff et al[24]	10/26	31	100 (TIMI 3 in 33)[a]	10	20	33
Costalat et al[25]	16/50	?	81 (TICI 3)	6.3	44	25
Dorn et al[26]	24/108	16	77.9	NA	NA	47.8[b]
Mordasini et al[27]	14/14	21	100	0	29	36
Espinosa et al[28]	18/18	20	94	0	50	22
Mourand et al[29]	31/31	38	74	16	35	32
Study group	24/24	24	87.5	8	33	29

Note:—N indicates number of patients; NA, not available; sICH, symptomatic intracerebral hemorrhage.
[a] TIMI (Thrombolysis In Myocardial Infarction) grade 2 or 3; [b]at discharge.

MATERIALS AND METHODS

Approval for prospective data collection of all interventional procedures reported in this study was given by the institutional review board. Patient informed consent for study inclusion was obtained from the patients or their legal representatives.

On the basis of the prospectively collected thrombolysis in stroke data base in Heidelberg since 1998, we analyzed angiographic and clinical data of patients with acute ischemic stroke caused by BAO undergoing endovascular stroke treatment with stent retrievers between December 2009 and May 2012. In our institution, the Solitaire FR Revascularization Device (Solitaire FR; Covidien, Dublin, Ireland) became available in March 2009 and the Revive SE thrombectomy device (Revive SE; Codman & Shurtleff, Raynham, Massachusetts) in October 2010 for endovascular stroke treatment.

On admission, a stroke neurologist performed physical neurologic examinations and detailed assessment of the NIHSS score. Cranial CT including CT angiography or multimodal stroke MR imaging including dynamic susceptibility contrast perfusion, DWI, and time-of-flight MR angiography was performed in all patients immediately after physical evaluation. Thereafter, intravenous thrombolysis with rtPA (0.9 mg/kg body weight for 40 minutes) was administered as bridging therapy in patients with no contraindications to rtPA. Patients who received intravenous thrombolysis in a tertiary institution and were referred to us for further endovascular therapy were also included in this study.

After the interventional procedure, patients were observed for at least 24 hours in a neurologic intensive care unit, and follow-up CT or MR imaging was routinely performed at 20–36 hours after treatment, or earlier if neurologic deterioration occurred. Postinterventional NIHSS and mRS were assessed by detailed physical examinations performed by an independent stroke neurologist at discharge. MR spectroscopy at 3 months was obtained during a standardized telephone follow-up or an outpatient visit. As a common definition of good outcome, an mRS score of 0–2 was adopted and for poor functional outcome a score of 3–6 was adopted.[15] Stroke etiology was classified according to TOAST criteria.[16]

Procedure

All interventions were performed by board-certified consultant neurointerventionalists on a biplanar system (Artis zee Biplane; Siemens, Erlangen, Germany) under general anesthesia. Using transfemoral access, a 6F guiding catheter (Envoy; Codman & Shurtleff or Neuron; Penumbra, Alameda, California) was placed into the dominant or most accessible vertebral artery. During the study period, mechanical thrombectomy was performed with the use of Solitaire FR or Revive SE. A microcatheter (Prowler Select Plus, Codman & Shurtleff; or Rebar 27, Covidien) with a 0.014-inch microwire (Transcend; Stryker, Kalamazoo, Michigan) was carefully advanced through the thromboembolic occlusion under fluoroscopic control. Angiographic runs were subsequently performed through the microcatheter to document the correct position of the microcatheter tip at least 0.5 cm beyond the distal end of the thrombus. Under fluoroscopic control, the stent retriever was advanced through the microcatheter across the vessel occlusion with the distal stent markers beyond the distal end of the occlusion. The stent was deployed/unsheathed completely by pulling back the microcatheter over the proximal marker, and angiographic runs were performed to control for flow restoration. The duration of stent deployment before its retrieval/thrombectomy maneuver varied between 1–5 minutes if thrombectomy/mechanical recanalization was the only aim (21/24 patients). If additional intra-arterial local administration of rtPA was performed, longer deployment times of up to 20 minutes were reached (3/24 patients). To perform the mechanical recanalization/thrombectomy maneuver, the microcatheter was withdrawn with the deployed/unsheathed stent retriever at fixed distance from the microcatheter tip under simultaneous aspiration with a 20-mL syringe at the guide catheter. In the case of persistent occlusion or incomplete vessel recanalization, the device was cleaned and reinserted for repeated thrombectomy.

As a supplement to thrombectomy, we used intra-arterial rtPA if distal branch occlusions persisted. If there was an underlying stenosis or insufficient recanalization, we eventually performed additional balloon angioplasty and permanent endovascular stent placement (Solitaire FR or Enterprise; Codman & Shurtleff). The maximum dose of intra-arterial rtPA was 21 mg. Other periprocedural medications in selected patients (12/24) included an IV bolus of 500 mg of aspirin or 5000 U of heparin or tirofiban (administered intravenously, at an initial rate of 0.4 μg/kg per minute for 30 minutes and continued at 0.1 μg/kg per minute for 24 or 48 hours). If permanent stent deployment was performed, postprocedural medication with 100 mg of aspirin and 300 mg of clopidogrel (subsequently 75 mg for 3 months) was initiated.

The extent of recanalization was classified according to the TICI grading scale.[17] TICI grades 2b and 3 were rated as sufficient

recanalization, whereas TICI grades 0–2a were rated as insufficient recanalization. Assessment of angiographic images was performed in consensus by 2 board-certified interventional neuroradiologists (M.M., S.S.) with more than 5 years of training.

The following time points were recorded for analysis: onset of symptoms, first angiogram, and achievement of final recanalization result. Time intervals from symptom onset to the first angiogram and procedure time to final recanalization (time to recanalization) were calculated. Furthermore, images were evaluated regarding level and length of the occlusion (in millimeters, by use of CTA or MRA), posterior circulation ASPECTS (by use of CT angiography source images or MR imaging DWI), and number of stent deployments necessary for recanalization.[18] Postprocedural hemorrhage was rated according to PROACT II criteria.

Statistics

Categoric data in contingency tables were analyzed by use of the Fisher exact test. Nonparametric pair-wise comparisons were performed with the use of the Wilcoxon test (procedure "rank sum" for unmatched data). Statistical analyses were performed by use of PASW Statistics, Version 18.0 (IBM, Armonk, New York). Statistical significance was assumed at an α level of $P < .05$ (2-sided). To test the effects of age, admission NIHSS score, time from symptom onset, and recanalization status on outcome, univariate logistic regression analyses were calculated ("logistic" procedure of STATA 12; StataCorp, College Station, Texas).

RESULTS

Between December 2009 and May 2012, endovascular therapy was performed on 31 patients for BAO. Of these, 7 patients were excluded because of endovascular treatment technique with either exclusive local intra-arterial thrombolysis or primary stent placement for high-grade basilar artery or distal vertebral artery stenosis. Twenty-four patients (17 male, 7 female; median age, 70; range, 33–83 years) underwent MT. In this group, 63.3% had hypertension, 50.0% had hypercholesterolemia, 33.3% had atrial fibrillation, 33.3% had a history of previous TIA or stroke, 23.3% had diabetes, 23.3% were current smokers, and 20% had coronary artery disease. Stroke etiology was categorized in accordance with TOAST classification: large-vessel disease in 7 (29.2%) patients, cardioembolic cause in 11 (45.8%) patients, both (large-vessel disease and cardioembolic) in 4 (16.7%) patients, and undetermined in 2 (8.3%) patients.

The site of BAO was partial basilar tip (1/24; 4.2%), distal to anterior ICA offspring to basilar tip (13/24; 54.2%), midbasilar without basilar tip (6/24; 25%), proximal basilar artery with 1 vertebral artery (2/24; 8.3%), and proximal basilar artery with both vertebral arteries (2/24; 8.3%). The median length of the occluded basilar artery segment was 17 mm (minimum, 5 mm; maximum, 50 mm).

Twenty-one patients (87.5%) received intravenous rtPA as bridging therapy before endovascular therapy, with a median dose of 50 mg (minimum, 36 mg; maximum, 90 mg), and local intra-arterial thrombolysis as an adjunctive therapy was given in 6 patients (25%), with median dose of 18 mg (minimum, 13 mg; maximum, 21 mg).

The median time interval from symptom onset to first angiogram was 254 minutes (range, 125–827 minutes), and median procedure time from first angiogram to recanalization was 77 minutes (range, 30–324 minutes).

Nine patients were treated with Solitaire FR, 12 patients with Revive SE, 2 patients with both devices, and in 1 patient delivery of the stent retriever was technically not feasible due to tortuous anatomy of aortic arch or right vertebral artery. The median number of passes for Solitaire FR or Revive SE was 2 (range, 1–10).

Initial TICI score before recanalization was 0 in 22 patients and 1 in 2 patients. After MT, successful recanalization defined as TICI score 2b or 3 was achieved in 18 patients (75%; TICI 2b in $n = 9$; TICI 3 in $n = 9$). Two of 24 patients were recanalized partially according to TICI 2a. Additional intracranial stent deployment after MT due to an underlying atherosclerotic stenosis was performed in 7 patients. In 3 of these patients, the TICI score subsequently improved from 0–2b ($n = 1$), from 1–2b ($n = 1$), and from 2a–2b ($n = 1$). In the remaining 4 patients, the TICI score did not differ from previous MT [TICI 2a ($n = 1$); 2b ($n = 1$); 3 ($n = 2$)]. Overall, after MT alone or in combination with intracranial stent placement, successful recanalization was achieved in 21 of 24 patients (87.5%; TICI 2b in $n = 12$; TICI 3 in $n = 9$). Extracranial stent placement was performed in 2 patients (in 1 patient with a severe 90% atherosclerotic stenosis in V1 and in another patient with dissection in V2 caused by the guiding catheter). Table 2 gives an overview of the patient angiographic and treatment data.

Asymptomatic postprocedure hemorrhage (HI1) occurred in 1 patient, and symptomatic intracranial hemorrhage (PH2) with lethal consequence appeared in another patient.

After stent retrieval, thromboembolic occlusion of a previously unaffected artery was observed in 4 of 24 (16%) patients (P2/P3 segment, $n = 1$; PICA, $n = 2$; superior cerebellar artery, $n = 1$). Severe vasospasm was detected in 2 patients, which resolved after intra-arterial administration of nimodipin.

Among all patients, median NIHSS score on admission was 24 (range, 7–42) and at discharge, 5 (range, 0–28), keeping in mind the impreciseness of this score in vertebrobasilar strokes and the arbitrary values in intubated patients. NIHSS improvement $\geq$10 points was reached in 54% of patients ($n = 13/24$). Mortality at discharge was 25% ($n = 6$) and at 3 months 29% ($n = 7$), respectively. After 3 months, 8 patients (33%) had a favorable clinical outcome (mRS 0–2), 4 patients (17%) were mRS 3, two patients (8%) were mRS 4, and 3 (13%) patients were mRS 5. Table 3 shows the outcome and complications of the treated patients. The strongest predictor of favorable outcome, with an odds ratio of 3.51 ($P = .10$; CI: 0.65–18.9), was recanalization status after thrombectomy as graded by the TICI scale. With an odds ratio of 0.58, the NIHSS score on admission also was a strong predictor of outcome with a trend toward statistical significance in this small sample ($P = .081$, CI: 0.31–1.06). Older patients tended to have worse outcome with an odds ratio of 0.93 (CI: 0.85–1.00; $P = .067$). Interestingly, time from symptom onset to endovascular treatment (range, 2 hours, 5 minutes to 13 hours, 47 minutes) did not exert a strong influence on outcome (odds ratio = 0.99; $P = .21$; CI: 0.98–1.00).

After dichotomization, by use of the posterior circulation ASPECTS score at a cutoff value of $\geq$9, NIHSS score at discharge

Table 2: Angiographic/treatment data

Patient No.	TICI at Baseline	TICI at End Point	No. of Passes	Type of Device	Intracranial Stent Placement	IV rtPA	IA rtPA	Concurrent Medication
1	0	3	1	S	0	54	20	0
2	0	3	4	S	0	0	0	A
3	0	2b	4	S	0	55	20	T
4	0	2b	2	S	1	35	21	T
5	0	2b	2	S	1	41	13	T
6	0	2a	1	S	1	47	16	T
7	0	3	2	S	1	52	0	T
8	0	2b	1	R	0	50	16	T
9	0	3	4	R	0	45	0	0
10	0	0	0	0	0	50	0	0
11	0	2b	7	R	1	0	0	T
12	0	2b	3	R	1	67	0	T
13	0	2b	2	R	0	50	0	0
14	0	3	1	R	0	90	0	0
15	0	2b	1	R	0	43	0	H
16	0	3	2	R	0	69	0	0
17	0	2b	2	R	0	90	0	0
18	0	3	6	R, S	0	0	0	0
19	1	2b	2	S	0	50	0	0
20	0	2b	3	R	0	38	0	0
21	0	3	1	S	1	73	0	T
22	0	3	2	R	0	60	0	0
23	0	0	10	R, S	0	68	0	T
24	1	2b	4	R	0	60	0	0

Note:—"No. of Passes" refers to the number of passes needed for recanalization. A indicates aspirin; H, heparin; R, Revive SE; S, Solitaire FR; T, tirofiban; IA, intra-arterial.

Table 3: Patient outcomes/complications

Patient No.	NHISS at Baseline	NHISS at Discharge	mRS at Discharge	mRS at 90 Days	ICH	Complication
1	17	0	1	0	0	0
2	38	7	5	5	0	0
3	35	[a]	6	6	AS	0
4	19	1	2	5	0	OUA
5	26	[a]	6	6	0	OUA
6	38	17	4	4	0	0
7	16	2	2	3	0	0
8	39	[a]	6	6	S	0
9	42	22	5	6	0	0
10	40	[a]	6	6	0	0
11	21	28	5	5	0	VAS
12	7	[a]	6	6	0	OUA
13	22	2	3	2	0	D V2
14	30	5	3	3	0	0
15	27	1	1	2	0	D V1
16	22	4	3	2	0	0
17	10	6	4	2	0	OUA
18	37	8	4	3	0	D V1
19	12	3	3	2	0	D V2
20	21	15	5	4	0	0
21	30	4	3	2	0	0
22	24	0	0	0	0	VAS
23	–	[a]	6	6	0	0
24	17	10	4	3	0	0

Note:—AS indicates asymptomatic; D, dissection; OUA, thromboembolic occlusion of a previously unaffected artery; S, symptomatic; V1, V2, segment of the vertebral artery; VAS, vasospasm; –, absent.
[a] Deceased.

($P = .03$), mRS at discharge ($P = .004$), and mRS at 3 months ($P = .02$) were significantly better in patients with ASPECTS ≥9. Mortality in patients with ASPECTS ≥9 was significantly lower: 9% versus 29%, $P = .034$.

DISCUSSION

The first description of the use of IAT in BAO was published in the early 1980s.[19] Since that time, multiple series describing the use of IAT in BAO have been published. A large meta-analysis that incorporated 10 studies including 316 patients reported an overall recanalization rate of 64% and overall mortality of 56%. The mortality was 87% in nonrecanalized patients and 37% in recanalized patients ($P < .001$).[20] In the most recent and largest series to date, the data of 180 adult patients with angiographically confirmed basilar occlusion treated with IAT at 5 German stroke centers were retrospectively evaluated. Patients with partial or complete recanalization had a significantly better neurologic outcome than nonrecanalized patients ($P < .001$), highlighting that complete or at least partial recanalization of the occlusion is essential for a favorable neurologic outcome. However, the overall recanalization rates of approximately 55% for IAT have remained low in these published series.[21] As a second major disadvantage of IAT, the time to recanalization is prolonged because it takes time to dissolve the thrombus after initial catheterization.[12] In accordance with these limitations, a previous meta-analysis showed that the overall proportion of patients achieving a favorable outcome after IAT remains low (good or favorable outcome in 24%).[22]

Therefore, various investigators have assessed the use of MT in small BAO case series (<16 patients with exception of the MERCI and Multi-MERCI trails) with different devices including simple clot disruption,[5] manual aspiration,[6] AngioJet catheter (Possis Medical, Minneapolis, Minnesota),[7] Amplatz Goose Neck Snare (Microvena, White Bear Lake, Minnesota),[8] Merci retriever (Concentric Medical, Mountain View, California),[9] and the Penumbra aspiration catheter.[10] In these studies, the successful recanalization rate varied between 50–100% and good clinical outcome ranged between 25–50%.

With the introduction of stent retrievers, which combine the advantages of temporary stent placement with immediate flow

restoration and thrombectomy with definite thrombus removal, increased recanalization rates of up to 100% have been reported.[11-14] However, only limited data about treatment of acute BAO with stent retrievers are presented in the literature (Table 1).[23-29]

Costalat et al[25] included 16 acute BAOs in their series of 50 patients with intracranial vessel occlusion and treated with the Solitaire FR. Successful recanalization (defined as TICI 3) was obtained in 81% (13/16), with a mean of 2.1 passes. One patient had a symptomatic intracranial hemorrhage. Good functional outcome (mRS of 0–2) at 3 months was achieved in 44% (7/16), and mortality rate was 25% (4/16).[25] Mordasini et al[27] presented a series with 14 acute BAOs treated with Solitaire FR. Successful recanalization (defined as TICI 2b or 3) was reached in all cases, with a mean of 1.3 passes. There was no symptomatic intracranial hemorrhage. At 3 months, good functional outcome (mRS 0–2) was observed in 28.6% (4/14) and overall mortality was 35.7% (5/14).[27] Espinosa de Rueda et al[28] treated 18 patients with Solitaire AB/FR or Trevo Pro (Stryker) with a mean of 1.7 passes. Successful recanalization (defined as TICI 2b or 3) was obtained in 94.4% (17/18) with good functional outcome (mRS 0–2) in 50% (9/17). No symptomatic intracranial hemorrhage was found, and mortality rate was 22.2% (5/17).[28]

In our series, we used 2 different stent retrievers. The first 9 patients were treated with the Solitaire FR and in the following 14 patients the Revive SE was used with changeover to the Solitaire FR in 2 cases. For both stent retrievers, the median number of passes was 2. In 1 of the 2 patients in which both devices (Solitaire FR after Revive SE) were used, successful recanalization was achieved only after the use of a slightly oversized Solitaire FR (6 mm in diameter) because the diameter of the basilar artery was very large, measuring nearly 5 mm. In the other patient, the basilar artery remained occluded despite 5 attempts with Revive SE, another 5 attempts with Solitaire FR, and even after eventual percutaneous transluminal angioplasty.

Thromboembolic events in previously unaffected proximal or distal portions of the posterior cerebral artery territories occurred in 2 patients distally (8%) and in 2 patients proximally (8%). Distal occlusion of previously patent branches is most likely to be explained by fragmentation and embolization of the clot during retrieval into the guiding catheter. This rate of embolism in our series is higher than what is reported for the anterior circulation.[30] One possible reason might be the different vessel anatomy in the posterior circulation, which is more tight and curved with possibly more tapering and deformation of the device while being withdrawn. To overcome this problem, we constantly attempted to advance the 6F guiding catheter as high/distal as possible so as to approach the deployed stent retriever as close as possible to optimize complete and effective aspiration of all thrombus material during retrieval. A potential drawback with this approach is possible vessel dissection occurring in 4 patients, emphasizing the application of a more flexible distal access catheter instead of stiffer guiding catheters.

In our series with 24 patients, successful recanalization was achieved in 75%, which is lower than the reported rate in the anterior circulation. Together with additional intracranial stent placement, we found that our successful recanalization of 87.5% is in line with the previous data (Table 1). These numbers reflect the higher incidence of a high-grade stenosis in the posterior circulation with consecutive atherothrombotic occlusions, caused by local thrombosis on the surface of ulcerated atherosclerotic plaques. The reported incidence in the literature of 35% of atherothrombotic lesions in patients with acute BAO is similar to our rate of 29%.[3]

After pretreatment intravenous thrombolysis with rtPA, no shift in occlusion site or recanalization rate was observed on preinterventional DSA compared with initial CTA or MRA. Whether pretreatment intravenous thrombolysis helped with recanalization cannot be proved in the face of the low recanalization failure rate.

However, despite the high successful recanalization rate, favorable clinical outcome was limited. The proportion of patients who gained independence (mRS 0–2) after 3 months was 33% ($n = 8$ /24). Two patients discharged with mRS 2, 1 week after onset, had subsequent MCA infarction during the follow-up period with the result of mRS 3 and mRS 5, respectively. Applying the definition of good neurologic outcome according to the SWIFT study, 54% of patients ($n = 13/24$) met the criteria for a good neurologic outcome.[31]

Some predictors influence clinical outcome independently from successful recanalization, such as high initial NIHSS/low Glasgow Coma Scale scores, age, thrombus volume, etiology, site of occlusion, time span from onset to recanalization, and brain stem DWI score or the posterior circulation ASPECTS.[18] In this study, NIHSS score on admission and age could be identified as predictors of outcome, however only with a trend toward statistical significance. This reflects one major limitation of our study, which is restriction to a single center and small sample size. Interestingly, time from onset to endovascular treatment did not exert a strong influence on outcome. This finding is in accordance with the observation that extended treatment windows of up to 12 hours in posterior circulation ischemic stroke are possible if irreversible extended brain stem infarction is ruled out by pretreatment DWI-MR imaging.[32] With the use of the posterior circulation ASPECTS in our series, patients with posterior circulation ASPECTS score ≥ 9 had a significantly better outcome (50%, $n = 6/12$, mRS 0–2 after 3 months) than patients with posterior circulation ASPECTS score ≤ 8 (17%, $n = 2/12$), which reveals that extensive and irreversible brain stem damage obviously will indicate poor prognosis regardless of recanalization success.

In 2 of 24 patients in our series (8%), intracranial hemorrhage (HI1, $n = 1$; PH2, $n = 1$; according to the PROACT II criteria) occurred with fatal outcome (mRS 6 in both; in 1 patient caused by PH2 and in the other patient caused by extensive brain stem infarction). Recanalization had been successful in both these patients (TICI 2b) and in both intravenous and intra-arterial lysis with rtPA, and, in addition, a standard dose rate of tirofiban had been given during and after the procedure. These observations in 2 cases of our series indicate that the risk of hemorrhage after recanalization/reperfusion might increase exceptionally with combined administration of intravenous/intra-arterial rtPA and glycoprotein IIb/IIIa antagonists and should therefore not be performed routinely in any interventional treatment of BAO.[33] However, the overall rate of intracranial hemorrhage compares favorably with the rates reported in other studies (Table 1).

CONCLUSIONS

Treatment of acute BAO with stent retrievers is safe and technically feasible, with high rates of recanalization. However, although feasible and safe, endovascular treatment still must show superiority to intravenous thrombolysis alone. The results encourage further prospective trials to evaluate the potential clinical benefit in patients with acute BAO.

Disclosures: Stefan Rohde—*UNRELATED: Payment for Lectures (including service on speakers bureaus):* Codman Neurovascular, MicroVention, AB Medica. Martin Bendszus—*RELATED: Consulting Fee or Honorarium:* Codman, Micrus; Comments: Honoraria for educational talks; *UNRELATED: Grants/Grants Pending:* Micrus,* Comments: IIS on aneurysm treatment with coils; *Payment for Lectures (including service on speakers bureaus):* Bayer, Guerbet, Novartis, Codman, Micrus, Comments: Educational talks. Peter Ringleb—*UNRELATED: Payment for Lectures (including service on speakers bureaus):* Boehringer Ingelheim, Paion, Ferrer, Sanofi, Bayer, GlaxoSmithKline, Comments: Lecture fees for talks about thrombolysis (**money paid to institution*).

REFERENCES

1. Mattle HP, Arnold M, Lindsberg PJ, et al. **Basilar artery occlusion.** *Lancet Neurol* 2011;10:1002–14
2. Ferbert A, Brückmann H, Drummen R. **Clinical features of proven basilar artery occlusions.** *Stroke* 1990;21:1135–42
3. Schonewille WJ, Wijman CA, Michel P, et al. **Treatment and outcomes of acute basilar artery occlusion in the Basilar Artery International Cooperation Study (BASICS): a prospective registry study.** *Lancet Neurol* 2009:8:724–30
4. Hacke W, Zeumer H, Ferbert A, et al. **Intra-arterial thrombolytic therapy improves outcome in patients with acute vertebrobasilar occlusive disease.** *Stroke* 1988;19:1216–22
5. Bergui M, Stura G, Daniele D, et al. **Mechanical thrombolysis in ischemic stroke attributable to basilar artery occlusion as first-line treatment.** *Stroke* 2006;37:145–50
6. Chapot R, Houdart E, Rogopoulos A, et al. **Thromboaspiration in the basilar artery: report of two cases.** *AJNR Am J Neuroradiol* 2002;23:282–84
7. Mayer TE, Hamann GF, Schulte-Altedorneburg G, et al. **Treatment of vertebrobasilar occlusion by a coronary waterjet thrombectomy device: a pilot study.** *AJNR Am J Neuroradiol* 2005;26:1389–94
8. Pfefferkorn T, Mayer TE, Opherk C, et al. **Staged escalation therapy in acute basilar artery occlusion: intravenous thrombolysis and on-demand consecutive endovascular mechanical thrombectomy: preliminary experience in 16 patients.** *Stroke* 2008;39:1496–500
9. Lutsep HL, Rymer MM, Nesbit GM. **Vertebrobasilar revascularization rates and outcomes in the MERCI and multi-MERCI trials.** *J Stroke Cerebrovasc Dis* 2008;17:55–57
10. Bose A, Henkes H, Alfke K, et al. **The Penumbra system: a mechanical device for the treatment of acute stroke due to thromboembolism.** *AJNR Am J Neuroradiol* 2008;29:1409–13
11. Castaño C, Dorado L, Guerrero C, et al. **Mechanical thrombectomy with the Solitaire AB device in large artery occlusions of the anterior circulation: a pilot study.** *Stroke* 2010;41:1836–40
12. Möhlenbruch M, Seifert M, Okulla T, et al. **Mechanical thrombectomy compared to local-intraarterial thrombolysis in carotid T and middle cerebral artery occlusions: a single center experience.** *Clin Neuroradiol* 2012;22:141–47
13. Stampfl S, Hartmann M, Ringleb PA, et al. **Stent placement for flow restoration in acute ischemic stroke: a single-center experience with the Solitaire stent system.** *AJNR Am J Neuroradiol* 2011;32:1245–48
14. Rohde S, Haehnel S, Herweh C, et al. **Mechanical thrombectomy in acute embolic stroke: preliminary results with the Revive device.** *Stroke* 2011;42:2954–56
15. Van Switen JC, Koudstaal PJ, Visser MC, et al. **Interobserver agreement for the assessment of handicap in stroke.** *Stroke* 1988;19:604–07
16. Adams HP Jr, Bendixen BH, Kappelle LJ, et al. **Classification of subtype of acute ischemic stroke: definitions for use in a multicenter clinical trial. TOAST: Trial of Org 10172 in Acute Stroke Treatment.** *Stroke* 1993;24:35–41
17. Higashida RT, Furlan AJ, Roberts H, et al. **Trial design and reporting standards for intra-arterial cerebral thrombolysis for acute ischemic stroke.** *Stroke* 2003;34:109–37
18. Puetz V, Sylaja PN, Coutts SB, et al. **Extent of hypoattenuation on CT angiography source images predicts functional outcome in patients with basilar artery occlusion.** *Stroke* 2008;39:2485–90
19. Zeumer H, Hacke W, Ringelstein EB. **Local intraarterial thrombolysis in vertebrobasilar thromboembolic disease.** *AJNR Am J Neuroradiol* 1983;4:401–04
20. Smith WS. **Intra-arterial thrombolytic therapy for acute basilar occlusion: pro.** *Stroke* 2007;38:701–03
21. Schulte-Altedorneburg G, Hamann GF, Mull M, et al. **Outcome of acute vertebrobasilar occlusions treated with intra-arterial fibrinolysis in 180 patients.** *AJNR Am J Neuroradiol* 2006;27:2042–47
22. Lindsberg PJ, Mattle HP. **Therapy of basilar artery occlusion: a systematic analysis comparing intra-arterial and intravenous thrombolysis.** *Stroke* 2006;37:922–28
23. Roth C, Papanagiotou P, Behnke S, et al. **Stent-assisted mechanical recanalization for treatment of acute intracerebral artery occlusions.** *Stroke* 2010;41:2559–67
24. Miteff F, Faulder KC, Goh AC, et al. **Mechanical thrombectomy with a self-expanding retrievable intracranial stent (Solitaire AB): experience in 26 patients with acute cerebral artery occlusion.** *AJNR Am J Neuroradiol* 2011;32:1078–81
25. Costalat V, Machi P, Lobotesis K, et al. **Rescue, combined, and standalone thrombectomy in the management of large vessel occlusion stroke using the Solitaire device: a prospective 50-patient single-center study: timing, safety, and efficacy.** *Stroke* 2011;42:1929–35
26. Dorn F, Stehle S, Lockau H, et al. **Endovascular treatment of acute intracerebral artery occlusions with the Solitaire stent: single-centre experience with 108 recanalization procedures.** *Cerebrovasc Dis* 2012;34:70–77
27. Mordasini P, Brekenfeld C, Byrne JV, et al. **Technical feasibility and application of mechanical thrombectomy with the Solitaire FR revascularization device in acute basilar artery occlusion.** *AJNR Am J Neuroradiol* 2013;34:159–63
28. Espinosa de Rueda M, Parrilla G, Zamarro J, et al. **Treatment of acute vertebrobasilar occlusion using thrombectomy with stent retrievers: initial experience with 18 patients.** *AJNR Am J Neuroradiol* 2013;34:1044–48
29. Mourand I, Machi P, Milhaud D, et al. **Mechanical thrombectomy with the Solitaire device in acute basilar artery occlusion.** *J Neurointerv Surg* 2014;6:200–04
30. Dávalos A, Pereira VM, Chapot R, et al. **Solitaire group: retrospective multicenter study of Solitaire FR for revascularization in the treatment of acute ischemic stroke.** *Stroke* 2012;43:2699–705
31. Saver JL, Jahan R, Levy EI, et al. **Solitaire flow restoration device versus the Merci retriever in patients with acute ischaemic stroke (SWIFT): a randomised, parallel-group, non-inferiority trial.** *Lancet* 2012;380:1241–49
32. Strbian D, Sairanen T, Silvennoinen H, et al. **Thrombolysis of basilar artery occlusion: impact of baseline ischemia and time.** *Ann Neurol* 2013;73:688–94
33. Kellert L, Hametner C, Rohde S, et al. **Endovascular stroke therapy: tirofiban is associated with risk of fatal intracerebral hemorrhage and poor outcome.** *Stroke* 2013;44:1453–55

Coil Occlusion of Wide-Neck Bifurcation Aneurysms Assisted by a Novel Intra- to Extra-Aneurysmatic Neck-Bridging Device (pCONus): Initial Experience

M. Aguilar-Pérez, W. Kurre, S. Fischer, H. Bäzner, and H. Henkes

ABSTRACT

BACKGROUND AND PURPOSE: The pCONus is a new stentlike self-expanding nitinol implant with 4 distal petals, which is fully retrievable and electrolytically detachable. The distal end is implanted inside the aneurysm at the neck. The shaft is anchored in the parent vessel. In selected wide-neck bifurcation aneurysms, the pCONus was used to assist coiling. The device was evaluated for its safety and efficacy.

MATERIAL AND METHODS: Twenty-eight patients with 28 wide-neck aneurysms (9 recently ruptured) were treated with pCONus-assisted coiling at the discretion of the operator. Other treatment options were considered but were discarded due to anticipated difficulties. Technical issues, immediate posttreatment angiographic findings, clinical outcome, and follow-up imaging were assessed.

RESULTS: There were 11 MCA, 7 anterior communicating artery, 1 posterior cerebral artery, 1 A2, and 8 basilar artery aneurysms. Insertion and deployment of the pCONus and subsequent coiling were possible in all cases. There were no clinically evident complications associated with the use of the device. Initial anatomic outcome showed 8 complete occlusions, 9 neck remnants, and 11 incomplete occlusions. Neurologic status remained unchanged at follow-up. Angiographic controls were obtained in 22 patients (mean, 7.5 months). Of these, 13 had complete occlusion, 9 showed improvement, and 7 were unchanged. Four died from SAH sequelae or other diseases, and 2 have not yet undergone follow-up. No intimal hyperplasia was observed.

CONCLUSIONS: The pCONus facilitates coil occlusion of unruptured and ruptured wide-neck bifurcation aneurysms. The device can be deployed safely. Coil retention is sufficient to protect the efferent vessels. So far, no intimal hyperplasia in the shaft has been observed.

ABBREVIATIONS: PCA = posterior cerebral artery; SCA = superior cerebellar artery; WNBA = wide-neck bifurcation aneurysm

Coil occlusion of intracranial aneurysms, both ruptured and unruptured, is safe and efficacious.[1,2] A major limitation of this treatment technique is related to the geometry of the target aneurysm. A neck of ≥4 mm and a fundus width/neck ratio of ≤1 mm are unfavorable for simple coiling.[3] Extrasaccular flow diversion has solved this issue for sidewall aneurysms.[4] Intra-aneurysmal flow diverters are promising but not yet fully established devices for selected bifurcation aneurysms.[5-7] For wide-neck bifurcation aneurysms (WNBAs), the techniques to assist coil occlusion include stent placement[8] and "balloon-remodeling,"[9] both requiring catheter access to at least 1 efferent vessel of the bifurcation. This catheterization can be difficult. Coil-assist techniques without efferent vessel access include the TriSpan device (Boston Scientific, Natick, Massachusetts),[10] which is no longer available, and the deployment of self-expanding stents with their distal end inside the aneurysm ("waffle cone" technique).[11] The stents used as waffle cones are not optimized for this purpose and are far from ideal. The pCONus (phenox, Bochum, Germany) is a dedicated neurovascular device that was designed to address the functional needs of an extra-intrasaccular neck-bridging aneurysm implant to assist the coil occlusion of WNBAs. This report summarizes our initial experience with the clinical use of this device.

MATERIALS AND METHODS

All patients were treated in a single institution by a team of 4 interventional neuroradiologists. The endovascular treatment was either proposed to the patient after interdisciplinary discussion or offered on the basis of the preference of the patient. The decision to assist the coil occlusion by a pCONus was made at the discretion of the senior author. In elective procedures, all patients

Received July 29, 2013; accepted after revision September 23.

From the Departments of Neuroradiology (M.A.-P., W.K., S.F., H.H.) and Neurology (H.B.), Klinikum Stuttgart, Stuttgart, Germany.

This article is dedicated to Professor Roland Felix for his 75th birthday.

Please address correspondence to Marta Aguilar-Pérez, MD, Department of Neuroradiology, Klinikum Stuttgart, Kriegsbergstr 60, D-70174 Stuttgart, Germany; e-mail: martaaguilarperez@yahoo.es

Indicates open access to non-subscribers at www.ajnr.org.

Indicates article with supplemental on-line table.

http://dx.doi.org/10.3174/ajnr.A3807

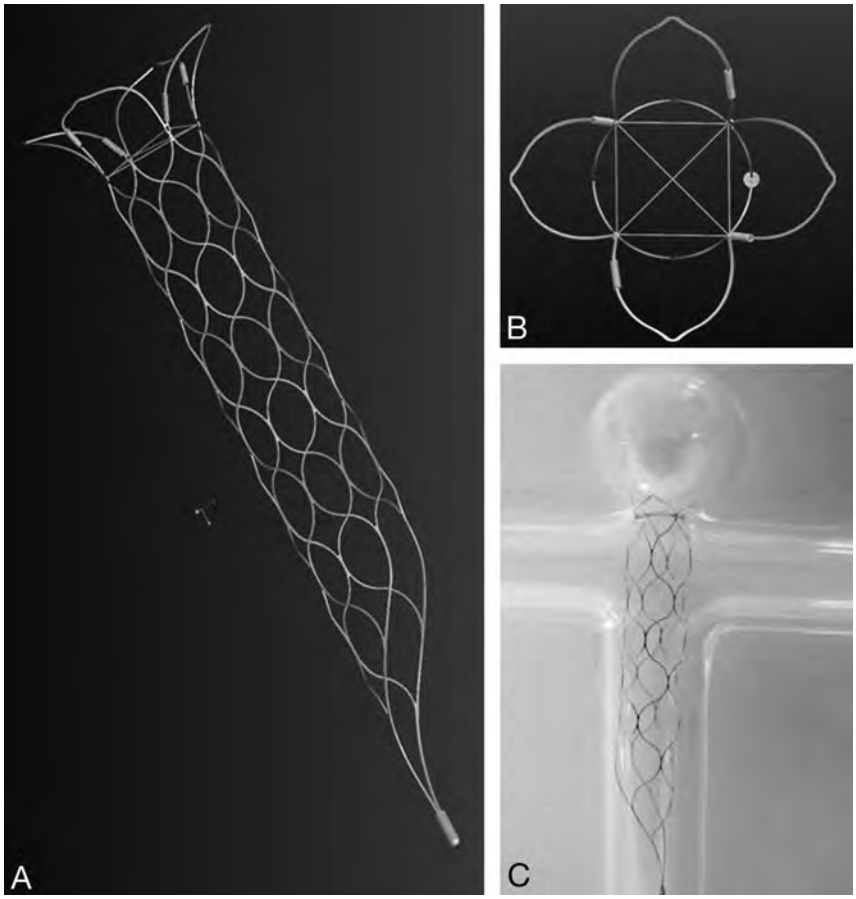

FIG 1. The pCONus is a self-expanding, completely retrievable, electrolytically detachable device with a proximal shaft (similar to stents) and 4 distal petals and a nylon cross in the distal end of the shaft (*A*). Similar to the waffle cone technique, the 4 distal loops of the pCONus are deployed inside the aneurysm at the level of the neck, assisting coil occlusion (*B*). The nylon cross (*C*) prevents coil protrusion into the shaft of the device.

had comprehensive consultations before the procedures. Microsurgery and conservative management were discussed with all elective patients. In patients in the acute phase after SAH, endovascular treatment, including the use of a pCONus, was performed as an emergency measure and, whenever possible, was explained to the relatives. Written informed consent was obtained from all elective patients, from 1 patient before the hemorrhage and from 1 authorized relative of a patient who presented with an SAH.

The pCONus is an endovascular implant for the bridging of intracranial WNBAs to enable coiling (Fig 1). The pCONus is a stentlike laser-cut vessel implant made of nitinol with 4 loops (petals) at its distal end, which are flared in a radial direction. The distal inner diameter of the pCONus is additionally crossed by 6 polyamide fibers, creating a mechanical barrier between the aneurysm and the parent vessel. The biocompatibility of these fibers is certified, and the same material is used for coils with attached nylon fibers (NXT Detachable Coil; ev3, Irvine, California). The proximal end of the implant and the 4 distal loops carry segmental radiopaque markers made of platinum-iridium wire. They allow visual control of the device under fluoroscopy. The pCONus ends proximally in 1 eccentric strut, which carries a detachment element connected to an insertion wire made of stainless steel. This detachment element consists of a cobalt chromium wire, which can be dissolved electrolytically by direct electric current by using available coil-detachment devices. The distal diameters of the expanded petals are available in 5, 6, 8, 10, 12, and 15 mm. The stentlike shaft has a 4-mm diameter and is 20 or 25 mm long. The pCONus is compatible with standard microcatheters with an inner diameter of 0.021 or 0.027 inches (eg, RapidTransit; Codman Neurovascular, Raynham, Massachusetts; and Marksman; Covidien, Dublin, Ireland). We used 0.021-inch microcatheters for easier access. The device allows controlled insertion, deployment, and eventual withdrawal into the microcatheter.

All patients were treated under general anesthesia by using a biplane DSA unit (Axiom Artis; Siemens, Erlangen, Germany). From a femoral access, a 6F or 8F guide catheter was inserted into the respective cervical vessel. The decision to use a pCONus in all patients was based on anatomic features of the target aneurysm. Single-vessel stent placement was weighed against pCONus usage. Kissing- or crossing-stent placement was not considered as a preferred alternative to the pCONus.

In unruptured aneurysms, a single dose of 500-mg acetylsalicylic acid and 600-mg clopidogrel was given the day before, and a Multiplate test (Verum Diagnostica, Munich, Germany) was performed before the procedure to confirm sufficient inhibition of the platelet function. Patients 19 and 21 did not show significant platelet-function inhibition and were reloaded with 30 mg prasugrel. Patient 24 was directly premedicated with 180 mg ticagrelor. In patients with severe SAH, the decision for an endovascular treatment was based on an interdisciplinary discussion. Arguments in favor of an endovascular approach were poor clinical condition after SAH or anticipated surgical difficulty. All patients with SAH were treated within 3 days after the index hemorrhage. After insertion of an external CSF drain, patients received 600 mg clopidogrel via a gastric tube and 500 mg acetylsalicylic acid; 5000 U of heparin was given intravenously as soon as the pCONus was deployed.

Postprocedural medication included a daily lifetime dose of 100 mg acetylsalicylic acid orally and 75 mg clopidogrel for 3 months. Patients 19 and 21 were continued with 10 mg prasugrel, and patient 24, with 2× 90-mg ticagrelor.

In a suitable working projection, calibrated measurements were made to determine the neck width, the aneurysm width, and the aneurysm height. The pCONus size was selected so that complete coverage of the aneurysm neck by the petals could be expected. A 0.021-inch microcatheter (eg, RapidTransit or Prowler Select Plus, Codman Neurovascular) was chosen. The distal end of the pCONus was deployed in the middle of the aneurysm fun-

dus, avoiding any impact with the aneurysm wall. As soon as the 4 petals were fully opened, the microcatheter was gently pulled back bringing the petals more proximal to the neck of the aneurysm. Without further movement, the insertion wire of the device was kept in place and the microcatheter was pulled back with complete deployment of the shaft of the pCONus. Thereafter, a second microcatheter was inserted through the shaft into the aneurysm fundus (eg, Echelon10, Covidien; or Excelsior SL10; Stryker, Kalamazoo, Michigan). Coil occlusion started with the attempt to create a frame or basket with the first coil (eg, Morpheus coil, Covidien/ev3; or Framing Coil, MicroVention, Tustin, California). The residual space was filled with long and soft coils (eg, HyperSoft; MicroVention). When the fundus was considered completely occluded, the coil catheter was withdrawn and the pCONus was electrolytically detached.

Patients with SAH were managed according to widely accepted Standards of Practice. Patients with unruptured aneurysms underwent an MR imaging examination within 48 hours after the procedure. Angiographic follow-up was scheduled for 3 and 9 months.

Feasibility of the treatment, rate of intraprocedural and postprocedural complications, morbidity and mortality, and immediate and follow-up angiographic outcome were evaluated and assessed by the operators and the first author. The authors made the analysis in retrospect.

RESULTS

Twenty-eight consecutive patients (13 women; median age, 57.35 years) and 28 aneurysms (9 ruptured) were included. Demographic data, aneurysm sizes, and treatment results are summarized in the On-line Table.

Insertion and controlled deployment of the pCONus were possible in all patients. Neither access failure nor aneurysm or vessel perforation occurred. Catheterization of the aneurysms through the shaft of the pCONus did not cause any difficulty. No coil loop protrusion between the petals was encountered.

In 25/28 aneurysms (89%), a single pCONus alone retained the coils inside the aneurysm sac and protected the efferent vessels. In 2/28 patients, another device was necessary to prevent the occlusion of the efferent vessels. In 1/28 patients, a second pCONus was necessary to protect the neck region of the aneurysm.

Patient 19 presented with a giant MCA aneurysm, for which a combination of a pCONus and a TriSpan was necessary for coil stabilization and protection of the M2 origins.

Patient 23 presented with a fusiform upper basilar trunk and bifurcation aneurysm with both posterior cerebral arteries (PCAs) and superior cerebellar arteries (SCAs) originating from the lateral aspect of the aneurysm. The pCONus alone appeared insufficient to protect the PCA and SCA origins. Just Y-crossing Solitaire stents (Covidien) in both PCAs were expected to incompletely protect the SCAs, with difficult control of the coil occlusion of the saccular component of the aneurysm. After positioning the pCONus petals within the lumen of the aneurysm, we catheterized both PCAs without difficulty and 2 Solitaire stents were deployed in a Y-technique. The resulting structure was stable and allowed a well-controlled coil occlusion of the aneurysm.

In patient 26, a large unruptured aneurysm of the basilar tip incorporated both PCA origins. The aneurysm was directed backward toward the brain stem, with a 90° angle between the axes of the basilar artery and the aneurysm fundus. Two 5-mm pCONus implants were deployed in a crossing position to protect the neck region of the aneurysm.

The 3-point scale of Raymond et al[12] was used to evaluate the initial occlusion rate. In 8/28 aneurysms (28.6%), the occlusion rate was graded as class 1 (complete), 9/28 aneurysms (32.1%) were graded as class 2 (neck remnant), and 11/28 aneurysms (39.3%), as class 3 (residual fundus perfusion). In patients 3 and 18, an early second treatment within the first week was necessary to achieve the occlusion of the aneurysm (Fig 2).

In 1 patient, a local thrombus formation was observed intraoperatively, which resolved with a body-weight-adapted bolus dose of eptifibatide. Thromboembolic incidents with new ischemic lesions on MR imaging occurred in 9/15 patients (60%) and remained clinically silent in all except 3 cases. Three of 28 patients (10.7%) showed transient ischemic symptoms after the treatment, which resolved within 1 week. No clinically evident complications with permanent neurologic deficits or death related to the pCONus deployment or coil occlusion occurred.

Of the 28 patients treated, 4 died (2 from SAH sequelae and 2 from other diseases) and 2 have not yet undergone follow-up. Angiographic follow-up was available in 22/28 patients (78.6%) between 2 and 19 months (mean, 7.5 months) after the treatment. Complete occlusion was seen in 13/22 aneurysms (59%); neck remnant, in 6/22 aneurysms (27.3%); and aneurysm remnant, in 3/22 aneurysms (13.6%). All aneurysm remnant regrowths occurred in large/giant, partially thrombosed aneurysms after initial partial occlusion. No intimal hyperplasia was observed inside the pCONus shaft. Of these 22 aneurysms, 9 showed improvement of at least 1 point on the Raymond grading scale, while 7 remained unchanged.

In the 3 aneurysms with recoiling, access through the implanted pCONus was again possible and coil retention was as reliable as it was during the initial procedure (Fig 3).

DISCUSSION

WNBAs have been challenging for the endovascular approach. 3D coils were an early and relatively easy-to-use solution for these aneurysms.[13] 3D coils alone work best in long aneurysms, but frequently do not have enough stability in shallow aneurysms and in those without any neck.

The "dual-catheter" technique is another straightforward and inexpensive strategy.[14] A known risk of this technique is the first coil not entirely protecting the vessel bifurcation and displacement of already detached coils by subsequent coils.

The balloon-remodeling technique was initially advocated for sidewall aneurysms.[9] The development of more flexible and atraumatic compliant balloon catheters allows the simultaneous use of multiple balloons.[15] Catheterization of the efferent vessels of a bifurcation, however, can be difficult, and the presence of 2 or 3 catheters in the parent vessel unavoidably causes a temporary interruption of the cerebral blood flow and may cause hemodynamic compromise and/or thromboembolic events. The coverage of the aneurysm neck by the inflated balloon is solid, but overinflation may cause vessel dissection; the risk of aneurysm rupture due to coil-induced pressure on the aneurysm wall might be increased.[16] Besides, the balloon coverage is temporary. If the coils

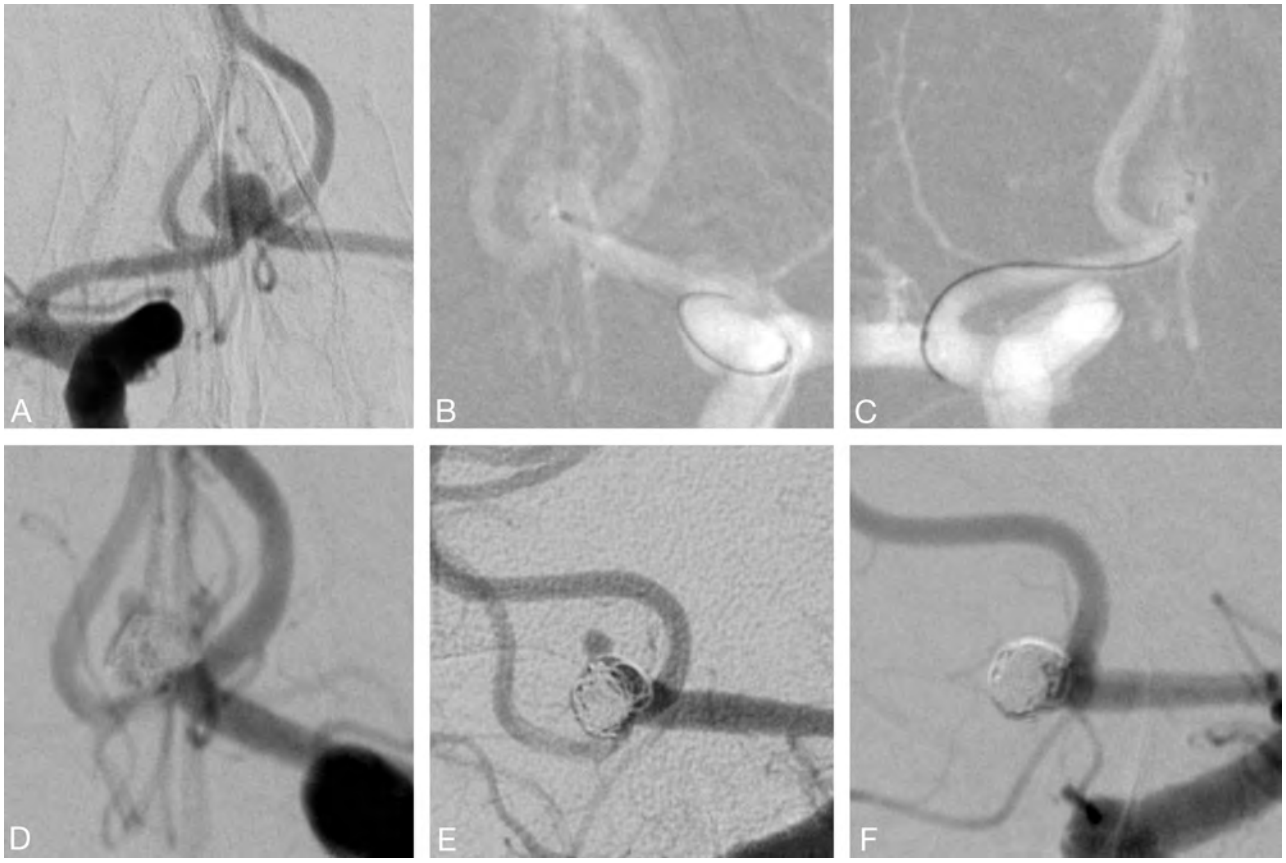

FIG 2. Wide-neck unruptured anterior communicating artery aneurysm in a 68-year-old man; neck diameter, 5.5 mm; fundus diameter, 7 mm (*A*). A 6-mm pCONus is inserted via the left A1 (*B*), with catheter access from the right A1 for coil occlusion (*C*). A minor neck remnant is accepted; the daughter aneurysm is still filling at the end of the procedure (*D*) and was expected to thrombose. For safety reasons, early angiographic follow-up was performed 4 days later and showed an incomplete coil occlusion (*E*). In a second session, complete occlusion of the aneurysm was achieved. The right A2 segment is filling from the ipsilateral ICA. Follow-up DSA 2 months later confirmed complete occlusion of the aneurysm, without compromise on the A1/A2 segment on both sides (*F*).

introduced under balloon protection do not stabilize each other, balloon deflation may be followed by coil prolapse into the parent vessel. In the available literature, the safety profile of balloon remodeling was similar to that of unassisted coiling.[17] If the follow-up occlusion rates post–stent placement are consistently better than those after balloon remodeling, then balloon remodeling remains open to further evaluation.[18] In our practice, we mainly use balloon remodeling for proximal sidewall aneurysms (eg, in cavernous/paraophthalmic locations).

In comparison with balloon remodeling, the use of the pCONus is easier and more controllable, without interruption of the blood flow and without the need to catheterize the efferent vessels. The need for dual medical antiaggregation for the pCONus is certainly a drawback, especially in ruptured aneurysms.

Neuroform (Stryker Neurovascular), Enterprise (Codman & Shurtleff), LEO+ (Balt Extrusion, Montmorency, France), Solitaire, and LVIS (MicroVention) are self-expanding stents for the treatment of WNBAs with different features.[19] Placing a stent over an aneurysm orifice may cause a neck-diameter reduction[20] and vessel straightening, improving the hemodynamic situation and stabilizing the occlusion rate after coil occlusion.[8,21] This effect is more important with closed-cell stents than with open-cell ones.[22] This technique can, however, be technically demanding[23] and may result in severe complications. In a retrospective analysis of a large series with 216 stented and coiled aneurysms, Piotin et al[21] found rates for procedure-related permanent neurologic morbidity and mortality of 7.4% and 6%, respectively. In their literature survey on stent-assisted aneurysm coiling, Shapiro et al[24] evaluated data from 39 articles with 1517 patients. They found a 9% rate of stent-related technical issues, 4% failure of stent deployment, a 19% overall procedure complication rate, and 2.1% periprocedural mortality.

The bridging of a vessel bifurcation by a single stent may provide insufficient coil retention. A more robust vessel reconstruction can be achieved if stents are deployed in both branching vessels (Y-stent placement). Descriptions of this technique were published for both unruptured and ruptured aneurysms.[25,26]

Cekirge et al[27] were the first to emphasize the hemodynamic effect of Y-stent placement. They observed reduced perfusion and final thrombosis of WNBAs after Y-stent placement with Enterprise stents without coiling. One of the reasons that stents such as the Enterprise with relatively large cells become hemodynamically active once they are used in a crossing fashion is the compression and deformation of the stents at their intersection.[28] For the same reason, catheterization for coiling through crossing an Enterprise can be very difficult if a "jailed catheter" technique was not used. In a recently published multicenter trial, Fargen et al[29] reported 45 (mostly basilar apex) aneurysms treated by Y-stent placement

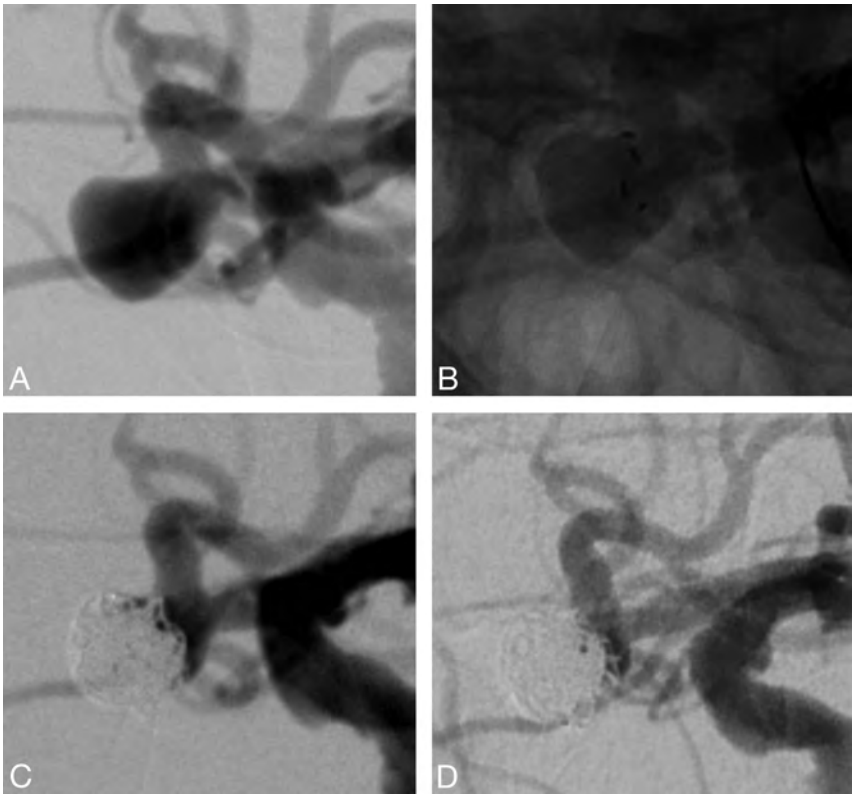

FIG 3. Wide-neck unruptured MCA bifurcation aneurysm in a 65-year-old woman, who rejected the proposed microsurgical clipping of the aneurysm (*A*). The aneurysm neck and fundus diameters are 5.7 and 8.7 mm, respectively. A 5-mm pCONus is deployed inside the aneurysm (*B*), which allows complete coil occlusion (*C*). Follow-up DSA 9 months later confirms the complete occlusion of the aneurysm (*D*), without intimal hyperplasia inside the shaft of the pCONus.

and coiling, with a rate of 84% of complete occlusion or neck remnant and an 11% procedural complication rate.

For Y-stent placement, hemodynamic effects are related to the metal construct in the parent artery and the alteration of the geometry of the efferent vessels. The formation of neointima over crossing stents appears at least unlikely.

The term "waffle cone technique" refers to a situation in which a self-expanding stent is deployed with its distal end inside an aneurysm instead of bridging the neck. Neuroform, Solitaire,[30] LEO+, and Enterprise[31] stents have been used for this purpose, but they share features that are far from ideal for this purpose. The Enterprise, for instance, has a smaller cell size and less radial force than the Solitaire and pCONus,[19] and stent migration has been observed.[32] The risk of migration is even higher if the distal end of the Enterprise stent is placed inside an aneurysm, with an axial outward force exerted by the coils. The intended use of the pCONus is similar to the waffle cone deployment of the above-mentioned stents, with the difference that the pCONus is made and optimized for this purpose. The Enterprise stent has flared distal ends, and the Solitaire AB has 4 sharp ends with radiopaque markers. Both are potentially more traumatic to the aneurysm wall than the pCONus petals. The waffle cone and pCONus techniques are theoretically superior to crossing-stent placement because less material is deployed inside the blood stream,[33] but it has been suggested that this technique can worsen the hemodynamic situation by directing the blood stream toward the aneurysm instead of diverting it away.[22,33] At this moment, this is a justified concern. Liu et al[34] reported good results from 10 aneurysms treated with the waffle cone technique; as in our series, angiographic follow-up showed a stable degree or improvement of occlusion in most aneurysms. An impaired occlusion at follow-up was mainly observed in large and giant partially thrombosed aneurysms. None of the aneurysms treated in the acute phase after SAH re-bled.

The TriSpan neck-bridging device was made of 3 nitinol loops (petals) coated with polyxylylene. Both ends of each petal were fixed to a central platinum coil ("umbilicus, stem"), which was attached to a stainless steel insertion wire. On withdrawal of the microcatheter, the petals of the TriSpan opened similar to a flower blossom. The device was positioned just beyond the level of the neck. Change, correction, or even withdrawal was possible. A second microcatheter was then inserted into the aneurysm between the petals and was used for coiling. Experimental[35] and early clinical results[10] were promising, but De Keukeleire et al[36] reported, in 14 patients, a complication rate of 37.5%, associated with a low primary complete occlusion rate and a high recurrence. A specific concern of this device was thromboembolic events, presumably related to the large foreign body surface in conjunction with inconsistent medical antiaggregation. The proper deployment of the TriSpan device was critical in aneurysms with a significant asymmetry or in the case of a steep angle between the longitudinal axis of the parent vessel and the aneurysm fundus. The TriSpan, once detached, had no further fixation. It was, therefore, necessary to either stabilize the device at the aneurysm wall or intermingle coils and TriSpan petals to create a self-stabilizing conglomerate. The TriSpan never gained FDA approval, and its production was terminated in 2007.

Similar to the TriSpan, the pCONus can be repositioned and/or withdrawn. The positions of the 4 pCONus petals (instead of 3 TriSpan loops) are, however, more stable due to their connection with the shaft. While TriSpan procedures were mostly performed without medical antiaggregation, the pCONus should only be implanted under dual antiaggregation. Aneurysm asymmetry is of less concern. Due to the firm connection between the distal petals and the proximal shaft, the device shows a tendency to center itself in asymmetric aneurysms. Similar to the behavior of TriSpan, the ability of the pCONus to retain small coils inside an aneurysm is poor at the proximity of the neck. The coil occlusion of an aneurysm after pCONus deployment should be started with at least 1 3D coil, which might be intermingled with the petals and should be completed with long and soft coils with a diameter of no less than 3 mm—just as was done previously with

the TriSpan. In the case of reperfusion of an aneurysm and endovascular retreatment, a previously detached TriSpan did not provide stability for further coils. In aneurysms treated with the pCONus, the petals of the first pCONus remain in the same position, again preventing coils from displacement.

The concept of intra-aneurysmal flow diversion has prompted the development of 2 similar devices: Woven EndoBridge (Sequent Medical, Aliso Viejo, California) and Luna (NFocus/Covidien). Both devices are spheric implants made from braided nitinol wires. They are introduced into the aneurysm fundus via a microcatheter. This concept will most likely play a role in the future treatment of WNBAs. There are, however, certain apparent issues. The device itself is more rigid than conventional stents or flow diverters, causing difficulty during the insertion. The sizing of these devices is critical, being less suitable for very large aneurysms and those with irregular shapes. Initial clinical results with Woven EndoBridge have been published,[5-7] but still little is known about the mid- and long-term results with this device and aneurysm regrowth after Woven EndoBridge occlusion has been reported.[37] In the case of recurrent or persistent perfusion of an aneurysm treated with these devices, retreatment can be difficult.

The aneurysm neck reconstruction device (PulseRider; Pulsar Vascular, San Jose, California) is a bifurcation stent that can be implanted in intracranial vessel bifurcations in front of wide-neck aneurysms to support coil occlusion. Turk et al[38] reported a good performance in an animal model. Clinical data are not yet available, and safety and efficacy are currently not known.

Limitations of This Series and the Device

This series reports a single-center experience, which was evaluated in retrospect. The retrospective nature of the data analysis precluded an ethics committee approval. No external institution was involved in the collection and analysis of the data. The decision to use a pCONus was at the operator's discretion and not under a given study protocol. We tried to avoid both crossing-stent placement and dual balloon remodeling, which is certainly an institutional preference and may be different at other centers. No effort was undertaken to compare the pCONus with other methods. A direct comparison of the pCONus and conventional single- or crossing-stent procedures is difficult to envision because both methods have different merits and drawbacks. Stent placement, for instance, has the advantage of permanently modifying the angulation of the vessel bifurcation, which may be advantageous. This particular aspect, however, cannot be expected from a pCONus treatment. The initial occlusion rate of pCONus-assisted coiling in this small series with 60% complete occlusion or a neck remnant is explained by the challenging anatomy of the treated aneurysms. Early retreatment in 2 patients was a result of the unfulfilled expectation that spontaneous thrombosis of residual filling of the aneurysm would occur. Short-term follow-up results, however, were encouraging. Long-term follow-up data for aneurysms treated with the pCONus are missing. Neither the incidence of intimal hyperplasia in the proximal stent shaft nor the long-term stability of the aneurysm occlusion is known following treatment.

The pCONus device is certainly not suitable for all WNBAs. We expect limitations if the aneurysm fundus is smaller than 5 mm and if the relation of the depth/width is >2. For aneurysms with a neck diameter of >15 mm, the 15-mm pCONus in its current design version may not provide sufficient coil retention. The additional use of a second pCONus or another stent may add safety under these rare circumstances. Recurrent perfusion of an aneurysm fundus after coiling may be an indication for microsurgical clipping.[39] After pCONus implantation and if the position of the device is unchanged, the aneurysm neck will remain bridged by the struts of the pCONus, which will most likely interfere with the proper closure of an aneurysm clip.

CONCLUSIONS

Deployment of the pCONus inside selected WNBAs, both ruptured and unruptured, is well-controlled and safe. The device does not interfere with the subsequent catheterization of the aneurysms and allows coil occlusion of the aneurysm fundus with reliable protection of the efferent vessels. A temporary dual medical platelet-function inhibition is required. Coil compaction and aneurysm reperfusion are not prevented by the pCONus, but the device does also assist re-coiling. Clip ligation of recurrent aneurysms after pCONus implantation is discouraged.

ACKNOWLEDGMENTS

The authors are most grateful to James Lago for language revision of the manuscript.

Disclosures: Marta Aguilar-Pérez—*RELATED*: *Consulting Fee or Honorarium*: phenox, *Comments*: Animal experience with pCONus in rabbits, *UNRELATED*: *Consultancy*: phenox, *Expert Testimony:* phenox, ev3, ab Medica, *Comments*: compensated for service as proctor, *Travel/Accommodations/Meeting Expenses Unrelated to Activities Listed*: phenox, MicroVention. Wiebke Kurre—*RELATED*: *Support for Travel to Meetings for the Study or Other Purposes*: phenox, *Comments*: travel expenses for the meeting of the American Society of Neuroradiology, *UNRELATED*: *Consultancy*: phenox, *Grants/Grants Pending*: Covidien,* *Comments*: grant for stroke research; *Payment for Lectures (including service on Speakers Bureaus)*: Covidien, Codman. Hansjörg Bäzner—*UNRELATED*: *Payment for Lectures (including service on Speakers Bureaus)*: Biogen Idec, Bayer Vital, UCB Pharma, Boehringer Ingelheim. Hans Henkes—*RELATED*: *Other*: phenox, *Comments*: Cofounder, shareholder, *UNRELATED*: *Board Membership:* phenox, *Payment for Lectures (including service on Speakers Bureaus)*: ev3/Covidien, phenox, Codman, ab Medica, *Comments*: modest compensation on a fee-for-service basis, *Travel/Accommodations/Meeting Expenses Unrelated to Activities Listed*: phenox, MicroVention, ev3/Covidien, *Other*: ev3/Covidien, phenox, ab Medica, *Comments*: proctoring. Money paid to the institution.

REFERENCES

1. Spetzler RF, McDougall CG, Albuquerque FC, et al. **The Barrow Ruptured Aneurysm Trial: 3-year results.** *J Neurosurg* 2013;119:146–57
2. Pierot L, Spelle L, Vitry F; for the ATENA Investigators. **Immediate clinical outcome of patients harboring unruptured intracranial aneurysms treated by endovascular approach: results of the ATENA study.** *Stroke* 2008;39:2497–504
3. Brinjikji W, Cloft HJ, Kallmes DF. **Difficult aneurysms for endovascular treatment: overwide or undertall?** *AJNR Am J Neuroradiol* 2009;30:1513–17
4. Fischer S, Vadja Z, Aguilar Perez M, et al. **Pipeline Embolization Device (PED) for neurovascular reconstruction: initial experience in the treatment of 101 aneurysms and dissections.** *Neuroradiology* 2012;54:369–82
5. Pierot L, Liebig T, Sychra V, et al. **Intrasaccular flow-disruption treatment of intracranial aneurysms: preliminary results of a multicenter clinical study.** *AJNR Am J Neuroradiol* 2012;33:1232–38
6. Lubicz B, Mine B, Collignon L, et al. **WEB device for endovascular**

treatment of wide-neck bifurcation aneurysms. *AJNR Am J Neuroradiol* 2013;34:1209–14
7. Pierot L, Klisch J, Cognard C, et al. **Endovascular WEB flow disruption in middle cerebral artery aneurysms: preliminary feasibility, clinical, and anatomical results in a multicenter study.** *Neurosurgery* 2013;73:27–34
8. Lubicz B, Bandeira A, Bruneau M, et al. **Stenting is improving and stabilizing anatomical results of coiled intracranial aneurysms.** *Neuroradiology* 2009;51:419–25
9. Moret J, Cognard C, Weill A, et al. **The "remodelling technique" in the treatment of wide neck intracranial aneurysms: angiographic results and clinical follow-up in 56 cases.** *Interv Neuroradiol* 1997;3:21–35
10. Raymond J, Guilbert F, Roy D. **Neck-bridge device for endovascular treatment of wide-neck bifurcation aneurysms: initial experience.** *Radiology* 2001;221:318–26
11. Horowitz M, Levy E, Sauvageau E, et al. **Intra/extra-aneurysmal stent placement for management of complex and wide-necked-bifurcation aneurysms: eight cases using the waffle cone technique.** *Neurosurgery* 2006;58(4 suppl 2):ONS-258–62, discussion ONS-262
12. Raymond J, Guilbert F, Weill A, et al. **Long-term angiographic recurrences after selective endovascular treatment of aneurysms with detachable coils.** *Stroke* 2003;34:1398–403
13. Cloft HJ, Joseph GJ, Tong FC, et al. **Use of three-dimensional Guglielmi detachable coils in the treatment of wide-necked cerebral aneurysms.** *AJNR Am J Neuroradiol* 2000;21:1312–14
14. Baxter BW, Rosso D, Lownie SP. **Double microcatheter technique for detachable coil treatment of large, wide-necked intracranial aneurysms.** *AJNR Am J Neuroradiol* 1998;19:1176–78
15. Arat A, Cil B. **Double-balloon remodeling of wide-necked aneurysms distal to the circle of Willis.** *AJNR Am J Neuroradiol* 2005;26:1768–71
16. Spiotta AM, Bhalla T, Hussain MS, et al. **An analysis of inflation times during balloon-assisted aneurysm coil embolization and ischemic complications.** *Stroke* 2011;42:1051–55
17. Pierot L, Cognard C, Spelle L, et al. **Safety and efficacy of balloon remodeling technique during endovascular treatment of intracranial aneurysms: critical review of the literature.** *AJNR Am J Neuroradiol* 2012;33:12–15
18. Chalouhi N, Starke RM, Koltz MT, et al. **Stent-assisted coiling versus balloon remodeling of wide-neck aneurysms: comparison of angiographic outcomes.** *AJNR Am J Neuroradiol* 2013;34:1987–92
19. Krischek O, Miloslavski E, Fischer S, et al. **A comparison of functional and physical properties of self-expanding intracranial stents [Neuroform3, Wingspan, Solitaire, Leo+, Enterprise].** *Minim Invasive Neurosurg* 2011;54:21–28
20. Adel JG, Sherma AK, Bendok BR. **CT angiography for assessment of intracranial basilar apex aneurysm neck diameter reduction post-stenting for treatment planning.** *Catheter Cardiovasc Interv* 2010;75:644–47
21. Piotin M, Blanc R, Spelle L, et al. **Stent-assisted coiling of intracranial aneurysms: clinical and angiographic results in 216 consecutive aneurysms.** *Stroke* 2010;41:110–15
22. Gao B, Baharoglu MI, Cohen AD, et al. **Stent-assisted coiling of intracranial bifurcation aneurysms leads to immediate and delayed intracranial vascular angle remodeling.** *AJNR Am J Neuroradiol* 2012;33:649–54
23. Henkes H, Kirsch M, Mariushi W, et al. **Coil treatment of a fusiform upper basilar trunk aneurysm with a combination of "kissing" Neuroform stents, TriSpan-, 3D- and fibered coils, and permanent implantation of the microguidewires.** *Neuroradiology* 2004;46:464–68
24. Shapiro M, Becske T, Sahlein D, et al. **Stent-supported aneurysm coiling: a literature survey of treatment and follow-up.** *AJNR Am J Neuroradiol* 2012;33:159–63
25. Thorell WE, Chow MM, Woo HH, et al. **Y-configured dual intracranial stent-assisted coil embolization for the treatment of wide-necked basilar tip aneurysms.** *Neurosurgery* 2005;56:1035–40
26. Lozen A, Manjila S, Rhiew R, et al. **Y-stent-assisted coil embolization for the management of unruptured cerebral aneurysms: report of six cases.** *Acta Neurochir (Wien)* 2009;151:1663–72
27. Cekirge HS, Yavuz K, Geyik S, et al. **A novel "Y" stent flow diversion technique for the endovascular treatment of bifurcation aneurysms without endosaccular coiling.** *AJNR Am J Neuroradiol* 2011;32:1262–68
28. Zhao KJ, Yang PF, Huang QH, et al. **Y-configuration stent placement (crossing and kissing) for endovascular treatment of wide-neck cerebral aneurysms located at 4 different bifurcation sites.** *AJNR Am J Neuroradiol* 2012;33:1310–16
29. Fargen KM, Mocco J, Neal D, et al. **A multicenter study of stent-assisted coiling of cerebral aneurysms with a Y configuration.** *Neurosurgery* 2013;73:466–72
30. Park HR, Yoon SM, Shim JJ, et al. **Waffle-cone technique using Solitaire AB stent.** *J Korean Neurosurg Soc* 2012;51:222–26
31. Gruber TJ, Ogilvy CS, Hauck EF, et al. **Endovascular treatment of a large aneurysm arising from a basilar trunk fenestration using the waffle-cone technique.** *Neurosurgery* 2010;67(3 suppl operative):ONS140–44, discussion ONS144
32. Kelly ME, Turner RD 4th, Moskowitz SI, et al. **Delayed migration of a self-expanding intracranial microstent.** *AJNR Am J Neuroradiol* 2008;29:1959–60
33. Sychra V, Klisch J, Werner M, et al. **Waffle-cone technique with SolitaireTM AB remodeling device: endovascular treatment of highly selected complex cerebral aneurysms.** *Neuroradiology* 2011;53:961–72
34. Liu W, Kung DK, Policeni B, et al. **Stent-assisted coil embolization of complex wide-necked bifurcation cerebral aneurysms using the "waffle cone" technique: a review of ten consecutive cases.** *Interv Neuroradiol* 2012;18:20–28
35. Turk AS, Rappe AH, Villar F, et al. **Evaluation of the TriSpan neck bridge device for the treatment of wide-necked aneurysms: an experimental study in canines.** *Stroke* 2001;32:492–97
36. De Keukeleire K, Vanlangenhove P, Defreyne L. **Evaluation of a neck-bridge device to assist endovascular treatment of wide-neck aneurysms of the anterior circulation.** *AJNR Am J Neuroradiol* 2008;29:73–78
37. Wallner AK, Broussalis E, Hauser T, et al. **Coiling after treatment with the Woven EndoBridge cerebral aneurysm embolization device: a case report.** *Interv Neuroradiol* 2012;18:208–12
38. Turk A, Turner RD, Tateshima S, et al. **Novel aneurysm neck reconstruction device: initial experience in an experimental preclinical bifurcation aneurysm model.** *J Neurointerv Surg* 2013;5:346–50
39. Nakamura M, Montibeller GR, Götz F, et al. **Microsurgical clipping of previously coiled intracranial aneurysms.** *Clin Neurol Neurosurg* 2013;115:1343–49

Fate of the Penumbra after Mechanical Thrombectomy

B. Friedrich, O. Kertels, D. Bach, S. Wunderlich, C. Zimmer, S. Prothmann, and A. Förschler

ABSTRACT

BACKGROUND AND PURPOSE: In acute stroke, CTP is often used to visualize the endangered brain areas, including the ischemic core and the penumbra. Our goal was to assess the evolution of the infarct after mechanical thrombectomy and to analyze the interventional factors determining the fate of the penumbra.

MATERIALS AND METHODS: All patients receiving mechanical thrombectomy in the anterior circulation and receiving CTP beforehand were identified. The infarct volume was specified. The clinical parameters, outcome, and interventional results were correlated with the CTP and the final infarct size.

RESULTS: In total, 73 patients were included. After mechanical thrombectomy, 78.1% reached a TICI score of 3/2b. The final infarct volume was significantly smaller, with a TICI score of 3/2b compared with less sufficient recanalization (19.60 ± 3 cm^3 versus 38.1 ± 9 cm^3; $P < .001$). After TICI 3/2b recanalization, 81% ± 5.2% of the potential infarct size (calculated as the sum of infarct core and penumbra) could be rescued. In patients with TICI scores of 2a or worse, only 39 ± 28.3 were salvaged ($P < .001$). The Alberta Stroke Program Early CT Score after successful recanalization TICI score of 3/2b resulted in a decline of 1.9 ± 1.4 compared with the significantly higher degradation score of 3.7 ± 1.7 after recanalization, with a TICI score of 2a or worse. A recanalization TICI score of 3/2b resulted in an NIHSS improvement of 7.3 ± 0.8 NIHSS points, whereas a poorer recanalization improved on the NIHSS by only 2.5 ± 1.5 points ($P < .01$).

CONCLUSIONS: Mechanical thrombectomy is a potent method to rescue large areas of penumbra in acute stroke.

ABBREVIATIONS: CCT = cranial CT; MTE = mechanical thrombectomy

Ischemic stroke caused by the acute occlusion of an intracranial blood vessel is a serious medical emergency. It can lead to severe disability and death in approximately one-fifth of all patients,[1,2] and, because of the often prolonged dependency of patients who have a stroke, the disease brings high economic costs.[3] Because of its ability to measure the infarct core by the diminished CBV and the penumbra and/or oligemia among others indicated by prolonged MTT, CTP has become a very useful and reliable tool in predicting final infarct sizes.[4,5] As a result, this technique is widely used to detect potentially rescuable endangered brain tissue and therefore to guide decisions about the use of recanalization therapy.[6]

The intravenous administration of tPA up to 4.5 hours after symptom onset can result in an overall reduction in the mortality and severe disability rate of up to 30%.[7] Despite this substantial improvement in ischemic stroke treatment by the introduction of tPA, the ability of this procedure to resolve large intracranial vessel occlusions has remained poor.[8-10] Whereas 63% of blood clots <4 mm were resolved by tPA, only 1% of clots >8 mm were successfully dissolved by tPA.[11] Additionally <10% of all patients with stroke are eligible for intravenous tPA.[12]

In recent years, mechanical thrombectomy (MTE) as a new treatment option has been very successful in the treatment of large-vessel occlusions. Especially with the help of a catheter-guided, second-generation, retractable stent retriever, it is possible to harbor the clot from the intracranial vessel, which leads to fast and lasting reperfusion. Some recent studies showed both the efficacy and safety of this method, reporting both significantly higher rates of recanalization and improved clinical outcomes compared with intravenous tPA alone.[13-20]

Received June 27, 2013; accepted after revision August 6.

From the Departments of Neuroradiology (B.F., O.K., D.B., C.Z., S.P., A.F.) and Neurology (S.W.), Klinikum Rechts der Isar, Munich, Germany.

B.F. and O.K. contributed equally to this work.

Data previously presented by Dr Friedrich at: Annual Meeting of the American Society of Neuroradiology, May 21, 2013; San Diego, California and awarded with the Michael Brothers Memorial Award.

Please address correspondence to Benjamin Friedrich, MD, Klinikum Rechts der Isar, Department of Neuroradiology, Ismaningerstraße 22, 81675 Munich, Germany; e-mail: benjamin.friedrich@tum.de

http://dx.doi.org/10.3174/ajnr.A3769

The aim of the present study was to determine the volume of infarction and amount of rescued brain tissue after MTE and to determine whether a correlation with the clinical course exists.

MATERIALS AND METHODS

The present retrospective, single-center cohort analysis was performed following the guidelines of and was approved by the local ethics committee.

The inclusion criteria are listed as follows:

Patients had an acute stroke in the anterior circulation between January 1, 2008, and May 1, 2012.
Patients were investigated with an imaging protocol including CTP before MTE.
Patients were treated with the use of MTE.
A cranial CT (CCT) at least 12 hours after MTE was available.

Exclusion criteria were:

Evidence of intracranial hemorrhage or intracranial mass, suspicious of tumor.
No sign of major artery occlusion in CTA.
Clearly visible sign of infarction in more than one-third of the corresponding vascular territory.
All patients fulfilling the above-mentioned criteria were consecutively enrolled in the present study. The CTP examination was performed by a routine stroke CT protocol including CCT, CTA, and CTP, with the following parameters: All scans were performed on a 64-section multidetector CT scanner (Philips, Best, the Netherlands). The CTP was acquired with a total of 4 scan sections and a section thickness of 10 mm. Forty milliliters of contrast agent followed by 60 mL of saline was injected during the 60-second scan. The volume of the infarct core and the penumbra were calculated automatically (IntelliSpace Portal V5, Philips; thresholds: 1.5 times increased MTT, reduced CBV: 2 mL/100 g, high permeability: 5 mL/min/100 g[21]).

Subsequent stent-retriever–based MTE was performed as described elsewhere.[22,23] Additionally, all patients were treated with a full dose of intravenous tPA ("bridging"). At 12 hours after MTE, the CCT and CTP images were fused with the use of commercial software (iPlan Cranial 3.0, BrainLAB AG, Germany) to match the angulation between pre-MTE CTP and post-MTE CCT and to limit the assessment of the post-MTE infarct size to the slides studied previously by CTP. Infarct size in CCT at 12 hours after MTE was measured 3 times on the corresponding slides by 2 experienced, board-certified neuroradiologists working independently, and the averages were calculated and used for further analysis. Additionally, the Alberta Stroke Program Early CT Score (ASPECTS)[24] was obtained on the initial CT and in the follow-up CT by the same neuroradiologists in consensus.

Clinical assessment was performed by use of the NIHSS both at admission and on the day of discharge. The quality and success of MTE was measured by the TICI score, in which a TICI score of 3 or 2b was considered a good recanalization.

Statistical Analysis

Statistical analysis was performed with the use of SPSS 20 (IBM, Armonk, New York) and SigmaPlot 11 (Systat). If not otherwise mentioned, a Kruskal-Wallis 1-way ANOVA on ranks was followed by multiple comparison procedures (Dunn method) to test for significant differences between groups. Statistical significance was assumed at $P < .05$. All data are presented as mean ± standard estimate of the mean, if not otherwise indicated.

RESULTS

In total, 73 patients were included in the present study. Women made up 52.1% of patients, and the mean age was 68 ± 2 years (minimum: 18; maximum: 96). The NIHSS score at admission was 13.2 ± 0.75 (Table 1). The performed CTP showed an average ischemic core of 29 ± 5 cm^3 and an average penumbra or tissue-at-risk of 85 ± 6 cm^3 (Fig 1*A*).

Table 1: Patient data

Age, y	68.2 ± 2 (minimum, maximum: 18, 96)
Sex	52.1% women
NIHSS on admission	13.2 ± 0.75
NIHSS at discharge	6.9 ± 0.71
Time to recanalization	254 ± 111 minutes

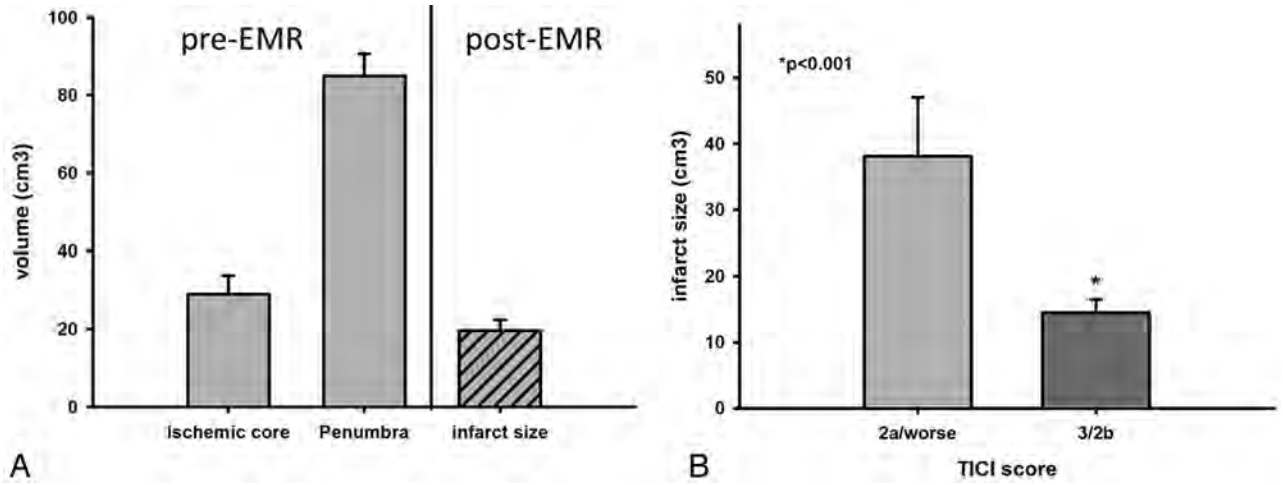

FIG 1. *A*, Chart shows initial sizes of the infarct core and the penumbra in CTP. The average final infarct size after MTE (striped pattern) is smaller than the predicted infarct core. *B*, Good recanalization of TICI score 3/2b results in a significantly smaller infarction compared with a less sufficient recanalization.

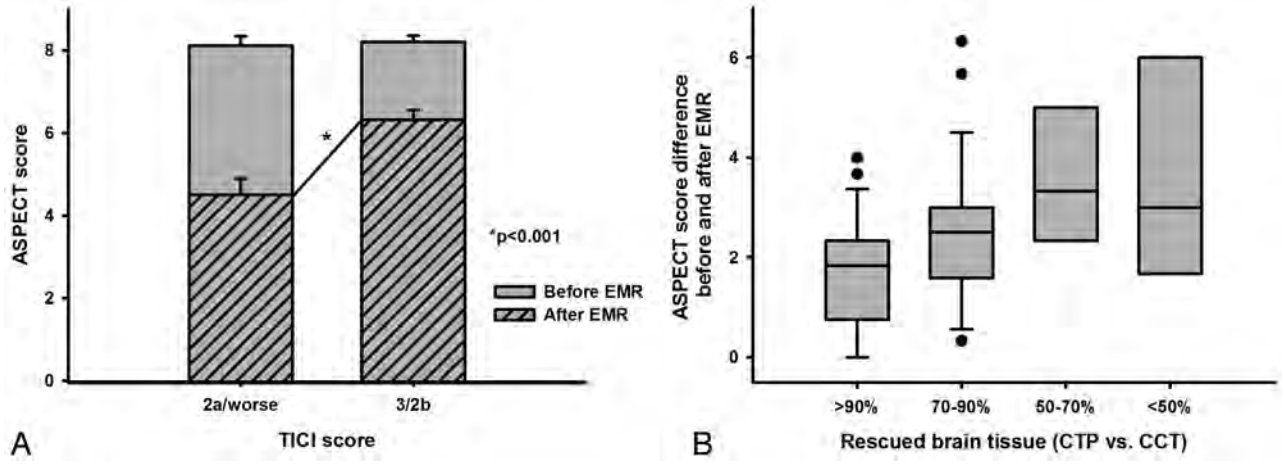

FIG 2. *A,* Successful recanalization resulted in a significantly lower deterioration of ASCPECTS after MTE compared with a less sufficient recanalization. *B,* There is a clear correlation between the amount of rescued tissue at risk identified by CTP and the final infarct growth measured by the difference in ASPECTS before and after MTE.

MTE was performed subsequently, and 78.1% of all patients could be sufficiently recanalized, with a TICI score of 3 or 2b (Table 1). There was no significant difference in baseline values concerning patients with a sufficient versus insufficient recanalization concerning either the epidemiologic data or the treatment modalities such as time to treatment or time to reperfusion. Also, there was no significant difference in the ASPECTS before MTE, with a score of 8.1 ± 0.9 in patients with a recanalization result of TICI 2a or worse and 8.2 ± 1.1 in patients with TICI 3/2b. The measured infarct size after MTE in our patient group was 19.60 ± 3 cm^3. The patients with a sufficient recanalization of TICI 3/2b had a significantly smaller infarct size of 14.5 ± 2.1 cm^3 compared with the infarct size of 38.1 ± 9 cm^3 ($P < .001$) after a poorer MTE result of TICI 2a or worse (Fig 1*B*). As an internal quality reference, the ASPECTS was assessed before and after MTE, and the difference was calculated. In analogy to our acquired infarct volumes, the difference in ASPECTS after successful recanalization TICI score of 3/2b resulted in a decline of 1.9 ± 1.4, compared with significantly higher degradation of 3.7 ± 1.7 after a less sufficient recanalization, with a resulting TICI score of 2a or worse (Fig 2*A*).

The sum of the infarct core and penumbra represents the potential size of the final infarction. Therefore, we were able to calculate the amount of rescued brain volume. A TICI score of 3/2b resulted in the rescue of 81% ± 5.2% of endangered brain tissue, whereas only 39% ± 28.3% could be salvaged after MTE TICI score of 2a or worse ($P < .001$) (Fig 3). The difference was especially dramatic in light of the group with large-tissue rescues. Furthermore, in 54.4% of the patients with a good MTE result, >90% of their potential infarction was rescued in contrast to only 6.25% of all patients with poorer MTE results (Fig 4). Again, the ASPECTS was used as an internal reference. There was a significant correlation between the difference in ASPECTS before and after MTE on the one hand and the corresponding amount of rescued brain tissue on the other. Whereas the rescue of >90% of endangered brain tissue resulted in a deterioration of ASPECTS of 1.6 ± 0.2, the ASPECTS worsened by 3.7 ± 2.4 points when <50% of endangered brain tissue could be rescued (Fig 2*B*) (Table 2).

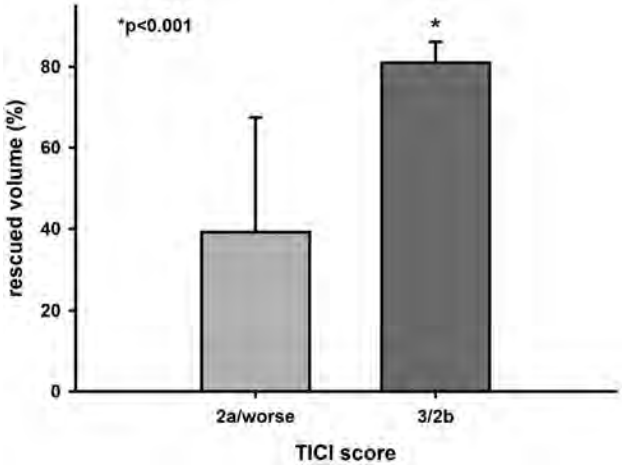

FIG 3. MTE of TICI score 3/2b was able to rescue >80% of the endangered brain tissue at risk (evaluated by pre-MTE CTP). Less than half of that tissue could be rescued by a poor MTE.

Three examples of different MTE results that led to different amounts of final infarct and rescued brain tissue are shown in Fig 5.

Regarding the short-term clinical outcome, there was a highly significant correlation between the percentage of rescued brain tissue and the difference in the NIHSS score between admission and discharge ($P < .02$) (Fig 6). The greater the amount of rescued brain tissue, the more dramatic was the clinical improvement (Fig 6*A*). Again, the post-MTE TICI score was highly significantly associated with short-term NIHSS development. A recanalization TICI score of 3/2b resulted in an NIHSS improvement of 7.3 ± 0.8 points, whereas a poorer recanalization improved on the NIHSS by only 2.5 ± 1.5 points ($P < .01$; Fig 6*B*) over time. Thus, the benefit of a good MTE result with consideration of the short-term NIHSS improvement was striking (global odds ratio, 1.4 for NIHSS improvement >10 points; 95% CI, 1.2–1.7).

DISCUSSION

CTP is an easy-to-use and widely available diagnostic tool for measuring and visualizing the amount of endangered brain tissue

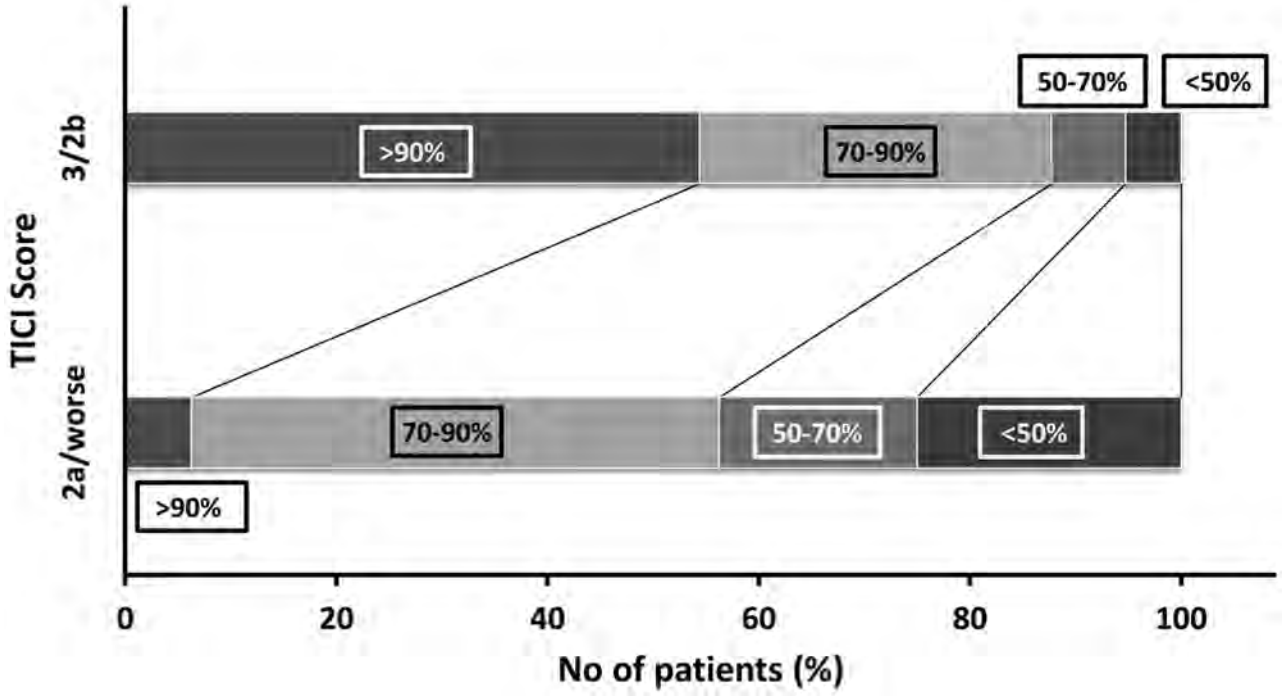

FIG 4. Stacked bar chart shows the grouped percentage of rescued brain tissue. After TICI score 3/2b recanalization in >50% of all cases, >90% of the tissue at risk could be rescued, whereas that rate dropped to <10% after MTE with a TICI score of 2a or less. Additionally, the number of cases in which <50% of tissue at risk could be rescued nearly quadrupled with a poor recanalization.

Table 2: Patient data after MTE

TICI Score after MTE	No. of Patients	Final Infarct Size, cm^3	Salvaged Penumbra
0	4.1% (3)	21 ± 25	67 ± 26%
1	1.4% (1)	NA	NA
2a	16.4% (12)	38 ± 44	69 ± 22%
2b	45.2% (33)	14 ± 11	89 ± 16%
3	32.9% (24)	9 ± 23	92 ± 20%

Note:—NA indicates not applicable.

after acute occlusion of an intracranial blood vessel and the subsequent breakdown in oxygen supply and other nutrients to neurons. Since its first description,[25] the concept of the penumbra has changed the view of ischemic stroke among treating physicians from a "catastrophe to be accepted" to a "treatable" disease. Generally, the penumbra is defined as a hypoperfused tissue in which the cerebral blood flow is too low to maintain neuronal electrophysiologic activity, which will lead to infarct after some time.

In the present study, we showed that the penumbra, as detected by CTP, is a potential target for rescue by endovascular mechanical recanalization. With a complete recanalization in 78.1% of our patient group, we found significantly higher recanalization rates than in the now more historical MERCI and the Multi-MERCI trials. Even compared with recently published studies such as IMS-III and MR RESCUE, we can show significantly higher recanalization rates with the use of second-generation stent retrievers compared with recanalization rates of <45% in IMS-III and 67% in MR RESCUE.[26,27] Both studies used a more generous definition of the term "successful" recanalization than the definition that we used, with a definition of TIMI 3/2 in IMS-III and TICI 3–2a in MR RESCUE. Both studies would have an even smaller recanalization rate with our definition of a "successful" recanalization with a TICI score of 3/2b. These low recanalization rates may be the main reason why both studies could not show the superiority of endovascular treatment compared with intravenous tPA alone; the SWIFT study proved that there is a clearly positive correlation between successful recanalization and clinical improvement, measured by the mRS[28] or the NIHSS, as we show in the present work. As a result of these trials, in our opinion, a fast and preferably complete recanalization is the main goal of every (not just endovascular) stroke therapy and is, besides the time to treatment,[29] the single most important independent prognostic factor.

In our study, the final infarct size after good recanalization was significantly smaller than after poor or unsuccessful MTE. Both subgroups did not show any significant differences between age, sex, initial NIHSS score, or initial infarct size measured by the ASPECTS. Parsons et al[4] showed in 2005 that without major reperfusion, the final infarct size closely matches the size initially predicted by CTP. Although this concept is still often discussed, it was successfully implemented in a recent study to select patients undergoing a new intravenous thrombolysis.[30] Hence, we can postulate that the difference between the initial deterioration in CTP and the final infarct size can be attributed predominantly to the treatment effect of endovascular mechanical recanalization. Although other factors (size of the clot, location of the clot, etc) might also play a role, the fact that we found a significant difference in the amount of rescued brain tissue between different MTE results further supports the conclusion that the benefit can be attributed to the treatment. Therefore, we suggest that the large difference between final infarct size and initial CTP must be attributed to the quality of recanalization.

Considering the impressive amount of rescued brain tissue

specified as possibly endangered, with a prolonged MTT in CTP, the highly significant difference between the recanalization results was striking. Although one must admit that the infarct size in early CCTs after MTE tends to be underestimated compared with that in DWI, and therefore the >80% rescue rate may be exaggerated, we performed a method less prone to examiner bias: the ASPECTS, which is known to be nearly as sensitive to ischemic changes as DWI[31] when used by trained examiners. With the help of this well-established tool, we found the same highly significant correlation between recanalization result and amount of rescued brain tissue. We tried to minimize the underestimation of the infarct by having 2 people independently assess the CCTs in 3 separate rounds. Nevertheless, one of the major weaknesses of the present study is the use of CT-based techniques rather than an MRI-based protocol. Although this MRI-based patient selection and protocol to investigate the development of the infarct lesions after endovascular treatment may be more advanced, it is a setup that few centers can keep on hand. Even in our high-volume neurointerventional center, follow-up MRI after MTE has been established as a routine for approximately 2 years. Therefore, our aim was to investigate whether it was possible to achieve the same goal with a technically less demanding and especially less time-consuming method.

Besides the limitations with the use of a CT-based evaluation rather than an MRI-based approach, we must admit that the present study is designed as retrospective and did not recruit in a prospective manner. All consecutive patients matching the inclusion and exclusion criteria were enrolled, minimizing the bias of a retrospective study. Additionally, we did not recruit a control group. However, in the present work, patients with a futile or partially successful recanalization served as an internal control group.

Although there have been some indications that the use of CBF is superior to CBV in determining and predicting the final infarct size and infarct core, respectively,[4] we used the MTT/CBV ratio on purpose because most commercial semi-automatic CTP evaluation tools in a clinical setup still use the ratio. Therefore, in our opinion, it was justified to use this somehow "old-fashioned" method.

Similar to recently published results,[32,33] we also found a clear correlation between the volume of rescued brain tissue and short-term clinical improvement, as measured by the difference in the NIHSS. In our opinion, this finding is particularly important because both successful recanalization and minimizing the infarct size for no clinical benefit may be

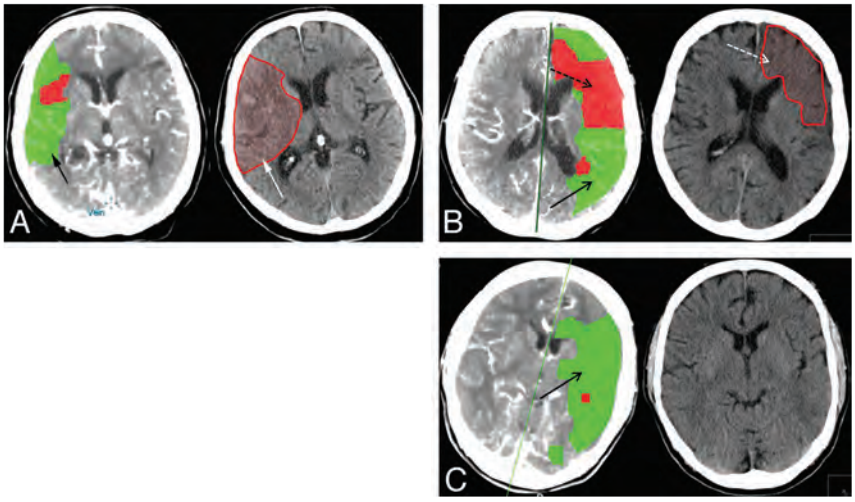

FIG 5. *A,* CTP indicated a large penumbra in the right MCA territory (*black arrow*). MTE was unsuccessful with a TICI score of 0. In the post-MTE CCT, a large infarction (larger than the initial penumbra, possibly caused by swelling effects) developed (*white arrow*). In the following days, a progressive herniation occurred and the patient died. *B,* In CTP, an infarct core in the left frontal MCA territory is detected (*black dashed arrow*) with a large surrounding penumbra (*black arrow*). After MTE TICI score of 3, the infarct core became infarcted (*white dashed arrow*) where the penumbra could be rescued. *C,* In CTP, a large area of tissue at risk in the left MCA territory without any significant infarct core can be detected (*black arrow*). After MTE TICI score of 3, no sign of infarction could be detected in post-MTE CCT.

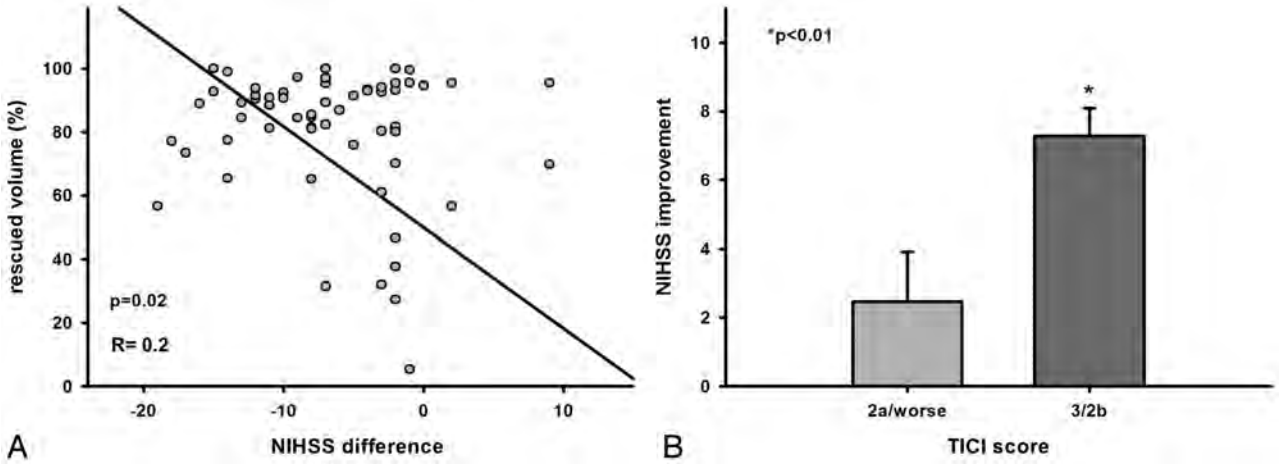

FIG 6. *A,* There is a clear correlation between the amount of rescued brain tissue and short-term NIHSS development: the greater the amount of brain tissue that was rescued, the more dramatic the clinical improvement, as measured by the difference in NIHSS at admission and on the day of discharge. *B,* Again, the results of MTE predict the short-term outcome, as measured by the improvement in NIHSS.

satisfying for the interventionalist but meaningless for the patient and the treating clinician. However, it would be useful to have a tool for early prediction of the short- to mid-term outcome. In light of our data and the above-mentioned previous studies, we propose that the evaluation of infarct size and amount of rescued brain tissue could be used as a tool to sensitively predict the clinical course over the days and possibly weeks after ischemic stroke.

CONCLUSIONS

In the present work, we found that acute ischemic stroke treatment with stent-retriever–based endovascular mechanical recanalization and subsequent fast and lasting cerebral reperfusion can result in the rescue of a large amount of endangered brain tissue with a highly significant correlation to the clinical improvement of the patients.

REFERENCES

1. Miniño AM, Murphy SL, Xu J, et al. **Deaths: final data for 2008.** *Natl Vital Stat Rep* 2011;59:1–126
2. Mullen MT, Pisapia JM, Tilwa S, et al. **Systematic review of outcome after ischemic stroke due to anterior circulation occlusion treated with intravenous, intra-arterial, or combined intravenous + intra-arterial thrombolysis.** *Stroke* 2012;43:2350–55
3. Pan F, Hernandez L, Ward A. **Cost-effectiveness of stroke treatments and secondary preventions.** *Exp Opin Pharmacother* 2012;13:1751–60
4. Parsons MW, Pepper EM, Chan V, et al. **Perfusion computed tomography: prediction of final infarct extent and stroke outcome.** *Ann Neurol* 2005;58:672–79
5. Wintermark M, Meuli R, Browaeys P, et al. **Comparison of CT perfusion and angiography and MRI in selecting stroke patients for acute treatment.** *Neurology* 2007;68:694–97
6. Campbell BC, Weir L, Desmond PM, et al. **CT perfusion improves diagnostic accuracy and confidence in acute ischaemic stroke.** *J Neurol Neurosurg Psychiatry* 2013;84:613–18
7. Wahlgren N, Ahmed N, Dávalos A, et al. **Thrombolysis with alteplase for acute ischaemic stroke in the Safe Implementation of Thrombolysis in Stroke-Monitoring Study (SITS-MOST): an observational study.** *Lancet* 2007;369:275–82
8. Smith WS, Tsao JW, Billings ME, et al. **Prognostic significance of angiographically confirmed large vessel intracranial occlusion in patients presenting with acute brain ischemia.** *Neurocrit Care* 2006;4:14–17
9. Abul-Kasim K, Brizzi M, Petersson J. **Hyperdense middle cerebral artery sign is an ominous prognostic marker despite optimal workflow.** *Acta Neurol Scand* 2010;122:132–39
10. Kharitonova T, Ahmed N, Thorén M, et al. **Hyperdense middle cerebral artery sign on admission CT scan: prognostic significance for ischaemic stroke patients treated with intravenous thrombolysis in the safe implementation of thrombolysis in Stroke International Stroke Thrombolysis Register.** *Cerebrovasc Dis* 2009;27:51–59
11. Riedel CH, Zimmermann P, Jensen-Kondering U, et al. **The importance of size: successful recanalization by intravenous thrombolysis in acute anterior stroke depends on thrombus length.** *Stroke* 2011;42:1775–77
12. de Los Ríos la Rosa F, Khoury J, Kissela BM, et al. **Eligibility for intravenous recombinant tissue-type plasminogen activator within a population: the effect of the European Cooperative Acute Stroke Study (ECASS) III Trial.** *Stroke* 2012;43:1591–95
13. Smith WS, Sung G, Starkman S, et al. **Safety and efficacy of mechanical embolectomy in acute ischemic stroke: results of the MERCI trial.** *Stroke* 2005;36:1432–38
14. Smith WS, Sung G, Saver J, et al. **Mechanical thrombectomy for acute ischemic stroke: final results of the Multi MERCI trial.** *Stroke* 2008;39:1205–12
15. Grunwald IQ, Walter S, Papanagiotou P, et al. **Revascularization in acute ischaemic stroke using the Penumbra system: the first single center experience.** *Eur J Neurol* 2009;16:1210–16
16. Penumbra Pivotal Stroke Trial Investigators. **The Penumbra Pivotal Stroke Trial: safety and effectiveness of a new generation of mechanical devices for clot removal in intracranial large vessel occlusive disease.** *Stroke* 2009;40:2761–68
17. Machi P, Costalat V, Lobotesis K, et al. **Solitaire FR thrombectomy system: immediate results in 56 consecutive acute ischemic stroke patients.** *J Neurointerv Surg* 2012;4:62–66
18. Mokin M, Dumont TM, Veznedaroglu E, et al. **Solitaire flow restoration thrombectomy for acute ischemic stroke: retrospective multicenter analysis of early postmarket experience after FDA approval.** *Neurosurgery* 2013;73:19–26
19. Ribo M, Molina CA, Jankowitz B, et al. **Stentrievers versus other endovascular treatment methods for acute stroke: comparison of procedural results and their relationship to outcomes.** *J Neurointerv Surg* 2014;6:265–69
20. Broussalis E, Trinka E, Hitzl W, et al. **Comparison of stent-retriever devices versus the Merci retriever for endovascular treatment of acute stroke.** *AJNR Am J Neuroradiol* 2013;34:366–72
21. Wintermark M, Flanders AE, Velthuis B, et al. **Perfusion-CT assessment of infarct core and penumbra: receiver operating characteristic curve analysis in 130 patients suspected of acute hemispheric stroke.** *Stroke* 2006;37:979–85
22. Dorn F, Stehle S, Lockau H, et al. **Endovascular treatment of acute intracerebral artery occlusions with the Solitaire stent: single-centre experience with 108 recanalization procedures.** *Cerebrovasc Dis* 2012;34:70–77
23. Prothmann S, Lockau H, Dorn F, et al. **The Phenox clot retriever as part of a multimodal mechanical thrombectomy approach in acute ischemic stroke: single center experience in 56 patients.** *Sci World J* 2012;2012:190763.
24. Barber PA, Demchuk AM, Zhang J, et al. **Validity and reliability of a quantitative computed tomography score in predicting outcome of hyperacute stroke before thrombolytic therapy. ASPECTS Study Group. Alberta Stroke Programme Early CT Score.** *Lancet* 2000;355:1670–74
25. Astrup J, Symon L, Branston NM, et al. **Cortical evoked potential and extracellular K+ and H+ at critical levels of brain ischemia.** *Stroke* 1977;8:51–57
26. Broderick JP, Palesch YY, Demchuk AM, et al. **Endovascular therapy after intravenous t-PA versus t-PA alone for stroke.** *N Engl J Med* 2013;368:893–903
27. Kidwell CS, Jahan R, Gornbein J, et al. **A trial of imaging selection and endovascular treatment for ischemic stroke.** *N Engl J Med* 2013;368:914–23
28. Saver JL, Jahan R, Levy EI, et al. **Solitaire flow restoration device versus the Merci retriever in patients with acute ischaemic stroke (SWIFT): a randomised, parallel-group, non-inferiority trial.** *Lancet* 2012;380:1241–49
29. Hassan AE, Chaudhry SA, Miley JT, et al. **Microcatheter to recanalization (procedure time) predicts outcomes in endovascular treatment in patients with acute ischemic stroke: when do we stop?** *AJNR Am J Neuroradiol* 2013;34:354–59
30. Parsons M, Spratt N, Bivard A, et al. **A randomized trial of tenecteplase versus alteplase for acute ischemic stroke.** *N Engl J Med* 2012;366:1099–107
31. Barber PA, Hill MD, Eliasziw M, et al. **Imaging of the brain in acute ischaemic stroke: comparison of computed tomography and magnetic resonance diffusion-weighted imaging.** *J Neurol Neurosurg Psychiatry* 2005;76:1528–33
32. Zaidi SF, Aghaebrahim A, Urra X, et al. **Final infarct volume is a stronger predictor of outcome than recanalization in patients with proximal middle cerebral artery occlusion treated with endovascular therapy.** *Stroke* 2012;43:3238–44
33. Yoo AJ, Chaudhry ZA, Nogueira RG, et al. **Infarct volume is a pivotal biomarker after intra-arterial stroke therapy.** *Stroke* 2012;43:1323–30

Hemorrhagic Complications after Endovascular Treatment of Cerebral Arteriovenous Malformations

H. Baharvahdat, R. Blanc, R. Termechi, S. Pistocchi, B. Bartolini, H. Redjem, and M. Piotin

ABSTRACT

BACKGROUND AND PURPOSE: Intracranial hemorrhage is the most severe complication of brain arteriovenous malformation treatment. We report our rate of hemorrhagic complications after endovascular treatment and analyze the clinical significance and potential mechanisms, with emphasis on cases of delayed hemorrhage after uneventful embolization.

MATERIALS AND METHODS: During a 10-year period, 846 embolization procedures were performed in 408 patients with brain AVMs. Any cases of hemorrhagic complications were identified and divided into those related or unrelated to a periprocedural arterial tear (during catheter navigation or catheter retrieval). We analyzed the following variables: sex, age, hemorrhagic presentation, Spetzler-Martin grade, size of the AVM, number of embolized pedicles, microcatheter used, type and volume of liquid embolic agent injected, and the presence of a premature venous occlusion. Univariate and multivariate multiple regression analyses were performed to identify risk factors for hemorrhagic complications.

RESULTS: A hemorrhagic complication occurred in 92 (11%) procedures. Forty-four (48%) complications were related to a periprocedural arterial perforation, and 48 (52%) were not. Hemorrhagic complications unrelated to an arterial perforation were located more commonly in the cerebral parenchyma, caused more neurologic deficits, and were associated with worse prognosis than those in the arterial perforation group. Only premature venous occlusion was identified as an independent predictor of hemorrhagic complication in the nonperforation group. Premature venous occlusion was significantly related to the ratio of Onyx volume to nidus diameter.

CONCLUSIONS: Higher injected volume of embolic agent and deposition on the venous outflow before complete occlusion of the AVM may account for severe hemorrhagic complications.

ABBREVIATIONS: AP = arterial perforation; EVT = endovascular treatment; HC = hemorrhagic complication; NAP = non-arterial perforation; S-M = Spetzler-Martin; V_{ea} = volume of liquid embolic agents

Treatment of cerebral arteriovenous malformation is challenging and requires a multidisciplinary approach involving surgery with AVM removal, endovascular treatment (EVT) with embolization, or radiosurgery. Each technique can be combined and has its own advantages and complications. A conservative approach is an important aspect of the management of AVMs. EVT can be used for presurgical or preradiosurgical treatment of AVMs or as a stand-alone procedure for curative purposes. Onyx (Covidien, Irvine, California) is currently the most commonly used embolic agent; in some instances, cyanoacrylate glue can be used. The most serious complication of AVM embolization is hemorrhage, reported in 4%–15% of patients treated by EVT.[1-3] The group of patients who experience delayed hemorrhage after EVT remains poorly understood, with multiple classifications[4-6] and explanations[7-9] and deserves further study. To investigate the potential mechanisms of hemorrhages following EVT, we report our rate of hemorrhagic complications (HCs) and their clinical significance and focus on those not related to an arterial lesion secondary to navigation or microcatheter retrieval.

Received July 29, 2013; accepted after revision September 29.

From the Department of Interventional Neuroradiology (H.B., R.B., S.P., B.B., H.R., M.P.), Fondation Adolphe de Rothschild, Paris, France; Neurosurgical Department (H.B.), Ghaem Hospital, Mashhad University of Medical Sciences, Iran; and Department of Neurology (R.T.), Vali-Asr Hospital, Tehran, Iran.

Please address correspondence to Raphaël Blanc, MD, MSc, Department of Interventional Neuroradiology Fondation Adolphe de Rothschild Hospital, Paris, France; e-mail rblanc@fo-rothschild.fr

http://dx.doi.org/10.3174/ajnr.A3906

MATERIALS AND METHODS

Patients and AVM Characteristics

Approval was obtained from our institutional ethics board to review the data from patients with AVMs who underwent endovascular procedures between January 2000 and March 2010. From our prospectively acquired data base, we collected patients' baseline characteristics, AVM modes of presentation, and total num-

ber of sessions per patient. The preprocedural neurologic condition was recorded, and outcomes were measured according to the modified Rankin Scale at patient discharge from the hospital and at 1 month.

AVMs were classified according to the Spetzler-Martin (S-M) grade.[10] The presence of intranidal aneurysms or aneurysms located on the arterial feeders to the malformations was recorded. The AVM venous outflow was scrutinized for venous ectasia or stenosis and the presence of a deep or single venous drainage. AVMs were localized as cortical, for cortical and subcortical supratentorial lesions; deep, for lesions located in the basal ganglia, thalamus, corpus callosum, and internal capsules; and infratentorial.

Endovascular Procedure

At our institution, patients were allocated to a treatment technique after multidisciplinary discussion, with EVT (with the goal of complete obliteration of the nidus in 1 or multiple sessions) being the first-choice treatment for cerebral AVMs. In very large cerebral AVMs, the objective was to reduce the risk of hemorrhage, seizure, and neurologic symptoms or to reduce the size of the nidus to permit another treatment technique. EVTs were performed with the patient under general anesthesia according to our standard protocol. In the study period, Onyx was the most commonly used agent for embolization of AVMs. Occasionally, cyanoacrylate glue (Histoacryl; Braun, Melsungen, Germany) or Glubran2 (GEM, Viareggio, Italy) was injected during the procedure for high-flow fistulas or arterial perforation. The number of pedicles catheterized and the total volume of liquid embolic agents (Onyx or cyanoacrylates) injected were recorded. For small or single-compartment AVMs, the procedure was stopped when complete occlusion was achieved or when there was >2-cm reflux of Onyx. For large AVMs, the goal was to embolize 30%–50% in 1 session. If necessary, multiple pedicles were embolized in 1 session. A head CT scan was performed (mobile CT scan until 2006, at which time the flat panel CT became available) in the operating room after each procedure or immediately if any perforation occurred.

After the procedure, all patients were admitted postoperatively to the intensive care unit with strict control of systolic blood pressure at <110 mm Hg for 24–48 hours. The patients were discharged within 4–5 days after embolization if there were no significant complications. The interval between the 2 procedures was 1–4 months. If an HC occurred, the patient was managed medically or surgically, depending on the volume of hematoma and the patient's condition. On the basis of the location of the hematoma, the surgery included hematoma evacuation or decompressive craniotomy. If patients were unconsciousness, intracranial pressure was monitored.

Data on procedural or postprocedural complications were collected, including catheter-related complications, the presence of a postembolization HC, or ischemic events. The angiographic results of AVM exclusion were considered complete if the nidus was excluded with no residual arteriovenous shunt and incomplete if any residual venous drainage was visible. The pattern of a premature venous occlusion, defined as occlusion of the venous drainage before complete nidal exclusion (either spontaneously or secondary to deposition of liquid embolic), was recorded. EVT was considered "completed" if complete angiographic occlusion of AVM was achieved, if endovascular access to the AVM was no longer possible, or if patients were sent for radiosurgery or surgery to complete the treatment. EVT was considered "ongoing" if another session was scheduled.

Hemorrhagic Complications

Any HC (subarachnoid, intraventricular, intraparenchymal hemorrhage) that occurred during or within 1 month of embolization was recorded.

The cause of the hemorrhage was categorized as either of the following:

1) Arterial perforation (AP) when related to an arterial perforation during microcatheterization or microcatheter retrieval (shown by extravasation of contrast during the procedure or visible on the CT scan after the procedure)
2. Nonarterial perforation (NAP) if the hemorrhage was not caused by arterial perforation during the procedure.

Statistical Analysis

Descriptive statistics were used to summarize the baseline characteristics of the procedures, patients, and procedures with HC. Continuous data are presented as means ± SDs. Statistical comparisons were performed by the χ^2 test, Student *t* test, and Fisher exact test for normally distributed data and the Mann-Whitney *U* test for data not normally distributed. Univariate analysis was performed to identify the effect of sex, age, hemorrhagic presentation, largest nidus diameter, injected volume of Onyx in each procedure, total injected volume of liquid embolic agents including Onyx and glue in each procedure (V_{ea}), ratio of Onyx volume to largest diameter of nidus, ratio of V_{ea} to the largest diameter of the nidus, number of embolized pedicles, premature venous occlusion, and microcatheter used on HC in the NAP group. Multivariate analysis was performed by logistic regression to test the real effect of the variables identified as risk factors of HC in univariate analysis. Model selection was performed by a stepwise continuous procedure. A P value < .05 was statistically significant. The data were analyzed by using the Statistical Package for Social Sciences (Version 16.0; IBM, Armonk, New York).

RESULTS

Between January 2000 and March 2010, four hundred eight patients with brain AVMs underwent 846 endovascular procedures; 230 were men (56%), and the mean age was 33.3 ± 14.1 years. Table 1 shows the basic characteristics of the patients and the AVMs. The median number of procedures for each case was 2 (range, 1–12). Nineteen procedures failed due to inability to access the appropriate point for embolization. Of the 827 successful procedures, Onyx 18 was used in 669 (81%) and cyanoacrylate in 251 (30%), including both liquid embolic agents in 93 (11%) sessions. The mean injected volume of Onyx in each procedure was 2.1 ± 2.0 mL. Of the 408 AVMs, EVT was completed in 282 (69%). Complete obliteration was achieved in 198 AVMs (ie, 70% AVMs with completed EVT or 49% of all AVMs). According to the Spetzler-Martin grade, overall cure (complete obliteration)

was 87% in grade I, 82% in grade II, 55% in grade III, 57% in grade IV, and 50% in grade V in 198 patients who completed EVT.

Overall, 22 (5%) of the 408 patients were sent to radiosurgery, and 15 (4%), to surgery.

Because no complication was noted during the 19 failed sessions, these procedures were excluded from the analysis and data from the remaining 827 procedures were analyzed.

Among 827 procedures, complications were reported in 206 (25%), including HCs in 92 (11%), postoperative ischemia in 53 (6%), catheter entrapment in 49 (6%), and catheter rupture in 12 (2%). Overall complications were 27% in grade I, 24% in grade II, 28% in grade III, 25% in grade IV, and 29% in grade V.

Among 408 patients, permanent disability was seen in 5% of S-M grade I, 6% of S-M grade II, 14% of S-M grade III, 19% of S-M grade IV, and 21% of S-M grade V. Fatal events occurred in 0% of S-M grades I and II, in 3% of S-M grade III, in 1% of S-M grade IV, and in 5% of S-M grade V.

Table 1: Basic characteristics of patients and AVMs

Variable[a]	Patients (*n* = 408)
Age (yr)	33.3 ± 14.1
Men	230 (56)
Presenting symptoms	
Hemorrhage	196 (48)
Seizure	115 (28)
Spetzler-Martin grade	
I	41 (10)
II	124 (30)
III	143 (35)
IV	81 (20)
V	19 (5)
AVM location	
Cortical	312 (76)
Deep	66 (16)
Infratentorial	30 (7)
Eloquent	231 (59)
AVM characteristics	
Deep drainage	159 (39)
Intranidal aneurysm	55 (14)
Number of procedure	
1 Session	157 (38)
2 Sessions	118 (29)
3 Sessions	75 (18)
≥ 3 Sessions	58 (14)

[a] No. (%); mean ± SD.

Characteristics of Hemorrhagic Complications

Hemorrhagic complications occurred in 92 of 827 (11.1%) procedures: 20% of S-M grade I, 11% grade II, 12% grade III, 8% grade IV, and 12% grade V (Table 2).

Forty-four (48%) HCs were classified as related to an AP, of which the most frequently reported was subarachnoid hemorrhage (71%). In most cases, the hemorrhage was detected during the procedure. Forty-eight (52%) HCs were classified as NAP, 39 (81%) of which occurred in the hours or days following the procedure (mean time between procedure and event, 34.4 ± 50.1 hours). Thirty-four of the NAP cases (71%) were intraparenchymal hemorrhage. The HCs in the NAP group were located more commonly in cerebral parenchyma compared with the AP group. Eight HCs (17%) occurred following a premature venous occlusion.

Outcomes of Hemorrhagic Complications

Procedures with HCs were associated with a new disability that was persistent at 1 month in 31 cases (patient morbidity related to an HC of 7.6%). Death occurred in 6 patients with HCs (patient mortality related to an HC of 1.6%) and in none of those without. As shown in Tables 2 and 3, compared with AP events, NAP events more commonly caused neurologic deficits and were associated with a worse prognosis (mRS > 2). Despite more deaths occurring in the NAP group, there was no statistical difference between the 2 groups.

In the AP group, 12 patients showed a new neurologic deficit after the procedure, which was transient in 9, and 1 death occurred.

In the NAP group, 37 patients showed a new neurologic deficit, including 28 cases (58%) of permanent disability; 5 (10%) patients died. Twenty-one (44%) patients were independent (mRS < 2) at the time of discharge.

Risk Factors for Hemorrhagic Complication in the NAP Group

Premature venous occlusion ($P < .001$), volume of Onyx injected ($P < .02$), total volume of embolic agent ($P < .03$), ratio of Onyx volume to the largest diameter of the nidus ($P < .01$), and ratio of V_{ea} to the largest diameter of nidus ($P < .01$) were associated with HC in univariate analysis (Table 4). Only premature venous oc-

Table 2: Characteristics of procedures with hemorrhagic complications

Variable[a]	Overall (*n* = 92)	AP (*n* = 44)	NAP (*n* = 48)	*P* Value
AVM location				
Cortical	77 (84)	41 (93)	36 (75)	<.041
Deep	11 (12)	3 (7)	8 (17)	
Infratentorial	4 (4)	0 (0)	4 (8)	
Eloquent	53 (58)	17 (39)	36 (75)	<.001
Type of HC				
Intraparenchymal hemorrhage	46 (50)	12 (27)	34 (71)	<.001
Subarachnoid hemorrhage	35 (38)	31 (71)	4 (8)	
Intraventricular hemorrhage	11 (12)	1 (1)	10 (21)	
Timing of rupture				
Hemorrhage during procedure	52 (59)	43 (98)	9 (18)	<.001
Delay between procedure and hemorrhagic events, hours (range)	17.2 (0–240)	0.05 (0–2)	34.4 (0–240)	<.001
Craniotomy for hematoma evacuation, decompressive craniotomy or EVD	15 (16)	3 (7)	12 (25)	<.019

Note:—EVD indicates external ventricular drainage.

[a] No. (%), mean ± SD or range.

Table 3: Outcomes in procedures with versus without hemorrhagic complications

Variable[a]	Overall (*n* = 827)	Without HC (*n* = 735)	With HC (*n* = 92)	*P* Value (without vs with HC)[b]	Type of Hemorrhagic Complications		
					AP (*n* = 44)	NAP (*n* = 48)	*P* Value (AP vs NAP)[b]
New disability	127 (15)	78 (11)	49 (53)	<.001	12 (27)	37 (77)	<.001
Transient	71 (9)	53 (7)	18 (20)		9 (20)	9 (19)	
Permanent	56 (7)	25 (3)	31 (34)		3 (7)	28 (58)	
Death	6 (1)	0 (0)	6 (7)	<.001	1 (2)	5 (10)	<.207

[a] No. (%).
[b] χ^2 or Fisher exact test for cells <5.

Table 4: Univariate predictors of hemorrhagic complications

Variable[a]	No Hemorrhagic Complications (*n* = 735)	NAP (*n* = 48)	*P* Value
Age (yr)	32.2 ± 13.7	33.9 ± 14.4	.405
Hemorrhagic presentation	316 (43)	18 (38)	.419
Nidus diameter (cm)	4.1 ± 3.8	3.9 ± 3.5	.553
Spetzler-Martin grade[b]	III	III	.874
AVM involving eloquent area	443 (60)	36 (75)	.164
Deep venous drainage	317 (43)	21 (44)	.660
Intranidal aneurysm presence	107 (15)	6 (13)	.513
Venous stenosis	40 (5)	5 (10)	.227
Venous ectasia	372 (51)	25 (3)	.596
Premature venous occlusion	3 (0.4)	8 (17)	<.001
Complete occlusion of AVM	181 (25)	18 (38)	.114
Detachable microcatheter	127 (17)	7 (15)	.606
Onyx volume (mL)	2.1 ± 2.0	2.9 ± 1.9	<.02
Total embolic agent volume (mL)[c]	2.5 ± 1.9	3.2 ± 1.6	<.03
Ratio of Onyx volume (mL)/nidus diameter (cm)	0.6 ± 0.6	0.8 ± 0.6	<.01
Ratio of V_{ea} (mL)/nidus diameter (cm)[c]	0.7 ± 0.6	0.9 ± 0.6	<.01
No. of pedicles embolized in each procedure[b]	1	1	.629

[a] Mean ± SD (median) (interquartile range) or count (%).
[b] Median.
[c] Sum of Onyx and glue used in each procedure.

Table 5: Independent predictors of hemorrhagic events in AVM size subdivisions of the no arterial perforation group

Variable	β	Odds Ratio	95% Confidential Interval	*P* Value[a]
Small AVM[b]				
Premature venous occlusion	3.8	44.3	4.24–462.04	<.001[c]
Total embolic agent volume	0.3	1.4	1.07–1.85	<.013[c]
Constant[d]	−3.6	0.03		<.001
Mid-size AVM[b]				
Premature venous occlusion	3.1	23.4	3.7–148.4	<.002[c]
Constant[d]	−2.7	0.06		<.001
Large AVM[b]				
Premature venous occlusion	24.2	3.2^{-10}	.00	1.00[e]
Constant[d]	−3.0	0.05		<.001

[a] Binary logistic regression.
[b] Small AVM, the largest diameter ≤3 cm; mid-size AVM, the largest diameters >3 cm and ≤6 cm; large AVM, the largest diameter >6 cm.
[c] Significant.
[d] A mathematic constant (no clinical interpretation).
[e] Nonsignificant.

clusion remained an independent predictor on multivariate analysis ($\beta = 3.8$; $P < .001$; 95% CI, 11–175). If premature venous occlusion occurred during the procedure, the probability of HCs increased by 45-fold.

Risk Factors for Hemorrhagic Complications according to AVM diameter

Both premature venous occlusion and total volume of embolic agents were independent risk factors on multivariate analysis only for small AVMs (Table 5). In the midsize AVMs, only premature venous occlusion was a risk factor of HC on univariate and multivariate analysis. In large AVMs, no variables were risk factors for HCs. The ratio of Onyx volume to the largest diameter of the nidus was an independent predictor of premature venous occlusion on multivariate analysis ($\beta = 1.4$; $P < .002$; 95% CI, 1.8–9.3).

DISCUSSION

In this series of 827 procedures, 11% were complicated by hemorrhage, which is consistent with the literature in which intracranial hemorrhage during or after the procedure was the most frequent complication of AVM embolization, reported in 2%–12.5% of procedures.[8,9,11-15] Intracranial hemorrhage was the most common cause of new disability after EVT.[16] Our strategy of embolization with curative intent in most patients leads to a higher cure rate compared with series with adjunctive embolization; nevertheless, this more aggressive approach could explain the higher rate of mortality and morbidity in this study. Periprocedural bleeding not only can causes neurologic deterioration but can also can result in poor outcome or death in many cases.[9,11,13,14] Aggressive treatment and early evacuation of the hematoma has minimized the neurologic morbidity in severe cases.[13,17,18] In our series, more than one-third of patients with HCs experienced a new permanent disability and a further 7% died. The overall rate of patient permanent morbidity due to a hemorrhagic complication following endovascular treatment for AVMs was, therefore, 7.6%, and the mortality rate was 1.6%.

Several studies classify HCs of AVM embolization into immediate (ie, occurring during or immediately after embolization) or delayed (occurring after uneventful and successful embolization and believed to be related to premature venous occlusion).[7,8,12] We included, in our study, any hemorrhage detected on immediate postprocedural CT or that occurred within the month following treatment. Almost half of the HCs were related to microwire or microcatheter perforation during navigation or arterial tear at catheter retrieval at the end of embolization, corresponding to a subarachnoid hemorrhage confirmed by flat panel CT with mostly a favorable outcome. In most instances, they are managed by reversal of heparin with protamine and lowering blood pressure, which

can stop the bleeding,[7] or they can be controlled by glue injection to prevent progression of hemorrhage. New detachable-tip catheters[19] or techniques with a second microcatheter placed in the same artery[20] are used for management of bleeding at retrieval of the wedged microcatheter. HCs occurring during catheterization are reported in 2% of EVT procedures, which is less than in our series (5%); however, it is likely that some of these complications are not mentioned because of their minor clinical significance, because they tend not to have clinical sequelae.[1,11,12,21] Also our standard technique of AVM treatment primarily uses Onyx and thus requires wire-directed navigation and dimethyl-sulfoxide–compatible catheters or detachable-tip microcatheters, which are stiffer. This navigation technique might account for the high incidence of periprocedural arterial perforation. Despite a benign prognosis in most cases, patients who develop HCs should be followed closely after the procedure to detect any hematoma progression or neurologic deterioration.

HCs not related to an arterial perforation clearly show different characteristics, with a delayed appearance, mostly symptomatic intraparenchymal hemorrhage, and with a much poorer clinical prognosis (58% permanent disability and 10% death).

Many terms from the surgical and endovascular literature have been proposed to explain the mechanisms of the NAP hemorrhagic group: normal perfusion breakthrough,[22] venous overload,[23] occlusive hyperemia,[24] nidus congestion,[6] venous occlusion by liquid embolic agents (Onyx or glue), progressive venous occlusion due to flow slowing and thrombosis, and inflammatory reaction or mural necrosis induced by the embolic material.[7,9,11,12,25] The importance of impaired venous drainage in the appearance of postoperative hemorrhage is well-recognized. al-Rodhan et al[24] reported that edema and hemorrhage after AVM resection are attributable to obstruction of the venous outflow system of brain tissue adjacent to the AVM, with subsequent worsening of the existing hypoperfusion and ischemia. The presence of impaired venous drainage before an operation has been recognized as a factor for the appearance of postoperative hemorrhage.[26] The brain parenchyma rendered hypoxic or ischemic by longstanding venous hypertension may not tolerate the increase in arterial flow after AVM resection. Careful examination of AVM drainage patterns is thus mandatory, with AVMs with more extensive patterns of draining veins requiring greater preoperative embolization and a staged return of normal circulatory patterns.

Ovalle et al[8] showed that of 13 potential factors, the volume of the embolic agent was the only one predictive of a delayed hemorrhagic complication. Our results agree with both univariate and multivariate analyses only in the subdivision of small AVMs (≤3 cm). In addition, we identified premature occlusion of the venous outflow before complete obliteration of the nidus as an independent predictor of hemorrhage, especially in small and midsize AVMs (≤6 cm). We also found that a predictive factor of premature venous occlusion is the ratio of Onyx volume to the largest diameter of the nidus. Using cyanoacrylates, Picard et al[9] reported that 80% of cases with a delayed hemorrhagic complication received ≥1 mL of glue, a much smaller quantity than commonly used now with Onyx (the mean volume by session was 2 mL in our study). This highlights the importance of careful delivery of liquid embolic agent and emphasizes the need for thorough anatomic and hemodynamic knowledge of the AVM compartment and veins draining the nidus.[27] Venous deposition of the embolic agent can be difficult to see when a large volume has been injected or when multiple embolizations have already been performed because the attenuation of Onyx prevents visualization.

Our study has some limitations. It is a retrospective analysis of the angioarchitecture of AVMs and of EVT results, which might not be simple with interobserver and intraobserver variability. This, combined with the relative small sample size of HC groups, could affect the analysis of the complications or result in nonsignificant differences.

CONCLUSIONS

Hemorrhagic complications are the most common and severe events following cerebral AVM embolization. Our study shows that premature venous occlusion is an independent predictive factor of hemorrhagic complications. Attention to the volume of the embolic agent used and prevention of premature venous occlusion by refined angioarchitecture analysis and liquid embolic delivery during EVT may reduce the incidence of these events. With regard to the risk of flow imbalance resulting in increased intranidal pressure and secondary rupture, our angiographic anatomic knowledge of the venous outflow of AVMs remains insufficient. There is, thus, a need for improvement of a preprocedural anatomic description of the nidus and its venous drainage as well as development of new embolic agents not obscuring the visualization of the nidal and venous anatomy.

ACKNOWLEDGMENTS

Sophie Rushton-Smith, PhD, provided editorial assistance in the final version of the manuscript and was funded by the authors. We thank Oriane Lambert and Said Akhlaghi for assistance in statistical analysis of the data of study.

Disclosures: Raphaël Blanc—*UNRELATED*: *Consultancy:* Covidien,* Stryker.* *Stock Options:* Lazarus Effect. Silvia Pistocchi—*UNRELATED*: *Consultancy*: Covidien,* Stryker.* Bruno Bartolini—*UNRELATED*: *Consultancy*: Covidien,* Stryker.* Michel Piotin—*UNRELATED*: *Consultancy*: Stryker,* Covidien.* *Payment for Manuscript Preparation*: Covidien,* *Payment for Development of Educational Presentations*: Covidien,* *Stock/Stock Options*: Lazarus Effect. *Money paid to the institution.

REFERENCES

1. Mounayer C, Hammami N, Piotin M, et al. **Nidal embolization of brain arteriovenous malformations using Onyx in 94 patients.** *AJNR Am J Neuroradiol* 2007;28:518–23
2. Debrun GM, Aletich V, Ausman JI, et al. **Embolization of the nidus of brain arteriovenous malformations with n-butyl cyanoacrylate.** *Neurosurgery* 1997;40:112–20
3. Weber W, Kis B, Siekmann R, et al. **Preoperative embolization of intracranial arteriovenous malformations with Onyx.** *Neurosurgery* 2007;61:244–52, discussion 252–244
4. Morgan MK, Winder M, Little NS, et al. **Delayed hemorrhage following resection of an arteriovenous malformation in the brain.** *J Neurosurg* 2003;99:967–71
5. Spetzler RF, Hargraves RW, McCormick PW, et al. **Relationship of perfusion pressure and size to risk of hemorrhage from arteriovenous malformations.** *J Neurosurg* 1992;76:918–23
6. Steiger HJ, Bruckmann H, Mayer T, et al. **Congested residual nidus after preoperative intranidal embolization in midsize cerebral ar-**

teriovenous malformations of 3–6 cm in diameter. *Acta Neurochir (Wien)* 2004;146:649–57
7. Haw CS, terBrugge K, Willinsky R, et al. **Complications of embolization of arteriovenous malformations of the brain.** *J Neurosurg* 2006;104:226–32
8. Ovalle F, Shay SD, Mericle RA. **Delayed intracerebral hemorrhage after uneventful embolization of brain arteriovenous malformations is related to volume of embolic agent administered: multivariate analysis of 13 predictive factors.** *Neurosurgery* 2012;70:313–20
9. Picard L, Da Costa E, Anxionnat R, et al. **Acute spontaneous hemorrhage after embolization of brain arteriovenous malformation with N-butyl cyanoacrylate.** *J Neuroradiol* 2001;28:147–65
10. Spetzler RF, Martin NA. **A proposed grading system for arteriovenous malformations.** *J Neurosurg* 1986;65:476–83
11. Saatci I, Geyik S, Yavuz K, et al. **Endovascular treatment of brain arteriovenous malformations with prolonged intranidal Onyx injection technique: long-term results in 350 consecutive patients with completed endovascular treatment course.** *J Neurosurg* 2011: 115;78–88
12. Purdy PD, Batjer HH, Samson D. **Management of hemorrhagic complications from preoperative embolization of arteriovenous malformations.** *J Neurosurg* 1991;74:205–11
13. Keller E, Yonekawa Y, Imhof HG, et al. **Intensive care management of patients with severe intracerebral haemorrhage after endovascular treatment of brain arteriovenous malformations.** *Neuroradiology* 2002;44:513–21
14. Deruty R, Pelissou-Guyotat I, Mottolese C, et al. **Therapeutic risk in multidisciplinary approach of cerebral arteriovenous malformations** [in French]. *Neurochirurgie* 1996;42:35–43
15. Biondi A, Le Jean L, Capelle L, et al. **Fatal hemorrhagic complication following endovascular treatment of a cerebral arteriovenous malformation: case report and review of the literature.** *J Neuroradiol* 2006;33:96–104
16. Panagiotopoulos V, Gizewski E, Asgari S, et al. **Embolization of intracranial arteriovenous malformations with ethylene-vinyl alcohol copolymer (Onyx).** *AJNR Am J Neuroradiol* 2009;30:99–106
17. Iwama T, Yoshimura K, Keller E, et al. **Emergency craniotomy for intraparenchymal massive hematoma after embolization of supratentorial arteriovenous malformations.** *Neurosurgery* 2003;53: 1251–58, discussion 1258–60
18. Carvi y Nievas M, Haas E, Hollerhage HG. **Severe intracranial bleedings during endovascular procedures: outcome of surgically treated patients.** *Neurol Res* 2007;29:81–90
19. Maimon S, Strauss I, Frolov V, et al. **Brain arteriovenous malformation treatment using a combination of Onyx and a new detachable tip microcatheter, SONIC: short-term results.** *AJNR Am J Neuroradiol* 2010;31:947–54
20. Abud DG, Abud TG, Nakiri GS. **Management of brain AVM procedural hemorrhagic complication by the "security" catheter technique.** *J Neuroradiol* 2013:40;45–49
21. n-BCA Trail Investigators. **N-butyl cyanoacrylate embolization of cerebral arteriovenous malformations: results of a prospective, randomized, multi-center trial.** *AJNR Am J Neuroradiol* 2002;23: 748–55
22. Spetzler RF, Wilson CB, Weinstein P, et al. **Normal perfusion pressure breakthrough theory.** *Clin Neurosurg* 1978;25:651–72
23. Wilson CB, Hieshima G. **Occlusive hyperemia: a new way to think about an old problem.** *J Neurosurg* 1993;78:165–66
24. al-Rodhan NR, Sundt TJ, Piepgras DG, et al. **Occlusive hyperemia: a theory for the hemodynamic complications following resection of intracerebral arteriovenous malformations.** *J Neurosurg* 1993;78: 167–75
25. Cronqvist M, Wirestam R, Ramgren B, et al. **Endovascular treatment of intracerebral arteriovenous malformations: procedural safety, complications, and results evaluated by MR imaging, including diffusion and perfusion imaging.** *AJNR Am J Neuroradiol* 2006;27: 162–76
26. Schaller C, Urbach H, Schramm J, et al. **Role of venous drainage in cerebral arteriovenous malformation surgery, as related to the development of postoperative hyperperfusion injury.** *Neurosurgery* 2002;51:921–27, discussion 927–29
27. Yamada S, Brauer FS, Colohan ART, et al. **Concept of arteriovenous malformation compartments and surgical management.** *Neurol Res* 2004;26:288–300

Temporary Solitaire Stent–Assisted Coiling: A Technique for the Treatment of Acutely Ruptured Wide-Neck Intracranial Aneurysms

F. Signorelli, B. Gory, and F. Turjman

ABSTRACT

BACKGROUND AND PURPOSE: Wide-neck intracranial aneurysms in patients with acute SAH are often challenging lesions to treat by neurosurgical and endovascular approaches. The aim of this study was to investigate the feasibility, safety, and efficacy of the use of temporary Solitaire AB stent–assisted technique with coiling for the treatment of acutely ruptured wide-neck aneurysms without perioperative antiplatelet therapy.

MATERIALS AND METHODS: A retrospective review of our endovascular data base identified all patients treated in the acute phase with a temporary stent–assisted technique by use of a fully resheathable Solitaire AB stent and coiling. One-year clinical and angiographic outcomes were evaluated.

RESULTS: Eight patients (5 women and 3 men; mean age, 57.5 years) with 8 ruptured wide-neck aneurysms were treated. There were 3 complications without clinical impact. Postoperative complete occlusion was achieved in 5 aneurysms, and 3 had a neck remnant. Three patients had an mRS score of 0, and 1 an mRS score of 3. Among the 4 patients admitted with a World Federation of Neurological Societies grade of V, 1 died, 1 improved to an mRS score of 1, and the other 2 achieved mRS scores of 4 and 5. Five had a stable occlusion, and 2 of the 3 incompletely occluded aneurysms underwent recanalization.

CONCLUSIONS: In this small series, temporary placement of the Solitaire AB stent during coiling was a feasible and effective treatment for acutely ruptured wide-neck aneurysms. This technique, avoiding the need for perioperative antiplatelet therapy, could be a valuable option for the treatment of such lesions when the balloon remodeling technique is either not an option or unsuccessful.

ABBREVIATIONS: EVD = external ventricular drain; SAC = stent-assisted coiling; WFNS = World Federation of Neurological Societies

Endovascular treatment of ruptured intracranial aneurysms is an established technique,[1] but it can be technically challenging when the neck is large. Numerous devices, including remodeling balloons[2-4] and stents,[5] have been developed to assist the endovascular treatment of wide-neck aneurysms. However, such techniques carry a great risk of hemorrhagic complications if they are applied in the acute phase of SAH because of the need for dual antiplatelet therapy.[6,7] In the recent review of acutely ruptured aneurysms treated with stent-assisted coiling (SAC) performed by Bodily et al,[7] clinically significant intracranial hemorrhagic complications occurred in 27 (8%) of 339 patients, including 9 (10%) of 90 patients known to have external ventricular drains (EVDs) who had ventricular drain–related hemorrhages.

To avoid the use of antiplatelet therapy in patients with acute SAH, the technique of temporary stent–assisted neck remodeling has been reported with the Enterprise stent (Codman & Shurtleff, Raynham, Massachusetts)[8] and recently with the support of the Solitaire AB stent (Covidien, Irvine, California) in 3 cases.[9] However, all patients received aspirin before the procedure, and 1 of 3 patients required antiplatelet therapy after the intervention.[9] The aim of this study was to investigate the feasibility, safety, and efficacy of the use of temporary Solitaire AB SAC for the treatment of acutely ruptured wide-neck aneurysms without perioperative antiplatelet therapy.

MATERIALS AND METHODS

The institutional review board of our hospital approved this study. A retrospective review of our data base identified all pa-

Received August 9, 2013; accepted after revision September 23.

From the Departments of Neurosurgery (F.S.) and Interventional Neuroradiology (B.G., F.T.), Hôpital Neurologique Pierre Wertheimer, Lyon, France; and Department of Experimental and Clinical Medicine (F.S.), University Magna Græcia, Catanzaro, Italy.

F.S. and B.G. contributed equally to this work.

Please address correspondence to Francesco Signorelli, MD, Hôpital Neurologique Pierre Wertheimer, Neurosurgery, 59 Bd Pinel, 69677 Bron, France; e-mail: signorelli2007@gmail.com

http://dx.doi.org/10.3174/ajnr.A3798

Table 1: Clinical and angiographic features

Patient	Sex/Age, y	Fisher Score	WFNS Grade	Aneurysm Location	Sac Size, mm	Neck Size, mm	Complementary Technique
1	Male/55	II	I	AcomA	4 × 2.5	4	RB
2	Male/51	III	V	Medium-basilar	21 × 13	8	
3	Female/58	IV	V	Right carotido-ophthalmic	12 × 10	6	
4	Female/77	II	I	Vertebrobasilar junction	9 × 10	10	
5	Female/43	IV	I	Left PcomA	4 × 3.5	3.5	
6	Female/81	IV	I	Left PcomA	3 × 2.5	3	
7	Female/52	III	V[a]	Right MCA	10 × 5	5	RB
8	Male/43	IV	V	Left PcomA	22 × 16	7	

Note:—AcomA indicates anterior communicating artery; RB, remodeling balloon; PcomA, posterior communicating artery.
[a] WFNS grade improved to III after EVD placement.

tients treated in the acute phase with a temporary stent–assisted technique by use of a fully resheathable Solitaire AB stent and coiling from April 2008 to December 2008. Patients presented with a ruptured aneurysm in the acute phase (≤72 hours) of SAH; a neck size of ≤4 mm and/or a dome-to-neck ratio of ≤1.0; and unfavorable anatomy, causing the balloon remodeling technique to be unsuccessful or unfeasible as the sole technique for supporting the coil mass. Patients were included with agreement of the treating neurosurgeon.

Characteristics of the Solitaire AB Stent

The Solitaire AB stent is a fully deployable and retrievable device that self-expands when the delivery microcatheter is withdrawn.[10] Its distal markers clearly show its position inside the artery at all times and in different projections. Its closed cell design and high cell deformation resistance provide flexibility and scaffolding to prevent coil herniation into the parent vessel. Moreover, it is provided with a system that allows for its retrieval.

Treatment Technique

All procedures were performed with the patient under general anesthesia and systemic heparinization (80 IU/kg). No antiplatelet therapy was given. A bilateral femoral approach by use of 6F or 8F guiding catheters was undertaken. One guiding catheter was used for the stent microcatheter (Prowler Select Plus, Codman & Shurtleff), and the other was used for the coil microcatheters (Echelon 14, Covidien and Prowler 14, Codman & Shurtleff). Coiling was achieved by a jailing technique with the use of a fully retrievable 4 × 20-mm stent, the Solitaire AB. The placement of the undetached stent was performed after microcatheter placement in the sac, and the neck was sufficiently covered in 6 patients. In the other 2 patients, a complementary balloon remodeling technique was used (HyperForm; Covidien) to prevent the coil from migrating distally into nearby arteries. In these 2 patients, the coil microcatheter and balloon were placed through the same guiding catheter. After packing of the aneurysm, the stent was retrieved by pushing the microcatheter and resheathing the stent, not by pulling the stent back.

Outcome Evaluation

Clinical outcome was assessed by means of the mRS at discharge; at 3, 6, and 12 months; and yearly thereafter (F.T.).[11]

Occlusion of the aneurysm was assessed angiographically at the end of the intervention, and at 3- and 12-month follow-up (F.T.). It was defined by use of the simplified 3-point Raymond classification scale: complete occlusion, neck remnant, and aneurysm remnant.[12] Recanalization was defined as a worsening of classification: complete occlusion to neck remnant, neck remnant to aneurysm remnant, or complete occlusion to aneurysm remnant.

RESULTS

Eight patients (5 women, 3 men; mean age, 57.5 years) with 8 aneurysms were treated with the temporary Solitaire AB SAC technique. Initial clinical features are summarized in Table 1. Among the 8 patients, 1 patient also presented with a bilateral subdural hematoma and 1 patient bled twice before treatment. Four patients were in good clinical condition (World Federation of Neurological Societies [WFNS] grade I) and 4 were in poor clinical condition (WFNS grade V). One patient with poor grade improved to grade III soon after EVD placement before embolization.

The mean aneurysm width was 10.6 mm (range, 3–22 mm), mean height of the sac 7.8 mm (range, 2.5–16 mm), and mean diameter of the neck was 5.8 mm (range, 3–10 mm) (Table 1).

Most aneurysms (75%) were located in the anterior circulation. Aneurysm locations are summarized in Table 1. All patients were treated successfully with the use of this technique. Placement of the undetached stent was easily performed and sufficiently covered the aneurysm neck in 6 patients, whereas concomitant balloon placement was required in 2 patients to protect a branch from distal coil migration (patients 1 and 7). The coil position was stable during and after stent retrieval in all patients.

Procedural Complications

One perforation of the aneurysm sac occurred during coil placement without clinical consequence (patient 5, mRS 0). One thromboembolic adverse event occurred during inflation of the balloon in the inferior MCA branch, which resulted in no clinical disability (patient 7, mRS 1). In another patient, premature detachment of 1 coil resulted in the placement of a portion of the coil in the basilar artery (patient 2, mRS 4). We did not retrieve the migrated coil because the free coil strand was stable in the basilar artery and did not cause distal flow reduction. Stent retrieval was uneventful.

Clinical Outcomes

Clinical outcomes are summarized in Table 2. Favorable outcome (mRS ≤2) was observed in 4 patients (50%). Among the 4 patients admitted with a WFNS grade of V, 1 died, 2 achieved mRS scores of 4 and 5 at discharge, respectively, and did not subsequently improve, and 1 improved to an mRS score of 1. Four patients required EVD placement after (and 1 before) SAC.

Table 2: Clinical and angiographic outcomes

Patient	mRS Score at Discharge	Aneurysmal Occlusion/ Initial 1-Year Follow-Up	Further Treatment
1	0	Complete/Complete	None
2	4	Complete/Complete	None
3	5	Neck remnant/Neck remnant	None
4	0	Neck remnant/Recanalization	SAC (complete occlusion)
5	0	Complete/Complete	None
6	3	Neck remnant/Recanalization	SAC (complete occlusion)
7	1	Complete/Complete	None
8	6	Complete/Complete	None

Angiographic Outcomes

Angiographic outcomes are summarized in Table 2. Postoperative angiographic results were the following: complete occlusion, 5 aneurysms (62.5%); and neck remnant, 3 aneurysms (37.5%). At 1-year follow-up, 2 of 3 patients showed recanalization and were treated electively with definitive stent placement, whereas 1 incomplete occlusion remained stable and was not treated because of the patient's persistent vegetative state.

Illustrative Cases

Case 1. A 55-year-old man (patient 1) presented with severe headaches and mild confusion (WFNS grade I). CT demonstrated SAH and bilateral subdural hematomas. The angiogram revealed an aneurysm of the anterior communicating artery associated with the median artery of the corpus callosum (Fig 1*A*). The broad-based aneurysm (dome, 4 × 2.5 mm; neck size, 4 mm) was impossible to coil by the conventional technique because the coils did not remain within the aneurysm, even with the balloon-assisted technique (Fig 1*B*). In the same setting, a 4 × 20-mm self-expanding Solitaire AB stent was placed but not detached in the left A1 and right A2 segments from the left. Coil implantation again resulted in coil herniation in the left A2. Thus, the stent was retrieved, a HyperForm balloon, 4 × 7 mm, was placed in the left A2, the stent was deployed again in the left A1–right A2 (Fig 1*C*), and 5 detachable coils were introduced. The balloon and then the stent were retrieved. The postprocedural angiogram demonstrated complete occlusion of the aneurysm (Fig 1*D*). Clinical examination at discharge and at 3- and 12-month follow-up revealed no neurologic deficits and an mRS score of 0.

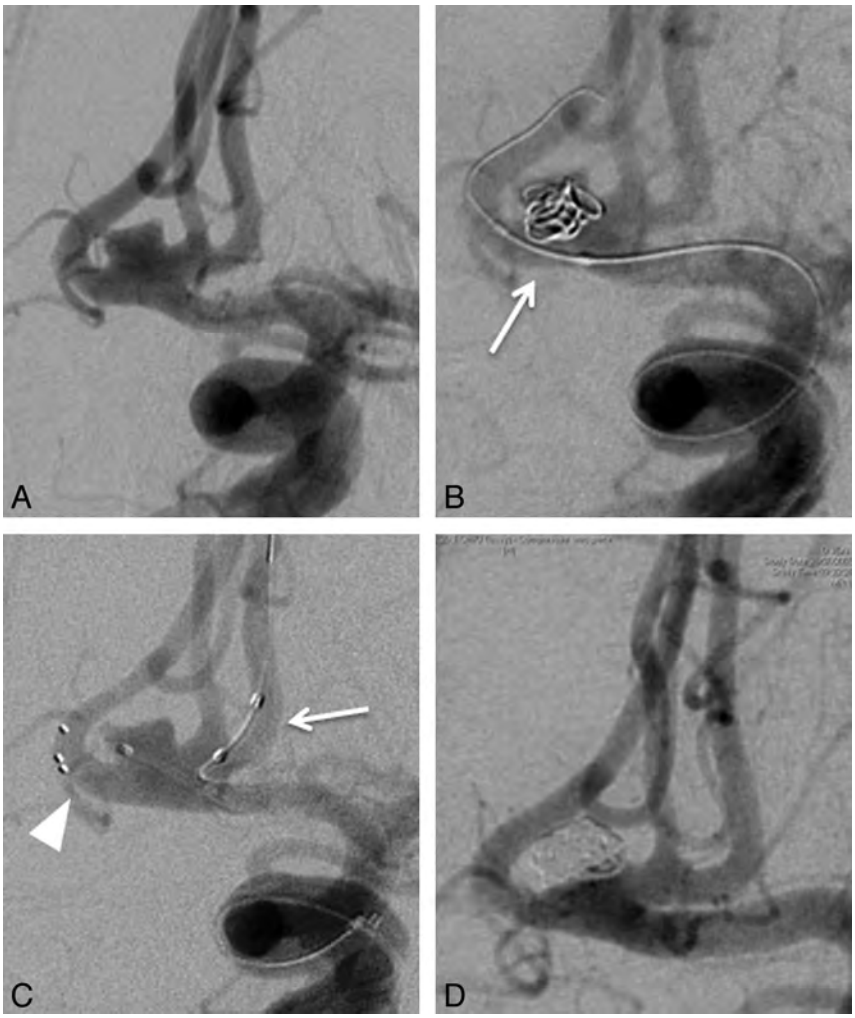

FIG 1. A 55-year-old man (patient 1) with a ruptured anterior communicating artery (AcomA) aneurysm. *A,* Initial angiogram shows a wide-neck AcomA aneurysm associated with the median artery of the corpus callosum. *B,* Balloon is positioned across the aneurysm neck and the first coil is inserted into the aneurysm with the balloon inflated. The first coil prolapses into the right A2 when the balloon is deflated (*arrow*). *C,* The deployed but undetached stent is positioned in the left A1 and right A2 segments from the left (*arrowhead*); the balloon is placed in the left A2 (*arrow*) and the microcatheter into the aneurysmal sac. *D,* Postprocedural angiogram demonstrates complete aneurysm occlusion after stent retrieval.

Case 2. A 52-year-old woman (patient 7) was admitted with a WFNS grade V SAH from a right bilobed, broad-based (dome, 10 × 5 mm; neck size, 5 mm) MCA bifurcation aneurysm (Fig 2*A, -B*). The patient had an additional paraophthalmic aneurysm, considered unruptured given its small size. Her WFNS grade improved to III after EVD placement. Embolization was carried out immediately thereafter. First, a HyperForm balloon, 4 × 7 mm, was placed to protect the inferior trunk from coil migration, and the undeployed stent was positioned across the superior trunk. The coil microcatheter was then positioned in the aneurysmal sac through the same guiding catheter as that used for the remodeling balloon, and the stent was deployed (Fig 2*C*). A vasospasm was observed in the stented artery. Aneurysm

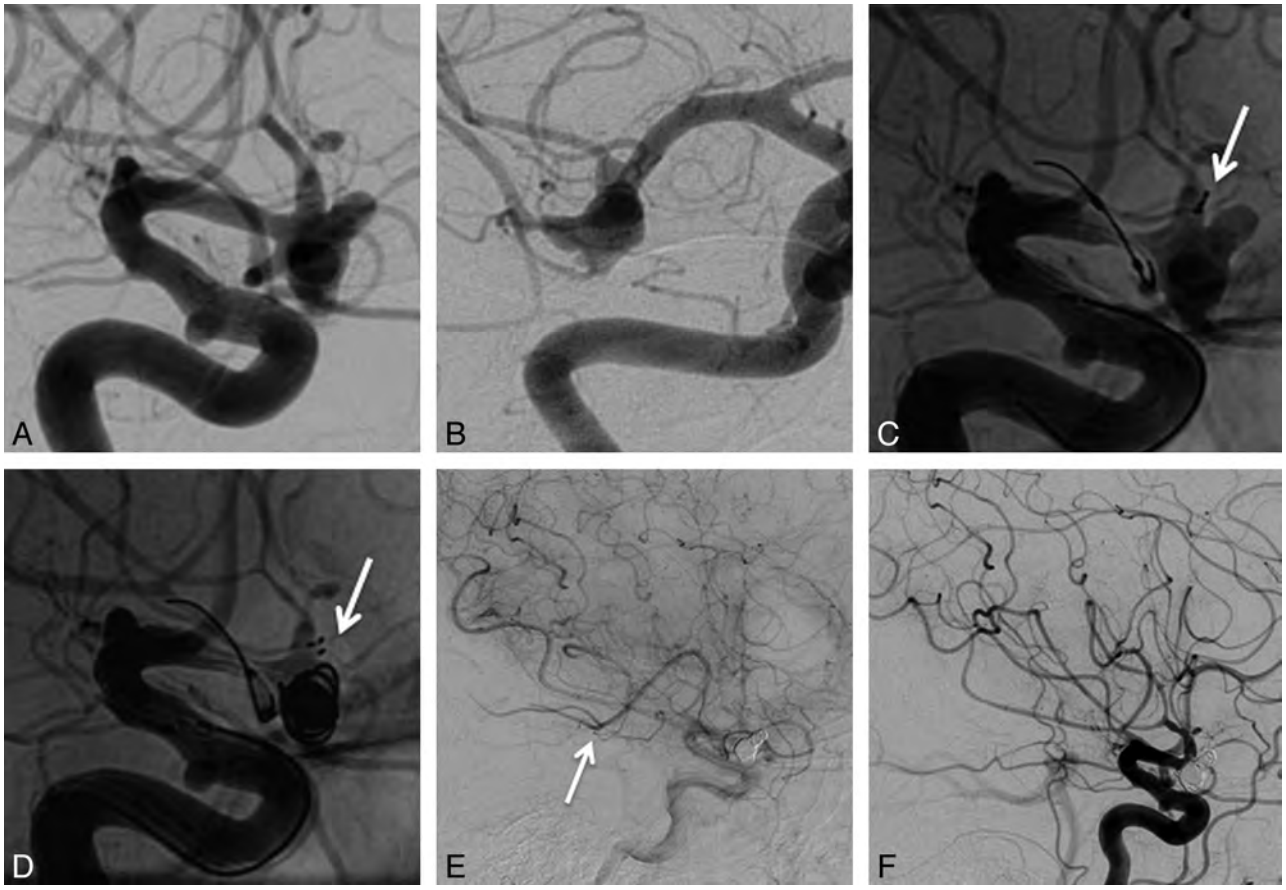

FIG 2. A 52-year-old woman (patient 7) with a complex MCA aneurysm. *A* and *B,* Initial angiogram shows a broad-based, bilobed MCA bifurcation aneurysm. An additional paraophthalmic aneurysm is noted. *C,* The undeployed stent is positioned across the superior trunk (*arrow*) and the balloon placed to protect the inferior trunk from coil migration. A vasospasm in the superior division of MCA was observed. *D,* The stent is deployed (*arrow*), and aneurysm packing is performed. The distal stent markers appear to be outside the vessel wall, an appearance that is related to vasospasm. *E* and *F,* A thromboembolic adverse event occurred during inflation of the balloon in the inferior MCA branch, which resulted in no clinical disability.

packing was then performed (Fig 2*D*), and the stent and balloon were retrieved. A thromboembolic adverse event was noted at the end of the procedure in the inferior MCA branch (Fig 2*E, -F*), without ischemic complications on the postoperative CT scan. At the 1-year follow-up, the patient had an mRS score of 1 and had resumed all previous activities.

DISCUSSION

Since the advent of self-expandable stents, SAC is a commonly adopted technique used in the coiling of wide-neck aneurysms.[5] In these cases, the most important function of the stent is to prevent herniation of coils into the parent artery.[13,14] However, perioperative antiplatelet treatment is mandatory to prevent in-stent thrombosis, which is a major concern in patients with acute SAH.[6,7,15] For this reason, stent placement is generally used only as a rescue technique in acutely ruptured aneurysms. In a recent systematic review of 339 patients with ruptured aneurysms who were treated acutely with SAC, clinically significant intracranial hemorrhagic complications occurred in 8% and clinically significant thromboembolic events occurred in 6%.[7]

The technique of temporary stent–assisted neck remodeling has been reported with the Enterprise stent[8] and recently with the Solitaire AB stent.[9] Contrary to a series by Almekhlafi et al,[9] we did not use antiplatelet therapy; thus theoretically reducing the risk of hemorrhagic complications linked to intraprocedural rupture of the aneurysm and to subsequent surgical interventions to treat intracranial hypertension such as EVD placement or decompressive craniectomy.[16] In our series, 4 of the 8 patients underwent emergent EVD placement, and no hemorrhagic complication was noted. Moreover, 1 patient had an intraoperative aneurysm rupture that was successfully managed by coil packing. The other concern with this technique is the patency of the stented parent artery during the deployment of the stent. In 1 of our 8 cases, there was an intraprocedural thromboembolic complication. This event occurred in the inferior branch of the MCA in which the balloon was inflated with no clinical impact.

The risk of entanglement of the coils was perceived as the major risk of this technique. After placement of a coil in contact with the stent, the latter was partially resheathed to assess this possibility. If the stent moved freely, the coil detachment was decided. After completing the coiling of the aneurysm, the stent was carefully completely resheathed to reduce the risk of endothelium damage and of subsequent vasospasm.

The balloon remodeling technique is the other option appli-

cable to treat wide-neck aneurysms[2-4]; it had a higher rate of adequate postoperative occlusion than did standard coiling with comparable safety[17] and had the advantage to overcome antiplatelet therapy. However, in our case series, we focused on wide-neck intracranial aneurysms in which the balloon remodeling technique had failed (patients 1 and 7) or was thought technically challenging because of the difficulty of navigating the balloon across the aneurysm neck. The Solitaire AB stent is a highly flexible device that easily conforms to vessel tortuosity and caliber variations because of its flexibility, which is not reduced by the closed cell design that offers a high outward radial force. Thus, the Solitaire AB efficiently accommodates curved and tapered vessels, bridging the aneurysm neck with virtually no limits in width and supporting the vessel lumen by avoiding recoil of coils.[10] There was no coil prolapse or herniation into the parent vessel during or after stent retrieval. Another advantage of this technique is the avoidance of anterograde flow arrest associated with repeated balloon inflations, which may cause ischemic stroke, given its reduced tolerance to ischemia in the setting of acute SAH.[5,18] Furthermore, balloon inflation may be associated with thromboembolic complications, especially when the parent artery diameter is small as in the illustrative case 2 of our series (patient 7).

Although this study has several limitations, including its retrospective nature, a relatively small number of cases, and limited follow-up duration, temporary SAC by use of the Solitaire AB stent has acceptable rates of technical failure and appears to be safe. Except for 1 case of asymptomatic vasospasm, there were no device-related adverse events, and the clinical outcome was favorable in 4 of 8 patients, whereas it was negatively affected by the clinical course of SAH in the other 4 patients. No rebleeding occurred during the observation period.

Complete aneurysm occlusion was achieved in most cases (62.5%); this suggests that this new technique could be an effective treatment. Although all aneurysms included in this series were ruptured, the recurrence rate is in line with the results of the systematic review of 7865 aneurysms coiled as performed by Ferns et al.[19]

CONCLUSIONS

Our preliminary experience with temporary SAC by use of the Solitaire AB stent suggests that it is a feasible, safe, and effective treatment alternative for wide-neck aneurysms in the setting of SAH when the balloon remodeling technique is either not an option or unsuccessful.

Disclosures: Francis Turjman—*RELATED: Support for Travel to Meetings for the Study or Other Purposes:* Covidien; *UNRELATED: Consultancy:* Codman; *Payment for Lectures (including service on speakers bureaus):* Codman; *Payment for Development of Educational Presentations:* Codman, Balt, Covidien; *Travel/Accommodations/Meeting Expenses Unrelated to Activities Listed:* Codman, Covidien.

REFERENCES

1. Li H, Pan R, Wang H, et al. **Clipping versus coiling for ruptured intracranial aneurysms: a systematic review and meta-analysis.** *Stroke* 2013;44:29–37
2. Moret J, Cognard C, Weill A, et al. **The "remodeling technique" in the treatment of wide neck intracranial aneurysms.** *Intervent Neuroradiol* 1997;3:21–35
3. Pierot L, Cognard C, Spelle L, et al. **Safety and efficacy of balloon remodeling technique during endovascular treatment of intracranial aneurysms: critical review of the literature.** *AJNR Am J Neuroradiol* 2012;33:12–15
4. Gory B, Kessler I, Seizem Nekiri G, et al. **Initial experience of intracranial aneurysm embolization using the balloon remodeling technique with Scepter C, a new double-lumen balloon.** *Intervent Neuroradiol* 2012;18:284–87
5. Shapiro M, Becske T, Sahlein D, et al. **Stent-supported aneurysm coiling: a literature survey of treatment and follow-up.** *AJNR Am J Neuroradiol* 2012;33:159–63
6. Tahtinen OI, Vanninen RL, Manninen HI, et al. **Wide-necked intracranial aneurysms: treatment with stent-assisted coil embolization during acute (<72 hours) subarachnoid hemorrhage: experience in 61 consecutive patients.** *Radiology* 2009;253:199–208
7. Bodily KD, Cloft HJ, Lanzino G, et al. **Stent-assisted coiling in acutely ruptured intracranial aneurysms: a qualitative, systematic review of the literature.** *AJNR Am J Neuroradiol* 2011;32:1232–36
8. Byun JS, Kim JK, Lee HY, et al. **Temporary semi-jailing technique for coil embolization of wide-neck aneurysm with small caliber parent artery following incomplete clipping.** *J Korean Neurosurg Soc* 2013;53:241–44
9. Almekhlafi MA, Hockley A, Wong JH, et al. **Temporary Solitaire stent neck remodeling in the coiling of ruptured aneurysms.** *J Neurointerv Surg* 2013;5(Suppl 3):iii76–78
10. Henkes H, Flesser A, Brew S, et al. **A novel microcatheter-delivered, highly-flexible and fully-retrievable stent, specifically designed for intracranial use.** *Intervent Neuroradiol* 2003;9:391–93
11. van Swieten JC, Koudstaal PJ, Visser MC, et al. **Interobserver agreement for the assessment of handicap in stroke patients.** *Stroke* 1988;19:604–07
12. Raymond J, Guilbert F, Weill A, et al. **Long-term angiographic recurrences after selective endovascular treatment of aneurysms with detachable coils.** *Stroke* 2003;34:1398–403
13. Piotin M, Blanc R, Spelle L, et al. **Stent-assisted coiling of intracranial aneurysms: clinical and angiographic results in 216 consecutive aneurysms.** *Stroke* 2010;41:110–15
14. Maldonado IL, Machi P, Costalat V, et al. **Neuroform stent-assisted coiling of unruptured intracranial aneurysms: short- and midterm results from a single-center experience with 68 patients.** *AJNR Am J Neuroradiol* 2011;32:131–36
15. Mahaney KB, Chalouhi N, Viljoen S, et al. **Risk of hemorrhagic complication associated with ventriculoperitoneal shunt placement in aneurysmal subarachnoid hemorrhage patients on dual antiplatelet therapy.** *J Neurosurg* 2013;119:937–42
16. Kung DK, Policeni BA, Capuano AW, et al. **Risk of ventriculostomy-related hemorrhage in patients with acutely ruptured aneurysms treated using stent-assisted coiling.** *J Neurosurg* 2011;114:1021–27
17. Pierot L, Cognard C, Anxionnat R, et al. **Remodeling technique for endovascular treatment of ruptured intracranial aneurysms had a higher rate of adequate postoperative occlusion than did conventional coil embolization with comparable safety.** *Radiology* 2011;258:546–53
18. Sluzewski M, van Rooij WJ, Beute GN, et al. **Balloon-assisted coil embolization of intracranial aneurysms: incidence, complications, and angiography results.** *J Neurosurg* 2006;105:396–99
19. Ferns SP, Sprengers ME, van Rooij WJ, et al. **Coiling of intracranial aneurysms: a systematic review on initial occlusion and reopening and retreatment rates.** *Stroke* 2009;40:523–29

Acute Basilar Artery Occlusion: Outcome of Mechanical Thrombectomy with Solitaire Stent within 8 Hours of Stroke Onset

J.M. Baek, W. Yoon, S.K. Kim, M.Y. Jung, M.S. Park, J.T. Kim, and H.K. Kang

ABSTRACT

BACKGROUND AND PURPOSE: Mechanical thrombectomy with a stent retriever applied shortly after symptom onset could increase good functional outcomes and improve survival in patients with acute basilar artery occlusion, but this has not yet been studied. This study evaluated the efficacy and safety of mechanical thrombectomy with a Solitaire stent within 8 hours of stroke onset in patients with acute basilar artery occlusion.

MATERIALS AND METHODS: We analyzed 25 consecutive patients with acute basilar artery occlusion who were treated with mechanical thrombectomy by use of the Solitaire stent within 8 hours of stroke symptom onset. Successful recanalization was defined as TICI grade 2b or 3. Good outcome was defined as mRS score of 0–2 at 3 months. Clinical and radiologic data in patients with good outcomes were compared with those with poor outcomes.

RESULTS: Successful recanalization was achieved in 96% (24/25) of patients, and 48% (12/25) of patients had good outcomes. Eighty-eight percent (22/25) of patients survived to 3 months. The median NIHSS score on admission was significantly lower in patients with good outcomes than in those with poor outcomes (9.5 versus 14, $P = .005$). Procedure-related complications occurred in 2 patients (8%). No symptomatic intracerebral hemorrhages occurred.

CONCLUSIONS: The current study suggests that mechanical thrombectomy by use of a Solitaire stent within 8 hours of stroke onset increases good outcomes and improves survival in patients with acute basilar artery occlusion.

ABBREVIATIONS: BAO = basilar artery occlusion; IA = intra-arterial; BASICS = Basilar Artery International Cooperation Study

Acute basilar artery occlusion (BAO) is associated with a very poor outcome and has the highest mortality rate among intracranial large-vessel occlusions.[1,2] In a prospective, observational study (BASICS [Basilar Artery International Cooperation Study]), 27 patients were treated conservatively because the patients were either comatose ($n = 26$) or tetraplegic ($n = 1$) at the time of presentation; 96.3% (26/27) of these patients died, and the 1 remaining patient had an mRS score of 5 at 1 month.[2]

Clinical outcomes were unsatisfactory, even when patients with acute BAO were treated with intravenous or intra-arterial (IA) pharmacologic thrombolysis. A systematic analysis including 420 patients showed that the rates of death or dependency were 78% (59/76) in patients treated with IV thrombolysis and 76% (260/344) in those treated with IA thrombolysis.[3]

In the past few years, the introduction of stent-type clot removal devices (stent retrievers) have initiated a new era in endovascular stroke therapy. Two randomized, controlled trials and many case series showed that stent retrievers can achieve a high rate of successful recanalization of up to 90%, thus improving the clinical outcome in patients with acute intracranial large-vessel occlusion.[4-11] Most studies were focused on anterior circulation stroke.

The efficacy of stent retrievers for treating acute BAO was reported in several recent case series.[12-14] These previous studies used a longer time window of up to 24 hours for mechanical thrombectomy in patients with acute BAO. However, BASICS showed that early recanalization therapy in patients with acute BAO is associated with a more favorable outcome, and all patients with severe stroke treated >9 hours after symptom onset had poor functional outcome despite IV or IA thrombolysis.[15] In this regard, the use of mechanical thrombectomy with a stent retriever within a shorter time period from symptom onset would increase

Received July 24, 2013; accepted after revision October 16.

From the Departments of Radiology (J.M.B., W.Y., S.K.K., M.Y.J., H.K.K.) and Neurology (M.S.P., J.T.K.), Chonnam National University Medical School, Chonnam National University Hospital, Gwangju, Republic of Korea.

Please address correspondence to Woong Yoon, MD, Department of Radiology, Chonnam National University Hospital, 671 Jebong-Ro, Dong-gu, Gwangju, 501–757, Republic of Korea; e-mail: radyoon@jnu.ac.kr

http://dx.doi.org/10.3174/ajnr.A3813

the patient's chances for a good functional outcome and decrease the mortality rate in patients with acute BAO, but this has not yet been studied. The aim of this study was to evaluate the efficacy and safety of mechanical thrombectomy with a stent retriever (Solitaire; Covidien, Irvine, California) as a first-line endovascular therapy within 8 hours of stroke onset in patients with acute BAO.

MATERIALS AND METHODS

Patients

Since December 2010, we prospectively collected data of patients with acute ischemic stroke treated with mechanical thrombectomy. The clinical and angiographic data for 25 patients who underwent mechanical thrombectomy with the Solitaire stent for acute BAO were identified from this data base between December 2010 and December 2012. During this period, a total of 133 consecutive patients with acute ischemic stroke caused by intracranial large-artery occlusion were treated with mechanical thrombectomy by use of the Solitaire stent as first-line endovascular therapy. The institutional ethics committee approved this retrospective analysis and waived informed consent on the basis of study design.

On admission, all patients were evaluated by a stroke neurologist and assessed by means of the NIHSS. All patients underwent an initial imaging protocol that included non-enhanced CT scan and multimodal MR imaging. The inclusion criteria for endovascular treatment were as follows: 1) baseline NIHSS score ≥4; 2) no intracerebral hemorrhage detected on the cranial CT or MR imaging; 3) BAO detected with MR angiography and conventional angiography; 4) no bilateral diffuse pontine ischemia on the DWI; and 5) the start of the procedure within 8 hours after symptom onset. IV rtPA (0.9 mg/kg) was administered in patients presenting within 4.5 hours from symptom onset. Subsequent endovascular treatment as a rescue therapy was considered within 1 hour of IV rtPA in patients with no neurologic improvement, defined as a NIHSS score unchanged from baseline or a worsening neurologic deficit.

Endovascular Treatment

All endovascular therapy was performed by 1 interventional neuroradiologist with 10 years of experience in neurovascular intervention. Written informed consent for endovascular therapy was obtained from a family member of all patients. Cerebral angiography and endovascular therapy were performed by means of a femoral approach under conscious sedation. In cases of agitation, an IV bolus of midazolam was given and repeated if necessary. After an arterial occlusion was demonstrated with diagnostic angiography, a diagnostic catheter was exchanged for a 6F or 7F guide catheter, which was placed in the most accessible or dominant vertebral artery. A balloon guide catheter was not used in any patient.

In all patients, mechanical thrombectomy with a Solitaire stent, which was 4 mm in diameter and 20 mm long, was used as a first-line endovascular treatment method. A microcatheter with a 0.021-inch internal diameter was navigated distal to the clot over a 0.014-inch microwire. The Solitaire stent was then introduced through the microcatheter and fully deployed across the occluded segment. After the stent was maintained in place for 1–3 minutes, the fully deployed stent and the delivery microcatheter were slowly pulled back together and withdrawn outside the body through the guide catheter. During clot retrieval, continuous manual aspiration with a 50-mL syringe at the guide catheter was performed. After removal of the Solitaire stent and microcatheter, another 10 mL of blood was aspirated from the guide catheter to prevent re-embolization of a vagrant clot. A control angiogram was performed to assess the recanalization status and possible distal embolic events. If recanalization was unsuccessful, the procedure was repeated. A maximum of 5 retrieval attempts was allowed.

When Solitaire thrombectomy was unsuccessful, additional rescue endovascular procedures were performed, including forced suction thrombectomy by use of a reperfusion catheter (Penumbra, Alameda, California) or aggressive mechanical clot disruption and IA urokinase infusion. The details of the technique for aggressive mechanical clot disruption have been described previously.[16] If an underlying atherosclerotic stenosis was revealed during the procedure, balloon angioplasty with or without stent placement was performed after the Solitaire thrombectomy.

During the procedure, heparin or glycoprotein IIb/IIIa inhibitor was not administered—IV or IA—in any patient. Patients who underwent intracranial angioplasty with or without stent placement received aspirin and clopidogrel (Plavix) for at least 3 months after the procedure. After the procedure, patients were admitted to an intensive care unit. All patients underwent non-enhanced CT scans immediately following and 24 hours after endovascular therapy. The start of endovascular therapy was defined as the moment the needle punctured the common femoral artery. Recanalization status was assessed on the final angiogram and classified according to the modified TICI scale.[17] Successful recanalization was defined as a TICI grade of 2b or 3. Assessment of angiographic images was performed by the consensus of 2 experienced neuroradiologists who were blinded to the procedure.

Outcome Measures

For all patients, we analyzed medical records to determine age, sex, risk factors, stroke subtype according to the Trial of Org 10172 in Acute Stroke Treatment classification, baseline NIHSS score, use of IV rtPA, time to IV rtPA and endovascular therapy, duration of the procedure, presence or absence of symptomatic hemorrhage, recanalization status, procedure-related vessel perforation and dissection, NIHSS score at discharge, and clinical outcome. Symptomatic hemorrhage was defined as a parenchymal hematoma that caused a mass effect on CT scans, with clinical deterioration defined as a ≥4-point increase in the NIHSS score or a 1-point deterioration in the level of consciousness. Vessel perforation was defined as obvious angiographic contrast extravasation that occurred during the procedure. Arterial dissection was defined as an identifiable intimal flap on the control angiogram obtained after mechanical thrombectomy. Neurologic evaluation was performed immediately by a stroke neurologist, 24 hours and 3 months after treatment, when any change occurred in clinical symptoms, and before the patient was discharged. Clinical outcome was assessed by means of the mRS by a stroke neurologist 3 months after treatment. Good clinical outcome was defined as an mRS score ≤2.

Baseline characteristics of the study population

	Good Outcome (n = 12)	Poor Outcome (n = 13)	Total (n = 25)	P
Age, y (mean ± SD)	63.2 ± 16.86	71.8 ± 11.92	68	NS
Sex, male, n (%)	6 (50%)	8 (61.5%)	14 (56%)	NS
Risk factors				
Hypertension	3 (25%)	12 (92.3%)	15 (60%)	.001
Atrial fibrillation	5 (41.7%)	4 (30.8%)	9 (36%)	NS
Diabetes mellitus	4 (33.3%)	4 (30.8%)	8 (32%)	NS
Dyslipidemia	4 (33.3%)	2 (15.4%)	6 (24%)	NS
Smoking	3 (25%)	3 (23.1%)	6 (24%)	NS
History of stroke or TIA	0%	4 (30.8%)	4 (16%)	NS
Coronary artery disease	0%	2 (15.4%)	2 (8%)	NS
Patent foramen ovale	1 (8.3%)	0%	1 (4%)	NS
Valvular heart disease	1 (8.3%)	0%	1 (4%)	NS
Atrioventricular block	0%	1 (8.3%)	1 (4%)	NS
Intravenous thrombolysis	3 (25%)	3 (23.1%)	6 (24%)	NS
Time to procedure, min	260 ± 100.32	290 ± 74.42	285 ± 88.48	NS
Procedure time, min	27.5 ± 24.21	30 ± 20.35	30 ± 21.91	NS
Time to recanalization, min	300 ± 110.03	310 ± 91.23	310 ± 99.91	NS
Rescue treatment				
Clot disruption with intra-arterial urokinase	1 (8.3%)	0%	1 (4%)	NS
Angioplasty with or without stenting	3 (25%)	3 (23.1%)	6 (24%)	NS
Baseline NIHSS score	9.5 ± 3.13	14 ± 5.75	11	.005
Discharge NIHSS score	2 ± 2.57	9 ± 8.21	4	.003
Stroke etiology				
Large-artery atherosclerosis	4 (33.3%)	5 (38.5%)	9 (36%)	NS
Cardioembolic	6 (50%)	6 (46.2%)	12 (48%)	NS
Undetermined	2 (8.3%)	2 (15.4%)	4 (16%)	NS

Note:—NS indicates non-significant.

Statistical Analysis

Statistical analyses were performed with the use of SPSS software (Version 19.0; IBM, Armonk, New York). The relationship between the characteristics and 3-month clinical outcome was determined by bivariate analysis. The χ^2 test was used for categoric variables and the Mann-Whitney U test for continuous variables. A value of $P < .05$ was considered significant.

RESULTS

Data from 25 patients (14 men and 11 women) were analyzed. Baseline patient characteristics according to clinical outcome are shown in the Table. Twenty-three patients had BAO only, and 2 patients had long segment occlusion from the distal intracranial segment of the vertebral artery to the basilar artery.

The median NIHSS score on admission was 11, with scores ranging from 3–25. The median time from symptom onset to endovascular therapy was 285 minutes (range, 110–470 minutes), the median procedure time was 30 minutes (range, 13–100 minutes), and the median time to recanalization was 310 minutes (range, 132–560). IV rtPA was administered in 6 patients (24%) before mechanical thrombectomy.

Successful recanalization was achieved in 96% (24/25) of patients, and complete recanalization (TICI grade 3) occurred in 76% (19/25) of patients. Successful recanalization with the Solitaire thrombectomy alone was achieved in 84% (21/25) of patients. In this study, rescue treatment was needed in 4 patients after Solitaire thrombectomy failed. One patient (patient 1) received aggressive mechanical clot disruption and low-dose IA urokinase infusion after unsuccessful Solitaire thrombectomy. Urokinase (80,000 IU) was given as a single bolus injection in this patient. Three patients (patients 10, 20, and 23) received forced suction thrombectomy with the Penumbra reperfusion catheter. Additional successful recanalization occurred in 3 of 4 patients who underwent rescue treatments. Three patients who underwent rescue forced suction thrombectomy with Penumbra reperfusion catheter achieved complete recanalization (TICI grade 3). One patient failed to achieve successful recanalization after aggressive mechanical clot disruption and IA urokinase infusion, and the patient's final recanalization grade was TICI 2a.

Six patients (24%) had underlying atherosclerotic stenosis in the distal intracranial vertebral artery ($n = 3$), basilar artery ($n = 2$), or both the distal vertebral and basilar arteries ($n = 1$). In these 6 patients, angioplasty, with or without stent placement, was performed to treat underlying stenosis after successful recanalization with a Solitaire thrombectomy. Of these 6 patients, 4 patients received angioplasty with stent placement and 2 patients received angioplasty alone. No angioplasty-related complication occurred in these 6 patients.

No patient had symptomatic hemorrhage during their hospital stay. At discharge, the NIHSS score was improved (decrease ≥4 points) in 15 patients (60%; range, 0–24; median, 4). At the 3-month follow-up, 12 patients (48%) showed a good clinical outcome. Eighty percent (12/15) of patients with hypertension had a poor clinical outcome and 90% (9/10) of those without hypertension had a good outcome; this difference was statistically significant ($P = .001$). Median NIHSS scores on admission (9.5 versus 14, $P = .005$) and at discharge (2 versus 9, $P = .003$) were significantly lower in patients with a good outcome than in those with a poor outcome. Other variables including age, sex, risk factors other than hypertension, stroke subtype, time to treatment, and procedure time were not statistically associated with a good clinical outcome. There was a good outcome in 50% (3/6) of patients who received a Solitaire thrombectomy after failed IV

thrombolysis and in 47% (9/19) of those who received a Solitaire thrombectomy as an initial treatment ($P = .910$). The median time from symptom onset to endovascular therapy tended to be shorter in patients with a good clinical outcome than in those with a poor clinical outcome (270 versus 313 minutes, $P = .301$).

Procedure-related complications occurred in 2 patients (8%). There was 1 vessel rupture unrelated to the Solitaire device. Active contrast extravasation caused by perforation of the thalamoperforating artery by a microwire was observed in 1 patient (patient 16). This patient exhibited a localized hematoma in the left paramedian thalamus, which was resolved on follow-up CT and had no neurologic worsening. One patient (patient 14) had SAH on the immediate posttherapeutic CT scan. This patient exhibited no postprocedural neurologic deterioration or associated symptomatic parenchymal hemorrhage. There were no device-related complications. The mortality rate was 12% (3/25) at 3 months. Two patients died 10 and 18 days after stroke onset because of extensive brain stem infarction. One patient with mRS score of 5 at discharge died 90 days after an initial stroke because of pneumonia.

DISCUSSION

The present study demonstrates that mechanical thrombectomy by use of the Solitaire stent within 8 hours of stroke onset in acute BAO is associated with increased rates of both good outcome and survival compared with previous studies. In our study, 88% (22/25) of patients survived for 3 months, and more than half of the survivors (55%, 12/22) had a good outcome.

There are still only a few studies that have investigated the clinical results of mechanical thrombectomy with stent retrievers in patients with acute BAO.[12-14] In contrast to our study, these previous studies included patients treated within 24 hours of stroke symptom onset. In a series of 14 patients treated with a Solitaire thrombectomy, Mordasini et al[12] reported that 28.6% (4/14) had a good outcome (mRS 0–2), and the mortality rate was 35.7% (5/14). In their study, a Solitaire thrombectomy was not the first-line endovascular treatment, and the median time from symptom onset to first angiogram was 414 minutes (range, 176–1440 minutes). Espinosa et al[13] reported a series of 18 patients with acute BAO who were directly treated with mechanical thrombectomy with either the Solitaire stent ($n = 10$) or the Trevo stent ($n = 8$). In their study, good functional outcome (mRS 0–2) was achieved in 50% (9/18), the mortality rate was 22.3% at 3 months, and time from symptom onset to groin puncture was 366 minutes. Most recently, in a series of 31 patients treated with Solitaire thrombectomy as the first-line endovascular treatment, Mourand et al[14] reported that 35% (11/31) had a good outcome, the mortality rate was 32% (10/31), and mean time from symptom onset to recanalization was 512 minutes. This group did not provide data regarding the time to treatment.

In comparison with these previous studies, the good outcome rate in our study is among the highest, and the mortality rate is among the lowest. In our study, the median time to treatment was <5 hours (285 minutes) and the median time to recanalization was <6 hours (310 minutes). The shorter time window for mechanical thrombectomy could be one of the factors that contributed to the good clinical results obtained in our study. A recent post hoc analysis of the BASICS trial found that early recanalization therapy in patients with BAO was associated with a more favorable outcome with a significantly increased chance of a poor outcome when recanalization therapy was started >6 hours after symptom onset.[15] In the BASICS trial, 85% of patients who were treated >9 hours after stroke onset had a poor functional outcome, whereas only 62% of those treated at ≤3 hours had a poor outcome.[15] The results of our study suggest that the same situation also holds true for mechanical thrombectomy with stent retrievers in patients with acute BAO.

Several other prognostic factors have been described that predict a good clinical outcome in patients with acute BAO receiving recanalization therapy and include recanalization status, baseline NIHSS score, and the extent of ischemic changes on the pretreatment imaging studies.[18-22]

A systematic review including 316 patients in 10 IA thrombolysis studies found that recanalization was associated with a substantial reduction in mortality rates in patients with acute BAO (mortality rate of 87% in non-recanalized compared with 39% in recanalized patients; $P < .001$).[18] The overall recanalization rate of these 10 studies was 64%, with a 56% mortality rate. Recent studies with the use of mechanical thrombectomy with stent retrievers reported significantly increased recanalization rates ranging from 74–100% in patients with acute BAO.[12-14] In our study, we achieved successful recanalization (TICI grades 2b to 3) in 96% (24/25) of patients, which is in line with previous reports. Successful recanalization with only the Solitaire stent occurred in 84% (21/25) of patients. This high rate of recanalization might also have contributed to the good results obtained in our study.

In a series of 106 patients with BAO treated with IA thrombolysis from 1992–2010, Jung et al[19] found that lower NIHSS score on admission was an independent predictor of good or moderate clinical outcome (mRS 0–3) ($P < .0001$) and survival ($P = .012$) at 3 months. The results of our study are in line with Jung's study. In our study, the median NIHSS score at admission was significantly lower in patients with a good outcome (mRS 0–2) than in those with a poor outcome (9.5 versus 14, $P = .005$). With regard to baseline NIHSS score, the median NIHSS score on admission in our study population was 11, which was lower than those of previous studies. Lower baseline NIHSS score could also be one of the factors that contributed to the good results obtained in our study.

The extent of early ischemic changes on pretreatment imaging studies can be used as a prognostic factor of clinical outcome in patients treated with recanalization therapy.[20-22] Puetz et al[20] showed that the posterior circulation ASPECTS on CT angiography source images predicts good outcome or death within 1 month in the subgroup of the BASICS registry population. Of 158 patients, 23% (18/78) of patients with a posterior circulation ASPECTS ≥8 had a good outcome, whereas 11% (9/80) of those with a posterior circulation ASPECTS <8 had a good outcome. The mortality rate was 32% (25/78) in patients with a posterior circulation ASPECTS ≥8 and 55% (44/80) in patients with a posterior circulation ASPECTS <8. We did not assess the extent of early ischemic changes on pretreatment CT or MR imaging in this study.

In our study, rescue treatment was needed in 4 patients (forced

suction thrombectomy in 3 and mechanical clot disruption with IA urokinase in 1) after unsuccessful Solitaire thrombectomy. Of these 4 patients, subsequent successful recanalization after a rescue treatment occurred in 3 patients who underwent forced suction thrombectomy with the Penumbra catheter, and 2 of these 4 patients showed a good outcome at 3 months. Therefore, adding suction thrombectomy with the Penumbra device appears to be promising in cases of unsuccessful thrombectomy with the Solitaire stent in patients with acute BAO. The effectiveness of such treatment must be confirmed in future studies.

Our study confirms the safety of mechanical thrombectomy with the Solitaire stent in patients with BAO. There was no symptomatic hemorrhage after mechanical thrombectomy in this study, and no vessel rupture or arterial dissections related to the Solitaire device occurred. There was 1 rupture of a perforating artery because of microwire perforation and 1 SAH, neither of which caused postprocedural neurologic deterioration. A recent study suggested that SAH might occur after mechanical thrombectomy with the Solitaire stent because of angiographically occult ruptures of small vessels caused by mechanical stretch during stent retrieval and that this had a benign clinical course.[23] Mordasini et al[12] reported no device-related complications or symptomatic hemorrhage. Espinosa de Rueda et al[13] reported 1 SAH in 18 patients with BAO treated with primary mechanical thrombectomy with the Solitaire stent. They reported a symptomatic hemorrhage rate of 0%, similar to that in our study. In a series of 31 patients with BAO treated with a Solitaire thrombectomy, Mourand et al[14] reported that vertebral artery dissection occurred in 1 patient, and no vessel perforation was observed. They also reported that symptomatic hemorrhage occurred in 16% (5/31) of patients, which is quite frequent compared with other reports. They did not describe the use of rescue treatments, including IA thrombolysis, in their report.

The limitations of our study included the small number of patients and the lack of a control group.

CONCLUSIONS

The current study suggests that a good clinical outcome can be safely achieved in nearly half of patients with acute BAO by use of mechanical thrombectomy with the Solitaire stent if treatment is started within 8 hours of symptom onset. In addition, such treatment can significantly reduce the mortality rate in this subset of patients with acute stroke, who otherwise have an extremely poor prognosis.

REFERENCES

1. Hacke W, Zeumer H, Ferbert A, et al. **Intra-arterial thrombolytic therapy improves outcome in patients with acute vertebrobasilar occlusive disease.** *Stroke* 1988;19:1216–22
2. Schonewille WJ, Wijman CA, Michel P, et al. **Treatment and outcomes of acute basilar artery occlusion in the basilar artery international cooperation study (BASICS): a prospective registry study.** *Lancet Neurol* 2009;8:724–30
3. Lindsberg PJ, Mattle HP. **Therapy of basilar artery occlusion: a systematic analysis comparing intra-arterial and intravenous thrombolysis.** *Stroke* 2006;37:922–28
4. Saver JL, Jahan R, Levy EI, et al. **Solitaire flow restoration device versus the Merci retriever in patients with acute ischaemic stroke (SWIFT): a randomized, parallel-group, non-inferiority trial.** *Lancet* 2012;380:1241–49
5. Nogueiro RG, Lutsep HL, Jovin TG, Aet al. **Trevo versus Merci retrievers for thrombectomy revascularization of large vessel occlusions in acute ischemic stroke (TREVO 2): a randomized trial.** *Lancet* 2012;380:1231–40
6. Castano C, Dorado L, Guerrero C, et al. **Mechanical thrombectomy with the Solitaire AB device in large artery occlusions of the anterior circulation: a pilot study.** *Stroke* 2010;41:1836–40
7. Roth C, Papanagiotou P, Behnke S, et al. **Stent-assisted mechanical recanalization for treatment of acute intracerebral artery occlusions.** *Stroke* 2010;41:2559–67
8. Costalat V, Machi P, Lobotesis K, et al. **Rescue, combined, and standalone thrombectomy in the management of large vessel occlusion stroke using the Solitaire device: a prospective 50-patient single-center study: timing, safety, and efficacy.** *Stroke* 2011;42:1929–35
9. Machi P, Costalat V, Lobotesis K, et al. **SolitaireFR thrombectomy system: immediate results in 56 consecutive acute ischemic stroke patients.** *J Neurointerv Surg* 2012;4:62–66
10. Miteff F, Faulder KC, Goh AC, et al. **Mechanical thrombectomy with a self-expanding retrievable intracranial stent (Solitaire AB): experience in 26 patients with acute cerebral artery occlusion.** *AJNR Am J Neuroradiol* 2011;32:1078–81
11. Yoon YH, Yoon W, Jung MY, et al. **Outcome of mechanical thrombectomy with Solitaire stent as first-line intra-arterial treatment in intracranial internal carotid artery occlusion.** *Neuroradiology* 2013;55:999–1005
12. Mordasini P, Brekenfeld C, Byrne JV, et al. **Technical feasibility and application of mechanical thrombectomy with the Solitaire FR revascularization device in acute basilar artery occlusion.** *AJNR Am J Neuroradiol* 2013;34:159–63
13. Espinosa de Rueda M, Parrilla G, Zamarro J, et al. **Treatment of acute vertebrobasilar occlusion using thrombectomy with stent retrievers: initial experience with 18 patients.** *AJNR Am J Neuroradiol* 2013;34:1044–48
14. Mourand I, Machi P, Milhaud D, et al. **Mechanical thrombectomy with the Solitaire device in acute basilar artery occlusion.** *J Neurointervent Surg* 2014;6:200–04
15. Vergouwen MD, Algra A, Pfefferkorn T, et al. **Time is brain(stem) in basilar artery occlusion.** *Stroke* 2012;43:3003–06
16. Yoon W, Park MS, Cho KH. **Low-dose intra-arterial urokinase and aggressive mechanical clot disruption for acute ischemic stroke after failure of intravenous thrombolysis.** *AJNR Am J Neuroradiol* 2010;31:161–64
17. Higashida RT, Furlan AJ, Roberts H, et al. **Trial design and reporting standards for intra-arterial cerebral thrombolysis for acute ischemic stroke.** *Stroke* 2003;34:e109–37
18. Smith WS. **Intra-arterial thrombolytic therapy for acute basilar artery occlusion: pro.** *Stroke.* 2007;38:701–03
19. Jung S, Mono ML, Fischer U, et al. **Three-month and long-term outcomes and their predictors in acute basilar artery occlusion treated with intra-arterial thrombolysis.** *Stroke* 2011;42:1946–51
20. Puetz V, Khomenko A, Hill MD, et al. **Extent of hypoattenuation on CT angiography source images in basilar artery occlusion: prognostic value in the Basilar Artery International Cooperation Study.** *Stroke* 2011;42:3454–59
21. Tei H, Uchiyama S, Usui T, et al. **Posterior circulation ASPECTS on diffusion-weighted MRI can be a powerful marker for predicting functional outcome.** *J Neurol* 2010;257:767–73
22. Strbian D, Sairanen T, Silvennoinen H, et al. **Thrombolysis of basilar artery occlusion: impact of baseline ischemia and time.** *Ann Neurol* 2013;73:688–94
23. Yoon W, Jung MY, Jung SH, et al. **Subarachnoid hemorrhage in a multimodal approach heavily weighted toward mechanical thrombectomy with Solitaire stent in acute stroke.** *Stroke* 2013;44:414–19

Temporal Correlation between Wall Shear Stress and In-Stent Stenosis after Wingspan Stent in Swine Model

M. Fujimoto, H. Takao, T. Suzuki, Y. Shobayashi, F. Mayor, S. Tateshima, M. Yamamoto, Y. Murayama, and F. Viñuela

ABSTRACT

BACKGROUND AND PURPOSE: A recent randomized clinical trial on intracranial atherosclerosis was discontinued because of the higher frequency of stroke and death in the angioplasty and stent placement group than in the medical treatment group. An in-depth understanding of the relationship between biologic responses and flow dynamics is still required to identify the current limitations of intracranial stent placement.

MATERIALS AND METHODS: Five Wingspan stents were deployed in tapered swine ascending pharyngeal arteries. Temporal wall shear stress distributions and in-stent stenosis were evaluated at days 0, 7, 14, and 28 after stent placement. The physiologic role of wall shear stress was analyzed regarding its correlation with in-stent stenosis.

RESULTS: In-stent stenosis reached a peak of nearly 40% at day 14 and decreased mainly at the distal stent segment until day 28. The wall shear stress demonstrated a characteristic pattern with time on the basis of the in-stent stenosis change. The wall shear stress gradient increased from the proximal to distal segment until day 14. At day 28, the trend was reversed dramatically, decreasing from the proximal to the distal segment. A significant correlation between the in-stent stenosis growth until day 14 and low wall shear stress values just after stent placement was detected. In-stent stenosis regression between days 14 and 28 was also associated with the high wall shear stress values at day 14.

CONCLUSIONS: These data suggest that the physiologic wall shear stress can control the biphasic in-stent stenosis change in tapered arteries.

ABBREVIATIONS: CFD = computational fluid dynamics; IS = in-stent stenosis; ISR = in-stent restenosis; WSS = wall shear stress

The Wingspan Stent System (Stryker, Kalamazoo, Michigan) is the only endovascular device for symptomatic intracranial atherosclerosis approved by the US Food and Drug Administration.[1] Although this system has achieved high technical success, the long-term (≥12-month) stroke complication rate ranges from 6.4%–20.5%.[2-7] Furthermore, the only randomized controlled trial, the Stent placement and Aggressive Medical Management for Preventing Recurrent stroke in Intracranial Stenosis (SAMMPRIS) trial, showed that aggressive medical treatment was superior to percutaneous transluminal angioplasty and stent placement. In particular, in-stent restenosis (ISR) occurred in approximately 30% of cases after stent treatments and was a major cause of late-phase stroke.[8-10] Although revascularization for ISR is relatively safe, 50% of treated patients experience recurrent restenosis.[11] An in-depth understanding of ISR after Wingspan stent placement is valuable to identify the current limitations of endovascular treatments of intracranial atherosclerosis and will help to improve this treatment methodology.

Stent placement can prevent arterial recoil and negative remodeling after angioplasty.[12] ISR mainly involves neointimal hyperplasia characterized by the migration of proliferating smooth muscle cells from the media. The neointimal hyperplasia is proportional to the degree of inflammation, such as that caused by medial damage or penetration of the stent into a lipid core.[13,14] In addition to the local stent-artery interaction, flow dynamics have been analyzed in their role in the biologic

Received April 30, 2013; accepted after revision August 26.

From the Division of Interventional Neuroradiology (M.F., H.T., Y.S., F.M., S.T., Y.M., F.V.), Department of Radiological Sciences, David Geffen School of Medicine, University of California, Los Angeles, California; Department of Neurosurgery (H.T., T.S., Y.M.), Jikei University School of Medicine, Tokyo, Japan; and Department of Mechanical Engineering (T.S., M.Y.), Graduate School of Engineering, Tokyo University of Science, Tokyo, Japan.

Funding from Division of Interventional Neuroradiology Research funds (F.V.) and research grant from Siemens Japan K.K. (Y.M., H.T.).

Please address correspondence to Motoaki Fujimoto, MD, PhD, Division of Interventional Neuroradiology, Department of Radiological Sciences, David Geffen School of Medicine at UCLA, 10833 Le Conte Ave, Los Angeles, California, 90095-1721; e-mail: moto.fujimo@gmail.com

http://dx.doi.org/10.3174/ajnr.A3773

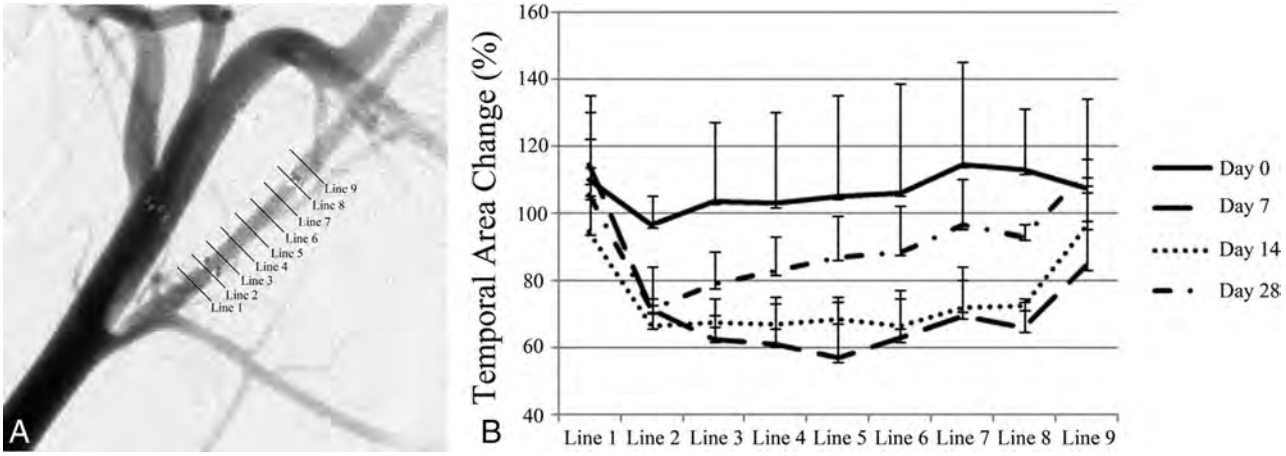

FIG 1. Nine cross-sectional areas at 1.5-mm intervals, including the 1.5 mm proximal and distal to the stent (*A*). Temporal area change after Wingspan stent placement, at days 0, 7, 14, and 28, was demonstrated in comparison with the preprocedural area (*B*).

response after endovascular treatment. In particular, low wall shear stress (WSS) reportedly correlates significantly with neointimal hyperplasia in both clinical and animal models.[15-19] Optimization of stent design on the basis of WSS has been attempted.[20]

Neointimal hyperplasia is suddenly initiated by arterial wall injury induced by endovascular devices and is stabilized for a limited period. Although drastic structural change can affect subsequent flow dynamics, there are no reports on evaluation of the temporal hemodynamic alterations that occur after stent placement. In our study, we focused the physiologic role of WSS on in-stent stenosis (IS) after Wingspan stent placement in a swine ascending pharyngeal artery.

MATERIALS AND METHODS

Animal Care

All animal experiments followed policies set by the Chancellor's Animal Research Committee of the University of California, Los Angeles. A total of 5 ascending pharyngeal arteries in 3 healthy Yorkshire swine (age range, 3–4 months; weight range, 30–40 kg) were included in this study. All endovascular procedures were performed by use of the Allura Xper FD10 System (Philips Healthcare, Best, the Netherlands) as described previously.[21] In brief, a 6F guiding catheter was positioned in the common carotid artery via the right femoral approach. Special interest was paid to the ascending pharyngeal artery, which corresponds to the human internal carotid artery. A segment without large branching and with a proximal diameter of > 2.0 to ≤ 3.0 mm was chosen, and the Wingspan stent was delivered. The Wingspan stent is a self-expandable straight stent with an open-cell design, which is made of nickel-titanium alloy. The stent diameter was followed to the manufacturer's recommendation to exceed the diameter of the referenced arterial diameter by 0–0.5 mm. Three 3.0 × 9-mm and two 2.5 × 9-mm stents were used. Three-dimensional rotational angiography was conducted before and after stent placement to construct the arterial models. As for 3D rotational angiography, the C-arm was rotated over 240° (120° right anterior oblique to 120° left anterior oblique) during 4.1 seconds with x-ray acquisition speed at 30 frames per second. During the rotational run, a total of 122 isocentric images were generated, resulting in a 256^3 isotropic image volume.

Nine cross-sectional areas at 1.5-mm intervals, including the 1.5 mm proximal and distal to the stent, were evaluated immediately after stent placement (Fig 1*A*). Follow-up angiograms were performed at days 7, 14, and 28 after stent placement. The cross-sectional area was measured from the 3D reconstructed image. IS was defined as a reduction of the sectional area, compared with the area just after stent placement.

Computational Fluid Dynamics Modeling and Analysis Condition

Steady- and pulsatile laminar-flow analyses were performed as described previously.[22] The ascending pharyngeal artery was extracted from the reconstructed 3D data and was converted to a stereolithography-triangulated surface by use of Real Intage (Cybernet Systems, Chiyoda, Tokyo). Surface smoothing was performed with Amira (Visage Imaging, San Diego, California). A volumetric mesh was prepared from the smoothed stereolithography by ICEM CFD 13.0 (ANSYS, Canonsburg, Pennsylvania). The mesh was composed of unstructured grids with mainly tetrahedrons. A mesh-convergence study focusing on the number of mesh elements was performed as reported previously.[22] The average number of nodes in these models was 1 million. Computational fluid dynamics (CFD) analysis was performed on the volumetric meshes by use of a finite-volume method solver from the general-purpose CFD analysis tool, CFX13.0 (ANSYS). For a typical geometry of the blood vessels, the laminar flow was assumed with a Reynolds number of 250. The Reynolds number was defined as the average velocity and the diameter of an inlet artery. Blood was applied to be a Newtonian fluid with an attenuation of 1100 kg/m^3 and viscous coefficient of 0.0036 Pa × s. The inlet condition was 0.0035 kg/second as a mass flow rate, which was comparable to the human wave form at a 0-second point.[23] Relative pressure on the outlet was set to 0 Pa. As for the time-stepping parameter, we calculated a total of 1.8 seconds as 2 pulsations and 3601 steps in a time-step size of 0.005 second. WSS value was evaluated as the average of WSS for the simulation time course. The Navier-Stokes equations were used to simulate blood flow on

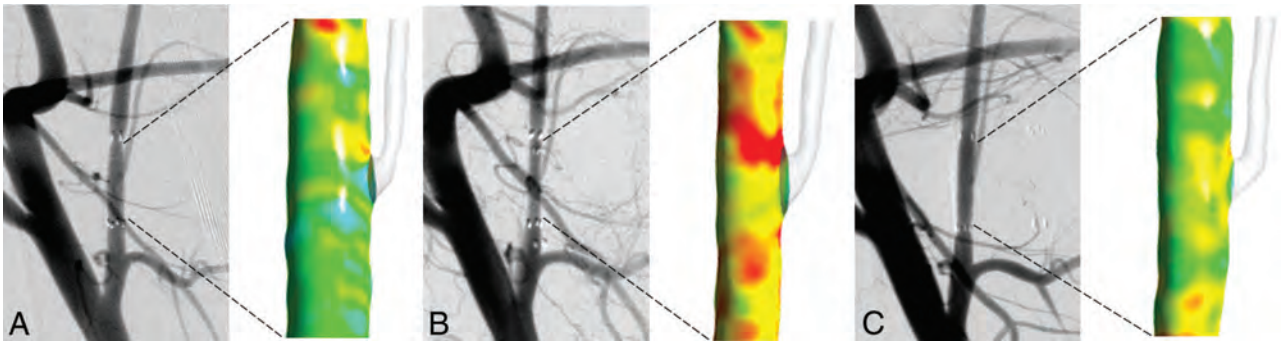

FIG 2. Temporal change of angiography and WSS distributions in a tapered artery. Immediately after stent placement (*A*) and at day 14 (*B*) and day 28 after stent placement (*C*).

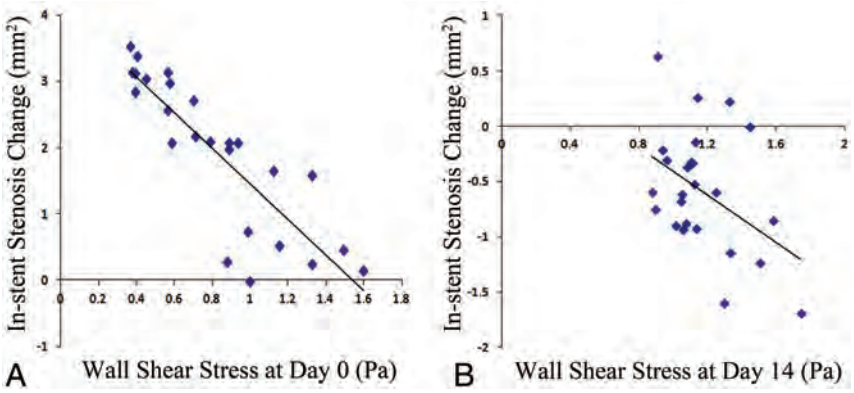

FIG 3. Correlation between IS change and the initial WSS for 2 terms, from days 0–14 (*A*) and days 14–28 (*B*).

the computational mesh. We applied a high-resolution scheme for the advection and a second-order backward Euler scheme for the transient term. The maximal calculation error was 1.7% between the result of CFX software and the theoretic value by use of the formula in a Poiseuille flow study.

Statistical Analysis

Statistical comparisons were conducted by use of STATA 12.0 (StataCorp, College Station, Texas). The normality was confirmed by the D'Agostino-Pearson test. The correlation between the area variation and WSS was evaluated by use of the Pearson correlation test. *P* values of $< .05$ were considered statistically significant.

RESULTS

Angiographic Change

The ascending pharyngeal artery showed a tapered shape. The preprocedural luminal ratio of the distal segment (Line 8) to the proximal segment (Line 2) was 81.3% ± 7.5% (Fig 1*A*). The temporal area changes at 1.5-mm intervals are shown in Fig 1*B*. Immediately after stent placement, the artery was dilated mainly at the distal stent segment. At days 7–14 after stent placement, IS reached a peak of nearly 40% for the entire stented artery. At day 28, the IS decreased by up to 4% at the distal stent segment.

CFD Simulations

Stent placement in a tapered artery resulted in marked hemodynamic changes with time (Fig 2). Just after stent placement, the WSS gradient increased from the proximal to the distal segment according to the tapering lumen. At day 14, WSS values were elevated because of the IS. The distribution pattern of WSS was almost identical to that immediately after stent placement. At day 28, the trend was dramatically reversed and decreased from the proximal to the distal segment.

Correlation between IS Change and WSS

The correlation between area variations of IS and the initial WSS values was analyzed in the following 2 periods: the growth period from days 0–14 and the regression period from days 14–28 (Fig 3). Between days 0 and 14, the IS growth correlated significantly with the low WSS values at day 0 ($R^2 = 0.73$; $P < .001$). A mild correlation between the IS regression between days 14 and 28 and the high WSS values at day 14 was observed ($R^2 = 0.19$; $P = .03$).

DISCUSSION

Shear stress is essential for maintenance of arterial wall function. Disturbed flow, such as that caused by low WSS or oscillatory shear stress, is reportedly associated with atheromatous plaque initiation, progression, and composition.[24,25] Hemodynamic stress is also responsible for the biologic response after endovascular treatment. From a clinical standpoint, WSS has been shown to correlate inversely with neointimal hyperplasia after coronary stent placement.[15,17] In addition to WSS, several hemodynamic factors such as the WSS gradients or oscillatory shear stress have been analyzed for their roles in IS in animal models.[16,18,19] Although atherosclerosis and ISR demonstrate many similarities in their process of formation, atherosclerosis is pathophysiologically characterized by progressive lipid accumulation, inflammation, and smooth muscle cell proliferation that continue for many years.[12] In contrast, neointimal hyperplasia is primarily a self-limited intimal hyperplastic process after arterial wall injury induced by endovascular devices. The physiologic role of WSS in ISR may not necessarily correspond to that in atherosclerotic disease. Temporal IS changes need to be clarified from a flow dynamics standpoint.

In our study, a characteristic gradient of IS with time was demonstrated after Wingspan stent placement in a tapered swine artery. The IS achieved a peak in whole at day 14 and regressed mainly at the distal stent segment at day 28. As a result, the WSS trend was dramatically reversed to demonstrate a decrease from the proximal to the distal segment at day 28. The WSS correlated significantly with both periods of growth and regression. In particular, the augmented IS in the growth phase correlated strongly with the low WSS. Low WSS was shown to upregulate proinflammatory genes, leading to smooth muscle cell proliferation and migration.[26] Our results of intracranial self-expandable Wingspan stent placement corresponded with those in previous reports of balloon-expandable stent placement.[15-19] Furthermore, a mild association between high WSS and the regression of IS between days 14 and 28 was demonstrated. Physiologic increases in WSS from IS may be involved in the regression process. High WSS decreased the inflammation associated with endothelial cell and smooth muscle cell proliferation.[27,28] Purposefully augmented WSS created by arterial venous shunting or flow-dividing devices has been demonstrated to decrease neointimal hyperplasia.[29-31] The residual IS at the proximal segment at day 28 may have been caused by both the growth of IS at the proximal segment with low WSS and the regression of IS at the distal segment with high WSS.

In clinical practice, there is often a marked difference in diameter between the proximal and distal segments of an artery, and in such cases of tapering, there is no option but to choose a stent that fits the proximal diameter. An oversized stent at the distal portion of an arterial wall injury can exaggerate the neointimal hyperplasia.[19] A straight stent with high solid mechanical value can be associated with a higher incidence of restenosis or asymptomatic occlusion than a tapered stent.[32,33] In addition to solid mechanics, WSS may contribute to both growth and regression of ISR. Further simulation study should evaluate which factors are most responsible for ISR after Wingspan stent placement. A temporal analysis of ISR may be required.

Study Limitations

Although the WSS change because of the IS can be a reasonable mechanism to explain the biologic response in a tapered artery, our results were limited by the simplified animal model, such as extremely small sample size, lack of any control information, and a straight arterial segment rather than a tortuous segment. Other flow dynamic parameters can be associated with the IS.[18] Furthermore, temporal IS regulation by WSS may not always be applied for clinical cases with a wide variety of characteristics. Exhaustive analysis with a larger sample size would be desired. Also, our technical limitation of this study was an evaluation method for IS. All area measurements were derived from 3D reconstructed images. The image artifacts by stent markers could make it difficult to evaluate the cross-sectional area at the ends of the stent.

CONCLUSIONS

We presented the temporal correlation between simulated WSS and IS elicited by Wingspan stent placement in a swine artery. The WSS showed a characteristic pattern in a tapered segment of the artery on the basis of change in IS. The physiologic WSS may play a large role in both the growth and decrement of IS. These insights into time-dependent flow dynamics will be useful for the understanding of biologic responses and for the development of an optimal stent design.

Disclosures: Hiroyuki Takao—*RELATED: Grant:* Siemens Japan K.K*; *UNRELATED: Grants/Grants Pending:* FujiFilm,* NTTdocomo.* Yuichi Murayama—*UNRELATED: Consultancy:* Stryker, ASAHI INTECC, Kakeka; *Grants/Grants Pending:* Siemens, FujiFilm; *Royalties:* Stryker. **Money paid to institution.*

REFERENCES

1. Bose A, Hartmann M, Henkes H, et al. **A novel, self-expanding, nitinol stent in medically refractory intracranial atherosclerotic stenoses: the Wingspan study.** *Stroke* 2007;38:1531–37
2. Chimowitz MI, Lynn MJ, Derdeyn CP, et al. **Stenting versus aggressive medical therapy for intracranial arterial stenosis.** *N Engl J Med* 2011;365:993–1003
3. Li J, Zhao ZW, Gao GD, et al. **Wingspan stenting with modified predilation for symptomatic middle cerebral artery stenosis.** *Catheter Cardiovasc Interv* 2011;78:286–93
4. Jiang WJ, Yu W, Du B, et al. **Outcome of patients with >/=70% symptomatic intracranial stenosis after Wingspan stenting.** *Stroke* 2011;42:1971–75
5. Costalat V, Maldonado IL, Vendrell JF, et al. **Endovascular treatment of symptomatic intracranial stenosis with the Wingspan stent system and Gateway PTA balloon: a multicenter series of 60 patients with acute and midterm results.** *J Neurosurg* 2011;115:686–93
6. Yu SC, Leung TW, Lee KT, et al. **Angioplasty and stenting of atherosclerotic middle cerebral arteries with Wingspan: evaluation of clinical outcome, restenosis, and procedure outcome.** *AJNR Am J Neuroradiol* 2011;32:753–58
7. Fiorella DJ, Turk AS, Levy EI, et al. **U.S. Wingspan Registry: 12-month follow-up results.** *Stroke* 2011;42:1976–81
8. Levy EI, Turk AS, Albuquerque FC, et al. **Wingspan in-stent restenosis and thrombosis: incidence, clinical presentation, and management.** *Neurosurgery* 2007;61:644–50; discussion 650–51
9. Albuquerque FC, Levy EI, Turk AS, et al. **Angiographic patterns of Wingspan in-stent restenosis.** *Neurosurgery* 2008;63:23–27; discussion 27–28
10. Turk AS, Levy EI, Albuquerque FC, et al. **Influence of patient age and stenosis location on Wingspan in-stent restenosis.** *AJNR Am J Neuroradiol* 2008;29:23–27
11. Fiorella DJ, Levy EI, Turk AS, et al. **Target lesion revascularization after Wingspan: assessment of safety and durability.** *Stroke* 2009;40:106–10
12. Kibos A, Campeanu A, Tintoiu I. **Pathophysiology of coronary artery in-stent restenosis.** *Acute Card Care* 2007;9:111–19
13. Farb A, Weber DK, Kolodgie FD, et al. **Morphological predictors of restenosis after coronary stenting in humans.** *Circulation* 2002;105:2974–80
14. Welt FG, Rogers C. **Inflammation and restenosis in the stent era.** *Arterioscler Thromb Vasc Biol* 2002;22:1769–76
15. Wentzel JJ, Krams R, Schuurbiers JC, et al. **Relationship between neointimal thickness and shear stress after Wallstent implantation in human coronary arteries.** *Circulation* 2001;103:1740–45
16. LaDisa JF Jr, Olson LE, Molthen RC, et al. **Alterations in wall shear stress predict sites of neointimal hyperplasia after stent implantation in rabbit iliac arteries.** *Am J Physiol Heart Circ Physiol* 2005;288:H2465–75
17. Papafaklis MI, Bourantas CV, Theodorakis PE, et al. **The effect of shear stress on neointimal response following sirolimus- and paclitaxel-eluting stent implantation compared with bare-metal stents in humans.** *JACC Cardiovasc Interv* 2010;3:1181–89
18. Morlacchi S, Keller B, Arcangeli P, et al. **Hemodynamics and in-stent restenosis: micro-CT images, histology, and computer simulations.** *Ann Biomed Eng* 2011;39:2615–26
19. Chen HY, Sinha AK, Choy JS, et al. **Mis-sizing of stent promotes**

intimal hyperplasia: impact of endothelial shear and intramural stress. *Am J Physiol Heart Circ Physiol* 2011;301:H2254–63
20. Gundert TJ, Marsden AL, Yang W, et al. **Optimization of cardiovascular stent design using computational fluid dynamics.** *J Biomech Eng* 2012;134:011002
21. Fujimoto M, Shobayashi Y, Tateshima S, et al. **Biomechanical responses after Wingspan stent deployment in swine ascending pharyngeal artery.** *Neurol Res* 2013;35:90–94
22. Takao H, Murayama Y, Otsuka S, et al. **Hemodynamic differences between unruptured and ruptured intracranial aneurysms during observation.** *Stroke* 2012;43:1436–39
23. Ford MD, Alperin N, Lee SH, et al. **Characterization of volumetric flow rate waveforms in the normal internal carotid and vertebral arteries.** *Physiol Meas* 2005;26:477–88
24. Samady H, Eshtehardi P, McDaniel MC, et al. **Coronary artery wall shear stress is associated with progression and transformation of atherosclerotic plaque and arterial remodeling in patients with coronary artery disease.** *Circulation* 2011;124:779–88
25. Eshtehardi P, McDaniel MC, Suo J, et al. **Association of coronary wall shear stress with atherosclerotic plaque burden, composition, and distribution in patients with coronary artery disease.** *J Am Heart Assoc* 2012;1:e002543
26. Chatzizisis YS, Coskun AU, Jonas M, et al. **Role of endothelial shear stress in the natural history of coronary atherosclerosis and vascular remodeling: molecular, cellular, and vascular behavior.** *J Am Coll Cardiol* 2007;49:2379–93
27. Ueba H, Kawakami M, Yaginuma T. **Shear stress as an inhibitor of vascular smooth muscle cell proliferation. Role of transforming growth factor-beta 1 and tissue-type plasminogen activator.** *Arterioscler Thromb Vasc Biol* 1997;17:1512–16
28. Sheikh S, Rainger GE, Gale Z, et al. **Exposure to fluid shear stress modulates the ability of endothelial cells to recruit neutrophils in response to tumor necrosis factor-alpha: a basis for local variations in vascular sensitivity to inflammation.** *Blood* 2003;102:2828–34
29. Carlier SG, van Damme LC, Blommerde CP, et al. **Augmentation of wall shear stress inhibits neointimal hyperplasia after stent implantation: inhibition through reduction of inflammation?** *Circulation* 2003;107:2741–46
30. Wentzel JJ, Gijsen FJ, Stergiopulos N, et al. **Shear stress, vascular remodeling and neointimal formation.** *J Biomech* 2003;36:681–88
31. Mattsson EJ, Kohler TR, Vergel SM, et al. **Increased blood flow induces regression of intimal hyperplasia.** *Arterioscler Thromb Vasc Biol* 1997;17:2245–49
32. Brown KE, Usman A, Kibbe MR, et al. **Carotid stenting using tapered and nontapered stents: associated neurological complications and restenosis rates.** *Ann Vasc Surg* 2009;23:439–45
33. Auricchio F, Conti M, De Beule M, et al. **Carotid artery stenting simulation: from patient-specific images to finite element analysis.** *Med Eng Phys* 2011;33:281–89

Reproducibility of Cerebrospinal Venous Blood Flow and Vessel Anatomy with the Use of Phase Contrast–Vastly Undersampled Isotropic Projection Reconstruction and Contrast-Enhanced MRA

E.M. Schrauben, K.M. Johnson, J. Huston, A.M. del Rio, S.B. Reeder, A. Field, and O. Wieben

ABSTRACT

BACKGROUND AND PURPOSE: The chronic cerebrospinal venous insufficiency hypothesis raises interest in cerebrospinal venous blood flow imaging, which is more complex and less established than in arteries. For accurate assessment of venous flow in chronic cerebrospinal venous insufficiency diagnosis and research, we must account for physiologic changes in flow patterns. This study examines day-to-day flow variability in cerebrospinal veins by use of 4D MR flow and contrast-enhanced MRA under typical, uncontrolled conditions in healthy individuals.

MATERIALS AND METHODS: Ten healthy volunteers were scanned in a test-retest fashion by use of a 4D flow MR imaging technique and contrast-enhanced MRA. Flow parameters obtained from phase contrast-vastly undersampled isotropic projection reconstruction and contrast-enhanced MRA scoring measurements in the head, neck, and chest veins were analyzed for internal consistency and interscan reproducibility.

RESULTS: Internal consistency was satisfied at the torcular herophili, with an input-output difference of 2.2%. Percentages of variations in flow were 20.3%, internal jugular vein; 20.4%, azygos vein; 6.8%, transverse sinus; and 5.1%, common carotid artery. Retrograde flow was found in the lower internal jugular vein (4.8%) and azygos vein (7.2%). Contrast-enhanced MRA interscan κ values for the internal jugular vein (left: 0.474, right: 0.366) and azygos vein (−0.053) showed poor interscan agreement.

CONCLUSIONS: Phase contrast–vastly undersampled isotropic projection reconstruction blood flow measurements are reliable and highly reproducible in intracranial veins and in the common carotid artery but not in veins of the neck (internal jugular vein) and chest (azygos vein) because of normal physiologic variation. Retrograde flow normally may be observed in the lower internal jugular vein and azygos vein. Low interrater agreement in contrast-enhanced MRA scans was observed. These findings have important implications for imaging diagnosis and experimental research of chronic cerebrospinal venous insufficiency.

ABBREVIATIONS: CCSVI = chronic cerebrospinal venous insufficiency; IJV = internal jugular vein; AV = azygos vein; PC-VIPR = phase contrast–vastly undersampled isotropic projection reconstruction; COM = conservation of mass; LOA = limits of agreement; CE = contrast-enhanced

In the hypothesis attributed to Zamboni et al[1] known as chronic cerebrospinal venous insufficiency (CCSVI),[1] obstructed venous outflow from the brain and spinal cord promotes tissue iron deposition that triggers the neuroinflammation characteristic of MS. Zamboni reported results of 100% sensitivity and specificity in distinguishing subjects with MS from non-MS subjects by use of cerebrospinal venous flow–specific criteria.[2] This hypothesis in the diagnosis and potential treatment of MS has increased interest in both intra- and extracranial venous flow measurements, namely in the deep cerebral veins, the internal jugular veins (IJVs), and the azygos vein (AV). In the wake of invasive venoplasty and "liberation" stent placement procedures being conducted and published results that are contrary to Zamboni's findings,[3,4] the CCSVI hypothesis has prompted much interest in the accuracy and reproducibility of cerebrospinal venous flow measurements, which have not yet been established.

The diagnosis of CCSVI uses duplex (gray-scale and color Doppler) ultrasonography. Intracranial arterial blood flow mea-

Received June 5, 2013; accepted after revision August 22.

From the Departments of Medical Physics (E.M.S., K.M.J., A.M.d.R., S.B.R., O.W.) and Radiology (J.H., S.B.R., A.F., O.W.), University of Wisconsin, Madison, Wisconsin.

Previously presented as "Reproducibility of Venous Luminography and Flow Quantification Related to the CCSVI Hypothesis" at: Annual Meeting of the International Society of Magnetic Resonance in Medicine, Melbourne, Australia, May 2012 and "Cerebrospinal Arterial and Venous Blood Flow Variability Assessed with 4D Flow MRI" at Annual Meeting of the ISMRM, Salt Lake City, Utah May 2013.

Grant support was provided by NMSS fund RC1003-A-one, NIH grant R01HL072260, and GE Healthcare.

Please address correspondence to Eric M. Schrauben, MS, 1122-P WIMR, Madison, WI 53705; e-mail: schrau24@gmail.com

Indicates open access to non-subscribers at www.ajnr.org

http://dx.doi.org/10.3174/ajnr.A3779

surements have well-known limitations including "acoustic window" issues and operator dependence. Special training for Zamboni's examination is required, and blinding of examiners to the disease status of subjects is difficult, potentially leading to study bias. MR can be implemented in the diagnosis of CCSVI to overcome these issues and is being used at some sites.[5] It has benefits compared with ultrasonography: it is established in MS diagnosis; acquires fewer user-dependent measurements with repeatable protocols from patient to patient; entire vessels can be assessed, including those inaccessible to sonography; and examiner bias can be removed through blinding. Drawbacks of MR imaging include non–real-time, electrocardiography-gated acquisitions that last several cardiac cycles, giving much lower temporal resolution compared with 2D ultrasonography. Additionally, all measurements must be conducted in the supine position, in which positional flow changes cannot be assessed.[2]

Phase contrast–vastly undersampled isotropic projection reconstruction (PC-VIPR)[6,7] is a 4D MR flow-sensitive technique that uses a 3D time-resolved radial acquisition scheme. The outer portions of *k*-space are undersampled, allowing for faster acquisition compared with a standard 3D Cartesian sampling scheme. Because of high image contrast and sparse signal representation, PC-VIPR has relatively benign undersampling artifacts that yield high temporal resolution capabilities, important in assessing blood velocity changes. PC-VIPR covers a large volume with high, isotropic spatial resolution. The acquisition allows for retrospective selection of flow analysis planes,[8] as detailed below. The accuracy and reproducibility of PC-VIPR has been established in arteries, specifically for velocity measurements in the carotid and cerebral arteries,[7] aorta,[9] liver,[10] and renal arteries[11] and for pulsatility in large cerebral arteries.[12] Venous PC-VIPR accuracy and reproducibility had yet to be investigated at the time of this study.

Although much has been made of potential diagnosis and treatment possibilities that CCSVI has to offer, relatively little effort has been made to investigate the reproducibility of venous blood flow measurements and luminography, especially by use of MR.[13] MR flow imaging and MRA have historically concentrated on arteries; therefore relatively little is known about the accuracy and reproducibility of venous flow assessment with phase-contrast MR and lumen assessment with MRA. Previous studies have shown that venous flow (particularly in the neck) is sensitive to body position,[14] head position/rotation,[15,16] respiratory state,[17] hydration level,[16] and other contributing factors.[14] Venous luminography is additionally difficult to accomplish because, unlike rigid, muscular arteries, veins have thin, nonmuscular walls that make for an easily compressible or distensible lumen.

The aims of this study were 3-fold: First, internal consistency of PC-VIPR venous blood flow measurements was evaluated in cerebral veins. Second, test-retest reproducibility of venous blood flow measurements by use of PC-VIPR was assessed in a healthy volunteer population and compared with arterial blood flow measurements. Finally, image quality and reproducibility of venous luminography by use of contrast-enhanced MRA (CE-MRA) were assessed.

MATERIALS AND METHODS

Experimental Subjects and Study Design

Under an institutional review board–approved protocol, 10 healthy adult volunteers (7 women; age, 36 ± 14 years) underwent anatomic CE-MRA and flow-sensitive (PC-VIPR) MR imaging on a 3T clinical scanner (Discovery MR750; GE Healthcare, Milwaukee, Wisconsin). Each subject was scanned twice on separate days in a test-retest fashion (14 ± 9 days between scans), yielding 10 matched pairs of acquired examinations. Subjects were selected to exclude any known vascular, neurologic, or psychiatric disorders.

Data Acquisition

A 3-station PC-VIPR examination was performed in the head, neck, and chest to obtain flow measurements in the cerebral veins, IJVs, and AV, respectively. To limit coil switching time, a high-definition 8-channel neurovascular coil (USA Instruments, Aurora, Ohio) was used for the head and neck scans. Cardiac triggers were recorded for retrospective cardiac gating. Sample MR imaging parameters for the PC-VIPR head scan were 3D radial free-breathing acquisition, TR = 15.9 ms, flip angle $\alpha = 25°$, FOV = $24 \times 24 \times 16$ cm^3, acquired spatial resolution = $(0.6\ \text{mm})^3$, 7:30 scan time. Similar parameters were used for the neck and chest scans; velocity encoding sensitization was set at 20 cm/s for the head and chest and 70 cm/s for the neck. These values were chosen to capture maximum possible velocities determined by test scans in the veins of interest in a healthy population. Because the purpose of this study was to examine the reproducibility of cerebrospinal venous blood flows under normal conditions, potential confounds were not controlled.

A 2-station CE-MRA neck and chest examination consisted of a single injection of gadofosveset trisodium (Ablavar; Lantheus Medical Imaging, North Billerica, Massachusetts) at a dose of 0.03–0.05 mmol/kg and rate of 3 mL/s. Ablavar binds to serum albumin, giving longer intravascular presence and allowing for a single injection to be used for all CE-MRA and PC-VIPR examinations. This requires less contrast volume than would be needed with the use of extravascular contrast agents.

Data Analysis

PC-VIPR datasets were reconstructed by use of a temporal filter as previously described for time-resolved CE-MRA with a 3D radial acquisition,[18] similar to view sharing in a Cartesian acquisition.[19] High frequency *k*-space contributions from neighboring timeframes increase the ability to visualize small vessels, but blood flow is captured almost entirely by low frequency and central *k*-space, collected during each TR with a radial acquisition. Twenty cardiac timeframes were reconstructed for each scan, giving velocity and magnitude images gated to the cardiac cycle. Temporal resolution is determined from the heart rate. For instance, a heart rate of 60 bpm gives 1 second per heartbeat divided by 20 frames per heartbeat or temporal resolution equal to 50 ms. Image sets were segmented by use of commercial software (Mimics; Materialise, Leuven, Belgium) and exported by use of an in-house magnitude and velocity conversion tool (Matlab; MathWorks, Natick, Massachusetts). Velocity data were then visualized (Ensight; CEI

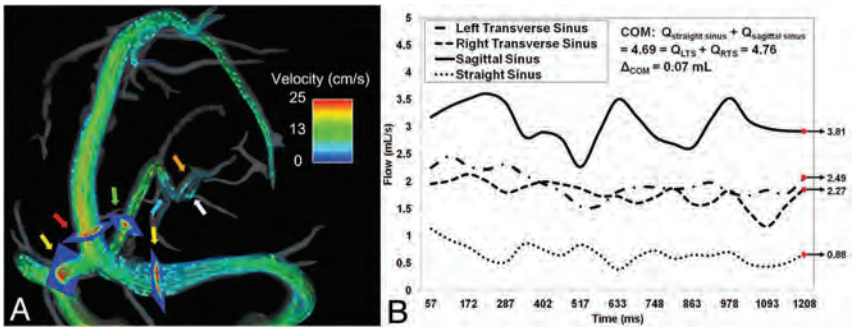

FIG 1. Example of flow visualization for COM (*A*). *Arrows*: yellow indicates left/right transverse sinus; red, sagittal sinus; green, straight sinus; blue, vein of Galen; internal cerebral veins: left (orange), right (white). Planes mark location of flow measurement. Blood flow waveforms (*B*) exemplify COM at the torcular herophili, with total flow measurements differing by only 0.37%.

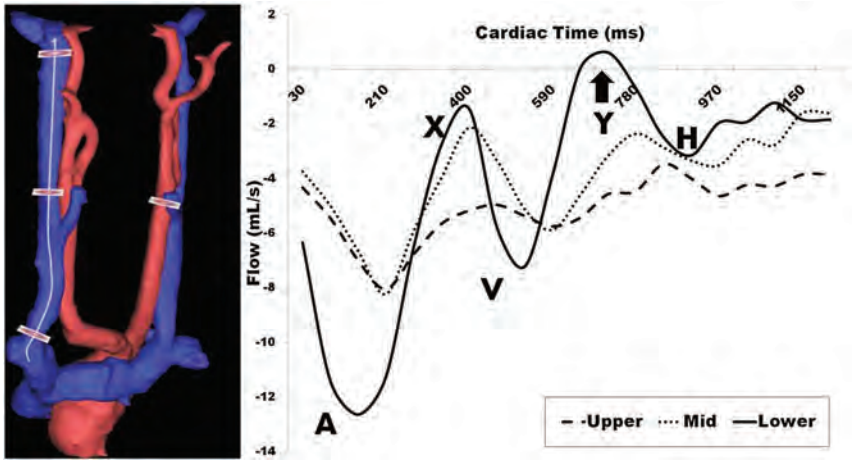

FIG 2. Left: Example placement of measurement planes in the right IJV down a centerline cubic spline and in the left common carotid artery. Right: Blood flow waveforms over the cardiac cycle indicate increasing pulsatility proximal to the heart, with a portion of the lower waveform showing retrograde flow (*arrow*). A indicates atrial systole; X, atrial relaxation; V, ventricular systole; Y, tricuspid reopening; H, atrial refilling.

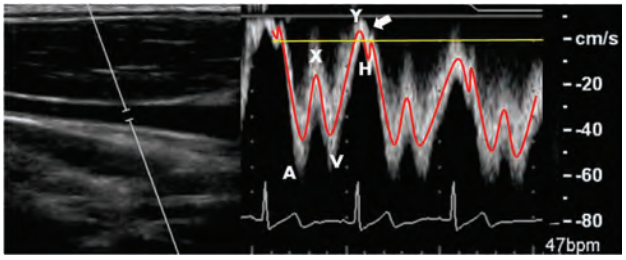

FIG 3. Left: B-mode anatomic location of right IJV blood flow. Right: Doppler ultrasonography displays triphasic IJV blood flow waveform as indicated in Fig 2. Arrow indicates minor normal reflux during the tricuspid valve reopening.

Software, Apex, North Carolina) and measured over the cardiac cycle[20] at specific 2D cut planes, retrospectively selected. PC-VIPR encodes velocity in 3D plus time, so that flow rate is integrated velocity within vessel area for a given cardiac timeframe. Vessel boundaries are hand-drawn over complex-difference 2D cut planes. To quantify reflux, percent retrograde flow (%RF) was calculated as total negatively directed flow (away from the heart) divided by total positively directed flow (toward the heart) over the cardiac cycle. Total flow (Q, in mL) was also calculated as the integration of flow rate over the cardiac cycle.

Cerebral Veins

As a test of internal consistency, a conservation of mass (COM) criterion was applied at the confluence of venous sinuses, or torcular herophili. COM requires that total flow entering and exiting the confluence must be equal. Figure 1*A* shows the placement of 2D cut planes used for these COM measurements: straight sinus, superior sagittal sinus, and left and right transverse sinuses (TS). Example blood flow waveforms for these 4 vessels are shown in Fig 1*B*. Thus, the COM formula to test becomes:

$$Q_{straight\ sinus} + Q_{sup.\ saggital\ sinus} = Q_{left\ TS} + Q_{right\ TS}$$

Twenty inflow and outflow measurements were compared to internally validate this equation, with mean percent difference between inflow and outflow averaged over all volunteers. Interscan reproducibility of Q in the same 4 veins was tested by use of Bland-Altman analysis.[21] A modification of Bland-Altman analysis accounting for repeated measurements within a subject was used for limits of agreement (LOA) calculations. The modification sums the between-subjects and within-subject variances to find single differences between pairs of measurements, slightly increasing the LOA. Finally, %RF over the cardiac cycle was determined for the same 4 veins as well as for the visualized deep cerebral veins.

Internal Jugular Veins

IJV flow measurement reproducibility was assessed. Similar to the analysis performed by Haacke (ms-mri.com), 3 measurement planes were placed along the length of a centerline cubic spline. Measurements were taken at the level just below the jugular bulb (upper), at the midpoint of the spline (mid), and just above the IJV junction with the subclavian vein (lower). An example 3D rendering and placement of planes along the spline are shown in Fig 2 (left). Interscan Bland-Altman 95% LOA and biases across all levels and volunteers were calculated. Figure 2 (right) shows sample IJV blood flow waveforms for each location (left), with detection of retrograde flow in the lower measurement plane. Comparing this lower waveform with a Doppler ultrasound–acquired jugular flow waveform (Fig 3), PC-VIPR is capable of resolving, both spatially and temporally, the triphasic flow waveform typical in the IJV.

Azygos Vein

As the primary outflow route of blood from the spinal cord in the upright position, Zamboni considered the detection of narrowing in the AV by use of invasive venography to be an inherent corol-

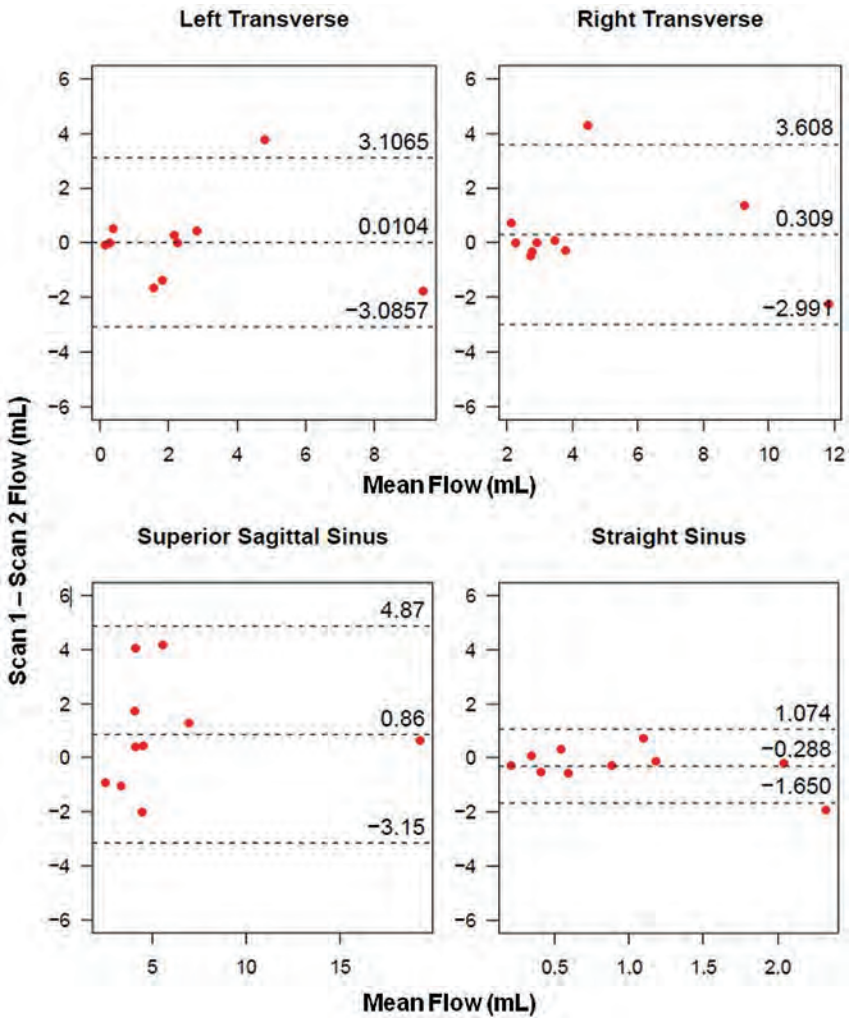

FIG 4. Interscan Bland-Altman plots for cerebral vein analysis within individual veins. Small biases and LOA indicate reproducibility of PC-VIPR in assessment of cerebral venous flow.

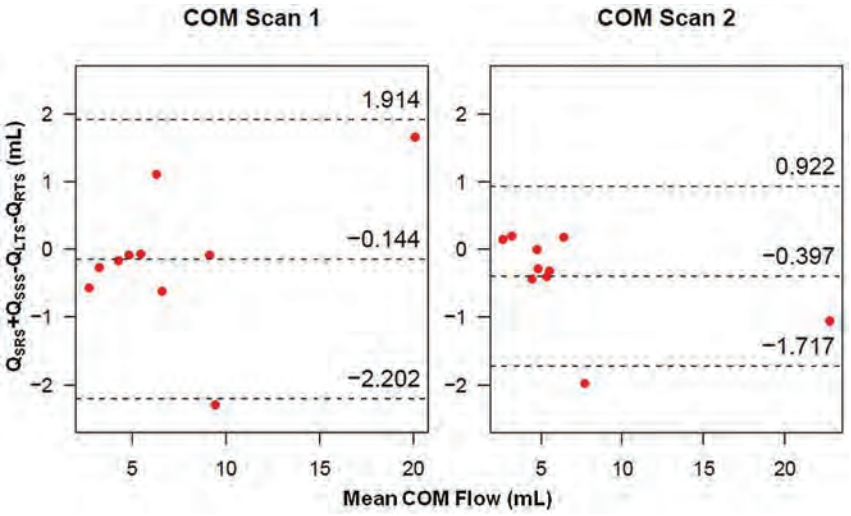

FIG 5. Bland-Altman plots of COM analysis for scan 1 (left) and scan 2 (right), showing small biases and LOA.

lary of CCSVI.[1] From the chest PC-VIPR scan, measurements of %RF were taken 2 cm from the AV junction with the superior vena cava and were compared between scans within each volunteer.

Venous/Arterial Comparison

To compare blood flow changes from one scan to the next throughout the cerebrospinal venous system, Q was measured in several locations: transverse sinuses, upper and lower IJV, and AV. To summarize flow in the cerebrospinal venous system, total flows were added from left and right transverse sinus and IJVs, providing total venous drainage at a single axial location. Flows through the common left and right carotid arteries were similarly analyzed to compare arterial and venous flow reproducibility across all volunteers. Percent change, calculated as interscan difference in total flow normalized to scan one flow, was calculated at all locations. Average percent difference between scans and paired *t* test *P* values were calculated across all volunteers.

Contrast-Enhanced MRA

To assess the reproducibility of semiquantitative assessments of venous caliber, CE-MRAs were scored by 2 experienced radiologists blinded to subject identity, date/sequence of scan, and each other's scores. The scoring followed the scale introduced by Zivadinov et al[23]: ability to assess the IJV and AV (1, poor; 2, acceptable; 3, good; 4, excellent), AV morphology (1, diffusely irregular/narrowed; 2, focally narrowed at central aspect; 3, caliber increasing from peripheral to central), and IJV morphology at its narrowest point (1, absent; 2, pinpoint; 3, flattened; 4, crescentic; 5, ellipsoidal/round). Cohen κ with linear weights was used to assess agreement between ratings in scan 1 and scan 2 (with both readers combined) and between readers (both scans combined). Kappa values were computed by means of the irr package, R statistical computing software (http://www.r-project.org/).

RESULTS

Cerebral Veins

Bland-Altman plots of cerebral venous flow measurements between scans within an individual volunteer and for individual vessels are shown in Fig 4. Interscan LOA for Q across all 20 scans (40 vessels) were small with respect to the mean (−2.924, 3.369 mL). Figure 5 displays Bland-Altman plots for COM analysis. Pooled COM LOA across both scans were also small (−1.985, 1.443 mL), with the average percent difference between inflow and outflow equal to 2.2%. All visualized deep cerebral veins and large cerebral veins (Fig 1) yielded zero retrograde flow (%RF = 0).

Table 1: Total flow (mL/cardiac cycle), delineated by side, measurement level, and scan, in all volunteers

	Left IJV						Right IJV					
	Upper		Mid		Lower		Upper		Mid		Lower	
Volunteer	S1	S2	S1	S2	S1	S2	S1	S2	S1	S2	S1	S2
1	0	0	0	0	0	0	1.90	8.36	2.00	7.15	3.95	3.07
2	4.36	4.42	4.45	2.80	4.63	4.11	6.03	6.40	4.56	3.34	9.59	8.47
3	3.35	2.63	4.39	1.41	1.99	0.31	0	0	0	0	0	0
4	2.09	2.82	0.80	3.34	2.14	3.70	3.40	3.02	2.99	6.53	2.78	8.75
5	3.89	2.03	1.84	1.74	2.46	1.09	2.37	0.46	2.73	1.86	1.47	0.37
6	1.00	1.68	0.98	1.44	2.26	2.82	3.53	5.37	2.90	4.27	1.39	3.48
7	0.49	0.46	0.82	0.33	0.57	0.50	6.35	4.31	4.91	2.82	5.25	3.63
8	4.18	4.77	3.60	4.01	2.95	4.24	4.54	5.39	3.42	5.72	2.69	5.53
9	2.87	0.74	2.54	1.14	0.64	0.34	0	0	0	0	0	0
10	3.09	3.25	2.60	2.59	1.03	0.99	3.99	3.33	3.75	2.35	1.28	1.19
Average/Max %RF	0.79/6.15		2.98/14.39		6.02/24.59		0.30/4.83		1.19/12.31		3.52/29.46	

Note:—Average and maximum retrograde flow percentages are presented (bottom row).

Internal Jugular Veins

Measurements of Q at the 3 measurement planes along the length of each IJV are presented in Table 1. "Zeroes" indicate no (or negligible) detection of flow. Large differences can be observed within single volunteers between scans. Asymmetric flow patterns were observed, with complete side dominance in volunteers 1, 3, and 9. Average and peak %RF calculations over all volunteers are shown (bottom row). Both increase as blood nears the heart. Bland-Altman analysis across all measurement planes yielded interscan large LOA in the left IJV (−2.06, 2.48 mL, bias: 0.21 mL) and in the right IJV (−5.08, 3.92 mL, bias: −0.58 mL). Interscan LOA for %RF in the left IJV were −14.187, 13.023%, bias: −0.58%; and in the right IJV were −10.130, 9.143%, bias: −0.49%. Large LOA relative to the mean are observed, indicating high variability between scan 1 and scan 2 and across all measurement locations.

Azygos Vein

For both scan 1 and scan 2, we were unable to visualize the AV for volunteers 8 and 10. From the remaining 16 measurements, 10 had significant (>1%) retrograde flow. The average detected %RF among the 8 visualized veins was 7.2%.

Venous/Arterial Comparison

Figure 6 includes boxplots of Q, with average percent differences from scan 1 to scan 2. Day-to-day variation in flow in the common carotid artery as measured by PC-VIPR is low (5.1 ± 4.2%). The venous flow measurements in the IJV and AV show much larger variations, whereas variations in the transverse sinus are comparable to those in the common carotid artery (6.8 ± 7.6%). Figure 7 displays percent change in total flows across all head/neck/chest veins and volunteers. Eight of 10 volunteers exhibited similar changes (increase/positive or decrease/negative) for 3 of the 4 venous flow measurements.

Contrast-Enhanced MRA

Scoring average for all acquired scores and Cohen κ for the blinded radiologist scoring of the CE-MRA are presented in Table 2. Higher variations for morphology scores are observed. Interscan results pooled for both radiologists indicate fair agreement for left IJV and right IJV morphology and slight to no agreement for the other 3 scores. Interrater results pooled for all scans show slight to no agreement across all scores.

DISCUSSION

Although it is well known that phase-contrast MRA has intravoxel dephasing because of the relatively long TE used,[24] PC-VIPR has isotropic resolution and small voxels. This allows for flow visualization and quantification in the cerebral venous system, including the relatively small deep cerebral veins such as the internal cerebral veins, as demonstrated in Fig 1. With PC-VIPR, the user can retrospectively select vessels to interrogate, unlike traditional MRV methods that require selecting a limited subset of vessels a priori. Sample cerebral venous flow waveforms in Fig 1*B* satisfy COM over the cardiac cycle. Waveforms show little variation through time, indicating low pulsatility far from the heart in the cerebral veins. This work confirms earlier 2D phase-contrast MR work in the cerebral veins performed by Stoquart-El Sankari et al.[25] The lack of retrograde flow in all deep cerebral veins and intracranial veins substantiates the work of Wattjes et al,[26] in which 2D phase-contrast MR was used to measure flow in the straight sinus and internal cerebral veins in both healthy control subjects and patients with MS.

From Bland-Altman analysis in each cerebral vessel (Fig 4), biases fall near the difference of zero, indicating that no consistent bias from the 2 independent measurements of vessel flow was detected. Tight interscan LOA with respect to mean values across all vessels provide evidence of reproducibility in PC-VIPR measurements of cerebral venous blood flow. In the Bland-Altman COM analysis (Fig 5), small interscan difference in cerebral vessels (2.2%) and tight LOA are further evidence of reproducibility of intracranial venous blood flow measurements by use of PC-VIPR. To our knowledge, this validation of internal consistency by use of a COM test is the first of its kind in venous vasculature by use of PC-VIPR. It points to the use of PC-VIPR as a reliable measurement tool for venous blood flow. Our findings indicate minimal day-to-day effect on the reproducibility of intracranial venous flow. This may be useful in future CCSVI studies or in other venous blood flow–related pathologies such as cerebral venous sinus thrombosis or idiopathic intracranial hypertension.

The tortuous and varied nature of the IJV causes difficulty in measuring blood flow at various locations along its length. PC-VIPR is ideal as a 4D flow measurement tool for this vascular territory. Figure 2 (left) demonstrates the use of a centerline cubic spline in the placement of measurement planes, permitting measurements orthogonal to the expected direction of flow. Figure 2

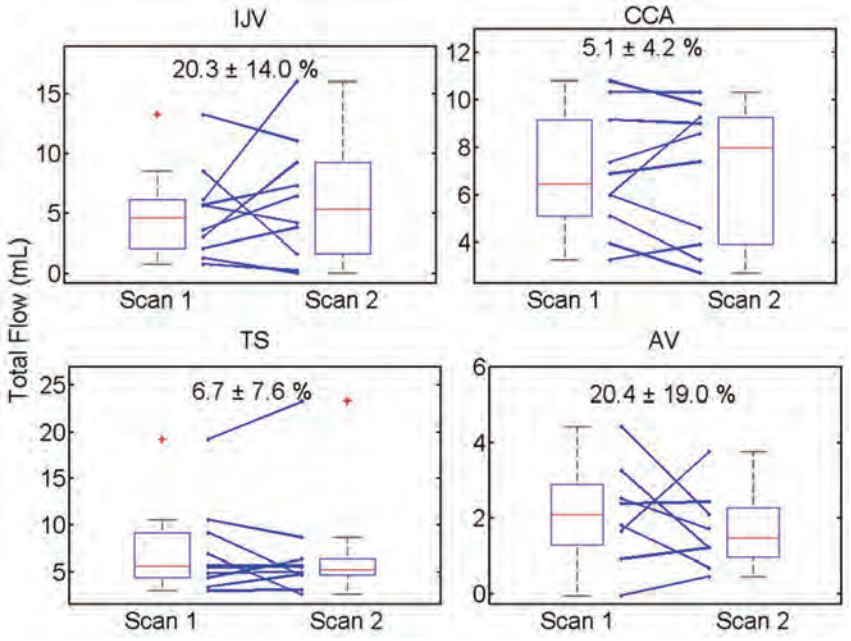

FIG 6. Boxplot results for all measurement locations. Individual changes (*blue lines*) show high variation in both the IJV and AV from scan to scan. No differences were considered significant ($P < .05$).

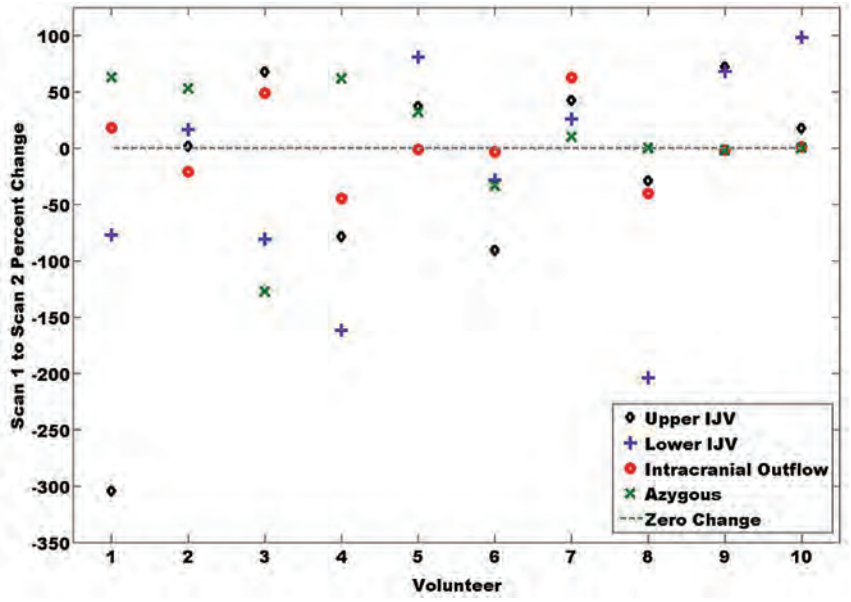

FIG 7. Percent change in total flow from scan 1 to scan 2 across volunteers. Volunteers 5–10 have similar directional changes in all measurements.

(right) reveals differing pulsatility that axial locations along the IJV exhibit. Each flow waveform is triphasic in nature. As we move closer toward the beating heart, and incidentally to locations in which the IJV is adjacent to and often physically touching the common carotid artery, the IJV exhibits greater pulsatility. The lower waveform of Fig 2 (right) exhibits retrograde flow over a short period of the cardiac cycle. The triphasic waveform is expected, corresponding to variations in carotid pulsatile motion.[27] An independent Doppler ultrasonographic examination of the jugular vein (Fig 3) confirms the triphasic waveform and minor retrograde flow seen in a healthy volunteer.

In analyzing %RF over the cardiac cycle (Table 1, bottom row), average and peak values increase as we measure in the superior to inferior direction. This larger %RF is in part caused by the greater pulsatility observed in "lower" measurement planes across and may reflect a normal result of greater oscillations in blood flow proximal to the beating heart. Larger %RF and slow flow also factor into Q values for a given axial location within a single IJV. We see a general lack of consistency within subject and between scan locations as a result of varying %RF and territories with slow flow, both appreciably affecting Q calculations. Other factors may contribute to retrograde flow seen in a healthy population, such as IJV valve incompetence.[28] Despite this finding, most measurement planes had less than 1% retrograde flow for all locations (81/120), indicating the strong tendency of constantly anterograde blood flow.

Table 1 illustrates the wide variance of Q values and varying side dominance in the IJV in a healthy control population, confirming earlier work[29] including flow measured by MR imaging.[25] The unpredictable nature of venous anatomy and blood flow characteristics are relevant because they convey difficulties that are likely to be encountered in clinical situations. Considering the variables that were not accounted for in this study, the interscan heterogeneity within a volunteer should be expected. These results are contrary to a previous work in ultrasonography[30] yet agree with a 3D MRV study.[26] This work points to the need for controlling of variables that may affect venous return.

The Bland-Altman results for the IJVs indicate that there are no systematic differences between test occasions. The small biases (left: 0.209, right: −0.58) between scans again lend support to the reproducibility of PC-VIPR; however, skewed distribution in the data indicate that IJV flow is not repeatable within subjects. Error proportional to the mean was observed in the interscan %RF Bland-Altman analysis.

In the AV, high variability in %RF was seen. AV visualization by means of PC-VIPR is difficult because of cardiorespiratory-induced motion. Of the 20 chest PC-VIPR scans taken, the AV was reliably visualized 80% of the time. The significant average %RF (7%) additionally suggests that retrograde flow may be a normal supine attribute of the AV measured 2 cm from its junction with the superior vena cava. This noninvasive probing of AV flow exemplifies another benefit of the use of PC-VIPR.

Table 2: Average (± standard deviation) scores from CE-MRA from both radiologists and across all scans

	IJV Image Quality	Left IJV Morphology	Right IJV Morphology	AV Image Quality	AV Morphology
Scoring, average ± standard deviation	3.70 ± 0.56	2.93 ± 1.00	3.40 ± 1.26	3.08 ± 0.89	2.95 ± 0.22
Interscan κ	−0.064	0.474	0.366	0.202	−0.053
Interrater κ	−0.042	−0.055	0.281	0.104	–

Note:—Interscan and interrater agreement is slight or nonexistent across scoring; κ <0 indicates no agreement; 0–0.20, slight; 0.21–0.40, fair; 0.41–0.60, moderate; 0.61–0.80, substantial; 0.81–1, almost perfect.

Individual variations of flow exhibited on the boxplots (Fig 6) reveal consistency in common carotid artery flow from one scan to the next while also showing the many varied venous changes. Low arterial variation (5.1 ± 4.2%) confirms both physiologic reproducibility of arterial flow and technical reproducibility of PC-VIPR. Small variation (6.8 ± 7.6%) was also observed in the transverse sinuses. In contrast, large variations in neck and chest venous flow (>20%) were observed, probably resulting from interscan physiologic changes. Whereas total venous outflow from the brain does not change, alternative drainage pathways probably arise for a certain physiologic state.[25] Figure 7 confirms these changes systemically affecting cerebrospinal venous blood flow. The number of similar, one-sided changes across veins indicate a physiologic (ie, not technical) change. These results strongly point to the necessity of controlling for venous flow-altering variables.

The scoring results from the CE-MRA analysis (Table 2) indicate good image quality for both the IJV and AV, with higher values for IJV (3.70 ± 0.56 versus 3.08 ± 0.89). This probably is a result of the mitigating motion in the chest during prospectively gated respiratory examinations versus the stationary neck examinations. AV caliber increased as it neared the junction with the superior vena cava. Turbulent flow from the much larger superior vena cava naturally increases the venous lumen in the AV near its junction with the superior vena cava. Left and right IJV morphology scores had higher variances and averaged to a flattened or crescentic appearance (3.0 ± 1.1 and 3.7 ± 1.3). Single volunteer variation is again corroborated by observing the low agreement from the interscan κ values. Low interrater agreement in the presence of good image quality points to a lack of reproducible identification of IJV and AV morphology, in large part caused by the varied sizes and shapes of venous structures across a healthy population.

This study is not without its limitations. First, for the sake of simplicity in measuring and presentation of data, vertebral veins were not included. Second, although our larger CCSVI study collects both ultrasonographic and PC-VIPR scans, this study did not use ultrasonography as a reference standard. The method of acquisition further limited the study not to investigate the "forced exhalation" that Zamboni uses to determine retrograde flow. This was planned because this study aimed to determine changes occurring in the cerebrospinal venous system under a normal physiologic state. Third, some of the chest scans and resulting AV image quality were poor. This is a direct result of respiratory motion effects purposefully not accounted for in each of the PC-VIPR scans. Fourth, to mitigate on the table scan time (and number of breath-holds) for each volunteer, Venc optimization scans were not performed before PC-VIPR scans. Although no phase aliasing was observed for any of the 60 PC-VIPR scans, low velocity in some of the IJVs caused both image quality- and the velocity-to-noise ratio to suffer, which would have been improved with a lower Venc setting. Finally, despite good image quality, CE-MRA results from this study differ from extracranial venous scoring by McTaggart et al,[31] in which a linearly increasing flattening scale[32] was used to assess the IJV caliber. Our semi-quantitative approach to venous lumen morphology, though borrowed from the literature, made decisions between available choices difficult. This may have led to poor interobserver and interscan agreement (Table 2), explaining the difference between this study's results and those of McTaggart et al. These results indicate that for venous CE-MRA to be valuable in assessing the CCSVI hypothesis, a set scoring system must be in place.

CONCLUSIONS

The use of PC-VIPR as a reliable measurement tool for venous flow has been demonstrated. Intracranial veins showed day-to-day reproducibility on the order of arteries. Normal venous flow in the neck (IJV) and chest (AV) has been shown to be much more variable, presumably because of confounding variables related to normal cardiorespiratory and positional effects that are dampened in the intracranial veins. The detection of retrograde flow has been shown to be a normal finding in the lower IJV and AV of healthy volunteers. CE-MRA scoring interrater agreement was low, indicating a need for a robust venous scoring system with added information gained through flow measurements. These findings have important implications in CCSVI in which normal variation in venous flow may be construed as diagnostically relevant.

Disclosure: Eric Schrauben—*RELATED: Other:* University of Wisconson-Madison Radiology R and D,* Comments: Study funded by the UW-Madison's Radiology Research and Development Funding. Kevin M. Johnson—*RELATED: Grant:* Multiple Sclerosis Society.* Alejandro Munoz del Rio—*RELATED: Grant:* National Multiple Sclerosis Society,* Comments: http://www.nationalmssociety.org/research/intriguing-leads-on-the-horizon/ccsvi/ccsvi-study-by-field-team/index.aspx; *UNRELATED: Consultancy:* Lippincott Williams & Wilkins, Comments: LWW publish *Annals of Surgery*, for which I am a statistical reviewer; *Grants/Grants Pending:* NIH, UW-Madison (Wisconsin Alumni Research Foundation), Comments: I am listed on several federally-funded research grants as a biostatistician. Aaron Field—*RELATED: Grant:* National Multiple Sclerosis Society,* Comments: Research grant (PI: Field). Oliver Wieben—*RELATED: Other:* GE Healthcare,* Comments: Research support from GE Healthcare.

REFERENCES

1. Zamboni P, Galeotti R, Menegatti E, et al. **Chronic cerebrospinal venous insufficiency in patients with multiple sclerosis.** *J Neurol Neurosurg Psychiatry* 2009;80:392–99
2. Zamboni P, Galeotti R. **The chronic cerebrospinal venous insufficiency syndrome.** *Phlebology* 2010;25:269–79
3. Baracchini C, Perini P, Causin F, et al. **Progressive multiple sclerosis is not associated with chronic cerebrospinal venous insufficiency.** *Neurology* 2011;77:844–50

4. Centonze D, Floris R, Stefanini M, et al. **Proposed chronic cerebrospinal venous insufficiency criteria do not predict multiple sclerosis risk or severity.** *Ann Neurol* 2011;70:51–58
5. Utriainen D, Feng W, Elias S, et al. **Using magnetic resonance imaging as a means to study chronic cerebral spinal venous insufficiency in multiple sclerosis patients.** *Tech Vasc Interv Radiol* 2012;15: 101–12
6. Johnson KM, Lum DP, Turski PA, et al. **Improved 3D phase contrast MRI with off-resonance corrected dual echo VIPR.** *Magn Reson Med* 2008;60:1329–36
7. Gu T, Korosec FR, Block WF, et al. **PC VIPR: a high-speed 3D phase-contrast method for flow quantification and high-resolution angiography.** *AJNR Am J Neuroradiol* 2005;26:743–49
8. Markl M, Frydrychowicz A, Kozerke S, et al. **4D flow MRI.** *J Magn Reson Imaging* 2012;36:1015–36
9. Frydrychowicz A, Niespodzany E, Reeder SB, et al. **Validation of 4D velocity mapping using 5-point PC-VIPR for blood flow quantification in the thoracic aorta and main pulmonary artery.** In: *Proceedings of the American Society of Neuroradiology 50th Annual Meeting Meeting & the Foundation of the ASNR Symposium*, New York, New York. April 21–26, 2012
10. Roldan-Alzate A, Frydrychowicz A, Niespodzany E, et al. **In vivo validation of 4D flow MRI for assessing the hemodynamics of portal hypertension.** *J Magn Reson Imaging* 2013;37:1100–08
11. Wentland AL, Grist TM, Wieben O. **Repeatability and internal consistency of abdominal 2D and 4D PC MR flow measurements.** In: *15th Annual SCMR Scientific Sessions.* 2012. Orlando, Florida
12. Wahlin A, Ambarki K, Birgander R, et al. **Measuring pulsatile flow in cerebral arteries using 4D phase-contrast MR imaging.** *AJNR Am J Neuroradiol* 2013;34:1740–45
13. Menegatti E, Genova V, Tessari M, et al. **The reproducibility of colour Doppler in chronic cerebrospinal venous insufficiency associated with multiple sclerosis.** *Int Angiol* 2010;29:121–26
14. Klabunde RE. *Cardiovascular Physiology Concepts.* 2nd ed. Philadelphia: Lippincott Williams & Wilkins/Wolters Kluwer; 2012:243
15. Khatri VP, Wagner-Sevy S, Espinosa MH, et al. **The internal jugular vein maintains its regional anatomy and patency after carotid endarterectomy: a prospective study.** *Ann Surg* 2001;233:282–86
16. Lu M, Raber L, Baus L, et al. **Ultrasound evaluations of chronic cerebrospinal venous insufficiency (CCSVI): important factors to consider.** In: *AAN Annual Meeting.* 2011. Honolulu, Hawaii
17. Nordenstrom B, Norhagen A. **Effect of respiration on venous return to the heart.** *Am J Roentgenol Radium Ther Nucl Med* 1965;95:655–61
18. Barger AV, Block WF, Toropov Y, et al. **Time-resolved contrast-enhanced imaging with isotropic resolution and broad coverage using an undersampled 3D projection trajectory.** *Magn Reson Med* 2002;48:297–305
19. Markl M, J Hennig J. **Phase contrast MRI with improved temporal resolution by view sharing: k-space related velocity mapping properties.** *Magn Reson Imaging* 2001;19:669–76
20. Stalder AF, Russe MF, Frydrychowicz A, et al. **Quantitative 2D and 3D phase contrast MRI: optimized analysis of blood flow and vessel wall parameters.** *Magn Reson Med* 2008;60:1218–31
21. Bland JM, Altman DG. **Agreement between methods of measurement with multiple observations per individual.** *J Biopharmaceutical Stat* 2007;17:571–82
22. Feng W, Utriainen D, Trifan G, et al. **Characteristics of flow through the internal jugular veins at cervical C2/C3 and C5/C6 levels for multiple sclerosis patients using MR phase contrast imaging.** *Neurol Res* 2012;34:802–09
23. Zivadinov R, Marr K, Cutter G, et al. **Prevalence, sensitivity, and specificity of chronic cerebrospinal venous insufficiency in MS.** *Neurology* 2011;77:138–44
24. Kim AC, Vu DG, Gonzalez RG, et al. **Conventional MRI and MR angiography of stroke.** In: *Acute Ischemic Stroke: Imaging and Intervention.* Springer-Verlag, Heidelberg, Germany 2011:123–44
25. Stoquart-Elsankari S, Legmann P, Villette A, et al. **A phase-contrast MRI study of physiologic cerebral venous flow.** *J Cereb Blood Flow Metab* 2009;29:1208–15
26. Wattjes MP, van Oosten VW, de Graaf WL, et al. **No association of abnormal cranial venous drainage with multiple sclerosis: a magnetic resonance venography and flow-quantification study.** *J Neurol Neurosurg Psychiatry* 2011;82:429–35
27. Garg N, Garg N. **Jugular venous pulse: an appraisal.** *Ind Acad Clin Med* 2000;1:260–69
28. Lin SK, Chang YJ, Yang FY. **Hemodynamics of the internal jugular vein: an ultrasonographic study.** *Tzu Chin Med J* 2009;21:317–22
29. Chung CP, Hsu HY, Chao AC, et al. **Flow volume in the jugular vein and related hemodynamics in the branches of the jugular vein.** *Ultrasound Med Biol* 2007;33:500–05
30. De Diego JI, Prim MP, Garcia-Raya P, et al. **Reproducibility of ultrasonographic measures in internal jugular veins of normal subjects.** *Auris Nasus Larynx* 2001;28:71–74
31. McTaggart RA, Fischbein NJ, Elkins CJ, et al. **Extracranial venous drainage patterns in patients with multiple sclerosis and healthy controls.** *AJNR Am J Neuroradiol* 2012;33:1615–20
32. Zaharchuk G, Fischbein NJ, Rosenberg J, et al. **Comparison of MR and contrast venography of the cervical venous system in multiple sclerosis.** *AJNR Am J Neuroradiol* 2011;32:1482–89

Cerebral Veins—Why Functional MR Imaging is Worth the Trouble

The incidence of multiple sclerosis in North America is approximately 5/100,000, and the peak of onset is 30 years of age. Hence, MS is one of the most frequent chronic neurologic diseases and the leading cause of disability in young and middle-aged individuals in the developed world.[1] Strategies to prevent, treat, or even cure MS are of the highest interest. Accordingly, the reintroduction of the chronic cerebrospinal venous insufficiency (CCSVI) hypothesis by Zamboni in 2006[2] has attracted enormous attention. Successive sonography and conventional angiography studies of intracranial, cervical, and thoracic veins in patients have suggested that there is a strong, previously unconsidered relationship between individual pathologic blood flow of extracranial veins and MS.[3] Moreover, consecutive publications have suggested that the so-called "liberation procedure" performed by percutaneous transluminal angioplasty in venous stenosis could, by improving individual hemodynamics, influence disease progression and thus offer a completely new approach for the treatment of multiple sclerosis.[4]

Unfortunately, correlations reported by one research group[2-4] were not reproducible by others by using venous sonography[5,6] or MR imaging.[7,8] This discrepancy has created reasonable doubts regarding the methodology used by Zamboni[2] and regarding the pathophysiologic concept of CCSVI.[9] 2D high-resolution sonography is ideally suited to study blood flow in extra- and intracranial veins.[10,11] It is limited due to the 2-dimensionality and operator dependency and requires a high level of experience and an adequate bone window for transcranial Doppler sonography. However, sonography allows a very accurate visualization and quantification of venous blood flow in both a supine or upright position and during free breathing or a Valsalva maneuver. Potential measurement errors can occur due to insufficient visualization of intracranial veins, insufficient angle correction, and compression of the extracranial veins by the sonography probe and are discussed in detail by Valdueza et al.[9]

MR imaging has the potential to overcome these limitations. However, previous MR venography studies were hampered by their low specificity: Extracranial large veins may collapse with the patient in a supine position and consequently lead to stenosis or occlusions in MR angiography, which is physiologic and only temporary.[12,13] In the current issue of the *American Journal of Neuroradiology,* Schrauben et al[14] evaluate the accuracy and reproducibility of blood flow analysis by using MR imaging in both intra- and extracranial veins in 10 healthy volunteers. They used both contrast-enhanced MR angiography and 3D phase-contrast MR imaging with 3D velocity-encoding. The latter technique (phase contrast with vastly undersampled isotropic projection reconstruction [PC-VIPR]) allows a time-resolved measurement of blood flow in vivo and 3D visualization and quantification of blood flow patterns, velocities, and flow. It is similar to another flow-sensitive MR angiography (4D flow MR imaging) that has been successfully applied to study blood flow within intracranial arteries,[15] carotid arteries,[16] and liver veins,[17] but not yet within the veins of the neck and head.

The current study of Schrauben et al[14] convincingly shows the feasibility of this MR imaging technique for the assessment of these vessels. It reveals plausible flow patterns that are familiar from sonographic examinations and accurate quantification of blood flow in the transverse sinus. In addition, tests for the "conservation of mass" at the confluence of the sinuses underscore this plausibility by demonstrating that blood flow in the draining proximal right and left transverse sinuses was very similar to blood flow in the supplying superior sagittal and straight sinuses. However, findings were limited if deep cerebral veins were evaluated in repeat MR imaging examinations; this limitation is probably due to the diameter of only ~2 mm in these vessels. In addition, results of PC-VIPR of the extracranial internal jugular and azygos veins showed strong day-to-day variations. Comparable with a previous MR venography study,[12] the accuracy of contrast-enhanced MR angiography of neck and thoracic veins in the study of Schrauben et al was low. Accordingly, the impact of MR angiography seems to be limited for the assessment of extracranial veins.

However, the strength of flow-sensitive MR angiography is the ability to evaluate blood flow in intracranial large and small veins. MR imaging provides the unique advantage of visualizing and quantifying blood flow in the superior sagittal sinus and in the superficial bridging veins that are hardly or not at all assessable by sonography due to the lack of a sufficient bone window.[10] Ac-

cordingly, little is known about physiologic flow or about pathologic changes at these sites in patients with acute brain edema, traumatic brain injury, sinus thrombosis, or idiopathic intracranial hypertension. A comparison with sonography in reliably accessible vessels such as the transverse sinus[10] or with high-resolution 2D phase-conventional angiography[8] as the reference method is a prerequisite before this MR imaging technique can be used in trials or in clinical routine. In particular, accurate quantification of blood flow in small cerebral veins (ie, straight sinus, internal cerebral veins, basal veins, and the vein of Galen) is challenging and requires a spatial resolution of <0.25 mm^3.

At present, to our knowledge, there is no evidence from high-level randomized controlled trials (RCTs) that has proved the value and safety of percutaneous transluminal venous angioplasty for the treatment of multiple sclerosis.[18] Patients with multiple sclerosis are typically young and closely follow new developments in diagnosis and treatment. Many are very open to undergoing experimental therapies to prevent further progression of disability, even if the efficacy has not yet been proved and if they potentially expose themselves to serious adverse effects. Due to the recent experience from several promising trials that have finally failed to show a benefit of interventional compared with medical treatment,[19-21] patients with multiple sclerosis should not be treated by venous angioplasty unless the 6 ongoing RCTs prove a clear benefit.[18] Until then, they should consistently receive established (eg, interferons, glatiramer acetate) or newer and more potent drugs (eg, natalizumab, fingolimod, fumaric acid) that have already proved their efficacy and safety in large RCTs.

REFERENCES

1. Koch-Henriksen N, Sørensen PS. **The changing demographic pattern of multiple sclerosis epidemiology.** *Lancet Neurol* 2010;9:520–32
2. Zamboni P. **The big idea: iron-dependent inflammation in venous disease and proposed parallels in multiple sclerosis.** *J R Soc Med* 2006;99:589–93
3. Zamboni P, Galeotti R, Menegatti E, et al. **Chronic cerebrospinal venous insufficiency in patients with multiple sclerosis.** *J Neurol Neurosurg Psychiatry* 2009;80:392–99
4. Zamboni P, Galeotti R, Menegatti E, et al. **A prospective open-label study of endovascular treatment of chronic cerebrospinal venous insufficiency.** *J Vasc Surg* 2009;50:1348–58.e1–3
5. Doepp F, Paul F, Valdueza JM, et al. **No cerebrocervical venous congestion in patients with multiple sclerosis.** *Ann Neurol* 2010;68:173–83
6. Tsivgoulis G, Mantatzis M, Bogiatzi C, et al. **Extracranial venous hemodynamics in multiple sclerosis: a case-control study.** *Neurology* 2011;77:1241–45
7. Sundström P, Wåhlin A, Ambarki K, et al. **Venous and cerebrospinal fluid flow in multiple sclerosis: a case control study.** *Ann Neurol* 2010;68:255–59
8. Wattjes MP, van Oosten BW, de Graaf WL, et al. **No association of abnormal cranial venous drainage with multiple sclerosis: a magnetic resonance venography and flow-quantification study.** *J Neurol Neurosurg Psychiatry* 2011;82:429–35
9. Valdueza JM, Doepp F, Schreiber SJ, et al. **What went wrong? The flawed concept of cerebrospinal venous insufficiency.** *J Cereb Blood Flow Metab* 2013;33:657–68
10. Stolz E, Kaps M, Kern A, et al. **Transcranial color-coded duplex sonography of intracranial veins and sinuses in adults: reference data from 130 volunteers.** *Stroke* 1999;30:1070–75
11. Schreiber SJ, Doepp F, Klingebiel R, et al. **Internal jugular vein valve incompetence and intracranial venous anatomy in transient global amnesia.** *J Neurol Neurosurg Psychiatry* 2005;76:509–13
12. Zivadinov R, Galeotti R, Hojnacki D, et al. **Value of MR venography for the detection of jugular vein abnormalities in multiple sclerosis: a pilot longitudinal study.** *AJNR Am J Neuroradiol* 2011;32:938–46
13. Niggemann P, Seifert M, Förg A, et al. **Positional venous MR angiography: an operator-independent tool to evaluate cerebral venous outflow hemodynamics.** *AJNR Am J Neuroradiol* 2012;33:246–51
14. Schrauben EM, Johnson KM, Huston J, et al. **Reproducibility of cerebrospinal venous blood flow and vessel anatomy with the use of phase-contrast–vastly undersampled isotropic projection reconstruction and contrast-enhanced MRA.** *AJNR Am J Neuroradiol* 2014;35:999–1006
15. Wetzel S, Meckel S, Frydrychowicz A, et al. **In vivo assessment and visualization of intracranial arterial hemodynamics with flow-sensitized 4D MR imaging at 3T.** *AJNR Am J Neuroradiol* 2007;28:433–38
16. Harloff A, Zech T, Wegent F, et al. **Comparison of blood flow velocity quantification by 4D flow MR imaging with ultrasound at the carotid bifurcation.** *AJNR Am J Neuroradiol* 2013;34:1407–13
17. Stankovic Z, Csatari Z, Deibert P, et al. **Normal and altered three-dimensional portal venous hemodynamics in patients with liver cirrhosis.** *Radiology* 2012;262:862–73
18. van Zuuren EJ, Fedorowicz Z, Pucci E, et al. **Percutaneous transluminal angioplasty for treatment of chronic cerebrospinal venous insufficiency in people with multiple sclerosis: a summary of a Cochrane systematic review.** *J Neurol Neurosurg Psychiatry* 2014;85:405–10
19. Chimowitz MI, Lynn MJ, Derdeyn CP, et al, for the SAMMPRIS Trial Investigators. **Stenting versus aggressive medical therapy for intracranial arterial stenosis.** *N Engl J Med* 2011;365:993–1003
20. Broderick JP, Palesch YY, Demchuk AM, et al, for the Interventional Management of Stroke (IMS) III Investigators. **Endovascular therapy after intravenous t-PA versus t-PA alone for stroke.** *N Engl J Med* 2013;368:893–903
21. Meier B, Kalesan B, Mattle HP, et al, for the PC Trial Investigators. **Percutaneous closure of patent foramen ovale in cryptogenic embolism.** *N Engl J Med* 2013;368:1083–91

A. Harloff
Department of Neurology
University Medical Center
Freiburg, Germany

http://dx.doi.org/10.3174/ajnr.A3811

Metrics and Textural Features of MRI Diffusion to Improve Classification of Pediatric Posterior Fossa Tumors

D. Rodriguez Gutierrez, A. Awwad, L. Meijer, M. Manita, T. Jaspan, R.A. Dineen, R.G. Grundy, and D.P. Auer

ABSTRACT

BACKGROUND AND PURPOSE: Qualitative radiologic MR imaging review affords limited differentiation among types of pediatric posterior fossa brain tumors and cannot detect histologic or molecular subtypes, which could help to stratify treatment. This study aimed to improve current posterior fossa discrimination of histologic tumor type by using support vector machine classifiers on quantitative MR imaging features.

MATERIALS AND METHODS: This retrospective study included preoperative MRI in 40 children with posterior fossa tumors (17 medulloblastomas, 16 pilocytic astrocytomas, and 7 ependymomas). Shape, histogram, and textural features were computed from contrast-enhanced T2WI and T1WI and diffusivity (ADC) maps. Combinations of features were used to train tumor-type-specific classifiers for medulloblastoma, pilocytic astrocytoma, and ependymoma types in separation and as a joint posterior fossa classifier. A tumor-subtype classifier was also produced for classic medulloblastoma. The performance of different classifiers was assessed and compared by using randomly selected subsets of training and test data.

RESULTS: ADC histogram features (25th and 75th percentiles and skewness) yielded the best classification of tumor type (on average >95.8% of medulloblastomas, >96.9% of pilocytic astrocytomas, and >94.3% of ependymomas by using 8 training samples). The resulting joint posterior fossa classifier correctly assigned >91.4% of the posterior fossa tumors. For subtype classification, 89.4% of classic medulloblastomas were correctly classified on the basis of ADC texture features extracted from the Gray-Level Co-Occurence Matrix.

CONCLUSIONS: Support vector machine–based classifiers using ADC histogram features yielded very good discrimination among pediatric posterior fossa tumor types, and ADC textural features show promise for further subtype discrimination. These findings suggest an added diagnostic value of quantitative feature analysis of diffusion MR imaging in pediatric neuro-oncology.

ABBREVIATIONS: EP = ependymoma; Gd = gadolinium; max = maximum; MB = medulloblastoma; PA = pilocytic astrocytoma; SVM = support vector machine; TA = texture analysis

Diffusion MR imaging discriminates different types of adult brain tumors.[1-3] In the pediatric literature, the diffusion restriction has also been suggested to differentiate primitive neuroectodermal tumor/medulloblastoma (MB) and other supra- and infratentorial tumors.[4] Several studies demonstrated that pilocytic astrocytomas (PAs) are characterized by significantly higher average ADC values than ependymomas (EPs) and medulloblastomas, but no clear difference was shown between EPs and MBs (Table 1).[3,5-7] However, by using the 75th percentile from the ADC histogram, instead of an average ADC, a promising discrimination of 90% was achieved,[7] suggesting that individual tumor components allow better classification or grading than averaged metrics. This concept is well in line with the known heterogeneity of underlying tumor biology and the current practice of histologic diagnosis based on the most characteristic tumor parts.

Texture analysis (TA) is another powerful approach to characterize and quantify the tumor matrix. TA features provide in-

Received June 17, 2013; accepted after revision August 20.

From the Division of Radiological and Imaging Sciences (D.R.G., A.A., M.M., R.A.D., R.G.G., D.P.A.), and Children's Brain Tumor Research Centre (D.R.G., L.M., R.G.G., D.P.A.), University of Nottingham, Nottingham, UK; and Nottingham University Hospital Trust (A.A., L.M., T.J., R.A.D.), Nottingham, UK.

This work was funded by grant C7809/A10342, Children's Cancer and Leukemia Group (Cancer Research United Kingdom and Engineering and Physical Sciences Research Council-CIP, in association with the Medical Research Council and England Department of Health).

Previously presented in part as a poster or oral presentations at: 36th European Society of Neuroradiology Annual Meeting, September 20–23, 2012; Edinburgh, Scotland; and European Society for Magnetic Resonance in Medicine and Biology 2012 Congress, October 4–6, 2012; Lisbon, Portugal.

Please address correspondence to Dorothee Auer, MD, Division of Radiological and Imaging Sciences, Room W/B 1441, Queens Medical Centre, Derby Rd, Nottingham NG7 2UH, United Kingdom; e-mail: dorothee.auer@nottingham.ac.uk

http://dx.doi.org/10.3174/ajnr.A3784

Table 1: Average tumor ADC values in pediatric posterior fossa tumors ($\times 10^{-3}$ mm^2/s)

	Yamasaki et al 2005[3]	Rumboldt et al 2006[6]	Schneider et al 2007[5]	Bull et al 2012[7]
No. (MB/EP/PA)	(9/6/6)	(8/5/17)	(7/2/4)	(16/5/11)
EP	1.05–1.33	0.97–1.29	−0.8–1.4	1.10–1.25
MB	0.68–0.99	0.48–0.93	−0.5–1.0	0.67–1.22
Sig. difference (MB/EP)	Yes	Yes	No	No

Note:—Sig. indicates significant.

Table 2: Demographics

	Total	PA	EP	MB
Sex (M/F)		9:7	2:5	9:8
Age (yr)				
Mean	8.4	9.4	8.2	7.8
Range	1.1–18.4	2.6–18.4	1.1–15.5	3.6–16.0

Table 3: No. of cases used in the analysis per MR imaging sequence

Type	Subtype	WHO Grade	T1WI+Gd	T2	ADC
PA		I	13	14	15
MB	Classic	IV	14	14	12
	Anaplastic	IV	3	3	3
EP	Classic	II	6	5	4
	Anaplastic	III	1	1	1
Total			37	37	35

Note:—WHO indicates World Health Organization.

formation about spatial patterns in the distribution of image intensities and have been successfully used to discriminate tumor types[8-11] and types of tissue for segmentation[12,13] and to predict prognosis.[14] Most important, texture features offer the potential to discriminate distinct genetic tumor subtypes[15-17] by using combinations of T1WI, gadolinium (Gd)-enhanced T1WI, T2WI or FLAIR, and diffusion imaging in adult oligodendroglial tumors.

Significant advances are being made in characterizing molecular genetic tumor subtypes that predict differential survival and treatment responsiveness, which are particularly promising for future treatment stratification in medulloblastomas.[18-20] There is a great interest in developing novel imaging tools to noninvasively predict tumor types and subtypes that may offer added value for first-line surgical treatment planning before histologic and molecular diagnosis is available and in follow-up decision-making when repeat biopsies are impractical. Most approaches to date demand a significant increase in acquisition time (eg, MR spectroscopy) and may be expensive and not widely available (eg, ^{18}F-PET). Dedicated advanced image processing may, instead, offer improved brain tumor classification without the time penalty based on the current standard brain tumor MR imaging protocol, which includes Gd-enhanced T1, T2, and diffusion MR imaging.

The purpose of our study was to investigate the value of quantitative analysis of standard clinical MR imaging to discriminate the main types of pediatric posterior fossa tumors (PA, MB, and EP) and subtypes (eg, to discriminate classic MB from other posterior fossa tumors). We compared the performance of individual or combined features derived from shape, texture, and histogram from anatomic T1WI and T2WI and diffusion map images. Multiple features were combined to train support vector machines (SVMs), a widely used supervised learning approach that has been previously suggested for tumor segmentation.[21,22] In SVM classifiers, features are represented as n-dimensional vectors and combined to create a model of a particular class by using true and false training examples.

MATERIALS AND METHODS

Patients

Before this study, informed consent was obtained from all participating patients or their guardians to allow data collection and analysis for research by the UK Child Cancer and Leukemia Group Functional Imaging Group data base, a UK National Health Service Research Ethics Committee–approved study. Forty patients with posterior fossa tumors (17 MBs, 16 PAs, and 7 EPs; Table 2) were included. Inclusion criteria were confirmed histologic diagnosis along with a World Health Organization grading/subtype when applicable and a preoperative clinical MR imaging (without previous therapy), including diffusion imaging (Table 3).

MR Imaging

Because we only included preoperative MR imaging, acquisition was undertaken by using standard pediatric neuro-oncologic protocols on several scanner platforms: 1.5T Signa (GE Healthcare, Milwaukee, Wisconsin); and 1.5T Intera or 3T Achieva (Philips Healthcare, Best, the Netherlands). For this analysis, Gd-enhanced spin-echo T1WI (TR = 598–647 ms, TE = 12–14 ms, and 0.4–0.5 × 0.4–0.5 × 4.0–5.0 mm^3 voxel size), fast spin-echo T2WI (TR = 3000 ms, TE = 14–85 ms, and 0.4–0.5 × 0.4–0.5 × 4.0–5.0 mm^3 voxel size), and diffusion data were used. Diffusion data were obtained with different sequences, ranging from 3-direction diffusion-weighted imaging to 15-direction diffusion tensor imaging, by using B0 = 0 s/mm^2 and either b_{max} = 1000 s/mm^2 or b_{max} = 800 s/mm^2, TR = 4883–5800 ms, TE = 59–89 ms, and 1.9–2.0 × 1.9–2.0 × 3.0–4.0 mm^3 voxel size. Missing data or exclusion due to motion artifacts reduced the total number of cases per imaging sequence (Table 3). ADC maps were generated by using the FMRIB Software Library toolbox (http://www.fmrib.ox.ac.uk/fsl/). Two sample cases can be seen in Fig 1.

Normalization

T2WI and ADC maps were registered, by using the FMRIB Linear Registration Tool (FLIRT), to the contrast-enhanced T1WI data (in general, T1WI was acquired with a voxel size of 0.5 × 0.5 × 4.0 mm^3; in 9 cases in which the dimensions were slightly different, these were interpolated to a grid with 0.5 × 0.5 × 4.0 mm^3 voxel size by using cubic interpolation). To minimize heterogeneity in image intensity caused by the use of different scanners and acquisition sequences, we intensity normalized the data to the mean value of normal-appearing white matter from 2 small ROIs drawn bilaterally above the ventricles.

Tumor Segmentation

Whole-tumor ROIs were manually drawn by 2 clinical research fellows with radiology training and 4 years (M.M.) and 1 year (A.A.) of experience in neuroimaging research by using NeuROI

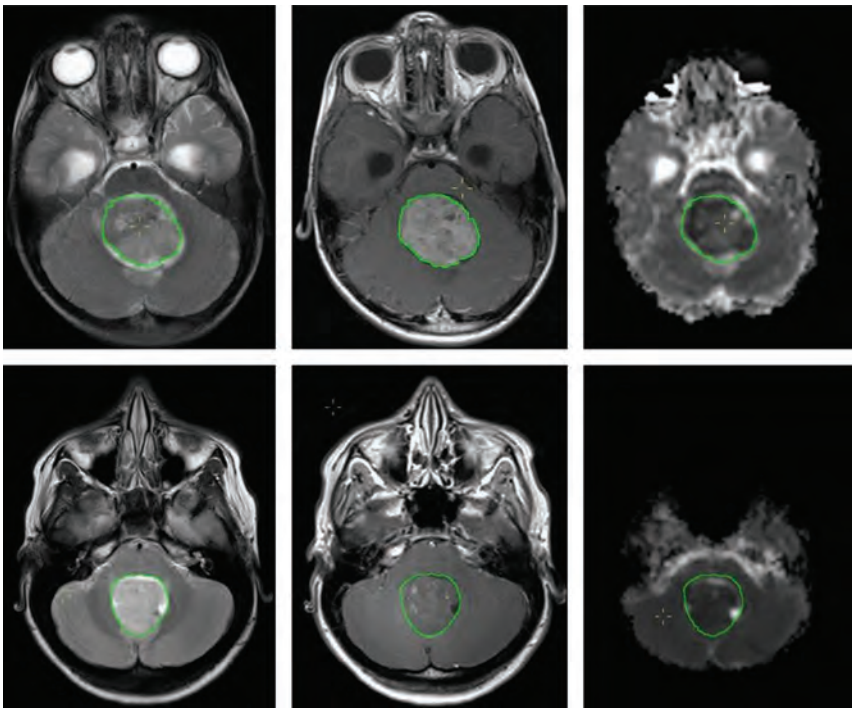

FIG 1. T1WI+Gd (left), T2WI (middle), and ADC map (right) of an anaplastic (top) and classic MB. The overlaid region of interest (inside the green outline) is used to derive shape features and to calculate histogram and texture features for each image sequence.

Table 4: Shape, histogram, and texture parameters used in analysis

Parameter	
Shape	Volume, compactness, solidity
Histogram	Mean variance, mode, maximum probability, skewness, kurtosis, energy, entropy; percentiles: 10%, 25%, 50%, 75%, and 90%
Gray-Level Co-Occurrence Matrix	Autocorrelation, contrast, correlation, cluster prominence, cluster shade, dissimilarity, energy, homogeneity, maximum probability, sum of squares variance, sum average, sum variance, sum entropy, difference variance, difference entropy, information measure of correlation, inverse difference normalized, inverse difference moment normalized

(http://www.nottingham.ac.uk/research/groups/clinicalneurology/neuroi.aspx). Tumor ROIs were defined on the T1WI+Gd images as areas of abnormal enhancement by using the coregistered precontrast T2WI to identify and exclude peripheral blood vessels adjacent to enhancing tumor and to include low-contrast tumor or necrotic tissue, excluding perilesional edema.

Shape, Histogram, and Texture Analysis

Shape, histogram, and texture features (Table 4) were extracted for each technique and patient by using in-house software developed in Matlab R2010a (MathWorks, Natick, Massachusetts). For shape features, values were computed on each section, and the mean value was used to characterize the whole tumor. Histogram-derived metrics and texture features were calculated from quantized data, by using 80 bins for the range ($0.5–4.5 \times 10^{-3}$ mm^2/s) (bin width = 0.05×10^{-3} mm^2/s). Histogram-derived metrics were calculated from whole-tumor ROIs. Texture features were calculated from Gray-Level Co-Occurrence Matrices, as per Haralick.[23] As per the shape measures, mean whole-tumor values were calculated across tumor sections. For each case, several co-occurrence matrices were calculated, corresponding to different distances (0.5, 1.0, 1.5, 2.0, and 2.5 mm). For each distance, co-occurrence matrices for several directions (0°, 45°, 90°) were computed.

The effect of the number of bins (ie, intensity quantization level) used for texture analysis on the ADC texture features was investigated by recomputing the co-occurrence matrices for different quantization levels (from 10 to 180 gray-level intensities). This is an important aspect in calculating co-occurrence matrices because it directly determines the pairs of pixels with the same intensity that may be found within a region of interest.

Tumor-Type SVM Classifiers

Shapes from region-of-interest, histogram, and TA features from ADC, T1WI+Gd, and T2WI were used independently or in combination to train tumor-type specific binary classifiers for MB, PA, and EP. The SVM classifiers used are part of the Bioinformatics Toolbox in Matlab. They were implemented as linear classifiers that produced a true/false classification for each tumor type.

Single-feature classifiers were created for every shape, histogram, and texture feature. In addition, combined classifiers (going only up to a maximum of 4 features, to avoid overtraining) were produced by a systematic combination of all features.

These individual tumor-type classifiers were combined to produce a joint posterior fossa classifier (3 posterior fossa tumor classifiers) by using a simple voting system based on single-classifier performance. A diagram of the process can be seen in Fig 2.

Training was performed by randomly choosing both true (n_T) and false (n_F) samples for each tumor type and by using the remaining samples as a test set. Each classifier was retrained with different-size training sets ($n_T = n_F = 2, 3, 4$) for each tumor type. For each tumor type and training set size, the training and testing process was repeated 500 times to obtain average classification rates for each classifier.

Radiologic reports at our institution were reviewed to investigate the accuracy of qualitative classification. Provisional diagnosis based on standard (including diffusion) MR imaging was recorded and matched to histopathology for MB, EP, and PA tumor types. Cases in which no provisional diagnosis was provided were considered as incorrectly classified.

Tumor-Subtype SVM Classifiers

In addition to tumor-type classifiers, a set of classic MB classifiers was produced to investigate tumor-subtype classification. The

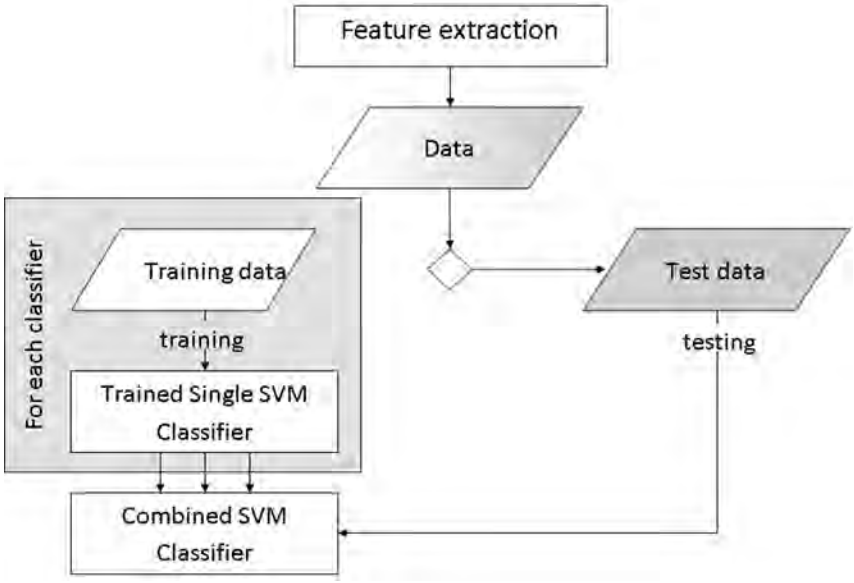

FIG 2. Training process to create single support vector machine classifiers for each tumor type and a combination step to produce a posterior fossa classifier to be tested on the remaining data.

Table 5: Average tumor ADC values ($\times 10^{-3}$mm^2/s)

	PA	EP	MB	*P* Value[a]
Tumor				
Mean/SD	1.70/0.26	1.34/0.29	0.85/0.18	<.05
Range	0.76–2.91	0.72–2.33	0.49–1.90	
Normal-appearing white matter				
Mean/SD	0.72/0.03	0.76/0.04	0.81/0.06	<.05
Range	0.63–0.87	0.62–0.95	0.59–0.93	

[a] Between-group means comparison for the 3 groups (using 1-way ANOVA and Tamhane T2 post hoc multiple comparisons correction) were all significant.

classic MB classifiers were based on ADC histogram and textural features.

Statistics

For both tumor type and subtype, we predefined <75% discrimination accuracy as futile for potential clinical use. Group mean differences for average ADC were calculated by using 1-way ANOVA and Tamhane T2 post hoc multiple comparison correction.

RESULTS

Between-Group Comparison of Metrics and Features

There was a substantial overlap among the 3 tumor types for all metrics and features on all histogram and TA features investigated. Group mean differences for average ADCs were significant (Table 5).

Tumor-Type Classifiers

Average classification rates for those classifiers yielding at least 75% correct classification performance are shown in Table 6 for joint posterior fossa classifiers based on T2WI and T1WI+Gd features with 8 sample randomly selected training sets tested on the remaining samples. The best classifier was based on a combination of size, histogram, and textural features, and it achieved <80% correct discrimination among the 3 groups. Classifiers trained with smaller sample sizes produced lower correct classification rates.

Average classification rates for the best performing joint posterior fossa classifiers based on ADC features with 8 sample randomly selected training sets and tested on the remaining samples can be seen in Table 7. Combined histogram-feature classifiers performed better than single-feature classifiers. Classifiers based on histogram metrics performed best with clinically useful 91% 3-way discrimination accuracy, which was better than that of classifiers built on either texture in isolation or combinations of histogram and textural features. The best performing ADC texture classifier based on entropy and homogeneity failed to reach the predefined minimum 75% accuracy level.

The best single-feature ADC classifier for our dataset was the 25th percentile of the ADC histogram (Table 7). Average ADC classification performance was substantially lower at 71.9% (PA 87.2%, MB 70.6%, and EP 59.0%). The best multiple-feature classifier was a combination of histogram percentiles and skewness. The distributions for the 25th and 75th percentiles (though the normalized distributions were used in the classifiers) and skewness can be seen in Fig 3.

Neuroradiologists' assessment at our institution according to clinical reports for the same dataset produced the following correct classification rates: PA 65%, MB 53%, and EP 60%.

Tumor-Subtype Classifiers

Due to the low number of nonclassic MBs, tumor-subtype classification was investigated by discriminating classic MB from other MBs (anaplastic MBs) and EPs, again by using a training set size of up to 8 randomly selected samples and by using the remaining samples as a test set. ADC texture-based features (best classifier: sum average + sum variance, 89.4% average correct classification) were more effective in discriminating classic MBs than ADC histogram features (best classifier: 75th percentile + max probability, 68.0%) or T2WI and T1WI+Gd derived classifiers (best classifier: 77.6%). The inclusion of shape features did not result in increased performance.

Effect of the Number of Bins on Classification

All the histogram and texture features were calculated by using 80 bins (bin size = 0.05×10^{-3}mm^2/s). The effect of the number of bins or the bin size on classification performance was investigated by training a series of PA classifiers on the basis of histogram features only (ADC 25th percentile) and another on the basis of texture features only (ADC entropy + homogeneity) by using different bin sizes. With a range from 10 bins (bin size = 0.4×10^{-3}mm^2/s) to 180 bins (bin size = 0.02×10^{-3}mm^2/s), classification rates can be seen in Fig 4. For classifiers based on histogram metrics, a higher number of bins resulted in higher classification rates. Texture-based classification decreased with both low and high numbers of bins. For this dataset, it was observed that the

Table 6: Average correct classification rates for joint posterior fossa classifiers (3-PFT) based on shape, T2WI, and T1WI+Gd histogram/texture features[a]

T1WI+Gd and T2WI Features	PA (%)	MB (%)	EP (%)	3-PFT C (%)
ROI volume + T1WI+Gd histogram energy + T1WI+Gd sum entropy	83.5	78.2	74.6	78.8
ROI volume + T1WI+Gd mean + T1WI+Gd sum entropy	80.0	81.9	69.7	76.4
T2WI histogram skewness + T2WI mean + T2WI cluster prominence + T2WI sum variance	76.7	78.1	71.3	75.2

Note:—3-PFT indicates 3 posterior fossa tumor; 3-PFT C, 3 posterior fossa tumor classifiers.
[a] The performance of the separate individual classifiers that make up the combined classifier is also shown.

Table 7: Average correct classification rates for joint posterior fossa classifiers (3-PFT) based on shape and ADC histogram/texture features[a]

ADC Features	PA (%)	MB (%)	EP (%)	3-PFT C (%)
Histogram 25th percentile + histogram 75th percentile + histogram skewness	96.9	95.8	94.3	91.4
Histogram 25th percentile + histogram median	95.6	92.0	91.8	89.2
ROI volume + histogram 75th percentile + histogram median + histogram entropy	96.2	91.3	83.9	87.4
Histogram 25th percentile	95.6	91.1	88.7	85.3
Histogram 75th percentile	96.1	89.7	85.1	83.5
Histogram median	92.3	89.9	82.2	78.9

Note:—3-PFT indicates 3 posterior fossa tumor; 3-PFT C, 3 posterior fossa tumor classifiers.
[a] The performance of the separate individual classifiers that make up the combined 3-PFT classifier is also shown. The bottom 3 rows correspond to the best single-feature classifiers.

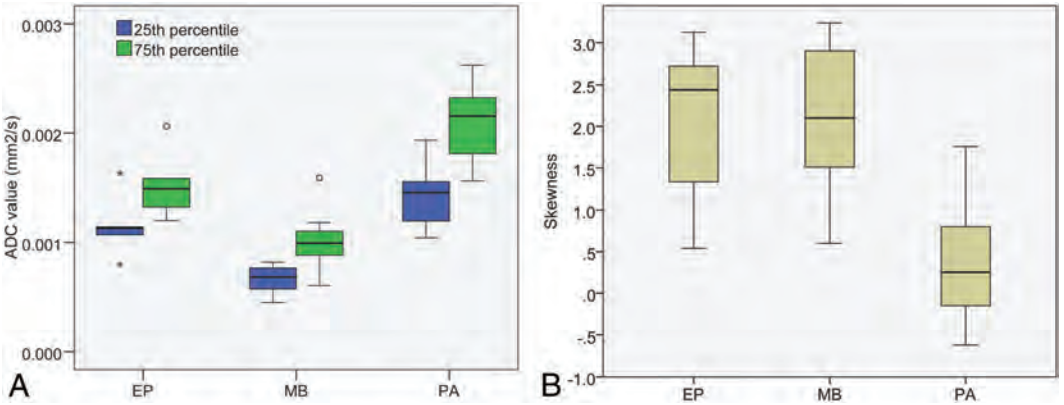

FIG 3. Distribution of 25th and 75th percentile values and skewness from ADC histograms for PAs, EPs, and MBs. White matter normalized values are used in the classifiers.

range of 60–90 bins (sized 0.07–0.04 × 10^{-3} mm^2/s) produced the best classification rates.

DISCUSSION

We show that quantitative feature analysis based on clinical MR imaging allows discriminating the main pediatric posterior fossa tumor types with an accuracy of 91% when using a combination of diffusion histogram metrics. These were found to be the best-performing metrics from a comparison of histogram and texture analysis features derived from ADC, Gd-enhanced T1WI, and T2WI scans. Conversely, textural ADC features predicted classic MB on average in 89% of test runs, demonstrating the potential for further tumor subtyping and highlighting the need for dedicated task-specific classifier optimization.

Features from diffusion MR imaging allowed better diagnosis of tumor type than textural features derived from conventional imaging. In agreement with Bull et al,[7] we found that histogram-derived metrics also outperformed mean tumor metrics. In this study, the 25th percentile expected to characterize the most cellular and hence most aggressive tumor part allowed the best classification. This is in partial contrast to the previously reported best discrimination based on the 75th percentile,[7] which also yielded a good discrimination in our study. The difference may be explained by the exclusion of cystic components in their study but deliberate inclusion in ours.

Quantitative analysis of tumor characteristics produced higher correct classification rates than clinical radiology reports provided by neuroradiologists in a tertiary neuroscience center. This difference likely reflects both the added value of quantitative analysis and the current lack of emphasis in radiology reporting of predicting tumor type provided by histology. The proposed approach yielding higher accuracy in predicting tumor types and possibly subtypes opens new avenues of research to explore the potential patient benefit based on noninvasive cancer classification. The surge of promising stratified care concepts highlight the need for parallel development of noninvasive classifiers to complement histologic and genetic classification systems. High-quality diagnosis of tumor type/subtype preoperatively would allow better planning of surgical resection extent and may become particularly useful for treatment guidance in residual/recurrent disease.

The possibility of combining several features by using SVMs was investigated to complement the discriminatory information and therefore increase classification rates. The best performance was achieved when combining the 25th percentile + 75th percentile + skewness (91.4% average correct classification). This per-

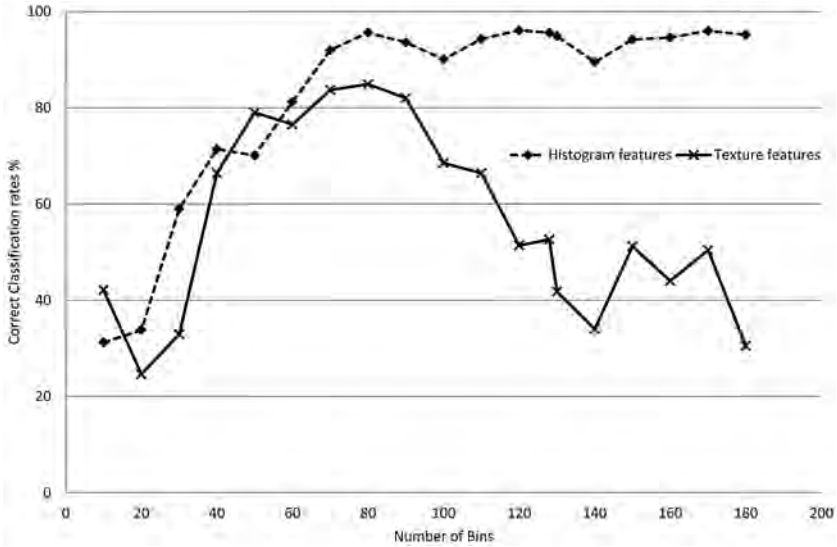

FIG 4. Average classification rates for 2 PA tumor-type classifiers as a function of the number of bins used to quantize the normalized ADC values. Classification rates for histogram feature-based classifiers are independent of the number of bins (as long as these are not very low). In contrast, if the number of bins is too large, classification based on Gray-Level Co-Occurrence textural features will be affected (insufficient pairs of pixels are found).

formance is similar to classifiers based on single-voxel proton MR spectroscopy studies of pediatric posterior fossa tumors (85%–93%).[5,24,25] To date, MR spectroscopy is available in most neuroimaging centers but comes at a significant increase of acquisition time and is limited to large nonhemorrhagic tumors. There is, however, the potential for even higher classification rates of up to 98%[26] when using well-defined research protocols with multiple TE MR spectroscopy with even longer acquisition times. In contrast, we show here that a short single-technique ADC scan that is applicable to all posterior fossa tumors regardless of size or hemorrhagic components affords a particular time-efficient classification of tumors.

The shape measures and ADC textural features, separately or in combination, neither yielded useful classification performance nor improved further ADC histogram metrics-based performance. Shape, textural, and histogram features from T1WI+Gd and T2WI data achieved moderate classification only (78.8% for the best classifier based on volume + T1WI+Gd histogram energy + T1WI+Gd sum entropy). This comparative quantitative analysis provides further evidence that diffusion MR imaging is particularly well-suited to tumor characterization, and, in conjunction with advanced postprocessing, may overcome current limitations in the discriminatory performance of conventional MR imaging for posterior fossa tumors.

Most interesting, ADC textural features and not histogram metrics provided the best tumor-subtype classification performance, namely 89% correct classification of classic MBs. This was achieved by using a combination of ADC textural features (sum average and sum variance of the Gray-Level Co-Occurrence Matrix). However, the classifier was only binary in that it specified whether a sample was a classic MB. There were insufficient data to train a similar anaplastic MB classifier, but these promising results suggest that it may be possible to train subtype classifiers and that there may be specific imaging features that best reflect specific tumor phenotypes. T2WI textural features have been found to be strongly predictive of genotype mutations in low-grade gliomas.[17]

Feature selection for the classifiers in this study consisted of a systematic combination of up to 4 individual features for each technique. Histogram and textural features from different imaging sequences (T1WI+Gd, T2WI, or ADC) were not cross-matched. Some of those features may provide an overlapping description of the tumor characteristics (eg, histogram percentiles describe slightly different aspects of the same distribution), and feature-reduction techniques such as principal component analysis that produce orthogonal features may improve classifier performance. Similarly, there are techniques that can be used to combine classifiers iteratively, such as AdaBoost,[27] which operates by weighting the combination of classifiers to minimize training error. These techniques produce strong classifiers from sets of weak classifiers that have the potential to further improve tumor type and subtype classification. Last, the SVM methodology proposed here is flexible and can be used to incorporate other shape and texture measures[28] and wavelets[29] and to combine multimodal imaging data.

Limitations

The main limitations are the relatively small datasets used, in which low numbers of tumor types (especially in EP) resulted in small training sets (maximum training set size $n_T + n_F = 8$). Using new data from other centers/scanners to train the SVM classifiers can help to improve their robustness. Most important, the presented classification is a best case scenario, given the data, and despite the promising accuracy, the generated classifiers from our dataset need to be prospectively tested on independent data to determine their robustness.

CONCLUSIONS

SVM-based classifiers by using a small set of ADC features (histogram and/or textural) and a small training dataset yielded very good discrimination among pediatric posterior fossa tumors, even though the individual features substantially overlapped. Features derived from ADC histograms yielded classification rates similar to those in reports based on MR spectroscopy and higher than those extracted from conventional T1WI+Gd or T2WI data. ADC textural features showed promise in discriminating tumor subtypes.

ACKNOWLEDGMENTS

The authors thank Gill Glen for data management.

Disclosures: Daniel Rodriguez Gutierrez—*RELATED*: *Grant*: Cancer Research United Kingdom,* Engineering and Physical Sciences Research Council.* Amir Awwad—*RELATED*: *Grant*: Cancer Research United Kingdom,* EPSRC.* Timothy Jaspan—

UNRELATED: *Consultancy*: Hoffman La Roche,* *Comments*: radiologist on HERBY study, a joint academia/pharma research study investigating the use of the antiangiogenic drug bevacizumab in pediatric high-grade glioma. Dorothee P. Auer—*RELATED*: *Grant*: Cancer Research UK,* Engineering and Physical Sciences Research Council UK,* *Comments*: includes some allowance for project-related travel, *UNRELATED*: *Board Membership*: Parkinson's UK, *Comments*: reimbursement of travel expenses to Parkinson's UK Research Advisory Panel Meetings, *Grants/Grants Pending*: MRC,* Engineering and Physical Sciences Research Council,* NIHR,* Stroke Association,* Arthritis Research UK,* Special Trustees NUHT,* Parkinson's UK* due to start. *Money paid to the institution.

REFERENCES

1. Heijmen L, Verstappen MC, Ter Voert EE, et al. **Tumour response prediction by diffusion-weighted MR imaging: ready for clinical use?** *Crit Rev Oncol Hematol* 2012;83:194–207
2. Gauvain KM, McKinstry RC, Mukherjee P, et al. **Evaluating pediatric brain tumor cellularity with diffusion-tensor imaging.** *AJR Am J Roentgenol* 2001;177:449–54
3. Yamasaki F, Kurisu K, Satoh K, et al. **Apparent diffusion coefficient of human brain tumors at MR imaging.** *Radiology* 2005;235:985–91
4. Erdem E, Zimmerman RA, Haselgrove JC, et al. **Diffusion-weighted imaging and fluid attenuated inversion recovery imaging in the evaluation of primitive neuroectodermal tumors.** *Neuroradiology* 2001;43:927–33
5. Schneider JF, Confort-Gouny S, Viola A, et al. **Multiparametric differentiation of posterior fossa tumors in children using diffusion-weighted imaging and short echo-time 1H-MR spectroscopy.** *J Magn Reson Imaging* 2007;26:1390–98
6. Rumboldt Z, Camacho DL, Lake D, et al. **Apparent diffusion coefficients for differentiation of cerebellar tumors in children.** *AJNR Am J Neuroradiol* 2006;27:1362–69
7. Bull JG, Saunders DE, Clark CA. **Discrimination of paediatric brain tumours using apparent diffusion coefficient histograms.** *Eur Radiol* 2012;22:447–57
8. Schad LR, Bluml S, Zuna I. **MR tissue characterization of intracranial tumors by means of texture analysis.** *Magn Reson Imaging* 1993;11:889–96
9. Eliat PA, Olivie D, Saikali S, et al. **Can dynamic contrast-enhanced magnetic resonance imaging combined with texture analysis differentiate malignant glioneuronal tumors from other glioblastoma?** *Neurol Res Int* 2012;2012:195176
10. Lerski RA, Straughan K, Schad LR, et al. **MR image texture analysis–an approach to tissue characterization.** *Magn Reson Imaging* 1993;11:873–87
11. Kassner A, Thornhill RE. **Texture analysis: a review of neurologic MR imaging applications.** *AJNR Am J Neuroradiol* 2010;31:809–16
12. Herlidou-Même S, Constans JM, Carsin B, et al. **MRI texture analysis on texture test objects, normal brain and intracranial tumors.** *Magn Reson Imaging* 2003;21:989–93
13. Assefa D, Keller H, Menard C, et al. **Robust texture features for response monitoring of glioblastoma multiforme on T1-weighted and T2-FLAIR MR images: a preliminary investigation in terms of identification and segmentation.** *Med Phys* 2010;37:1722–36
14. Drabycz S, Roldan G, de Robles P, et al. **An analysis of image texture, tumor location, and MGMT promoter methylation in glioblastoma using magnetic resonance imaging.** *Neuroimage* 2010;49:1398–405
15. Choi KY, Jung TY, Jung S, et al. **Prognosis of oligodendroglial tumor with ring enhancement showing central necrotic portion.** *J Neurooncol* 2011;103:103–10
16. Jenkinson MD, Smith TS, Brodbelt AR, et al. **Apparent diffusion coefficients in oligodendroglial tumors characterized by genotype.** *J Magn Reson Imaging* 2007;26:1405–12
17. Brown R, Zlatescu M, Sijben A, et al. **The use of magnetic resonance imaging to noninvasively detect genetic signatures in oligodendroglioma.** *Clin Cancer Res* 2008;14:2357–62
18. Leary SE, Olson JM. **The molecular classification of medulloblastoma: driving the next generation clinical trials.** *Curr Opin Pediatr* 2012;24:33–39
19. Gajjar A, Hernan R, Kocak M, et al. **Clinical, histopathologic, and molecular markers of prognosis: toward a new disease risk stratification system for medulloblastoma.** *J Clin Oncol* 2004;22:984–93
20. Gibson P, Tong Y, Robinson G, et al. **Subtypes of medulloblastoma have distinct developmental origins.** *Nature* 2010;468:1095–99
21. Hoisak JD, Koh E-S, Yu E, et al. **An image similarity-guided correspondence correction for voxel-wise analysis applied to MR imaging of glioblastoma multiforme acquired pre- and post-chemoradiotherapy.** In: *Proceedings of the 18th Annual Meeting of the International Society for Magnetic Resonance in Medicine*, Stockholm, Sweden. May 1–7, 2010
22. Luts J, Heerschap A, Suykens JA, et al. **A combined MRI and MRSI based multiclass system for brain tumour recognition using LS-SVMs with class probabilities and feature selection.** *Artif Intell Med* 2007;40:87–102
23. Haralick RM. **Statistical and structural approaches to texture.** *Proceedings of the IEEE* 1979;67:786–804
24. Wang Z, Sutton LN, Cnaan A, et al. **Proton MR spectroscopy of pediatric cerebellar tumors.** *AJNR Am J Neuroradiol* 1995;16:1821–33
25. Davies NP, Wilson M, Harris LM, et al. **Identification and characterisation of childhood cerebellar tumours by in vivo proton MRS.** *NMR Biomed* 2008;21:908–18
26. Vicente J, Fuster-Garcia E, Tortajada S, et al. **Accurate classification of childhood brain tumours by in vivo (1)H MRS: a multi-centre study.** *Eur J Cancer* 2013;49:658–67
27. Freund Y, Schapire RE. **A decision-theoretic generalization of on-line learning and an application to boosting.** *Journal of Computer and System Sciences* 1997;55:119–39
28. Tang XO. **Texture information in run-length matrices.** *IEEE Trans Image Process* 1998;7:1602–09
29. Manjunath BS, Ma WY. **Texture features for browsing and retrieval of image data.** *IEEE Trans Image Process* 1996;18:837–42

Evaluation of SWI in Children with Sickle Cell Disease

A.M. Winchell, B.A. Taylor, R. Song, R.B. Loeffler, P. Grundlehner, J.S. Hankins, W.C. Wang, R.J. Ogg, C.M. Hillenbrand, and K.J. Helton

ABSTRACT

BACKGROUND AND PURPOSE: SWI is a powerful tool for imaging of the cerebral venous system. The SWI venous contrast is affected by blood flow, which may be altered in sickle cell disease. In this study, we characterized SWI venous contrast in patients with sickle cell disease and healthy control participants and examined the relationships among SWI venous contrast, and hematologic variables in the group with sickle cell disease.

MATERIALS AND METHODS: A retrospective review of MR imaging and hematologic variables from 21 patients with sickle cell disease and age- and sex-matched healthy control participants was performed. A Frangi vesselness filter was used to quantify the attenuation of visible veins from the SWI. The normalized visible venous volume was calculated for quantitative analysis of venous vessel conspicuity.

RESULTS: The normalized visible venous volume was significantly lower in the group with sickle cell disease vs the control group ($P < .001$). Normalized visible venous volume was not associated with hemoglobin, percent hemoglobin F, percent hemoglobin S, absolute reticulocyte count, or white blood cell count. A hypointense arterial signal on SWI was observed in 18 of the 21 patients with sickle cell disease and none of the 21 healthy control participants.

CONCLUSIONS: This study demonstrates the variable and significantly lower normalized visible venous volume in patients with sickle cell disease compared with healthy control participants. Decreased venous contrast in sickle cell disease may reflect abnormal cerebral blood flow, volume, velocity, or oxygenation. Quantitative analysis of SWI contrast may be useful for investigation of cerebrovascular pathology in patients with sickle cell disease, and as a tool to monitor therapies. However, future studies are needed to elucidate physiologic mechanisms of decreased venous conspicuity in sickle cell disease.

ABBREVIATIONS: BOLD = blood oxygen level–dependent; mIP = minimum intensity projection; NVVV = normalized visible venous volume; SCD = sickle cell disease

Stroke is one of the most devastating complications in children with sickle cell disease (SCD).[1] The cause of stroke in SCD has both occlusive and hemodynamic contributions.[2,3] The pathophysiology of vaso-occlusion is related to the poor deformability of sickled red blood cells and the increased endothelial interactions of erythrocytes and inflammatory cells, which can induce vascular injury.[4] Hemodynamic contributions arise from a hemolytic anemia, creating a hyperemic state to satisfy cerebral oxygen demands.[2,3,5] Transcranial Doppler sonography is routinely used to screen for the risk for stroke, as the increase in cerebral blood flow in the hyperemic state is known to increase the risk for stroke.[3,6-9] MR imaging and MRA are also routinely used to assess parenchymal injury and the vascular integrity of the cerebrovascular system to assess the risk for stroke in patients with SCD.[10]

In addition to MRA, SWI has evolved into an important technique for imaging of the cerebrovascular system.[11] SWI enhances the venous contrast in the brain by taking advantage of the difference in magnetic susceptibility between deoxyhemoglobin and oxyhemoglobin. Because SWI is a blood oxygen level–dependent (BOLD) sensitive technique, the image can be affected by CBF changes, as reported in studies that have used carbogen or caffeine challenges or anesthesia.[12-14] Hyperemia is a well-described condition in SCD.[5,9,15,16] SWI has not been systematically investigated in SCD and may be a useful tool to study venous flow in conditions in which CBF is increased.

Received May 2, 2013; accepted after revision September 24.

From the Departments of Radiological Sciences (A.M.W., B.A.T., R.S., R.B.L., P.G., R.J.O., C.M.H., K.J.H.) and Hematology (J.S.H., W.C.W.), St. Jude Children's Research Hospital, Memphis, Tennessee.

Grant support: NIH HL070590 (Comprehensive Sickle Center Scholar), NIH R01HD049888, and American Lebanese Syrian Associated Charities (ALSAC).

Please address correspondence to Kathleen J. Helton, St. Jude Children's Research Hospital, 262 Danny Thomas Place, Mail Stop 220, Memphis, TN 38105; e-mail: Kathleen.helton@stjude.org

http://dx.doi.org/10.3174/ajnr.A3794

Correlation of NVVV with hematologic parameters

Parameter	*N*	Interval between SWI and Laboratory Measurements (d)	Value	*R* (*P* Value)*
Hemoglobin (g/dL)	21	−0.05 ± 2.4	8.51 ± 1.10	0.25 (.28)
Absolute reticulocyte count ($\times 10^6$/L)	21	−0.05 ± 2.4	0.23 ± 0.10	0.10 (.66)
White blood cell count ($\times 10^6$/L)	21	−0.05 ± 2.4	10.10 ± 4.50	0.19 (.40)
Hemoglobin F (%)	18	−3.22 ± 9.38	12.84 ± 9.40	−0.09 (.71)
Hemoglobin S (%)	18	−3.22 ± 9.38	68.06 ± 18.22	−0.25 (.31)

Note:—Results presented as mean ± standard deviation.

* *R*(*P* Value) value for the correlation of each hematologic parameter and NVVV.

In this study, we quantitatively compared the venous contrast in patients with SCD with that of age- and sex-matched healthy control participants. The visible venous volume calculated in each SWI examination was correlated with hematologic variables to determine whether this quantitative SWI measurement could be used as a biomarker of disease severity.

MATERIALS AND METHODS

Patient Demographics and MR Imaging

This retrospective study was approved by our hospital institutional review board. We analyzed diagnostic SWI scans from patients with SCD treated at our institution between March 2010 and December 2010. Patients who were sedated,[14] received supplemental oxygen for the MR examination, had a history of stroke, Moyamoya vasculopathy, encephalomalacia, or who had severe stenosis (> 75%) or occlusion of major intracranial vessels of the circle of Willis by MRA were excluded from analysis. Of the 29 eligible patients, 7 were excluded because of severe motion artifacts on SWI, and 1 patient was excluded for the hemoglobin SC genotype, yielding a final cohort of 21 patients with genotype hemoglobin SS (12 female, mean age, 12.9 ± 3.7 years; 9 male, mean age, 12.3 ± 3.9 years). Patients were also categorized by treatment: hydroxyurea, long-term transfusion therapy, or no therapy. Hemoglobin, percent hemoglobin F, percent hemoglobin S, absolute reticulocyte count, and white blood cell count (Table 1) obtained within 30 days of the MR examination were used as covariates for SWI analysis in the SCD group. SWI examinations were also analyzed from 21 sex- and age-matched healthy control participants (12 females, mean age, 12.7 ± 4.1 years; 9 males, mean age, 12.3 ± 3.5 years). The healthy control participants were enrolled from the community in an institutional review board–approved clinical trial examining neural substrates of reading (National Institutes of Health R01HD049888). Hematologic parameters were not available for the control group.

In the SCD group, 12 examinations were performed at 1.5T (Avanto and Symphony; Siemens, Erlangen, Germany) and 9 examinations at 3T (Trio; Siemens). All control examinations were performed at 3T. The SWI acquisition involved a 3D T2*-weighted gradient-echo sequence with the following parameters: TE, 25 ms; TR, 56 ms at 3T and TE, 40 ms; TR, 60 ms at 1.5T; flip angle, 20°; section thickness, 2 mm; matrix size, 384 × 257 × 72; FOV, 210 × 210 mm^2; and a parallel imaging acceleration factor of 2. Sliding minimum intensity projections (mIP, 16-mm thick) were used in the image analysis.

Because SWI was performed at 1.5T and 3T in the SCD group, another set of healthy adult volunteers underwent scanning at 1.5T and 3T by use of the respective SWI parameters to evaluate any potential differences in the SWI signal as a function of field strength. Twelve healthy volunteers (3 females, mean age, 53.0 ± 5.2 years; 9 males, mean age, 38.1 ± 14.9 years) were recruited and underwent scanning consecutively at 1.5T and 3T after informed written consent was obtained.

Image Analysis

The apparent venous contrast was quantified by segmentation of the venous structures by a Frangi vesselness filter[17] in Matlab (MathWorks, Natick, Massachusetts). The mathematic basis of the Frangi vesselness filter pertaining to vessel segmentation has been shown previously,[17-19] including the evaluation of SWI contrast in multiple sclerosis.[20] In general, the line intensity profile of the hypointense vein seen in SWI can be described as a Gaussian function with a uniform intensity along the vessel. The second partial derivative of the image provided by the Hessian matrix describes the local curvature along the vessel and its cross-section. The degree of curvature is described in the eigenvalues of the Hessian matrix. The Frangi vesselness filter analyzes the relationship of the eigenvalues to remove "blob" or circlelike features and determines the likelihood of tubelike structures.

Vein maps were created by first removing the skull from the mIP images with the Brain Extraction Tool (FMRIB Software Library; www.fmrib.ox.ac.uk/fsl).[21] To provide a similar signal intensity range for all images, the mIP images were normalized to 98% of the maximum signal intensity before applying the 2D Frangi vesselness filter. The 2 filter parameters (β and c), used to suppress bloblike structures and background noise, were set to $\beta = 0.5$ and $c = 20$, as suggested in previous studies.[17,22] The spatial scale of the filter was equal to the in-plane spatial resolution of the mIP (0.55 mm). The filter result is a probability estimate of the venous vesselness. Vein maps were created by accepting a probability estimate of > 60%. The volume identified as veins above the level of the M1 segment of the MCA was divided by the total intracranial volume above the M1 segment to create a quantitative normalized visible venous volume (NVVV). NVVV is a dimensionless ratio. Only the sections above the M1 segment were used to avoid possible misidentification of these structures as veins due to inflow effects that are sometimes seen in gradient recalled-echo acquisitions. This also avoided susceptibility artifacts at the level of the paranasal sinuses.

All SCD and healthy control examinations were qualitatively graded for hypointense arterial contribution above the M1 segments on the mIP. An examination with no hypointense arterial vessels on the mIP SWI in the Sylvian fissure received a grade of zero. Examinations with a few arterial vessels in the anterior Sylvian fissure received a grade of I. If the arterial vessels extended through the Sylvian fissure to the posterior temporal lobe, the examination received a grade of II. An examination received a grade of III if multiple tertiary arterial branches were present in the Sylvian fissure.

Finally, to evaluate potential differences in the apparent venous contrast due to field strength and respective SWI parameters, calculated NVVVs at 1.5T and 3T were compared in the same volunteer. The NVVV was calculated following the same

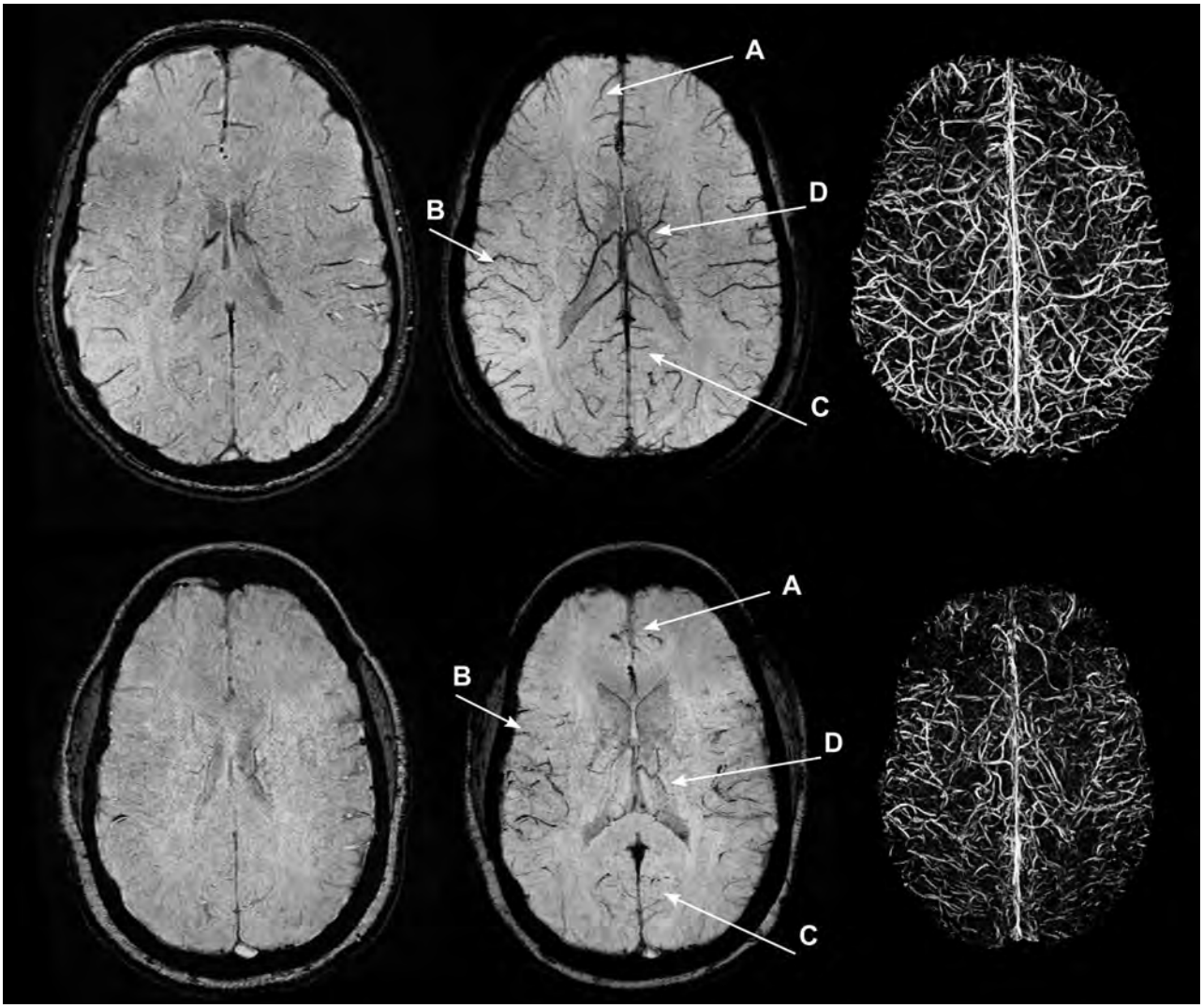

FIG 1. SWI, mIP SWI, and segmented vein maps for a representative control (top row, NVVV = 0.032) and patient with SCD (bottom row, NVVV = 0.013). In the mIP SWI and segmented vein maps, there is visually less venous contrast in the examination from the patient with SCD. The arrows point to loss of cortical venous conspicuity in the frontal (*A*), temporal (*B*), occipital (*C*), and deep medullary (*D*) areas, indicating a global decrease in signal.

procedure as described above. However, to ensure similar section position above the M1 segment, the 1.5T mIP images were realigned to the 3T mIP images by use of FLIRT (FMRIB Software Library)[23] before the NVVV calculation.

Statistical Analyses

Statistical analysis was performed by use of Matlab. Variables were expressed as means ± standard deviations. Group differences were assessed by use of the Wilcoxon rank sum test. Differences between 1.5T and 3T NVVV in the healthy volunteers were assessed by the Wilcoxon signed rank test. Linear dependencies of other physiologic markers with NVVV were tested by the Pearson correlation coefficient. Group differences or linear relationships were considered significant if $P < .05$.

RESULTS

Of the 21 patients with SCD, 15 were receiving hydroxyurea therapy (mean years of therapy, 5.4 ± 1.8 years; 1.5T = 7; 3T = 8), 2 were receiving long-term transfusion therapy (mean years of therapy, 3.85 ± 0.91 years; 1.5T = 2), and 4 were not receiving therapy (1.5T = 3; 3T = 1).

The SCD group had a visually lower venous contrast and overall visible venous vasculature than the control group (Fig 1). The loss of visible venous vasculature in the SCD group appeared to be global, with loss of venous contrast in both the deep medullary and regional cortical veins. By radiologic review, there were no focal regions of decreased or increased venous contrast. However, the presence of arteries (grade I, II, or III) in the mIP SWI was observed in 18 (grade I = 7; grade II = 9; grade III = 2) of the 21 SCD examinations and in none of the 21 healthy control examinations. Larger arterial contributions (grade II or III) were more prominent in the 1.5T cohort (all grades: grade 0 = 1; grade I = 1; grade II = 8; grade III = 2) than in the 3T cohort (all grades: grade 0 = 2; grade I = 6; grade II = 1; grade III = 0). Arterial signal contributions in the mIP SWI originated from hypointense signal in the SWI magnitude images and not from the phase mask multiplication. Figure 2 illustrates that many of the hypointense-ap-

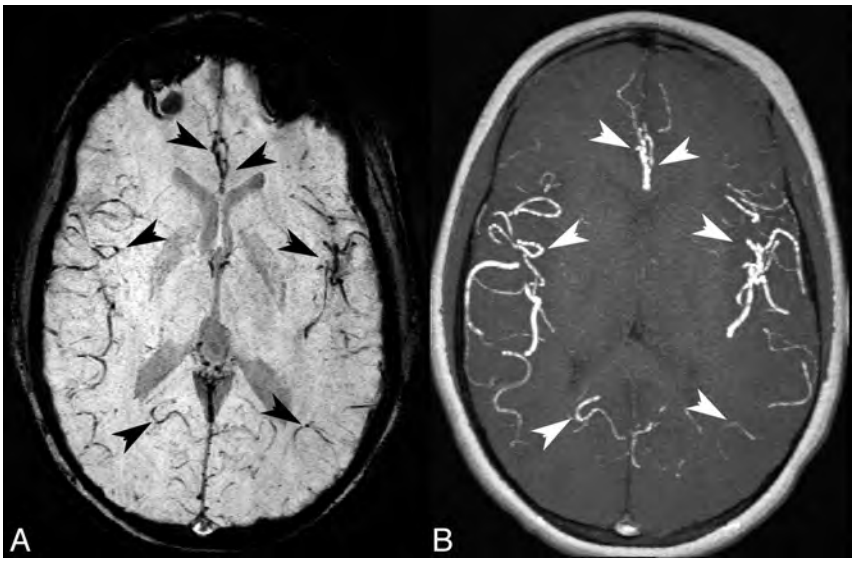

FIG 2. An SCD mIP SWI (*A*) with several hypointense-appearing vessels that could be interpreted as veins (*black arrowheads*). The corresponding MIP TOF (*B*) indicated that many of the hypointense-appearing vessels on the mIP SWI correlate with a hyperintense arterial signal from the TOF (*white arrowheads*). The arrows indicated arterial contribution of more distal branches of the left and right (anterior to posterior) bilateral anterior, middle, and posterior cerebral arteries. This example received a grade of II because of a hypointense arterial signal on the mIP SWI in the anterior Sylvian fissure through to the posterior temporal lobe.

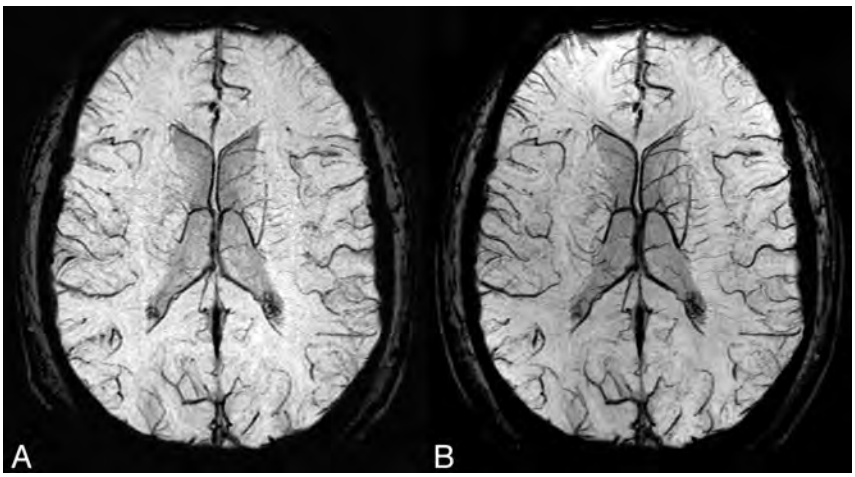

FIG 3. Representative mIP SWI from the same volunteer who underwent scanning at 1.5T (*A*) and 3T (*B*) depicts similar venous anatomy. The combination of higher SNR and venous contrast at 3T results in an improved venous conspicuity and a higher venous vessel likelihood from the Frangi filter. Several veins (eg, deep medullary veins) appear larger at 3T. The combination of larger-appearing veins and a higher vessel likelihood we believe were attributed to the increased conspicuity of NVVV at 3T.

pearing vessels on the mIP SWI corresponded to a hyperintense arterial signal on the mIP MRA. Because the arterial contribution could not be removed from the mIP SWI, NVVV is overestimated in the SCD groups because of the inclusion of these hypointense arterial vessels.

Because the examinations in the SCD group were acquired at 2 magnetic field strengths, the first test analyzed differences in the NVVV by using the segmented vein mask of healthy volunteers who underwent scanning at 1.5T and 3T. There was a significant difference ($P = .03$) in the NVVV between the 1.5T (0.024 ± 0.006) and 3T (0.028 ± 0.009) examinations. This finding indicates a bias toward higher NVVV at 3T. Figure 3 depicts a representative mIP SWI from the same volunteer who underwent scanning at 1.5T and 3T.

The measured NVVV in the SCD group was 0.013 ± 0.004 ($n=12$) and 0.011 ± 0.006 ($n=9$) at 1.5T and 3T, respectively. The measured NVVV in the healthy control participants at 3T was 0.031 ± 0.009 ($n=21$; Fig 4). There was no significant difference in NVVV measured at 1.5T and 3T in the SCD group ($P = .21$). The field strength bias detected in the volunteers was not observed in the SCD group. No sex differences ($P = .65$) or age-related changes ($P = .38$) in NVVV were observed in the healthy control participants and volunteers at 3T.

Because of the field bias observed in the volunteer measurements, cohort differences were only analyzed from the 9 patients with SCD at 3T and their corresponding 9 sex- and age-matched healthy control participants. There was a significantly lower NVVV in the 3T SCD group when compared with the healthy control group (0.034 ± 0.011; $n=9$; $P < .001$). So we would not further reduce our SCD sample size, we correlated NVVV with hematologic variables from all SCD examinations. The correlation of NVVV with hematologic variables was evaluated to determine parameters that may influence venous contrast in the SCD group. There was no significant correlation of NVVV (Table) with hemoglobin concentration ($R = 0.25$; $P = .28$), hemoglobin F ($R = -0.09$; $P = .71$), hemoglobin S ($R = -0.25$; $P = .31$), absolute reticulocyte count ($R = 0.10$; $P = .66$), or white blood cell count ($R = 0.19$; $P = .40$).

DISCUSSION

This study was undertaken to compare the BOLD-sensitive SWI venous contrast between patients with SCD and an age- and sex-matched healthy population and correlate these findings with hematologic variables in patients with SCD. We found that SCD affects the venous conspicuity of SWI. The NVVV was significantly lower in patients with SCD than in healthy control participants. From a qualitative perspective, SWI in patients with SCD produced a global isointense signal, which was similar in appearance to the diminished venous conspicuity reported in high-flow conditions found during anesthesia[14] and carbogen challenges.[12] To better understand the pathophysiology of decreased venous conspicuity in SCD, we investigated the relationship between SCD SWI venous contrast and hematologic variables. There were no correlations between the hematologic variables and SCD

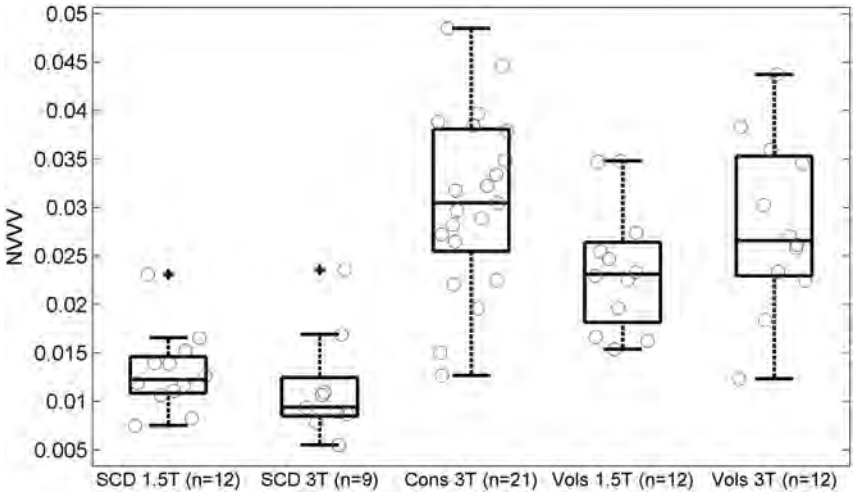

FIG 4. Boxplot of the NVVV in the SCD group (1.5T = 0.013 ± 0.004; 3T = 0.011 ± 0.006), control group (3T = 0.031 ± 0.009), and volunteers (1.5T = 0.024 ± 0.006; 3T = 0.028 ± 0.009). The difference in NVVV between the 3T SCD and control groups was significant ($P < .001$) when assessed by the Wilcoxon rank sum test. Volunteer measurements at 1.5T and 3T indicate increased conspicuity of NVVV at 3T ($P = .03$) when assessed by the Wilcoxon signed rank test.

NVVV, suggesting that other or more complex mechanisms affect venous conspicuity.

The Frangi vesselness filter was used to quantify venous contrast.[17] The automated vesselness filter method is superior to a qualitative categoric grading system of weak or strong contrast because it provides a continuous variable with which physiologic parameters can be correlated and is not subject to user-dependent segmentation methods. The mIP images were used in the analysis because they had higher conspicuity of the venous vasculature than SWI, allowing better sensitivity of venous segmentation. The use of mIP images with the same section thickness in both the SCD and control groups allowed a direct comparison between the groups. However, the use of mIP images will overestimate a true venous volume because the same venous vessels are replicated on multiple sections.

In this study, there was a significant difference in NVVV between patients with SCD and healthy control participants. This difference is unlikely the result of a morphologic decrease in the venous vasculature in patients with SCD but, instead, may be caused by decreased venous contrast. We excluded patients with a history of stroke, Moyamoya, encephalomalacia, severe stenosis, or major vessel occlusion to eliminate any confounding variance from known macrovasculature or microvasculature disease that could influence NVVV. Failure of the linear flow compensation observed in 86% of the SCD examinations resulted in the inclusion of an arterial vessel signal in the NVVV. This results in an overestimation of the true apparent NVVV and indicates a larger difference between patients with SCD and healthy control participants. A hypointense signal from arteries in a fully flow-compensated SWI sequence could indicate nonlinear flow or high flow acceleration. The tortuous arterial vessels reported in SCD[24,25] could attribute to the difference in flow compensation performance between the patients with SCD and healthy control participants.

Given that SCD can affect the concentration of paramagnetic deoxyhemoglobin,[26] the source of contrast in SWI, it was expected that hematologic variables such as hemoglobin levels or absolute reticulocyte count might correlate with the amount of venous contrast in SWI. However, we did not find any significant correlation between the hematologic variables and NVVV, which may be due to the relatively small number of patients in our study and the included arterial signal contributions. However, changes in hematologic variables such as hemoglobin concentration can affect other important parameters such as CBF,[16,27] which may play a more primary role in affecting NVVV. In this retrospective study, blood flow or perfusion values were not available to investigate this relationship. From a physiologic standpoint, because of the lower oxygen-carrying capacity of hemoglobin S and the chronic anemic state in SCD, CBF increases to maintain a constant oxygen extraction fraction.[2,28] SWI is sensitive to CBF changes,[12-14] and CBF could be a cause for altered SWI contrast in SCD. The elevated CBF reported in SCD,[15,28] combined with the decreased concentration of deoxyhemoglobin,[26] may represent a complex multifactorial physiologic mechanism that results in diminished SWI contrast in SCD.

There were no significant sex differences or age-related changes in NVVV in either the patients with SCD or healthy control participants and volunteers at 3T. Volunteer measurements at 1.5T and 3T detected a bias of higher NVVV at 3T. One possible mechanism for the difference is that the TEs were not scaled proportionally for the change in magnetic field. To produce similar phase effects, the product of magnetic field strengths and TE should be equal.[29] A TE of 40 ms at 1.5T only produces 80% of the phase offset of a TE of 25 ms at 3T. SNR also increases with higher field. The combination of higher SNR and larger-phase offset at 3T improved contrast to noise and conspicuity of smaller venous vessels at 3T and, thus, a larger NVVV. However, NVVV was higher at 1.5T than at 3T in the SCD cohort. The higher NVVV could be attributed to a larger degree of arterial contribution (grade II or III) in the 1.5T SCD examinations than in the 3T SCD examinations.

A limitation of this retrospective study was the small number of patients with SCD. Several factors could have impeded our ability to elucidate hematologic effects with NVVV, which included a small sample size, data at 2 different fields, and arterial contribution. Further SWI sequence design to include acceleration compensation or postprocessing techniques would be necessary in future studies to eliminate an arterial signal to provide a better estimate of NVVV. Another study limitation was the absence of flow data to determine its relationship with NVVV. The small number of patients with SCD who did not receive treatment or received transfusions did not allow an analysis of treatment-related NVVV effects. A longitudinal prospective study at a single field across different SCD treatment groups is needed with quantitative measures of cerebral flow to determine the relationship of

NVVV in SCD, and to assess if quantitative SWI measures could be used as surrogate markers of disease severity and treatment success.

CONCLUSIONS

Our study is the first to describe a spectrum of SWI changes in children with SCD across multiple therapies. SWI venous conspicuity (NVVV) was significantly lower in patients with SCD than in healthy age- and sex-matched control participants. Given that SCD produces a complex physiologic response to maintain adequate cerebral oxygenation, several factors, particularly cerebral blood flow and perfusion, may play a role in this decreased contrast in SWI. Prospective studies that include concomitant longitudinal hematologic and flow measurements are required to determine the physiologic mechanisms of decreased venous conspicuity in SCD and their usefulness as a possible biomarker of disease severity.

ACKNOWLEDGMENTS

We thank Dr. Vani Shanker for editing the manuscript and Dr. James Langston for his insightful discussion. We would also like to thank Melissa Jones and Dr. Axel Krafft for assistance in volunteer recruitment scanning.

Disclosures: Adam M. Winchell—*Grant:* NIH,* HL070590. Paul Grundlehner— Comments: I was supported in part by 5R25CA02394 from the National Cancer Institute of the NIH. Ralf B. Loeffler—*Grant:* NIH,* HL070590. Winfred C. Wang—*Grant:* NIH HL070590.* Robert J. Ogg—*Grant:* NIH (R01HD049888).* Claudia M. Hillenbrand—*Grant:* NIH,* HL070590 (Comprehensive Sickle Center Scholar). Kathleen J. Helton—*Grant:* NIH R01HD049888.* **Money paid to institution.*

REFERENCES

1. Ohene-Frempong K, Weiner SJ, Sleeper LA, et al. **Cerebrovascular accidents in sickle cell disease: rates and risk factors.** *Blood* 1998;91:288–94
2. Debaun MR, Derdeyn CP, McKinstry RC 3rd. **Etiology of strokes in children with sickle cell anemia.** *Ment Retard Dev Disabil Res Rev* 2006;12:192–99
3. Doepp F, Kebelmann-Betzing C, Kivi A, et al. **Stenosis or hyperperfusion in sickle cell disease—ultrasound assessment of cerebral blood flow volume.** *Ultrasound Med Biol* 2012;38:1333–38
4. Verduzco LA, Nathan DG. **Sickle cell disease and stroke.** *Blood* 2009;114:5117–25
5. Ausavarungnirun P, Sabio H, Kim J, et al. **Dynamic vascular analysis shows a hyperemic flow pattern in sickle cell disease.** *J Neuroimaging* 2006;16:311–17
6. Kirkham FJ, Lerner NB, Noetzel M, et al. **Trials in sickle cell disease.** *Pediatr Neurol* 2006;34:450–58
7. Adams RJ. **TCD in sickle cell disease: an important and useful test.** *Pediatr Radiol* 2005;35:229–34
8. Lowe LH, Bulas DI. **Transcranial Doppler imaging in children: sickle cell screening and beyond.** *Pediatr Radiol* 2005;35:54–65
9. Kwiatkowski JL, Granger S, Brambilla DJ, et al. **Elevated blood flow velocity in the anterior cerebral artery and stroke risk in sickle cell disease: extended analysis from the STOP trial.** *Br J Haematol* 2006;134:333–39
10. Arkuszewski M, Melhem ER, Krejza J. **Neuroimaging in assessment of risk of stroke in children with sickle cell disease.** *Adv Med Sci* 2010;55:115–29
11. Haacke EM, Xu Y, Cheng YC, et al. **Susceptibility weighted imaging (SWI).** *Magn Reson Med* 2004;52:612–18
12. Sedlacik J, Kutschbach C, Rauscher A, et al. **Investigation of the influence of carbon dioxide concentrations on cerebral physiology by susceptibility-weighted magnetic resonance imaging (SWI).** *Neuroimage* 2008;43:36–43
13. Sedlacik J, Helm K, Rauscher A, et al. **Investigations on the effect of caffeine on cerebral venous vessel contrast by using susceptibility-weighted imaging (SWI) at 1.5, 3 and 7 T.** *Neuroimage* 2008;40:11–18
14. Sedlacik J, Lobel U, Kocak M, et al. **Attenuation of cerebral venous contrast in susceptibility-weighted imaging of spontaneously breathing pediatric patients sedated with propofol.** *AJNR Am J Neuroradiol* 2010;31:901–06
15. Helton KJ, Paydar A, Glass J, et al. **Arterial spin-labeled perfusion combined with segmentation techniques to evaluate cerebral blood flow in white and gray matter of children with sickle cell anemia.** *Pediatr Blood Cancer* 2009;52:85–91
16. Prohovnik I, Pavlakis SG, Piomelli S, et al. **Cerebral hyperemia, stroke, and transfusion in sickle cell disease.** *Neurology* 1989; 39:344–48
17. Frangi A, Niessen W, Vincken K, et al. **Multiscale vessel enhancement filtering.** In: Wells W, Colchester A, Delp S, eds. *Medical Image Computing and Computer-Assisted Intervention — MICCAI'98*. Berlin Heidelberg:Springer Verlag;1998:130–37
18. Sato Y, Nakajima S, Shiraga N, et al. **Three-dimensional multi-scale line filter for segmentation and visualization of curvilinear structures in medical images.** *Med Image Anal* 1998;2:143–68
19. Koopmans PJ, Manniesing R, Niessen WJ, et al. **MR venography of the human brain using susceptibility weighted imaging at very high field strength.** *MAGMA* 2008;21:149–58
20. Zivadinov R, Poloni GU, Marr K, et al. **Decreased brain venous vasculature visibility on susceptibility-weighted imaging venography in patients with multiple sclerosis is related to chronic cerebrospinal venous insufficiency.** *BMC Neurol* 2011;11:128
21. Smith SM. **Fast robust automated brain extraction.** *Hum Brain Mapp* 2002;17:143–55
22. Koopmans P, Manniesing R, Norris D, et al. **Vein segmentation from 3D high resolution MR venograms by using vessel enhancing diffusion.** Presented at the Annual Meeting of ESMRMB, September 21–23, 2006; Warsaw, Poland. pg. 361
23. Jenkinson M, Smith S. **A global optimisation method for robust affine registration of brain images.** *Med Image Anal* 2001;5:143–56
24. Steen RG, Langston JW, Ogg RJ, et al. **Ectasia of the basilar artery in children with sickle cell disease: relationship to hematocrit and psychometric measures.** *J Stroke Cerebrovasc Dis* 1998;7:32–43
25. Steen RG, Emudianughe T, Hankins GM, et al. **Brain imaging findings in pediatric patients with sickle cell disease.** *Radiology* 2003;228:216–25
26. Zou P, Helton KJ, Smeltzer M, et al. **Hemodynamic responses to visual stimulation in children with sickle cell anemia.** *Brain Imaging Behav* 2011;5:295–306
27. Ibaraki M, Shinohara Y, Nakamura K, et al. **Interindividual variations of cerebral blood flow, oxygen delivery, and metabolism in relation to hemoglobin concentration measured by positron emission tomography in humans.** *J Cereb Blood Flow Metab* 2010;30: 1296–305
28. Oguz KK, Golay X, Pizzini FB, et al. **Sickle cell disease: continuous arterial spin-labeling perfusion MR imaging in children.** *Radiology* 2003;227:567–74
29. Haacke EM, Mittal S, Wu Z, et al. **Susceptibility-weighted imaging: technical aspects and clinical applications, part 1.** *AJNR Am J Neuroradiol* 2009;30:19–30

Quantitative Cerebral Perfusion Imaging in Children and Young Adults with Moyamoya Disease: Comparison of Arterial Spin-Labeling–MRI and $H_2[^{15}O]$-PET

R. Goetti, G. Warnock, F.P. Kuhn, R. Guggenberger, R. O'Gorman, A. Buck, N. Khan, and I. Scheer

ABSTRACT

BACKGROUND AND PURPOSE: Cerebral perfusion assessment is important in the preoperative evaluation and postoperative follow-up of patients with Moyamoya disease. The objective of this study was to evaluate the correlation of quantitative CBF measurements performed with arterial spin-labeling–MR imaging and $H_2[^{15}O]$-PET in children and young adults with Moyamoya disease.

MATERIALS AND METHODS: Thirteen children and young adults (8 female patients; age, 9.7 ± 7.1 years; range, 1–23 years) with Moyamoya disease underwent cerebral perfusion imaging with $H_2[^{15}O]$-PET (Discovery STE PET/CT, 3D Fourier rebinning filtered back-projection, 128 × 128 × 47 matrix, 2.34 × 2.34 × 3.27 mm^3 voxel spacing) and arterial spin-labeling (3T scanner, 3D pulsed continuous arterial spin-labeling sequence, 32 axial sections, TR = 5.5 seconds, TE = 25 ms, FOV = 24 cm, 128 × 128 matrix, 1.875 × 1.875 × 5 mm^3 voxel spacing) within less than 2 weeks of each other. Perfusion of left and right anterior cerebral artery, MCA, and posterior cerebral artery territories was qualitatively assessed for arterial spin-labeling–MR imaging and $H_2[^{15}O]$-PET by 2 independent readers by use of a 3-point-Likert scale. Quantitative correlation of relative CBF with cerebellar normalization between arterial spin-labeling–MR imaging and $H_2[^{15}O]$-PET was evaluated in a volume-based approach for each vascular territory after 3D image coregistration.

RESULTS: Interreader agreement was good (κ = 0.67–0.69), and strong and significant correlations were found between arterial spin-labeling–MR imaging and $H_2[^{15}O]$-PET for both qualitative perfusion scoring (ρ = 0.77; $P < .001$) and quantitative perfusion assessment of relative CBF with cerebellar normalization (r = 0.67, $P < .001$).

CONCLUSIONS: In children and young adults with Moyamoya disease, quantitative evaluation of CBF is possible with the use of arterial spin-labeling–MR imaging without ionizing radiation or contrast injection with a good correlation to $H_2[^{15}O]$-PET after cerebellar normalization.

ABBREVIATIONS: ASL = arterial spin-labeling; rCBF = relative CBF

Children and young adults with Moyamoya disease have progressive bilateral stenosis of the supraclinoid ICA, anterior cerebral artery, MCA, and to a much lesser extent, the posterior cerebral artery, with formation of netlike collateral vessel networks, termed "Moyamoya" vessels.[1] "Moyamoya" is the Japanese term for "puff of smoke" and describes the characteristic angiographic appearance of the collateral vessel networks typically formed at the skull base and around the basal ganglia in Moyamoya disease. The condition is rare; however, it is implicated in approximately 6% of childhood strokes.[2] The main goal of treatment of children with Moyamoya is the prevention of future strokes by means of surgical revascularization.

To determine the optimal targets for revascularization procedures as well as for postoperative follow-up, CBF studies with the use of Xe-CT, SPECT, or PET have been shown to be of high clinical value.[3-7] However, these methods are associated with ionizing radiation, which should be minimized or avoided whenever possible and especially in young patients. Recently, interest in MR imaging techniques for CBF assessment has grown, and initial evaluation of these techniques has been undertaken in patients with Moyamoya disease. MR perfusion imaging by use of dynamic susceptibility contrast imaging, on the basis of the decrease of T2/T2* times of tissue during the first pass of a gadolinium-containing contrast agent through the cerebral capillary bed, has been shown to correlate well with the reference standard of

Received August 27, 2013; accepted after revision September 25.

From the Departments of Diagnostic Imaging (R. Goetti, R. Guggenberger, I.S.), Diagnostic and Interventional Radiology (R. Goetti, F.P.K., R. Guggenberger), and Nuclear Medicine (G.W., F.P.K., A.B.), Center for MR Research (R.O.); and the Moyamoya Center, Division of Neurosurgery, Department of Surgery (N.K.), University Children's Hospital Zurich, Zurich, Switzerland.

Please address correspondence to Robert Goetti, MD, Department of Diagnostic and Interventional Radiology, University Hospital Zurich, Raemistr 100, CH-8091 Zurich, Switzerland; e-mail: robertpaul.goetti@usz.ch

http://dx.doi.org/10.3174/ajnr.A3799

$H_2[^{15}O]$-PET[8] in the assessment of cerebrovascular occlusive disease. Arterial spin-labeling (ASL) is an alternative MR imaging technique for CBF imaging that is based on the T1 magnetization state of electromagnetically tagged (ie, spin-labeled), freely diffusible arterial water. Blood flow measurements with ASL have been shown to correlate well with those from DSC imaging in children with Moyamoya disease.[9]

As a method requiring neither ionizing radiation nor exogenous contrast material injection, ASL could represent an ideal technique for the assessment of cerebral perfusion in children. The purpose of the present study was thus to assess the comparability of ASL and the reference standard of $H_2[^{15}O]$-PET imaging in children and young adults with Moyamoya disease.

MATERIALS AND METHODS

Patients

Children and young adults with angiographically proven Moyamoya disease who underwent both MR imaging with ASL imaging as well as $H_2[^{15}O]$-PET for preoperative assessment or postoperative follow-up after surgical revascularization as a routine work-up at our institutions between January 2011 and December 2012 were included in this retrospective study. The informed consent requirement was waived by the institutional review board because of the retrospective nature of the study.

Exclusion criteria were patient age >25 years ($n = 0$), $H_2[^{15}O]$-PET not performed within 2 weeks of ASL ($n = 11$), interventions or cerebrovascular incidents (ie, transient ischemic attacks or strokes) between the 2 examinations ($n = 0$), postoperative status <6 months ($n = 0$), contraindications to sedation in children <6 years old as evaluated by a board-certified anesthesiologist ($n = 0$), contraindications to contrast-enhanced MR imaging, such as noncompatible metallic implants or known previous allergic reactions to gadolinium-based contrast material ($n = 0$), and nondiagnostic image quality of either ASL or $H_2[^{15}O]$-PET studies ($n = 1$: nondiagnostic image quality of ASL caused by motion artifacts).

Thirteen children and young adults (8 female patients and 5 male patients; age, 9.7 ± 7.1 years; range, 1–23 years) met all criteria and were thus included in the study. Suzuki stages of the angiographically confirmed Moyamoya disease in these patients were II ($n = 4$), III ($n = 4$), IV ($n = 3$), and V ($n = 2$). Anterior watershed infarctions were present in 4 patients unilaterally and in 1 patient bilaterally. The mean time interval between the 2 examinations was 2 ± 3 days (range, 1–13 days). $H_2[^{15}O]$-PET was performed first in 3 patients, whereas ASL was performed first in 10 patients. Because of the retrospective nature of the study, the order of acquisition was not randomized.

MR Imaging Protocol and Image Reconstruction

MR imaging was performed with the use of a 3T scanner (HD.xt TwinSpeed; GE Healthcare, Milwaukee, Wisconsin) equipped with an 8-channel receive-only head coil for signal reception in all patients. Patients under the age of 6 years ($n = 6$), were sedated with propofol (Propofol-Lipuro; Braun Medical, Melsungen, Germany) and monitored by a board-certified anesthesiologist during the examination. A standardized MR imaging protocol for patients with Moyamoya disease consisting of multiplanar T2WI, T1WI, FLAIR, DWI, 3D-TOF, ASL, and contrast-enhanced DSC as well as multiplanar postcontrast T1WI was performed in all patients without complications.

ASL images were acquired as 32 axial sections by use of a background-suppressed, pulsed continuous arterial spin-labeling sequence, with a 3D stack of spiral fast spin-echo readout.[10] The labeling duration was 1.5 seconds, and a postlabeling delay of 1.5 seconds was used to reduce errors from transit time effects.[11] Further imaging parameters of the ASL sequence were TR, 5500 ms; TE, 25 ms; FOV, 24 cm; matrix, 128 × 128; section thickness, 5 mm; and number of excitations, 3. The reconstructed voxel spacing was 1.875 × 1.875 × 5 mm^3. The total scan time was 5 minutes, 34 seconds.

Quantitative CBF maps were calculated from the ASL data by use of the standard on-line perfusion image reconstruction provided by the scanner manufacturer. This reconstruction calculates the perfusion images according to the model described by Wang et al,[12] with an additional factor included to correct for incomplete recovery of the magnetization in the reference image caused by a saturation pulse applied 2 seconds before imaging.[13] No further preprocessing was performed. CBF was calculated according to the following equation.[11,13]

$$f = \frac{\lambda}{2\alpha T_{1b}\left(1 - e^{-\frac{\tau}{T_{1b}}}\right)} \frac{(S_{ctrl} - S_{lb1})\left(1 - e^{-\frac{t_{sat}}{T_{1g}}}\right)}{S_{ref}} e^{\frac{w}{T_{1b}}}$$

In this equation, f is blood flow (in mL/min per 100 mg), S_{ctrl}-S_{lbl} is the difference image (control-label), and S_{ref} is a proton-attenuation–weighted reference image; λ is the blood-brain partition coefficient (0.9), α is the inversion efficiency, T_{1b} is the T1 of blood (1600 ms), T_{1g} is the T1 of gray matter (1200 ms), w is the postlabeling delay (1.5 seconds), and τ is the labeling duration (1.5 seconds).[9,12,13] To investigate the effects of variations in blood T1 across the patient group, the blood T1 was calculated for $n = 11$ patients from venous hematocrit levels according to the equation T1 = 1/(0.83 Hct + 0.28). ASL perfusion values were calculated by use of an assumed blood T1 of 1600 ms and by use of the individual blood T1 for the patients in whom hematocrit data were available.

PET Protocol and Image Reconstruction

The PET data were acquired in 3D mode on a full-ring PET/CT scanner (Discovery STE; GE Healthcare) and corrected for attenuation, scatter, random photons, and dead time by use of the corresponding low-dose CT (120 kV/80 mA). The scanner's axial FOV covered 15.3 cm, and transaxial images were reconstructed by use of a 3D Fourier rebinning filtered back-projection algorithm resulting in a 128 × 128 × 47 matrix with 2.34 × 2.34 × 3.27 mm^3 voxel spacing; 400–800 MBq $H_2[^{15}O]$ was administered intravenously by use of an automatic injection device that delivered the predefined tracer dose over a period of 20 seconds. Patients under the age of 6 years ($n = 6$, the same as in ASL) were sedated with the use of Propofol-Lipuro and monitored by a board-certified anesthesiologist during the examination. The emission data were acquired as a series of eighteen, 10-second frames.

Parametric images of CBF were generated by means of a reported method[14] in which a standardized arterial input function

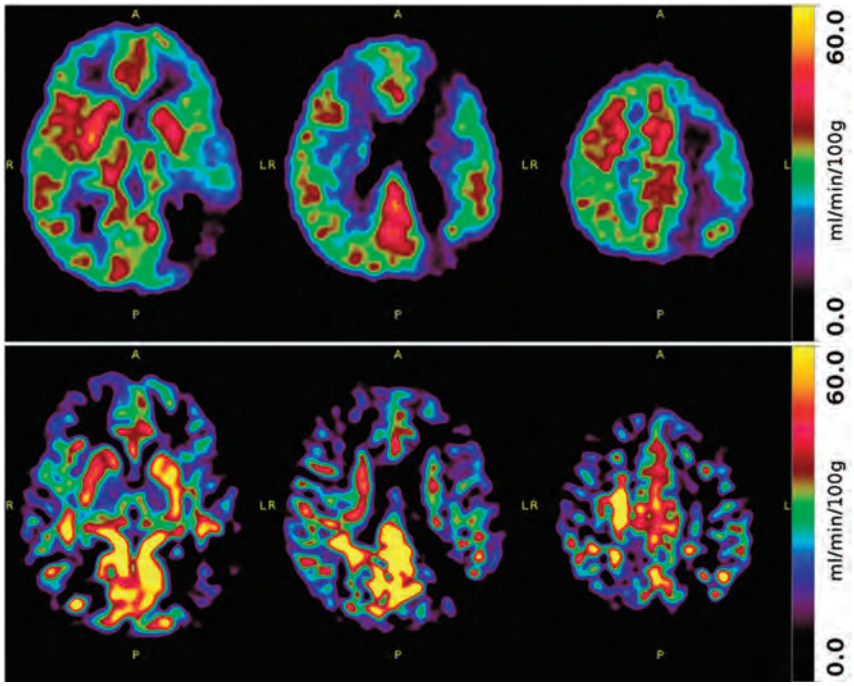

FIG 1. Example of CBF maps from $H_2[^{15}O]$-PET (upper row) and ASL (lower row) in the same 2-year-old girl with Moyamoya disease show reduced perfusion in the bilateral anterior and middle cerebral artery territories, more pronounced on the left (score 3) than on the right (score 2).

and image scaling on the basis of the washout rate (k2) of $H_2[^{15}O]$ are used to derive CBF. This technique, which is based on the Alpert method, exploits the fact that k2 is related to the shape and not the scale of the arterial input function and proportional to relative CBF (rCBF): (k2 = K1/p, where p is the partition coefficient).[15]

MR Imaging and PET Image Analysis

Qualitative Analysis. ASL and $H_2[^{15}O]$-PET CBF maps were assessed separately by 2 blinded and independent radiologists with 5 years and 7 years of experience. CBF was visually categorized on a 3-point Likert scale (1: normal, 2: reduced, 3: severely reduced) in the color-coded CBF maps (Fig 1) of each technique for anterior cerebral artery, MCA, and posterior cerebral artery territories on each side by comparison to cerebellar perfusion, which was assumed to be normal.

Quantitative Image Analysis. Semi-automated image analysis was performed in PMOD (version 3.4; PMOD Technologies, Zurich, Switzerland). With the use of a PET perfusion template image (SPM5, average $H_2[^{15}O]$ image from 12 subjects), ASL and PET perfusion maps were normalized to the stereotaxic spatial array of the Montreal Neurological Institute brain template by applying a mutual information–based registration including 12-parameter affine and elastic transformations and transitional image smoothing with a 6-mm full width at half maximum Gaussian kernel. Successful normalization was verified visually with the aid of image-outlining contours. After normalization, a volume-of-interest template defining the vascular territories (left/right, anterior cerebral artery, MCA, and posterior cerebral artery) and cerebellum was used to extract average perfusion by territory. This volume-of-interest template was generated by attributing the predefined brain regions outlined by the Hammer N30R83 atlas[16] to the respective vascular territories and was identical in size and shape for both $H_2[^{15}O]$-PET and ASL data (Fig 2). Relative CBF values (rCBF), that is, cerebellar normalized values, were calculated by dividing the CBF value of the respective supratentorial territory by cerebellar CBF.

Statistical Analysis

Cohen κ statistics were used for the assessment of interreader agreement in the evaluation of qualitative cerebral perfusion. Kappa values were interpreted as follows: $\kappa \geq 0.81$, excellent; $\kappa = 0.61$–0.80, good; $\kappa = 0.41$–0.60, moderate; $\kappa = 0.21$–0.40, fair; and $\kappa \leq 0.20$, poor agreement.

The correlation between $H_2[^{15}O]$-PET and ASL was assessed by use of Spearman rank correlation coefficient for qualitative perfusion scores and by Pearson correlation coefficient for quantitative CBF values and quantitative relative CBF values after cerebellar normalization. Bland-Altman analysis was used to compare mean differences in CBF and rCBF between $H_2[^{15}O]$-PET and ASL.

Paired *t* tests were used to compare CBF and rCBF values between $H_2[^{15}O]$-PET and ASL, and unpaired *t* tests were used to compare CBF and rCBF between territories with normal (qualitative perfusion score of 1) and reduced perfusion (score of 2 or 3) for both $H_2[^{15}O]$-PET and ASL. Differences in CBF and rCBF between territories grouped by perfusion scores were assessed by means of 1-way ANOVA with Tukey honestly significant differences post hoc analysis. All statistical tests were performed with the use of the statistical package R[17] (http://www.r-project.org/) and the R frontend RKWard Version 0.6.1 (http://rkward.sourceforge.net/). Statistical significance was inferred at $P < .05$.

RESULTS

Qualitative Image Analysis

Interreader agreement for qualitative perfusion assessment was good for both $H_2[^{15}O]$-PET ($\kappa = 0.67$) and ASL ($\kappa = 0.69$). A strong and significant correlation between perfusion scores in ASL and $H_2[^{15}O]$-PET was found ($\rho = 0.77$; $P < .001$). No posterior circulation involvement that could have influenced cerebellar normalization was found in our patient cohort.

Reduced perfusion in the visual qualitative assessment was found in 33 of 78 (42%) territories in 11 of 13 (85%) patients with $H_2[^{15}O]$-PET and in 32 of 78 (41%) territories in the same 11 of 13 (85%) patients with ASL. An overview of the qualitative perfusion assessment per vascular territory in both $H_2[^{15}O]$-PET and ASL is provided in the Table.

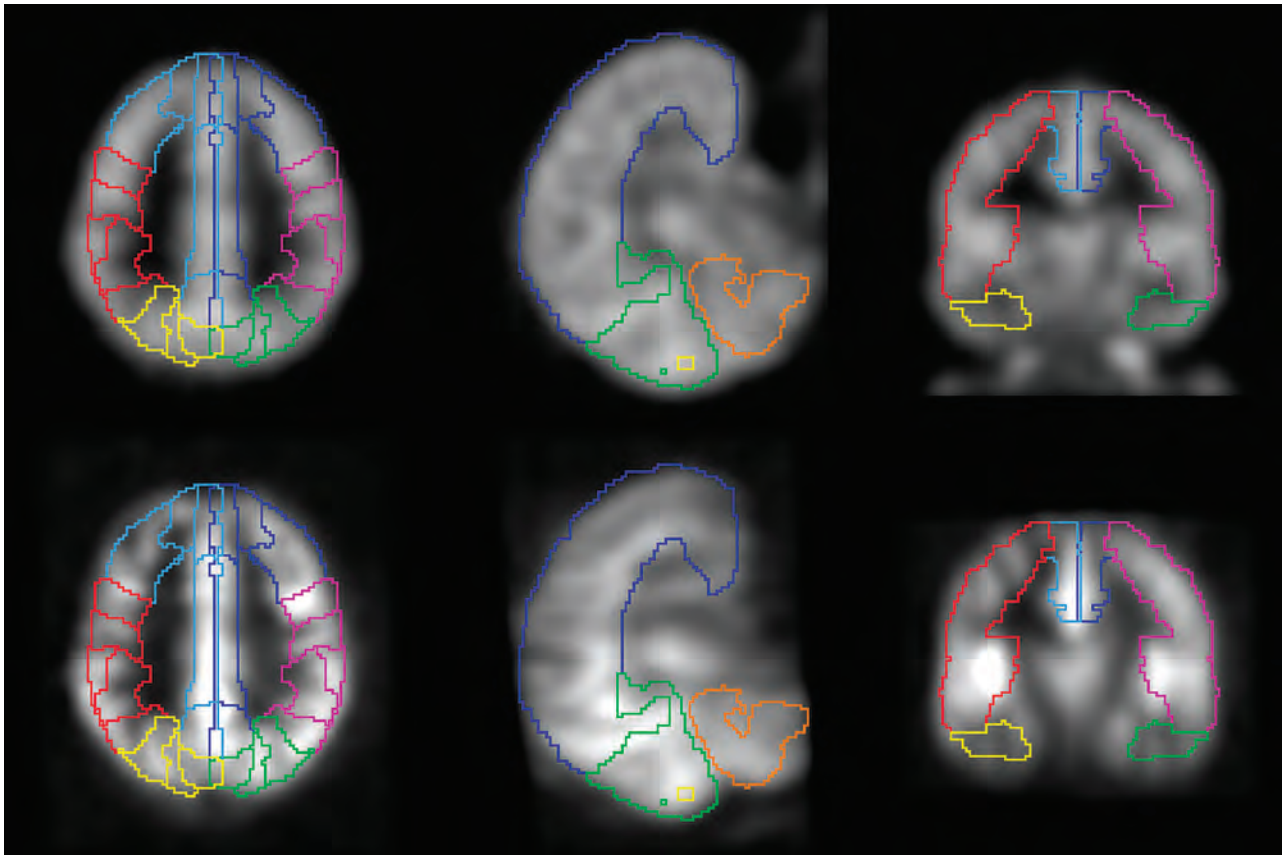

FIG 2. Volume-of-interest definition for quantitative CBF assessment per territory (upper row: $H_2[^{15}O]$-PET; lower row: arterial spin-labeling).

Overview of qualitative perfusion scores and quantitative perfusion in $H_2[^{15}O]$-PET and ASL

Qualitative Perfusion	Quantitative Perfusion	Territory		
		ACA	MCA	PCA
PET				
Normal	CBF: 31.51 ± 6.87[a] rCBF: 1.011 ± 0.112	9/26 (35%)	13/26 (50%)	23/26 (88%)
Reduced	CBF: 28.20 ± 6.97[a] rCBF: 0.943 ± 0.163	12/26 (46%)	9/26 (35%)	3/26 (12%)
Severely Reduced	CBF: 23.00 ± 3.70[a] rCBF: 0.677 ± 0.161	5/26 (19%)	4/26 (15%)	
ASL				
Normal	CBF: 31.88 ± 8.24[a] rCBF: 1.059 ± 0.159	6/26 (23%)	15/26 (57%)	25/26 (96%)
Reduced	CBF: 24.76 ± 7.58[a] rCBF: 0.853 ± 0.249	15/26 (58%)	8/26 (31%)	1/26 (4%)
Severely Reduced	CBF: 16.06 ± 5.18[a] rCBF: 0.507 ± 0.098	5/26 (19%)	3/26 (12%)	None

Note:—ACA indicates anterior cerebral artery; PCA, posterior cerebral artery; rCBF, relative CBF (values are given as ratios to cerebellar CBF).

[a] CBF values are given as mL/min per 100 g.

Quantitative Image Analysis

Quantitative image analysis revealed a strong and significant correlation between $H_2[^{15}O]$-PET and ASL ($r = 0.67$, $P < .001$) after cerebellar normalization (rCBF), with a regression slope of 1.0061 and intercept of −0.0057 (Fig 3). For absolute CBF values, the correlation was much weaker ($r = 0.26$, $P = .015$) using a literature value (1600 ms) for the blood T1 in the ASL perfusion quantification. The correlation was not improved with the use of an individual blood T1 on the basis of the hematocrit ($r = 0.14$, $P = .025$).

Mean CBF values (across all perfusion territories) were 30.58 ± 7.56 mL/min per 100 g in $H_2[^{15}O]$-PET and 28.38 ± 9.15 mL/min per 100 g in ASL. Bland-Altman analysis showed a mean difference of 2.19 ± 10.23 mL/min per 100 g between $H_2[^{15}O]$-PET and ASL ($P = .062$). After cerebellar normalization, mean rCBF values (all territories) were 0.958 ± 0.165 for $H_2[^{15}O]$-PET and 0.951 ± 0.247 for ASL, with a mean difference of 0.007 ± 0.186 ($P = .737$) (Fig 4).

Territories with normal qualitative perfusion (score 1) showed similar values in $H_2[^{15}O]$-PET and ASL ($P = .497$). Similar values were also found for territories with reduced perfusion (score 2) in $H_2[^{15}O]$-PET and ASL ($P = .162$). For territories with severely reduced perfusion (score 3), values tended to be higher in $H_2[^{15}O]$-PET (CBF: 23.00 ± 3.70 mL/min per 100 g; rCBF: 0.677 ± 0.161) than in ASL (CBF: 16.06 ± 5.18 mL/min per 100 g; rCBF: 0.507 ± 0.098), though not at a statistically significant level ($P = .085$). An overview of all quantitative perfusion values is provided in the Table. Quantitative perfusion values were significantly lower in territories with reduced qualitative perfusion scores (ie, scores 2 and 3) compared with those with normal qualitative perfusion for both $H_2[^{15}O]$-PET (CBF: $P = .025$, rCBF:

$P = .016$) and ASL (CBF: $P = .010$, rCBF: $P = .004$). Significant differences between territories with reduced perfusion (score 2) and severely reduced perfusion (score 3) were found for ASL ($P = .03$) but not for $H_2[^{15}O]$-PET ($P = .17$).

DISCUSSION

In the present study, we compared MR imaging–based and PET-based methods for the evaluation of cerebral perfusion in children and young adults with Moyamoya disease, through the use of qualitative and quantitative approaches. Our results demonstrate that CBF assessment by use of ASL-MR imaging with cerebellar normalization correlates well with the reference standard $H_2[^{15}O]$-PET method. This suggests that ASL-MR imaging could be a valuable alternative to $H_2[^{15}O]$-PET, while avoiding the use of ionizing radiation and injection of an exogenous contrast agent. However, absolute values of CBF may differ between the modalities.

The most widely used MR imaging technique is gadolinium-enhanced DSC, which is based on the decrease of T2/T2* signal intensity of cerebral tissue during the first pass of gadolinium through the capillary bed. It has been shown to reveal alterations in perfusion even in apparently (structurally) normal cerebral parenchyma in patients with Moyamoya disease and may be used in the targeting of revascularization approaches.[18] In a recent study, quantitative CBF values obtained with DSC were shown to strongly correlate with CBF values from $H_2[^{15}O]$-PET in patients with Moyamoya disease or ICA occlusions, though with a slight underestimation of CBF values in DSC.[8]

Arterial spin-labeling is a well-established method for the quantitative assessment of cerebral perfusion. It does not require the injection of an exogenous contrast agent but instead uses the water in arterial blood as an endogenous tracer through electromagnetic tagging with radiofrequency pulses. For the calculation of blood flow, the amount of labeled blood arriving in the cerebral tissue after a predefined transit time is measured by subtraction from a previously acquired control image.[19] A high correlation between ASL and DSC has been reported, with correlation coefficients between ASL and DSC of 0.62–0.79 in patients with acute ischemic stroke.[20] In a recent study with the use of DSC as the standard of reference in children with Moyamoya disease, it could be demonstrated that ASL-based measurements of CBF showed a similarly strong and significant correlation with DSC-based perfusion ($r = 0.79$, $P < .001$), enabling the detection of impaired perfusion per cerebral vascular territory with a high diagnostic accuracy.[9] In a direct comparison of ASL and $H_2[^{15}O]$-PET, one study found similar cortical perfusion values with no significant

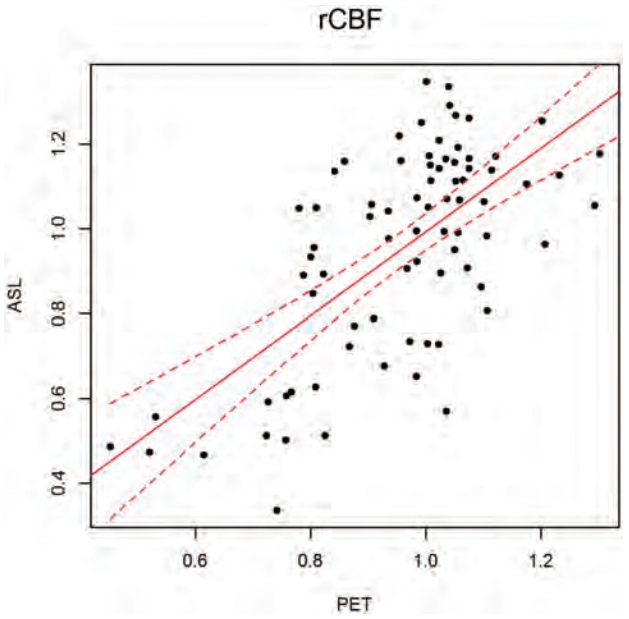

FIG 3. Correlation of relative CBF after cerebellar normalization (rCBF) between $H_2[^{15}O]$-PET and arterial spin-labeling ($r = 0.67$, $P < .001$). Linear regression fit line is shown in red (dashed lines show 95% confidence limits).

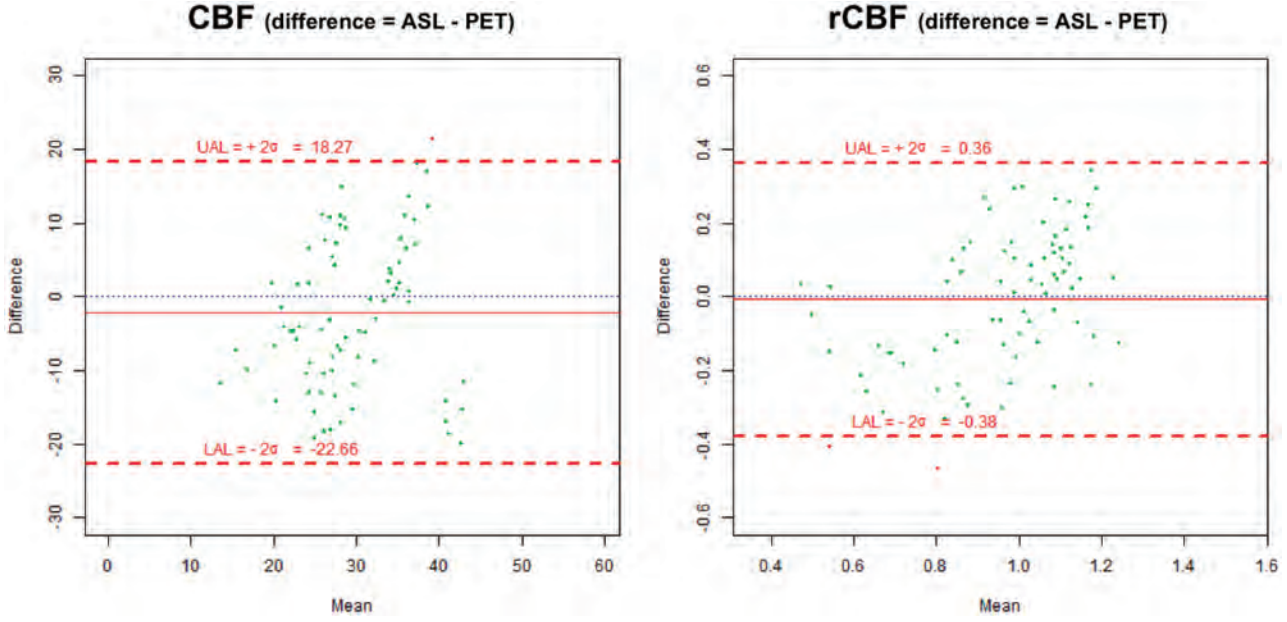

FIG 4. Bland-Altman plots of CBF (mL/100 g per minute) and relative CBF after cerebellar normalization (rCBF).

differences between the 2 modalities in 12 healthy subjects.[21] However, to the best of our knowledge, there has been no study comparing cerebral perfusion imaging with ASL and the current reference standard of $H_2[^{15}O]$-PET in children and young adults with Moyamoya disease.

Assessment of CBF with ASL imaging has been shown to correlate with (^{123}I-IMP)-SPECT in patients with Moyamoya disease, though the absolute values of CBF were found to be slightly lower in ASL.[22] Our results show a similar trend toward underestimation of CBF in ASL compared with $H_2[^{15}O]$-PET, particularly in territories with severely reduced perfusion in the qualitative visual assessment. This could be partly due to long transit times caused by the presence of collateral vessel networks feeding these territories, leading to a loss of perfusion signal in which the labeled blood does not arrive between the time of labeling and image acquisition, resulting in artificially low CBF values.[23] However, because transit time errors would not be expected to affect the cerebellar perfusion in Moyamoya disease, the observation that cerebellar normalization improves the correlation between ASL and PET suggests that lengthened transit times are not the major source of the discrepancy in absolute perfusion values between the 2 modalities. Rather, our observation that cerebellar normalization improves the agreement between ASL and PET suggests that errors in global scaling factors (which would affect the cerebellum and cortical/subcortical regions equally) are likely to underlie the differences in absolute ASL and PET perfusion values. Because the reliability of ASL perfusion values is most affected by errors in the labeling efficiency, the equilibrium magnetization of blood and tissue, and the blood T1 used for perfusion scaling,[24] errors in these factors may contribute to the difference in perfusion values measured between ASL and PET observed in the present study. However, accounting for differences in blood T1 did not improve the correlation between ASL and PET perfusion values in our study, suggesting that the discrepancy observed between the perfusion measurements from the 2 modalities without cerebellar normalization are likely to arise from other effects. Future studies should investigate if MR angiographic flow measurements can reduce these errors by correcting the labeling efficiency values used for quantification.

Alternatively, the difference in ASL-derived and $H_2[^{15}O]$-PET–derived CBF values could also be caused by the use of a mean arterial input function–based method for $H_2[^{15}O]$-PET.[14] Whereas this method substantially reduces the invasive nature of $H_2[^{15}O]$-PET, it does not measure the individual activity in arterial blood. Indeed, CBF measured with the less invasive technique was shown to overestimate true perfusion by approximately 11%. Because this difference is substantially larger than that between ASL and PET in our study, the underestimation that we found could be considered negligible. This is supported by the lack of a significant difference in CBF or rCBF in territories with qualitatively normal perfusion.

Generally, comparisons of quantitative values between different modalities with different quantification models must be interpreted with caution. To minimize bias caused by different quantification models, we normalized the CBF values found in the supratentorial vascular territories to cerebellar CBF (rCBF). In patients with Moyamoya disease, which predominantly affects the anterior circulation, cerebellar perfusion may be assumed to be normal and act as an intraindividual reference for the detection of reduced perfusion. In our study, the mean difference in perfusion values between $H_2[^{15}O]$-PET and ASL was reduced from approximately 13% to a mere 0.7% after cerebellar normalization, leading to a regression slope of 1.0061 (intercept of −0.0057) and allowing for a more meaningful comparison between the 2 modalities.

Limitations

A limitation of our study is the rather small study cohort. However, this is inherent to the low prevalence of this disease. Second, ASL and $H_2[^{15}O]$-PET were not performed in an integrated PET/MR imaging scanner in the same examination or on the same day, but up to 13 days apart. However, there were no interventions or cerebrovascular incidents between the 2 examinations in any of the patients. Because we had no patients with both preoperative and postoperative examinations with both ASL and $H_2[^{15}O]$-PET, we could not evaluate the correlations of ASL and $H_2[^{15}O]$-PET for the assessment of postoperative improvement of perfusion.

CONCLUSIONS

Our results demonstrate that the assessment of CBF after cerebellar normalization by use of arterial spin-labeling MR imaging correlates well with the $H_2[^{15}O]$-PET reference standard method in children and young adults with Moyamoya disease. Therefore, ASL may prove to be a valuable alternative for preoperative assessment and postoperative follow-up in these patients without the use of ionizing radiation or the need for injection of an exogenous contrast agent.

Disclosures: Geoffrey Warnock—*OTHER RELATIONSHIPS:* Teaching consultant for PMOD Technologies. Alfred Buck—*UNRELATED: Royalties:* Medrad Inc.

REFERENCES

1. Suzuki J, Takaku A. **Cerebrovascular "Moyamoya" disease: disease showing abnormal net-like vessels in base of brain.** *Arch Neurol* 1969;20:288–99
2. Smith ER, Scott RM. **Spontaneous occlusion of the circle of Willis in children: pediatric Moyamoya summary with proposed evidence-based practice guidelines: a review.** *J Neurosurg Pediatr* 2012;9:353–60
3. Feole JB, Ali A, Fordham EW, et al. **Serial SPECT imaging in Moyamoya using I-123 IMP: a method of noninvasive evaluation and follow-up.** *Clin Nucl Med* 1993;18:43–45
4. Ikezaki K, Matsushima T, Kuwabara Y, et al. **Cerebral circulation and oxygen metabolism in childhood Moyamoya disease: a perioperative positron emission tomography study.** *J Neurosurg* 1994;81:843–50
5. Nambu K, Suzuki R, Hirakawa K. **Cerebral blood flow: measurement with xenon-enhanced dynamic helical CT.** *Radiology* 1995;195:53–57
6. Nariai T, Suzuki R, Hirakawa K, et al. **Vascular reserve in chronic cerebral ischemia measured by the acetazolamide challenge test: comparison with positron emission tomography.** *AJNR Am J Neuroradiol* 1995;16:563–70
7. Weber B, Westera G, Treyer V, et al. **Constant-infusion H(2)15O PET and acetazolamide challenge in the assessment of cerebral perfusion status.** *J Nucl Med* 2004;45:1344–50
8. Vakil P, Lee JJ, Mouannes-Srour JJ, et al. **Cerebrovascular occlusive disease: quantitative cerebral blood flow using dynamic suscepti-**

bility contrast MR imaging correlates with quantitative H2[15O] PET. *Radiology* 2013;266:879–86
9. Goetti R, O'Gorman R, Khan N, et al. **Arterial spin labelling MRI for assessment of cerebral perfusion in children with Moyamoya disease: comparison with dynamic susceptibility contrast MRI.** *Neuroradiology* 2013;55:639–47
10. Dai W, Garcia D, de Bazelaire C, et al. **Continuous flow-driven inversion for arterial spin labeling using pulsed radio frequency and gradient fields.** *Magn Reson Med* 2008;60:1488–97
11. Alsop DC, Detre JA. **Reduced transit-time sensitivity in noninvasive magnetic resonance imaging of human cerebral blood flow.** *J Cereb Blood Flow Metab* 1996;16:1236–49
12. Wang J, Zhang Y, Wolf RL, et al. **Amplitude-modulated continuous arterial spin-labeling 3.0-T perfusion MR imaging with a single coil: feasibility study.** *Radiology* 2005;235:218–28
13. Jarnum H, Steffensen EG, Knutsson L, et al. **Perfusion MRI of brain tumours: a comparative study of pseudo-continuous arterial spin labelling and dynamic susceptibility contrast imaging.** *Neuroradiology* 2010;52:307–17
14. Treyer V, Jobin M, Burger C, et al. **Quantitative cerebral H2(15)O perfusion PET without arterial blood sampling, a method based on washout rate.** *Eur J Nucl Med Mol Imaging* 2003;30:572–80
15. Arigoni M, Kneifel S, Fandino J, et al. **Simplified quantitative determination of cerebral perfusion reserve with H2(15)O PET and acetazolamide.** *Eur J Nucl Med* 2000;27:1557–63
16. Hammers A, Allom R, Koepp MJ, et al. **Three-dimensional maximum probability atlas of the human brain, with particular reference to the temporal lobe.** *Hum Brain Mapp* 2003;19:224–47
17. R Core Team. **R: A language and environment for statistical computing.** R Vienna, Austria: Foundation for Statistical Computing. http://www.R-project.org/.2013
18. Calamante F, Ganesan V, Kirkham FJ, et al. **MR perfusion imaging in Moyamoya syndrome: potential implications for clinical evaluation of occlusive cerebrovascular disease.** *Stroke* 2001;32:2810–16
19. Huisman TA, Sorensen AG. **Perfusion-weighted magnetic resonance imaging of the brain: techniques and application in children.** *Eur Radiol* 2004;14:59–72
20. Wang DJ, Alger JR, Qiao JX, et al. **The value of arterial spin-labeled perfusion imaging in acute ischemic stroke: comparison with dynamic susceptibility contrast-enhanced MRI.** *Stroke* 2012;43:1018–24
21. Ye FQ, Berman KF, Ellmore T, et al. **H(2)(15)O PET validation of steady-state arterial spin tagging cerebral blood flow measurements in humans.** *Magn Reson Med* 2000;44:450–56
22. Noguchi T, Kawashima M, Irie H, et al. **Arterial spin-labeling MR imaging in Moyamoya disease compared with SPECT imaging.** *Eur J Radiol* 2011;80:e557–562
23. Calamante F, Thomas DL, Pell GS, et al. **Measuring cerebral blood flow using magnetic resonance imaging techniques.** *J Cereb Blood Flow Metab* 1999;19:701–35
24. Wu WC, St Lawrence KS, Licht DJ, et al. **Quantification issues in arterial spin labeling perfusion magnetic resonance imaging.** *Top Magn Reson Imaging* 2010;21:65–73

Spinal Cord Injury after Blunt Cervical Spine Trauma: Correlation of Soft-Tissue Damage and Extension of Lesion

R. Martínez-Pérez, I. Paredes, S. Cepeda, A. Ramos, A.M. Castaño-León, C. García-Fuentes, R.D. Lobato, P.A. Gómez, and A. Lagares

ABSTRACT

BACKGROUND AND PURPOSE: In patients with spinal cord injury after blunt trauma, several studies have observed a correlation between neurologic impairment and radiologic findings. Few studies have been performed to correlate spinal cord injury with ligamentous injury. The purpose of this study was to retrospectively evaluate whether ligamentous injury or disk disruption after spinal cord injury correlates with lesion length.

MATERIALS AND METHODS: We retrospectively reviewed 108 patients diagnosed with traumatic spinal cord injury after cervical trauma between 1990–2011. Plain films, CT, and MR imaging were performed on patients and then reviewed for this study. MR imaging was performed within 96 hours after cervical trauma for all patients. Data regarding ligamentous injury, disk injury, and the extent of the spinal cord injury were collected from an adequate number of MR images. We evaluated anterior longitudinal ligaments, posterior longitudinal ligaments, and the ligamentum flavum. Length of lesion, disk disruption, and ligamentous injury association, as well as the extent of the spinal cord injury were statistically assessed by means of univariate analysis, with the use of nonparametric tests and multivariate analysis along with linear regression.

RESULTS: There were significant differences in lesion length on T2-weighted images for anterior longitudinal ligaments, posterior longitudinal ligaments, and ligamentum flavum in the univariate analysis; however, when this was adjusted by age, level of injury, sex, and disruption of the soft tissue evaluated (disk, anterior longitudinal ligaments, posterior longitudinal ligaments, and ligamentum flavum) in a multivariable analysis, only ligamentum flavum showed a statistically significant association with lesion length. Furthermore, the number of ligaments affected had a positive correlation with the extension of the lesion.

CONCLUSIONS: In cervical spine trauma, a specific pattern of ligamentous injury correlates with the length of the spinal cord lesion in MR imaging studies. Ligamentous injury detected by MR imaging is not a dynamic finding; thus it proved to be useful in predicting neurologic outcome in patients for whom the MR imaging examination was delayed.

ABREVIATIONS: ALL = anterior longitudinal ligament; ASIA = American Spinal Injury Association Impairment Scale; LF = ligamentum flavum; PLL = posterior longitudinal ligament; SCI = spinal cord injury; SCIWORA = spinal cord injury without radiological abnormalities

Acute traumatic spinal cord injury (SCI) is located at the cervical level in 45–75% of cases.[1,2] Thus, cervical trauma is potentially the source of long-term disability because of its associated risk of SCI.[2] The internal architecture of the spinal cord, as well as soft tissue injury, is best visualized with MR imaging. However, MR imaging performed after the cervical trauma has prognostic implications for the therapeutic management of this disease; hence, it has become part of the standard imaging protocol for patients with acute cervical spine injury.[3] Since the early 1990s, several studies have investigated the role of several radiologic findings in SCI.[3,4] Previous published reports have described the mechanism and biomechanics of spinal stability after blunt trauma.[5-7] It is believed that the degree of soft-tissue damage is related to the severity of the SCI. However, very few studies have similarly shown this association.

Instead, the correlation between lesion length and neurologic outcome has been sufficiently demonstrated in the acute phase after cervical trauma.[8,9] In fact, it has been recommended that the first MR imaging should be performed 24–72 hours after injury.[10] The prognostic value of MR imaging in later stages is less clear because of the dynamic nature of edema and the dependence on the lesion length after trauma.[11] Therefore, we designed this study to detect soft-tissue injuries that are related to more pronounced

Received February 5, 2013; accepted after revision September 9.

From the Departments of Neurosurgery (R.M.-P., I.P., S.C., AM.C.-L., R.D.L., P.A.G., A.L.) and Radiology (A.R.), and Intensive Care Unit (C.G.-F.), Hospital 12 de Octubre, Universidad Complutense de Madrid, Madrid, Spain.

Please address correspondence to Rafael Martínez-Pérez, MD, Hospital 12 de Octubre. Andalucía s/n, 28041, Madrid, Spain; e-mail: rafa11safin@hotmail.com

http://dx.doi.org/10.3174/ajnr.A3812

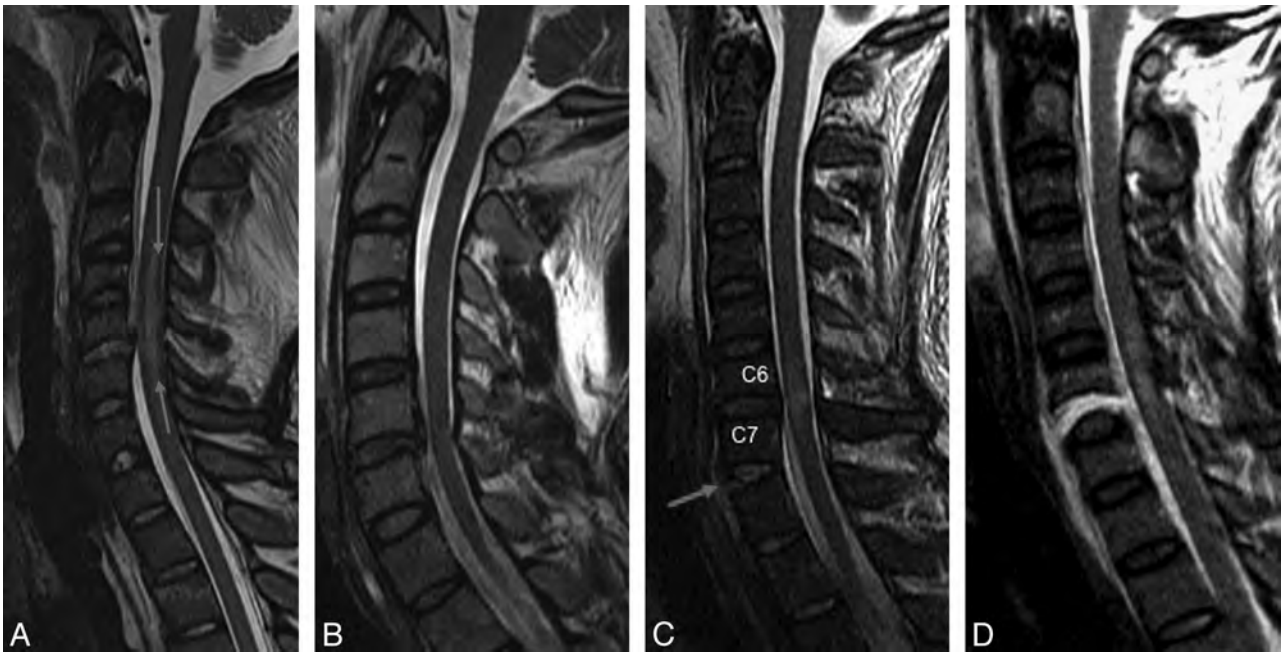

FIGURE. *A,* Traumatic herniation disk producing spinal cord compression at the same level; it is seen as hyperintensity in the T2-weighted image. Lesion length is measured in millimeters from the most cephalad level to the lowest (*arrows*). *B,* Sagittal projection on T2-weigthed images. Disruption of posterior longitudinal ligament is visualized at level C5–C6. *C,* Sagittal projection on T2-weighted image. At level C7–T1, the injured anterior longitudinal ligament (*arrow*) is seen. Signal changes are shown at level C6–C7. *D,* Damage in anterior longitudinal ligament, posterior longitudinal ligament, ligamentum flavum, and disk are represented by a disruption in low signal intensity corresponding to this structure.

lesions, which MR imaging can detect, including more severe SCI. Soft-tissue injury is a more static finding than is cord edema and can convey potentially relevant information when MR imaging is delayed (Fig 1).

MATERIALS AND METHODS

Patients with known SCI after non-penetrating cervical spine trauma over a 21-year period were recruited in the clinical, retrospective data base. Only patients in whom cervical MR imaging was performed within 96 hours after trauma were selected for further analysis.

Patients who were neurologically intact, or whose MR imaging was performed after the fourth day of the injury, were excluded. Patients with severe traumatic brain injury or upper cervical spine injuries (C1–C2 fractures) were also excluded from the analysis. Thoracic injuries were not included either.

We recorded clinical variables, including age, sex, mechanism of injury, and neurologic status. Epidemiologic data also examined age, sex, and mechanism of injury from the medical records. Neurologic status was assessed clinically during the first examination by using the American Spinal Injury Association Impairment Scale (ASIA) (Table 1).

Plain radiographs, CT scans, and MR images were consensually assessed by a neurosurgeon trained in cervical trauma images (I.P.) and an experimental neuroradiologist (A.R.). Both observers were blinded to patient clinical and neurologic data.

To diagnose the level and extension of injury and determine the number of fractures, plain radiographs, MR imaging, and CT were used. The presence of fracture and bone integrity was assessed in the CT scan.

Soft-tissue injury was assessed with the use of MR imaging and analyzed with anterior longitudinal ligament (ALL), posterior longitudinal ligament (PLL), and ligamentum flavum (LF), and the intervertebral disk was examined. In all patients, MR imaging was performed within the first 4 days after trauma. MR imaging was performed with the use of a 1.5T magnet and 3-mm section thickness for axial and sagittal planes. We analyzed ligamentous injury by assessing disruption in T1- and T2-weighted images (in a sagittal plane), including axial T2- and T2*-weighted images. In all patients, lesion length was determined by intramedullary cord signal intensity change in T2-weighted images and was defined as the distance in millimeters between the most caudal and cephalad signal intensity change in the cord. Soft-tissue disruption was defined as a clear MR imaging signal with complete discontinuity of the structure in all appropriate imaging sections.

The segment affected was defined as fracture level with only 1 fracture: if there was more than 1, it was defined as the fracture

Table 1: American Spinal Injury Association Impairment Scale

Grade A	Complete: No sensory or motor function is preserved in the sacral segments S4–S5
Grade B	Incomplete: Sensory but not motor function is preserved below the neurological level and includes the sacral segments S4–S5
Grade C	Incomplete: Motor function is preserved below the neurological level, and more than half of key muscles below the neurological level have a muscle grade <3
Grade D	Incomplete: Motor function is preserved below the neurological level, and at least half of key muscles below the neurological level have a muscle grade ≥ 3
Grade E	Normal: Sensory and motor function is normal

level that produced the most cord compression. In cases with SCI but without radiologic abnormalities (SCIWORA), we considered the segment to be affected when the soft tissues were most injured.

We analyzed the data with univariate and multivariate methods to compare the damage of soft-tissue structures (LF, ALL, PLL, and disk), including the extent of SCI. ALL, PLL, LF, and disk injuries were independently analyzed as dichotomous variables (damaged or intact); the extent of SCI (distance between the most caudal and cephalad of the cord signal intensity change [hyperintensity] in a sagittal plane, T2-weighted image measured in millimeters) was considered to be a continuous variable. Levels of injury, age, and sex were analyzed as potential covariates. Sex (male/female) and level of injury (upper lesion, C3-C4-C5 and lower lesion, C6-C7-C8) were considered dichotomous variables, whereas age was seen as a continuous variable. The Mann-Whitney *U* test compared lesion length of each predefined qualitative variable (ALL, PLL, LF, and disk damage, sex, and level of injury). Spearman ρ was calculated to demonstrate the correlation between lesion length and age. Variables with a value of $P < .1$ were included in the multivariate analysis. Linear regression was used for the multivariate analysis as well.

The Kruskall-Wallis test could also probe a possible association between how many ligaments were affected (none, 1, 2, or 3 ligaments), including lesion length.

The association between lesion length and neurologic status was also analyzed. Lesion length was considered a continuous variable, as stated previously. Neurologic status at admission was separated as complete SCI (ASIA A) and incomplete SCI (ASIA B, C, and D). We used a *t* test to compare the lesion length for the 2 groups. The threshold for statistical significance was $P < .05$, and all tests were calculated by use of SPSS v20 (IBM, Armonk, New York).

RESULTS

We retrospectively reviewed 331 patients with known or suspected SCI or with radiculopathy after a non-penetrating cervical spine trauma who presented to the emergency department or the intensive care unit at our institution between 1990–2011. MR imaging was performed on 186 patients within 96 hours after trauma who were then selected for further analysis. We excluded 40 patients with severe traumatic brain injury from the analysis. In addition, 38 patients with upper cervical spine trauma (C1–C2 fractures) were also excluded. Finally, data analysis included 108 patients (87 men and 21 women, ages 17–86 years; overall mean age, 40.5 years) (Table 2). Seventy-four patients had 1 fracture, 13 patients had 2, and 3 patients had 3 noncontiguous fractures, respectively. In 18 patients, there was no evidence of any fracture after radiologic examination: all patients were diagnosed with SCI without radiologic abnormalities (SCIWORA). The most common mechanism of injury was motor vehicle crash (Table 2). The C5–C6 spinal level was most commonly involved (Table 2). As stated, MR imaging was performed within 96 hours after the trauma occurred in all patients, whereas in 81.4% of these patients, it was performed within the first 72 hours. According to ASIA, there were 39 patients with ASIA A, 10 patients with ASIA B, 22 patients with ASIA C, and 37 patients with ASIA D (Table 2).

Table 2: Characteristics of patients with acute traumatic cervical SCI

Characteristic	No. of Patients (%)
Mean age, y	40.5 (17–86)
Male	87 (80.6)
Female	21 (19.4)
Severity of SCI	
ASIA A	39 (36.1)
ASIA B	10 (9.3)
ASIA C	22 (20.3)
ASIA D	37 (34.3)
Spinal level of SCI	
C3–C4	16 (14.8)
C4–C5	22 (20.3)
C5–C6	31 (28.7)
C6–C7	24 (22.2)
C7–T1	15 (13.8)
Cause of SCI	
Motor vehicle crash	61 (56.4)
Car crash	35 (32.4)
Pedestrians	8 (7.4)
Motorcyclists	18 (16.6)
Falls	33 (30.6)
Sport injury	9 (8.3)
Aggression/assault	5 (4.6)

Table 3: Univariate analysis: Qualitative variables (soft tissues)

	No. of Cases (%)		Mean Length of Lesion, mm		*P*
Structure	Intact	Disrupted	Intact	Disrupted	Value
ALL	51 (47.2)	57 (52.8)	43.22	64.60	<.001
PLL	45 (41.7)	63 (58.3)	47.64	59.40	.05
LF	56 (51.9)	52 (48.1)	35.96	74.46	<.001
Disk	46 (42.6)	62 (57.4)	47.48	59.71	.044

Table 4: Multivariate analysis: Linear regression

Dependent Variable	Independent Variable	*P* Value
Lesion length (mm)	ALL	.395
	PLL	.525
	LF	<.001
	Disk	.464
	Age	.215

Note:—R^2 value of prediction model number 1 = 0.365.

Age was correlated with lesion length ($P = .036$) in the univariate analysis and was included in the multivariate analysis as a covariate. The level of lesion ($P = .449$) and sex ($P = .398$) were not associated with larger lesions in the univariate analysis. Eighteen patients did not show hyperintensity changes in T2-weighted images. ALL was disrupted in 52.8% of cases, PLL in 58.3%, LF in 48.1%, and disk in 57.4%. Average cord lesion length (in mm) for disrupted and non-disrupted soft tissue was 64.60 and 43.22 for ALL, 59.40 and 47.64 for PLL, 74.46 and 35.96 for LF, 59.71 and 47.48 for disk, respectively. All structures showed a greater mean lesion length when there was soft-tissue disruption, compared with when there was not disruption. With the use of univariate analysis, LLA, PLL, LF, and disk disruption were related to a significantly larger lesion length (Table 3). However, in multivariate analysis, LF was the only structure showing a significant association between the ligament injured and greater lesion length (Table 4).

There were 22 patients without disrupted ligaments, 34 with 1

disrupted ligament, 17 with 2 disrupted ligaments, and 35 with 3 disrupted ligaments. Mean lesion lengths in millimeters were 29.75, 50.15, 56.38, and 73.37 for none, 1, 2, and 3 disrupted ligaments, respectively. The number of disrupted ligaments correlated with lesion length (Pearson correlation coefficient, 0.49; $P < .01$).

Patients with complete SCI at admission had a larger intramedullary lesion ($P < .001$) than did patients with incomplete SCI.

DISCUSSION

Previous studies show that lesion lengths measured in sagittal T2-weighted images are related to patient prognosis.[9,12-14] Edema is seen in T2 MR imaging sequences as hyperintensity of the signal within the cord, whereas a low intensity area on T2-weighted images in the acute stage is thought to indicate intramedullary hemorrhage, attributed to deoxyhemoglobin.[15,16] In addition, because hemorrhage is almost always concurrent with edema, it is common to measure signal hyperintensity in T2-weighted images to determine the length of the lesion.[17] It is not clear whether these signal changes are a result of primary or secondary spinal cord damage.[18]

MR imaging may be a useful tool in the management of cervical trauma, especially in cases of questionable structural instability, because it is extremely useful in detecting soft-tissue injury.[19,20] Patients without demonstrated abnormalities in plain radiographs or CT may show signs of instability with MR imaging, as determined by soft-tissue involvement. Some authors have demonstrated that different ligamentous injuries are associated with spinal instability; therefore, this could serve as a guide for surgical treatment of traumatic instability of the spinal cord. Greater posterior vertebral body translation and angulation are related to disruption of the posterior ligamentous complex[21,22] and are indirect signs of spinal instability.

For assessing disruption of ligaments, T2-weighted images in the sagittal plane should be included in all MR imaging protocols.[3] Other sequences have been described in the literature to rule out soft-tissue injuries, such as fat-suppressed T2 images (STIR).[19,20] In acute cervical trauma, MR imaging has moderate to high sensitivity for injury of specific ligamentous structures but low specificity for intraoperative findings of the same injuries.[23,24] The posterior ligamentous complex consists of supraspinous and interspinous ligaments: the LF, the facet capsules, and the cervical fascia.[25-28] In several studies, MR imaging was also sensitive for the evaluation of injury of the posterior ligamentous complex[19,24]; this suggests that injury to ALL may be underestimated with the use of MR imaging, if the findings are considered in isolation. The explanation is that ALL and PLL adhere to the disk, whereas only the ALL adheres to the vertebrae, such that the PLL is easier to identify.[3]

We have discussed the importance of MR imaging in the detection of ligamentous injury after cervical trauma: it also determines the structural stability of the cervical spine. Spinal instability is related to neurologic injury and therefore to cord injury because the involvement of soft tissue may play a role in the extent of SCI. This report shows that damage to soft tissue such as LF, ALL, PLL, and disk is related to longer-length cord hyperintensity as measured in T2-weighted images; when this was adjusted for age, level of injury, sex, and ligamentous or disk injury in a multivariate analysis, only LF injury was found to be significantly associated with lesion length.

We hypothesize that LF injury is more strongly correlated with extension of cord damage, in that posterior elements are associated with increased instability and therefore with greater SCI. Another possible explanation is that the LF is more elastic and that more pressure is needed to break it. The force required for this kind of injury would be responsible for SCI; it is probably the result of a combination of the 2 mechanisms because they are not mutually exclusive. We excluded patients with upper cervical fractures because these lesions are the result of different injury mechanisms.[18]

Several prognostic factors have been described as predictive of traumatic spinal cord damage.[10,13,17,29-32] Some studies have focused on particular clinical features, such as SCIWORA,[29,33] Central Cord syndrome,[29] or Brown-Sequard syndrome.[34] Evidence in the literature shows that more severe abnormalities seen through MR imaging have been associated with more severe neurologic status. Excessive edema, changes in T2-weighted images, greater degree of cord compression, and hemorrhage have been related to worse neurologic outcomes.[9,35-38] Gain in motor strength at follow-up has been seen to correlate with a decrease in T2-weighted hyperintensity in serial MR imaging studies.[39] Some authors have described a close correlation between level of injury and severity of SCI.[30] Miranda et al[34] found an association between MR imaging signal changes and level of injury. Therefore, because the level of injury is related anatomically with the level of fracture, we also introduced this factor in the multivariate analysis. To our knowledge, there is 1 paper in the literature that relates the severity of ligamentous injury with degree of SCI.[6] In this study, we found that the severity of PLL, versus ALL injury, was correlated with more severe SCI, especially in patients with extension fractures.

Our study found that patients without signal changes in the spinal cord had few neurologic deficits. Patients with complete SCI showed larger lesions than did those with incomplete SCI. This in turn highlights the correlation between radiologic and clinical findings.

Limitations

The first limitation of our study may be related to the timing of the MR imaging. Clinical instability associated with cervical trauma sometimes impedes the reliability of MR imaging in the first hours. A review of the literature by Bozzo et al[3] concluded that MR imaging should be done in the acute period after SCI for better prognostication. It has also been recommended that the first MR imaging should be performed 24–72 hours after trauma.[10] However, there is a lack of evidence supporting precise guidelines.[3,23] In fact, transferring critical or unstable patients from the intensive care unit to an x-ray room presents an unacceptable risk during the first days, especially in patients with trauma. Length of edema in T2-weighted images depends on the time when the MR imaging was performed after trauma.[11] The extension of the lesion may be overestimated in patients in whom MR imaging was performed at a later point in time. To focus on

acute traumatic injury, and to minimize potential bias introduced with chronic injury, we only included patients who had undergone MR imaging during the first 96 hours after injury. In 82.4% of these patients, MR imaging was performed within 72 hours after trauma.

The second limitation of our study could be correct identification and diagnosis of ligament disruption. T2-weighted images have shown moderate to high sensitivity with low specificity when compared with intraoperative findings in ligament disruption.[23,24] Other sequences have been described in the literature that rule out soft-tissue injuries, such as STIR. One study showed a high correlation between STIR sequences and intraoperative findings in detecting soft-tissue injury.[27] Unfortunately, the STIR sequence was not included in all cervical trauma protocols during the initial years of this study; in this sense, not all patients were observed for STIR sequence, even though most were. We used STIR for assessment of soft tissue when it was available. Any assessment of the extent of damage in spinal cord and ligament injuries is subjective, which poses another potential limitation and source of bias.

Third, this study comprised a select group of cases that were managed in the intensive care or neurosurgery units. Minor cervical trauma with a lesser degree of lesion does not require MR imaging by protocol in most cases. Furthermore, this study does not include all patients with cervical spine trauma, but it does involve most patients with more severe cervical trauma.

Fourth, steroids were not included in our treatment protocol after Bracken et al[40] could not corroborate statistically significant benefits from steroids. Most patients did not receive steroids, and it was therefore not possible to access this information in relation to the time of imaging; thus, this factor could not be adequately analyzed because it could have affected length of abnormal cord signals.

Finally, lesion length represents the degree of SCI but is not a measure of neurologic outcome at follow-up. In this light, interpretation of these results should be taken with caution. Nevertheless, initial neurologic examination tends to have a certain degree of subjectivity: in patients with trauma, sedation, distractive pain, or clinical condition confounds reliable interpretation of the neurologic state at admission. This is often the case when it is necessary to differentiate between ASIA A (complete SCI) and ASIA B (incomplete, but no motor function preserved) in sedated patients. In the acute phase, lesion length is a measure that has been well correlated with neurologic recovery.[9,11] Reliability issues, as the result of feasibility of clinical examination for initial assessment of cervical spine trauma, were better determined in our study when MRI was performed within 96 hours after trauma. We prefer to use a continuous quantitative variable to indirectly appraise the degree of SCI. Our results correlate with those of previous works,[8,9,36] and larger lesions statistically correlate with more severe neurologic deficits with complete SCI in the acute phase ($P < .001$). However, other investigators have found that lesion length depends on the time of MR imaging after trauma.[11] The value of the extent of the lesion may be overestimated in patients for whom MR imaging was performed later. Therefore, we must determine which soft-tissue injury is associated with a greater degree of SCI, given that this is a static finding; however, intramedullary signal changes are dynamic, and their prognostic value decreases over time. Injury of the LF is a feature perdurable over time. It can also be detected when MR imaging is performed at a more delayed stage if the patient is clinically unstable during the acute phase and the MR imaging is not able to be obtained at an earlier stage. It could also be helpful in predicting neurologic outcome in these cases.

CONCLUSIONS

We have presented the first study that correlates ALL, PLL, LF, and disk lesions according to the degree of spinal cord damage. Patients who had disruption of the LF showed greater length of lesion as measured by MR imaging. Additionally, the statistical association between number of ligaments injured and greater signal changes in T2-weighted images of the spinal cord has been demonstrated.

We still have several concerns (timing of imaging, poor specificity in measurement method, short follow-up period, lack of objectivity); however, findings suggest that the extent of the T2 signal (after cervical spine trauma) correlates to a specific pattern of ligamentous injury. This might help determine neurologic outcome when MR imaging is performed after the acute phase, in that other features have less predictive potential.

Carefully designed studies, including neurologic outcome at follow-up, are needed to confirm some of our preliminary observations.

Disclosures: Ana Ramos—*UNRELATED: Grants/Grants Pending:* FIS* (**money paid to institution*).

REFERENCES

1. Hasler RM, Exadaktylos AK, Bouamra O, et al. **Epidemiology and predictors of spinal injury in adult major trauma patients: European cohort study.** *Eur Spine J* 2011;20:2174–80
2. Milby AH, Halpern CH, Guo W, et al. **Prevalence of cervical spinal injury in trauma.** *Neurosurg Focus* 2008;25:E10
3. Bozzo A, Marcoux J, Radhakrishna M, et al. **The role of magnetic resonance imaging in the management of acute spinal cord injury.** *J Neurotrauma* 2011;28:1401–11
4. Boldin C, Raith J, Fankhauser F, et al. **Predicting neurologic recovery in cervical spinal cord injury with postoperative MR imaging.** *Spine* 2006;31:554–59
5. Pizones J, Izquierdo E, Sanchez-Mariscal F, et al. **Sequential damage assessment of the different components of the posterior ligamentous complex after magnetic resonance imaging interpretation: prospective study 74 traumatic fractures.** *Spine* 2012;37:E662–67
6. Song KJ, Kim GH, Lee KB. **The efficacy of the modified classification system of soft tissue injury in extension injury of the lower cervical spine.** *Spine* 2008;33:E488–93
7. Vaccaro AR, Madigan L, Schweitzer ME, et al. **Magnetic resonance imaging analysis of soft tissue disruption after flexion-distraction injuries of the subaxial cervical spine.** *Spine* 2001;26:1866–72
8. Flanders AE, Spettell CM, Tartaglino LM, et al. **Forecasting motor recovery after cervical spinal cord injury: value of MR imaging.** *Radiology* 1996;201:649–55
9. Miyanji F, Furlan JC, Aarabi B, et al. **Acute cervical traumatic spinal cord injury: MR imaging findings correlated with neurologic outcome: prospective study with 100 consecutive patients.** *Radiology* 2007;243:820–27
10. Bondurant FJ, Cotler HB, Kulkarni MV, et al. **Acute spinal cord injury: a study using physical examination and magnetic resonance imaging.** *Spine* 1990;15:161–68
11. Leypold BG, Flanders AE, Burns AS. **The early evolution of spinal**

cord lesions on MR imaging following traumatic spinal cord injury. *AJNR Am J Neuroradiol* 2008;29:1012–16
12. Andreoli C, Colaiacomo MC, Rojas Beccaglia M, et al. **MRI in the acute phase of spinal cord traumatic lesions: relationship between MRI findings and neurological outcome.** *Radiol Med* 2005;110: 636–45
13. Ramon S, Dominguez R, Ramirez L, et al. **Clinical and magnetic resonance imaging correlation in acute spinal cord injury.** *Spinal Cord* 1997;35:664–73
14. Shimada K, Tokioka T. **Sequential MR studies of cervical cord injury: correlation with neurological damage and clinical outcome.** *Spinal Cord* 1999;37:410–15
15. Flanders AE, Schaefer DM, Doan HT, et al. **Acute cervical spine trauma: correlation of MR imaging findings with degree of neurologic deficit.** *Radiology* 1990;177:25–33
16. Kulkarni MV, Bondurant FJ, Rose SL, et al. **1.5 Tesla magnetic resonance imaging of acute spinal trauma.** *Radiographics* 1988;8: 1059–82
17. Flanders AE, Spettell CM, Friedman DP, et al. **The relationship between the functional abilities of patients with cervical spinal cord injury and the severity of damage revealed by MR imaging.** *AJNR Am J Neuroradiol* 1999;20:926–34
18. Alday R, Lobato, RD, Gomez PA. **Cervical spine fractures.** In: *Neurosurgery*. New York: Churchill Livingstone; 1996
19. Pizones J, Sanchez-Mariscal F, Zuniga L, et al. **Prospective analysis of magnetic resonance imaging accuracy in diagnosing traumatic injuries of the posterior ligamentous complex of the thoracolumbar spine.** *Spine* 2013;38:745–51
20. Pizones J, Zuniga L, Sanchez-Mariscal F, et al. **MRI study of posttraumatic incompetence of posterior ligamentous complex: importance of the supraspinous ligament. prospective study of 74 traumatic fractures.** *Eur Spine J* 2012;21:2222–31
21. Radcliff K, Su BW, Kepler CK, et al. **Correlation of posterior ligamentous complex injury and neurological injury to loss of vertebral body height, kyphosis, and canal compromise.** *Spine* 2012;37: 1142–50
22. Samartzis D, Wein SM, Shen FH, et al. **A revisitation of distractive-extension injuries of the subaxial cervical spine: a cadaveric and radiographic soft tissue analysis.** *Spine* 2010;35:395–402
23. Goradia D, Linnau KF, Cohen WA, et al. **Correlation of MR imaging findings with intraoperative findings after cervical spine trauma.** *AJNR Am J Neuroradiol* 2007;28:209–15
24. Rihn JA, Fisher C, Harrop J, et al. **Assessment of the posterior ligamentous complex following acute cervical spine trauma.** *J Bone Joint Surg Am* 2010;92:583–89
25. Carrino JA, Manton GL, Morrison WB, et al. **Posterior longitudinal ligament status in cervical spine bilateral facet dislocations.** *Skeletal Radiol* 2006;35:510–14
26. Haba H, Taneichi H, Kotani Y, et al. **Diagnostic accuracy of magnetic resonance imaging for detecting posterior ligamentous complex injury associated with thoracic and lumbar fractures.** *J Neurosurg* 2003;99:20–26
27. Lee HM, Kim HS, Kim DJ, et al. **Reliability of magnetic resonance imaging in detecting posterior ligament complex injury in thoracolumbar spinal fractures.** *Spine* 2000;25:2079–84
28. Vaccaro AR, Hulbert RJ, Patel AA, et al. **The subaxial cervical spine injury classification system: a novel approach to recognize the importance of morphology, neurology, and integrity of the disco-ligamentous complex.** *Spine* 2007;32:2365–74
29. Collignon F, Martin D, Lenelle J, et al. **Acute traumatic central cord syndrome: magnetic resonance imaging and clinical observations.** *J Neurosurg* 2002;96:29–33
30. Liao CC, Lui TN, Chen LR, et al. **Spinal cord injury without radiological abnormality in preschool-aged children: correlation of magnetic resonance imaging findings with neurological outcomes.** *J Neurosurg* 2005;103:17–23
31. Silberstein M, Hennessy O. **Implications of focal spinal cord lesions following trauma: evaluation with magnetic resonance imaging.** *Paraplegia* 1993;31:160–67
32. Yamashita Y, Takahashi M, Matsuno Y, et al. **Acute spinal cord injury: magnetic resonance imaging correlated with myelopathy.** *Br J Radiol* 1991;64:201–09
33. Dare AO, Dias MS, Li V. **Magnetic resonance imaging correlation in pediatric spinal cord injury without radiographic abnormality.** *J Neurosurg* 2002;97:33–39
34. Miranda P, Gomez P, Alday R, et al. **Brown-Sequard syndrome after blunt cervical spine trauma: clinical and radiological correlations.** *Eur Spine J* 2007;16:1165–70
35. Dai L, Jia L. **Central cord injury complicating acute cervical disc herniation in trauma.** *Spine* 2000;25:331–35
36. Marciello MA, Flanders AE, Herbison GJ, et al. **Magnetic resonance imaging related to neurologic outcome in cervical spinal cord injury.** *Arch Phys Med Rehabil* 1993;74:940–46
37. Selden NR, Quint DJ, Patel N, et al. **Emergency magnetic resonance imaging of cervical spinal cord injuries: clinical correlation and prognosis.** *Neurosurgery* 1999;44:785–92
38. Shepard MJ, Bracken MB. **Magnetic resonance imaging and neurological recovery in acute spinal cord injury: observations from the National Acute Spinal Cord Injury Study 3.** *Spinal Cord* 1999; 37:833–37
39. Miranda P, Gomez P, Alday R. **Acute traumatic central cord syndrome: analysis of clinical and radiological correlations.** *J Neurosurg Sci* 2008;52:107–12
40. Bracken MB, Shepard MJ, Collins WF, et al. **A randomized, controlled trial of methylprednisolone or naloxone in the treatment of acute spinal-cord injury: results of the Second National Acute Spinal Cord Injury Study.** *N Engl J Med* 1990;322:1405–11

Characterization of Peripheral Nerve Sheath Tumors with 3T Proton MR Spectroscopy

L.M. Fayad, X. Wang, J.O. Blakeley, D.J. Durand, M.A. Jacobs, S. Demehri, T.K. Subhawong, T. Soldatos, and P.B. Barker

ABSTRACT

BACKGROUND AND PURPOSE: The characterization of peripheral nerve sheath tumors is challenging. The purpose here was to investigate the diagnostic value of quantitative proton MR spectroscopy at 3T for the characterization of peripheral nerve sheath tumors as benign or malignant, compared with PET.

MATERIALS AND METHODS: Twenty participants with 24 peripheral nerve sheath tumors underwent MR spectroscopy by use of a point-resolved sequence (TE, 135 ms). Six voxels were placed in 4 histologically proven malignant peripheral nerve sheath tumors and 22 voxels in 20 benign peripheral nerve sheath tumors (9 histologically proven, 11 with documented stability). The presence or absence of a trimethylamine signal was evaluated, the trimethylamine concentration estimated by use of phantom replacement methodology, and the trimethylamine fraction relative to Cr measured. MR spectroscopy results for benign and malignant peripheral nerve sheath tumors were compared by use of a Mann-Whitney test, and concordance or discordance with PET findings was recorded.

RESULTS: In all malignant tumors and in 9 of 18 benign peripheral nerve sheath tumors, a trimethylamine peak was detected, offering the presence of trimethylamine as a sensitive (100%), but not specific (50%), marker of malignant disease. Trimethylamine concentrations (2.2 $\pm$ 2.8 vs 6.6 $\pm$ 5.8 institutional units; $P < .049$) and the trimethylamine fraction (27 $\pm$ 42 vs 88 $\pm$ 22%; $P < .012$) were lower in benign than malignant peripheral nerve sheath tumors. A trimethylamine fraction threshold of 50% resulted in 100% sensitivity (95% CI, 58.0%–100%) and 72.2% (95% CI, 59.5%–75%) specificity for distinguishing benign from malignant disease. MR spectroscopy and PET results were concordant in 12 of 16 cases, (2 false-positive results for MR spectroscopy and PET each).

CONCLUSIONS: Quantitative measurement of trimethylamine concentration by use of MR spectroscopy is feasible in peripheral nerve sheath tumors and shows promise as a method for the differentiation of benign and malignant lesions. Trimethylamine presence within a peripheral nerve sheath tumor is a sensitive marker of malignant disease, but quantitative measurement of trimethylamine content is required to improve specificity.

ABBREVIATIONS: MPNST = malignant peripheral nerve sheath tumor; NF-1 = neurofibromatosis type 1; PNST = peripheral nerve sheath tumor; SUV = standard uptake values; TMA = trimethylamine

Peripheral nerve sheath tumors (PNSTs) are commonly encountered in the general population, and most PNSTs are benign schwannomas and neurofibromas, rather than malignant peripheral nerve sheath tumors (MPNSTs).[1-3] However, the characterization of PNSTs by anatomic imaging methods and clinical features is challenging, given that the features of various benign tumors are shared,[4] and the features of benign PNSTs and MPNSTs overlap. Recent literature suggests some specific anatomic imaging features with MR imaging[5-8] and specific metabolic imaging features with PET[9-13] to be associated with malignant disease in PNSTs. Yet, noninvasive characterization of malignant disease remains problematic, especially in patients with neurofibromatosis type 1 (NF-1), who may have both benign and malignant tumors simultaneously and have greater risk for the development of MPNSTs than the general population.[7] Proton

Received May 30, 2013; accepted after revision August 13.

From The Russell H. Morgan Department of Radiology and Radiological Science (L.M.F., X.W., D.J.D., S.D., M.A.J., P.B.B.), Orthopedic Surgery (L.M.F.), Oncology (L.M.F., M.A.J.), The Johns Hopkins Hospital Comprehensive Neurofibromatosis Center and Department of Neurology (J.O.B.), The Johns Hopkins University School of Medicine, Baltimore, Maryland; Department of Radiology (T.K.S.), University of Miami Miller School of Medicine, Miami, Florida; and Research Unit of Radiology and Medical Imaging (T.S.), National and Capodestrian University of Athens, Evgenidion Hospital, Athens, Greece.

Funding information: L.M. Fayad: GE Radiology Research Fellowship (GERRAF), Siemens Medical Systems, The William M.G. Gatewood M.D. Fellowship, The SCBT/MR Young Investigator Award.

Paper previously presented at: Annual Meeting of the Society for Skeletal Radiology, March 18–21, 2012; Miami Beach, Florida.

Please address correspondence to Laura M. Fayad, MD, The Russell H. Morgan Department of Radiology and Radiological Science, The Johns Hopkins Medical Institutions, 601 North Wolfe St, Baltimore, MD 21287; e-mail: lfayad1@jhmi.edu

Indicates article with supplemental on-line table.

http://dx.doi.org/10.3174/ajnr.A3778

MR spectroscopy has been used extensively to characterize brain tumors, but far less has been done to evaluate musculoskeletal lesions with MR spectroscopy[14] and, specifically, PNSTs.[15-18] The detection of a signal from trimethylamine (TMA) and choline-containing compounds by MR spectroscopy has been established as a valuable indicator of malignant disease in other musculoskeletal lesions from alterations in the metabolism of phosphocholine and phosphatidylcholine.[16-23]

We hypothesized that MPNSTs would show high TMA content but that benign PNSTs would show undetectable or low levels of TMA when quantified. This study investigates the feasibility of performing quantitative MR spectroscopy in PNSTs and assesses the differential TMA measures of benign and MPNSTs, particularly in patients with NF-1. TMA measurements were also assessed between benign schwannomas and neurofibromas, given prior reports that these entities may have different metabolic profiles by FDG-PET imaging.[24] Finally, we compared MR spectroscopy measurements with the FDG-PET results in a subset of patients who underwent PET imaging as part of their routine clinical evaluation.

MATERIALS AND METHODS

Study Design

This study was approved by the Institutional Review Board, and informed consent was obtained from each participant. Twenty participants with 24 PNSTs (histologically proven, or with clinical presentation and longitudinal imaging features consistent with neurofibroma in patients with NF-1 or schwannomas in patients with schwannomatosis) underwent MR imaging and quantitative proton MR spectroscopy at 3T. Two observers reviewed the MR imaging and MR spectroscopy data for each tumor. TMA measurements were compared between benign and MPNSTs, as well as among benign PNSTs, to determine the diagnostic performance of MR spectroscopy for the characterization of PNSTs. TMA content was also compared with maximal standard uptake values (SUVmax) when FDG-PET scans were available.

Patient Population

Research was performed at a tertiary care center having a comprehensive neurofibromatosis center and specialized care for patients with PNSTs. Participants were prospectively enrolled between August 2009 and April 2012, in a nonconsecutive manner. Inclusion criteria consisted of patients with suspected or known PNSTs with available histologic confirmation; patients with a documented history of NF-1, neurofibromatosis type 2, or schwannomatosis (diagnosed by clinical criteria and with genetic confirmation when available) with stable peripheral nerve tumors, and target lesions $> 1 \times 1 \times 1$ cm^3; and patients with no contraindication for MR imaging. Exclusion criteria were a contraindication for MR imaging, prior treatment for the PNST, or PNSTs with no subsequent histologic confirmation or definitive follow-up.

Patient medical records were reviewed for demographics, underlying diagnoses, and history of prior therapies to identify inclusion and exclusion criteria. Patient records were also reviewed to determine if FDG-PET imaging was performed as part of the patients' routine clinical care within 1 month of the MR spectroscopy examination, to assess the agreement of MR spectroscopy findings with FDG-PET.

Lesions were classified as malignant after surgical resection (4 MPNSTs with 6 voxel locations; 1 participant had a very large MPNST in which 3 single voxels were placed). Lesions were classified as benign neurofibromas if they had either histologic confirmation (3 histologically confirmed neurofibromas; in 2 of these cases, 2 MR spectroscopy voxels were located within the neurofibroma), or if the patient had a documented history of NF-1 and a stable clinical and imaging appearance consistent with neurofibroma (stable on follow-up evaluation between 5 and 7 months). Lesions were classified as benign schwannomas if the patient had either histologic confirmation (6 histologically proven schwannomas) or a documented history of schwannomatosis and a stable clinical and imaging appearance consistent with schwannoma (1 schwannoma stable for 18 months).

Imaging and MR Spectroscopy Acquisition

All studies were performed on a 3T MR system (Magnetom Trio or Magnetom Verio; Siemens, Erlangen, Germany) by use of a flexible phased-array body-matrix coil. Axial fat-suppressed T2-weighted images (spin echo: TR, 2886 ms; TE, 100 ms; FOV, 18; section thickness, 6 mm) and coronal STIR images (inversion recovery: TR, 2462 ms; TE, 100 ms; TI, 200 ms; FOV, 20; section thickness, 6 mm) of the body part in question were performed.

After the anatomic imaging was performed, water-suppressed MR spectroscopy was performed by use of a single-voxel point-resolved spectroscopy sequence (CHESS water suppression, 128 averages; TR, 2000 ms; TE, 135 ms; scan time, 4 minutes 16 seconds). The voxel size and location were determined by a radiologist to encompass most of the lesion, with careful attention to exclude structures outside the perimeter of the lesion, including adjacent bone cortex, muscle, and vascular structures. The range of voxel sizes used varied from 1–25 cm^3. For the estimation of TMA concentrations, a phantom replacement technique was used; signals from the lesion were compared with those from a 20-mmol/L solution of TMA recorded separately. To account for the different radiofrequency coil loading between the phantom and in vivo, the water signal was also recorded (without suppression, 16 averages) from the localized volume by use of transmit body coil receive and phased-array receive, as described previously.[25,26] No lipid suppression was applied. Shimming up to second order was performed to optimize the field homogeneity by a physicist with 8 years of experience. In 2 PNSTs, spectra were recorded by use of multivoxel MR spectroscopic imaging once it became available, with the same acquisition parameters, except that the nominal voxel size was smaller (1 cm^3, FOV of 16 cm, and 16×16 phase-encoding steps, 1 signal average, scan time 7 minutes 40 seconds).

MR Spectroscopy Data Processing

Spectra were analyzed by a physicist with 8 years of experience in MR spectroscopy and a radiologist with 9 years of experience in MR spectroscopy and 11 years of experience in imaging of musculoskeletal tumors, in consensus. The quality of the spectra was determined by the visibility of discrete TMA and Cr peaks, the degree of separation of the peaks, and the presence or absence of

Accuracy of proton MR spectroscopy for distinction of benign and malignant PNSTs

MR Spectroscopy Method of Analysis	Sensitivity (%)	Specificity (%)	Positive Predictive Value (%)	Negative Predictive Value (%)
Qualitative (presence of TMA peak)	100.0	50.0	40.0	100.0
Quantitative (TMA fraction > 50%)	100.0	72.2	54.5	100.0

artifacts. The signals evaluated included water (4.7 ppm), lipid (1.3 and 0.9 ppm), TMA (3.2 ppm), and Cr (3.0 ppm). Before analysis, each spectrum was judged for sufficient quality subjectively; if it had resolved TMA, Cr, water, and lipid peaks with no uncorrectable baseline distortions; and the absence of artifacts that might interfere with the TMA or Cr peak measurements. The presence or absence of a TMA peak was noted based on visual assessment.

Analysis of the spectra was performed by use of the "advanced method for accurate, robust, efficient spectral fitting" routine (AMARES)[12] in the "java-based Magnetic Resonance User's Interface" (jMRUI; www.mrui.uab.es/mrui/mrui_download/) package,[13] which fits the time-domain spectroscopy data as a model of exponentially decaying oscillators by use of a nonlinear least-squares algorithm. TMA and Cr concentrations were estimated by use of the phantom replacement method,[25,26] modified from previous use in normal skeletal muscle.[27] Metabolite concentrations were estimated by use of the formula:

$$[M] = [P] \times \frac{A_M}{A_P} \times \frac{n_P}{n_M} \times \frac{k_P}{k_M} \frac{TA_M}{TA_P} CF_{vol}$$

where M and P subscripts represent the in vivo (metabolite, M) and phantom (P) scans, respectively. $[M]$ is the estimated in vivo (TMA or Cr) molar concentrations in "institutional units" (i.u.), $[P]$ is the known (molar) concentration of the phantom, A represents the spectral peak area, n represents the number of protons in the molecular functional group ($n=9$ for TMA, $n=3$ for Cr), k is a term correcting for T1 and T2 relaxation times, TA is the radiofrequency transmitter amplitude (voltage) required for a 90° pulse in the phantom (P) and in vivo (M) MR spectroscopy acquisitions collection, and CF_{vol} is a correction factor for the relative presence of water and fat within the voxel. T1 and T2 relaxation times were taken from the literature.[28] Please see the Online Appendix for additional information.

PET Imaging

Eight patients, 7 having NF-1 and 1 having schwannomatosis, had FDG-PET scans available for comparison. All but 1 FDG-PET study was performed with early and delayed acquisitions, as described previously,[11,13] at the same institution where MR spectroscopy was acquired, and interpreted by nuclear medicine physicians; 1 FDG-PET study was performed with delayed imaging only, at a different institution, but was reinterpreted by the study institution's nuclear medicine physician.

PET results were recorded as "suspicious" (SUVs increased on delayed compared with early acquisition, or values ≥3.5[11,13]) or "not suspicious" (SUVs not meeting criteria for suspicious activity) by 1 observer (with 14 years of experience in image interpretation).

Statistical Analysis Methods

Descriptive statistics were reported for each PNST, including demographic information, anatomic lesion characteristics, clinical characteristics, and results of PET imaging. Qualitative MR spectroscopy results (presence or absence of a TMA signal) were compared for benign and malignant lesions, as well as among benign lesions, with use of the Fisher exact test. Quantitative MR spectroscopy results for each PNST were recorded as the metabolite concentrations when metabolite peaks were found. A percentage "TMA fraction" was determined from the metabolite concentration ratios as [TMA]/([TMA] + [Cr]) × 100. Note that this is slightly different from the more commonly used metric in prior MR spectroscopy studies of a TMA/Cr ratio; the TMA fraction was used here because it is a more stable measurement when Cr concentrations are either very low or are zero. Quantitative results were compared between benign and MPNSTs, and between neurofibromas and schwannomas, by the Wilcoxon 2-sampled (Mann-Whitney) test. The level of statistical significance was set at $P < .05$. Finally, MR spectroscopy and FDG-PET findings were recorded as concordant if MR spectroscopy and FDG-PET both classified lesions as malignant/suspicious or as benign/nonsuspicious.

RESULTS

The On-line Table lists the clinical, histologic, and imaging characteristics for the patients and imaged tumor(s), with documentation of follow-up. The median age of the participants was 42 years (age range, 11–78 years); there were 12 men and 8 women. Eight participants had NF-1, and 1 had schwannomatosis.

Two patients were excluded because of an aborted MR spectroscopy by patient preference ($n=1$), and nondiagnostic quality ($n=1$). Two additional participants were excluded because of a lack of histologic confirmation or definitive follow-up. Hence, a total of 6 voxels were placed in 4 MPNSTs and 18 voxels placed in 16 benign PNSTs. Diagnostic quality spectra were achieved for 22 of 24 included voxel locations.

A discrete TMA peak was identified in 9 of 18 voxels placed in benign PNSTs (4 schwannomas, 5 neurofibromas) and in 6 of 6 voxels placed in MPNSTs, suggesting that the absence of a detectable TMA signal is a useful sign of a benign PNST ($P = .02$). Sensitivity, specificity, positive predictive value, and negative predictive value to distinguish benign and malignant lesions, based on qualitative MR spectroscopy results, were 100%, 50.0%, 40.0%, and 100%, respectively (Table).

TMA concentrations were significantly lower in benign PNSTs (mean, 2.2 ± 2.8; range, 0–9.2) than in MPNSTs (mean, 6.6 ± 5.8; range, 1.6–14.0) ($P < .049$). There was also a significant difference in the TMA fraction of benign PNSTs (27% ± 42%; range, 0%–100%) and MPNSTs (88% ± 22%; range, 51%–100%) ($P < .012$). Taking a TMA fraction > 50%

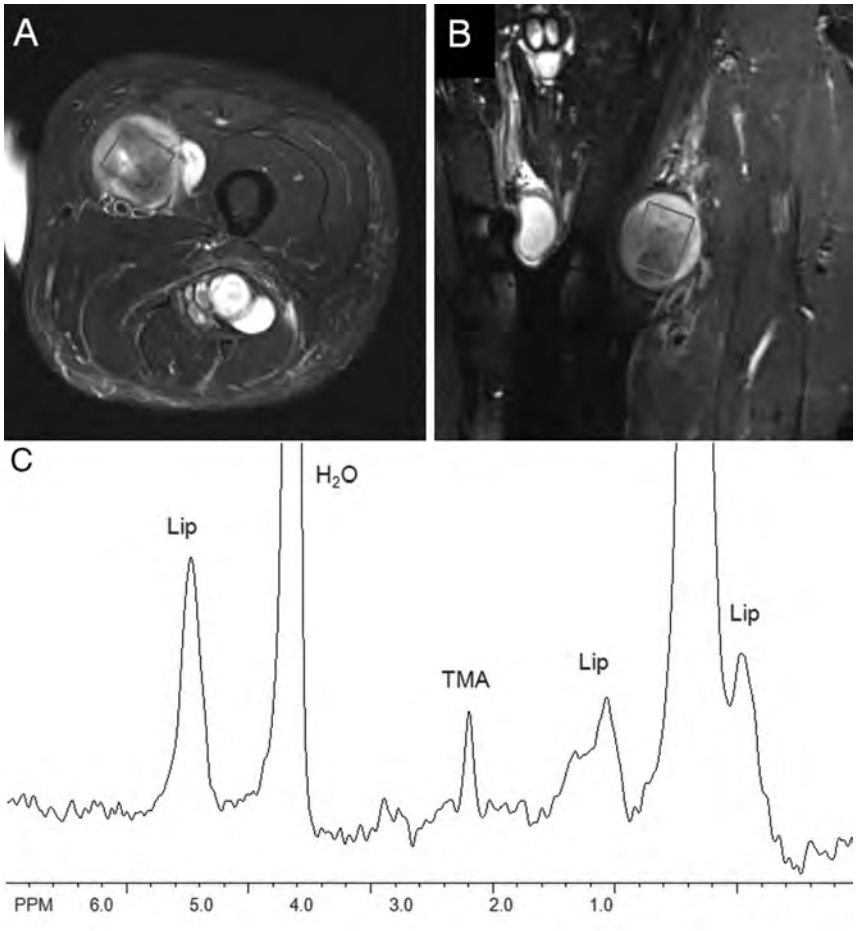

FIG 1. A 53-year old man with NF-1 and a left anterior thigh MPNST. Axial fat-suppressed T2-weighted (*A*) and coronal STIR (*B*) images show a heterogeneous mass within the left anterior thigh. Single-voxel placement is shown. (*C*) MR spectroscopy revealed a detectable TMA peak, with a TMA concentration of 14.0 institutional units and a TMA fraction of 74%.

as a definition for malignant disease resulted in a 100% negative predictive value and a sensitivity, specificity, and positive predictive value of 100%, 72.2%, and 54.5%, respectively. Figures 1 and 2 show examples of benign PNSTs and MPNSTs. Figure 3 is a graphic representation of TMA content between schwannomas, neurofibromas, and MPNSTs.

In patients with a history of NF-1, lower TMA concentrations were found in benign neurofibromas compared with MPNSTs, though the differences were not statistically significant (0.9 ± 1.8 vs 6.6 ± 5.8, respectively; $P < .61$), but the spectral pattern in the TMA fraction was significantly different (23% ± 43% vs 88% ± 22%, respectively; $P = .005$). Taking a TMA fraction > 50% as a definition for malignant disease in the patients with NF-1 resulted in a sensitivity, specificity, positive predictive value, and negative predictive value for diagnosis of an MPNST of 100%, 77.8%, 75.0%, and 100%, respectively.

Schwannomas had 2 distinct patterns, either showing an absence of detectable metabolite signals (in 4/7), or a high TMA fraction (> 50% in 3/7), similar to that found in MPNSTs. For neurofibromas, most cases showed a TMA fraction < 10%, but 2 patients had a TMA fraction of 100%. Hence, comparing all schwannomas with all neurofibromas, differences in the TMA concentrations (3.0 ± 3.5 vs 1.5 ± 2.1, respectively; $P < .66$) and TMA fraction (46% ± 50% vs 12% ± 31%, respectively; $P < .27$) were not significant.

A total of 9 patients (16 lesions in total) with NF-1 or schwannomatosis also underwent FDG-PET. In the schwannoma case studied by FDG-PET ($n=1$), PET correctly classified the lesion as nonsuspicious, whereas MR spectroscopy suggested malignant disease (TMA fraction, 60%). For the benign neurofibromas (9 lesions), MR spectroscopy and FDG-PET results were concordant (and agreed with the final diagnosis) in 6 of 9 lesions, and were discordant in 3 of 9 lesions. In 1 case, MR spectroscopy produced a false-positive result, and in 2 cases, FDG-PET produced false-positive results (Table 1); however, in one of these cases, the FDG-PET was a single time point (rather than early and delayed acquisitions), possibly accounting for the discrepancy. For MPNSTs, results of MR spectroscopy and FDG-PET were concordant in all cases.

DISCUSSION

PNSTs are among the most common soft tissue tumors that occur in the musculoskeletal system.[1,29] Most nerve sheath tumors are benign, with schwannomas and neurofibromas accounting for 6% of soft tissue tumors, but MPNSTs are rare. However, patients with NF-1 carry a lifetime risk of up to 10% for the development of an MPNST.[28] Unfortunately, the ability to distinguish benign PNSTs and MPNSTs with current clinical and imaging tools remains challenging, with only a few anatomic features[6-8] or markers of metabolic activity by PET[10,13,24] assisting in the diagnosis of malignant disease. Our present study offers preliminary evidence that proton MR spectroscopy is feasible in PNSTs and is a potentially valuable method for their characterization. Although qualitative interpretation of the presence or absence of a TMA signal on MR spectroscopy appears to have a high sensitivity for diagnosis of malignant disease, it offers poor specificity because many benign lesions also show a detectable TMA signal. The specificity of MR spectroscopy is increased by quantitative estimates of either the TMA concentration or TMA fraction.

In musculoskeletal masses, previous proton MR spectroscopy studies have established TMA as a marker for malignant disease.[18] The TMA peak resonating at 3.2 ppm is a composite peak with contributions from phosphocholine, glycerophosphocholine, and free choline itself, metabolites that are involved in the synthesis and degradation of cell membranes. During malignant transformation, several alterations in TMA metabolism are known to occur, including increases in the synthesis of phosphocholine due to choline-kinase activation, as well as upregulation of phosphatidylcholine metabolism by *ras* mutations, found in multiple tumor

types, including sarcomas.[30] Of note, the loss of neurofibromin that occurs as a result of the *Nf1* mutation results in constitutive activation of ras.[31] Consistent with prior investigations, all MPNSTs in the current series showed detectable levels of TMA, with a high TMA content reflected both in elevated TMA concentrations as well as in TMA fractions > 50%. However, several of the benign PNSTs in this study showed detectable TMA peaks consistent with a recent review that included 9 benign PNSTs,[18] all of which had discrete TMA peaks. Quantitative analysis of TMA content in this study allowed further characterization because most benign PNSTs showed lower TMA concentrations and TMA fractions than those of MPNSTs, though there were outliers that had a similar TMA profile to MPNSTs. These results may be the result of a lack of specificity of the technique or the result of the heterogeneity of the tumor with some regions harboring atypical, but not yet malignant, histologic patterns.[32] The cumulative results of this study suggest that MR spectroscopy has a high negative predictive value for malignant disease in PNSTs: When no detectable TMA peak was present, or TMA content (concentration or fraction) was low, a benign diagnosis was found in all cases.

FDG-PET, along with MR imaging, is a key technique used to assess for malignant transformation in the setting of NF-1 based on a sensitivity of 0.89 (95% CI, 0.76–0.96) and a specificity of 0.95 (95% CI, 0.88–0.98) in this patient population.[11] In this study, FDG-PET findings were concordant with the MR spectroscopy findings in all cases of malignant disease (with no false-negative findings); however, both MR spectroscopy and

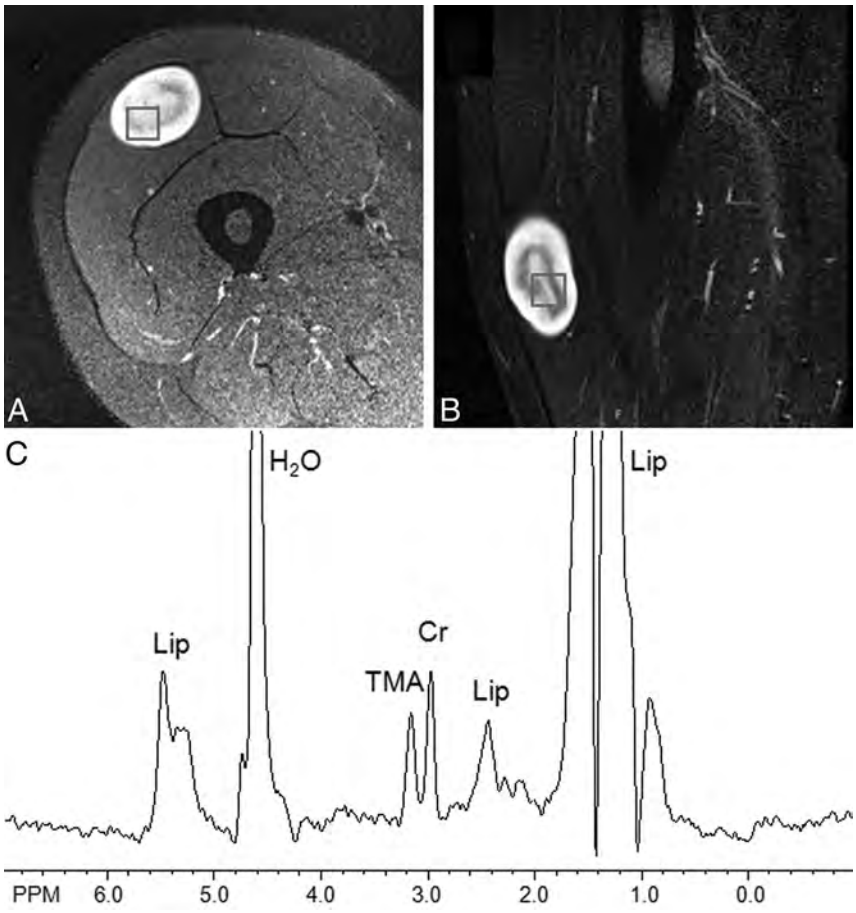

FIG 2. A 41-year-old woman with a biopsy-proven neurofibroma. Axial fat-suppressed T2 weighted (*A*) and sagittal STIR (*B*) images of the right thigh show a soft tissue mass with a low internal signal and a high peripheral signal. Voxel placement is shown, from multivoxel MR spectroscopic imaging in this lesion. *C*, MR spectroscopy revealed a detectable TMA peak within the mass, with a TMA concentration of 3.5 institutional units and a TMA fraction of 7%.

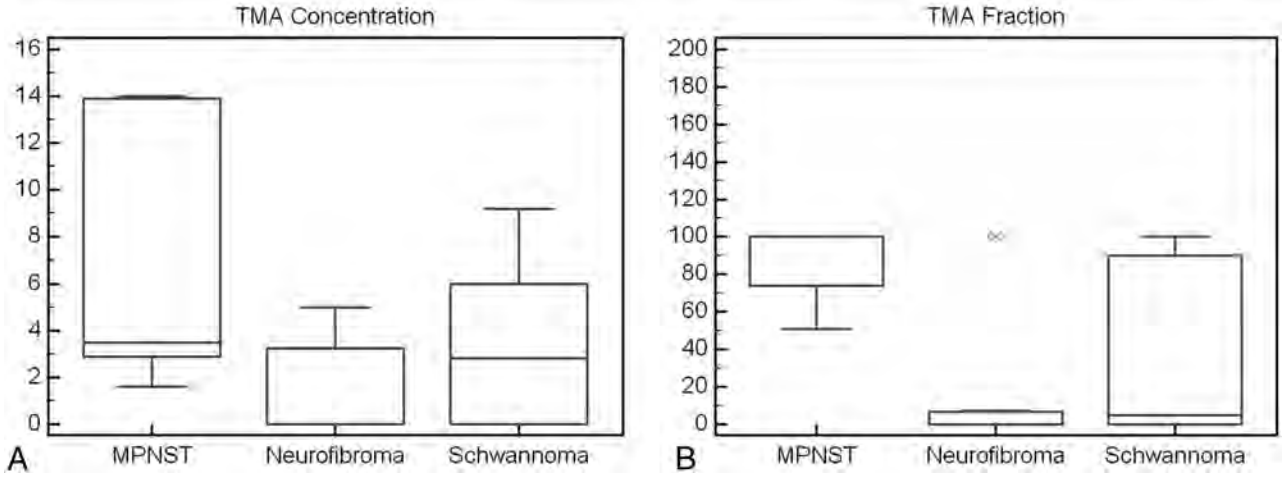

FIG 3. Comparison of the TMA concentrations (*A*) and TMA fractions (*B*) of MPNSTs, neurofibromas, and schwannomas. These results indicate that both the TMA concentration and the TMA fraction are sensitive for the detection of malignant disease, but the TMA fraction is more specific for distinguishing benign neurofibromas from MPNSTs. TMA content does not reliably distinguish between schwannomas and neurofibromas.

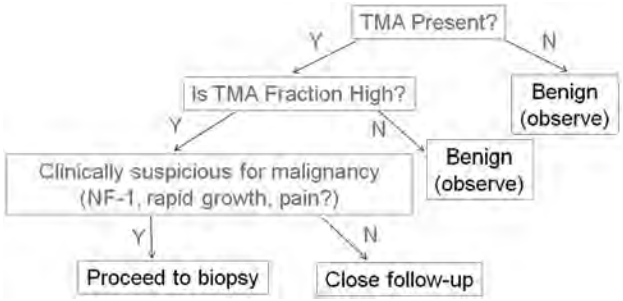

FIG 4. Flow chart suggesting the potential usefulness of proton MR spectroscopy for the assessment of PNSTs. Because MR spectroscopy offers a negative predictive value of 100%, the absence of detectable TMA within a PNST indicates a benign diagnosis. However, when a detectable TMA peak is present, quantitative results are helpful: A low TMA fraction indicates a benign PNST, whereas a high TMA fraction supports the diagnosis of malignant disease. In a patient with suspicious clinical features or risk factors for malignant disease (such as a history of NF-1), a high TMA fraction signifies the need for a biopsy. In a patient without suspicious clinical features or a history of NF-1 but with a high TMA fraction, close follow-up rather than biopsy may be entertained.

FDG-PET had false-positive results and were discordant in 3 cases of benign neurofibromas. Hence, MR spectroscopy has initial results similar to FDG-PET for a diagnosis of malignant disease in patients with NF-1, and may be used clinically to further characterize FDG-avid lesions as either neurofibroma or MPNST. Further investigations are needed to assess the additive role and cost-effectiveness of MR spectroscopy and PET, alone or in combination, in patients with NF-1. It is interesting to note that metabolic activity within some schwannomas has been found to be similar to that of MPNSTs by PET,[24] and this finding may explain why some schwannomas in the current series were metabolically active by MR spectroscopy, to a level similar to that of MPNSTs. Figure 4 shows a potential diagnostic algorithm for the incorporation of MR spectroscopy into the characterization of PNSTs, though further study is needed to determine the interplay of FDG-PET and MR spectroscopy in the characterization of PNSTs.

Another important clinical dilemma lies with the characterization of benign PNSTs, as no MR imaging finding is sufficiently specific to allow confident discrimination between neurofibromas and schwannomas,[4] though their distinction carries therapeutic implications. Schwannomas may be amenable to nerve-sparing resection, whereas the resection of a neurofibroma has the potential for greater morbidity.[33] Unfortunately, our investigations showed no significant differences in either TMA concentration or TMA fraction between schwannomas and neurofibromas, suggesting that other techniques will be required to assist in this distinction.

The small sample size of patients recruited from a single-center, tertiary institution in this study was a limitation, but the results provided preliminary data as a framework for future investigations with a larger number of participants and variety of PNST histologic features. Although all malignant cases in this study had histologic confirmation, several benign cases did not have a tissue diagnosis because these patients all had NF-1 or schwannomatosis, and there is rarely indication for surgical intervention for lesions that are behaving in a benign clinical fashion. All patients without histologic confirmation had clinical and radiographic follow-up confirming benign lesion behavior. However, the lack of histologic confirmation for these benign cases and the relatively short-term follow-up available remains a limitation of this study. It is challenging to determine when malignant transformation occurs within a benign neurofibroma in patients with NF-1, and, though rare, schwannomas may occur in NF-1 and neurofibromas may occur in schwannomatosis such that clinical diagnosis on the basis of tumor behavior and imaging features is not always accurate. Second, in patients with NF-1, the use of single-voxel MR spectroscopy may be suboptimal for the identification of MPNSTs, given that MPNSTs typically arise within benign neurofibromas and these tumors are large and heterogeneous. In the future, higher-spatial resolution multivoxel MR spectroscopic imaging (shown to be feasible in this study) may be used to map out lesion heterogeneity and may be a helpful approach to identify high-risk regions to biopsy. Finally, the performance of MR spectroscopy requires availability of a dedicated physicist familiar with the technique, and optimization before implementation clinically, given the complexities of the approach.

CONCLUSIONS

Quantitative MR spectroscopy measurements of Cho content in PNSTs provides good separation between benign and malignant nerve sheath tumors, offering a high negative predictive value when Cho content is negligible, and a high sensitivity when the Cho fraction is $>$ 50%. With quantitative methodology, the specificity of MR spectroscopy to distinguish benign and MPNSTs is increased compared with a qualitative assessment of Cho content (the presence of detectable Cho). MR spectroscopy may prove to be especially useful in patients with NF-1 who are at high risk for malignant transformation of benign neurofibromas, and may offer supporting or complementary information to interpret FDG-PET results in this regard. Although MR spectroscopy is a promising technique, the true value of MR spectroscopy to clinical decision-making in the work-up of PNSTs remains to be elucidated with larger studies.

Disclosures: Laura M. Fayad—*UNRELATED: Grants/Grants Pending:* Gerard (2008–2010),* Siemens (2011).* Jaishri O. Blakeley—*UNRELATED: Grants/Grants Pending:* Children's Tumor Foundation,* National Institutes of Health (NIH),* GlaxoSmithKline,* Lilly,* Sanifo.* Daniel Durand—*RELATED: Grant:* Radiological Society of North America (RSNA) R&E Foundation, Comments: During the period in which I worked on this manuscript, I received 50% salary support from the RSNA Research & Education Foundation; *UNRELATED: Consultancy:* Osiris Therapeutics, Med IQ, Comments: I have served as a consultant for these companies at various points during the past 8 years; *Employment:* McKinsey & Company, Evolent Health, Comments: I work full time as a healthcare consultant and have held positions with McKinsey & Company, Evolent Health; *Payment for Development of Educational Presentations:* Usmlerx.com, McGraw-Hill, Comments: I was a longtime editor of the McGraw-Hill First Aid for Boards Study series. Michael Jacobs—*UNRELATED: Grants/Grants Pending:* NIH,* Comments: U01CA070095, U01CA140204, P50CA103175. Peter Barker—*UNRELATED: Consultancy:* Olea Medical; *Grants/Grants Pending:* NIH*; *Payment for Lectures (including service on speaker bureaus):* Philips Healthcare; *Royalties:* Cambridge University Press. **Money paid to institution.*

REFERENCES

1. Kransdorf MJ. **Benign soft-tissue tumors in a large referral population: distribution of specific diagnoses by age, sex, and location.** *AJR Am J Roentgenol* 1995;164:395–402
2. Kransdorf MJ, Murphey MD, Smith SE. **Imaging of soft tissue neo-**

plasms in the adult: benign tumors. *Semin Musculoskelet Radiol* 1999;3:21–38
3. Murphey MD, Kransdorf MJ, Smith SE. **Imaging of soft tissue neoplasms in the adult: malignant tumors.** *Semin Musculoskelet Radiol* 1999;3:39–58
4. Jee WH, Oh SN, McCauley T, et al. **Extraaxial neurofibromas versus neurilemmomas: discrimination with MRI.** *AJR Am J Roentgenol* 2004;183:629–33
5. Bhargava R, Parham DM, Lasater OE, et al. **MR imaging differentiation of benign and malignant peripheral nerve sheath tumors: use of the target sign.** *Pediatr Radiol* 1997;27:124–29
6. Li CS, Huang GS, Wu HD, et al. **Differentiation of soft tissue benign and malignant peripheral nerve sheath tumors with magnetic resonance imaging.** *Clin Imaging* 2008;32:121–27
7. Matsumine A, Kusuzaki K, Nakamura T, et al. **Differentiation between neurofibromas and malignant peripheral nerve sheath tumors in neurofibromatosis 1 evaluated by MRI.** *J Cancer Res Clin Oncol* 2009;135:891–900
8. Wasa J, Nishida Y, Tsukushi S, et al. **MRI features in the differentiation of malignant peripheral nerve sheath tumors and neurofibromas.** *AJR Am J Roentgenol* 2010;194:1568–74
9. Bensaid B, Giammarile F, Mognetti T, et al. **Utility of 18 FDG positron emission tomography in detection of sarcomatous transformation in neurofibromatosis type 1.** *Ann Dermatol Venereol* 2007;134:735–41
10. Bredella MA, Torriani M, Hornicek F, et al. **Value of PET in the assessment of patients with neurofibromatosis type 1.** *AJR Am J Roentgenol* 2007;189:928–35
11. Ferner RE, Golding JF, Smith M, et al. **[18F]2-fluoro-2-deoxy-D-glucose positron emission tomography (FDG PET) as a diagnostic tool for neurofibromatosis 1 (NF1) associated malignant peripheral nerve sheath tumours (MPNSTs): a long-term clinical study.** *Ann Oncol* 2008;19:390–94
12. Karabatsou K, Kiehl TR, Wilson DM, et al. **Potential role of 18fluorodeoxyglucose-positron emission tomography/computed tomography in differentiating benign neurofibroma from malignant peripheral nerve sheath tumor associated with neurofibromatosis 1.** *Neurosurgery* 2009;65:A160–70
13. Warbey VS, Ferner RE, Dunn JT, et al. **[18F]FDG PET/CT in the diagnosis of malignant peripheral nerve sheath tumours in neurofibromatosis type-1.** *Eur J Nucl Med Mol Imaging* 2009;36:751–57
14. Fayad LM, Jacobs MA, Wang X, et al. **Musculoskeletal tumors: how to use anatomic, functional, and metabolic MR techniques.** *Radiology* 2012;265:340–56
15. Hascalik S, Celik O, Erdem G, et al. **Proton magnetic resonance spectroscopy findings of a sacrococcygeal schwannoma.** *Int J Gynecol Cancer* 2006;16 Suppl 1:344–48
16. Qi ZH, Li CF, Li ZF, et al. **Preliminary study of 3T 1H MR spectroscopy in bone and soft tissue tumors.** *Chin Med J (Engl)* 2009;122:39–43
17. Lee CW, Lee JH, Kim DH, et al. **Proton magnetic resonance spectroscopy of musculoskeletal lesions at 3 T with metabolite quantification.** *Clin Imaging* 2010;34:47–52
18. Subhawong TK, Wang X, Durand DJ, et al. **Proton MR spectroscopy in metabolic assessment of musculoskeletal lesions.** *AJR Am J Roentgenol* 2012;198:162–72
19. Wang CK, Li CW, Hsieh TJ, et al. **Characterization of bone and soft-tissue tumors with in vivo 1H MR spectroscopy: initial results.** *Radiology* 2004;232:599–605
20. Fayad LM, Wang X, Salibi N, et al. **A feasibility study of quantitative molecular characterization of musculoskeletal lesions by proton MR spectroscopy at 3 T.** *AJR Am J Roentgenol* 2010;195:W69–75
21. Fayad LM, Bluemke DA, McCarthy EF, et al. **Musculoskeletal tumors: use of proton MR spectroscopic imaging for characterization.** *J Magn Reson Imaging* 2006;23:23–28
22. Fayad LM, Barker PB, Jacobs MA, et al. **Characterization of musculoskeletal lesions on 3-T proton MR spectroscopy.** *AJR Am J Roentgenol* 2007;188:1513–20
23. Fayad LM, Barker PB, Bluemke DA. **Molecular characterization of musculoskeletal tumors by proton MR spectroscopy.** *Semin Musculoskelet Radiol* 2007;11:240–45
24. Benz MR, Czernin J, Dry SM, et al. **Quantitative F18-fluorodeoxyglucose positron emission tomography accurately characterizes peripheral nerve sheath tumors as malignant or benign.** *Cancer* 2010;116:451–58
25. Bonekamp D, Smith MA, Zhu H, et al. **Quantitative SENSE-MRSI of the human brain.** *Magn Reson Imaging* 2010;28:305–13
26. Natt O, Bezkorovaynyy V, Michaelis T, et al. **Use of phased array coils for a determination of absolute metabolite concentrations.** *Magn Reson Med* 2005;53:3–8
27. Fayad LM, Salibi N, Wang X, et al. **Quantification of muscle choline concentrations by proton MR spectroscopy at 3 T: technical feasibility.** *AJR Am J Roentgenol* 2010;194:W73–79
28. Perrin RG, Guha A. **Malignant peripheral nerve sheath tumors.** *Neurosurg Clin N Am* 2004;15:203–16
29. Kransdorf MJ. **Malignant soft-tissue tumors in a large referral population: distribution of diagnoses by age, sex, and location.** *AJR Am J Roentgenol* 1995;164:129–34
30. Glunde K, Artemov D, Penet MF, et al. **Magnetic resonance spectroscopy in metabolic and molecular imaging and diagnosis of cancer.** *Chem Rev* 2010;110:3043–59
31. Thomas L, Richards M, Mort M, et al. **Assessment of the potential pathogenicity of missense mutations identified in the GTPase-activating protein (GAP)-related domain of the neurofibromatosis type-1 (NF1) gene.** *Hum Mutat* 2012;33:1687–96
32. Beert E, Brems H, Daniëls B, et al. **Atypical neurofibromas in neurofibromatosis type 1 are premalignant tumors.** *Genes Chromosomes Cancer* 2011;50:1021–32
33. Murphey MD, Smith WS, Smith SE, et al. **From the archives of the AFIP. Imaging of musculoskeletal neurogenic tumors: radiologic-pathologic correlation.** *Radiographics* 1999;19:1253–80

AJNR

Go Green!

AJNR urges American Society of Neuroradiology members to reduce their environmental footprint by voluntarily suspending their print subscription.

The savings in paper, printing, transportation, and postage not only help members cut down on clutter, but go to fund new electronic enhancements and expanded content.

The digital edition of *AJNR* presents the print version in its entirety, along with extra features including:

- Publication Preview
- Case of the Week
- Podcasts
- Special Collections
- The *AJNR* Blog
- Weekly Poll

It also **reaches subscribers much faster than print**. An **electronic table of contents** will be sent directly to your mailbox to notify you as soon as it publishes.

Readers can **search, reference, and bookmark** current and archived content 24 hours a day on www.ajnr.org, rather than thumb through stacks of accumulated paper issues for articles and images they need.

http://www.ajnr.org/cgi/feedback

ASNR members who wish to opt out of print can do so by using the Feedback form on the *AJNR* Website (**http://www.ajnr.org/cgi/feedback**). Just type "Go Green" in the subject line to stop print and spare our ecosystem.

Target® Detachable Coils

See package insert for complete indications, contraindications, warnings and instructions for use.

INTENDED USE / INDICATIONS FOR USE

Target Detachable Coils are intended to endovascularly obstruct or occlude blood flow in vascular abnormalities of the neurovascular and peripheral vessels. Target Detachable Coils are indicated for endovascular embolization of:

- Intracranial aneurysms
- Other neurovascular abnormalities such as arteriovenous malformations and arteriovenous fistulae
- Arterial and venous embolizations in the peripheral vasculature

CONTRAINDICATIONS

None known.

POTENTIAL ADVERSE EVENTS

Potential complications include, but are not limited to: allergic reaction, aneurysm perforation and rupture, arrhythmia, death, edema, embolus, headache, hemorrhage, infection, ischemia, neurological/intracranial sequelae, post-embolization syndrome (fever, increased white blood cell count, discomfort), TIA/stroke, vasospasm, vessel occlusion or closure, vessel
perforation, dissection, trauma or damage, vessel rupture, vessel thrombosis. Other procedural complications including but not limited to: anesthetic and contrast media risks, hypotension, hypertension, access site complications.

WARNINGS

- Contents supplied STERILE using an ethylene oxide (EO) process. Do not use if sterile barrier is damaged. If damage is found, call your Stryker Neurovascular representative.
- For single use only. Do not reuse, reprocess or resterilize. Reuse, reprocessing or resterilization may compromise the structural integrity of the device and/or lead to device failure which, in turn, may result in patient injury, illness or death. Reuse, reprocessing or resterilization may also create a risk of contamination of the device and/or cause patient infection or cross-infection, including, but not limited to, the transmission of infectious disease(s) from one patient to another. Contamination of the device may lead to injury, illness or death of the patient.
- After use, dispose of product and packaging in accordance with hospital, administrative and/or local government policy.
- **This device should only be used by physicians who have received appropriate training in interventional neuroradiology or interventional radiology and preclinical training on the use of this device as established by Stryker Neurovascular.**
- Patients with hypersensitivity to 316LVM stainless steel may suffer an allergic reaction to this implant.
- MR temperature testing was not conducted in peripheral vasculature, arteriovenous malformations or fistulae models.
- The safety and performance characteristics of the Target Detachable Coil System (Target Detachable Coils, InZone Detachment Systems, delivery systems and accessories) have not been demonstrated with other manufacturer's devices (whether coils, coil delivery devices, coil detachment systems, catheters, guidewires, and/or other accessories). Due to the potential incompatibility of non Stryker Neurovascular devices with the Target Detachable Coil System, the use of other manufacturer's device(s) with the Target Detachable Coil System is not recommended.
- To reduce risk of coil migration, the diameter of the first and second coil should never be less than the width of the ostium.
- In order to achieve optimal performance of the Target Detachable Coil System and to reduce the risk of thromboembolic complications, it is critical that a continuous infusion of appropriate flush solution be maintained between a) the femoral sheath and guiding catheter, b) the 2-tip microcatheter and guiding catheters, and c) the 2-tip microcatheter and Stryker Neurovascular guidewire and delivery wire. Continuous flush also reduces the potential for thrombus formation on, and crystallization of infusate around, the detachment zone of the Target Detachable Coil.
- Do not use the product after the "Use By" date specified on the package.
- Reuse of the flush port/dispenser coil or use with any coil other than the original coil may result in contamination of, or damage to, the coil.
- Utilization of damaged coils may affect coil delivery to, and stability inside, the vessel or aneurysm, possibly resulting in coil migration and/or stretching.
- The fluoro-saver marker is designed for use with a Rotating Hemostatic Valve (RHV). If used without an RHV, the distal end of the coil may be beyond the alignment marker when the fluoro-saver marker reaches the microcatheter hub.
- If the fluoro-saver marker is not visible, do not advance the coil without fluoroscopy.
- Do not rotate delivery wire during or after delivery of the coil. Rotating the Target® Detachable Coil delivery wire may result in a stretched coil or premature detachment of the coil from the delivery wire, which could result in coil migration.
- Verify there is no coil loop protrusion into the parent vessel after coil placement and prior to coil detachment. Coil loop protrusion after coil placement may result in thromboembolic events if the coil is detached.
- Verify there is no movement of the coil after coil placement and prior to coil detachment. Movement of the coil after coil placement may indicate that the coil could migrate once it is detached.
- Failure to properly close the RHV compression fitting over the delivery wire before attaching the InZone® Detachment System could result in coil movement, aneurysm rupture or vessel perforation.
- Verify repeatedly that the distal shaft of the catheter is not under stress before detaching the Target Detachable Coil. Axial compression or tension forces could be stored in the 2-tip microcatheter causing the tip to move during coil delivery. Microcatheter tip movement could cause the aneurysm or vessel to rupture.
- Advancing the delivery wire beyond the microcatheter tip once the coil has been detached involves risk of aneurysm or vessel perforation.
- The long term effect of this product on extravascular tissues has not been established so care should be taken to retain this device in the intravascular space.
- To reduce risk of coil migration, the diameter of the first and second coil should never be less than the width of the ostium.
- In order to achieve optimal performance of the Target Detachable Coil System and to reduce the risk of thromboembolic complications, it is critical that a continuous infusion of appropriate flush solution be maintained between a) the femoral sheath and guiding catheter, b) the 2-tip microcatheter and guiding catheters, and c) the 2-tip microcatheter and Stryker Neurovascular guidewire and delivery wire. Continuous flush also reduces the potential for thrombus formation on, and crystallization of infusate around, the detachment zone of the Target Detachable Coil.
- Do not use the product after the "Use By" date specified on the package.
- Reuse of the flush port/dispenser coil or use with any coil other than the original coil may result in contamination of, or damage to, the coil.

Damaged delivery wires may cause detachment failures, vessel injury or unpredictable distal tip response during coil deployment. If a delivery wire is damaged at any point during the procedure, do not attempt to straighten or otherwise repair it. Do not proceed with deployment or detachment. Remove the entire coil and replace with undamaged product.

- Verify repeatedly that the distal shaft of the catheter is not under stress before detaching the Target Detachable Coil. Axial compression or tension forces could be stored in the 2-tip microcatheter causing the tip to move during coil delivery. Microcatheter tip movement could cause the aneurysm or vessel to rupture.
- After use, dispose of product and packaging in accordance with hospital, administrative and/or local government policy.

CAUTIONS / PRECAUTIONS

- Federal Law (USA) restricts this device to sale by or on the order of a physician.
- Besides the number of InZone Detachment System units needed to complete the case, there must be an extra InZone Detachment System unit as back up.
- Removing the delivery wire without grasping the introducer sheath and delivery wire together may result in the detachable coil sliding out of the introducer sheath.
- Failure to remove the introducer sheath after inserting the delivery wire into the RHV of the microcatheter will interrupt normal infusion of flush solution and allow back flow of blood into the microcatheter.
- Some low level overhead light near or adjacent to the patient is required to visualize the fluoro-saver marker; monitor light alone will not allow sufficient visualization of the fluoro-saver marker.
- Advance and retract the Target Detachable Coil carefully and smoothly without excessive force. If unusual friction is noticed, slowly withdraw the Target Detachable Coil and examine for damage. If damage is present, remove and use a new Target Detachable Coil. If friction or resistance is still noted, carefully remove the Target Detachable Coil and microcatheter and examine the microcatheter for damage.
- If it is necessary to reposition the Target Detachable Coil, verify under fluoroscopy that the coil moves with a one-to-one motion. If the coil does not move with a one-to-one motion or movement is difficult, the coil may have stretched and could possibly migrate or break. Gently remove both the coil and microcatheter and replace with new devices.
- Increased detachment times may occur when:
  – Other embolic agents are present.
  – Delivery wire and microcatheter markers are not properly aligned.
  – Thrombus is present on the coil detachment zone.
- Do not use detachment systems other than the InZone Detachment System.
- Increased detachment times may occur when delivery wire and microcatheter markers are not properly aligned.
- Do not use detachment systems other than the InZone Detachment System.

Stryker Neurovascular
47900 Bayside Parkway
Fremont, CA 94538-6515
stryker.com/neurovascular

Date of Release: FEB/2014
EX_EN_US

Trevo® XP ProVue Retrievers

See package insert for complete indications, complications, warnings, and instructions for use.

INDICATIONS FOR USE

The Trevo Retriever is intended to restore blood flow in the neurovasculature by removing thrombus in patients experiencing ischemic stroke within 8 hours of symptom onset. Patients who are ineligible for intravenous tissue plasminogen activator (IV t-PA) or who fail IV t-PA therapy are candidates for treatment.

COMPLICATIONS

Procedures requiring percutaneous catheter introduction should not be attempted by physicians unfamiliar with possible complications which may occur during or after the procedure. Possible complications include, but are not limited to, the following: air embolism; hematoma or hemorrhage at puncture site; infection; distal embolization; pain/headache; vessel spasm, thrombosis, dissection, or perforation; emboli; acute occlusion; ischemia; intracranial hemorrhage; false aneurysm formation; neurological deficits including stroke; and death.

COMPATIBILITY

3x20 mm retrievers are compatible with Trevo® Pro 14 Microcatheters (REF 90231) and Trevo® Pro 18 Microcatheters (REF 90238). 4x20 mm retrievers are compatible with Trevo® Pro 18 Microcatheters (REF 90238). Compatibility of the Retriever with other microcatheters has not been established. Performance of the Retriever device may be impacted if a different microcatheter is used. The Merci® Balloon Guide Catheters are recommended for use during thrombus removal procedures. Retrievers are compatible with the Abbott Vascular DOC® Guide Wire Extension (REF 22260).

WARNINGS

- Contents supplied STERILE, using an ethylene oxide (EO) process. Nonpyrogenic.
- To reduce risk of vessel damage, adhere to the following recommendations:
  – Take care to appropriately size Retriever to vessel diameter at intended site of deployment.
  – Do not perform more than six (6) retrieval attempts in same vessel using Retriever devices.
  – Maintain Retriever position in vessel when removing or exchanging Microcatheter.
- To reduce risk of kinking/fracture, adhere to the following recommendations:
  – Immediately after unsheathing Retriever, position Microcatheter tip marker just proximal to shaped section. Maintain Microcatheter tip marker just proximal to shaped section of Retriever during manipulation and withdrawal.
  – Do not rotate or torque Retriever.
  – Use caution when passing Retriever through stented arteries.
- Do not resterilize and reuse. Structural integrity and/or function may be impaired by reuse or cleaning.
- The Retriever is a delicate instrument and should be handled carefully. Before use and when possible during procedure, inspect device carefully for damage. Do not use a device that shows signs of damage. Damage may prevent device from functioning and may cause complications.
- Do not advance or withdraw Retriever against resistance or significant vasospasm. Moving or torquing device against resistance or significant vasospasm may result in damage to vessel or device. Assess cause of resistance using fluoroscopy and if needed resheath the device to withdraw.
- If Retriever is difficult to withdraw from the vessel, do not torque Retriever. Advance Microcatheter distally, gently pull Retriever back into Microcatheter, and remove Retriever and Microcatheter as a unit. If undue resistance is met when withdrawing the Retriever into the Microcatheter, consider extending the Retriever using the Abbott Vascular DOC guidewire extension (REF 22260) so that the Microcatheter can be exchanged for a larger diameter catheter such as a DAC® catheter. Gently withdraw the Retriever into the larger diameter catheter.
- Administer anti-coagulation and anti-platelet medications per standard institutional guidelines.

PRECAUTIONS

- Prescription only – device restricted to use by or on order of a physician.
- Store in cool, dry, dark place.
- Do not use open or damaged packages.
- Use by "Use By" date.
- Exposure to temperatures above 54°C (130°F) may damage device and accessories. Do not autoclave.
- Do not expose Retriever to solvents.
- Use Retriever in conjunction with fluoroscopic visualization and proper anti-coagulation agents.
- To prevent thrombus formation and contrast media crystal formation, maintain a constant infusion of appropriate flush solution between guide catheter and Microcatheter and between Microcatheter and Retriever or guidewire.
- Do not attach a torque device to the shaped proximal end of DOC® Compatible Retriever. Damage may occur, preventing ability to attach DOC® Guide Wire Extension.

Concentric Medical
301 East Evelyn
Mountain View, CA 94041

Stryker Neurovascular
47900 Bayside Parkway
Fremont, CA 94538-6515
stryker.com/neurovascular

Date of Release: FEB/2014
EX_EN_US

stryker® Neurovascular

Trevo® XP
PROVUE RETRIEVER

Take Control. Capture More.

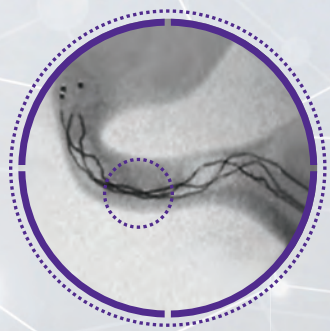

Easy to Deliver

- **48% less delivery force** required as demonstrated in bench testing*

Easy to Place

- **Distal FlexCell Design** including softer distal segment,† shorter landing zone‡ and bright radiopaque markers

Easy to See

- **Full-length radiopacity††** for precise placement, visible integration and interactive retrieval

See for Yourself: TrevoXP.com

All photographs taken by Stryker Neurovascular.
Bench test results may not necessarily be indicative of clinical performance.
Testing completed by Stryker Neurovascular. Data on file and available upon request.

* Compared to Solitaire FR, 4x20mm.
† Bench testing included Trevo XP ProVue, 4x20mm (n=57) and Solitaire FR, 4x20mm and 4x15mm (n=8).
‡ Compared to Trevo® ProVue Retriever.
†† Bench model photo.
Solitaire is a trademark of Tyco Healthcare Group LP composed of Covidien, Inc.

Stroke: *Our Only Focus. Our Ongoing Promise.*